frontiers | Research Topics

# Molecular mechanisms in ocular development and disease

**Edited by**
Rajalekshmy Shyam, Elizabeth Zuniga-Sanchez, Deepika Vasudevan and Daisy Y. Shu

**Published in**
Frontiers in Cell and Developmental Biology

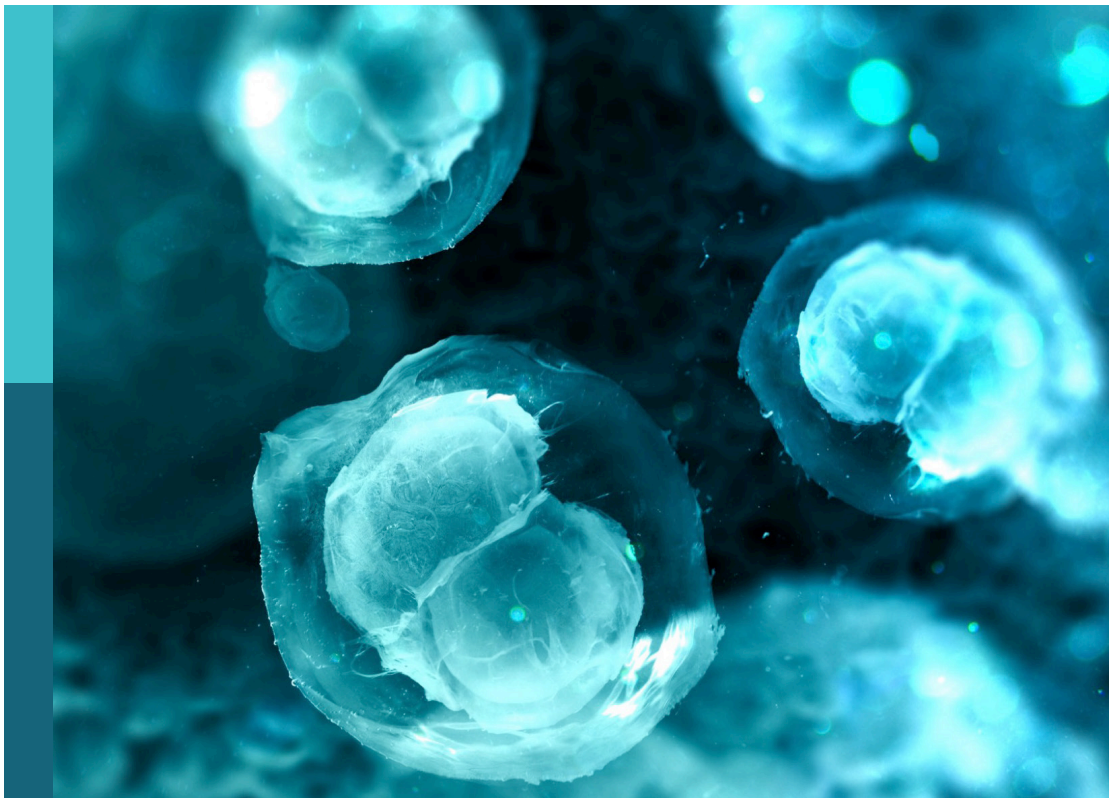

ISSN 1664-8714
ISBN 978-2-8325-2875-4
DOI 10.3389/978-2-8325-2875-4

## About Frontiers

Frontiers is more than just an open access publisher of scholarly articles: it is a pioneering approach to the world of academia, radically improving the way scholarly research is managed. The grand vision of Frontiers is a world where all people have an equal opportunity to seek, share and generate knowledge. Frontiers provides immediate and permanent online open access to all its publications, but this alone is not enough to realize our grand goals.

## Frontiers journal series

The Frontiers journal series is a multi-tier and interdisciplinary set of open-access, online journals, promising a paradigm shift from the current review, selection and dissemination processes in academic publishing. All Frontiers journals are driven by researchers for researchers; therefore, they constitute a service to the scholarly community. At the same time, the *Frontiers journal series* operates on a revolutionary invention, the tiered publishing system, initially addressing specific communities of scholars, and gradually climbing up to broader public understanding, thus serving the interests of the lay society, too.

## Dedication to quality

Each Frontiers article is a landmark of the highest quality, thanks to genuinely collaborative interactions between authors and review editors, who include some of the world's best academicians. Research must be certified by peers before entering a stream of knowledge that may eventually reach the public - and shape society; therefore, Frontiers only applies the most rigorous and unbiased reviews. Frontiers revolutionizes research publishing by freely delivering the most outstanding research, evaluated with no bias from both the academic and social point of view. By applying the most advanced information technologies, Frontiers is catapulting scholarly publishing into a new generation.

## What are Frontiers Research Topics?

Frontiers Research Topics are very popular trademarks of the *Frontiers journals series*: they are collections of at least ten articles, all centered on a particular subject. With their unique mix of varied contributions from Original Research to Review Articles, Frontiers Research Topics unify the most influential researchers, the latest key findings and historical advances in a hot research area.

Find out more on how to host your own Frontiers Research Topic or contribute to one as an author by contacting the Frontiers editorial office: frontiersin.org/about/contact

# Molecular mechanisms in ocular development and disease

**Topic editors**

Rajalekshmy Shyam — Indiana University Bloomington, United States
Elizabeth Zuniga-Sanchez — Baylor College of Medicine, United States
Deepika Vasudevan — University of Pittsburgh, United States
Daisy Y. Shu — Schepens Eye Research Institute, Harvard Medical School, United States

**Citation**

Shyam, R., Zuniga-Sanchez, E., Vasudevan, D., Shu, D. Y., eds. (2023). *Molecular mechanisms in ocular development and disease*. Lausanne: Frontiers Media SA. doi: 10.3389/978-2-8325-2875-4

# Table of contents

05 Editorial: Molecular mechanisms in ocular development and disease
Rajalekshmy Shyam, Daisy Y. Shu, Elizabeth Zuniga-Sanchez and Deepika Vasudevan

08 Valproic Acid Reduces Neuroinflammation to Provide Retinal Ganglion Cell Neuroprotection in the Retina Axotomy Model
James R. Tribble, Elizabeth Kastanaki, A. Berşan Uslular, Carola Rutigliani, Tim J. Enz and Pete A. Williams

18 From Bench to Bed: The Current Genome Editing Therapies for Glaucoma
Meihui He, Rong Rong, Dan Ji and Xiaobo Xia

32 Connexin Mutants Cause Cataracts Through Deposition of Apatite
Peter J. Minogue, Andre J. Sommer, James C. Williams Jr, Sharon B. Bledsoe, Eric C. Beyer and Viviana M. Berthoud

42 Deficiency of the bZIP transcription factors Mafg and Mafk causes misexpression of genes in distinct pathways and results in lens embryonic developmental defects
Shaili D. Patel, Deepti Anand, Hozumi Motohashi, Fumiki Katsuoka, Masayuki Yamamoto and Salil A. Lachke

61 The pathophysiological mechanisms underlying diabetic retinopathy
Lindan Wei, Xin Sun, Chenxi Fan, Rongli Li, Shuanglong Zhou and Hongsong Yu

73 Dysfunctional peroxisomal lipid metabolisms and their ocular manifestations
Chuck T. Chen, Zhuo Shao and Zhongjie Fu

97 Eyes on CHARGE syndrome: Roles of CHD7 in ocular development
Laura A. Krueger and Ann C. Morris

117 Methodologies to unlock the molecular expression and cellular structure of ocular lens epithelial cells
Justin Parreno, Grace Emin, Michael P. Vu, Jackson T. Clark, Sandeep Aryal, Shaili D. Patel and Catherine Cheng

134 Analysis of mitochondrial dynamics and function in the retinal pigment epithelium by high-speed high-resolution live imaging
Li Xuan Tan, Jianlong Li, Colin J. Germer and Aparna Lakkaraju

150 Porcn is essential for growth and invagination of the mammalian optic cup
Sabine Fuhrmann, Sara Ramirez, Mirna Mina Abouda and Clorissa D. Campbell

162 Chemical signaling in the developing avian retina: Focus on cyclic AMP and AKT-dependent pathways
A. T. Duarte-Silva, L. G. R. Ximenes, M. Guimarães-Souza, I. Domith and R. Paes-de-Carvalho

183 Blimp-1/PRDM1 and Hr3/RORβ specify the blue-sensitive photoreceptor subtype in *Drosophila* by repressing the hippo pathway
Joseph Bunker, Mhamed Bashir, Sydney Bailey, Pamela Boodram, Alexis Perry, Rory Delaney, Maria Tsachaki, Simon G. Sprecher, Erik Nelson, Gerald B. Call and Jens Rister

199 Patterning of the *Drosophila* retina by the morphogenetic furrow
Jasmine Warren and Justin P. Kumar

frontiers | Frontiers in Cell and Developmental Biology

TYPE Editorial
PUBLISHED 29 June 2023
DOI 10.3389/fcell.2023.1244123



OPEN ACCESS

EDITED AND REVIEWED BY
Ana Cuenda,
Spanish National Research Council (CSIC), Spain

*CORRESPONDENCE
Rajalekshmy Shyam,
rashyam@iu.edu
Deepika Vasudevan,
deepika.vasudevan@pitt.edu

RECEIVED 21 June 2023
ACCEPTED 22 June 2023
PUBLISHED 29 June 2023

CITATION
Shyam R, Shu DY, Zuniga-Sanchez E and Vasudevan D (2023), Editorial: Molecular mechanisms in ocular development and disease.
*Front. Cell Dev. Biol.* 11:1244123.
doi: 10.3389/fcell.2023.1244123



# Editorial: Molecular mechanisms in ocular development and disease

Rajalekshmy Shyam[1]*, Daisy Y. Shu[2,3], Elizabeth Zuniga-Sanchez[4] and Deepika Vasudevan[5]*

[1]Indiana University School of Optometry, Bloomington, IN, United States, [2]Schepens Eye Research Institute of Massachusetts Eye and Ear, Boston, MA, United States, [3]Department of Ophthalmology, Harvard Medical School, Boston, MA, United States, [4]Department of Ophthalmology, Baylor College of Medicine, Houston, TX, United States, [5]Department of Cell Biology, University of Pittsburgh School of Medicine, Pittsburgh, PA, United States

KEYWORDS

**eye developent, retina, cornea, ophthalmological disease, optic nerve, photoreceptor**

Editorial on the Research Topic
Molecular mechanisms in ocular development and disease

## Introduction

From developmental defects that affect infants and children to age-related defects that impact older adults, a vast and complex range of ophthalmological disorders affects nearly 2.2 billion individuals globally. Each step in light perception and processing involves multiple cell types and signaling pathways that we collectively refer to as the visual system. A substantial portion of our understanding of this remarkable system comes from basic research using model organisms such as mice, rats, zebrafish and fruit flies. Such research has been crucial not only in identifying signaling pathways that instruct normal development and functioning of the eye, but also in tracing the etiology of ocular pathologies. This Research Topic presents a collection of new research and comprehensive review articles that describe recent advancements in our understanding of visual development and ocular diseases.

The articles in this Research Topic can be broadly classified into three groups: a set of review articles summarizing recent progress in specific disorders, a set of research articles focused on disease etiology and interventions, and a third set of research articles focused on the development of the visual system.

The first of the review articles by He et al. provides a comprehensive overview of technological advances in gene therapy as a promising approach to treating glaucoma, which is the leading cause of blindness worldwide. The current mainstay for treating glaucoma is through topical medications or surgery to lower the intraocular pressure (IOP). However, there are many risk factors outside of elevated IOP that drive glaucoma, which call for new gene therapy-based strategies targeting pathogenic genes that have been linked to primary open angle glaucoma (MYOC, NTF4, OPTN, WDR36).

Next, Wei et al. review the multifactorial mechanisms underlying diabetic retinopathy including oxidative stress, inflammation, neovascularization and

neurodegeneration. They extensively discuss the key role of the "gut-retinal axis" in maintaining normal metabolic function and immune regulation in the retina. This is critical because hyperglycemia in diabetic patients can lead to dysregulation of the gut microbiota, resulting in intestinal inflammation and changes in the metabolome. The authors also highlight key areas of research that will inform the development of therapeutic strategies that prevent disease progression while treating patient symptoms. Krueger and Morris outline the unanswered questions on the pathogenesis of CHARGE syndrome, a genetic disorder characterized by ocular coloboma, heart defects, choanal atresia, growth retardation, genital abnormalities, and ear abnormalities. The authors place special emphasis on pathogenic variations in the protein Chromodomain helicase DNA binding protein 7 (CHD7), which causes the majority of CHARGE syndrome cases. Consistent with the theme of this Research Topic, the article discusses known molecular roles for CHD7 and its effects on vertebrate ocular development and function. Finally, an article by Chen et al. discusses the need to study the role of lipid metabolism, as effected by peroxisomes, in eye diseases. Notably, the authors summarize cases of ocular symptoms in patients with peroxisomal disorders. Peroxisomes are highly specialized enzyme-rich organelles that mediate degradation of long-chain fatty acids amongst other substrates, and communicate extensively with other organelles critical for retinal function such as the endoplasmic reticulum, mitochondria and lysosomes.

In the cluster of research articles focused on disease etiology and treatment strategies, Tribble et al. propose a new pharmacological approach using valproic acid as a neuroprotective agent for retinal ganglion cells. Treatment with valproic acid improved microglial architecture and prevented astrocyte remodeling in the retina, indicating the potential of this treatment modality for ocular neurodegenerative diseases such as glaucoma. Next, Minogue et al. examined the protein composition of the lens in two mouse models that develop cataracts due to mutations in connexin46 and connexin50. They use micro-computed tomography to show that there is calcium phosphate present in the form of apatite in the lens of mutant mice but not in the wildtype. This work supports the idea that cataracts form due to abnormal mineralization within the lens. Another cutting edge study by Tan et al. team utilize live cell imaging to analyze mitochondrial dynamics and functions in Retinal Pigment Epithelial (RPE) cells. Strikingly, they show that typical lab fixation protocols disrupt mitochondria integrity, thus highlighting the suitability of live-cell imaging for studying mitochondrial dynamics in RPE cells. Their results find substantial loss in mitochondrial integrity in albino mice compared to pigmented mice, suggesting critical roles for pigmentation in cellular metabolism. This cluster was home to another methods paper by Parreno et al. who provide detailed experimental protocols to investigate the molecular expression patterns and cellular structures in lens epithelial cells. The lens of the eye is covered by a thin layer of epithelial cells. One of the complications associated with cataract surgery is that the lens epithelial cells undergo an epithelial-mesenchymal transition resulting in the formation of a secondary cataract. Their protocols span multiple lens epithelia systems including native, primary culture, and immortalized cells, making this an excellent resource for studying lens cell biology.

The third set of research articles showcased mouse and *Drosophila* models to study the development of the visual system. Patel et al. used a compound mouse knockout model to show that the bZIP transcription factors, MafG and MafK are required for lens development. They dissect the underlying mechanism using transcriptomics to reveal clusters of target genes associated with cytoskeletal and extracellular matrix functions that likely mediate the effects of MafG and MafK in lens development. Fuhrmann et al. research group similarly uses a mouse model to investigate the role of Porcn, a regulator of the Wnt signaling pathway during early stages of ocular development. Dysregulation of signaling cascades that regulate the morphogenetic events during early development results in congenital ocular malformations such as microphthalmia, anophthalmia, and coloboma. This work finds that temporal loss of Porcn in ocular tissues during development acutely recapitulates severe microphthalmia seen in Focal Dermal Hypoplasia. Importantly, their work sets the stage for future studies to identify the specific cell types where Porcn is required for optic cup development. This section was also home to such advanced studies on cell type specific gene regulation such as Bunker et al., who pinpoint a role for the evolutionarily conserved transcription complexes Blimp-1 and Hr3 in blue-light sensitive photoreceptor specification. In the case of the *Drosophila* eye, as with the vertebrate eye, the proportion of blue- and -green-light sensitive photoreceptors is determined by seemingly stochastic expression of transcription factors. The authors use elegant *Drosophila* genetics to show that Blimp-1 and Hr3 act as repressors of wrts, a well-known modulator of photoreceptor specification, to stochastically designate blue light-sensitive photoreceptors. This original research work is perfectly complemented by a review where Warren and Kumar artfully discuss two contrasting models for how the *Drosophila* retina is patterned: the first model makes a case for morphogen-driven gradients across stationary cells, and the second argues that mechanically driven cell flow contributes to retinal pattern formation.

## Summary

The research findings and proposed questions emanating from this Research Topic are highly relevant to understanding the complexity that underlies development, function, and diseases in the visual system. In a field that has spanned decades yet continues to pursue fundamentally formative problems, Research Topic articles such as this one hopefully serves as an influential frame of a reference within the coordinates of basic vision science.

## Author contributions

All authors listed have made a substantial, direct, and intellectual contribution to the work and approved it for publication.

## Funding

RS is funded by the National Eye Institute (K99EY032974). DS is funded by the BrightFocus Foundation Postdoctoral Fellowship Program in Macular Degeneration Research (M2021010F). EZ-S is funded by the National Eye Institute (R00EY028200, R01EY033037), Research to Prevent Blindness (RPB), and an ARVO Genentech Career Development Award. DV is funded by the National Eye Institute (R00EY029013).

## Acknowledgments

The editors would like to thank all the authors, reviewers, and editorial staff that made this Research Topic a success.

## Conflict of interest

The authors declare that the research was conducted in the absence of any commercial or financial relationships that could be construed as a potential conflict of interest.

## Publisher's note

frontiers | Frontiers in Cell and Developmental Biology

BRIEF RESEARCH REPORT
published: 12 May 2022
doi: 10.3389/fcell.2022.903436

# Valproic Acid Reduces Neuroinflammation to Provide Retinal Ganglion Cell Neuroprotection in the Retina Axotomy Model

*James R. Tribble†, Elizabeth Kastanaki†, A. Berşan Uslular, Carola Rutigliani, Tim J. Enz and Pete A. Williams**

*Department of Clinical Neuroscience, Division of Eye and Vision, St. Erik Eye Hospital, Karolinska Institutet, Stockholm, Sweden*

OPEN ACCESS

**Edited by:**
*Rajalekshmy Shyam, Indiana University Bloomington, United States*

**Reviewed by:**
*Ruchi Sharma, National Eye Institute (NIH), United States*
*Davide Ortolan, National Eye Institute (NIH), United States*
*Shahna Shahul Hameed, Indiana University-Purdue University Indianapolis, United States*

***Correspondence:**
*Pete A. Williams*
*pete.williams@ki.se*

*†These authors have contributed equally to this work*

**Specialty section:**
*This article was submitted to Cell Death and Survival, a section of the journal Frontiers in Cell and Developmental Biology*

**Received:** *24 March 2022*
**Accepted:** *18 April 2022*
**Published:** *12 May 2022*

**Citation:**
*Tribble JR, Kastanaki E, Uslular AB, Rutigliani C, Enz TJ and Williams PA (2022) Valproic Acid Reduces Neuroinflammation to Provide Retinal Ganglion Cell Neuroprotection in the Retina Axotomy Model. Front. Cell Dev. Biol. 10:903436. doi: 10.3389/fcell.2022.903436*

Neuroinflammation is a critical and targetable pathogenic component of neurodegenerative diseases, including glaucoma, the leading cause of irreversible blindness. Valproic acid has previously been demonstrated to reduce neuroinflammation and is neuroprotective in a number of experimental settings. To determine whether valproic acid can limit retinal neuroinflammation and protect retinal neurons we used an *ex vivo* retina explant (axotomy) model to isolate resident glial responses from blood-derived monocytes. Neuroinflammatory status was defined using high resolution confocal imaging with 3D morphological reconstruction and cytokine protein arrays. Valproic acid significantly reduced microglia and astrocyte morphological changes, consistent with a reduction in pro-inflammatory phenotypes. Cytokine profiling demonstrated that valproic acid significantly attenuated or prevented expression of pro-inflammatory cytokines in injured retina. This identifies that the retinal explant model as a useful tool to explore resident neuroinflammation in a rapid timescale whilst maintaining a complex system of cell interactions and valproic acid as a useful drug to further explore anti-neuroinflammatory strategies in retinal disease.

**Keywords: neuroinflammation, microglia, astrocyte, retina, glaucoma**

## BACKGROUND

Neuroinflammation is emerging as a critical and targetable pathogenic component of neurodegenerative diseases including Alzheimer's disease and glaucoma. The anti-epileptic drug valproic acid (VPA) has received renewed interest for its anti-inflammatory properties (Zhang et al., 2008). Across immune cell subtypes, including monocytes, macrophages, and T-cells, VPA has been demonstrated to drive a reduction in proinflammatory cytokine release and reduced expression of immune cell surface receptors (Soria-Castro et al., 2019). In the CNS, VPA has demonstrated both neuroprotective and anti-inflammatory effects in diverse animal models of neurodegenerative conditions including spinal cord injury, traumatic brain injury, stroke, Parkinson's disease, and optic neuritis (Kim et al., 2007; Liu et al., 2017; Chen S et al., 2018; Chen X et al., 2018; Chang et al., 2019; Kim et al., 2019). Using a comparative transcriptomics approach, we recently identified VPA as a potential modifier of expression of genes common to retinal ganglion cell axon degeneration (Enz, Tribble and Williams, 2021) (the susceptible neuron in many optic neuropathies including glaucoma, Leber's hereditary optic neuropathy, and autosomal dominant optic atrophy). Pathway analysis of genes revealed neuroinflammatory signaling pathways to be the most commonly shared element and,

as hypothesized, VPA provided significant neuroprotection to retinal ganglion cells post-axotomy. Supporting this, VPA has previously been demonstrated to reduce retinal ganglion cell apoptosis in models of glaucoma (Alsarraf et al., 2014; Kimura et al., 2015), a common neurodegenerative disease in which retinal ganglion cells degenerate. A pathogenic feature of glaucoma (in humans and animal models) is progressive retinal ganglion cell degeneration accompanied by progressive neuroinflammation (Williams et al., 2017b). Ourselves and others have identified pro-inflammatory activation of microglia and astrocytes, infiltration of monocytes from the blood, and upregulation of cytokines and neuroinflammatory molecules as key pathological components of glaucoma (Tezel et al., 2010; Bosco, Steele and Vetter, 2011; Breen et al., 2016; Gramlich et al., 2016; Williams et al., 2016; Williams et al., 2019; Cooper et al., 2020; Tribble et al., 2020; Tribble et al., 2021a). Importantly, inhibiting these processes can provide some level of neuroprotection in multiple animal models. However, this neuroprotection is not complete, and often neuroinflammatory strategies provide short-term protection but fail to provide long-term protection. Retina and optic nerve neuroinflammation in glaucoma is highly temporal and context dependent, caveated by the difference in rodent-to-human immune cell sub-types and the ongoing debate of infiltrating monocytes vs proliferative microglia in disease. As such, an anti-neuroinflammatory strategy has yet to make it to glaucoma patients.

Separating resident from infiltrating inflammatory responses in ocular tissue is a non-trivial task. Microglia and tissue macrophages share many common genetic signatures and antigens, making cell specific labeling or sorting difficult without transgenic reporter lines (which are still unlikely to be conclusively accurate and still require verification and refinement in the retina). This approach is not amenable to testing potential anti-inflammatory therapeutics for effects on resident microglia. Thus, we present a modification of the retinal explant model as a simple tool to explore only resident glia activity. Using this model, we demonstrate that VPA significantly reduces microglial morphological changes and significantly attenuates resident glial release of pro-inflammatory cytokines in response to retinal ganglion cell injury.

# METHODS

## Animal Strain and Husbandry

All breeding and experimental procedures were performed in accordance with the Association for Research for Vision and Ophthalmology (ARVO) Statement for the Use of Animals in Ophthalmic and Research. Individual study protocols were approved by Stockholm's Committee for Ethical Animal Research (10389-2018). Male C57BL/6J mice were purchased from The Jackson Laboratory (ME, United States, through SCANBUR AB, Sweden). All mice were housed in a 12 h light/12 h dark cycle with food and drinking water available *ad libitum*. All mice were used at 12-20 weeks of age.

## Retinal Explant Model

The retinal explant axotomy model has been described previously (Tribble et al., 2021c). The model was adapted for the analysis of glial responses (removal of N2 and B27 supplements from the media recipe yielded greater numbers of ramified microglia at 1 day *ex vivo* (*data not shown*)). Mice were euthanized by cervical dislocation, and eyes were enucleated immediately. Retinas were removed and flat mounted onto cell culture inserts ganglion cell layer up (Millicell 0.4 µm pore; Merck). Culture inserts were suspended in 6-well plates so that retinas were supplied by culture media from below. Neurobasal-A media supplemented with 2 mM L-glutamate (GlutaMAX, Gibco) and 1% penicillin/streptomycin (Gibco) was used, and plates were maintained at (37°C, 5% $CO_2$) for either 1 or 2 days *ex vivo*. Retinas were treated with either lipopolysaccharide (LPS; from *Salmonella enterica* serotype *typhimurium*, cell culture grade, 100 ng/ml; Sigma) or VPA (valproic acid, sodium salt, 1 mM; Merck Millipore) which was dissolved in the culture media. For controls, eyes were used immediately without culture. All eyes were either fixed in ice-cold PFA (3.7%) in PBS for histology or homogenized for cytokine array at the end time point.

## Immunofluorescent Labelling and Microscopy

Following fixation, retinas were transferred to slides and isolated using a hydrophobic barrier pen. Retinas were permeabilized with 0.5% Triton X-100 (VWR) in PBS for 60 min and blocked in 2% bovine serum albumin (Fisher Scientific) in PBS for 60 min. Primary antibodies were applied overnight at 4°C. The primary antibodies were anti-RBPMS (Rabbit, Novusbio # NBP2-20112, 1:500), anti-Iba1 (Rabbit, Abcam # 178846, 1:500), anti-GFAP (Chicken, Novusbio # NBP1-05198, 1:500), and Isolectin GS-$IB_4$ (IsoB4; Invitrogen #I21414, 0.1 mg/ml). Retinas were washed 5 times for 10 min in PBS, and secondary antibodies were applied for 4 h at room temperature. The secondary antibodies were Goat anti-Rabbit AF 568 (Invitrogen # A11011, 1:500), Goat anti-Chicken AF 647 (Abcam # ab150171, 1:500), and Streptavidin AF 488 conjugate (Invitrogen #S11223, 4 µg/ml). Retinas were washed 5 times for 10 min in PBS, DAPI nuclear stain (1 µg/ml in 1M PBS) was applied for 10 min, and tissue washed again once in PBS. Retinas were mounted using Fluoromount-G, glass coverslips were applied, and slides were sealed with nail-varnish.

## Morphological Analysis

RGC density was determined as an average of RBPMS + cells *en face* in six regions of interest per retina, as described previously (Tribble et al., 2021b). Images were acquired on a Leica DMi8 microscope with a CoolLED pE-300 white LED-based light source and a Leica DFC7000 T fluorescence color camera (all Leica). For morphological analysis of microglia and astrocytes, images were acquired on a on a Zeiss LSM800-Airy (20×, image field 532.42 × 532.42 µm, voxel size 0.26 × 0.26 × 0.47 µm). For microglia, four regions of interest were imaged at 1,000 µm from the optic nerve head as *Z*-stacks through the nerve fiber layer to the beginning of the outer nuclear layer to capture all three

microglial niches. For astrocytes, *Z*-stacks were acquired through the nerve fiber layer to the beginning of the ganglion cell layer. Microglia images were cropped in *Z* to separate the distinct microglia niches using the nuclear layers as a guide. Microglia morphology was reconstructed semi-automatically using Imaris (Bitplane, version 9.3.2), and individual microglia were analyzed. Number of filaments (processes), total filament (process) length, filament (field) area, and filament volume were calculated automatically and exported. Filament volume was divided by total length to differentiate complex and amoeboid-like microglia. Astrocyte morphology was reconstructed manually with automatic volume filling due to the difficulty in automated pathfinding along filaments. Astrocytes were treated as a network for analysis purposes. Total number of filaments, total filament length, and total filament volume were calculated automatically and exported. The degree of space-filling and filament density was determined using the Imaris cell function to isolate discrete areas enclosed by filaments (Membrane Detection algorithm, where the created astrocyte filaments were detected as cell boundaries). Enclosed area sizes and counts were calculated automatically and exported.

## Cytokine Array

Retinas were transferred to HBSS containing protease and phosphatase inhibitors and lysed by ultrasonification (Vibra-Cell). Samples were frozen at −80°C. Samples were thawed and protein was quantified by Bradford assay. Proteome Profiler Mouse XL Cytokine Arrays (R&D Systems) were used according to the manufacturer's instructions. For each sample, 100 µg of protein was used. Array membranes were imaged on a ChemiDoc iMP system (Bio-Rad) and analyzed by densitometry in FIJI following background subtraction (FIJI; (Schindelin et al., 2012). Spots were analyzed in duplicates and normalized to the reference spots as per the manufacturer's instructions.

## Statistical Analysis

All statistical analyses were performed in R software. Data were tested for normality with a *Shapiro–Wilk* test. Normally distributed data were analyzed by *Student's t*-test or *ANOVA* (with *Tukey's* HSD). Non-normally distributed data were analyzed by a *Kruskal–Wallis* test followed by *Dunn's* tests with *Benjamini and Hochberg* correction. For microglial morphology, where multiple observations (*i.e.,* individual microglia) come from the same sample (*i.e.,* same retina) a linear mixed effects model was used to reduce intra-class correlation and limit *p* value inflation (Wilson et al., 2017; Tribble et al., 2021a) using the *lme4* package in R (Bates et al., 2015). For protein array data, one-way ANOVA was performed, *p* values were adjusted for multiple comparisons to a false discovery rate (FDR; *q*). Unless otherwise stated, * = $p < 0.05$, ** = $p < 0.01$, ***$p < 0.001$, NS = non-significant ($p > 0.05$). For box plots, the center hinge represents the median, with upper and lower hinges representing the first and third quartiles; whiskers represent 1.5 times the interquartile range. Violin plots show data distribution by density with accompanying boxplots (as previously mentioned).

# RESULTS

## Retinal Ganglion Cell Axotomy Results in Microglia Neuroinflammation

In the mouse retinal axotomy model, enucleation of the eye results in complete axotomy of all retinal ganglion cell (RGC) axons, which drives rapid neurodegeneration from as early as day 1 as the retina is maintained in tissue culture. This includes fragmentation of RGC axons in the nerve fiber layer (NFL), apoptosis of RGCs in the ganglion cell layer (GCL), and atrophy of RGC dendrites in the inner plexiform layer (IPL) (Tribble et al., 2021c). Apoptosis of other retinal neurons does not occur within the first 7 days of explant (Bull et al., 2011; Binley et al., 2016). Microglia reside in three distinct niches in the retina, in the NFL/GCL, IPL, and outer plexiform layer (OPL; photoreceptor synaptic layer) where they perform homeostatic surveillance roles for synaptic and metabolic activity, and for immune or cellular debris antigens. When surveilling, microglia are ramified with numerous low volume processes, but change to a more voluminous, amoeboid morphology when activated. This is associated with a change towards pro-inflammatory and phagocytic phenotypes. By 1 day *ex vivo* (D1) microglia in the NFL/GCL, IPL, and OPL had retracted processes and decreased morphological complexity (**Figure 1A–D**) suggesting a retina wide inflammatory environment (~60% average loss of processes, total process length, field area, and ~60% increase in normalized volume in the NFL/GCL; ~70% average loss of processes, total process length, field area, and ~60% increase in normalized volume in the IPL/INL; ~65% average loss of processes, total process length, field area, and ~80% increase in normalized volume in the OPL). Microglia counts within niches demonstrated no significant net gain (proliferation or migration), or loss of microglia between layers by D1 (**Figure 1D**) (*i.e.,* in this context microglia are non-proliferative and non-migratory). By D2, microglia morphology in the NFL/GCL was distinct from that of *in vivo* native or activated phenotypes in retinal neuroinflammation and instead resembled microglia in cell culture (**Figures 1A–D**). By D2 microglia process number, process length, and field area had increased significantly over D1 and were comparable to D0, suggesting an outgrowth of processes. The processes were thick, as demonstrated by the significant increase in normalized volume over D1 microglia. This also occurred in the IPL/INL but was much less pronounced (**Figure 1A–D**). In the OPL, there were no detectable significant differences in morphology between D1 and D2 microglia. However, there was a significant decrease in microglia density in the OPL, and IPL/INL (**Figure 1D**). Together, these suggest a deviation from what would be expected *in vivo* with relevance to the NFL/GCL. We subsequently focused on D1 as a timepoint for the modeling and investigation of early neuroinflammation. We focused on the GCL/NFL as the predominant site of neurodegeneration relevant to RGCs. We tested the anti-neuroinflammatory capacity of VPA in the explant model, and compared this to LPS, a putative positive control for inducing inflammation. At D1, significant RGC death has occurred (33% average loss relative to D0

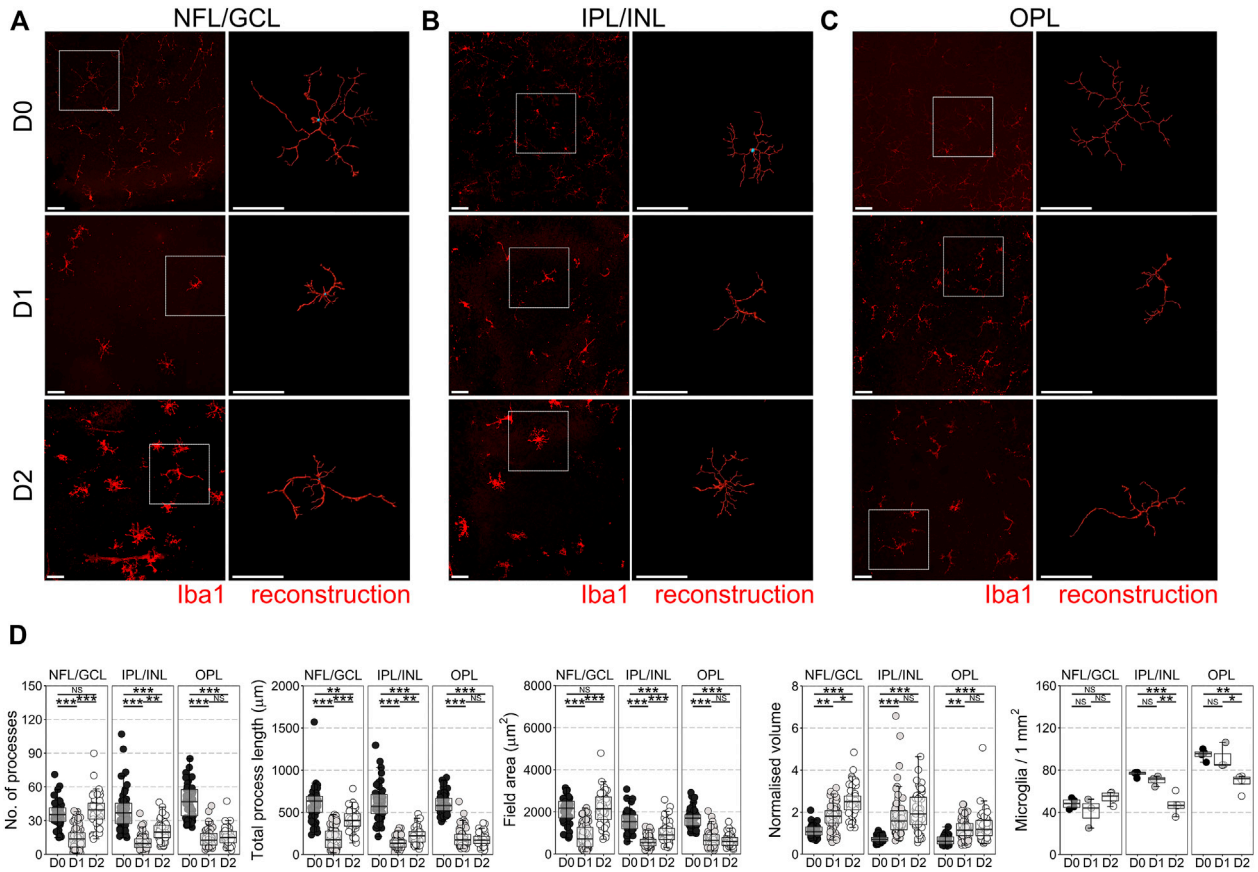


**FIGURE 1 |** Microglial morphological changes associated with pro-inflammatory phenotypes occur in all retinal microglia niches in retinal explants. Retinal explants were maintained for 1 day (D1) or 2 days (D2) *ex vivo* and compared to D0 controls (eyes fixed immediately after enucleation). IBA1 labeled microglia were imaged and individually reconstructed using Imaris software from the three retinal microglia niches **(A)** nerve fiber layer/ganglion cell layer (NFL/GCL) **(B)** inner plexiform layer/inner nuclear layer (IPL/INL), and **(C)** outer plexiform layer (OPL). **(D)** Across all microglial niches, at D1 there was a significant reduction in the number of microglia processes, total process length, field area, and normalized volume, demonstrating that microglia became less complex and more voluminous, as occurs with a shift towards pro-inflammatory phenotypes. The degree of change was no greater in any one layer, suggesting a global retinal inflammatory environment. There was no significant difference in microglial density within niches demonstrating that there is no active proliferation, migration, or apoptosis of microglia by D1. By D2, microglia in the NFL/GCL had significantly increased number of microglia processes, total process length, field area, and normalized volume, demonstrating an outgrowth of processes reminiscent of microglia in cell culture. This was similar in the IPL/INL, but not in the OPL. Iba1 = microglia specific marker, $n = 4$ retinas for all conditions, scale bars = 50 µm, * = $p < 0.05$, ** = $p < 0.01$, *** = $p < 0.001$, NS = non-significant.

controls). LPS did not significantly increase RGC death relative to untreated D1 retinas (**Supplementary Figure S1**). VPA significantly reduced RGC death at D1 compared to D1 untreated retinas, and the remaining density of RGCs was not significantly different from D0 controls (13% average loss relative to D0 controls) (**Supplementary Figure S1**).

## Valproic Acid Reduces Loss of Microglial Complexity

We next determined whether VPA reduced resident inflammation in the NFL/GCL in response to RGC injury. Individual Iba1 labeled microglia were imaged and reconstructed (**Figure 2A**). VPA significantly reduced microglial morphological changes but did not completely prevent remodeling (*i.e.,* suggesting a lowered, but not anti-inflammatory, immune cell state). Microglia in VPA treated retinas demonstrated a significantly greater number of processes (40% greater on average) and a significantly lower normalized volume (33% less on average) compared to D1 untreated retinas, without a significant difference in total process length and field area (**Figure 2B**). This demonstrates that VPA preserved a more branched morphology in microglia (*i.e.,* closer to a surveilling state than an activated state). LPS did not significantly alter microglial morphological changes at D1 relative to untreated D1 retinas (**Figure 2B**). VPA and LPS did not change microglial density in the NFL/GCL (**Figure 2B**).

## Valproic Acid Prevents Astrocyte Remodeling

Inflammatory microglial responses are strongly linked to direct activation of astrocytes, and astrocyte upregulation of GFAP (gliosis) is a prominent feature of retinal neurodegeneration.

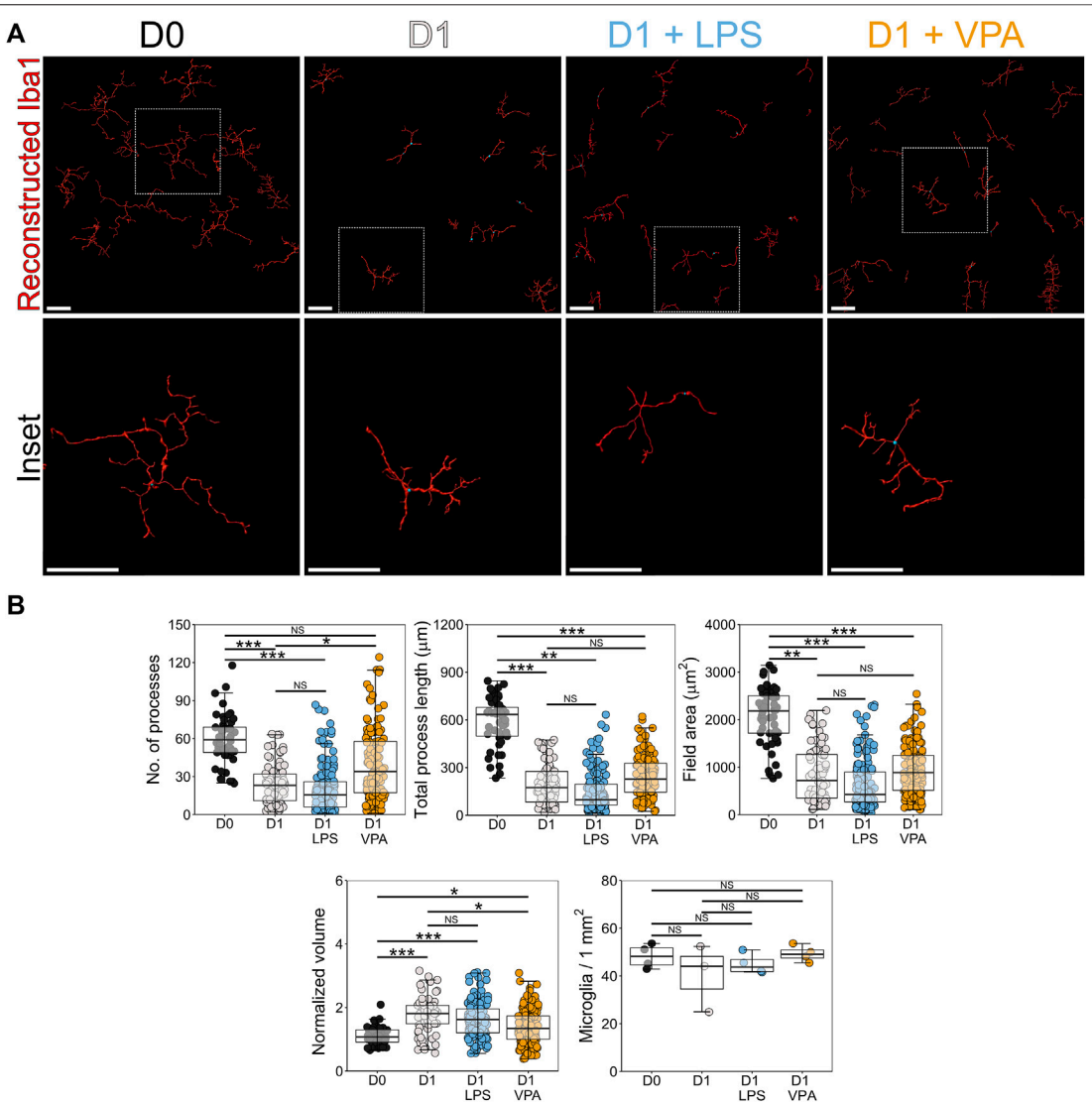


**FIGURE 2 |** Valproic acid reduces microglial morphological changes associated with pro-inflammatory phenotypes. **(A)** Retinal explants were exposed to LPS, VPA, or untreated and assessed at D1 in comparison to D0 controls. Individual IBA1 labeled microglia were reconstructed using Imaris software. **(B)** At D1 there was a significant reduction in the number of microglia processes, total process length, field area, and normalized volume, demonstrating that microglia became less complex and more voluminous, as occurs with a shift towards pro-inflammatory phenotypes. LPS treatment did not significantly enhance this morphological change. Addition of VPA significantly attenuated these morphological changes, as the number of processes remained higher, and volume was lower than in D1 controls. Total process length and field area were unchanged. There were no significant changes in microglial numbers in retinas exposed to VPA or LPS. These suggest a reduction in the magnitude of a pro-inflammatory shift and a retention of some morphological aspects associated with microglial support functions. $n = 4$ retinas for all conditions, scale bars = 50 µm, * = $p < 0.05$, ** = $p < 0.01$, *** = $p < 0.001$, NS = non-significant.

In the retina astrocytes reside only within the NFL where they support RGC axons. Astrocytes also demonstrated remodeling by D1, with increased number and total volume of GFAP fibers (both ~90% higher on average) in absence of a change to total filament length (**Figure 3A,B**). This suggests a global thickening of filaments and an increase in small filaments, thus increasing the density of GFAP fibers as is typical of reactive gliosis. Supporting this increase in filament density, astrocyte processes increased space filling of the retina, with a significant decrease in the average area enclosed by crossing filaments (52% less on average), and a significant increase in the number of areas enclosed by crossing filaments (120% higher on average) (**Figure 3B**). VPA significantly reduced astrocyte remodeling. VPA treated retinas were statistically similar to D0 controls, and VPA also significantly prevented the increase in number of filaments (3% change relative to D0), filament volume (5% change relative to D0), and decreased number and areas enclosed by crossing filaments (0.5% change relative to D0) (**Figure 3B**). LPS did not significantly alter astrocyte morphological changes at D1 relative to untreated D1 retinas (**Figure 3B**).

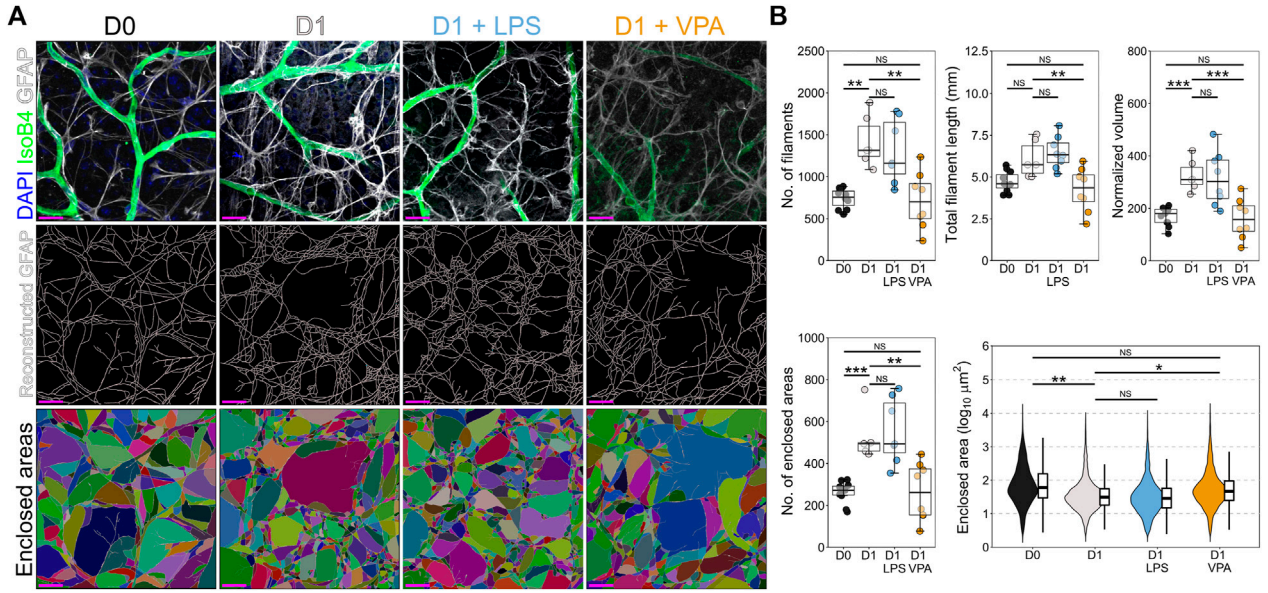


**FIGURE 3 |** Valproic acid reduces astrocyte morphological changes associated with inflammation and gliosis. **(A)** Retinal explants were exposed to LPS, VPA, or untreated and assessed at D1 in comparison to D0 controls. Individual GFAP fibers were reconstructed to generate astrocyte networks using Imaris software. Areas enclosed by these fibers were generated in Imaris to measure space filling (individual areas are demonstrated by a unique color). **(B)** At D1 there was a significant increase in the number of filaments and the normalized volume, with no significant change in total filament length. This suggests a thickening of GFAP filaments and an increase in filament intersection. Supporting this, the number of enclosed areas was significantly increased, and these were significantly smaller (decreased enclosed area) suggesting an increase in filament volume and space filling by the astrocyte network, as is typical in gliosis. Addition of LPS to the media had no significant effect on astrocyte morphology compared to those in untreated D1 retinas. Addition of VPA significantly attenuated changes to the astrocyte network, with a reduction in the number of filaments, total filament length, and the normalized volume relative to untreated D1 retinas. The number of enclosed areas was significantly reduced, and the area of these was significantly higher than in untreated D1 retinas. There was no significant difference to D0 controls. Together, these suggest a protection against astrocyte morphological change and attenuation of pro-inflammatory and gliotic astrocyte changes. GFAP = astrocyte specific marker in NFL when labeled as flat mounts, $n = 4$ retinas for all conditions, scale bars = 20 µm, * = $p < 0.05$, ** = $p < 0.01$, *** = $p < 0.001$, NS = non-significant. Individual enclosed areas demonstrated by condition as violin plots.

## Valproic Acid Attenuates Pro-inflammatory Cytokine Expression

VPA treated retina demonstrated some glial morphological changes relative to control retinas which suggests that a mild inflammatory phenotype remained. To better resolve this we profiled a panel of 111 murine chemokines and cytokines to understand the neuroinflammatory changes that occur in response to VPA treatment (**Supplementary Dataset S1**). Hierarchical clustering demonstrated that VPA treated retinas were most similar to D0 controls, and distinct from D1 untreated, and D1 LPS treated retinas (**Figure 4A**). Principle component analysis revealed that cytokine profiles were distinct across conditions with a continuum of increasing pro-inflammatory change (**Figure 4B**) predominantly determined by differences in Ccl5 and Cxcl10 (**Figure 4C**). One-way ANOVA identified 10 significantly altered cytokines ($q < 0.05$) (**Figure 4D**). Individual comparisons demonstrated an increase in pro-inflammatory cytokines at D1 compared to D0 control. Addition of LPS significantly increased Ccl5, Cxcl10, and Igfbp-1 relative to D1 untreated retinas and caused a significant increase in Il12, which was not altered in any other condition. Addition of VPA significantly reduced Ccl5, Cxcl10, Ccl2, Cxcl1, and cystatin C relative to D1 untreated controls (**Figure 4D**). There was no statistically significant difference in Ccl5, Cxcl10, Ccl2, or Icam-1-1 expression between D0 controls and D1 VPA treated retinas, all of which were significantly increased relative to control in D1 untreated retinas (**Figure 4E**), demonstrating that VPA significantly attenuated pro-inflammatory cytokine expression. However, VPA did not significantly reduce Il1a, nor prevent changes in Fgf1 or cystatin-C relative to D0 controls (**Figure 4E**). The cytokine changes observed in the explant model (D0 compared to D1 untreated) replicate findings of *in vivo* RGC injury (DBA/2J mouse model of glaucoma (Howell et al., 2011)) in the optic nerve head (ONH) and retina (**Figure 4F**). None of these genes were differentially expressed in monocytes in the DBA/2J ONH (Williams et al., 2019), further supporting that the changes identified reflected resident glial inflammation (**Figure 4F**). The % overlap with whole tissue was higher in the ONH than the retina, which occurred earlier in disease in the ONH than the retina, and was highest in later part of the disease in both cases (**Figure 4F**). This supports the utility of the explant method as a model of RGC injury and the potential to replicate findings *in vivo*.

Taken together, the retinal explant model allows for the assessment of neuroinflammation in a mature tissue system without the caveat of a systemic immune response (*i.e.,* monocyte infiltration) with which to explore resident glia responses. Using this model, we identify VPA

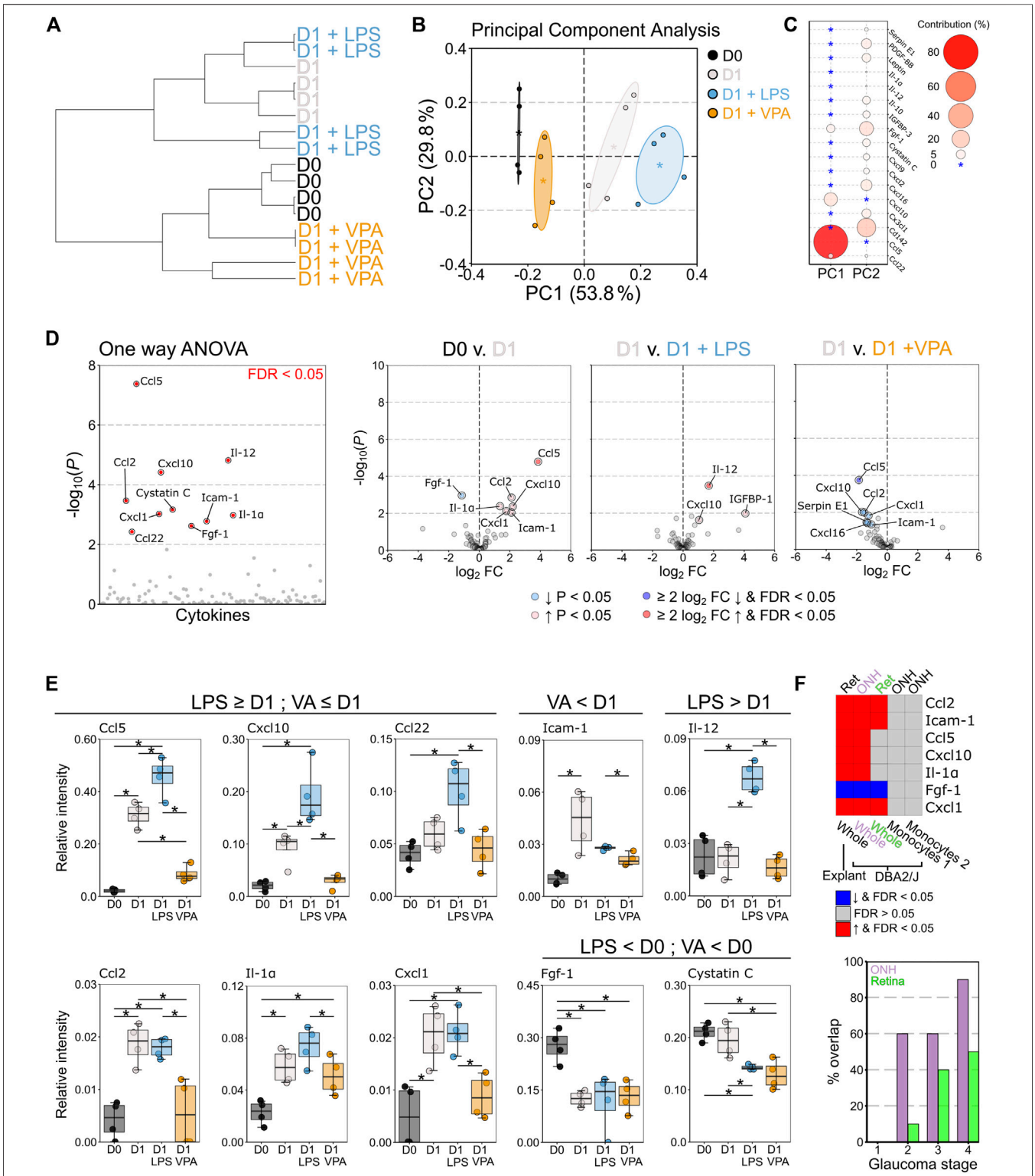


**FIGURE 4 |** Valproic acid attenuates pro-inflammatory cytokine responses from resident glia. Retinal explants were exposed to LPS, VPA, or untreated and assessed at D1 in comparison to D0 controls. Whole retinal homogenates were probed by cytokine array (111 cytokines and chemokines). **(A)** Hierarchical clustering (*Pearson* correlation) demonstrated that D0 and D1 retinas had discrete global cytokine profiles and that LPS treated retinas were most similar to D1 retinas. VPA treated retinas clustered with D0, demonstrating a protection against global cytokine changes, and a profile most similar to naïve retina. **(B)** Principle component (PC) analysis demonstrated a continuum of change from D0 retina, with D1 VPA least altered, followed by D1, and D1 LPS the most significantly changed. **(C)** This separation

(*Continued*)

**FIGURE 4 |** was predominantly driven by CCL5 and CXCL10 levels (PC 1) with small contributions from a number of cytokines across PC 2. **(D)** One-way ANOVA demonstrated 10 significantly altered cytokines between conditions (FDR <0.05). Volcano plots for individual comparisons demonstrate significant upregulation of five pro-inflammatory cytokines at D1, with a further increase in three pro-inflammatory cytokines under LPS treatment. VPA treatment significantly reduced six pro-inflammatory cytokines relative to untreated D1 retina **(E)** CCL5, CXCL10, CC122, and IL-1A demonstrated discrete graded responses by condition where D1 > D0, LPS > D1, and VPA < D1 (and not significantly changed from D0). VPA also reduced ICAM1, but did not affect FGF1 or cystatin **(C)**. LPS significantly enhanced IL12 over all conditions. Collectively, these demonstrate that LPS enhanced the pro-inflammatory response to injury in the retina even if this did not result in detectible morphological change over untreated D1 retinas. VPA demonstrated both a morphological and pro-inflammatory cytokine expression attenuation, but with a greater effect on cytokine profile. **(F)** To validate these findings against an *in vivo* model of RGC injury, significantly changed cytokines between D0 and D1 retina (ret, whole tissue, explant model) were compared to gene array data (ONH/Ret, whole tissue, DBA/2J) and RNA-sequencing data from sorted monocytes (ONH, monocytes, DBA/2J) in the DBA/2J mouse model of glaucoma. Common significant changes and the directionality of change are demonstrated as a heatmap. There was complete overlap with the optic nerve head (ONH) and 4/7 in the retina (ret) when compared to late-stage disease (stage 5 for ONH, four for retina). Monocytes do not differentially express any of these genes (monocytes 1 = enriched for pro-inflammatory changes, monocytes 2 = fewer pro-inflammatory changes), further supporting that the explant model can identify resident glia-specific changes. The % overlap in whole tissue was greatest for later disease stages, and greatest in the ONH, but there was overlap with early stages. This supports that the explant changes reflect real *in vivo* changes from early to late disease. $n = 4$ retinas for all conditions, FC = fold change, FDR = false discovery rate ($q$), * = $p < 0.05$, ** = $p < 0.01$, *** = $p < 0.001$, NS = non-significant. In **B** * = group centroid, and the cloud = 95% CI. In **C** * = 0% contribution to a principle component.

as a potent retinal anti-neuroinflammatory agent that provides RGC neuroprotection even in context of severe acute insult.

## DISCUSSION

The retinal explant model has previously been demonstrated to be a useful tool for the rapid exploration of neurodegenerative and neuroprotective mechanisms in mouse, rat, pig, and human retina (Bull et al., 2011; Bell et al., 2016; Binley et al., 2016; Osborne et al., 2016; Williams et al., 2017a; Tribble et al., 2021c; Enz, Tribble and Williams, 2021). Our data demonstrate that it is also highly amenable in investigating neuroinflammation without the loss of spatial interaction that occurs in cell culture or direct insult to glial and astrocytes that may occur from cutting brain slices for culture (as, in this model, only retinal ganglion cell axons are axotomized). However, the utility of this model may be limited to short-term investigation of RGC relevant insult since changes at D2 resembled cell culture-like outgrowth more than *in vivo* inflammatory changes. Inflammation could be successfully modulated within a 1 day time window by the addition of test compounds to the media. Using this model, we demonstrated that VPA provides significant protection against neuroinflammation. VPA significantly attenuated pro-inflammatory cytokine release and reduced glial remodeling caused by retinal ganglion cell axotomy. As a putative positive control, retinas were treated with LPS. LPS further exacerbated inflammation at D1, although this was not a strong effect. There was high overlap with inflammatory changes identified in the explant and the DBA2/J mouse model of glaucoma (Howell et al., 2011), at early and late molecular stages of disease, suggesting that this model recapitulates *in vivo* retinal inflammation well. Greater overlap in the ONH than retina reflects that the primary insult is to retinal ganglion cell axons (as the ONH is enriched for retinal ganglion cell axons). That overlap was greater in the later molecular disease stages and reflects the acute insult of the explant model. Significantly, none of the genes identified are differentially expressed by monocytes in early disease stages, further supporting that the explant model can identify resident glia-specific changes.

VPA has previously demonstrated neuroprotection of RGCs in optic nerve crush, normal tension glaucoma, and optic neuritis (Biermann et al., 2010; Kimura et al., 2015; Liu et al., 2017). VPA treatment of optic neuritis, reduced optic nerve mRNA expression of TNF-α and Il-1β, inhibited upregulation of phosphorylated NF-κB p65 and downregulation of IκB suggesting a suppression of the NF-κB signaling pathway (Liu et al., 2017). The NF-κB signaling pathway is a major driver of pro-inflammatory cytokine expression. VPA has been demonstrated to inactivate the NF-κB pathway inflammatory response by inhibiting histone deacetylase (HDAC) 3, which increases STAT1 and NF-κB acetylation (inactivating NF-κB signalling; (Chen S et al., 2018)). VPA is a broad HDAC inhibitor, with reported inhibition of HDAC1 and 2 (Class Ia), HDAC 3 (Class Ib), HDAC 8 (Class Ic), and HDAC 4, 5, and 7 (Class IIa) resulting in epigenetic inhibition of cell cycle, cell differentiation, and apoptotic genes (although the effects are cell type specific (Soria-Castro et al., 2019)). Administration of VPA to microglia *in vitro* results in apoptosis (Chen et al., 2007), although this has not been reported in animal models where neuroinflammation is a feature (*i.e.,* this may purely be a feature of isolated microglia outside of a mature tissue context). We observed no significant change in microglia numbers in VPA treated retinas which further support the need to explore inflammation in the context of *in vivo* or *ex vivo* systems where cell interactions remain intact. VPA improved RGC survival which could be a result of both HDAC mediated suppression of RGC apoptosis and a reduction in neuroinflammation. Broad and targeted inhibition of HDACs has demonstrated significant protection against apoptosis in RGCs (Biermann et al., 2010; Pelzel, Schlamp and Nickells, 2010; Chindasub et al., 2013), although targeted deletion of specific HDCAs (1-3) does not protect against injury-induced gene silencing (Schmitt et al., 2014), suggesting that the neuroprotective effects of broad-spectrum inhibitors such as VPA act through multiple mechanisms. Whether this includes suppression of glial inflammation is yet to be determined *in vivo*. Future comparison of the anti-inflammatory properties of VPA to other HDAC inhibitors (*e.g.* trichostatin A, sodium butyrate) would allow for the development of targeted HDCA inhibition of glial neuroinflammatory responses.

VPA significantly attenuated RGC apoptosis and inflammation in the explant model. Since we observed no clear difference in the degree of microglial activation between the retinal layers, this suggests that the degree of neuron insult/death is not the determinant of the degree of inflammation (since only

RGCs are injured and only RGCs have degenerated by D1). This suggests that inflammation was suppressed as a direct glial effect, rather than as secondary to improved RGC survival. We cannot preclude survival bias which would require definitive testing (*e.g.* where RGCs do not degenerate such as in mice carrying $Bax^{-/-}$ alleles and/or the Wallerian degeneration slow allele ($Wld^{S}$) in RGCs, or targeted HDAC inhibition of glia). VPA inhibition of HDAC 3 also upregulates the Nrf2/ARE pathway, promoting autophagy and antioxidative responses (Chen X et al., 2018). Owing to its simple chemical structure, VPA may also modulate metabolism, particularly the use of glucose, fatty acids, and glutamine in the brain. Chronic administration of VPA drastically reduces brain glucose consumption (Leiderman et al., 1991). Shifting retinal metabolism away from glucose using a ketogenic diet is both neuroprotective and anti-inflammatory in glaucoma (Harun-Or-Rashid et al., 2018; Harun-Or-Rashid and Inman, 2018). These support multiple mechanisms of neuroprotection and anti-inflammation action of VPA.

## CONCLUSION

The retinal explant model is a useful tool to explore resident neuroinflammation. Neuroinflammation can be modulated and explored on a rapid timescale whilst maintaining a complex system of cell interactions. VPA can attenuate resident glial inflammation in the retina and is a useful tool to further explore inhibition of pro-inflammatory glia in neurodegenerative disease.

## DATA AVAILABILITY STATEMENT

The original contributions presented in the study are included in the article/**Supplementary Materials**, further inquiries can be directed to the corresponding author.

## ETHICS STATEMENT

The animal study was reviewed and approved by Stockholm's Committee for Ethical Animal Research (10389-2018).

## AUTHOR CONTRIBUTIONS

JT conceived, designed, and performed experiments, analyzed data, and wrote the manuscript; EK performed experiments, analyzed data, and wrote the manuscript; ABU, CR, and TE performed experiments; PW conceived and designed experiments, wrote the manuscript. All authors have read and agreed to the published version of the manuscript.

## FUNDING

This research was funded by Vetenskapsrådet 2018-02124 (PAW), KI Foundation Grant for Eye Research, and KI Research Foundation Grant (JT). PW is supported by Karolinska Institutet in the form of a Board of Research Faculty Funded Career Position and by St. Erik Eye Hospital philanthropic donations.

## ACKNOWLEDGMENTS

The authors would like to thank Teresa Lejenäs for assistance with animal husbandry and maintenance and St. Erik Eye Hospital for financial support for research space and animal facilities.

## SUPPLEMENTARY MATERIAL

The Supplementary Material for this article can be found online at: https://www.frontiersin.org/articles/10.3389/fcell.2022.903436/full#supplementary-material

**Supplementary Figure S1 |** Valproic acid provides robust protection against retinal ganglion cell death following axotomy. **(A)** Using a retinal explant model, where retinas are maintained in tissue culture following eye enucleation, the effect of Valproic acid (VPA) and Lipopolysaccharide (LPS) on retinal ganglion cell (RGC) survival were assessed. **(B)** At 1 day *ex vivo* (D1), significant retinal ganglion cell death has occurred compared to naïve control retina (D0, eyes fixed immediately following enucleation). Addition of LPS to the culture media did not significantly increase RGC death at D1 (D1 + LPS). Addition of VPA significantly reduced RGC death at D1 (D1 + VPA). RBPMS = RGC specific marker, $n = 6$ retinas for all conditions, scale bars = 20 μm, * = $P < 0.05$, ** = $P < 0.01$, *** = $P < 0.001$, NS = non-significant.

## REFERENCES

Alsarraf, O., Fan, J., Dahrouj, M., Chou, C. J., Yates, P. W., and Crosson, C. E. (2014). Acetylation Preserves Retinal Ganglion Cell Structure and Function in a Chronic Model of Ocular Hypertension. *Invest. Ophthalmol. Vis. Sci.* 55 (11), 7486–7493. doi:10.1167/iovs.14-14792

Bates, D., Mächler, M., Bolker, B., and Walker, S. (2015). Fitting Linear Mixed-Effects Models Using Lme4. *J. Stat. Softw.* 67 (1), 48. doi:10.18637/jss.v067.i01

Bell, K., Wilding, C., Funke, S., Perumal, N., Beck, S., Wolters, D., et al. (2016). Neuroprotective Effects of Antibodies on Retinal Ganglion Cells in an Adolescent Retina Organ Culture. *J. Neurochem.* 139 (2), 256–269. doi:10.1111/jnc.13765

Biermann, J., Grieshaber, P., Goebel, U., Martin, G., Thanos, S., Di Giovanni, S., et al. (2010). Valproic Acid-Mediated Neuroprotection and Regeneration in Injured Retinal Ganglion Cells. *Invest. Ophthalmol. Vis. Sci.* 51 (1), 526–534. doi:10.1167/iovs.09-3903

Binley, K. E., Ng, W. S., Barde, Y. A., Song, B., and Morgan, J. E. (2016). Brain-derived Neurotrophic Factor Prevents Dendritic Retraction of Adult Mouse Retinal Ganglion Cells. *Eur. J. Neurosci.* 44 (3), 2028–2039. doi:10.1111/ejn.13295

Bosco, A., Steele, M. R., and Vetter, M. L. (2011). Early Microglia Activation in a Mouse Model of Chronic Glaucoma. *J. Comp. Neurol.* 519 (4), 599–620. doi:10.1002/cne.22516

Breen, K. T., Anderson, S. R., Steele, M. R., Calkins, D. J., Bosco, A., and Vetter, M. L. (2016). Loss of Fractalkine Signaling Exacerbates Axon Transport Dysfunction in a Chronic Model of Glaucoma. *Front. Neurosci.* 10, 526. doi:10.3389/fnins.2016.00526

Bull, N. D., Johnson, T. V., Welsapar, G., DeKorver, N. W., Tomarev, S. I., and Martin, K. R. (2011). Use of an Adult Rat Retinal Explant Model for Screening

of Potential Retinal Ganglion Cell Neuroprotective Therapies. *Invest. Ophthalmol. Vis. Sci.* 52 (6), 3309–3320. doi:10.1167/iovs.10-6873

Chang, P., Williams, A. M., Bhatti, U. F., Biesterveld, B. E., Liu, B., Nikolian, V. C., et al. (2019). Valproic Acid and Neural Apoptosis, Inflammation, and Degeneration 30 Days after Traumatic Brain Injury, Hemorrhagic Shock, and Polytrauma in a Swine Model. *J. Am. Coll. Surg.* 228 (3), 265–275. doi:10.1016/j.jamcollsurg.2018.12.026

Chen, P. S., Wang, C.-C., Bortner, C. D., Peng, G.-S., Wu, X., Pang, H., et al. (2007). Valproic Acid and Other Histone Deacetylase Inhibitors Induce Microglial Apoptosis and Attenuate Lipopolysaccharide-Induced Dopaminergic Neurotoxicity. *Neuroscience* 149 (1), 203–212. doi:10.1016/j.neuroscience.2007.06.053

Chen, S., Ye, J., Chen, X., Shi, J., Wu, W., Lin, W., et al. (2018). Valproic Acid Attenuates Traumatic Spinal Cord Injury-Induced Inflammation via STAT1 and NF-Kb Pathway Dependent of HDAC3. *J. Neuroinflammation* 15 (1), 150. doi:10.1186/s12974-018-1193-6

Chen, X., Wang, H., Zhou, M., Li, X., Fang, Z., Gao, H., et al. (2018). Valproic Acid Attenuates Traumatic Brain Injury-Induced Inflammation *In Vivo*: Involvement of Autophagy and the Nrf2/ARE Signaling Pathway. *Front. Mol. Neurosci.* 11, 117. doi:10.3389/fnmol.2018.00117

Chindasub, P., Lindsey, J. D., Duong-Polk, K., Leung, C. K., and Weinreb, R. N. (2013). Inhibition of Histone Deacetylases 1 and 3 Protects Injured Retinal Ganglion Cells. *Invest. Ophthalmol. Vis. Sci.* 54 (1), 96–102. doi:10.1167/iovs.12-10850

Cooper, M. L., Pasini, S., Lambert, W. S., D'Alessandro, K. B., Yao, V., Risner, M. L., et al. (2020). Redistribution of Metabolic Resources through Astrocyte Networks Mitigates Neurodegenerative Stress. *Proc. Natl. Acad. Sci. U.S.A.* 117 (31), 18810–18821. doi:10.1073/pnas.2009425117

Enz, T. J., Tribble, J. R., and Williams, P. A. (2021). Comparison of Glaucoma-Relevant Transcriptomic Datasets Identifies Novel Drug Targets for Retinal Ganglion Cell Neuroprotection. *J. Clin. Med.* 10 (17), 3938. doi:10.3390/jcm10173938

Gramlich, O. W., Teister, J., Neumann, M., Tao, X., Beck, S., von Pein, H. D., et al. (2016). Immune Response after Intermittent Minimally Invasive Intraocular Pressure Elevations in an Experimental Animal Model of Glaucoma. *J. Neuroinflammation* 13 (1), 82. doi:10.1186/s12974-016-0542-6

Harun-Or-Rashid, M., and Inman, D. M. (2018). Reduced AMPK Activation and Increased HCAR Activation Drive Anti-inflammatory Response and Neuroprotection in Glaucoma. *J. Neuroinflammation* 15 (1), 313. doi:10.1186/s12974-018-1346-7

Harun-Or-Rashid, M., Pappenhagen, N., Palmer, P. G., Smith, M. A., Gevorgyan, V., Wilson, G. N., et al. (2018). Structural and Functional Rescue of Chronic Metabolically Stressed Optic Nerves through Respiration. *J. Neurosci.* 38 (22), 5122–5139. doi:10.1523/jneurosci.3652-17.2018

Howell, G. R., Walton, D. O., King, B. L., Libby, R. T., and John, S. W. (2011). Datgan, a Reusable Software System for Facile Interrogation and Visualization of Complex Transcription Profiling Data. *BMC Genomics* 12, 429. doi:10.1186/1471-2164-12-429

Kim, H. J., Rowe, M., Ren, M., Hong, J.-S., Chen, P.-S., and Chuang, D.-M. (2007). Histone Deacetylase Inhibitors Exhibit Anti-inflammatory and Neuroprotective Effects in a Rat Permanent Ischemic Model of Stroke: Multiple Mechanisms of Action. *J. Pharmacol. Exp. Ther.* 321 (3), 892–901. doi:10.1124/jpet.107.120188

Kim, T., Song, S., Park, Y., Kang, S., and Seo, H. (2019). HDAC Inhibition by Valproic Acid Induces Neuroprotection and Improvement of PD-like Behaviors in LRRK2 R1441G Transgenic Mice. *Exp. Neurobiol.* 28 (4), 504–515. doi:10.5607/en.2019.28.4.504

Kimura, A., Guo, X., Noro, T., Harada, C., Tanaka, K., Namekata, K., et al. (2015). Valproic Acid Prevents Retinal Degeneration in a Murine Model of normal Tension Glaucoma. *Neurosci. Lett.* 588, 108–113. doi:10.1016/j.neulet.2014.12.054

Leiderman, D. B., Balish, M., Bromfield, E. B., and Theodore, W. H. (1991). Effect of Valproate on Human Cerebral Glucose Metabolism. *Epilepsia* 32 (3), 417–422. doi:10.1111/j.1528-1157.1991.tb04671.x

Liu, Q., Li, H., Yang, J., Niu, X., Zhao, C., Zhao, L., et al. (2017). Valproic Acid Attenuates Inflammation of Optic Nerve and Apoptosis of Retinal Ganglion Cells in a Rat Model of Optic Neuritis. *Biomed. Pharmacother.* 96, 1363–1370. doi:10.1016/j.biopha.2017.11.066

Osborne, A., Hopes, M., Wright, P., Broadway, D. C., and Sanderson, J. (2016). Human Organotypic Retinal Cultures (HORCs) as a Chronic Experimental Model for Investigation of Retinal Ganglion Cell Degeneration. *Exp. Eye Res.* 143, 28–38. doi:10.1016/j.exer.2015.09.012

Pelzel, H. R., Schlamp, C. L., and Nickells, R. W. (2010). Histone H4 Deacetylation Plays a Critical Role in Early Gene Silencing during Neuronal Apoptosis. *BMC Neurosci.* 11, 62. doi:10.1186/1471-2202-11-62

Schindelin, J., Arganda-Carreras, I., Frise, E., Kaynig, V., Longair, M., Pietzsch, T., et al. (2012). Fiji: an Open-Source Platform for Biological-Image Analysis. *Nat. Methods* 9 (7), 676–682. doi:10.1038/nmeth.2019

Schmitt, H. M., Pelzel, H. R., Schlamp, C. L., and Nickells, R. W. (2014). Histone Deacetylase 3 (HDAC3) Plays an Important Role in Retinal Ganglion Cell Death after Acute Optic Nerve Injury. *Mol. Neurodegeneration* 9, 39. doi:10.1186/1750-1326-9-39

Soria-Castro, R., Schcolnik-Cabrera, A., Rodríguez-López, G., Campillo-Navarro, M., Puebla-Osorio, N., Estrada-Parra, S., et al. (2019). Exploring the Drug Repurposing Versatility of Valproic Acid as a Multifunctional Regulator of Innate and Adaptive Immune Cells. *J. Immunol. Res.* 2019, 9678098. doi:10.1155/2019/9678098

Tezel, G., Yang, X., Luo, C., Kain, A. D., Powell, D. W., Kuehn, M. H., et al. (2010). Oxidative Stress and the Regulation of Complement Activation in Human Glaucoma. *Invest. Ophthalmol. Vis. Sci.* 51 (10), 5071–5082. doi:10.1167/iovs.10-5289

Tribble, J. R., Harder, J. M., Williams, P. A., and John, S. W. M. (2020). Ocular Hypertension Suppresses Homeostatic Gene Expression in Optic Nerve Head Microglia of DBA/2 J Mice. *Mol. Brain* 13 (1), 81. doi:10.1186/s13041-020-00603-7

Tribble, J. R., Kokkali, E., Otmani, A., Plastino, F., Lardner, E., Vohra, R., et al. (2021a). When Is a Control Not a Control? Reactive Microglia Occur throughout the Control Contralateral Pathway of Retinal Ganglion Cell Projections in Experimental Glaucoma. *Trans. Vis. Sci. Tech.* 10 (1), 22. doi:10.1167/tvst.10.1.22

Tribble, J. R., Otmani, A., Kokkali, E., Lardner, E., Morgan, J. E., and Williams, P. A. (2021b). Retinal Ganglion Cell Degeneration in a Rat Magnetic Bead Model of Ocular Hypertensive Glaucoma. *Trans. Vis. Sci. Tech.* 10 (1), 21. doi:10.1167/tvst.10.1.21

Tribble, J. R., Otmani, A., Sun, S., Ellis, S. A., Cimaglia, G., Vohra, R., et al. (2021c). Nicotinamide Provides Neuroprotection in Glaucoma by Protecting against Mitochondrial and Metabolic Dysfunction. *Redox Biol.* 43, 101988. doi:10.1016/j.redox.2021.101988

Williams, P. A., Tribble, J. R., Pepper, K. W., Cross, S. D., Morgan, B. P., Morgan, J. E., et al. (2016). Inhibition of the Classical Pathway of the Complement cascade Prevents Early Dendritic and Synaptic Degeneration in Glaucoma. *Mol. Neurodegener* 11, 26. doi:10.1186/s13024-016-0091-6

Williams, P. A., Braine, C. E., Kizhatil, K., Foxworth, N. E., Tolman, N. G., Harder, J. M., et al. (2019). Inhibition of Monocyte-like Cell Extravasation Protects from Neurodegeneration in DBA/2J Glaucoma. *Mol. Neurodegeneration* 14 (1), 6. doi:10.1186/s13024-018-0303-3

Williams, P. A., Harder, J. M., Foxworth, N. E., Cochran, K. E., Philip, V. M., Porciatti, V., et al. (2017a). Vitamin B 3 Modulates Mitochondrial Vulnerability and Prevents Glaucoma in Aged Mice. *Science* 355 (6326), 756–760. doi:10.1126/science.aal0092

Williams, P. A., Marsh-Armstrong, N., Howell, G. R., Bosco, A., Danias, J., Simon, J., et al. (2017b). Neuroinflammation in Glaucoma: A New Opportunity. *Exp. Eye Res.* 157, 20–27. doi:10.1016/j.exer.2017.02.014

Wilson, M. D., Sethi, S., Lein, P. J., and Keil, K. P. (2017). Valid Statistical Approaches for Analyzing Sholl Data: Mixed Effects versus Simple Linear Models. *J. Neurosci. Methods* 279, 33–43. doi:10.1016/j.jneumeth.2017.01.003

Zhang, Z., Zhang, Z. Y., Fauser, U., and Schluesener, H. J. (2008). Valproic Acid Attenuates Inflammation in Experimental Autoimmune Neuritis. *Cell. Mol. Life Sci.* 65 (24), 4055–4065. doi:10.1007/s00018-008-8521-4

**Conflict of Interest:** The authors declare that the research was conducted in the absence of any commercial or financial relationships that could be construed as a potential conflict of interest.

frontiers | Frontiers in Cell and Developmental Biology

REVIEW
published: 16 May 2022
doi: 10.3389/fcell.2022.879957

# From Bench to Bed: The Current Genome Editing Therapies for Glaucoma

*Meihui He*[1,2,3†], *Rong Rong*[1,2,3†], *Dan Ji*[1,2,3*] *and Xiaobo Xia*[1,2,3*]

[1]Eye Center of Xiangya Hospital, Central South University, Changsha, China, [2]Hunan Key Laboratory of Ophthalmology, Changsha, China, [3]National Clinical Research Center for Geriatric Disorders, Xiangya Hospital, Central South University, Changsha, China

Glaucoma is a group of optic neuropathies featured by degeneration of retinal ganglion cells and loss of their axons in the optic nerve. The only currently approved therapies focus on lowering intraocular pressure with medication and surgery. Over the previous few decades, technological advances and research progress regarding pathogenesis has brought glaucomatous gene therapy to the forefront. In this review, we discuss the three current genome editing methods and potential disease mechanisms of glaucoma. We further summarize different genome editing strategies that are being developed to target a number of glaucoma-related genes and pathways from four aspects including strategies to lower intraocular pressure, neuroprotection, RGC and optic nerve neuro-regeneration, and other strategies. In summary, genome therapy is a promising therapy for treating patients with glaucoma and has great potential to be widely applied in clinical practice.

**Keywords: glaucoma, gene therapy, CRISPR, eye, aqueous humor, optic nerve, retina**

OPEN ACCESS

***Edited by:***
*Daisy Y. Shu,*
*Schepens Eye Research Institute and Harvard Medical School, United States*

***Reviewed by:***
*Anton Lennikov,*
*University of Missouri, United States*
*Krish Kizhatil,*
*Jackson Laboratory, United States*

***Correspondence:**
*Xiaobo Xia*
*xbxia21@163.com*
*Dan Ji*
*475393400@qq.com*

†*These authors share first authorship*

***Specialty section:***
*This article was submitted to Molecular and Cellular Pathology, a section of the journal Frontiers in Cell and Developmental Biology*

***Received:*** *20 February 2022*
***Accepted:*** *25 April 2022*
***Published:*** *16 May 2022*

***Citation:***
*He M, Rong R, Ji D and Xia X (2022) From Bench to Bed: The Current Genome Editing Therapies for Glaucoma. Front. Cell Dev. Biol. 10:879957. doi: 10.3389/fcell.2022.879957*

## INTRODUCTION

Glaucoma is a group of optic neuropathies featured by degeneration of retinal ganglion cells (RGCs) and loss of their axons in the optic nerve (Jonas et al., 2017). By 2020, there were an estimated 80 million glaucoma patients with approximately 11.2 million people being blind, making glaucoma a leading cause of irreversible blindness worldwide (Quigley and Broman, 2006; Cook and Foster, 2012). In addition, there are a tremendous number of asymptomatic early-stage individuals, which is supported by surveys revealing that only 10–50% of people with glaucoma are aware of the disease. As a result, by the time many individuals with glaucoma come to the hospital due to eye discomfort, they often have apparent optic nerve damage and irreversible loss of visual function.

Glaucoma is classified as primary glaucoma, secondary glaucoma and congenital glaucoma, based on pathogenesis, age of onset. Primary glaucoma is further classified as open-angle and angle-closure (or closed-angle) glaucoma, according to the trabecular meshwork (TM) function and iridocorneal angle. Increased cup-disk ratio (CDR), CDR asymmetry, elevated intraocular pressure (IOP), specific genetic backgrounds, and reduced corneal thickness each raise the risk of primary glaucoma (Stein et al., 2021). Secondary glaucoma can result from trauma, tumors, use of corticosteroids, or inflammation. There are a number of secondary glaucoma variety including pigmentary, hemolytic, pseudoexfoliative, uveitic, neovascular, ciliary-block glaucoma and so on. Primary congenital glaucoma is caused by developmental abnormalities in the anterior segment and aqueous outflow pathway during fetal development. Among glaucoma, primary open-angle glaucoma (POAG) is the most common type worldwide.

**TABLE 1 |** Clinical trials investigating human genome editing for ocular diseases. Target means the diseases targeted in ophthalmology. Strategy means the experimental process by genome editing to treat the targeted disease.

| Identifier | Phase | Title | Conditions | Intervention | Status |
|---|---|---|---|---|---|
| NCT04560790 | Phase1/2 | CRISPR/Cas9 mRNA Instantaneous Gene Editing Therapy Assisted Corneal Transplantation in the Treatment of Refractory Viral Keratitis | Viral KeratitisBlindness Eye | BD111 CRISPR/Cas9 mRNA Instantaneous Gene Editing Therapy | Recruiting |
| NCT01949324 | Phase 2 | A Phase 2 Multicenter Randomized Clinical Trial of Ciliary Neurotrophic Factor (CNTF) for Macular Telangiectasia Type 2 (MacTel) | Macular Telangiectasia Type 2 | Ciliary neurotrophic factor released from NT-501 encapsulated cell implant | Completed |
| NCT02862938 | Phase 2 | Study of NT-501 Encapsulated Cell Therapy for Glaucoma Neuroprotection and Vision Restoration | glaucoma | Ciliary neurotrophic factor released from NT-501 encapsulated cell implant | Active |
| NCT04577300 | Phase 2 | Dual Intravitreal Implantation of NT-501 Encapsulated Cell Therapy for Glaucoma | glaucoma | Ciliary neurotrophic factor released from NT-501 encapsulated cell implant | Not yet recruiting |
| NCT03872479 | Phase1/2 | Open-Label, Single Ascending Dose Study to Evaluate the Safety, Tolerability, and Efficacy of EDIT-101 in Adult and Pediatric Participants with Leber Congenital Amaurosis Type 10 (LCA10) | Leber Congenital Amaurosis 10 | EDIT-101 (subretinal injection), a candidate genome-editing therapeutic, to remove the aberrant splice donor created by the IVS26 mutation in the CEP290 gene and restore normal CEP290 expression | Recruiting |

Despite the great adverse impact of glaucoma on human health, there is still no adequate treatment for completely preventing glaucoma progression and no way currently to reverse the damage. Clinical treatments focus on lowering IOP using medication or surgery. However, risk factors beyond the elevation of IOP may aggravate glaucoma. Therefore, lowering IOP in many cases fails to halt further damage to RGCs and their axons. The extent and duration of medical and surgery therapy efficacy are limited.

With recent advancements in technology and the discovery of specific disease mechanisms, there is growing possibility that future glaucoma treatment will focus more on the direct protection of RGCs and the optic nerve and neuron regeneration to reverse glaucomatous injury. This potential propels gene therapy and genome editing into the spotlight of the glaucoma field as they can be tailored to target specific disease pathways and exert lasting and effective outcomes. Of the 22 gene therapy products that had been approved worldwide as of 2019 (Ma et al., 2020), Luxturna™ by Spark Therapeutics, Inc. was the first viral ocular gene therapy. Luxturna™received FDA approval in December 2017 to treat Leber congenital amaurosis type 2 (LCA2), which is an inherited retinal disease (IRD) caused by mutations in the RPE65 gene, leading to severely impaired vision at birth. In Luxturna™ therapy, RPE65 complementary DNA (cDNA) is administrated to the subretinal space of both eyes to treat the retinal dystrophy, which has achieved great vision improvement.

Gene therapy, historically defined as the transfer of genetic material to cells, has extended into three fields, gene augmentation, gene suppression, and genome editing, of which genome editing stands out for its characteristic of precise manipulation of targeted genes. Although antiviral and anti-cancer strategies account for most clinical trials of genome editing, there have been some clinical trials regarding ocular diseases (see in **Table 1**). The eyeball has the characteristics of self-sealing, the scope of influence after gene drug injection is small, and the eye to a certain extent is an immune privileged site. Clinical trials have shown that the use of adeno-associated virus (AAV) or lentiviral (LV) vectors to deliver gene therapy in the eye do not cause systemic side effects or a significant immune response against the vectors. Therefore, the application of gene therapy in the eye for genetic-based diseases has been the first to mature. Moreover, genome editing in ophthalmology is gaining momentum with the accumulation of promising advancements in preclinical studies (see in **Table 2**).

## GENOME EDITING METHODS

Since the discovery of genes being the basic genetic unit that controls biological traits, it has become an aspiration of humans to modify them in order to cure diseases fundamentally. Gene therapy is the optimal indicated approach for diseases rooted in mutated genes. The areas in which gene therapy has been most commonly applied include cancers, monogenic diseases, cardiovascular diseases, infectious diseases, neurological diseases, and ocular diseases, among others. Gene therapy to date can be characterized as the knock-down of deleterious genes and augmentation of necessary or desirable genes and has included the genetic modification of mutated genes using site-specific editing.

### Endogenous DNA Repair Mechanisms

The realization that a targeted DNA double-strand break (DSB) can stimulate endogenous DNA repair mechanisms forms the foundation of genome editing. There are two main types of DNA repair, homology-directed repair (HDR) and non-homologous end-joining (NHEJ). HDR utilizes templates from either exogenously supplied donor sequence or sister chromatid for precise DNA repair, which leads to the insertion and correction of the relevant gene/DNA. In contrast to the predictable gene-editing that results from HDR, NHEJ functions to repair DSBs in a template-independent manner through direct ligation of DNA ends. This process is error-prone and has a high possibility of introducing insertions and/

**TABLE 2 |** Representative preclinical studies of gene editing for ocular diseases.

| Target | Strategy | References |
|---|---|---|
| Leber congenital amaurosis type 10 | Removal the aberrant splice donor created by the IVS26 mutation in the CEP290 gene | Maeder et al. (2019) |
| Meesmann's epithelial corneal dystrophy | Allele-specificdisruption of KRT12-L1$^{32}$P gene by CRISPR/Cas9 | Courtney et al. (2016) |
| Fuchs' endothelial corneal dystrophy | Reduction of intronic CTG triplet repeat expansion in the TCF4 gene by CRISPR/Cas9 | Rong et al. (2020) |
| Retinitis pigmentosa | Correctionof the Pde6b-rd1 mutation in the mouse retina | Wu et al. (2016) |
| Retinitis pigmentosa | Disruption of dominant mutation inRho-S334 gene | Bakondi et al. (2016) |
| Retinitis pigmentosa | Inserting a copy of Mertk exon 2 into intron 1 | Suzuki et al. (2016) |
| Laser-induced choroid neovascularization | Edition of genomic Vegfaand Hif1a in vivowhich abolished angiogenesis | Kim et al. (2017) |
| Autosomal dominant cone-rod dystrophy (CORD6) | Disruption of GUCY2D to alter retinal function and structure by CRISPR/Cas9 | McCullough et al. (2019) |
| Leber congenital amaurosis | Correction of a disease-associated nonsense mutation in Rpe65 in rd12 mice by CRISPR-Cas9 | Jo et al. (2019) |
| X-linked juvenile retinoschisis | Correction of the disease-associated RS1-C625T mutation in a 3D retinal organoid by CRISPR/Cas9 | Huang et al. (2019), Yang et al. (2020) |
| X-linked juvenile retinoschisis | Knocking in of the RS1 gene with the homology-independent targeted integration (HITI) strategy by CRISPR/Cas9 | Chou et al. (2020) |
| Usher syndrome type II | Deletion of the exon 12 of mouse Ush2a gene (corresponding to exon 13 of human USH2A) using CRISPR/Cas9-based exon-skipping approach | Pendse et al. (2019) |
| Usher syndrome (USH) type III | Excision of the mutated intronic CLRN1 splicing mutation | Panagiotopoulos et al. (2020) |
| Non-disease condition | Knockout of both PXDN by CRISPR in mice showed completely or almost closed eyelids with small eyes, having no apparent external morphological defects in other organs | Kim et al. (2019) |
| Enhanced S-cone syndrome | Correction of disease-causing NR2E3 mutations in patient-derived induced pluripotent stem cells (iPSCs) by CRISPR/Cas9 | Bohrer et al. (2019) |
| Non-disease condition | 11-base pair deletions to the homologous PMEL in zebrafish by CRISPR/Cas9 caused profound pigmentation defects (Pigmentary glaucoma in human) | Lahola-Chomiak et al. (2019) |
| Glaucoma | Disruption of mutant MYOC by CRISPR/Cas9 in cultured human trabecular meshwork cells resulted in lower IOP and prevents further glaucomatous damage | Jain et al. (2017) |
| Glaucoma | Disruption Aquaporin 1 resulted in reduced IOP in treated eyes by CRISPR/Cas9 | Wu et al. (2020) |
| Glaucoma | CRISPR-Cas9-mediated connective tissue growth factor (CTGF) suppression reduced glaucoma filtration surgery (GFS) fibrosisand improved human GFS outcomes | Lee et al. (2020) |
| Non-disease condition | RGCs differentiated from OPTN(E50K) mutated hPSCs by CRISPR/Cas9 exhibitednumerous neurodegenerative defects (glaucoma) | VanderWall et al. (2020) |
| Inherited retinal diseases | Correction of nonsense mutation in the Rpe65 gene regained retinal and visual functions | Suh et al. (2020) |
| Aniridia | Germline correction of the Pax6 small eye(Sey) mutation alone rescues the mutant phenotype | Mirjalili Mohanna et al. (2020) |
| Best disease, a dominant macular dystrophy | Normalization of BEST1 channel activity by CRISPR-Cas9 editing of the mutant allele | Sinha et al. (2020) |

or deletions (indels) at the site of the break. These indels may cause gene mutations leading to frameshifts and premature stop codons. It is possible to cause gene deletions through NHEJ with large DNA segments.

To stimulate endogenous cellular DNA repair, current genome editing methods focus on various types of sequence-specific nucleases that form site-specific DSBs. For genome editing, novel nucleases are used, including zinc finger nucleases (ZFNs), transcription activator-like effector nucleases (TALENs), and clustered regularly interspaced short palindromic repeats (CRISPR)/Cas9.

## ZFNs

The technology using ZFNs for genome editing was made possible with the discovery of the precise DNA-binding domain and FokI restriction endonuclease. The zinc finger protein is a type of transcription factor with the zinc finger domain forming the basis for the necessary DNA-binding specificity. The modular design of DNA-binding proteins makes it relatively easy to generate chimeric sequence-specific nucleases by replacing the FokI DNA-binding domain with a zinc finger domain.

## TALENs

Similar to ZFNs, TALENs are programmable DNA-binding nucleases with the catalytic domain of the FokI endonuclease fused to transcription activator-like effector (TALE) repeats. Different from that of ZFNs, the highly conserved 34 amino acid TALE repeats are responsible for the DNA-binding specificities of TALENs instead of zinc finger domains. Each TALE repeat specifies a single base pair and makes it possible to target any DNA sequence of choice.

## CRISPR/Ca9

CRISPR/Ca9 technology was initially derived from an adaptive immune system in bacteria that is used to defend against invading viruses. Among the main components of the technology, CRISPR RNAs (crRNAs) and trans-activating crRNAs (tracrRNAs) recognize specific DNA base pairs and the CRISPR-associated (Cas) proteins act as nucleases to perform precise cleavage of the DNA. After *in vitro* modification, the CRISPR/Ca9 has been simplified to two components by fusing the crRNAs and tracrRNAs as guide RNAs (gRNAs). The CRISPR/Cas system also requires a

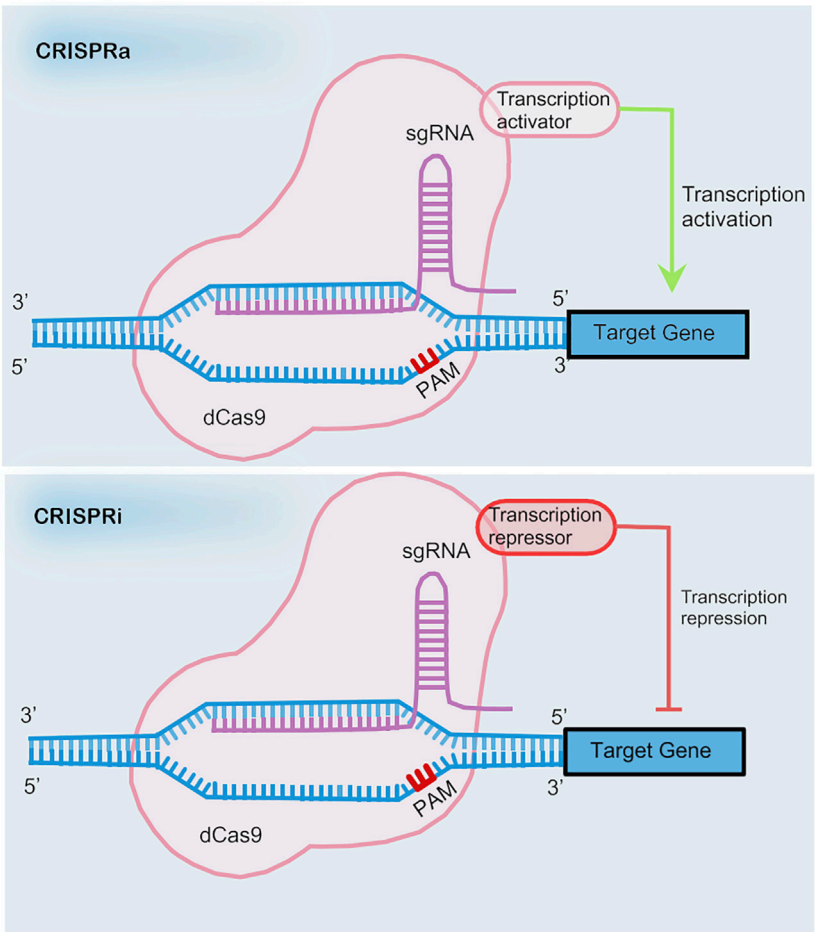


**FIGURE 1 |** The mechanism of CRISPRa and CRISPRi.

protospacer-adjacent motif (PAM) situated immediately 3′ to the target site. Cas9 has six domains of which the PAM interacting domain specifically recognizes PAM to initiate the targeted binding to the DNA. The Rec I domain of Cas9 acts as the gRNA binding domain. Domains HNH and RuvC are nuclease domains that cut single-stranded DNA. Once Cas9 finds a specific PAM, the gRNA attempts to pair with the target DNA sequence and consequently forms a DSB. Compared with the nuclease systems discussed above, Cas9 complexed with gRNAs is free of novel chimeric nucleases. Instead, the target sites are altered by simply modifying a few base pairs of the gRNAs.

Scientists today have recognized the potential ability to control genetic mutations using powerful biotechnology to modify the DNA in living cells and even modify the genetic code of all species on the planet. In addition to the NHEJ and HDR strategies, many novel CRISPR strategies have been developed. Among the many gene-editing tools, the latest and possibly most effective is CRISPR-Cas9. The development, transformation, and application of gene editing tools based on the CRISPR system have shown explosive growth, which allows for precise gene editing to better serve humans. The discovery of new Cas orthologues and variants, such as VRER SpCas9, VQR SpCas9 (Anders et al., 2016; Hu et al., 2018), Cas13 (Abudayyeh et al., 2017) and xCas9 (Hu et al., 2018), even further broadens the scope of recognition sequences in the genome and increases editing specificity.

CRISPR interference (CRISPRi) and CRISPR activation (CRISPRa) are types of safe pattern reformative CRISPR systems that avoid permanent sequence mutations (Dominguez et al., 2016) (see in **Figure 1**). Gene regulation can be achieved through a transcription depressor or transcription activator being fused with a nuclease-deficient Cas9 (dCas9). The fusion of dCas9 and the Krüppel associated box (KRAB) contributes to the down-regulation of transcription by binding with the promoter or downstream of the transcription start site via the guidance of single guide RNA (sgRNA). In the same way, a complex comprised of dCas9 and the p65 transactivating subunit of NF-kappa B or the transcriptional activation domain VP64 promotes the up-regulation of transcription.

However, application of CRISPRi is limited due to the large sizes of the coding sequences of dCas9 fusion proteins. Incorporation of RNA-protein interacting systems into gRNA helps resolve the limitation by recruiting effector proteins. The

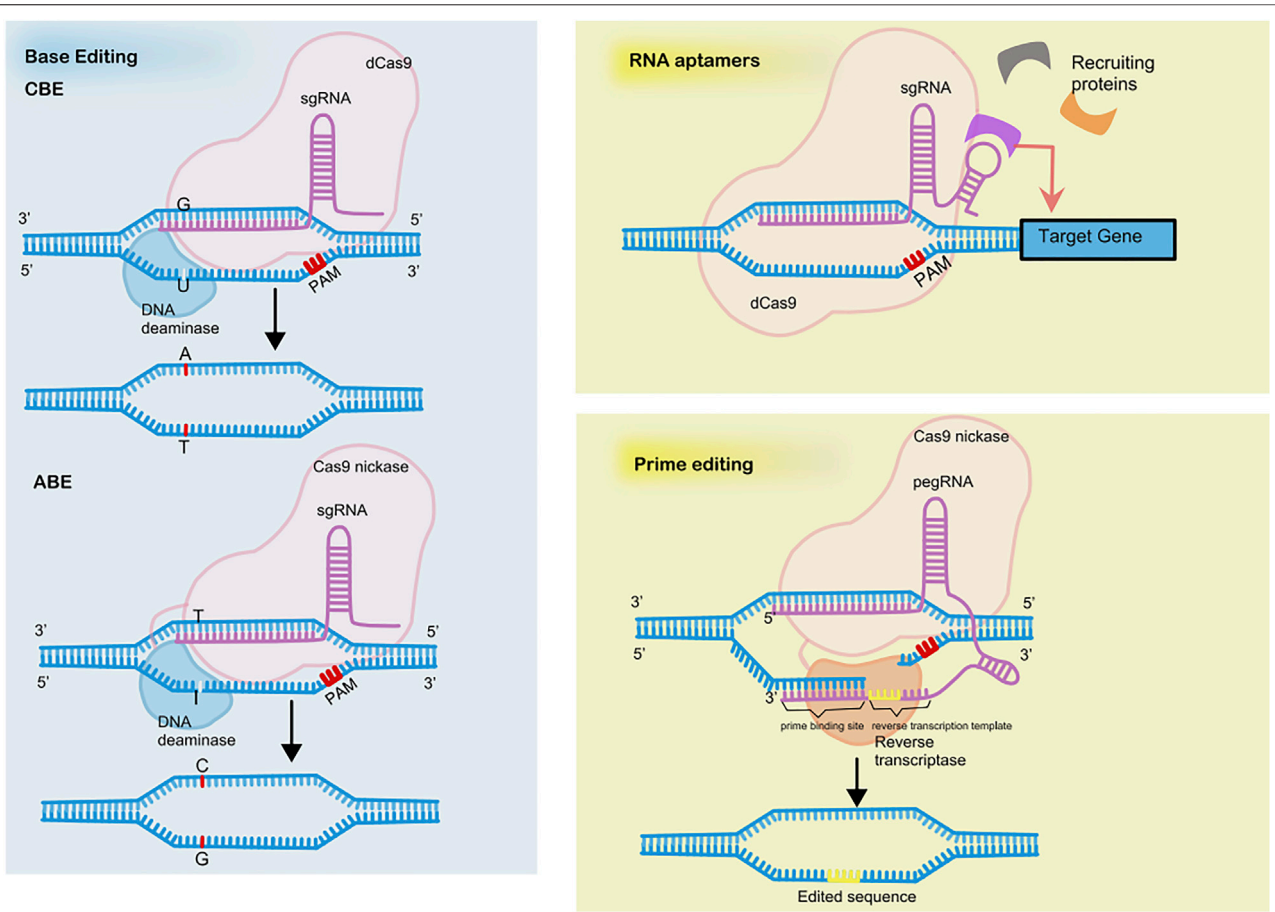


**FIGURE 2 |** The mechanisms of base editing, prime editing and RNA aptamers.

recruitment of RNA-binding proteins by RNA aptamers allows for the independent regulation of multiple genes simultaneously (Zalatan et al., 2015) (see in **Figure 2**).

Homology-independent targeting integration is a novel evolution of the NHEJ pathway, which directly ligates exogenous DNA fragments to DSBs. DSBs are generated in the genome targeting sequence, as well as both ends of the inserted DNA fragments, due to a pair of flanking CRISPR targeting sequences of the inserted DNA matching the genome targeting sequence (Suzuki et al., 2016).

The novel genome editing approach of base editing achieves precise base mutations without creating DSBs or the need of delivering templates (see in **Figure 2**). The base editor is a fusion of dCas9 with DNA deaminase plus DNA repairing proteins, if necessary. Two types of base editors have been developed, cytosine base editors (CBEs) and adenine base editors (ABEs), which allow the conversion of cytosine (C) to thymine (T) and adenine (A) to guanine (G), respectively (Komor et al., 2016; Gaudelli et al., 2017). The nucleotide position that can be effectively edited is called the active window and is located at positions four to eight downstream of the pre-interval sequence. Cas9 nickase is an H840A mutant of Cas9 and cleaves only the PAM-containing DNA strand. The innovation of combining uracil-DNA glycosylase inhibitor (UGI) and Cas9 nickase to cleave the unedited complementary strand vastly increases editing efficiency.

A brand-new genome editing tool based on CRSIPR is prime editing, which is reported to repair 89% of all 75,000 pathogenic human genetic variations (Anzalone et al., 2019) (see in **Figure 2**). Prime editing enables 12 kinds of base-to-base conversions, insertions up to 44 bases long, and deletions up to 80 bases long. The prime editor (PE) consists of a reverse transcriptase fused to a Cas9nickase and a gRNA with added RNA sequence at 3′ ends called prime editing guide RNA (pegRNA). The RNA sequence at 3′ ends includes a primer binding site to initiate reverse transcription and serves as a template for reverse transcription.

CRISPR off is a reversible and inheritable epigenetic memory editor based on the CRISPR system (Nuñez et al., 2021) (see in **Figure 3**). With guidance from gRNA, CRISPR off promotes the methylation of the targeting DNA to repress gene transcription without the generation of DSBs. Furthermore, the epigenetic memory by CRISPR off can be reversed by CRISPR on, which applies demethylase to relieve the transcription repression. This method can even silence

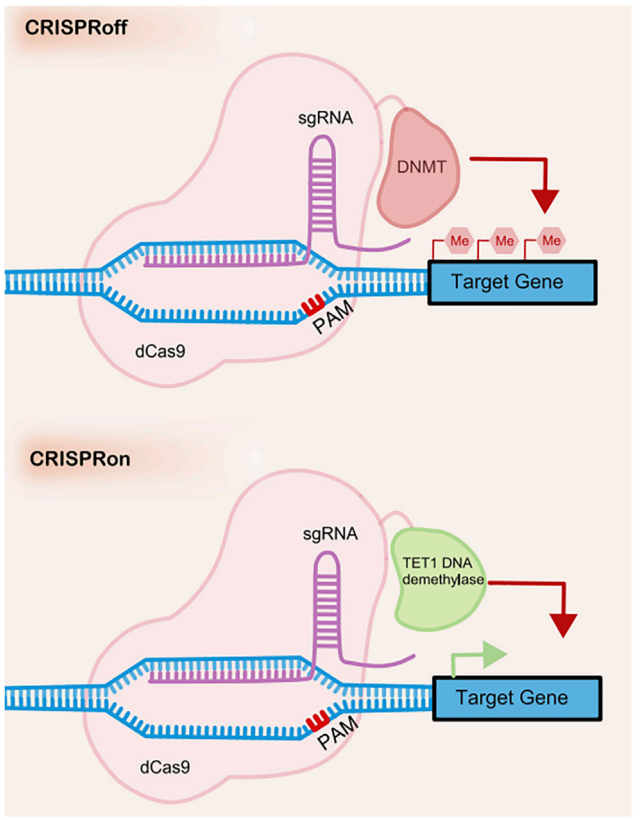


**FIGURE 3 |** The mechanism of CRISPRoff and CRISPRon.

genes that do not have large methylated regions (CpG islands), which significantly broadens the scope of its application.

## Gene Delivery Vectors

Currently, adenoviruses, adeno-associated viruses (AAVs), and lentiviral vectors represent the majority of viral vectors used for gene therapy. AAV is a group of replication-defective, non-pathogenic virus containing a single-stranded DNA genome comprised of 4.7 kilo nucleotides (4.7knt) (Srivastava et al., 1983). Due to their non-pathogenicity, low immunogenicity and the ability of mediating persistent transgene expression, AAV vectors are currently the most widely used and the most efficient vehicle for *in vivo* gene delivery (Gaj et al., 2016). The availability of 13 AAV serotypes and hundreds of variants has greatly expanded the scope and speed of transduction (Wang et al., 2019). However, the main drawback of AAV is the limited packaging capacity which is less than ~4.8 kb of DNA. This has posed a challenge for the delivery of large nucleases such as TALENs and CRISPR-Cas9, which has to be delivered using a dual-AAV approach.

Compared to AAVs, adenoviral vectors have larger genome size (~30–40 kb pairs) so as to deliver much larger transgenes (Maggio et al., 2014). Adenoviral vectors do not integrate to the genome but can achieve persistent expression using its variants (Wang et al., 2019). In a glaucoma gene therapy study, adenovirus five vectors were used for delivery of CRISPR/SpCas9 system to knock out human MYOC gene (Jain et al., 2017). However, one limitation of adenoviruses is their relatively high immunogenicity and the high prevalence of neutralizing antibodies in population, resulting in the limited application for ocular gene therapy (Yang et al., 1996).

Lentivirus is also a promising system for delivery of transgenes. Lentiviral vector gene–carrying capacity (8–10 kb) is between that of adenoviruses and AAVs, allowing for the delivery of most transgenes (Balaggan and Ali, 2012). Lentiviruses can achieve persistent gene expression by integrating to the genome, which may also cause risk of insertional mutagenesis (Romano, 2012). Lentiviruses have been applied in several ocular gene therapies, where they are able to transduce trabecular meshwork (Khare et al., 2008), RPE cells (Yin et al., 2022), photoreceptor cells (Hanke-Gogokhia et al., 2021), Müller cells and ganglion cells (Zhou et al., 2021). The lower transducing efficiency in ocular gene delivery limited the clinical application.

Recently, the cell-specific targeting of these gene vectors has greatly advanced to pave the way for successful clinical trials in future. The current strategies of cell-specific targeting include modifying tropism of delivery vectors, designing to target the specific molecular markers and carrying cell-specific promoter in the viruses (Hulliger et al., 2020; Johari et al., 2021). A previous study found that due to the high expression of heparin sulfate proteoglycan in RGCs, which mediates attachment to AAV2, AAV2 has a high tropism for RGCs (Summerford and Samulski, 1998). Another example is an optimized hypoxia regulated, RPE cell-specific gene therapy to inhibit choroidal neovascularization (Biswal et al., 2018). Researchers achieved production of human endostatin (a powerful angiostatic protein) in RPE through AAV2, which comprised a RPE-specific promoter and HIF-1 response elements (HRE).

# PATHOGENESIS OF GLAUCOMA

## Genetics

It is well known that glaucoma is markedly affected by genetic factors and is a complex genetic disease (Aboobakar and Wiggs, 2022). There has been evidence suggesting that small variations, including single nucleotide polymorphisms (SNPs) may be underlying cause of glaucoma. Besides, these SNPs may play highly pathogenic, mildly pathogenic or protective role in causing glaucoma. Genome-wide association studies (GWAS) is a genome-wide method that compares the genetic profile of SNPs between glaucoma cases and normal groups, aimed at identifying glaucoma-associated genomic regions (Aboobakar and Wiggs, 2022). Thus far, findings of GWAS have implicated 127 genetic loci that show strong associations with primary open-angle glaucoma (Gharahkhani et al., 2021). Among them, only four pathogenic genes, MYOC, NTF4, OPTN and WDR36 have been definitively linked to POAG. Similarly, multiple GWASs have been performed for PACG and 13 loci strongly associated with risk for developing PACG have been

identified (Khor et al., 2016). Except for POAG and PACG, primary congenital glaucoma (PCG), which has significant genetic basis, has been identified five distinct loci through linkage analyses (Souma et al., 2016). Generally speaking, glaucoma is a complex polygenetic disease. Multiple genes with small effect sizes and possible environmental influences are necessary for disease pathogenesis.

## Glaucoma-Related Changes in the TM

Elevated IOP, which is commonly identified in glaucoma, is caused by an imbalance between the production of aqueous humor by ciliary epithelial cells and its drainage mainly through the TM or to a lesser extent through the uveoscleral outflow pathway. In patients with POAG, increased resistance to aqueous humor outflow through the TM is responsible for the elevation of IOP. The TM is a series of fenestrated beams and sheets of extracellular matrix (ECM) covered with endothelial-like trabeculocytes. There is a growing consensus that the TM plays a central role in the pathogenesis of glaucoma. Many changes have been elucidated in the TM structure and function regarding glaucoma.

Disturbances in extracellular matrix (ECM) homeostasis are known to occur in glaucomatous TM, but the mechanism remains unclear. Studies of transforming growth factor-beta 2 (TGFβ2) have revealed its effects on increasing cross-linking enzymes and ECM deposition and a potential glaucoma-TGFβ2 relationship (Wallace et al., 2013; Pattabiraman et al., 2014). Other explanations for the accumulation of ECM also exist, including the abnormal endocytic recycling of ECM components. As they are associated with glaucoma, caveolin-1 (CAV-1) and caveolin−2(CAV-2) are significant endocytosis-related proteins and their knockdown or mutation contributes to increased levels of ECM components and altered aqueous humor outflow rates (Loomis et al., 2014).

In addition to ECM abnormalities, studies and gene analysis of human TM cells have identified changes in cellular metabolism and expression levels of some genes. For instance, oxidative stress detected in TM epithelium cells is involved in early stage of glaucoma. The free radicals cause damage to the TM epithelium cells, which consequently leads to impaired outflow capabilities (Joe et al., 2003). Furthermore, the attack by free radicals on oxide-sensitive mitochondrial DNA causes mitochondrial dysfunction. The MYOC gene encodes myocilin and a MYOC mutation is known to impair mitochondria function in glaucomatous TM cells (He et al., 2009). Furthermore, MYOC is one of the pathogenic genes definitely linked to glaucoma. It is reported that the MYOC mutation is detected in 2–4% of POAG cases. However, the role of the MYOC mutation in glaucoma remains elusive. One hypothesis is that mutant myocilin is involved in mitochondrial depolarization and subsequent calcium overload, which leads to endothelial dysfunction in the TM. Another hypothesis includes intracellular aggregation of misfolded myocilin in the endoplasmic reticulum, which then leads to endoplasmic reticulum stress and potential cytotoxicity in TM cells (Joe et al., 2003).

## Glaucoma-Related Changes in RGCs

Common to all kinds of glaucoma is the degeneration of RGCs and optic neuropathy. Increased IOP is the main risk factor for glaucoma progression and the acceleration of optic neuropathy. Increased IOP leads to the eventual compression, deformation, and remodeling of the lamina cribrosa with mechanical axonal damage and disrupted bidirectional axonal transport within the optic nerve leading to neurotrophin deprivation. For instance, the retrograde transport of the neurotrophin brain-derived neurotrophic factor (BDNF) is blocked in RGCs (Quigley et al., 2000). Even with effective IOP control, the RGCs continue to degenerate. The mechanism by which RGCs die remains unknown. In addition to increased IOP, other mechanisms may include low ocular perfusion pressure (Zheng et al., 2010), apoptosis (Cordeiro et al., 2004), altered immunity, inflammation, excitotoxicity, and oxidative stress (Tezel, 2006), as well as excessive intracellular calcium and changes in glial cells (Rojas et al., 2014). Several genes are associated with glaucomatous RGC damage, such as optineurin (OPTN). OPTN is widely expressed in RGCs, has been identified as an autophagy receptor, and interacts with many proteins. Mutation of OPTN, such as E50K-OPTN, results in functional defects of vesicle trafficking and autophagy, leading to the death of RGCs by apoptosis (Sirohi and Swarup, 2016). Other mutations are also likely to cause glaucoma via different pathogenic mechanisms (Bansal et al., 2015).

RGCs do not have the capacity for self-renewal and self-repair following their degeneration and death. It has been suggested that a combination of intrinsic cellular properties and environmental factors limits the repair and regeneration of the optic nerve. Phosphatase and tensin homolog (PTEN) is a negative regulator of the mammalian target of rapamycin (mTOR) pathway and may account for the intrinsic inability of central nervous system axons to regenerate (Park et al., 2008). As for environmental factors, excessive myelin within the optic nerve (Wang et al., 2002) and reactive glial scarring and inflammation serve as a mechanical barrier to axonal growth. A study found that inhibition of microRNA miR-21 ameliorates excessive astrocyte activation and glial scar formation, which consequently promotes axonal regeneration (Li et al., 2018). Based on the information available, there has been an increasing consensus regarding the importance of neuroprotection in treating glaucoma fundamentally.

## Impact of the Biomechanical Property of Fibrous Layer

Considerable evidence indicates that deformation, remodeling, and mechanical failure of the fibrous layer, consisting of the cornea, sclera, and lamina cribrosa, is associated with glaucoma susceptibility and progression (Yang et al., 2017). Animal models provide the ability to evaluate the effects of alterations in the ocular connective tissues on glaucoma progression. Alteration in the biomechanical property of the cornea is an important risk factor for glaucoma progression in humans (Rahman et al., 2020). Scleral weakness with low fibrous density attributable to mutations in a disintegrin and metalloproteinase domain with

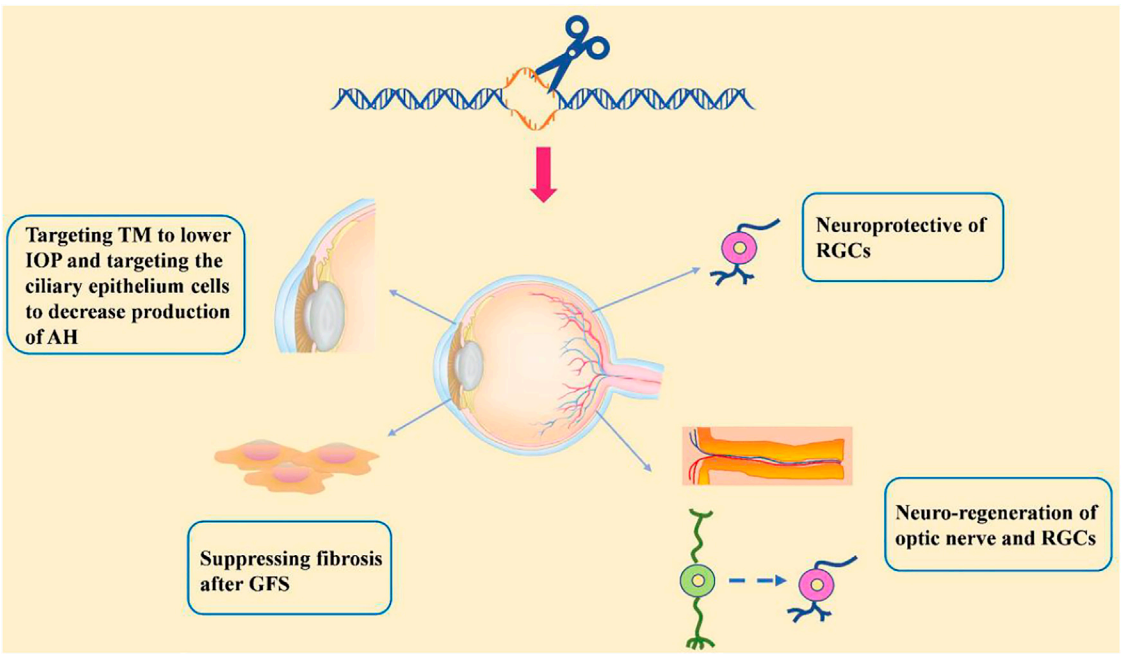


**FIGURE 4 |** An overview illustration of the review.

thrombospondin type-1 motifs (ADAMTS10) can slow the course of glaucoma progression following increased IOP (Palko et al., 2013). It has also been reported that treatment of the sclera with cross-linking agents makes glaucomatous RGC axon damage worse (Kimball et al., 2014). Another study has revealed that peripapillary scleral stiffening reduces the biomechanical tension within the lamina cribrosa and exerts a neuroprotective effect (Coudrillier et al., 2016). Experimental studies have demonstrated that a chronic increase in IOP results in stiffness of the peripapillary sclera and remodeling of the collagen structure of the sclera. However, whether glaucoma-related scleral changes are protective or damaging is currently unknown. In general, the sclera is a dynamic structure and altering its structure and behavior in response to IOP changes may provide new treatment targets; however, this requires further research.

## GENOME EDITING OF GLAUCOMA

Progress based on studies of the pathogenic mechanisms of glaucoma makes the possibility of gene therapy more viable. Gene therapy in treating glaucoma would be a great improvement over that of daily eye drops and surgery and would allow for more effective, targeted, and fundamental therapeutic outcomes following a one-time injection of the vector. Among gene therapy approaches, genome editing stands out for its characteristic of allowing the precise manipulation of target genes. Here, we discuss the recent advancements in genome editing for treating glaucoma (see in **Figure 4**).

### TM Targeting to Lower IOP

Impaired TM may cause resistance for aqueous humor drainage and subsequently lead to elevated IOP. Accordingly, therapy that targets the TM is attracting attention. In a recent study, the CRISPR/Cas9 system was used to disrupt the mutant MYOC gene in human and mouse TM cells and Ad5-crMYOC was intravitreally injected into transgenic POAG mice expressing mutant myocilin (Tg-MYOC$^{Y437H}$) (Jain et al., 2017). Ad5-crMYOC treatment is able to increase the aqueous humor outflow rate, prevent IOP elevation, and improve RGC function. This indicates that disrupting mutant MYOC leads to improved TM cell function and prevents further glaucomatous damage (Jain et al., 2017). In addition to repairing damaged TM through gene therapy, advancements in stem cell therapy provides the ability to transfer stem cell-derived TM cells to the anterior chamber for glaucoma therapy. Transplantation of induced pluripotent stem cell (iPSC)-derived TM cells restores TM cellularity and function and promotes the proliferation of endogenous TM cells in both young and aged POAG mice in the Tg-MYOC$^{Y437H}$ transgenic mouse model (Zhu et al., 2017; Zhu et al., 2020).

Expect for TM, the aqueous fluid outflow through the Schlemm's canal and distal vessels. The angiopoietin (ANGPT)-TEK (tunica interna endothelial cell kinase) system is an endothelial growth factor pathway and both of ANGPT and TEK are highly expressed by SC endothelial cells. Studies have found that delivery of a recombinant ANGPT1-mimetic promoted developmental SC expansion in healthy and Angpt1 deficient eyes, suppressed intraocular pressure (IOP) elevation and RGC loss in a mouse model of PCG (Thomson et al., 2021).

## Other Strategies to Lower IOP

Based on the mechanism of IOP elevation, other strategies have been used to lower IOP, including the targeting of ciliary epithelium cells to decrease aqueous humor production and the use of trabecular bypass to increase the aqueous humor outflow capacity. In general, most glaucoma treatments focus on two main ways to lower IOP in effort to control the progression of glaucoma, increasing aqueous humor drainage and decreasing aqueous humor production by the ciliary body epithelium. Aquaporins are a family of water-transporting transmembrane proteins and play a significant role in the formation of aqueous humor. Efficient aquaporin 1 (Aqp1) disruption by CRISPR/Cas9 in the mouse ciliary body epithelium following intravitreal injection is able to lower IOP and prevent RGC loss in a micro-bead glaucoma mouse model (Wu et al., 2020).

Glaucoma filtration surgery (GFS) is a common choice for controlling IOP. Aqueous humor drainage is increased through GFS, typically by diversion of the drainage under the conjunctiva and the formation of a filtration bleb. However, surgery failures commonly occur due to excessive sub-conjunctival fibrosis at the filtration bleb. Connective tissue growth factor (CTGF) is responsible for the fibrogenic reaction induced by fibroblasts; therefore, targeting CTGF to suppress fibrosis would potentially be an effective treatment to facilitate GFS success (Yamanaka et al., 2008). Permanent knockout of the CTGF gene using CRISPR/Cas9 system was performed by injecting viral vectors into the sub-conjunctival tissues of animals in a GFS rabbit model (Lee et al., 2020). It was demonstrated that disruption of CTGF promotes survival of the filtering blebs, improves bleb function, and reduces the overall degree of sub-conjunctival fibrosis.

## Neuroprotection

Novel neuroprotective therapies may be promising approaches for neurodegenerative disorders, including glaucoma (Nafissi and Foldvari, 2015). Neurotrophins, such as BDNF, ciliary neurotrophic factor (CNTF), and glial cell-line derived neurotrophic factor (GDNF), increase the survival of RGCs. However, the rapid clearance of neurotrophins limits their application. Genome editing therapy, which transports edited living cells that persistently express neurotrophins, overcomes this limit. Renexus® is an encapsulated cell therapy-based NT-501intravitreal implant in which the NT-501 contains a genetically modified retinal pigment epithelium cell line that permanently secretes CNTF (Emerich and Thanos, 2008). NT-501 is being evaluated in two phase II clinical trials for the treatment of glaucoma (NCT02862938, NCT04577300). Osborne et al. designed a novel AAV gene therapy (AAV2 TrkB-2A-mBDNF) that not only increased BDNF level but also exerted long-term neuroprotection by increasing expression of the BDNF receptor (TrkB) within the inner retina (Osborne et al., 2018). In addition to neurotrophins, anti-axon retraction, anti-inflammation treatment, anti-apoptosis treatment, antioxidation treatment, and gene transfer of MAX, BRN3B, Hsp-70, PDEF, and EpoR76E also have the ability to protect RGC survival. Based on the finding that decreased content of the transcription factor Myc-associated protein X (MAX) is associated with degeneration of RGCs, a recent study demonstrated that overexpression of human MAX had a neuroprotective effect against RGC injury (Lani-Louzada et al., 2022).

Recently, mitochondrial dysfunction within the RGCs have been elucidated to be the one of the mechanisms of glaucoma (Abu-Amero et al., 2006). Reduced nicotinamide adenine dinucleotide (NAD+) levels have been closely related to mitochondrial dysfunction and have become features of neurodegenerative diseases including glaucoma. NAD + has been shown to be protective against axon degeneration *in vitro* and *in vivo* (Williams et al., 2017a). Various pathways are implicated to influence the NAD + levels, including NAD + synthesising enzyme and NAD + consuming enzymes. Upregulation of NAD + synthesising enzymes (QPRT, NADSYN1, NAPRT, NAMPT, NMRK, NMNAT) or downregulation of NAD + consuming enzymes such as SIRTS, PARPs, CD38/CD157, and SARM1 would result in increased NAD + levels. Subretinal injection of a normal copy of human NMNAT1 via AAV–mediated gene augmentation rescued retinal structure and function in Nmnat1-mutated mice (Greenwald et al., 2020). Overexpression of Nmnat1 in RGCs of D2 mice also prevented glaucomatous nerve damage in >70% of treated eyes (Williams et al., 2017b). On the other hand, suppression of SARM1 has been demonstrated to protect against mitochondrial dysfunction, leading to preservation of axon degeneration and retaining of visual function in an *in vivo* mouse model of RGC degeneration (Finnegan et al., 2022).

Except for gene therapy, direct supplement of NAD + have been evaluated, including treatment with the NAD + precursors nicotinamide (NAM), nicotinamide riboside (NR), or nicotinamide mononucleotide (NMN). Among them, oral administration of the NAM vitamin B3 in mice has very strong axonal protective effects (Williams et al., 2017b). Furthermore, NAD + has been applied in several clinical trials.

A recent small randomised trial of 57 glaucoma patients, demonstrated that oral NAM (1.five to three g/d) for 3 months significantly improved retinal function in glaucoma determined by photopic negative response (PhNR) parameters (Hui et al., 2020). Another clinical trial of 125 patients with POAG will be conducted to address whether daily nicotinamide riboside (NR) intake at 300 mg/day for 24 months has a neuroprotective effect in glaucoma patients (Leung et al., 2022).

## RGC and Optic Nerve Neuro-Regeneration

To overcome the irreversible loss of RGCs and optic nerve due to their inability of regeneration requires neuro-regenerative therapy. Gene therapies have been developed that modify axonogenesis-related genes, such as PTEN, SOCS3 (Sun et al., 2011), c-myc (Belin et al., 2015) and Nogo receptor (Dickendesher et al., 2012). There have also been a few attempts at using novel genome editing to promote axon regeneration. For instance, it has been demonstrated that the specific repression of PTEN by CRISPR/dCas9 promotes axon regeneration in rat neural crest-derived PC-12 cells (Moses et al., 2020).

As a result of the lack of regenerative ability of the human retina, the transplantation of living cells is the only way to recover

vision loss after RGC death. The development of stem cell therapies allow for the replacement of degenerated and dead cells in glaucomatous retina using RGCs derived from stem cells, including human embryonic stem cells, iPSCs, and Müller glia cells. The discovery of Müller glia cell has generated great excitement in the field of cell replacement therapy as Müller glia cell can dedifferentiate to allow for their proliferation and differentiation into cell types that were damaged and thereby serve as retina progenitors.

Obstacles to neuro-regeneration that need to be overcome before successful application include RGCs being present at low proportions and hard-to-purify in stem cell-derived cultures and regenerated optic nerves have difficulty in exiting eyes and connecting with brain nuclei. Several proteins, non-coding RNAs (La Torre et al., 2013; Konar et al., 2020), and signals have been implicated in the difficulties associated with RGC transplantation. Therefore, cell replacement therapy may need the assistance of genome editing therapy and molecules that promote RGC survival and direct axon growth.

A recent study determined that down-regulation of a single RNA-binding protein, polypyrimidine tract-binding protein 1 (Ptbp1), by the *in vivo* delivery of the CRISPR system CasRx promotes expression of neuron-specific transcription factors, thereby increasing the efficiency of conversion of Müller glia cells to RGCs (Zhou et al., 2020). Notably, the Müller glia-derived RGCs established central projections to the brain and restored visual functions in an N-methyl-D-aspartate (NMDA)-induced retina injury mouse model. Another study revealed that trans-activation of the transcription factors Brn2, Ascl1, and Myt1l (BAM factors) by CRISPR/Cas9-based transcriptional activators can promotes epigenetic remodeling and gene over-expression, which thereby directly reprograms mouse embryonic fibroblasts to induced neuronal cells (Black et al., 2016). Furthermore, over-expression of Atoh7, an essential basic helix–loop–helix (bHLH) transcription factor for RGC differentiation, significantly increases the proportion of RGCs differentiated from Müller glia-derived stem cells (Song et al., 2013; Song et al., 2015). Similarly, Ngn2 is also a pro-neuralbHLH transcription factor expressed in retinal progenitor cells throughout retinal neurogenesis (Hufnagel et al., 2010) and transduction of Ascl1, Brn3b, and Ngn2 promotes the conversion of mouse fibroblasts to RGCs (Meng et al., 2013).

As discussed above, genome editing therapy can assist cell replacement therapy. Recent studies have suggested that applying the proper chemicals can convert fibroblasts to photoreceptors without the need of stem cells, thus opening a timesaving and clinically easy avenue for cell replacement therapy (Mahato et al., 2020). It was revealed that a combination of five small molecules, including Wnt/β-catenin pathway inhibitor IWR1, Repsox (VCR) combined with FSK (VCRF), and Sonic hedgehog, taurine, and retinoic acid (STR), is able to convert mouse embryonic fibroblasts into functional chemically induced photoreceptor-like cells (CiPCs). Subretinal transplantation of CiPCs into animals of a rod degeneration mouse model leads to long-term improvement in pupil reflex and partial restoration of visual function. The underlying mechanism indicates that mitochondria-translocated axis inhibition protein 2 (AXIN2) induces increased generation of reactive oxygen species, activation of NF-κB, and upregulation of Ascl1, which leads to the conversion of fibroblasts to photoreceptors. Therefore, combining pharmacologic reprogramming with genome editing is a prospective approach for converting fibroblasts to RGCs in the treatment of glaucoma.

Recently, investigators performed single-cell RNA sequencing (scRNA-seq) to construct the gene regulatory networks controlling Müller glia reprogramming (Hoang et al., 2020). They first conducted RNA-seq, scRNA-seq, and ATAC-seq of NMDA-induced or light-induced damaged mouse, zebrafish and chick retinas to profile the changes in gene expression and chromatin accessibility. Ten modules of differentially expressed genes and Müller glia-expressed transcription factors were then obtained to construct the regulatory networks for mice and zebrafish. A significant number of genes were identified that are highly related in the resting, reactivity, and reversion to resting statuses in mice and related to progression of the neurogenic status in zebrafish. For instance, hmga1a, smarca5, and yap1 in zebrafish and fatty acid-binding proteins (FABPs) in chicks are essential in reactive Müller glia for neurogenesis. Furthermore, nuclear factor I (NFI) in mice maintains Müller glia quiescence and reverts reactive Müller glia to the resting status. Deletion of NFI relieves the neurogenic barrier and promotes the development of multiple Müller glia-derived retinal neurons, including RGCs.

Research on the regeneration of RGCs and optic nerve is an essential component of curing glaucoma, but a long way remains before it can be truly applied to the clinical setting. Currently, scRNA-seq technology can be used to identify molecular changes after damage at the cellular level and then combined with the CRISPR/Cas9 gene editing system, which can achieve remarkable intervention effects by precisely targeting the relative key molecules. It is believed that with the continuing development of sequencing technology and gene editing technology, the application of RGCs and optic nerve regeneration therapy will become possible in the clinic setting and will facilitate the complete cure of glaucoma.

## Other Therapies

As noted above, ocular biomechanical properties influence glaucoma susceptibility and progression. Therefore, targeting the fibrous layer consisting of the cornea, sclera, and lamina cribrosa in patients with glaucoma is an alternative avenue for treatment. While genome editing therapy targeting the sclera and lamina cribrosa has not yet been performed, corneal gene modification using the CRISPR/Cas9 system has recently been successfully executed in several disease models, including for Meesmann's epithelial corneal dystrophy (Courtney et al., 2016) and Fuchs' endothelial corneal dystrophy (Rong et al., 2020), and has even entered clinical trials for viral keratitis (NCT04560790). The investigation of glaucoma-related cross-linking proteins, such as lysyl oxidase (LOX)/lysyl oxidase-like 1 (LOXL1), tissue trans-glutaminase (TG2), and advanced glycation end products, will allow corneal gene therapy to be further developed into a promising treatment of glaucoma.

Finally, anti-neovascular gene therapies may be useful for the prevention of neovascularization and uveitis and the treatment of secondary glaucoma after cataract surgery. A few such gene therapies have already been developed. For example, genome editing of vascular endothelial growth factor A (Vegfa) and hypoxia-inducible factor 1-alpha (Hif1a) by CRISPR/CjCas9 *in vivo* is able to abolish angiogenesis in an age-related macular degeneration model, supporting the possibility of applying this approach for treating secondary glaucoma after cataract surgery.

## LIMITATIONS AND PROSPECTS

As we described, different genome editing therapies targeting different ocular components in glaucoma currently exist, but many limitations remain resulting in their limited application. First, the most important limitation is the safety concern regarding off-target effects. Gene modification beyond the pathogenic site would result in the disruption of normal genes and off-target mutations, which may result in oncogenesis. Several studies have raised concerns regarding the potential for AAV vectors to cause pro-oncogenic events in treating hematological system diseases (Logan et al., 2017; Dalwadi et al., 2021). However, in all of the clinical studies of ocular gene therapy reported to date, ocular malignancies have not been found after injection of AAV or lentiviral vectors. Second, complications of genome editing therapies include gene therapy associated uveitis, there is a growing number of studies reporting immune responses and intraocular inflammation (Bainbridge et al., 2015; Tummala et al., 2021) and/or loss of efficacy after ocular delivery of clinical grade AAV (Bainbridge et al., 2015; Boyd et al., 2016). Besides, precise modification of the chosen gene may cause disappointing and detrimental outcomes due to the partial understanding of the complicated gene crosstalk. One example is that a clinical trial of 312 macular edema participants reported that 8.0% had IOP elevation more than 10 mmHg after intravitreal anti-VEGF injections (Aref et al., 2021), which reminds us to be cautious to apply anti-VEGF treatment for secondary glaucoma after cataract surgery as mentioned above. Third, many of the novel gene therapies discussed in this review were administrated simultaneously or even prior to the onset of optic nerve damage. In most cases of glaucoma, irreversible damage occurs before medical intervention is administered (Harvey et al., 2002). The efficacy of the gene therapies after damage occurs is unknown. Fourth, although AAV2 is considered the most efficient delivery system for gene therapy in rodents as mentioned above, transduction of RGCs is still largely inefficient by AAV2 in both large animals and humans (Ramachandran et al., 2017), which limits clinical applications of gene therapy for inner retinal diseases including glaucoma. Fifth, the specific disease mechanisms of glaucoma and pathways involved in its pathogenesis have not been fully elucidated. Therefore, the precise genome editing needs require further investigation. Finally yet importantly, the ethical, legal, and social implications of germline editing are always controversial topics and under continuous debate.

In summary, genome editing therapy has advanced greatly in recent years and has enormous potential in the treatment of glaucoma. With technological advancements and the obstacles addressed, genome editing will surely become a promising therapy for treating patients with glaucoma and will be widely applied in clinical practice.

## AUTHOR CONTRIBUTIONS

All authors listed have made a substantial, direct, and intellectual contribution to the work and approved it for publication.

## FUNDING

National key research and development program of China (2020YFC2008205, 2021YFA1101200, and 2021YFA1101202); National Natural Science Foundation of China (82171058); National Natural Science Foundation of China (81974134); Key R&D plan of Hunan Province of China (2020SK2076).

## REFERENCES

Aboobakar, I. F., and Wiggs, J. L. (2022). The Genetics of Glaucoma: Disease Associations, Personalised Risk Assessment and Therapeutic opportunities-A Review. *Clin. Exper Ophthalmol.* 50 (2), 143–162. doi:10.1111/ceo.14035

Abu-Amero, K. K., Morales, J., and Bosley, T. M. (2006). Mitochondrial Abnormalities in Patients with Primary Open-Angle Glaucoma. *Invest. Ophthalmol. Vis. Sci.* 47 (6), 2533–2541. doi:10.1167/iovs.05-1639

Abudayyeh, O. O., Gootenberg, J. S., Essletzbichler, P., Han, S., Joung, J., Belanto, J. J., et al. (2017). RNA Targeting with CRISPR-Cas13. *Nature* 550 (7675), 280–284. doi:10.1038/nature24049

Anders, C., Bargsten, K., and Jinek, M. (2016). Structural Plasticity of PAM Recognition by Engineered Variants of the RNA-Guided Endonuclease Cas9. *Mol. Cell* 61 (6), 895–902. doi:10.1016/j.molcel.2016.02.020

Anzalone, A. V., Randolph, P. B., Davis, J. R., Sousa, A. A., Koblan, L. W., Levy, J. M., et al. (2019). Search-and-replace Genome Editing without Double-Strand Breaks or Donor DNA. *Nature* 576 (7785), 149–157. doi:10.1038/s41586-019-1711-4

Aref, A. A., Scott, I. U., VanVeldhuisen, P. C., King, J., Ip, M. S., Blodi, B. A., et al. (2021). Intraocular Pressure-Related Events after Anti-Vascular Endothelial Growth Factor Therapy for Macular Edema Due to Central Retinal Vein Occlusion or Hemiretinal Vein Occlusion: SCORE2 Report 16 on a Secondary Analysis of a Randomized Clinical Trial. *JAMA Ophthalmol.* 139 (12), 1285–1291. doi:10.1001/jamaophthalmol.2021.4395

Bainbridge, J. W., Mehat, M. S., Sundaram, V., Robbie, S. J., Barker, S. E., Ripamonti, C., et al. (2015). Long-term Effect of Gene Therapy on Leber's Congenital Amaurosis. *N. Engl. J. Med.* 372 (20), 1887–1897. doi:10.1056/NEJMoa1414221

Bakondi, B., Lv, W., Lu, B., Jones, M. K., Tsai, Y., Kim, K. J., et al. (2016). *In Vivo* CRISPR/Cas9 Gene Editing Corrects Retinal Dystrophy in the S334ter-3 Rat Model of Autosomal Dominant Retinitis Pigmentosa. *Mol. Ther.* 24 (3), 556–563. doi:10.1038/mt.2015.220

Balaggan, K. S., and Ali, R. R. (2012). Ocular Gene Delivery Using Lentiviral Vectors. *Gene Ther.* 19 (2), 145–153. doi:10.1038/gt.2011.153

Bansal, M., Swarup, G., and Balasubramanian, D. (2015). Functional Analysis of Optineurin and Some of its Disease-Associated Mutants. *IUBMB Life* 67 (2), 120–128. doi:10.1002/iub.1355

Belin, S., Nawabi, H., Wang, C., Tang, S., Latremoliere, A., Warren, P., et al. (2015). Injury-induced Decline of Intrinsic Regenerative Ability Revealed by Quantitative Proteomics. *Neuron* 86 (4), 1000–1014. doi:10.1016/j.neuron.2015.03.060

Biswal, M. R., Prentice, H. M., Smith, G. W., Zhu, P., Tong, Y., Dorey, C. K., et al. (2018). Cell-specific Gene Therapy Driven by an Optimized Hypoxia-Regulated Vector Reduces Choroidal Neovascularization. *J. Mol. Med.* 96 (10), 1107–1118. doi:10.1007/s00109-018-1683-0

Black, J. B., Adler, A. F., Wang, H.-G., D'Ippolito, A. M., Hutchinson, H. A., Reddy, T. E., et al. (2016). Targeted Epigenetic Remodeling of Endogenous Loci by CRISPR/Cas9-Based Transcriptional Activators Directly Converts Fibroblasts to Neuronal Cells. *Cell Stem Cell* 19 (3), 406–414. doi:10.1016/j.stem.2016.07.001

Bohrer, L. R., Wiley, L. A., Burnight, E. R., Cooke, J. A., Giacalone, J. C., Anfinson, K. R., et al. (2019). Correction of NR2E3 Associated Enhanced S-Cone Syndrome Patient-specific iPSCs Using CRISPR-Cas9. *Genes (Basel)* 10 (4), 278. doi:10.3390/genes10040278

Boyd, R. F., Boye, S. L., Conlon, T. J., Erger, K. E., Sledge, D. G., Langohr, I. M., et al. (2016). Reduced Retinal Transduction and Enhanced Transgene-Directed Immunogenicity with Intravitreal Delivery of rAAV Following Posterior Vitrectomy in Dogs. *Gene Ther.* 23 (6), 548–556. doi:10.1038/gt.2016.31

Chou, S. J., Yang, P., Ban, Q., Yang, Y. P., Wang, M. L., Chien, C. S., et al. (2020). Dual Supramolecular Nanoparticle Vectors Enable CRISPR/Cas9-Mediated Knockin of Retinoschisin 1 Gene-A Potential Nonviral Therapeutic Solution for X-Linked Juvenile Retinoschisis. *Adv. Sci.* 7 (10), 1903432. doi:10.1002/advs.201903432

Cook, C., and Foster, P. (2012). Epidemiology of Glaucoma: What's New? *Can. J. Ophthalmol.* 47 (3), 223–226. doi:10.1016/j.jcjo.2012.02.003

Cordeiro, M. F., Guo, L., Luong, V., Harding, G., Wang, W., Jones, H. E., et al. (2004). Real-time Imaging of Single Nerve Cell Apoptosis in Retinal Neurodegeneration. *Proc. Natl. Acad. Sci. U.S.A.* 101 (36), 13352–13356. doi:10.1073/pnas.0405479101

Coudrillier, B., Campbell, I. C., Read, A. T., Geraldes, D. M., Vo, N. T., Feola, A., et al. (2016). Effects of Peripapillary Scleral Stiffening on the Deformation of the Lamina Cribrosa. *Invest. Ophthalmol. Vis. Sci.* 57 (6), 2666–2677. doi:10.1167/iovs.15-18193

Courtney, D. G., Moore, J. E., Atkinson, S. D., Maurizi, E., Allen, E. H. A., Pedrioli, D. M. L., et al. (2016). CRISPR/Cas9 DNA Cleavage at SNP-Derived PAM Enables Both *In Vitro* and *In Vivo* KRT12 Mutation-specific Targeting. *Gene Ther.* 23 (1), 108–112. doi:10.1038/gt.2015.82

Dalwadi, D. A., Torrens, L., Abril-Fornaguera, J., Pinyol, R., Willoughby, C., Posey, J., et al. (2021). Liver Injury Increases the Incidence of HCC Following AAV Gene Therapy in Mice. *Mol. Ther.* 29 (2), 680–690. doi:10.1016/j.ymthe.2020.10.018

Dickendesher, T. L., Baldwin, K. T., Mironova, Y. A., Koriyama, Y., Raiker, S. J., Askew, K. L., et al. (2012). NgR1 and NgR3 are Receptors for Chondroitin Sulfate Proteoglycans. *Nat. Neurosci.* 15 (5), 703–712. doi:10.1038/nn.3070

Dominguez, A. A., Lim, W. A., and Qi, L. S. (2016). Beyond Editing: Repurposing CRISPR-Cas9 for Precision Genome Regulation and Interrogation. *Nat. Rev. Mol. Cell Biol.* 17 (1), 5–15. doi:10.1038/nrm.2015.2

Emerich, D. F., and Thanos, C. G. (2008). NT-501: An Ophthalmic Implant of Polymer-Encapsulated Ciliary Neurotrophic Factor-Producing Cells. *Curr. Opin. Mol. Ther.* 10 (5), 506–515.

Finnegan, L. K., Chadderton, N., Kenna, P. F., Palfi, A., Carty, M., Bowie, A. G., et al. (2022). SARM1 Ablation is Protective and Preserves Spatial Vision in an *In Vivo* Mouse Model of Retinal Ganglion Cell Degeneration. *Int. J. Mol. Sci.* 23 (3), 1606. doi:10.3390/ijms23031606

Gaj, T., Epstein, B. E., and Schaffer, D. V. (2016). Genome Engineering Using Adeno-Associated Virus: Basic and Clinical Research Applications. *Mol. Ther.* 24 (3), 458–464. doi:10.1038/mt.2015.151

Gaudelli, N. M., Komor, A. C., Rees, H. A., Packer, M. S., Badran, A. H., Bryson, D. I., et al. (2017). Programmable Base Editing of AT to GC in Genomic DNA without DNA Cleavage. *Nature* 551 (7681), 464–471. doi:10.1038/nature24644

Gharahkhani, P., Jorgenson, E., Hysi, P., Khawaja, A. P., Pendergrass, S., Han, X., et al. (2021). Genome-wide Meta-Analysis Identifies 127 Open-Angle Glaucoma Loci with Consistent Effect across Ancestries. *Nat. Commun.* 12 (1), 1258. doi:10.1038/s41467-020-20851-4

Greenwald, S. H., Brown, E. E., Scandura, M. J., Hennessey, E., Farmer, R., Pawlyk, B. S., et al. (2020). Gene Therapy Preserves Retinal Structure and Function in a Mouse Model of NMNAT1-Associated Retinal Degeneration. *Mol. Ther. Methods Clin. Dev.* 18, 582–594. doi:10.1016/j.omtm.2020.07.003

Hanke-Gogokhia, C., Lehmann, G. L., Benedicto, I., de la Fuente-Ortega, E., Arshavsky, V. Y., Schreiner, R., et al. (2021). Apical CLC-2 in Retinal Pigment Epithelium is Crucial for Survival of the Outer Retina. *FASEB J.* 35 (7), e21689. doi:10.1096/fj.202100349R

Harvey, A. R., Kamphuis, W., Eggers, R., Symons, N. A., Blits, B., Niclou, S., et al. (2002). Intravitreal Injection of Adeno-Associated Viral Vectors Results in the Transduction of Different Types of Retinal Neurons in Neonatal and Adult Rats: A Comparison with Lentiviral Vectors. *Mol. Cell. Neurosci.* 21 (1), 141–157. doi:10.1006/mcne.2002.1168

He, Y., Leung, K. W., Zhuo, Y. H., and Ge, J. (2009). Pro370Leu Mutant Myocilin Impairs Mitochondrial Functions in Human Trabecular Meshwork Cells. *Mol. Vis.* 15, 815–825.

Hoang, T., Wang, J., Boyd, P., Wang, F., Santiago, C., Jiang, L., et al. (2020). Gene Regulatory Networks Controlling Vertebrate Retinal Regeneration. *Science* 370 (6519), 370. doi:10.1126/science.abb8598

Hu, J. H., Miller, S. M., Geurts, M. H., Tang, W., Chen, L., Sun, N., et al. (2018). Evolved Cas9 Variants with Broad PAM Compatibility and High DNA Specificity. *Nature* 556 (7699), 57–63. doi:10.1038/nature26155

Huang, K.-C., Wang, M.-L., Chen, S.-J., Kuo, J.-C., Wang, W.-J., Nhi Nguyen, P. N., et al. (2019). Morphological and Molecular Defects in Human Three-Dimensional Retinal Organoid Model of X-Linked Juvenile Retinoschisis. *Stem Cell Rep.* 13 (5), 906–923. doi:10.1016/j.stemcr.2019.09.010

Hufnagel, R. B., Le, T. T., Riesenberg, A. L., and Brown, N. L. (2010). Neurog2 Controls the Leading Edge of Neurogenesis in the Mammalian Retina. *Dev. Biol.* 340 (2), 490–503. doi:10.1016/j.ydbio.2010.02.002

Hui, F., Tang, J., Williams, P. A., McGuinness, M. B., Hadoux, X., Casson, R. J., et al. (2020). Improvement in Inner Retinal Function in Glaucoma with Nicotinamide (Vitamin B3) Supplementation: A Crossover Randomized Clinical Trial. *Clin. Exp. Ophthalmol.* 48 (7), 903–914. doi:10.1111/ceo.13818

Hulliger, E. C., Hostettler, S. M., and Kleinlogel, S. (2020). Empowering Retinal Gene Therapy with a Specific Promoter for Human Rod and Cone ON-Bipolar Cells. *Mol. Ther. Methods Clin. Dev.* 17, 505–519. doi:10.1016/j.omtm.2020.03.003

Jain, A., Zode, G., Kasetti, R. B., Ran, F. A., Yan, W., Sharma, T. P., et al. (2017). CRISPR-Cas9-based Treatment of Myocilin-Associated Glaucoma. *Proc. Natl. Acad. Sci. U.S.A.* 114 (42), 11199–11204. doi:10.1073/pnas.1706193114

Jo, D. H., Song, D. W., Cho, C. S., Kim, U. G., Lee, K. J., Lee, K., et al. (2019). CRISPR-Cas9-mediated Therapeutic Editing of Rpe65 Ameliorates the Disease Phenotypes in a Mouse Model of Leber Congenital Amaurosis. *Sci. Adv.* 5 (10), eaax1210. doi:10.1126/sciadv.aax1210

Joe, M. K., Sohn, S., Hur, W., Moon, Y., Choi, Y. R., and Kee, C. (2003). Accumulation of Mutant Myocilins in ER Leads to ER Stress and Potential Cytotoxicity in Human Trabecular Meshwork Cells. *Biochem. Biophys. Res. Commun.* 312 (3), 592–600. doi:10.1016/j.bbrc.2003.10.162

Johari, Y. B., Mercer, A. C., Liu, Y., Brown, A. J., and James, D. C. (2021). Design of Synthetic Promoters for Controlled Expression of Therapeutic Genes in Retinal Pigment Epithelial Cells. *Biotech. Bioeng.* 118 (5), 2001–2015. doi:10.1002/bit.27713

Jonas, J. B., Aung, T., Bourne, R. R., Bron, A. M., Ritch, R., and Panda-Jonas, S. (2017). Glaucoma. *Lancet* 390 (10108), 2183–2193. doi:10.1016/s0140-6736(17)31469-1

Khare, P. D., Loewen, N., Teo, W., Barraza, R. A., Saenz, D. T., Johnson, D. H., et al. (2008). Durable, Safe, Multi-Gene Lentiviral Vector Expression in Feline Trabecular Meshwork. *Mol. Ther.* 16 (1), 97–106. doi:10.1038/sj.mt.6300318

Khor, C. C., Do, T., Jia, H., Nakano, M., George, R., Abu-Amero, K., et al. (2016). Genome-wide Association Study Identifies Five New Susceptibility Loci for Primary Angle Closure Glaucoma. *Nat. Genet.* 48 (5), 556–562. doi:10.1038/ng.3540

Kim, E., Koo, T., Park, S. W., Kim, D., Kim, K., Cho, H.-Y., et al. (2017). *In Vivo* genome Editing with a Small Cas9 Orthologue Derived from Campylobacter Jejuni. *Nat. Commun.* 8, 14500. doi:10.1038/ncomms14500

Kim, H. K., Ham, K. A., Lee, S. W., Choi, H. S., Kim, H. S., Kim, H. K., et al. (2019). Biallelic Deletion of Pxdn in Mice Leads to Anophthalmia and Severe Eye Malformation. *Int. J. Mol. Sci.* 20 (24), 6144. doi:10.3390/ijms20246144

Kimball, E. C., Nguyen, C., Steinhart, M. R., Nguyen, T. D., Pease, M. E., Oglesby, E. N., et al. (2014). Experimental Scleral Cross-Linking Increases Glaucoma Damage in a Mouse Model. *Exp. Eye Res.* 128, 129–140. doi:10.1016/j.exer.2014.08.016

Komor, A. C., Kim, Y. B., Packer, M. S., Zuris, J. A., and Liu, D. R. (2016). Programmable Editing of a Target Base in Genomic DNA without Double-Stranded DNA Cleavage. *Nature* 533 (7603), 420–424. doi:10.1038/nature17946

Konar, G. J., Ferguson, C., Flickinger, Z., Kent, M. R., and Patton, J. G. (2020). miRNAs and Müller Glia Reprogramming during Retina Regeneration. *Front. Cell Dev. Biol.* 8, 632632. doi:10.3389/fcell.2020.632632

La Torre, A., Georgi, S., and Reh, T. A. (2013). Conserved microRNA Pathway Regulates Developmental Timing of Retinal Neurogenesis. *Proc. Natl. Acad. Sci. U. S. A.* 110 (26), E2362–E2370. doi:10.1073/pnas.1301837110

Lahola-Chomiak, A. A., Footz, T., Nguyen-Phuoc, K., Neil, G. J., Fan, B., Allen, K. F., et al. (2019). Non-Synonymous Variants in Premelanosome Protein (PMEL) Cause Ocular Pigment Dispersion and Pigmentary Glaucoma. *Hum. Mol. Genet.* 28 (8), 1298–1311. doi:10.1093/hmg/ddy429

Lani-Louzada, R., Marra, C., Dias, M. S., de Araújo, V. G., Abreu, C. A., Ribas, V. T., et al. (2022). Neuroprotective Gene Therapy by Overexpression of the Transcription Factor MAX in Rat Models of Glaucomatous Neurodegeneration. *Invest. Ophthalmol. Vis. Sci.* 63 (2), 5. doi:10.1167/iovs.63.2.5

Lee, E. J., Han, J. C., Park, D. Y., Cho, J., and Kee, C. (2020). Effect of Connective Tissue Growth Factor Gene Editing Using Adeno-Associated Virus-Mediated CRISPR-Cas9 on Rabbit Glaucoma Filtering Surgery Outcomes. *Gene Ther.* 28, 277. doi:10.1038/s41434-020-0166-4

Leung, C. K. S., Ren, S. T., Chan, P. P. M., Wan, K. H. N., Kam, A. K. W., Lai, G. W. K., et al. (2022). Nicotinamide Riboside as a Neuroprotective Therapy for Glaucoma: Study Protocol for a Randomized, Double-Blind, Placebo-Control Trial. *Trials* 23 (1), 45. doi:10.1186/s13063-021-05968-1

Li, H.-J., Pan, Y.-B., Sun, Z.-L., Sun, Y.-Y., Yang, X.-T., and Feng, D.-F. (2018). Inhibition of miR-21 Ameliorates Excessive Astrocyte Activation and Promotes Axon Regeneration Following Optic Nerve Crush. *Neuropharmacology* 137, 33–49. doi:10.1016/j.neuropharm.2018.04.028

Logan, G. J., Dane, A. P., Hallwirth, C. V., Smyth, C. M., Wilkie, E. E., Amaya, A. K., et al. (2017). Identification of Liver-specific Enhancer-Promoter Activity in the 3′ Untranslated Region of the Wild-type AAV2 Genome. *Nat. Genet.* 49 (8), 1267–1273. doi:10.1038/ng.3893

Loomis, S. J., Kang, J. H., Weinreb, R. N., Yaspan, B. L., Cooke Bailey, J. N., Gaasterland, D., et al. (2014). Association of CAV1/CAV2 Genomic Variants with Primary Open-Angle Glaucoma Overall and by Gender and Pattern of Visual Field Loss. *Ophthalmology* 121 (2), 508–516. doi:10.1016/j.ophtha.2013.09.012

Ma, C.-C., Wang, Z.-L., Xu, T., He, Z.-Y., and Wei, Y.-Q. (2020). The Approved Gene Therapy Drugs Worldwide: from 1998 to 2019. *Biotechnol. Adv.* 40, 107502. doi:10.1016/j.biotechadv.2019.107502

Maeder, M. L., Stefanidakis, M., Wilson, C. J., Baral, R., Barrera, L. A., Bounoutas, G. S., et al. (2019). Development of a Gene-Editing Approach to Restore Vision Loss in Leber Congenital Amaurosis Type 10. *Nat. Med.* 25 (2), 229–233. doi:10.1038/s41591-018-0327-9

Maggio, I., Holkers, M., Liu, J., Janssen, J. M., Chen, X., and Gonçalves, M. A. F. V. (2014). Adenoviral Vector Delivery of RNA-Guided CRISPR/Cas9 Nuclease Complexes Induces Targeted Mutagenesis in a Diverse Array of Human Cells. *Sci. Rep.* 4, 5105. doi:10.1038/srep05105

Mahato, B., Kaya, K. D., Fan, Y., Sumien, N., Shetty, R. A., Zhang, W., et al. (2020). Pharmacologic Fibroblast Reprogramming into Photoreceptors Restores Vision. *Nature* 581 (7806), 83–88. doi:10.1038/s41586-020-2201-4

McCullough, K. T., Boye, S. L., Fajardo, D., Calabro, K., Peterson, J. J., Strang, C. E., et al. (2019). Somatic Gene Editing of GUCY2D by AAV-CRISPR/Cas9 Alters Retinal Structure and Function in Mouse and Macaque. *Hum. Gene Ther.* 30 (5), 571–589. doi:10.1089/hum.2018.193

Meng, F., Wang, X., Gu, P., Wang, Z., and Guo, W. (2013). Induction of Retinal Ganglion-like Cells from Fibroblasts by Adenoviral Gene Delivery. *Neuroscience* 250, 381–393. doi:10.1016/j.neuroscience.2013.07.001

Mirjalili Mohanna, S. Z., Hickmott, J. W., Lam, S. L., Chiu, N. Y., Lengyell, T. C., Tam, B. M., et al. (2020). Germline CRISPR/Cas9-Mediated Gene Editing Prevents Vision Loss in a Novel Mouse Model of Aniridia. *Mol. Ther. Methods Clin. Dev.* 17, 478–490. doi:10.1016/j.omtm.2020.03.002

Moses, C., Hodgetts, S. I., Nugent, F., Ben-Ary, G., Park, K. K., Blancafort, P., et al. (2020). Transcriptional Repression of PTEN in Neural Cells Using CRISPR/dCas9 Epigenetic Editing. *Sci. Rep.* 10 (1), 11393. doi:10.1038/s41598-020-68257-y

Nafissi, N., and Foldvari, M. (2015). Neuroprotective Therapies in Glaucoma: II. Genetic Nanotechnology Tools. *Front. Neurosci.* 9, 355. doi:10.3389/fnins.2015.00355

Nuñez, J. K., Chen, J., Pommier, G. C., Cogan, J. Z., Replogle, J. M., Adriaens, C., et al. (2021). Genome-wide Programmable Transcriptional Memory by CRISPR-Based Epigenome Editing. *Cell* 184 (9), 2503–2519. doi:10.1016/j.cell.2021.03.025

Osborne, A., Khatib, T. Z., Songra, L., Barber, A. C., Hall, K., Kong, G. Y. X., et al. (2018). Neuroprotection of Retinal Ganglion Cells by a Novel Gene Therapy Construct that Achieves Sustained Enhancement of Brain-Derived Neurotrophic Factor/tropomyosin-Related Kinase Receptor-B Signaling. *Cell Death Dis.* 9 (10), 1007. doi:10.1038/s41419-018-1041-8

Palko, J. R., Iwabe, S., Pan, X., Agarwal, G., Komáromy, A. M., and Liu, J. (2013). Biomechanical Properties and Correlation with Collagen Solubility Profile in the Posterior Sclera of Canine Eyes with anADAMTS10Mutation. *Invest. Ophthalmol. Vis. Sci.* 54 (4), 2685–2695. doi:10.1167/iovs.12-10621

Panagiotopoulos, A.-L., Karguth, N., Pavlou, M., Böhm, S., Gasparoni, G., Walter, J., et al. (2020). Antisense Oligonucleotide- and CRISPR-Cas9-Mediated Rescue of mRNA Splicing for a Deep Intronic CLRN1 Mutation. *Mol. Ther. Nucleic Acids* 21, 1050–1061. doi:10.1016/j.omtn.2020.07.036

Park, K. K., Liu, K., Hu, Y., Smith, P. D., Wang, C., Cai, B., et al. (2008). Promoting Axon Regeneration in the Adult CNS by Modulation of the PTEN/mTOR Pathway. *Science* 322 (5903), 963–966. doi:10.1126/science.1161566

Pattabiraman, P. P., Maddala, R., and Rao, P. V. (2014). Regulation of Plasticity and Fibrogenic Activity of Trabecular Meshwork Cells by Rho GTPase Signaling. *J. Cell. Physiol.* 229 (7), 927–942. doi:10.1002/jcp.24524

Pendse, N. D., Lamas, V., Pawlyk, B. S., Maeder, M. L., Chen, Z.-Y., Pierce, E. A., et al. (2019). *In Vivo* Assessment of Potential Therapeutic Approaches for USH2A-Associated Diseases. *Adv. Exp. Med. Biol.* 1185, 91–96. doi:10.1007/978-3-030-27378-1_15

Quigley, H. A., and Broman, A. T. (2006). The Number of People with Glaucoma Worldwide in 2010 and 2020. *Br. J. Ophthalmol.* 90 (3), 262–267. doi:10.1136/bjo.2005.081224

Quigley, H. A., McKinnon, S. J., Zack, D. J., Pease, M. E., Kerrigan-Baumrind, L. A., Kerrigan, D. F., et al. (2000). Retrograde Axonal Transport of BDNF in Retinal Ganglion Cells Is Blocked by Acute IOP Elevation in Rats. *Invest Ophthalmol. Vis. Sci.* 41 (11), 3460–3466.

Rahman, N., O'Neill, E., Irnaten, M., Wallace, D., and O'Brien, C. (2020). Corneal Stiffness and Collagen Cross-Linking Proteins in Glaucoma: Potential for Novel Therapeutic Strategy. *J. Ocular Pharmacol. Ther.* 36 (8), 582–594. doi:10.1089/jop.2019.0118

Ramachandran, P. S., Lee, V., Wei, Z., Song, J. Y., Casal, G., Cronin, T., et al. (2017). Evaluation of Dose and Safety of AAV7m8 and AAV8BP2 in the Non-Human Primate Retina. *Hum. Gene Ther.* 28 (2), 154–167. doi:10.1089/hum.2016.111

Rojas, B., Gallego, B. I., Ramírez, A. I., Salazar, J. J., de Hoz, R., Valiente-Soriano, F. J., et al. (2014). Microglia in Mouse Retina Contralateral to Experimental Glaucoma Exhibit Multiple Signs of Activation in All Retinal Layers. *J. Neuroinflammation* 11, 133. doi:10.1186/1742-2094-11-133

Romano, G. (2012). Development of Safer Gene Delivery Systems to Minimize the Risk of Insertional Mutagenesis-Related Malignancies: a Critical Issue for the Field of Gene Therapy. *ISRN Oncol.* 2012, 616310. doi:10.5402/2012/616310

Rong, Z., Gong, X., Hulleman, J. D., Corey, D. R., and Mootha, V. V. (2020). Trinucleotide Repeat-Targeting dCas9 as a Therapeutic Strategy for Fuchs' Endothelial Corneal Dystrophy. *Trans. Vis. Sci. Tech.* 9 (9), 47. doi:10.1167/tvst.9.9.47

Sinha, D., Steyer, B., Shahi, P. K., Mueller, K. P., Valiauga, R., Edwards, K. L., et al. (2020). Human iPSC Modeling Reveals Mutation-Specific Responses to Gene Therapy in a Genotypically Diverse Dominant Maculopathy. *Am. J. Hum. Genet.* 107 (2), 278–292. doi:10.1016/j.ajhg.2020.06.011

Sirohi, K., and Swarup, G. (2016). Defects in Autophagy Caused by Glaucoma-Associated Mutations in Optineurin. *Exp. Eye Res.* 144, 54–63. doi:10.1016/j.exer.2015.08.020

Song, W.-t., Zhang, X.-y., and Xia, X.-b. (2013). Atoh7 Promotes the Differentiation of Retinal Stem Cells Derived from Müller Cells into Retinal Ganglion Cells by Inhibiting Notch Signaling. *Stem Cell Res. Ther.* 4 (4), 94. doi:10.1186/scrt305

Song, W.-t., Zhang, X.-y., and Xia, X.-b. (2015). Atoh7 Promotes the Differentiation of Müller Cells-Derived Retinal Stem Cells into Retinal Ganglion Cells in a Rat Model of Glaucoma. *Exp. Biol. Med. (Maywood)* 240 (5), 682–690. doi:10.1177/1535370214560965

Souma, T., Tompson, S. W., Thomson, B. R., Siggs, O. M., Kizhatil, K., Yamaguchi, S., et al. (2016). Angiopoietin Receptor TEK Mutations Underlie Primary Congenital Glaucoma with Variable Expressivity. *J. Clin. Invest* 126 (7), 2575–2587. doi:10.1172/jci85830

Srivastava, A., Lusby, E. W., and Berns, K. I. (1983). Nucleotide Sequence and Organization of the Adeno-Associated Virus 2 Genome. *J. Virol.* 45 (2), 555–564. doi:10.1128/jvi.45.2.555-564.1983

Stein, J. D., Khawaja, A. P., and Weizer, J. S. (2021). Glaucoma in Adults-Screening, Diagnosis, and Management. *JAMA* 325 (2), 164–174. doi:10.1001/jama.2020.21899

Suh, S., Choi, E. H., Leinonen, H., Foik, A. T., Newby, G. A., Yeh, W. H., et al. (2020). Restoration of Visual Function in Adult Mice with an Inherited Retinal Disease via Adenine Base Editing. *Nat. Biomed. Eng.* 5, 169. doi:10.1038/s41551-020-00632-6

Summerford, C., and Samulski, R. J. (1998). Membrane-associated Heparan Sulfate Proteoglycan is a Receptor for Adeno-Associated Virus Type 2 Virions. *J. Virol.* 72 (2), 1438–1445. doi:10.1128/jvi.72.2.1438-1445.1998

Sun, F., Park, K. K., Belin, S., Wang, D., Lu, T., Chen, G., et al. (2011). Sustained Axon Regeneration Induced by Co-deletion of PTEN and SOCS3. *Nature* 480 (7377), 372–375. doi:10.1038/nature10594

Suzuki, K., Tsunekawa, Y., Hernandez-Benitez, R., Wu, J., Zhu, J., Kim, E. J., et al. (2016). *In Vivo* genome Editing via CRISPR/Cas9 Mediated Homology-independent Targeted Integration. *Nature* 540 (7631), 144–149. doi:10.1038/nature20565

Tezel, G. (2006). Oxidative Stress in Glaucomatous Neurodegeneration: Mechanisms and Consequences. *Prog. Retin. Eye Res.* 25 (5), 490–513. doi:10.1016/j.preteyeres.2006.07.003

Thomson, B. R., Liu, P., Onay, T., Du, J., Tompson, S. W., Misener, S., et al. (2021). Cellular Crosstalk Regulates the Aqueous Humor Outflow Pathway and Provides New Targets for Glaucoma Therapies. *Nat. Commun.* 12 (1), 6072. doi:10.1038/s41467-021-26346-0

Tummala, G., Crain, A., Rowlan, J., and Pepple, K. L. (2021). Characterization of Gene Therapy Associated Uveitis Following Intravitreal Adeno-Associated Virus Injection in Mice. *Invest. Ophthalmol. Vis. Sci.* 62 (2), 41. doi:10.1167/iovs.62.2.41

VanderWall, K. B., Huang, K.-C., Pan, Y., Lavekar, S. S., Fligor, C. M., Allsop, A. R., et al. (2020). Retinal Ganglion Cells with a Glaucoma OPTN(E50K) Mutation Exhibit Neurodegenerative Phenotypes when Derived from Three-Dimensional Retinal Organoids. *Stem Cell Rep.* 15 (1), 52–66. doi:10.1016/j.stemcr.2020.05.009

Wallace, D. M., Clark, A. F., Lipson, K. E., Andrews, D., Crean, J. K., and O'Brien, C. J. (2013). Anti-connective Tissue Growth Factor Antibody Treatment Reduces Extracellular Matrix Production in Trabecular Meshwork and Lamina Cribrosa Cells. *Invest. Ophthalmol. Vis. Sci.* 54 (13), 7836–7848. doi:10.1167/iovs.13-12494

Wang, K. C., Koprivica, V., Kim, J. A., Sivasankaran, R., Guo, Y., Neve, R. L., et al. (2002). Oligodendrocyte-myelin Glycoprotein is a Nogo Receptor Ligand that Inhibits Neurite Outgrowth. *Nature* 417 (6892), 941–944. doi:10.1038/nature00867

Wang, D., Tai, P. W. L., and Gao, G. (2019). Adeno-associated Virus Vector as a Platform for Gene Therapy Delivery. *Nat. Rev. Drug Discov.* 18 (5), 358–378. doi:10.1038/s41573-019-0012-9

Williams, P. A., Harder, J. M., and John, S. W. M. (2017). Glaucoma as a Metabolic Optic Neuropathy. *J. Glaucoma* 26 (12), 1161–1168. doi:10.1097/ijg.0000000000000767

Williams, P. A., Harder, J. M., Foxworth, N. E., Cochran, K. E., Philip, V. M., Porciatti, V., et al. (2017). Vitamin B 3 Modulates Mitochondrial Vulnerability and Prevents Glaucoma in Aged Mice. *Science* 355 (6326), 756–760. doi:10.1126/science.aal0092

Wu, W.-H., Tsai, Y.-T., Justus, S., Lee, T.-T., Zhang, L., Lin, C.-S., et al. (2016). CRISPR Repair Reveals Causative Mutation in a Preclinical Model of Retinitis Pigmentosa. *Mol. Ther.* 24 (8), 1388–1394. doi:10.1038/mt.2016.107

Wu, J., Bell, O. H., Copland, D. A., Young, A., Pooley, J. R., Maswood, R., et al. (2020). Gene Therapy for Glaucoma by Ciliary Body Aquaporin 1 Disruption Using CRISPR-Cas9. *Mol. Ther.* 28 (3), 820–829. doi:10.1016/j.ymthe.2019.12.012

Yamanaka, O., Saika, S., Ikeda, K., Miyazaki, K.-i., Kitano, A., and Ohnishi, Y. (2008). Connective Tissue Growth Factor Modulates Extracellular Matrix Production in Human Subconjunctival Fibroblasts and Their Proliferation and Migration *In Vitro*. *Jpn. J. Ophthalmol.* 52 (1), 8–15. doi:10.1007/s10384-007-0497-3

Yang, Y., Jooss, K. U., Su, Q., Ertl, H. C., and Wilson, J. M. (1996). Immune Responses to Viral Antigens versus Transgene Product in the Elimination of Recombinant Adenovirus-Infected Hepatocytes *In Vivo*. *Gene Ther.* 3 (2), 137–144.

Yang, H., Reynaud, J., Lockwood, H., Williams, G., Hardin, C., Reyes, L., et al. (2017). The Connective Tissue Phenotype of Glaucomatous Cupping in the Monkey Eye - Clinical and Research Implications. *Prog. Retin. Eye Res.* 59, 1–52. doi:10.1016/j.preteyeres.2017.03.001

Yang, T.-C., Chang, C.-Y., Yarmishyn, A. A., Mao, Y.-S., Yang, Y.-P., Wang, M.-L., et al. (2020). Carboxylated Nanodiamond-Mediated CRISPR-Cas9 Delivery of Human Retinoschisis Mutation into Human iPSCs and Mouse Retina. *Acta Biomater.* 101, 484–494. doi:10.1016/j.actbio.2019.10.037

Yin, L., Ma, C., Hou, S., and Ma, X. (2022). Methyltransferase-like (METTL)14-mediated N6-Methyladenosine Modification Modulates Retinal Pigment Epithelial (RPE) Activity by Regulating the Methylation of Microtubule-Associated Protein (MAP)2. *Bioengineered* 13 (3), 4773–4785. doi:10.1080/21655979.2022.2032968

Zalatan, J. G., Lee, M. E., Almeida, R., Gilbert, L. A., Whitehead, E. H., La Russa, M., et al. (2015). Engineering Complex Synthetic Transcriptional Programs with CRISPR RNA Scaffolds. *Cell* 160 (1-2), 339–350. doi:10.1016/j.cell.2014.11.052

Zheng, Y., Wong, T. Y., Mitchell, P., Friedman, D. S., He, M., and Aung, T. (2010). Distribution of Ocular Perfusion Pressure and its Relationship with Open-Angle Glaucoma: the singapore Malay Eye Study. *Invest. Ophthalmol. Vis. Sci.* 51 (7), 3399–3404. doi:10.1167/iovs.09-4867

Zhou, H., Su, J., Hu, X., Zhou, C., Li, H., Chen, Z., et al. (2020). Glia-to-Neuron Conversion by CRISPR-CasRx Alleviates Symptoms of Neurological Disease in Mice. *Cell* 181 (3), 590–603. doi:10.1016/j.cell.2020.03.024

Zhou, Y., Cai, L.-j., Xu, L.-h., Guo, Y., Chen, N., and Yao, Q. (2021). The Role of Sirt1 in the Retinal Ganglion Cells Cultured by High Glucose. *Int. Ophthalmol.* 41 (3), 845–852. doi:10.1007/s10792-020-01638-4

Zhu, W., Jain, A., Gramlich, O. W., Tucker, B. A., Sheffield, V. C., and Kuehn, M. H. (2017). Restoration of Aqueous Humor Outflow Following Transplantation of iPSC-Derived Trabecular Meshwork Cells in a Transgenic Mouse Model of Glaucoma. *Invest. Ophthalmol. Vis. Sci.* 58 (4), 2054–2062. doi:10.1167/iovs.16-20672

Zhu, W., Godwin, C. R., Cheng, L., Scheetz, T. E., and Kuehn, M. H. (2020). Transplantation of iPSC-TM Stimulates Division of Trabecular Meshwork Cells in Human Eyes. *Sci. Rep.* 10 (1), 2905. doi:10.1038/s41598-020-59941-0

**Conflict of Interest:** The authors declare that the research was conducted in the absence of any commercial or financial relationships that could be construed as a potential conflict of interest.

**Publisher's Note:** All claims expressed in this article are solely those of the authors and do not necessarily represent those of their affiliated organizations, or those of the publisher, the editors and the reviewers. Any product that may be evaluated in this article, or claim that may be made by its manufacturer, is not guaranteed or endorsed by the publisher.

frontiers | Frontiers in Cell and Developmental Biology

ORIGINAL RESEARCH
published: 22 July 2022
doi: 10.3389/fcell.2022.951231

# Connexin Mutants Cause Cataracts Through Deposition of Apatite

*Peter J. Minogue[1], Andre J. Sommer[2], James C. Williams Jr[3], Sharon B. Bledsoe[3], Eric C. Beyer[1†] and Viviana M. Berthoud[1*†]*

[1]Department of Pediatrics, University of Chicago, Chicago, IL, United States, [2]Molecular Microspectroscopy Laboratory, Department of Chemistry and Biochemistry, Miami University, Oxford, OH, United States, [3]Department of Anatomy, Cell Biology and Physiology, Indiana University School of Medicine, Indianapolis, IN, United States

Cataracts are lens opacities that are among the most common causes of blindness. It is commonly believed that cataracts develop through the accumulation of damage to lens proteins. However, recent evidence suggests that cataracts can result from calcium ion accumulation and the precipitation of calcium-containing salts. To test for the presence of precipitates and to identify their components, we studied the lenses of mice that develop cataracts due to mutations of connexin46 and connexin50. Micro-computed tomography showed the presence of radio-dense mineral in the mutant lenses, but not in wild-type lenses. Three-dimensional reconstructions of the scans showed that the distribution of the radio-dense mineral closely paralleled the location and morphology of the cataracts. The mutant lens homogenates also contained insoluble particles that stained with Alizarin red (a dye that stains $Ca^{2+}$ deposits). Using attenuated total internal reflection micro–Fourier transform infrared spectroscopy, we identified the mineral as calcium phosphate in the form of apatite. Taken together, these data support the novel paradigm that cataracts are formed through pathological mineralization within the lens.

**Keywords: cataracts, mineralization, calcification, computed tomography, connexin, Fourier transform IR, gap junction channel, lens**

OPEN ACCESS

***Edited by:***
*Deepika Vasudevan, University of Pittsburgh, United States*

***Reviewed by:***
*Anaclet Ngezahayo, Leibniz University Hannover, Germany*
*Xinbo Li, Oregon Health and Science University, United States*

***Correspondence:**
*Viviana M. Berthoud*
*vberthou@peds.bsd.uchicago.edu*

*†These authors share senior authorship*

***Specialty section:***
*This article was submitted to Molecular and Cellular Pathology, a section of the journal Frontiers in Cell and Developmental Biology*

***Received:*** *23 May 2022*
***Accepted:*** *22 June 2022*
***Published:*** *22 July 2022*

***Citation:***
*Minogue PJ, Sommer AJ, Williams JC Jr, Bledsoe SB, Beyer EC and Berthoud VM (2022) Connexin Mutants Cause Cataracts Through Deposition of Apatite. Front. Cell Dev. Biol. 10:951231. doi: 10.3389/fcell.2022.951231*

## INTRODUCTION

Cataracts are the leading cause of blindness worldwide (Resnikoff et al., 2004). They represent areas of cloudiness or opacification within the lens that prevent the proper transmission of light entering the eye onto the retina. Cataracts are frequently associated with aging and can develop as consequences of various diseases or in response to environmental insults. They can also result from genetic mutations of major lens proteins. The prevailing hypothesis has been that cataracts develop through accumulation of modifications in lens proteins (including oxidation, deamidation, cross-linking, cleavage, fragmentation, and glycation) and formation of insoluble high molecular weight protein aggregates (reviewed in Sharma and Santhoshkumar, 2009; Truscott and Friedrich, 2019).

The lens is an avascular organ comprised of an anterior epithelial cell layer and fiber cells that lose their organelles during differentiation. Because the lens has no direct blood supply, its homeostasis depends on a microcirculatory system that is responsible for the flow of water, ions and solutes into,

**Abbreviations:** ATR-μFTIR, attenuated total internal reflection micro–Fourier transform infrared spectroscopy; Cx46, connexin46; Cx50, connexin50; micro-CT, micro-computed tomography.

within and out of the lens (reviewed in Mathias et al., 2007). In the circulation model, water and ions enter into the lens at the anterior and posterior poles; they flow through extracellular spaces into the lens center; and, they flow back to the surface and leave the lens through epithelial cells at the equator. This circulation is driven by ion pumps in the lens surface cells. As ions and water flow into the lens, they enter the cytoplasm of cells, following the electrochemical potentials of the ions, whereas outflow occurs by fiber cell-to-fiber cell diffusion through intercellular channels composed of the gap junction proteins, connexin46 (Cx46) and connexin50 (Cx50).

We have been characterizing two mouse cataract models that mimic connexin mutations found in humans, a Cx46 mutant (Cx46fs380) and a Cx50 mutant (Cx50D47A) (Berthoud et al., 2013; Berthoud et al., 2014; Gao et al., 2018; Berthoud et al., 2019). In heterozygous and homozygous lenses of both models, gap junction-mediated communication between lens fiber cells is significantly decreased (Minogue et al., 2017; Berthoud et al., 2019). The reduced intercellular communication impairs the lens microcirculation leading to disruptions of normal ion gradients, including that of calcium ions. The calcium ions accumulate to levels beyond the solubility product of some of its salts. After reaction of these lenses with Alizarin red (a dye used to detect calcified material in tissues like bone), we have observed red staining that closely corresponds to the locations of the opacities detected by darkfield microscopy (Gao et al., 2018; Berthoud et al., 2019). This led us to propose the novel hypothesis that cataracts result from accumulation of calcium ions and pathological mineralization within the organ by formation of deposits of calcium salts. Further support for our hypothesis that pathological mineralization is a common mechanism for cataract formation has been provided by studies of other mouse models in which Alizarin red-stained material is found in cataractous lenses (Li et al., 2021; Zhou et al., 2021).

The current study was designed to test the hypothesis that cataractous lenses expressing mutant lens fiber cell connexins contain mineralized material. Several approaches were applied to detect crystals or mineralized deposits within the connexin mutant lenses and to identify the inorganic components of these deposits. Part of these data was previously presented in abstract form (Beyer et al., 2019).

# RESULTS

## The Cataractous Lenses Contain Radio-Dense Mineralized Material

We used high energy, micro-computed tomography (micro-CT) scanning to examine the lenses for the presence and distribution of mineralized material. We studied homozygous animals, because they have more severe cataracts than the heterozygotes. The Cx46fs380 animals that were studied were older than the Cx50D47A, because they develop severe cataracts later. We obtained darkfield microscopy images of freshly dissected wild-type and homozygous Cx46fs380 and Cx50D47A lenses. Then, the lenses were fixed and studied by micro-CT scanning. The wild-type lenses appeared transparent by darkfield microscopy and showed no radio-dense material in the micro-CT images (**Figures 1A**, **2A**). In contrast, the homozygous mutant lenses had cataracts (**Figures 1B**, **2B,E**), and they contained abundant radio-dense material (**Figures 1C,D**, **2C,F**). Although the examples shown are from male mice, X-ray dense material was observed in mice of both sexes.

Cataracts in the homozygous Cx46fs380 lenses were composed mostly of several large opacities within the anterior region of the lens nucleus (**Figure 1**). Three-dimensional reconstruction of the micro-CT scans of the lenses from 5-6-month-old homozygous Cx46fs380 mice showed relatively large mineral bodies concentrated in a plane corresponding to the anterior region of the lens nucleus and scattered bits of mineral spread out towards the posterior pole of the lens (**Figure 1**; **Supplementary Movie S1**). In the lens shown in **Figure 1**, the mineral bodies were arranged roughly into a flattened ring that encircled the anterior region of the lens. The distribution of the mineral particles (detected by micro-CT) corresponded nearly perfectly to the morphology of the cataracts (seen by darkfield microscopy) (**Figure 1**). In Cx46fs380 lenses, the length of the mineral bodies ranged from 73–2,936 μm and the width ranged from 41–240 μm ($n$ = 7). Consistent with the appearance and restricted location of the Cx46fs380 cataracts, the proportion of the lens volume that contained mineral as determined from the micro-CT data was 0.31% (range 0.09%–1.03%; $n$ = 7).

The distribution of mineral and the appearance of the radio-dense deposits in homozygous Cx50D47A lenses were very different from the Cx46fs380 lenses. Homozygous Cx50D47A animals showed a rather severe cataract that optically appeared diffuse and occupied the entire lens nucleus (**Figure 2**). While wild-type lenses showed no X-ray dense material in any region, Cx50D47A lenses showed widely dispersed particles with a dim X-ray density and some particles that were more intensely X-ray dense. The more X-ray dense particles extended into curved, needle-like shapes or coalesced into thin, spherical shells. On average, the X-ray dense material in the Cx50D47A lenses occupied only 0.24% of the lens volume (range 0.08%–0.51%; $n$ = 6) in lenses from 2-month-old mice and 0.84% (range 0.45%–1.33%; $n$ = 8) in 102-day-old lenses. The total X-ray dense material (a combination of scattered particles of dimly X-ray dense material extending up to the center of the lens nucleus in between thin, spherical baskets of higher X-ray density) occupied a spherical volume that closely matched the region of the cataract in each lens (**Figure 2**; **Supplementary Movies S2, S3**). The elongated appearance of some of the X-ray dense regions resembled the shapes and orientations of fiber cells. The lengths of highly X-ray dense deposits in the spherical layers ranged from 58–458 μm ($n$ = 6) in 2-month-old lenses and 160–348 μm ($n$ = 8) in 102-day-old lenses, and the widths ranged from 8–65 μm ($n$ = 6) and 21–61 μm ($n$ = 8), respectively, suggesting that their dimensions increased with age (as expected, because the cataracts become more severe with age). Interestingly, the average widths of the mineral layers were significantly thinner than the average widths of the mineral bodies in the Cx46fs380 lenses ($p < 0.02$).

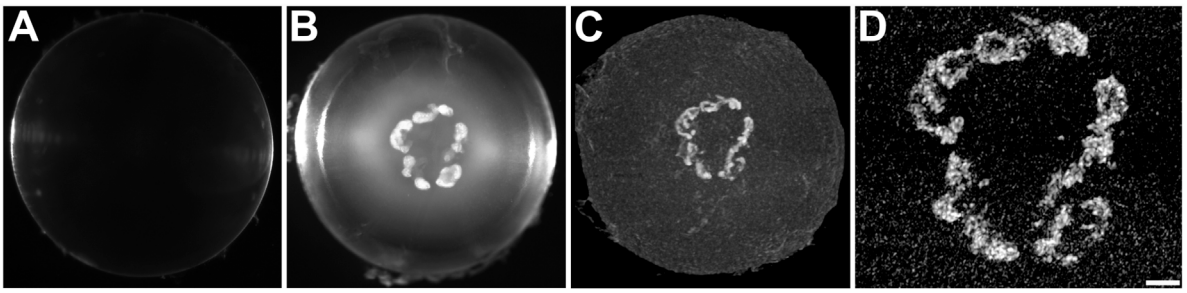


**FIGURE 1 |** The distribution of the high X-ray attenuating material in Cx46fs380 lenses coincides with that of the cataract. **(A,B)** Darkfield images of Cx46fs380 lenses from 171-day-old wild-type **(A)** and homozygous **(B)** male mice. **(C)** Three-dimensional projection of the micro-CT images from the homozygous lens shown in **(B)**. **(D)** Magnified view of the central region of the three-dimensional projection of the homozygous lens shown in **(C)**. The scale bar represents 331 μm for panels **(A,B)**, 300 μm for panel **(C)**, and 100 μm for panel **(D)**.

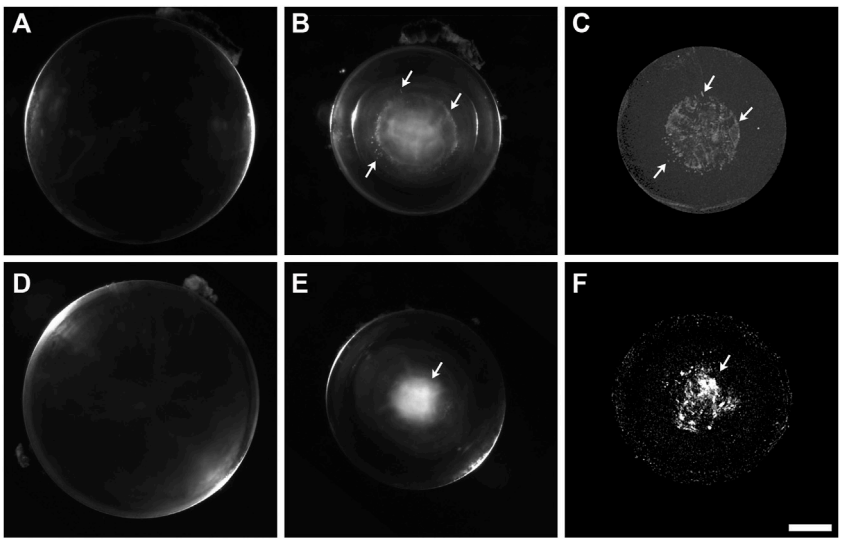


**FIGURE 2 |** The cataractous Cx50D47A lenses present high X-ray attenuating material. **(A,B)** Darkfield images of Cx50D47A lenses from a 59-day-old wild-type **(A)** and a 56-day-old homozygous **(B)** male mouse. **(C)** View from a three-dimensional projection of the micro-CT images from the lens shown in **(B)**. A 3D-reconstruction movie of the mineral densities found in the lens shown in **(B)** is shown in **Supplementary Movie S2**. **(D,E)** Darkfield images of Cx50D47A lenses from 102-day-old wild-type **(D)** and homozygous **(E)** male mice. **(F)** View from a three-dimensional projection of the micro-CT images from the lens shown in **(E)**. A 3D-reconstruction movie of the mineral densities found in the lens shown in **(E)** is shown in **Supplementary Movie S3**. Arrows in panels **(B,C)** and **(E,F)** indicate positions of close correspondence between opacities seen in the darkfield images and X-ray dense material in the respective micro-CT images. The scale bar represents 357 μm for panels **(A,B)**, 418 μm for panel **(C)**, 448 μm for panels **(D,E)**, and 378 μm for panel **(F)**.

## Cataractous Lenses Have Insoluble Particles That Stain With Alizarin Red

We also sought to further characterize the Alizarin red-stained material that we had previously detected after wholemount staining of homozygous Cx50D47A and Cx46fs380 lenses (Gao et al., 2018; Berthoud et al., 2019). For this purpose, we prepared insoluble fractions from lens homogenates from wild-type and homozygous Cx50D47A and Cx46fs380 mice by centrifugation and stained them with Alizarin red. No significant stained material was detected in the insoluble fraction from wild-type lenses of either mouse line (**Figures 3A**, **4A**). In contrast, the samples from homozygous lenses of both lines contained particles that stained with Alizarin red (**Figures 3**, **4**). In the homogenates of the Cx46fs380 lenses, the Alizarin red-stained objects varied widely in size, but the size range was within the dimensions determined by micro-CT (i.e., 22–310 μm in the longest dimension for the examples shown in **Figure 3**). Many of the particles in the Cx46fs380 insoluble fractions had distinct, sharp edges. In the homogenates from the Cx50D47A lenses, most of the Alizarin red-stained particles appeared as irregularly shaped red objects of various sizes (ranging from <8 to 70 μm in the longest dimension for the examples shown in **Figure 4**). Some of the particles had dark, sharp, linear edges suggestive of` crystals (shown at higher magnification in **Figures 4F–H**).

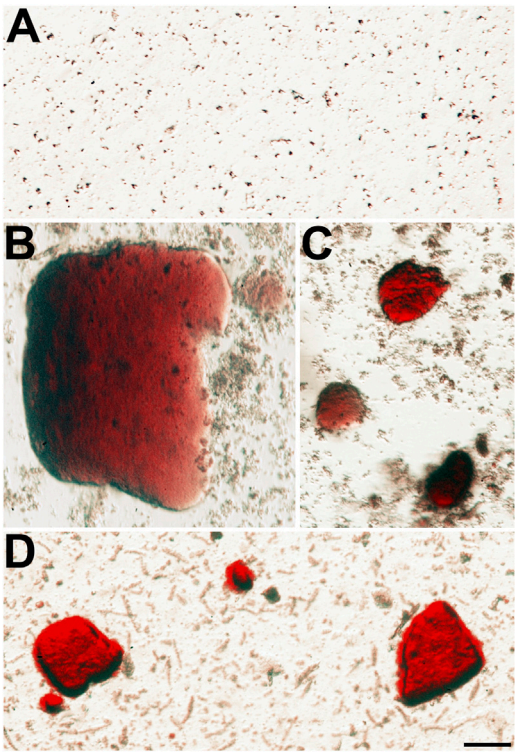


**FIGURE 3 |** Alizarin red-stained crystals are present in the insoluble fraction of homozygous Cx46fs380 lenses. **(A)** Image shows the absence of Alizarin red-stained material in the lens insoluble fraction of a 191-day-old wild-type Cx46fs380 male mouse. **(B–D)** Images show the presence of Alizarin red-stained crystals of different sizes in the lens insoluble fraction of a homozygous Cx46fs380 female littermate. The images were modified to decrease the reddish background from the Alizarin red solution in which the insoluble fraction was resuspended. The scale bar represents 54 μm.

## Identification of the Lens Mineral

To determine the composition of the mineral particles, sections from homozygous Cx46fs380 or Cx50D47A lenses were mounted on low-E glass slides. These sections were then analyzed using Attenuated Total Internal Reflection micro–Fourier transform infrared spectroscopy (ATR-μFTIR) imaging. Localization of $Ca^{2+}$-containing material in Yasue-stained sections facilitated identification of regions in adjacent sections to analyze by ATR-μFTIR (**Figures 5A–C** and **Figures 6A–C**). Sections from the lenses of at least three homozygous Cx46fs380 and Cx50D47A mice were analyzed using this technique.

Representative spectra extracted from the non-mineral regions and the mineral-rich regions in sections of homozygous Cx46fs380 lenses are shown in **Figure 5D**. The spectra extracted from the non-mineral regions are characteristic for normal protein. Prominent features in these spectra include the combined N-H and O-H stretch located near 3,270 $cm^{-1}$ and the amide I and II absorptions located near 1,633 and 1,521 $cm^{-1}$, respectively. The spectra extracted from the mineral-rich regions showed additional absorptions besides those observed in spectra

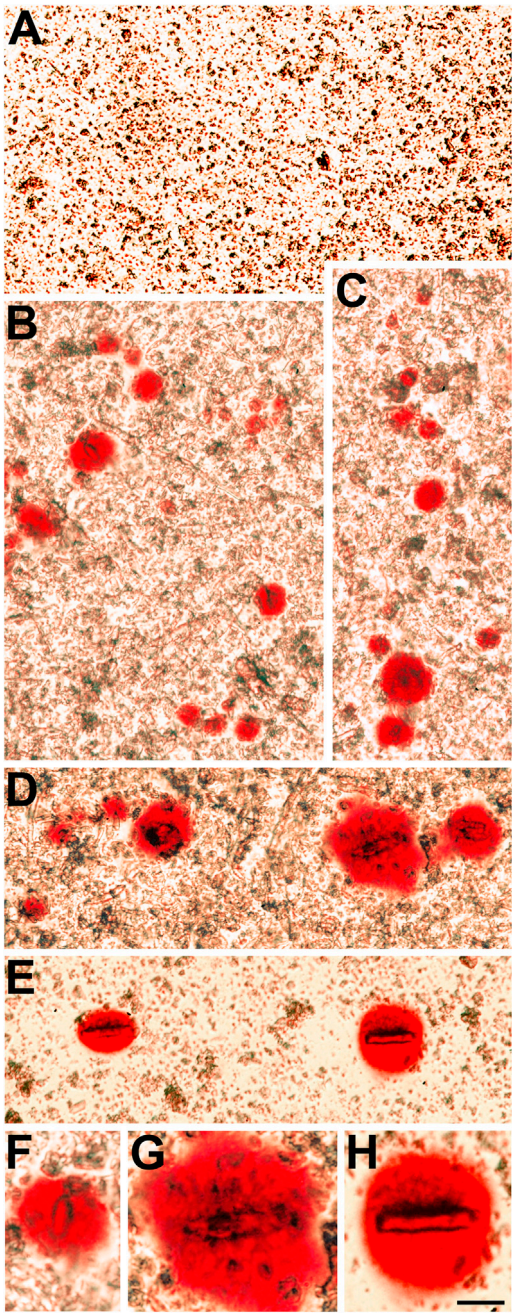


**FIGURE 4 |** The insoluble fraction of homozygous Cx50D47A lenses contains Alizarin red-stained crystals. **(A)** Image shows the lack of Alizarin red-stained material in the lens insoluble fraction from a 93-day-old wild-type Cx50D47A female mouse. **(B–E)** Images show several Alizarin red-stained crystals present in the insoluble fraction of Cx50D47A homozygous lenses from a 60-day-old female mouse **(E)** and a 93-day-old male mouse **(B–D)**. **(F–H)** Higher magnification images of selected Alizarin red-stained crystals from panels **(B,D,E)**. The images were modified to decrease the reddish background from the Alizarin red solution used to resuspend the insoluble fraction. The scale bar represents 54 μm in panels **(A–E)**, and 27 μm in panels **(F–H)**.

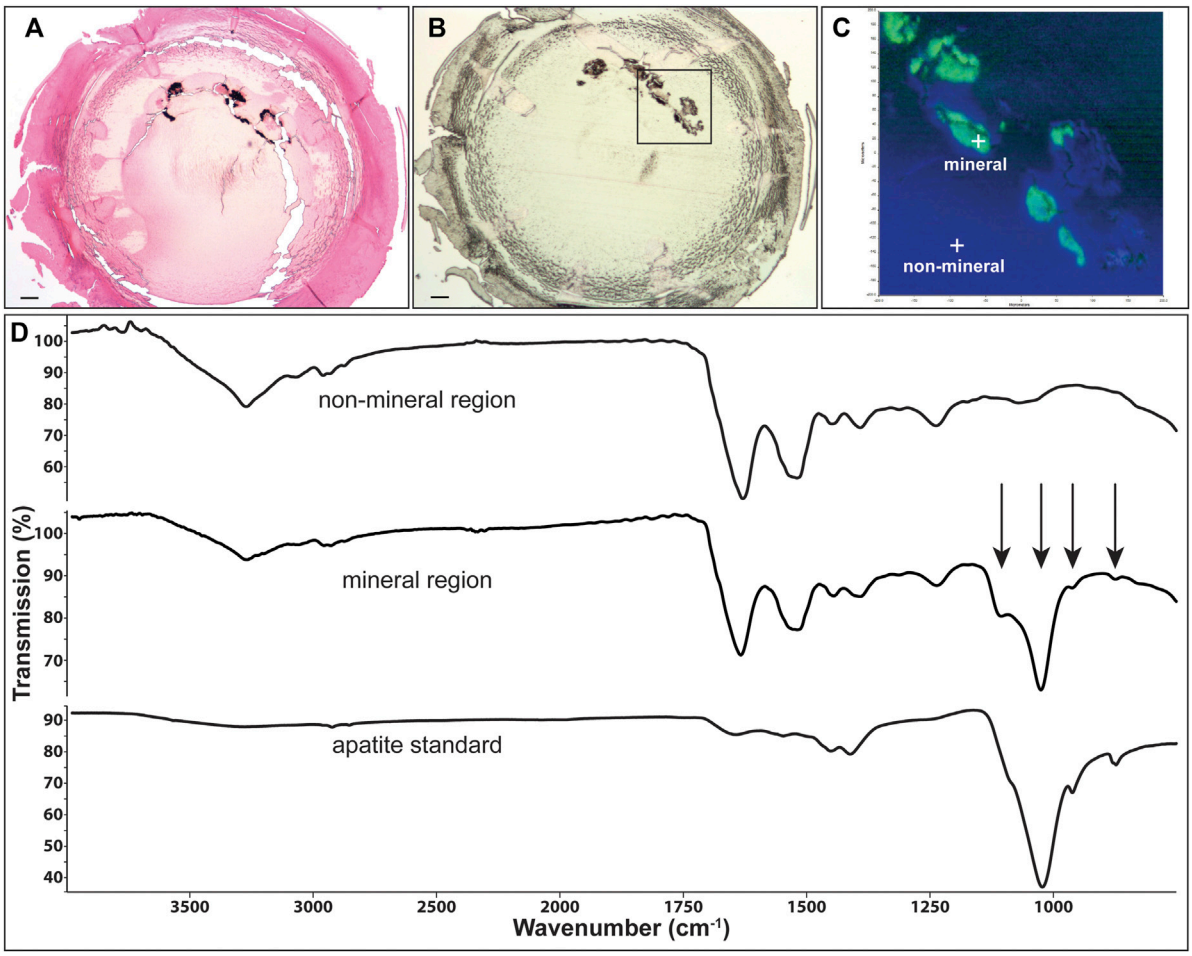


**FIGURE 5 |** Identification of mineral type in Cx46fs380 lenses. **(A)** Image showing Yasue staining of a section from the lens of the 171-day old homozygous Cx46fs380 male mouse shown in **Figure 1**. The black stained material corresponds to calcifications. **(B)** Image of an unstained section of the same lens on low emissivity glass that was used for infrared imaging. **(C)** Image shows the infrared signal map obtained of the boxed region shown on **(B)** by collecting 65,746 infrared spectra with a pixel resolution of 1.56 μm. Green areas are mineral regions and blue areas are protein regions. **(D)** Graphs show the spectra of a non-mineral region, a mineral region, and the apatite standard. Arrows point to features characteristic of apatite mineral in the lens. The scale bars in **(A,B)** represent 100 μm.

from the non-mineral regions. These additional absorptions are located at 1,106, 1,024, 961, and 873 $cm^{-1}$, which are characteristic for calcium apatite. A reference spectrum of apatite is also shown in **Figure 5D** for comparison. Similarly, in sections of homozygous Cx50D47A lenses the infrared spectra of the mineral regions showed the absorption bands characteristic of protein and of calcium apatite (**Figure 6D**).

Thus, these analyses revealed that the composition of the mineral present in both Cx46fs380 and Cx50D47A lenses contains calcium phosphate in the form of apatite.

## DISCUSSION

In this manuscript, we have demonstrated that cataracts resulting from mutations in the lens fiber cell connexins, Cx46 and Cx50, form by deposition of calcium phosphate. We found insoluble, calcium-containing material in homogenates and X-ray dense material only in samples from cataractous lenses. In addition, in both mutant mouse lines, we identified the mineral component as apatite.

The current data from micro-computed tomographic scans show that the distributions of radio-dense material (mineral) closely correspond to the cataract morphologies in both mouse models. In addition, the three-dimensional distribution of the X-ray dense material observed by micro-CT scanning of cataractous lenses from Cx46fs380 and Cx50D47A mice closely resembles the Alizarin red staining pattern of these lenses (Gao et al., 2018; Berthoud et al., 2019). Thus, the micro-CT scanning data provide conclusive evidence that cataracts reflect the formation of calcified deposits.

ATR-μFTIR allowed us to study the chemical composition of the cataracts in the Cx46fs380 and Cx50D47A mice. The ATR-μFTIR spectral data show that the inorganic component of the mineralized particles in the lenses of both mouse lines is calcium phosphate (apatite). This mineral form of calcium is often found

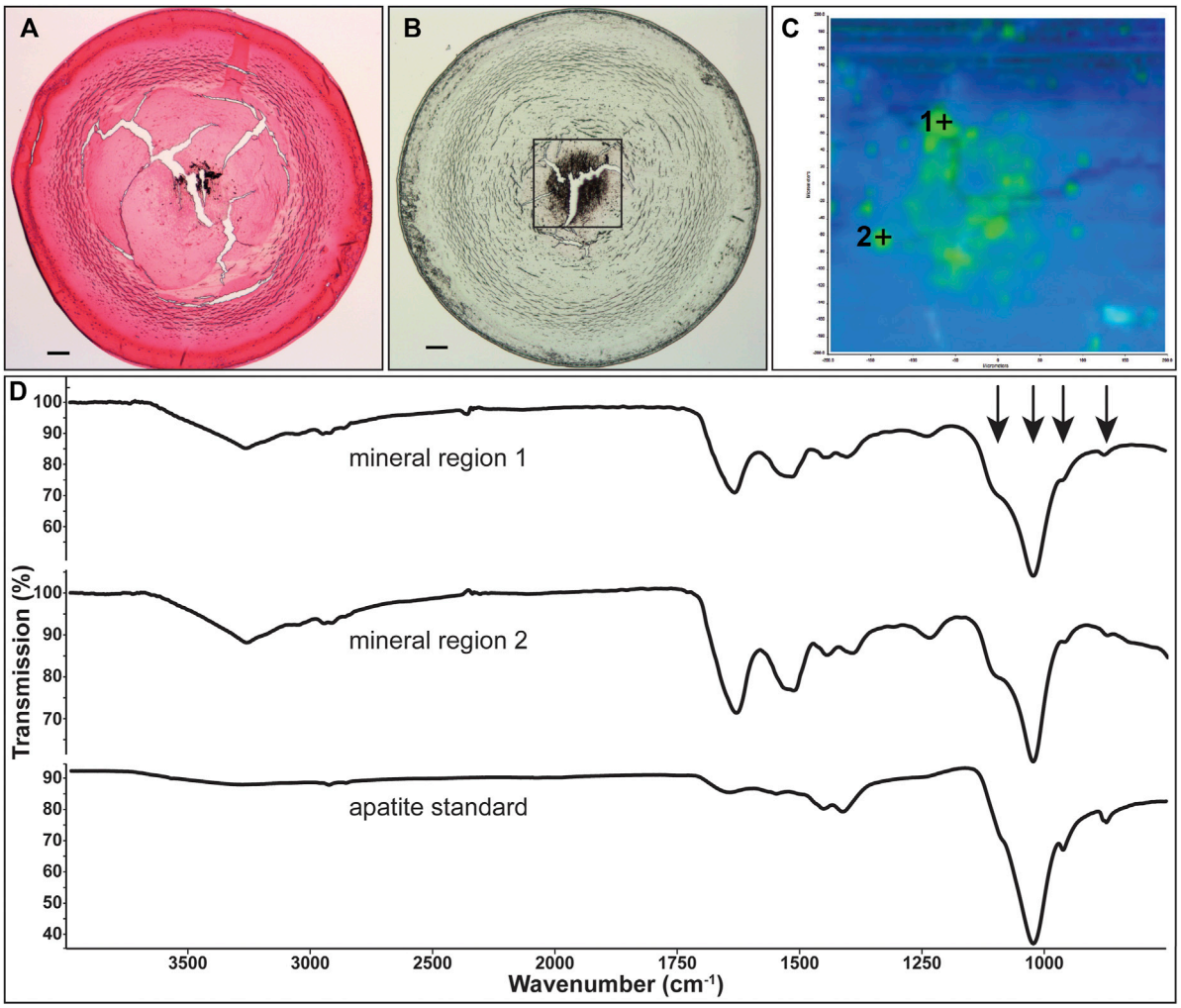


**FIGURE 6 |** Identification of mineral type in Cx50D47A lenses. **(A)** Image showing Yasue staining of a section from the lens of the 102-day-old homozygous Cx50D47A male mouse shown in **Figure 2E**. The stained material that appears black corresponds to calcifications. **(B)** Image of an unstained section of the same lens on low emissivity glass used for infrared imaging. **(C)** Image shows the infrared signal map of the boxed region shown on **(B)** generated by collecting 4,096 infrared spectra with a pixel resolution of 6.24 μm. Green areas are mineral regions and blue areas are protein regions. **(D)** Graphs show the spectra of two mineral regions and the apatite standard. Arrows point to features characteristic of apatite mineral in the lens. The scale bars in **(A,B)** represent 100 μm.

in other body tissues/fluids where calcium deposits have been reported. Typically, apatite forms acicular crystallites (~0.1 μm in length) that are closely bound with proteins (LeGeros, 2001; Ryall, 2008). Our ATR-μFTIR spectral data also showed amide I and amide II bands at the sampled locations. The spatial resolution of the method is diffraction limited to 6 μm at 1,650 $cm^{-1}$ and to ~3 μm at 3,400 $cm^{-1}$ in the x-y plane. In the z plane, the infrared beam penetrates the sample to depths of 0.67 and 0.33 μm at those wavenumbers, respectively, but the penetration depth into the sample in the ATR method increases from the short wavelength (high wavenumber) to the long wavelength (low wavenumber) end of the spectrum (e.g., 1.1 μm at 1,000 $cm^{-1}$). Therefore, based on the large size of many of the particles relative to the spatial limitations of the method and the avidity of apatite crystallites for protein, it is likely that proteins are associated with the mineral. These proteins may be integral components of the mineral, but it is also possible that the proteins surround the crystals or are trapped inside them during their formation. The detection of both a calcium salt and protein at locations of mineral deposits is consistent with the deposition of crystals on a macromolecular matrix as occurs during physiological biomineralization of tissues like bone and teeth. Since the formation of calcium depositions within the lens corresponds to a pathological phenomenon that is detrimental to lens function, we consider this process to be "pathological mineralization."

Precipitation of calcium salts requires supersaturating concentrations of calcium ions (and an anion). We have previously shown that the Cx46fs380 and Cx50D47A lenses contain increased levels of intracellular calcium ions and that these levels surpass the *Ksp* for some of its salts (Gao et al., 2018; Berthoud et al., 2019). We have developed a model to explain the

mechanism of formation of the calcium precipitates in connexin mutant lenses that is presented in **Figure 7**. The lens microcirculation is impaired in homozygous connexin mutant lenses, because gap junctional intercellular communication, which provides the outflow pathway for ions to exit the lens, is significantly decreased (Minogue et al., 2017; Berthoud et al., 2019). Consequently, ions accumulate in the lens. In the case of calcium ions, the intracellular concentration of free calcium ions reaches values above 2 μM in the center of the lens in both fiber cell connexin mutant lenses, whereas in surface fiber cells it is similar to wild-type in homozygous Cx46fs380 lenses and more than twice the value in wild-type lenses in homozygous Cx50D47A lenses (Gao et al., 2018; Berthoud et al., 2019). The high intracellular concentration of calcium ions reacts with intracellular inorganic free phosphate to form calcium phosphate (apatite).

Several lines of evidence suggest that an increase in the concentration of calcium to supersaturating levels followed by formation of calcium deposits is a common and necessary step in the formation of lens opacities of many different etiologies. Increased levels of $Ca^{2+}$ have been reported in human and mouse lenses with cataracts of various etiologies (Duncan and van Heyningen, 1977; Hightower and Reddy, 1982; Duncan and Jacob, 1984; Gao et al., 2004; Li et al., 2010; Liu et al., 2015). Indeed, many years ago cataracts were reported to contain insoluble material that appeared like scales or needles (which were suggested to be composed of different substances, including phosphate of lime (a term used then for calcium phosphate) and cholesterine) (reviewed and discussed in Jacob, 1851). Subsequent studies have reported increased levels of calcium ions in the insoluble fraction of human cataractous lenses compared with non-cataractous lenses (Duncan and van Heyningen, 1977), X-ray dense material and calcium-rich regions in the cortical region of canine cataractous lenses (Antunes et al., 2006), and radio-dense material accumulated in the anterior Y suture of Cx46-null mice (Li et al., 2021). Similar to our previous studies of lens fiber cell connexin mutant mice (Gao et al., 2018; Berthoud et al., 2019), material that stains with Alizarin red has been detected in cataractous lenses from mice carrying a mutation in the transient-receptor-potential cation channel, subfamily M, member 3 (TRPM3) and in Cx46-null mice (Li et al., 2021; Zhou et al., 2021).

Our study provides evidence for cataractogenesis through formation of insoluble, calcified material in which the counterion is phosphate. Similar to our findings in connexin mutant lenses, several case reports have identified mineral composed of calcium and phosphate in the cataracts of both younger and older people (Fagerholm et al., 1982; Fagerholm et al., 1986; Chen et al., 2005). Although calcium precipitates may be a common finding in cataracts of different etiologies, the counterion in the precipitates might differ as the presence of calcium oxalate has been reported in Morgagnian cataracts (Zimmerman and Johnson, 1958; Bron and Habgood, 1976; Pau, 1984). Nevertheless, the presence of apatite or another precipitated calcium salt in the lens (whether deposited so densely that it effectively blocks X-rays or deposited less abundantly so that it causes a much lower total X-ray attenuation (Williams et al., 2021)) would alter the gradient of refractive index and cause density fluctuations and light scattering.

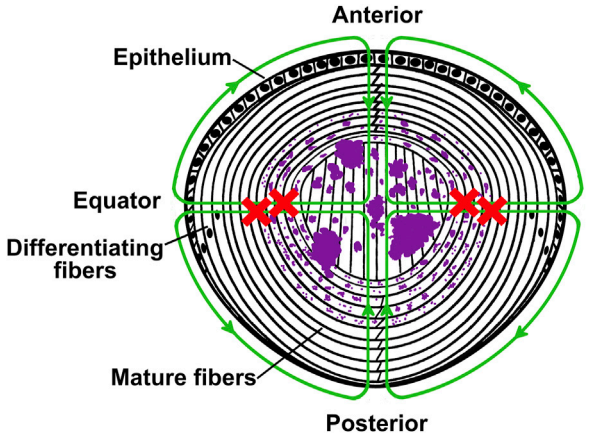


**FIGURE 7 |** Model illustrating the mechanism of formation of apatite deposits in the lens. The diagram depicts a cross sectional view of a mouse lens in which the lens circulation is impaired due to expression of a mutant connexin in the fiber cells. In the healthy lens, ions and fluid enter into the lens from the anterior and posterior poles and move to the lens center through the extracellular spaces, and they exit across epithelial cell membranes at the equator. The green lines with arrowheads illustrate the circulation and the direction of flow of ions and fluid in a normal healthy lens. The red crosses indicate that outflow of ions through fiber cell-to-fiber cell gap junctions is impaired due to the expression of the mutant connexin. This disruption leads to accumulation of calcium ions. As their concentration increases, the calcium ions react with the intracellular phosphate to form apatite precipitates (illustrated in purple). The crystals are initially small, but they become larger with aging.

Thus, our current data suggest that the formation of cataracts in two different mouse models occurs through pathological mineralization of the organ, and consideration of published reports implies that this process may be a general mechanism contributing to the formation of cataracts of many different etiologies.

## MATERIALS AND METHODS

### Animals

Cx46fs380 animals were generated and maintained as described by Berthoud et al. (2014). Cx50D47A mice (also known as *No2* or ENU-326) (Favor, 1983) were maintained in the C3H mouse strain as described previously (Berthoud et al., 2013). Animals of both sexes were used for all experiment types. The sex of the animal is indicated in the legends for the data shown in the figures. Cx46fs380 animals were studied at 157, 167, 171 and 191 days. Cx50D47A animals were studied at 56, 59, 60, 63, 93 and 102 days. All animal procedures were approved by the University of Chicago Animal Care and Use Committee and followed its guidelines.

## Light Microscopy Analysis

Before fixation, lenses were viewed using a Zeiss Stemi-2000C stereo microscope (Carl Zeiss, München, Germany) equipped with a halogen lighting system for transmitted illumination. Images were acquired with a Zeiss AxioCam digital camera using Zeiss AxioVision software using identical settings (i.e., magnification, illumination, and exposure time) to photograph the wild-type and homozygous lenses in each group (Berthoud et al., 2013; Berthoud et al., 2014).

## High Resolution Micro-CT

Lenses were fixed in 5% paraformaldehyde in PBS for 48 h and scanned by high resolution micro-CT to detect the presence or absence of high X-ray attenuating (mineralized) material using a Skyscan 1172 Micro CT System at 60 kV with a final image stack resolution of 3–6 μm cubic voxels. We examined a total of 6 wild-type and 7 homozygous Cx46fs380 mouse lenses (157–171 days of age), and 14 wild-type and 14 homozygous Cx50D47A mouse lenses (56–102 days of age). The micro-CT scans were performed under blinded conditions by an investigator who was unaware of the genotypes. Three-dimensional image stacks were viewed using ImageJ (as distributed through fiji. sc) (Schindelin et al., 2012), and overall mineral density and distributions of deposit sizes were quantified. Movies from the three-dimensional scan stacks were generated using 3D Slicer (Fedorov et al., 2012).

## Alizarin Red Staining of the Lens Water-Insoluble Fraction

Wild-type and homozygous Cx46fs380 lenses from 191-day-old mice and wild-type and homozygous Cx50D47A lenses from 60 and 93 days of age were homogenized in PBS containing cOmplete EDTA-free protease inhibitor cocktail (Roche Applied Science, Indianapolis, IN, United States) at a concentration of 1 tablet/7 ml using a glass-glass homogenizer. The homogenates were centrifuged at 16,000 g for 20 min. The supernatant was discarded, and the pellet was resuspended in homogenization buffer. Equal amounts of the resuspended pellet and a filtered solution of 2% Alizarin red in water pH 4.1–4.3 were added to a glass slide and mixed by pipetting up and down. Glass slides and the glass-glass homogenizer were pretested to make sure they did not contain any material that interacted with Alizarin red and cleaned with deionized water prior to the experiment. The specimens were observed using a DIAPHOT inverted Nikon microscope (Nikon Instruments Inc., Melville, NY) equipped with epifluorescence and Hoffman modulation contrast optics. Phase-contrast and fluorescence images were obtained with a 10X objective using a Nikon D70 digital camera (Nikon). These experiments were performed once for Cx46fs380 lenses and twice for Cx50D47A lenses. The longest dimension of the Alizarin red-stained particles was determined using ImageJ (Schindelin et al., 2012).

## Yasue Staining

After micro-CT scanning, each lens was dehydrated and embedded in paraffin. Five-μm sections were obtained from each lens, and alternating sections were deposited on regular glass for staining with the Yasue method to show calcium salts (Yasue, 1969) and on low-emissivity (low-E) glass for infrared microspectroscopy.

## Fourier-Transform Infrared Microspectroscopy

The composition of crystals in Cx46fs380 lenses (157–171 days of age) and Cx50D47A lenses (102 days of age) was determined by Attenuated Total Internal Reflection Fourier-transform infrared microspectroscopy (ATR-μFTIR) on lens sections mounted on low-E glass slides. The unstained tissue sections were imaged using the visible CCD camera and frame grabber on the Spectrum Spotlight (Gulley-Stahl et al., 2010). Infrared images over the selected area were collected with a Perkin-Elmer Spotlight 400 infrared microscope interfaced to a Perkin-Elmer Frontier Fourier transform infrared spectrometer (FTIR). The system employed a 16 × 1, liquid nitrogen cooled, mercury cadmium telluride (HgCdTe) array detector. The ATR imaging accessory is based on a germanium internal reflection element which enables infrared spectra to be collected at a pixel resolution of 1.56 μm or 6.24 μm. Each spectrum in the image represents the average of four individual scans collected at a spectral resolution of 8 wavenumbers ($cm^{-1}$).

## Statistics

Data are presented as a range or mean (with its range in the case of percentages). Statistical analysis of the width and length of X-ray dense material was performed using unpaired two-tailed Student's t-test. A $p$ value $< 0.05$ was considered significant. Data from both sexes were combined because no sex differences were detected in the parameters studied.

# DATA AVAILABILITY STATEMENT

The original contributions presented in the study are included in the article/**Supplementary Material**, further inquiries can be directed to the corresponding author.

# ETHICS STATEMENT

The animal study was reviewed and approved by the University of Chicago Animal Care and Use Committee.

# AUTHOR CONTRIBUTIONS

PM, EB and VB conceived the project. PM, JW, AS, EB and VB designed the experiments. PM, JW, SB, AS and VB performed experiments. PM, JW, AS and VB performed data analysis. VB and EB coordinated the project. VB wrote the initial draft of the paper. All authors made significant contributions to the writing of the manuscript. All authors approved the final version of the paper.

## FUNDING

This work was supported by National Institutes of Health grants R01-EY030914 (to EB and VB) and S10 RR023710 (to JW). The content of this article is solely the responsibility of the authors and does not necessarily represent the official views of the National Institutes of Health.

## ACKNOWLEDGMENTS

The authors thank Jennifer Stashevsky for excellent technical assistance.

## SUPPLEMENTARY MATERIAL

The Supplementary Material for this article can be found online at: https://www.frontiersin.org/articles/10.3389/fcell.2022.951231/full#supplementary-material

**Supplementary Movie S1: |** Animation of the series of scans through the lens of a 157-day-old homozygous Cx46fs380 male mouse. In this animation, the lens has been oriented with its anterior face towards the bottom.

**Supplementary Movie S2: |** Animation of the series of scans through the lens from a 56-day-old homozygous Cx50D47A male mouse shown in **Figure 2B**.

**Supplementary Movie S3: |** Animation of the series of scans through the lens from a 102-day-old homozygous Cx50D47A male mouse shown in **Figure 2E**.

## REFERENCES

Antunes, A., Safatle, A. M. V., Barros, P. S. M., and Morelhão, S. L. (2006). X-Ray Imaging in Advanced Studies of Ophthalmic Diseases. *Med. Phys.* 33, 2338–2343. doi:10.1118/1.2207135

Berthoud, V. M., Gao, J., Minogue, P. J., Jara, O., Mathias, R. T., and Beyer, E. C. (2019). The Connexin50D47A Mutant Causes Cataracts by Calcium Precipitation. *Invest. Ophthalmol. Vis. Sci.* 60, 2336–2346. doi:10.1167/iovs.18-26459

Berthoud, V. M., Minogue, P. J., Yu, H., Schroeder, R., Snabb, J. I., and Beyer, E. C. (2013). Connexin50D47A Decreases Levels of Fiber Cell Connexins and Impairs Lens Fiber Cell Differentiation. *Invest. Ophthalmol. Vis. Sci.* 54, 7614–7622. doi:10.1167/iovs.13-13188

Berthoud, V. M., Minogue, P. J., Yu, H., Snabb, J. I., and Beyer, E. C. (2014). Connexin46fs380 Causes Progressive Cataracts. *Invest. Ophthalmol. Vis. Sci.* 55, 6639–6648. doi:10.1167/iovs.14-15012

Beyer, E. C., Gao, J., Minogue, P. J., Jara, O., Bledsoe, S., Gardner, T., et al. (2019). Connexin Mutants Impair the Lens Circulation Leading to Calcium Accumulation/Precipitation and Cataracts. Abstract Retrieved from the Program for The 6th International Conference on the Lens, p. 50.

Bron, A. J., and Habgood, J. O. (1976). Morgagnian Cataract. *Trans. Ophthalmol. Soc. U. K.* 96, 265–277.

Chen, K.-H., Cheng, W.-T., Li, M.-J., Yang, D.-M., and Lin, S.-Y. (2005). Calcification of Senile Cataractous Lens Determined by Fourier Transform Infrared (FTIR) and Raman Microspectroscopies. *J. Microsc.* 219, 36–41. doi:10.1111/j.1365-2818.2005.01491.x

Duncan, G., and Jacob, T. J. (1984). Calcium and the Physiology of Cataract. *Ciba Found. Symp.* 106, 132–152. doi:10.1002/9780470720875.ch8

Duncan, G., and van Heyningen, R. (1977). Distribution of Non-Diffusible Calcium and Sodium in Normal and Cataractous Human Lenses. *Exp. Eye Res.* 25, 183–193. doi:10.1016/0014-4835(77)90130-0

Fagerholm, P., Lundevall, E., Trocmé, S., and Wroblewski, R. (1986). Human and Experimental Lens Repair and Calcification. *Exp. Eye Res.* 43, 965–972. doi:10.1016/0014-4835(86)90074-6

Fagerholm, P., Philipson, B., and Carlström, D. (1982). Calcification in the Human Lens. *Curr. Eye Res.* 1, 629–633. doi:10.3109/02713688109001866

Favor, J. (1983). A Comparison of the Dominant Cataract and Recessive Specific-Locus Mutation Rates Induced by Treatment of Male Mice with Ethylnitrosourea. *Mutat. Res.* 110, 367–382. doi:10.1016/0027-5107(83)90153-7

Fedorov, A., Beichel, R., Kalpathy-Cramer, J., Finet, J., Fillion-Robin, J.-C., Pujol, S., et al. (2012). 3D Slicer as an Image Computing Platform for the Quantitative Imaging Network. *Magn. Reson. Imaging* 30, 1323–1341. doi:10.1016/j.mri.2012.05.001

Gao, J., Minogue, P. J., Beyer, E. C., Mathias, R. T., and Berthoud, V. M. (2018). Disruption of the Lens Circulation Causes Calcium Accumulation and Precipitates in Connexin Mutant Mice. *Am. J. Physiol. Cell Physiol.* 314, C492–C503. doi:10.1152/ajpcell.00277.2017

Gao, J., Sun, X., Martinez-Wittinghan, F. J., Gong, X., White, T. W., and Mathias, R. T. (2004). Connections Between Connexins, Calcium, and Cataracts in the Lens. *J. Gen. Physiol.* 124, 289–300. doi:10.1085/jgp.200409121

Gulley-Stahl, H. J., Bledsoe, S. B., Evan, A. P., and Sommer, A. J. (2010). The Advantages of an Attenuated Total Internal Reflection Infrared Microspectroscopic Imaging Approach for Kidney Biopsy Analysis. *Appl. Spectrosc.* 64, 15–22. doi:10.1366/000370210792966161

Hightower, K. R., and Reddy, V. N. (1982). Calcium Content and Distribution in Human Cataract. *Exp. Eye Res.* 34, 413–421. doi:10.1016/0014-4835(82)90087-2

Jacob, A. (1851). *Cataract. Structure of the Lens and the Nature of Its Opacity. On Cataract, and the Operation of Its Removal by Absorption With the Fine Needle Through the Cornea*. Dublin: Medical Press Office, 1–60.

LeGeros, R. Z. (2001). Formation and Transformation of Calcium Phosphates: Relevance to Vascular Calcification. *Z. Kardiol.* 90 (Suppl. 3), 116–124. doi:10.1007/s003920170032

Li, L., Cheng, C., Xia, C.-h., White, T. W., Fletcher, D. A., and Gong, X. (2010). Connexin Mediated Cataract Prevention in Mice. *PLoS ONE* 5, e12624. doi:10.1371/journal.pone.0012624

Li, Y., Parkinson, D. Y., Feng, J., Xia, C.-h., and Gong, X. (2021). Quantitative X-Ray Tomographic Analysis Reveals Calcium Precipitation in Cataractogenesis. *Sci. Rep.* 11, 17401. doi:10.1038/s41598-021-96867-7

Liu, K., Lyu, L., Chin, D., Gao, J., Sun, X., Shang, F., et al. (2015). Altered Ubiquitin Causes Perturbed Calcium Homeostasis, Hyperactivation of Calpain, Dysregulated Differentiation, and Cataract. *Proc. Natl. Acad. Sci. U.S.A.* 112, 1071–1076. doi:10.1073/pnas.1404059112

Mathias, R. T., Kistler, J., and Donaldson, P. (2007). The Lens Circulation. *J. Membr. Biol.* 216, 1–16. doi:10.1007/s00232-007-9019-y

Minogue, P. J., Gao, J., Zoltoski, R. K., Novak, L. A., Mathias, R. T., Beyer, E. C., et al. (2017). Physiological and Optical Alterations Precede the Appearance of Cataracts in Cx46fs380 Mice. *Invest. Ophthalmol. Vis. Sci.* 58, 4366–4374. doi:10.1167/iovs.17-21684

Pau, H. (1984). Die Sphärolithen der Linse. *Klin. Monatsbl. Augenheilkd.* 184, 159–162. doi:10.1055/s-2008-1054431

Resnikoff, S., Pascolini, D., Etya'ale, D., Kocur, I., Pararajasegaram, R., Pokharel, G. P., et al. (2004). Global Data on Visual Impairment in the Year 2002. *Bull. World Health Organ.* 82, 844–851. doi:10.1590/S0042-96862004001100009

Ryall, R. L. (2008). The Future of Stone Research: Rummagings in the Attic, Randall's Plaque, Nanobacteria, and Lessons from Phylogeny. *Urol. Res.* 36, 77–97. doi:10.1007/s00240-007-0131-3

Schindelin, J., Arganda-Carreras, I., Frise, E., Kaynig, V., Longair, M., Pietzsch, T., et al. (2012). Fiji: An Open-Source Platform for Biological-Image Analysis. *Nat. Methods* 9, 676–682. doi:10.1038/nmeth.2019

Sharma, K. K., and Santhoshkumar, P. (2009). Lens Aging: Effects of Crystallins. *Biochim. Biophys. Acta.* 1790, 1095–1108. doi:10.1016/j.bbagen.2009.05.008

Truscott, R. J. W., and Friedrich, M. G. (2019). Molecular Processes Implicated in Human Age-Related Nuclear Cataract. *Invest. Ophthalmol. Vis. Sci.* 60, 5007–5021. doi:10.1167/iovs.19-27535

Williams, J. C., Jr., Lingeman, J. E., Daudon, M., and Bazin, D. (2021). Using Micro Computed Tomographic Imaging for Analyzing Kidney Stones. *C. R. Chim.* 24, 1–12. doi:10.5802/crchim.89

Yasue, T. (1969). Histochemical Identification of Calcium Oxalate. *Acta Histochem. Cytochem.* 2, 83–95. doi:10.1267/ahc.2.83

Zhou, Y., Bennett, T. M., and Shiels, A. (2021). Mutation of the TRPM3 Cation Channel Underlies Progressive Cataract Development and Lens Calcification Associated with Pro-Fibrotic and Immune Cell Responses. *FASEB J.* 35, e21288. doi:10.1096/fj.202002037R

Zimmerman, L. E., and Johnson, F. B. (1958). Calcium Oxalate Crystals Within Ocular Tissues. A Clinicopathologic and Histochemical Study. *AMA Arch. Ophthalmol.* 60, 372–383. doi:10.1001/archopht.1958.00940080388005

**Conflict of Interest:** The authors declare that the research was conducted in the absence of any commercial or financial relationships that could be construed as a potential conflict of interest.

**Publisher's Note:** All claims expressed in this article are solely those of the authors and do not necessarily represent those of their affiliated organizations, or those of the publisher, the editors and the reviewers. Any product that may be evaluated in this article, or claim that may be made by its manufacturer, is not guaranteed or endorsed by the publisher.

frontiers | Frontiers in Cell and Developmental Biology

TYPE Original Research
PUBLISHED 26 August 2022
DOI 10.3389/fcell.2022.981893



OPEN ACCESS

EDITED BY
Deepika Vasudevan,
University of Pittsburgh, United States

REVIEWED BY
Amit Kumar,
Albert Einstein College of Medicine, United States
Frank James Lovicu,
The University of Sydney, Australia

*CORRESPONDENCE
Salil A. Lachke,
salil@udel.edu

SPECIALTY SECTION
This article was submitted to Morphogenesis and Patterning, a section of the journal Frontiers in Cell and Developmental Biology

RECEIVED 29 June 2022
ACCEPTED 28 July 2022
PUBLISHED 26 August 2022

CITATION
Patel SD, Anand D, Motohashi H, Katsuoka F, Yamamoto M and Lachke SA (2022), Deficiency of the bZIP transcription factors Mafg and Mafk causes misexpression of genes in distinct pathways and results in lens embryonic developmental defects. *Front. Cell Dev. Biol.* 10:981893. doi: 10.3389/fcell.2022.981893



# Deficiency of the bZIP transcription factors Mafg and Mafk causes misexpression of genes in distinct pathways and results in lens embryonic developmental defects

Shaili D. Patel[1], Deepti Anand[1], Hozumi Motohashi[2], Fumiki Katsuoka[3], Masayuki Yamamoto[4] and Salil A. Lachke[1,5]*

[1]Department of Biological Sciences, University of Delaware, Newark, DE, United States, [2]Department of Gene Expression Regulation, Institute of Development, Aging, and Cancer, Tohoku University, Sendai, Japan, [3]Department of Integrative Genomics, Tohoku University Tohoku Medical Megabank Organization, Sendai, Japan, [4]Department of Medical Biochemistry, Tohoku University Graduate School of Medicine, Sendai, Japan, [5]Center for Bioinformatics and Computational Biology, University of Delaware, Newark, DE, United States

Deficiency of the small Maf proteins Mafg and Mafk cause multiple defects, namely, progressive neuronal degeneration, cataract, thrombocytopenia and mid-gestational/perinatal lethality. Previous data shows *Mafg*$^{-/-}$:*Mafk*$^{+/-}$ compound knockout (KO) mice exhibit cataracts age 4-months onward. Strikingly, *Mafg*$^{-/-}$:*Mafk*$^{-/-}$ double KO mice develop lens defects significantly early in life, during embryogenesis, but the pathobiology of these defects is unknown, and is addressed here. At embryonic day (E)16.5, the epithelium of lens in *Mafg*$^{-/-}$:*Mafk*$^{-/-}$ animals appears abnormally multilayered as demonstrated by E-cadherin and nuclear staining. Additionally, *Mafg*$^{-/-}$:*Mafk*$^{-/-}$ lenses exhibit abnormal distribution of F-actin near the "fulcrum" region where epithelial cells undergo apical constriction prior to elongation and reorientation as early differentiating fiber cells. To identify the underlying molecular changes, we performed high-throughput RNA-sequencing of E16.5 *Mafg*$^{-/-}$:*Mafk*$^{-/-}$ lenses and identified a cohort of differentially expressed genes that were further prioritized using stringent filtering criteria and validated by RT-qPCR. Several key factors associated with the cytoskeleton, cell cycle or extracellular matrix (e.g., *Cdk1*, *Cdkn1c*, *Camsap1*, *Col3a1*, *Map3k12*, *Sipa1l1*) were mis-expressed in *Mafg*$^{-/-}$:*Mafk*$^{-/-}$ lenses. Further, the congenital cataract-linked extracellular matrix peroxidase *Pxdn* was significantly overexpressed in *Mafg*$^{-/-}$:*Mafk*$^{-/-}$ lenses, which may cause abnormal cell morphology. These data also identified the ephrin signaling receptor *Epha5* to be reduced in *Mafg*$^{-/-}$:*Mafk*$^{-/-}$ lenses. This likely contributes to the *Mafg*$^{-/-}$:*Mafk*$^{-/-}$ multilayered lens epithelium pathology, as loss of an ephrin ligand, Efna5 (ephrin-A5), causes similar lens defects. Together, these findings uncover a novel early function of Mafg and Mafk in lens development and identify their new downstream regulatory relationships with key cellular factors.

KEYWORDS

lens, MAFG, MAFK, transcription, development, epithelium, bZIP transcription factors, eph signaling

## Introduction

Lens development and homeostasis is important for the establishment and maintenance of its transparency, the perturbation of which causes cataract—defined as opacification of the lens (Lachke and Maas, 2010; Cvekl and Zhang, 2017; Shiels and Hejtmancik, 2019). Depending on its early or late onset in life, cataract is classified as congenital/pediatric or age-related. Deficiency or alterations in several genes and genomic loci have been associated with both congenital and age-related cataract (Hammond et al., 2000, 2001; Congdon et al., 2005; Shiels and Hejtmancik, 2019, 2021; Choquet et al., 2021; Lachke, 2022). An estimated 8–25% of congenital/pediatric cataract are hereditary, suggesting the perturbation of the lens developmental pathways (Haargaard et al., 2004; Yi et al., 2011; Berry et al., 2020). Thus, defining the genetic pathways controlling lens development and/or homeostasis is important for fully understanding the factors contributing toward lens defects and cataract pathobiology. Thus far, the function of several transcriptional factors and post-transcriptional regulators in lens development has been characterized (Dash et al., 2016; Anand and Lachke, 2017; Cvekl and Zhang, 2017; Lachke, 2022).

The *MAF* (musculoaponeurotic fibrosarcoma) gene family encodes basic leucine zipper transcription factors (TFs) and is classified into two subgroups, namely "small" and "large" MAF proteins (Blank, 2008; Kannan et al., 2012; Katsuoka and Yamamoto, 2016). While both small and large MAF proteins contain DNA-binding domains called the Basic Region (BR) domain, small MAFs lack the transactivation domain that is present in large MAFs. Indeed, mutations or deficiency in the large-MAF subgroup gene *MAF* (also known as c-MAF) causes congenital cataract in humans and animal models (Kawauchi et al., 1999; Kim et al., 1999; Ring et al., 2000; Jamieson et al., 2002; Anand et al., 2018a). On the other hand, deficiencies of the small Maf TFs Mafg (OMIM: 602020) and Mafk (OMIM: 600197) in specific combination of knockout alleles are linked to cataract (Agrawal et al., 2015), in addition to other developmental defects such as progressive neuronal degeneration and thrombocytopenia (Blank, 2008; Kannan et al., 2012; Katsuoka and Yamamoto, 2016). Indeed, while individual germline knockout (KO) of either Mafg or Mafk do not lead to discernable defects in the lens, their compound deletion in mice, specifically as $Mafg^{-/-}$:$Mafk^{+/-}$, results in cataracts from age 4-months onward (Agrawal et al., 2015). Interestingly, $Mafg^{-/-}$:$Mafk^{+/-}$ compound KO mice do not exhibit defects in early lens stages.

In contrast, in the present study, we find that Mafg and Mafk double KO ($Mafg^{-/-}$:$Mafk^{-/-}$) mice exhibit severe lens defects starting from early stages of lens embryonic development. We report a detailed characterization of the lens defects in $Mafg^{-/-}$:$Mafk^{-/-}$ double KO mice that has revealed the necessity of these small Maf TFs in formation of a uniform monolayered epithelium in lens development. Further, these data suggest that Mafg and Mafk also have a role in coordinating cytoskeletal events in the early stages of epithelial to fiber cell differentiation. RNA-sequencing (RNA-seq) analysis of embryonic lens revealed misexpression of several key genes, including the extracellular matrix peroxidase Pxdn and the Eph signaling receptor Epha5, thereby providing novel insights into the molecular mechanisms underlying the lens defects in $Mafg^{-/-}$:$Mafk^{-/-}$ double KO mice. Together, these data identify new regulatory relationships between key factors that are associated with the maintenance of a monolayered epithelium and cellular differentiation, and therefore may of significance in non-ocular tissues, in addition to the lens.

## Methods

### Generation of *Mafg*:*Mafk* knockout mice

Double heterozygous $Mafg^{+/-}$:$Mafk^{+/-}$ germline knockout (KO) mice, which were generated in a previous study (Shavit et al., 1998; Onodera et al., 2000), were used to derive double knockout ($Mafg^{-/-}$:$Mafk^{-/-}$) and compound KO ($Mafg^{-/-}$:$Mafk^{+/-}$) mouse strains used in this study. Animals were housed in the Office of Laboratory Animal Medicine (OLAM) at the University of Delaware and experiments involving animals adhered to the Association of Research in Vision and Ophthalmology (ARVO) statement for the use of animals in ophthalmic and vision research and were approved by the Institutional Animal Care and Use Committee (IACUC) (IACUC Protocol No. 1226). Unless otherwise mentioned, mice were maintained on an ICR background. Animals were housed at a temperature range of 20–23°C in 12:12-h light-dark cycles with free access to water and food. $Mafg^{+/-}$:$Mafk^{+/-}$ double heterozygous mice were crossed to $Mafg^{+/-}$:$Mafk^{-/-}$ compound KO to generate various KO allele combinations. Genotyping was performed as previously described (Onodera et al., 2000; Agrawal et al., 2015). Briefly, genotyping was performed on tail-DNA prepared from post-natal or embryonic tissue using a commercial DNA-extraction kit (Qiagen, Catalog#158908 (Cell lysis solution), 158,912 (Protein precipitation

TABLE 1 Antibodies and immunostaining conditions.

| Target | Fixation | Wash | Permeabilization | Blocking buffer | Diln. Buffer | Primary antibody | Catalog | Wash | Secondary antibody | Nuclear staining | Wash |
|---|---|---|---|---|---|---|---|---|---|---|---|
| MIP (Aquaporin 0 or Aqp0) | 4% PFA for 20 min | 1X PBS 5 min, 3x each | NA | 10% Horse serum (Abcam, Cambridge, MA) in 1X PBS for 1.5 h at RT | NA | 1:200 20 h 4°C | Millipore, #AB3071 | 1X PBS 10 min, 3x each | Alexa 568 Gt anti Rb 1:200 (Alexa Goat anti Rabbit 568, Thermo Fisher Scientific, Catalog # A-11011); incubated with Nuclear Stain for 1.5 h | DAPI 1: 1,000 | 1X PBS 10 min, 3x each |
| Beta-catenin | 4% PFA for 20 min | 1X PBS 5 min, 3x each | NA | 5% Chicken serum (Abcam, Cambridge, MA), 0.3% TritonX-100, 2% BSA in 1X PBS for 1.5 h at RT | NA | 1:50 16 h 4°C | BD Biosciences #610153 | 1X PBS 10 min, 3x each | Rhodamine Red-X 568 Ch anti Ms 1:200 (Molecular probes, Eugene Oregon United States, R-6388); incubated with Nuclear Stain for 1.5 h | DAPI 1: 1,000 | 1X PBS 10 min, 3x each |
| Cdkn1c ($p57^{Kip2}$) | 4% PFA for 20 min | 1X PBS 5 min, 3x each | 0.1% TritonX-100 for 5 min | 5% Chicken Serum (Abcam, Cambridge, MA), 0.3% TritonX-100, 2% BSA in 1X PBS for 1.5 h at RT | NA | 1:50 18 h 4°C | Santa Cruz Biotechnology #sc-8298 | 1X PBS 10 min, 3x each | Alexa 568 Gt anti Rb 1:200 (Alexa Goat anti Rabbit 568, Thermo Fisher Scientific, Catalog # A-11011); incubated with Nuclear Stain for 1.5 h | DAPI 1: 1,000 | 1X PBS 10 min, 3x each |
| E-cadherin | 4% PFA for 20 min | 1X PBS 5min, 3x each | NA | 5% Normal Goat Serum (Abcam, Cambridge, MA), 0.3% TritonX-100 (Sigma, Catalog#T8787), 0.3% BSA in 1X PBS for 2 h at RT | NA | 1:100 18 h 4°C | Cell Signaling Technology, #3195S | 1X PBS 10 min, 3x each | Alexa 568 Gt anti Rb 1:200 (Alexa Goat anti Rabbit 568, Thermo Fisher Scientific, Catalog # A-11011); incubated with Nuclear Stain for 1.5 h | DAPI 1: 1,000 | 1X PBS 10 min, 3x each |
| F-actin | 4% PFA for 20 min | 1X PBS 5 min, 3x each | NA | 5% Chicken serum (Abcam, Cambridge, MA), 0.1% TritonX-100 in 1X PBS for 1.5 h at RT | NA | NA | Conjugated | 1:40 at 1.5 h s at RT | 1:40 at 1.5 h at RT (Thermo Fisher Scientific #A12380, Conjugate); incubated with Nuclear Stain for 1.5 h | DAPI 1: 1,000 | 1X PBS 10 min, 3x each |
| Foxe3 | 4% PFA for 20 min | 1X PBS 5 min, 3x each | 0.3% TritonX-100 for 10 min | 5% Chicken Serum (Abcam, Cambridge, MA), 0.3% TritonX-100 in 1X PBS for 1.5 h | NA | 1:200 20 h 4°C | Santa Cruz Biotechnology #sc-48162 | 1X PBS 10 min, 3x each | Alexa 568 Gt anti Rb 1:200 (Alexa Goat anti Rabbit 568, Thermo Fisher Scientific, Catalog # A-11011); incubated with Nuclear Stain for 1.5 h | DAPI 1: 1,000 | 1X PBS 10 min, 3x each |
| Gamma-crystallin | 4% PFA for 20 min | 1X PBS 5 min, 3x each | NA | 5% Chicken serum (Abcam, Cambridge, MA), 0.3% TritonX-100, 1% BSA in 1X PBS for 1.5 h at RT | NA | 1:100 18 h 4°C | Santa Cruz Biotechnology #sc-22415 | 1X PBS 10 min, 3x each | Alexa 568 Dn anti Gt 1:200 (Alexa Dn anti Gt 568, Thermo Fisher Scientific Catalog # A-11057); incubated with Nuclear Stain for 1.5 h | DAPI 1: 1,000 | 1X PBS 10 min, 3x each |
| Ki-67 | 4% PFA for 20 min | 1X PBS 5 min, 3x each | 0.1% TritonX-100 in 1X PBS for 2 min at RT | 5% Normal goat serum (NGS) (Abcam, Cambridge, MA), 0.3% TritonX-100 in 1X PBS for 1.5 h at RT | 2% BSA, 0.3% TritonX-100 in 1X PBS | 1:100 18 h 4°C | Cell Signaling Technology # 9129S | 1X PBS 10 min, 3x each | Alexa 568 Gt anti Rb 1:200 (Alexa Goat anti Rabbit 568, Thermo Fisher Scientific, Catalog # A-11011); incubated with Nuclear Stain for 1.5 h | DAPI 1: 1,000 | 1X PBS 10 min, 3x each |





10.3389/fcell.2022.981893

solution), 158,916 (DNA hydration solution)) and by using the following primers: *Mafg* WT: Forward 5′-GCATGACTC GCCAGGAACAG-3′, *Mafg* WT: Reverse- 5′-CCCAAGCCC AGCCTCTCTAC-3′, *Mafk* WT: Forward 5′-CCTACCGTT TCTGTCTTTCCAG-3′, *Mafk* WT: Reverse 5′-AATTCC TGAGGACAAAGCTGAC-3′, and LacZ: 5′-CCTGTAGCC AGCTTTCATCAAC-3'.

## Tissue collection and immunostaining

Pregnant female mice collected from crosses between $Mafg^{+/-}$:$Mafk^{+/-}$ and $Mafg^{+/-}$:$Mafk^{-/-}$ mice were harvested for obtaining embryonic tissue at different stages. Observation of the vaginal plug was considered embryonic day (E) 0.5, and tissues was collected at E12.5, E14.5, and E16.5. Mouse embryonic head tissues were embedded without fixation in Optimal Cutting Temperature (OCT) (Fisher Scientific, Catalog# 14-373-65) and stored at -80°C until downstream applications. Tissue was sectioned to obtain coronal sections of the eye using a Leica CM3050 cryostat (Leica Microsystems, Buffalo Grove, IL, United States). Tissue sections were collected on Colorfrost Plus slides (Fisher Scientific, Hampton, NH, United States, Catalog #12-500-18) at chamber temperature of -18°C, at 12 µm thickness for E12.5 and 14 µm thickness for E14.5 and E16.5. For immunostaining, after thawing and air-drying the slides with sections, they were immediately fixed in 4% Paraformaldehyde (PFA) (Fisher Scientific, Catalog# AC416780010) in 1x phosphate buffer saline (PBS) (Corning, Catalog#21-031-CV) for 20 min at room temperature, which was followed by three washes in 1x PBS (5 min each wash). The slides were blocked for 1.5–2 h in blocking buffer (Table 1) followed by overnight incubation at 4°C with the specific primary antibody at the appropriate concentration in blocking or dilution buffer. The following day, section slides were subjected to three washes in 1x PBS (10 min each wash) and incubated for 1.5 h with secondary antibody at 1:200 dilution in blocking or dilution buffer (Table 1) along with the nuclear counterstain 4',6-diamidino-2-phenylindole (DAPI, 1:1,000 dilution) (Thermo Fisher Scientific; Catalog# 62,248). The specific conditions for different primary antibodies are listed in Table 1. Slides were washed three times in 1x PBS for 10 min each after the secondary antibody incubation followed in mounting media and sealing with cover slips. Slides were stored at −20°C until they were imaged using a Zeiss LSM 880 confocal configured with Argon/Krypton laser (358 and 561 nm excitation wavelengths) (Carl Zeiss Inc., Göttingen, Germany).

## *In situ* hybridization and histology

*In situ* hybridization was performed as previously described (Lachke et al., 2012b). Briefly, mouse embryonic tissue was isolated and fixed in 4% para-formaldehyde, overnight. The tissue freezing media OCT (Tissue Tek, Torrance, CA) was used to embed and freeze the tissue in an orientation to yield coronal sections (16 µm). Oligomers that included T7 promoter sequence upstream of the gene-specific region were used to amplify cDNA that was used as template in an *in vitro* transcription reaction to prepare an antisense digoxygenin-labeled RNA probe. Frozen tissue was thawed and subjected to the previously described *in situ* protocol and images were imaged using light microscope. For hematoxylin and eosin (H&E) staining, mouse embryonic head tissue were fixed in Pen-Fix (Richard Allan Scientific, Kalamazoo, MI) overnight, followed by dehydration using ethanol, and embedding in paraffin. Sagittal paraffin sections (5 µm) were stained with H&E as previously described (Siddam et al., 2018) and visualized using light microscopy.

## Fluorescence quantification and statistical analysis

Fiji ImageJ software (v1.52P, NIH, Bethesda, MD) was used to quantify the differences in the mean fluorescence signal intensity between control ($Mafg^{+/-}$:$Mafk^{+/-}$) and $Mafg^{-/-}$:$Mafk^{-/-}$ KO lens sections. Images were split into a single channel to measure and quantify the mean fluorescence intensity (Ki67, $p57^{Kip2}$, Phalloidin), counting the average cell number, or counting the average number of nuclei (Ki67, $p57^{Kip2}$) as previously described (Shihan et al., 2021). The background subtraction was performed for normalization after the Threshold application, and the fluorescence intensity was measured in the red channel depending on the criteria for each section in at least three biological replicates for control and $Mafg^{-/-}$:$Mafk^{-/-}$ KO lenses. Finally, all statistics were assessed using either Student's two sample *t*-test (correct for multiple comparisons using the Holm-Sídák method) or one-way ANOVA. Data are presented as mean ± SE (SEM) and differences were considered significant at $p \leq 0.05$.

## RNA isolation and quality control

For RNA isolation for downstream assays namely, RNA-sequencing (RNA-Seq) and/or RT-qPCR, embryonic lenses at E16.5 ($n$ = 8 lenses per biological replicate; total three biological replicates) were collected from control ($Mafg^{+/-}$:$Mafk^{+/-}$), compound ($Mafg^{-/-}$:$Mafk^{+/-}$) and double KO ($Mafg^{-/-}$:$Mafk^{-/-}$) mice. Total RNA isolation was performed using the mirVana™ RNA isolation kit (Thermo Fisher Scientific, Catalog#AM1560), followed by removal of small molecular weight RNA according to the manufacturer's

TABLE 2 Primers used in RT-qPCR assays.

| Gene | Forward 5′-3′ primer | Reverse 5′-3′ primer | cDNA Amplicon (bp) |
|---|---|---|---|
| *Camsap1* | TATTGCCCAGAGCAGATGAAA | CCTCAGAAGGCGGATGTTATAG | 90 |
| *Cdk1* | AAAGCGAGGAAGAAGGAGTG | CCATGGACAGGAACTCAAAGA | 144 |
| *Cdkn1c* | TGAAGGACCAGCCTCTCT | TCCTGCGCAGTTCTCTTG | 99 |
| *Col3a1* | CCCTTCTTCATCCCACTCTTATT | GATCCTGAGTCACAGACACATATT | 139 |
| *Epha5* | ACCTGCATCTGTGTATGTCTTC | ACTGACACTGGTGTGGTTTC | 99 |
| *Gapdh* | GATCGTGGAAGGGCTAATGA | GACCACCTGGTCCTCTGTG | 340 |
| *Hmox1* | GTACACATCCAAGCCGAGAA | TGGTACAAGGAAGCCATCAC | 98 |
| *Lars2* | GACAAGGAAGGATGTGGAGAAG | GGAACATGGAGAGCAAGTAGAA | 110 |
| *Mafk* | TGTTGTTCTTCGCCGAGTC | ACAAGCGCTTCTGCTCTC | 88 |
| *Mafg* | GAGGCCCTGCAGAACTTT | AGCATCCGTCTTGGACTTTAC | 147 |
| *Map3k12* | GAGTGACAAGAGCACCAAGAT | GGACCAGATGTCAACCTTCTC | 103 |
| *Sipa1l1* | GTCGGTGGAGAGCTTCATTAG | CCATTTCTTCGCAGAGTCATTTC | 108 |
| *Trex1* | CAGGGAATGGTTCGAGGAAA | TGAGCAGGGTTAGAACATCAC | 111 |

instructions. RNA quality was analyzed using fragment analyzer (Advanced Analytical Technologies, AATI FEMTO Pulse) and samples with RNA quality number (RQN) greater than 7.2 were used for library preparation and RNA-seq.

## RNA-sequencing

Lens RNA at E16.5 from control (*Mafg*$^{+/-}$:*Mafk*$^{+/-}$), compound (*Mafg*$^{-/-}$:*Mafk*$^{+/-}$) and double KO (*Mafg*$^{-/-}$:*Mafk*$^{-/-}$) mice was used to generate strand-specific, paired-end 101 bp-length libraries which were sequenced by DNA Link, United States (901 Morena Blvd. Ste 730 San Diego, CA 92117, United States) on a NovaSeq 6000 (San Diego, CA, United States). The processed reads were aligned against *Mus musculus* reference genome (mm39) using HISAT2 (Kim et al., 2015). The aligned reads were assembled using StringTie (Pertea et al., 2015) to obtain transcript-level expression counts. The count file was imported in edgeR package using R-statistical environment (Robinson et al., 2010) to analyze differential gene expression in control, compound and double KO datasets. In edgeR, reads that were lowly expressed, i.e. < 1 count per million in less than two samples were filtered out. The RNA-seq data is deposited in GEO and the accession number is: GSE207853.

## Gene ontology analysis for *Mafg*$^{-/-}$:*Mafk*$^{-/-}$ dfferentially expressed genes

The Database for Annotation, Visualization and Integrated Discovery (DAVID, v6 .8) was used for functional annotation by Gene Ontology (GO) categories (Huang et al., 2009). The pathways and GO categories identified were prioritized based on Benjamini corrected significant *p*-values. All GO comparisons were made against the 14 October 2020 release of the Gene Ontology Consortium (GOC) database (Ashburner et al., 2000), specifically KEGG (Kanehisa and Goto, 2000).

## cDNA synthesis and RT-qPCR

The isolated mouse embryonic lens RNA was used for cDNA synthesis using iScript cDNA Synthesis Kit (Bio-Rad, Catalog#1708890) followed by quantitative PCR (RT-qPCR). iScript reaction [5x iScript reaction mixture (4 µL), iScript reverse transcriptase (1 µL), Total RNA Template (300 ng), Nuclease-free $H_2O$ (to make to total volume 20 µL)] was performed using a custom program [25°C (5 min), 42°C (30 min), 85°C (5 min), 4°C (hold)]. RT-qPCR was performed using cDNA-specific primer sets (Table 2) and a Power SYBR Green kit (Fisher Scientific, Catalog # A25742). The RT-PCR reaction [PowerUp SYBR master mix (12.5 µL), Forward Primer (0.5 µL of 10 µM), Reverse Primer (0.5 µL of 10 µM), cDNA (1 µL of 400 ng), Nuclease-free $H_2O$ (10.5 µL to bring volume to total 20 µL volume)] using a custom program [95°C (2 min), followed by 40 cycles of 95°C (5 s) followed by 58°C (20 s), and terminal cycle of 95°C (15 s), 60°C (1 min), 95°C (15s) and hold at room temperature] was analyzed on a 7500 Fast PCR system (Applied Biosystems, Foster City, California). Three biological replicates (each biological replicate having two technical replicates) were used for control and KO samples. Fold-change was calculated using the ΔΔCT-method using *Gapdh* as a house-keeping gene and statistical significance was determined using a two-sample Student's t-test.

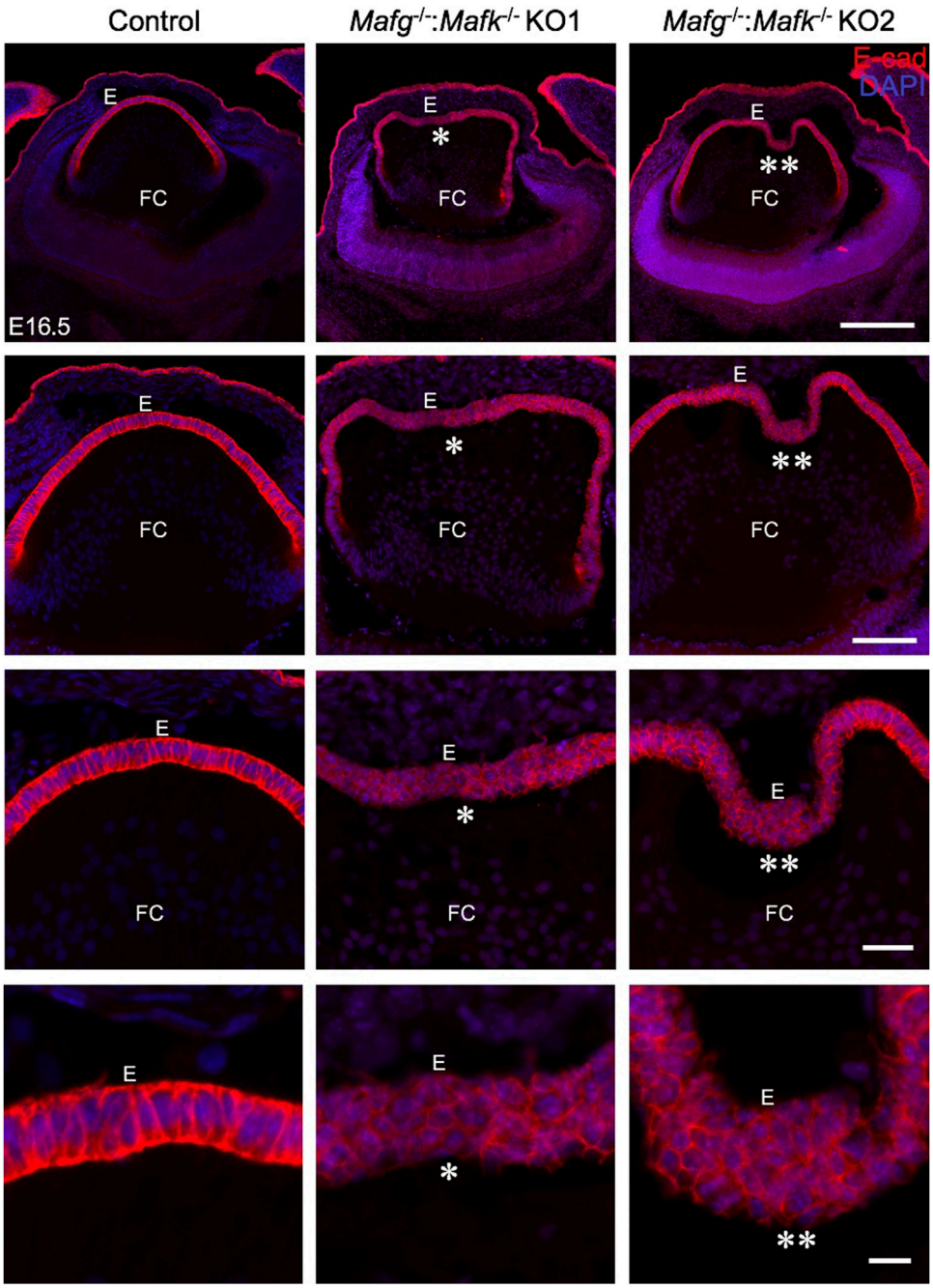


FIGURE 1
Mafg and Mafk deficiency results in an abnormally multilayered epithelium of the lens. Immunostaining for E-cadherin reveals cellular abnormalities (indicated by asterisks) in the lens epithelium of *Mafg*$^{-/-}$:*Mafk*$^{-/-}$ but not control at embryonic day (E)16.5. *Mafg*$^{-/-}$:*Mafk*$^{-/-}$KO #1 and KO #2 are shown as representative of the severity of epithelial defects. Sections are co-stained with DAPI for visualization of nuclei. Higher magnification images in row 2 (20X), row 3 (40X), and row 4 (63X) demonstrate the variable extent of multilayered epithelium in the *Mafg*$^{-/-}$:*Mafk*$^{-/-}$ lenses compared to control. Abbreviation: E, Epithelium of the lens; FC, Fiber cells of the lens. Scale bar for Row 1, 10 μm; Row 2, 20 μm; Row 3, 10 μm; Row 4, 8 μm.

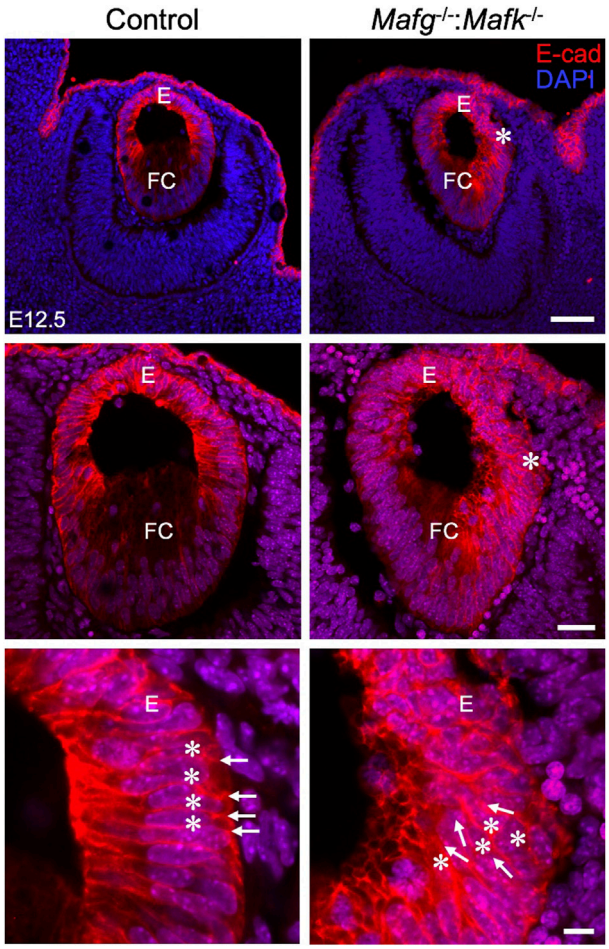


FIGURE 2
*Mafg*$^{-/-}$:*Mafk*$^{-/-}$ mice exhibit abnormalities in the lens epithelium at E12.5. Immunostaining for E-Cadherin and co-staining with DAPI shows that early in lens development, at stage E12.5, *Mafg*$^{-/-}$:*Mafk*$^{-/-}$ lens exhibits regions of disorganization in the epithelium (asterisks in row 1, row 2) compared to control. In row 3, cell boundaries (arrows) revealed by E-cadherin staining and nuclei stained by DAPI (asterisks) appear in a uniform manner in the control, but not in *Mafg*$^{-/-}$:*Mafk*$^{-/-}$ lens, wherein they appear disorganized. Abbreviation: E, Epithelium of the lens; FC, Fiber cells of the lens. Scale bar for Row 1, 20 μm; Row 2, 10 μm; Row 3, 8 μm.

# Results

## *Mafg*$^{-/-}$:*Mafk*$^{-/-}$ KO mice exhibit abnormal multilayered lens epithelium

iSyTE (integrated Systems Tool for Eye gene discovery) expression analysis has indicated that Mafg and Mafk are significantly expressed in mouse lens embryonic development (Supplementary Figure S1A). The expression of *Mafg* in mouse embryonic lens development is confirmed by *in situ* hybridization (Supplementary Figure S1B). Further, examination of previous generated RNA-seq data from isolated epithelium and fiber cells at E14.5, E16.5, E18.5 and P0 (Zhao et al., 2018) shows that *Mafg* and *Mafk* are both expressed in the epithelium and fiber cells (Supplementary Figure S1C). This analysis shows that as relative expression of *Mafg* decreases, that of *Mafk* increases, in progressive stages of development. Together, these data suggesting a role for Mafg and Mafk in lens embryonic development. Therefore, to examine the impact of Mafg and Mafk deficiency on lens development, we generated *Mafg*$^{-/-}$:*Mafk*$^{-/-}$ double KO mice and first characterized the lens tissue with marker analysis. Immunostaining for the epithelial marker, E-cadherin (also known as Cdh1), demonstrated profound abnormalities in the appearance of the epithelium in *Mafg*$^{-/-}$:*Mafk*$^{-/-}$ lenses. At E16.5, control lenses exhibit uniform E-cadherin protein expression and localization in the epithelium, which appears monolayered, as also suggested by nuclei stained with DAPI (Figure 1). In contrast, the *Mafg*$^{-/-}$:*Mafk*$^{-/-}$ lenses exhibit nuclear staining that indicates multilayered epithelium wherein the E-cadherin protein expression pattern also appears abnormal. E-cadherin staining reveals that *Mafg*$^{-/-}$:*Mafk*$^{-/-}$ epithelial cells appear irregularly shaped and aggregated compared to control. While this defect is observed in the vast majority of *Mafg*$^{-/-}$:*Mafk*$^{-/-}$ lenses (92%, $n$ = 12), the extent of the multilayered epithelium cellular abnormalities and cell shape changes varies between individual embryos (Figure 1). In *Mafg*$^{-/-}$:*Mafk*$^{-/-}$ lenses that exhibit a comparatively milder defect, the abnormal multilayered cellular region is flanked by normal-appearing mononucleated epithelium. To identify the onset of these defects, we examined embryos at earlier stages. While less severe when compared to the defects observed at E16.5, the E-cadherin protein staining pattern appears abnormal in *Mafg*$^{-/-}$:*Mafk*$^{-/-}$ epithelium at E12.5 (Figure 2) and E14.5 (Supplementary Figure S2). Interestingly, the E12.5 *Mafg*$^{-/-}$:*Mafk*$^{-/-}$ epithelium exhibits early indications of multilayer formation of cells (Figure 2), suggesting that the lens defects may initiate at this stage and become progressively severe in development. Additionally, when compared to control lenses, the population of E-cadherin expressing cells appears to extend further toward the posterior region in *Mafg*$^{-/-}$:*Mafk*$^{-/-}$ lenses (Figures 1, 2). Care was taken to analyze centrally located sections, avoiding peripheral sections. However, it should be noted that not all *Mafg*$^{-/-}$:*Mafk*$^{-/-}$ lenses had an abnormal expansion of epithelial cells in the posterior region of the lens. It should also be noted that no overt changes were observed between control and *Mafg*$^{-/-}$:*Mafk*$^{-/-}$ lenses with respect to E-cadherin's localization within the cells. In contrast to *Mafg*$^{-/-}$:*Mafk*$^{-/-}$ animals, *Mafg*$^{-/-}$:*Mafk*$^{+/-}$ compound mice did not exhibit such severe lens defects at E16.5 (Supplementary Figure S3),

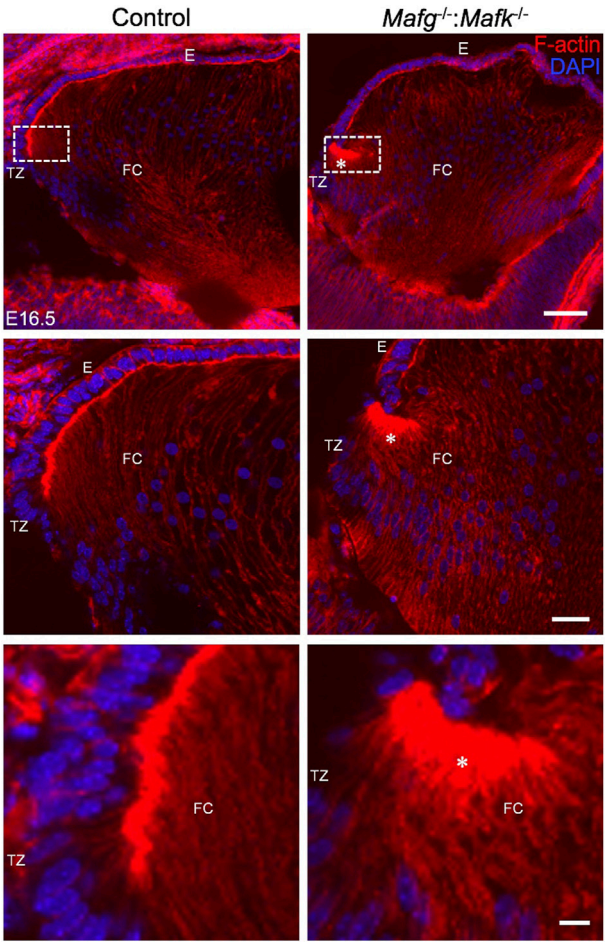


FIGURE 3
*Mafg*$^{-/-}$:*Mafk*$^{-/-}$ mice exhibit abnormal F-actin distribution in differentiating lens fiber cells. Staining with phalloidin for visualizing F-actin and co-staining with DAPI to visualize nuclei demonstrate that E16.5 *Mafg*$^{-/-}$:*Mafk*$^{-/-}$ mice exhibit non-uniform distribution (asterisk) of F-actin at the apical tips of the fiber cells near the transition zone. The area shown in the broken-line box in control and test was used for measurement of fluorescence signal intensity shown in Figure 4B. Abbreviation: E, Epithelium of the lens; FC, Fiber cells of the lens; TZ, Transition zone of the lens. Scale bar for Row 1, 20 μm; Row 2, 10 μm; Row 3, 8 μm.

suggesting that the absence of both alleles of Mafg and Mafk is necessary to cause these severe lens defects.

## *Mafg*$^{-/-}$:*Mafk*$^{-/-}$ KO mouse lenses have abnormal F-actin distribution in fiber cells

We next analyzed *Mafg*$^{-/-}$:*Mafk*$^{-/-}$ mice for potential defects in lens fiber cells. Near the equator of the lens, at a region termed the transition zone, cells of the epithelium exit the cell cycle and begin differentiation into fiber cells. At the initial stage of differentiation, as fiber cells begin to migrate toward the interior of the lens, they undergo a sharp re-orientation in their position relative to the epithelium. At the lens equator location termed "the fulcrum" or "modiolus", the apical regions of epithelial cells constrict to form an anchor point prior to elongation during their differentiation into fiber cells (Zampighi et al., 2000; Sugiyama et al., 2009). As a result, at this location, early fiber cells first begin to get positionally re-oriented so that their apical regions face the apical regions of cells of the epithelium. We sought to examine this region in *Mafg*$^{-/-}$:*Mafk*$^{-/-}$ mouse lens. Staining for phalloidin (which stains F-actin) showed that E16.5 *Mafg*$^{-/-}$:*Mafk*$^{-/-}$ mice exhibit abnormal F-actin distribution in cells near the fulcrum region of the lens (Figure 3). While all E16.5 *Mafg*$^{-/-}$:*Mafk*$^{-/-}$ mice that were examined showed this defect on at least one side of the lens, in about one-third of the animals it was observed on both sides. Further, while in E16.5 control lenses, F-actin appears uniformly distributed at the apical junctions of epithelial and fiber cells, it appears reduced in the region anterior to the fulcrum in *Mafg*$^{-/-}$:*Mafk*$^{-/-}$ lenses (Figure 3). This abnormal F-actin staining pattern was also observed earlier in development, at E14.5, in *Mafg*$^{-/-}$:*Mafk*$^{-/-}$ lenses (Figure 4A). In control lenses, F-actin staining intensity is highest at the initial junction region of epithelial and differentiating fiber cells. In contrast, in *Mafg*$^{-/-}$:*Mafk*$^{-/-}$ lenses, the highest staining intensity of F-actin is observed anterior to this region (Figures 4B–E). It should be noted that the quantitative analysis serves to demonstrate that F-actin levels are abnormally distributed in the area measured and are not necessarily a reflection of change in the total actin levels in the lens. Further, histological analysis shows that while in control, the fulcrum region appears normal, in E16.5 *Mafg*$^{-/-}$:*Mafk*$^{-/-}$ mice, the fiber cell organization in this region, and beyond, is abnormal, suggestive of suboptimal interactions with the overlying epithelium (Supplementary Figure S4A). Moreover, in control lens, fiber cells appear to "curve" in the same direction as the overall structure of the lens (Supplementary Figure S4B). In contrast, fiber cells do not follow this natural curvature and their appearance is somewhat sigmoidal in *Mafg*$^{-/-}$:*Mafk*$^{-/-}$ mice (Supplementary Figure S4B,C). Together, these data indicate that Mafg and Mafk deficiency results in abnormal abundance of F-actin in distinct regions of early differentiating fiber cells, which in turn impacts their organization in the lens.

## Beta-catenin and gamma crystallin proteins are unaltered in *Mafg*$^{-/-}$:*Mafk*$^{-/-}$ KO mouse lenses

Because E-cadherin is known to interact with beta-catenin, and both are implicated in cell-cell adhesion, we next sought to examine whether beta-catenin was altered in *Mafg*$^{-/-}$:*Mafk*$^{-/-}$ lenses. Immunostaining for beta-catenin demonstrated no change in the levels of its expression in *Mafg*$^{-/-}$:*Mafk*$^{-/-}$ lenses

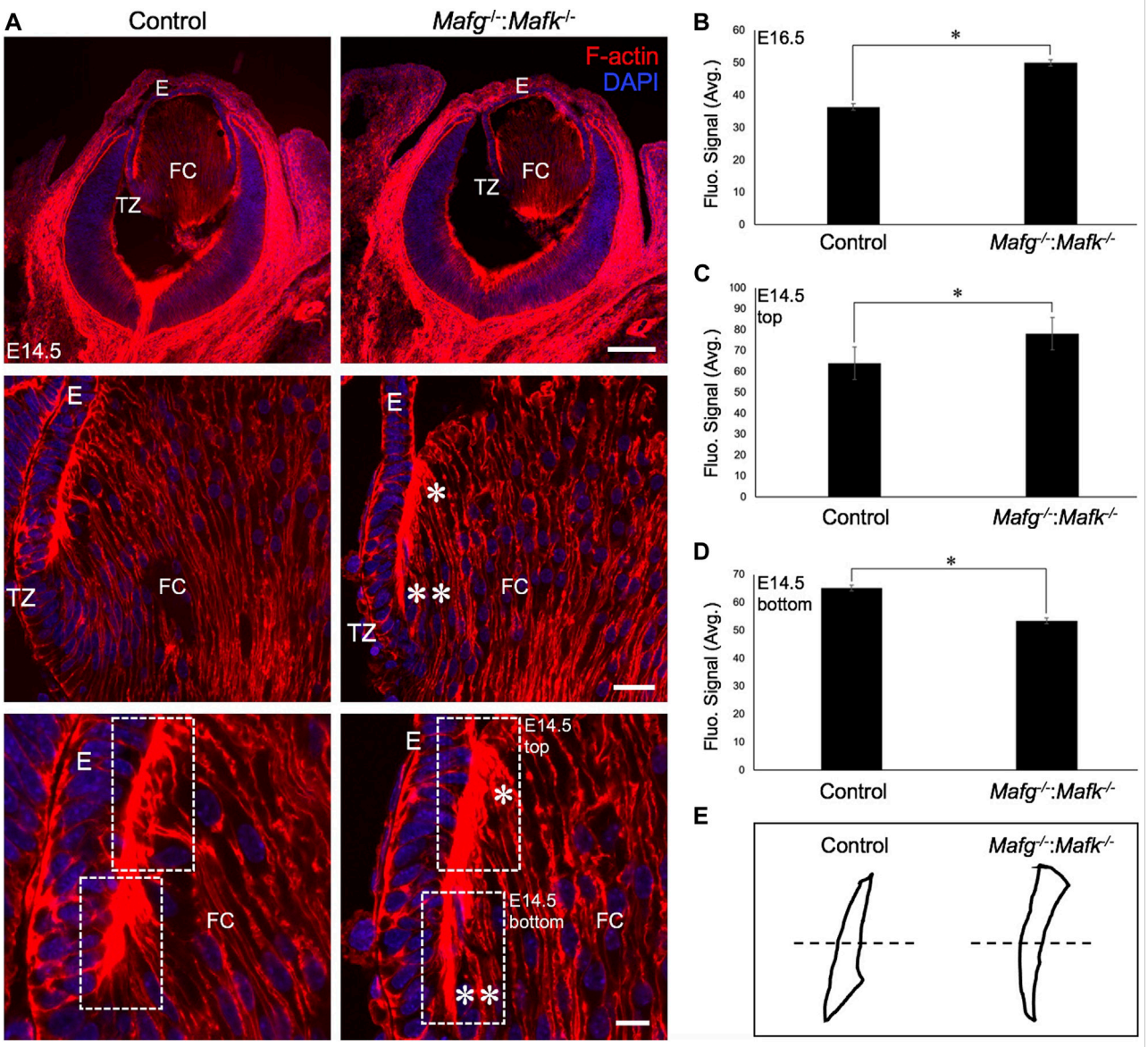


FIGURE 4
The F-actin distribution defects are detected in earlier stages of lens development in *Mafg*$^{-/-}$:*Mafk*$^{-/-}$ mice. **(A)** Staining with phalloidin for visualizing F-actin and co-staining with DAPI to visualize nuclei demonstrate that *Mafg*$^{-/-}$:*Mafk*$^{-/-}$ lenses at stage E14.5 exhibit abnormally reduced F-actin distribution (two asterisks) near the transition zone and the fulcrum region compared to the control. Further, *Mafg*$^{-/-}$:*Mafk*$^{-/-}$ lenses exhibit abnormally elevated F-actin distribution (asterisk) in fiber cells that have progressed further in differentiation. **(B)** Measurement of fluorescence intensity signal near the transition zone region of E16.5 *Mafg*$^{-/-}$:*Mafk*$^{-/-}$ lenses indicates elevated F-actin levels compared to control. **(C)** Measurement of fluorescence intensity signal in fiber cells progressed further in differentiation (represented by broken-line box termed "top") of E14.5 *Mafg*$^{-/-}$:*Mafk*$^{-/-}$ lenses indicates elevated F-actin levels compared to control. **(D)** Measurement of fluorescence intensity signal in fiber cells near the transition zone and the fulcrum region (represented by broken-line box termed "bottom") of E14.5 *Mafg*$^{-/-}$:*Mafk*$^{-/-}$ lenses indicates reduced F-actin levels compared to control. **(E)** Schematic of the differential distribution of F-actin in the top and bottom region (separated by broken line) of control and *Mafg*$^{-/-}$:*Mafk*$^{-/-}$ lenses at E14.5. Statistical significance was determined using a two-sample Student's *t*-test. Abbreviation: E, Epithelium of the lens; FC, Fiber cells of the lens; TZ, Transition zone of the lens. Scale bar for Row 1, 20 μm; Row 2, 10 μm; Row 3, 8 μm.

at E14.5 (Supplementary Figure S5A) or E16.5 (Supplementary Figure S5B). However, because beta-catenin is localized to the membrane, these data offer independent validation of these defects and their impact on the lens through the view of the cell membrane in *Mafg*$^{-/-}$:*Mafk*$^{-/-}$ mice. These data corroborate that while in control lenses, epithelium and fiber cell organization appears uniform, in *Mafg*$^{-/-}$:*Mafk*$^{-/-}$ lenses, cells in these regions appear disorganized at E14.5 (Supplementary Figure S5A',A") and E16.5 (Supplementary Figure S5B',B"). At E16.5, the cortical fiber cell nuclei appear different between control and *Mafg*$^{-/-}$:

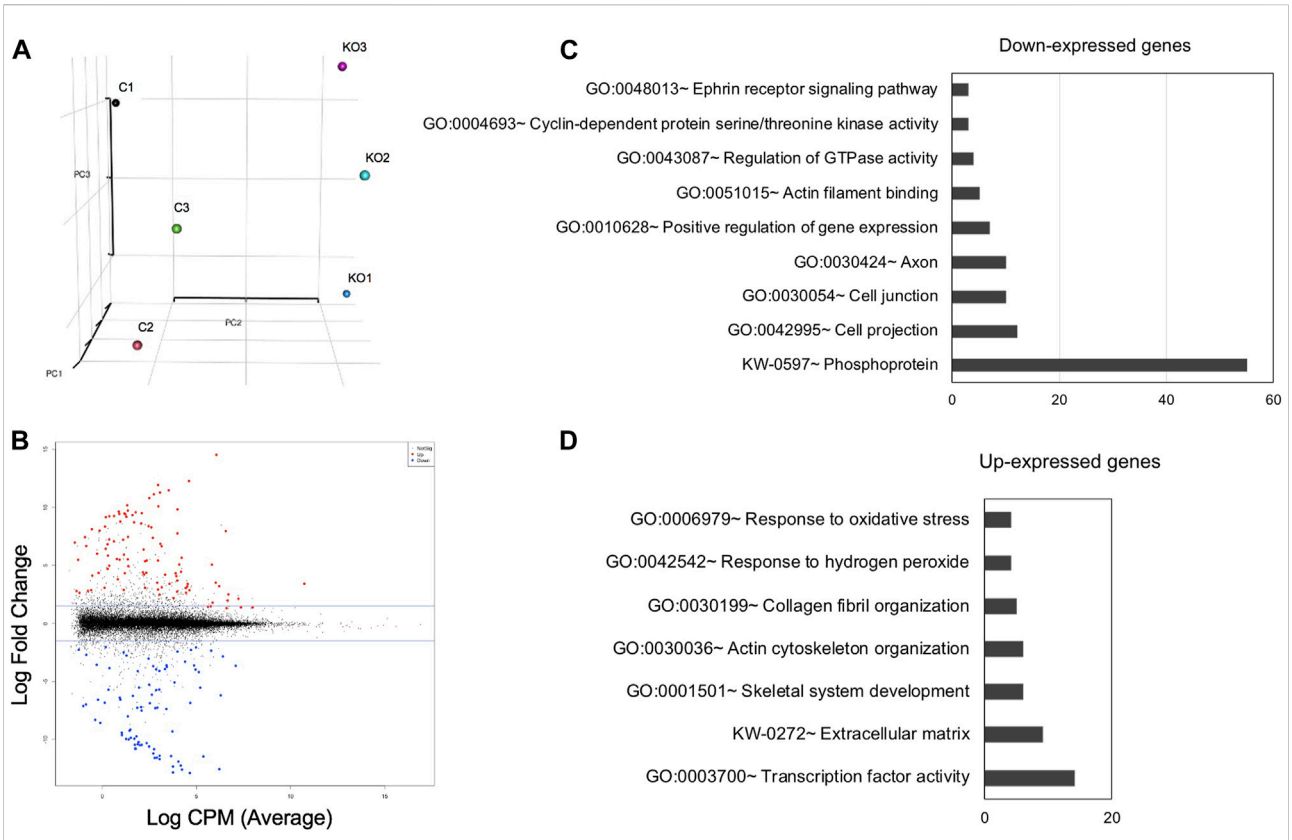


FIGURE 5
High-throughput RNA-sequencing analysis identifies genes misexpressed in *Mafg*$^{-/-}$:*Mafk*$^{-/-}$ lenses. **(A)** Principal Component Analysis (PCA) shows that the RNA-sequencing (RNA-seq) datasets representing *Mafg*$^{+/-}$:*Mafk*$^{+/-}$ (control) and *Mafg*$^{-/-}$:*Mafk*$^{-/-}$ (double KO) lens cluster based on their genotypes. **(B)** Plot of differentially expressed genes (DEGs) in *Mafg*$^{-/-}$:*Mafk*$^{-/-}$ lens compared to control. **(C)** Gene Ontology (GO) and pathway analysis of down-regulated genes in *Mafg*$^{-/-}$:*Mafk*$^{-/-}$ lens. **(D)** Gene Ontology (GO) and pathway analysis of up-regulated genes in *Mafg*$^{-/-}$:*Mafk*$^{-/-}$ lens.

*Mafk*$^{-/-}$ lenses. Together with the findings on E-cadherin, these data suggest a general loss of normal epithelium architecture in *Mafg*$^{-/-}$:*Mafk*$^{-/-}$ lenses. Furthermore, expression of the fiber cell marker, gamma crystallin, was unaltered in *Mafg*$^{-/-}$:*Mafk*$^{-/-}$ lenses at E16.5 or earlier stages (Supplementary Figure S6A,B). Together, these data suggest that while the morphology of lens cells is abnormal, certain aspects of fiber cell gene expression are unaltered in *Mafg*$^{-/-}$:*Mafk*$^{-/-}$ lenses.

## *Mafg*$^{-/-}$:*Mafk*$^{-/-}$ KO mouse lenses exhibit altered transcriptome

To identify the specific RNA changes resulting from Mafg and Mafk deficiency, we next took an unbiased genome-wide approach and performed high-throughput RNA-sequencing (RNA-seq) of E16.5 *Mafg*$^{-/-}$:*Mafk*$^{-/-}$ lenses. Principle component analysis showed that control and *Mafg*$^{-/-}$:*Mafk*$^{-/-}$ lens replicates clustered away from each other (Figure 5). Further, as expected, compared to control, RNA-seq identified *Mafg* and *Mafk* to be severely reduced in *Mafg*$^{-/-}$:*Mafk*$^{-/-}$ lenses. Comparative analysis showed that *Mafg*$^{-/-}$:*Mafk*$^{-/-}$ exhibit 241 differentially expressed genes (DEGs) (±≥1.5-fold, $p \leq 0.05$) with 144 being elevated and 97 being reduced in the absence of Mafg and Mafk (Supplementary Table S1).

## Validation of key *Mafg*$^{-/-}$:*Mafk*$^{-/-}$ DEGs relevant to lens biology

Next, to further prioritize candidate genes relevant to lens biology so as to uncover the underlying molecular changes associated with *Mafg*$^{-/-}$:*Mafk*$^{-/-}$ lens defects, we applied various selection criteria to the list of DEGs identified by RNA-seq. These include gene ontology (GO) and pathway analysis as well as iSyTE analysis, which informs on the expression of candidate genes in normal lens development and its altered expression in various gene perturbation mouse models with lens defects/cataract, and has been shown to be effective in prioritizing key genes and pathways in the lens

TABLE 3 Functional significance of select *Mafg*$^{-/-}$:*Mafk*$^{-/-}$ differentially expressed candidates.

| Gene | Effect in *Mafg*$^{-/-}$:*Mafk*$^{-/-}$ lens | Description | Functional significance | References |
|---|---|---|---|---|
| *Camsap1* | Up | Calmodulin regulated spectrin associated protein 1 | Involved in cytoskeletal control | [Jiang et al., 2014; King et al., 2014; Xiang et al. (2016)] |
| *Cdk1* | Down | Cyclin dependent kinase 1 | Involved in cell cycle progression | Santamaría et al. (2007) |
| *Cdkn1c* | Up | Cyclin dependent kinase inhibitor 1C | Involved in cell cycle inhibition | Zhang et al. (1998) |
| *Col3a1* | Up | Collagen type III alpha 1 chain | Involved in extracellular matrix control | Kuivaniemi and Tromp, (2019) |
| *Epha5* | Down | Eph receptor A5 (Tyrosine kinase) | Involved in signaling with Efna5 (ephrin-A5 ligand) to control cell-cell contract mediated events | Akaneya et al. (2010) |
| *Hmox1* | Up | Heme oxygenase | Involved in oxidative stress response | Zheng et al. (2010) |
| *Lars2* | Down | Mitochondrial leucyl-tRNA synthetase | Involved in mitochondrial protein synthesis; homolog associated with autophagy | Pierce et al. (2013) |
| *Map3k12* | Down | Mitogen-activated protein kinase kinase 12 (Leucine-zipper domain and serine/threonine protein kinase) | Involved in cell cycle control and differentiation | [Robitaille et al., 2005, Robitaille et al., 2010; Daviau et al. (2011)] |
| *Pxdn* | Up | Peroxidasin | Involved in extracellular matrix formation | [Khan et al., 2011; Yan et al. (2014)] |
| *Sipa1l1* | Down | Signal induced proliferation associated 1 like 1 | Potentially involved in actin cytoskeleton organization | [Pak et al., 2001; Matsuura et al. (2021)] |
| *Trex1* | Down | Three prime repair exonuclease 1 | Potentially involved in DNA repair | Yang et al. (2007) |

(Lachke et al., 2011, 2012a, 2012b; Wolf et al., 2013; Manthey et al., 2014; Agrawal et al., 2015; Anand et al., 2015, 2018b, 2021; Audette et al., 2016; Cavalheiro et al., 2017; Patel et al., 2017; Kakrana et al., 2018; Krall et al., 2018; Siddam et al., 2018; Padula et al., 2019; Aryal et al., 2020; Barnum et al., 2020; Choquet et al., 2021). We also considered the potential relevance of the candidate genes to lens biology based on their function described in the published literature. In particular, we prioritized candidates that were starkly altered in *Mafg*$^{-/-}$:*Mafk*$^{-/-}$ double KO lenses as opposed to in *Mafg*$^{-/-}$:*Mafk*$^{+/-}$ compound KO lenses. GO analysis of *Mafg*$^{-/-}$:*Mafk*$^{-/-}$ lens DEGs identified several potentially important categories such as "ephrin receptor signaling pathway", "extracellular matrix", "cell projection", "cell junction", "response to oxidative stress", "cyclin-dependent protein serine/threonine kinase activity", "actin filament binding" and "positive regulation of gene expression", among others (Figure 5). Based on their differential expression in *Mafg*$^{-/-}$:*Mafk*$^{-/-}$ lenses and potential significance to lens development, several candidates from these categories were selected for further analysis by iSyTE and independent validation by RT-qPCR (Table 3). iSyTE analysis showed that majority of these candidates exhibit significant expression or "enriched" expression in normal lens development (Supplementary Figure S7). Further, several of these candidates were found to also be misexpressed in specific gene perturbation mouse models with lens defects or cataract (Supplementary Figure S8). RT-qPCR analysis showed over 10-fold reduction of *Mafg* and *Mafk* transcripts in *Mafg*$^{-/-}$:*Mafk*$^{-/-}$ lenses. As reported previously for *Mafg*$^{-/-}$:*Mafk*$^{+/-}$ compound KO lenses (Agrawal et al., 2015), RT-qPCR confirmed elevated expression of *Hmox1* and reduced expression of *Trex1* in *Mafg*$^{-/-}$:*Mafk*$^{-/-}$ double KO lenses, suggesting that some genes were similarly differentially expressed regardless of whether one or both copies of Mafk were absent in the context of homozygous deletion of Mafg (Figure 6). Importantly, we sought to confirm the differential expression of those genes that were starkly altered only in *Mafg*$^{-/-}$:*Mafk*$^{-/-}$ double KO lenses compared to control and *Mafg*$^{-/-}$:*Mafk*$^{+/-}$ compound lenses, as these would likely contribute to the early onset lens defects observed only in the double KO animals. Among these candidate genes, the peroxidase enzyme *PXDN*—secreted in the extracellular matrix, identified as lens-enriched by iSyTE and shown to linked to congenital cataract and other ocular defects in human or animal models—was found to be significantly overexpressed in *Mafg*$^{-/-}$:*Mafk*$^{-/-}$ lenses (Figure 7). Furthermore, the ephrin signaling receptor, *Epha5*, was found to be significantly reduced in *Mafg*$^{-/-}$:*Mafk*$^{-/-}$ double KO lenses. This is interesting because iSyTE analysis shows that Epha5 exhibits enriched expression in the lens, second only to the other ephrin receptor, Epha2, the perturbation of which is linked to cataract in humans and animal models (Figure 8). Moreover, Epha5 is known to be the receptor for the ligand Efna5 (ephrin-A5), the perturbation of which is linked to lens defects (Cheng and Gong, 2011; Cheng et al., 2017) resembling those observed in *Mafg*$^{-/-}$:*Mafk*$^{-/-}$ lenses. Additionally, several other

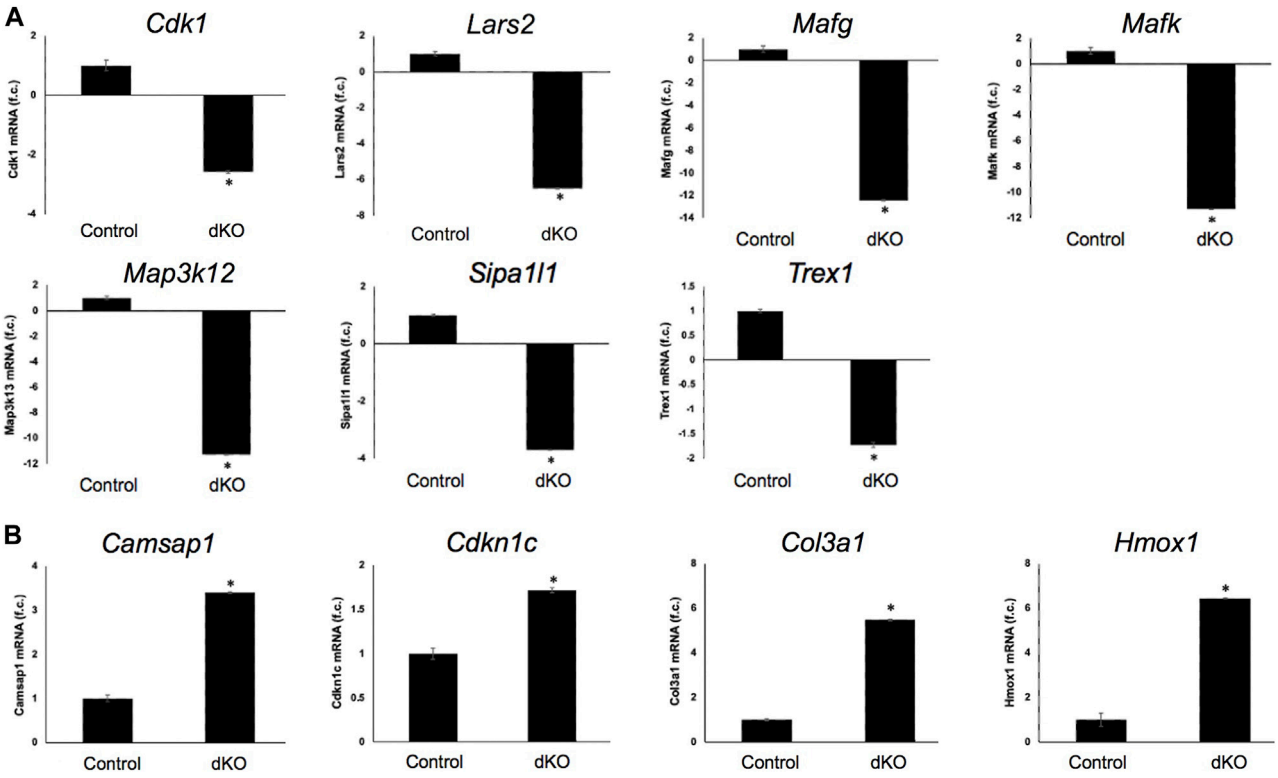


FIGURE 6
RT-qPCR-based validation of differentially expressed genes in *Mafg*$^{-/-}$:*Mafk*$^{-/-}$ lens. Validation by RT-qPCR of several RNA-seq analysis-identified candidate genes that are **(A)** down-regulated and **(B)** upregulated in *Mafg*$^{-/-}$:*Mafk*$^{-/-}$ lenses. Fold-change was calculated using the ΔΔCT-method using *Gapdh* as a house-keeping gene and statistical significance was determined using a two-sample Student's *t*-test. Asterisk indicates $p \leq 0.05$.

genes that may contribute to the lens defects were found to be differentially expressed in *Mafg*$^{-/-}$:*Mafk*$^{-/-}$ lenses. These include cyclin-dependent kinase *Cdk1*, leucyl t-RNA synthase *Lars2*, mitogen-activated protein kinase *Map3k12* and signal-induced proliferation protein *Sipal1l*, all exhibiting reduced expression in *Mafg*$^{-/-}$:*Mafk*$^{-/-}$ lenses (Figure 6). In contrast, the genes that were found to be sharply elevated in *Mafg*$^{-/-}$:*Mafk*$^{-/-}$ lenses were calmodulin-regulated spectrin associated protein *Camsap1*, collagen *Col3a1* and cyclin-dependent kinase inhibitor *Cdkn1c* (p57$^{Kip2}$) (Figure 6). Further, compared to control, E16.5 *Mafg*$^{-/-}$:*Mafk*$^{-/-}$ lenses exhibit elevated levels of Cdkn1c (p57$^{Kip2}$) protein in the transition zone and in differentiating fiber cells (Figures 9A,B). Cdkn1c (p57$^{Kip2}$) protein levels were also elevated in fiber cells located deeper in the *Mafg*$^{-/-}$:*Mafk*$^{-/-}$ lens tissue, compared to control. Together, misexpression of these genes likely contribute to the lens defects in *Mafg*$^{-/-}$:*Mafk*$^{-/-}$ mice. To examine whether increased cell numbers contributed to the multilayered epithelium defects observed in *Mafg*$^{-/-}$:*Mafk*$^{-/-}$ lenses, we next performed staining with the established cell proliferation marker Ki67 (Gerdes et al., 1984). Compared to control, *Mafg*$^{-/-}$:*Mafk*$^{-/-}$ lenses exhibit elevated number of cells with Ki67 staining and these were restricted to the epithelium region of the lens (Supplementary Figure S9). However, no stark difference was observed in the percent subset of cells that were Ki67 positive between control and *Mafg*$^{-/-}$:*Mafk*$^{-/-}$ lenses at E16.5 (data not shown), suggesting that any change in rate of proliferation had ceased by this stage.

## Discussion

Previous work showed that loss of the small Maf transcription factors Mafg and Mafk, either individually, or in different allelic combinations result in distinct cellular defects (Blank, 2008; Kannan et al., 2012; Katsuoka and Yamamoto, 2016). However, the role of small Mafs in embryonic lens development remained unaddressed. In an earlier study, we demonstrated that removal of two copies of *Mafg* and one copy of *Mafk* cause lens defects late in life resulting in cataract (Agrawal et al., 2015). Here, we report that mice carrying homozygous deletion of *Mafg* and *Mafk* exhibit embryonic lens defects. We find that *Mafg*$^{-/-}$:*Mafk*$^{-/-}$ lens defects are detectable at E12.5 that get progressively severe, such that, by E16.5, the epithelium appears multilayered and there is abnormal

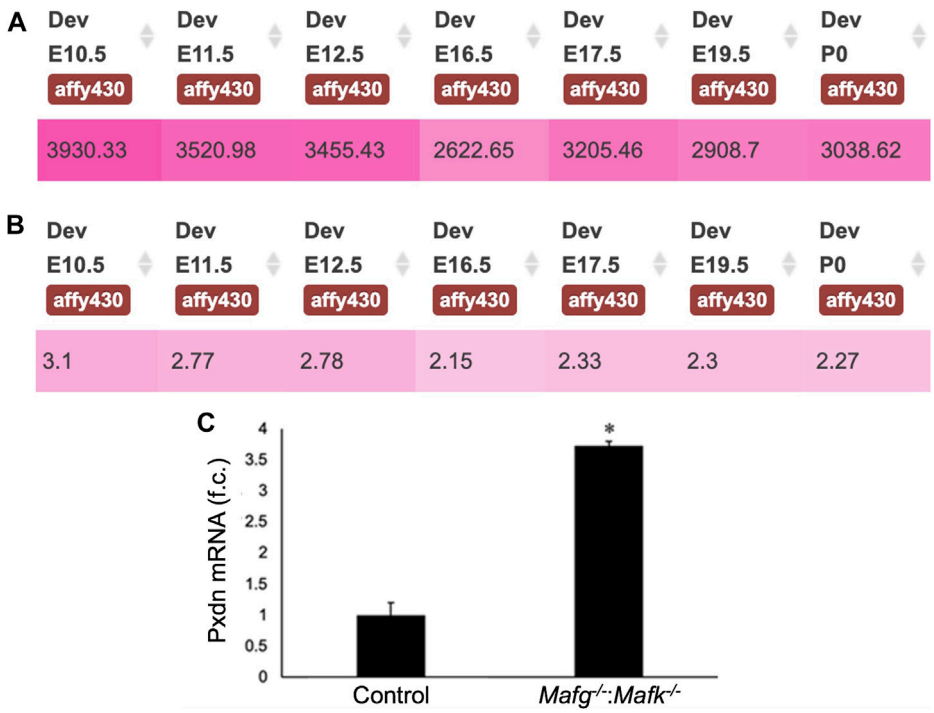


FIGURE 7
*Pxdn* expression in normal lens development and validation of its abnormally elevated expression in *Mafg*$^{-/-}$:*Mafk*$^{-/-}$ lens. **(A)** iSyTE analysis shows that the cataract and ocular defects-linked heme-containing peroxidase enzyme, Pxdn, which is identified by RNA-seq analysis among the DEGs in *Mafg*$^{-/-}$:*Mafk*$^{-/-}$ lenses, exhibits robust absolute expression, and **(B)** lens-enriched expression, in various stages of normal mouse embryonic lens development. **(C)** RT-qPCR validation of abnormally elevated expression of *Pxdn* in *Mafg*$^{-/-}$:*Mafk*$^{-/-}$ lenses. Numbers in **(A)** represent normalized microarrays fluorescence intensity units as described in Kakrana and coworkers (2018). Fold-change was calculated using the ΔΔCT-method using *Gapdh* as a house-keeping gene and statistical significance was determined using a two-sample Student's *t*-test. Asterisk indicates $p \leq 0.05$.

accumulation of F-actin in early differentiating fiber cells that appear disorganized. We took an unbiased approach to gain insights into the molecular basis of these defects and performed high-throughput RNA-seq on *Mafg*$^{-/-}$:*Mafk*$^{-/-}$ lenses. GO analysis of *Mafg*$^{-/-}$:*Mafk*$^{-/-}$ lens DEGs identified several candidates in distinct pathways, involved in cell proliferation, extracellular matrix, cell junction and cytoskeleton control, whose misregulation can help explain the cellular basis of the lens defects, as described in the proposed model (Figure 10). These include the extracellular matrix heme peroxidase Pxdn, mutations in which are linked to human ocular defects, including cataract (Khan et al., 2011; Yan et al., 2014). Pxdn is found to be elevated in several types of cancer and is associated with its poor prognosis and indeed, its overexpression is involved in promoting cell proliferation (Zheng and Liang, 2018). Further, co-expression of Pxdn along with Hmox1, which is also found to be elevated in *Mafg*$^{-/-}$:*Mafk*$^{-/-}$ lens, is thought to promote cell proliferation (Tauber et al., 2010). Interestingly, Pxdn has recently been recognized to be a target of the TF Nrf2 (Hanmer and Mavri-Damelin, 2018), which is an established partner protein of small Mafs, binding together of which impact their downstream control over target genes (Katsuoka et al., 2005). Further, Nrf2 deficiency is associated with lens defects and cataract (Rowan et al., 2021). Thus, overexpression of Pxdn, resulting from Mafg, Mafk deletion, may impact cell proliferation and altered ECM, which together contribute to the epithelial defects observed in *Mafg*$^{-/-}$:*Mafk*$^{-/-}$ lens. It can be further postulated that the recruitment of Mafg and Mafk for regulation of Pxdn in the lens suggest that multiple pathways may converge to ensure optimal levels of this important protein in the lens.

In addition to Pxdn, an eph signaling receptor, Epha5, was found to be significantly downregulated in *Mafg*$^{-/-}$:*Mafk*$^{-/-}$ lens. It has been shown that loss of an established ligand—Ephrin A5 (also known as Efna5)—results in lens defects and cataract in mouse (Cooper et al., 2008; Son et al., 2013; Biswas et al., 2016). Further, the Eph signaling receptor, Epha2, is known to be involved in lens development and cataract (Shiels et al., 2008; Jun et al., 2009; Cheng and Gong, 2011; Shi et al., 2012; Cheng et al., 2013). The lens defects observed in the knockout models of these Eph pathway genes—albeit influenced by the specific mouse strains in which the experiments were carried out on—overlap with the lens defects observed in *Mafg*$^{-/-}$:*Mafk*$^{-/-}$ lens. Interestingly, careful studies of Epha2 and Ephrin-A5 double knockout mouse lenses (Cheng et al.,

**A**

| Symbol | Dev E10.5 affy430 | Dev E11.5 affy430 | Dev E12.5 affy430 | Dev E16.5 affy430 | Dev E17.5 affy430 | Dev E19.5 affy430 | Dev P0 affy430 |
|---|---|---|---|---|---|---|---|
| Epha1 | 51.73 | 38.54 | 40.14 | 52.43 | 39.97 | 45.43 | 40.53 |
| Epha2 | 201.09 | 217.08 | 230.87 | 414.55 | 339.27 | 388.52 | 351.25 |
| Epha3 | 32.64 | 56.31 | 40.89 | 18.19 | 18.91 | 29.05 | 11.27 |
| Epha4 | 36.48 | 29.72 | 27.28 | 31.98 | 28.47 | 33.9 | 36.08 |
| Epha5 | 40.42 | 70.29 | 69.95 | 106.09 | 153.25 | 170.81 | 172.11 |
| Epha6 | 9.35 | 10.37 | 9.03 | 9.63 | 11.22 | 8.43 | 10.18 |
| Epha7 | 38.45 | 41 | 34.63 | 32.23 | 32.21 | 35.16 | 30.43 |

**B**

| Symbol | Dev E10.5 affy430 | Dev E11.5 affy430 | Dev E12.5 affy430 | Dev E16.5 affy430 | Dev E17.5 affy430 | Dev E19.5 affy430 | Dev P0 affy430 |
|---|---|---|---|---|---|---|---|
| Epha1 | 1.12 | -1.16 | -1.14 | 1.08 | -1.19 | -1.06 | -1.13 |
| Epha2 | 2.96 | 3.35 | 3.54 | 7.08 | 5.68 | 6.63 | 5.87 |
| Epha3 | -28.92 | -16.65 | -22.88 | -59.96 | -51.84 | -33.48 | -80.45 |
| Epha4 | -6.66 | -8.42 | -9.31 | -7.55 | -7.78 | -7.21 | -6.87 |
| Epha5 | -1.2 | 1.53 | 1.57 | 2.92 | 3.93 | 4.02 | 3.76 |
| Epha6 | -1.25 | -1.13 | -1.3 | -1.22 | -1.03 | -1.38 | -1.12 |
| Epha7 | -2.32 | -2.26 | -2.51 | -2.72 | -2.74 | -2.49 | -2.86 |

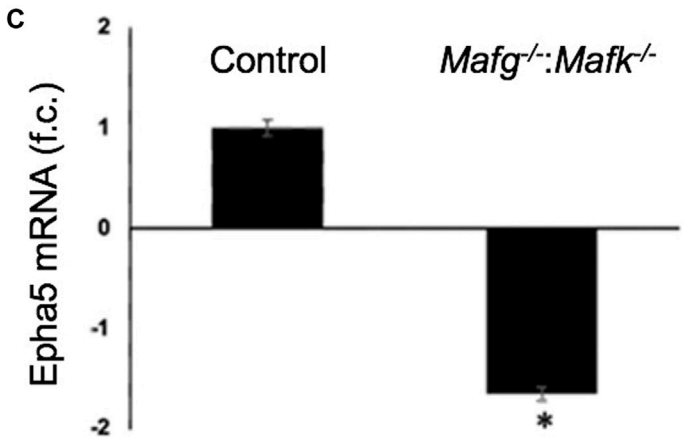


FIGURE 8
Expression of Eph-signaling receptors in normal lens development and the reduced expression of Epha5 in *Mafg*$^{-/-}$:*Mafk*$^{-/-}$ lens. **(A)** iSyTE analysis of various Eph-signaling receptors shows that Epha5, which is identified by RNA-seq analysis among the DEGs in *Mafg*$^{-/-}$:*Mafk*$^{-/-}$ lenses, exhibits high expression and **(B)** high lens-enriched expression, second only to Epha2 that is linked to congenital cataract in humans and in animal models. **(C)** RT-qPCR validation of abnormally reduced expression of *Epha5* in *Mafg*$^{-/-}$:*Mafk*$^{-/-}$ lenses. Numbers in **(A)** represent normalized microarrays fluorescence intensity units as described in Kakrana and coworkers (2018). Fold-change was calculated using the ΔΔCT-method using *Gapdh* as a house-keeping gene and statistical significance was determined using a two-sample Student's *t*-test. Asterisk indicates $p \leq 0.05$.

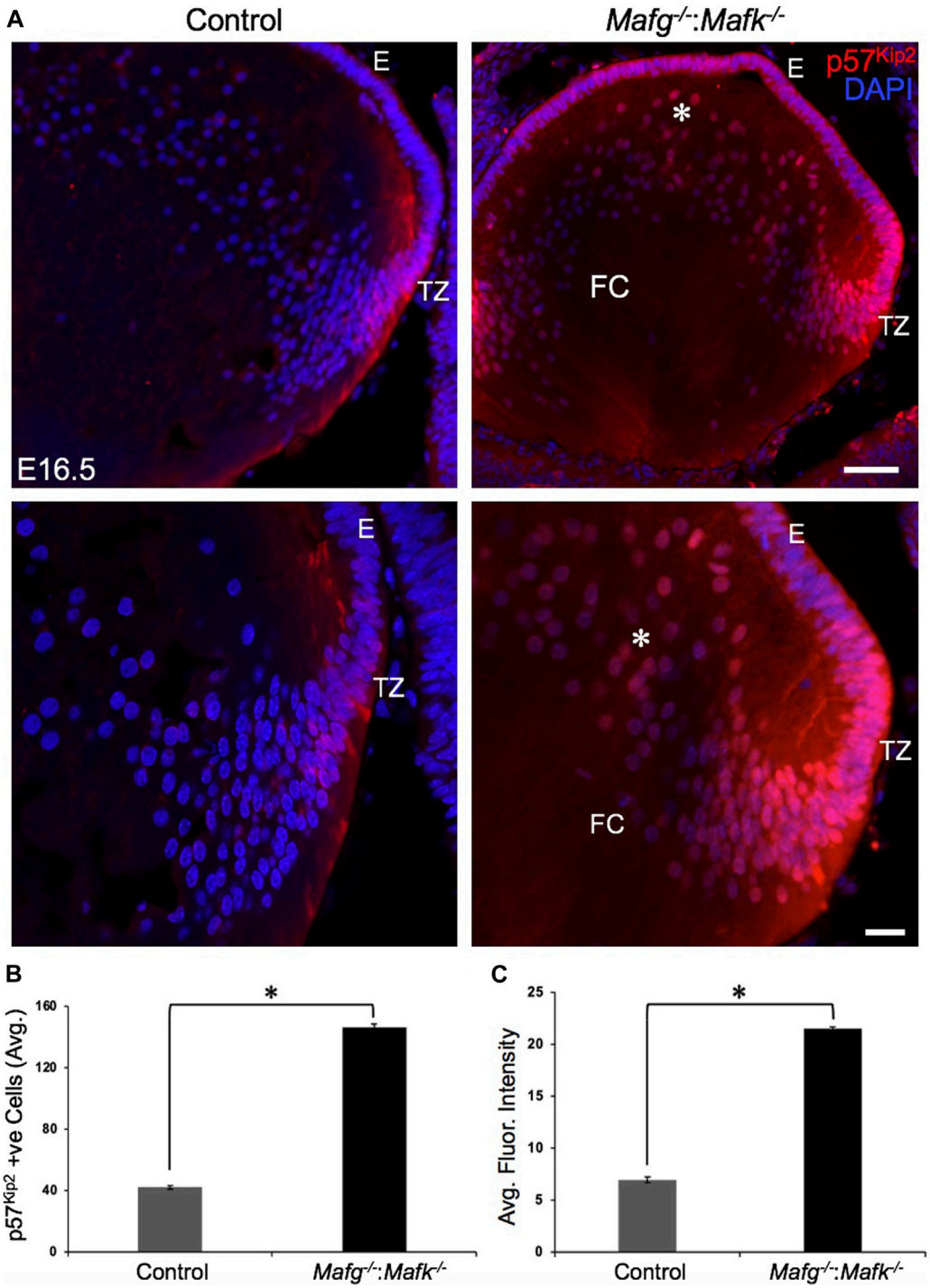


FIGURE 9
Cdkn1c ($p57^{Kip2}$) protein levels are elevated in $Mafg^{-/-}$:$Mafk^{-/-}$ lens. **(A)** Immunostaining shows Cdkn1c ($p57^{Kip2}$) protein levels are elevated in the transition zone and in fiber cells (asterisk) in E16.5 $Mafg^{-/-}$:$Mafk^{-/-}$ lenses compared to control. **(B)** Quantification of cells from transition zone and fiber compartment exhibiting Cdkn1c ($p57^{Kip2}$) signal in $Mafg^{-/-}$:$Mafk^{-/-}$ lenses compared to control. **(C)** Quantification of average fluorescence intensity of Cdkn1c ($p57^{Kip2}$) signal in $Mafg^{-/-}$:$Mafk^{-/-}$ lenses compared to control. Statistical significance was determined using a two-sample Student's *t*-test. Abbreviation: E, Epithelium of the lens; FC, Fiber cells of the lens; TZ, Transition zone of the lens. Scale bar for Row 1, 10 μm; Row 2, 8 μm. Asterisk in **(B)** and **(C)** indicates $p \leq 0.05$.

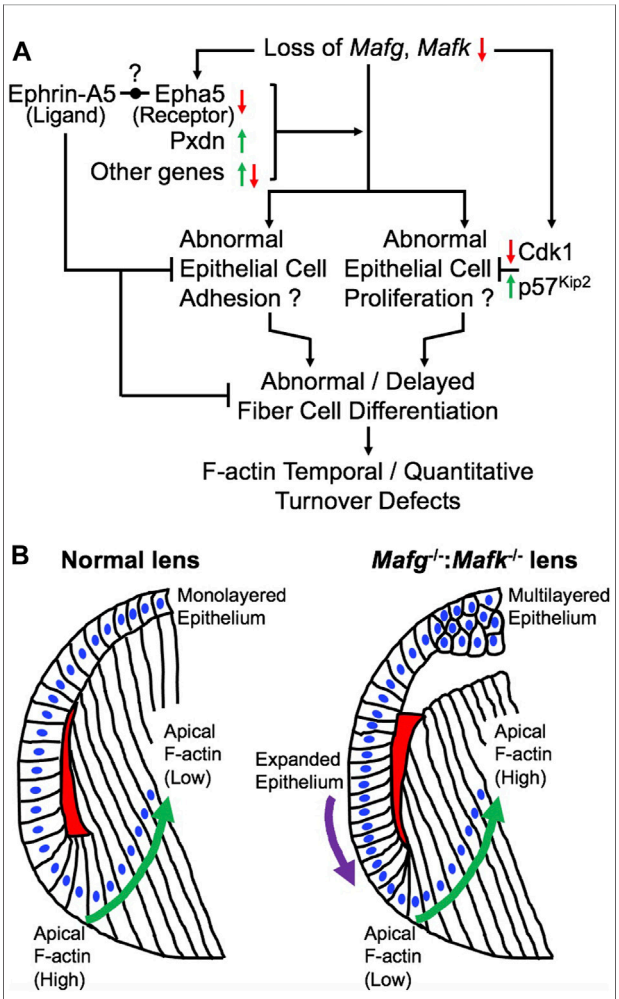


FIGURE 10
Model for the role of Mafg and Mafk in embryonic lens development. **(A)** Based on the findings in this report, a model is proposed for the role of Mafg and Mafk in lens development. Loss of Mafg and Mafk results in misexpression of several genes, including the cataract-linked extracellular matrix peroxidase enzyme Pxdn and Eph-signaling receptor Epha5. Interestingly, previous work has shown that loss of an ephrin ligand, Efna5 (Ephrin-A5), causes similar lens defects. It was recently proposed by Cheng and co-workers (2017) that an Eph receptor—other that Epha2—may be involved in interactions with Efna5 (Ephrin-A5). Based on these new data, it is tempting to propose Epha5 could represent this receptor. Further, it can be speculated that correct dosage of the cataract-linked gene Pxdn, which is involved in extracellular matrix organization and which is also involved in cell proliferation, may be necessary for proper lens epithelium formation, and its over or under-expression results in lens defects, thus explaining the recruitment of Mafg and Mafk to ensure correct dosage of Pxdn in the lens. These, together with misexpression of other genes result in abnormal epithelial cell adhesion in the lens. It is possible that reduced expression of Cdk1 (positive regulator of the cell cycle) and the elevated expression of $p57^{Kip2}$ (negative regulator of the cell cycle) may reflect perturbations in the cell cycle in *Mafg*$^{-/-}$:*Mafk*$^{-/-}$ lenses. Together these epithelial defects may contribute to abnormal or delayed fiber cell differentiation that impacts the optimal distribution of F-actin in these cells. **(B)** In normal lens, the epithelium is maintained as a uniform monolayer. Epithelial cells exit the cell cycle in the transition zone that commence differentiation into fiber cells. In early stages of fiber

(*Continued*)

FIGURE 10
cell differentiation, F-actin (indicated by red) in the apical region of the cells is observed to be high (Note: the red region is a schematic representative of the overall F-actin staining pattern in this region and further cellular details, such as how cells form the fulcrum region, are not shown). As cells progress in the differentiation program (indicated by green arrow), F-actin levels in their apical regions get reduced. In contrast, *Mafg*$^{-/-}$:*Mafk*$^{-/-}$ lenses exhibit loss of a uniformed, monolayer of epithelium (indicated by purple arrow). Further, in *Mafg*$^{-/-}$:*Mafk*$^{-/-}$ lenses, F-actin levels are low in the apical region of fiber cells in early stages of differentiation. In contrast to normal lenses, F-actin levels in the apical regions are not observed to be reduced as cells progress in the differentiation program. It will be important in future studies to examine how the crosstalk between small Mafs and their downstream targets control these cell differentiation events.

2017; Zhou and Shiels, 2018; Murugan and Cheng, 2022) have suggested that additional Eph signaling receptors, besides Epha2, may be involved in lens development. Our iSyTE analysis shows that Epha5 is the second most abundant Eph signaling receptor—after Epha2—in embryonic lens development. Thus, our observations of high lens-enriched expression of Epha5, along with its reduction in *Mafg*$^{-/-}$:*Mafk*$^{-/-}$ lens, which exhibit epithelial and fiber defects that overlap with those observed in Ephrin A5 (Efna5) ligand knockout mice, together present a provocative hypothesis that Epha5 may be an additional receptor involved in Eph signaling in the lens—which can be tested in future studies. The potential relevance of Epha5 downregulation upon Mafg, Mafk KO mice, in different KO allelic combinations, can also be explored further in the context of neurological defects observed in these animals.

Misexpression of other downstream targets of Mafg and Mafk may also contribute to the defects observed in *Mafg*$^{-/-}$:*Mafk*$^{-/-}$ lens. For example, based on its known role in other cells (Pak et al., 2001; Matsuura et al., 2021), Sipa1l1 may be involved in regulation of the actin cytoskeleton, and its reduced expression may contribute to the cytoskeletal defects in *Mafg*$^{-/-}$:*Mafk*$^{-/-}$ lens. Interestingly, Sipa1l1 is found to be in the eph receptor signaling pathway according to GO analysis. Similarly, misexpression of Camsap1, known to be involved in cytoskeletal control by binding to spectrin (Jiang et al., 2014; King et al., 2014; Xiang et al., 2016), may contribute to the observed lens defects. Further, overexpression of the collagen encoding gene *Col3a1* in *Mafg*$^{-/-}$:*Mafk*$^{-/-}$ may result in ECM defects and thus contribute to the lens defects (Kuivaniemi and Tromp, 2019).

Dimerization of small Maf transcription factors with other bZIP family members are known to control their specific function. Interestingly, we find a leucine zipper containing mitogen-activated serine/threonine protein kinase, *Map3k12*, to have significantly reduced expression in *Mafg*$^{-/-}$:*Mafk*$^{-/-}$ lens. Map3k12 is potentially involved in cell differentiation and control of the cell cycle (Robitaille et al., 2005, 2010; Daviau et al., 2011). Thus, its reduced expression may contribute to the lens defects in *Mafg*$^{-/-}$:*Mafk*$^{-/-}$ lens. The proposed model outline the various downstream events that

help provide a molecular and cellular explanation for understanding the pathology observed in *Mafg*$^{-/-}$:*Mafk*$^{-/-}$ mouse lenses (Figure 10). In particular, it is interesting to note that in *Mafg*$^{-/-}$:*Mafk*$^{-/-}$ lenses, F-actin levels are low in the apical region of fiber cells in early stages of differentiation and are not reduced as cells progress in the differentiation program. This suggests that Mafg and Mafk contribute to the spatiotemporal control over F-actin deposition and/or turnover in early lens fiber differentiation (Figure 10). It will be interesting to explore, in future, the potential crosstalk of Mafg, Mafk and Eph-signaling, as well as other factors (e.g., Pxdn) in regulating these cytoskeletal events in the lens. Other finer aspects of the *Mafg*$^{-/-}$:*Mafk*$^{-/-}$ lens defects, such as the abnormal "dip-like" appearance in the central epithelium, may be a result of diverse—not necessarily mutually exclusive—events (e.g., secondary to abnormal epithelial cell activity or change in extracellular matrix proteins or as an indirect result due to fiber cells not expanding optimally to accommodate epithelial cells as a monolayer, etc.) that are areas that can be characterized in the future. Also, it should be noted that in the present study RNA-seq was performed on whole lens tissue and therefore subtle changes in gene expression that occur specifically in epithelial or fiber cells may not be detected. Therefore, future RNA-seq studies on isolated epithelium or fiber cells using laser capture microdissection (LCM) or on single cells may provide new molecular insights into these defects. In sum, these data suggest new directions wherein it can be examined whether these regulatory relationships between small Mafs and their downstream mis-expressed genes, especially those involving Eph-signaling, extracellular matrix proteins and cell cycle regulators, are present in the development and/or homeostasis of other tissues.

## Data availability statement

The datasets presented in this study can be found in online repositories (Gene expression omnibus). "Accession Number: GSE207853".

## Ethics statement

The animal study was reviewed and approved by Institutional Animal Care and Use Committee (IACUC).

## Author contributions

SP, DA, HM, FK, MY, and SL contributed to the generation and interpretation of the data. SP, DA, HM, FK, MY, and SL analysed the data. SP, DA, and SL wrote the manuscript. All authors reviewed the manuscript.

## Funding

This work was supported by National Institutes of Health (R01 EY021505 and R01 EY029770 to SL) to SL. DA was supported by a Knights Templar Pediatric Ophthalmology Career Starter Grant Award. SP was supported by a Graduate Scholars Award from the University of Delaware. Support from the University of Delaware Core Imaging facility was made possible through funding from the State of Delaware and National Institutes of Health/National Institute of General Medical Sciences INBRE Program Grant (P20 GM103446). Acquisition of the confocal microscope used in this study was funded by the National Institutes of Health/National Center for Research Resources grant (1S10 RR027273–01).

## Conflict of interest

The authors declare that the research was conducted in the absence of any commercial or financial relationships that could be construed as a potential conflict of interest.

## Publisher's note



## Supplementary material

The Supplementary Material for this article can be found online at: https://www.frontiersin.org/articles/10.3389/fcell.2022.981893/full#supplementary-material

## References

Agrawal, S. A., Anand, D., Siddam, A. D., Kakrana, A., Dash, S., Scheiblin, D. A., et al. (2015). Compound mouse mutants of bZIP transcription factors Mafg and Mafk reveal a regulatory network of non-crystallin genes associated with cataract. *Hum. Genet.* 134, 717–735. doi:10.1007/s00439-015-1554-5

Akaneya, Y., Sohya, K., Kitamura, A., Kimura, F., Washburn, C., Zhou, R., et al. (2010). Ephrin-A5 and EphA5 interaction induces synaptogenesis during early hippocampal development. *PLoS One* 5, e12486. doi:10.1371/journal.pone.0012486

Anand, D., Agrawal, S. A., Slavotinek, A., and Lachke, S. A. (2018a). Mutation update of transcription factor genes FOXE3, HSF4, MAF, and PITX3 causing cataracts and other developmental ocular defects. *Hum. Mutat.* 39, 471–494. doi:10.1002/humu.23395

Anand, D., Agrawal, S., Siddam, A., Motohashi, H., Yamamoto, M., and Lachke, S. A. (2015). An integrative approach to analyze microarray datasets for prioritization of genes relevant to lens biology and disease. *Genom. Data* 5, 223–227. doi:10.1016/j.gdata.2015.06.017

Anand, D., Al Saai, S., Shrestha, S. K., Barnum, C. E., Chuma, S., and Lachke, S. A. (2021). Genome-wide analysis of differentially expressed miRNAs and their associated regulatory networks in lenses deficient for the congenital cataract-linked tudor domain containing protein TDRD7. *Front. Cell Dev. Biol.* 9, 615761. doi:10.3389/fcell.2021.615761

Anand, D., Kakrana, A., Siddam, A. D., Huang, H., Saadi, I., and Lachke, S. A. (2018b). RNA sequencing-based transcriptomic profiles of embryonic lens development for cataract gene discovery. *Hum. Genet.* 137, 941–954. doi:10.1007/s00439-018-1958-0

Anand, D., and Lachke, S. A. (2017). Systems biology of lens development: A paradigm for disease gene discovery in the eye. *Exp. Eye Res.* 156, 22–33. doi:10.1016/j.exer.2016.03.010

Aryal, S., Anand, D., Hernandez, F. G., Weatherbee, B. A. T., Huang, H., Reddy, A. P., et al. (2020). MS/MS *in silico* subtraction-based proteomic profiling as an approach to facilitate disease gene discovery: Application to lens development and cataract. *Hum. Genet.* 139, 151–184. doi:10.1007/s00439-019-02095-5

Ashburner, M., Ball, C. A., Blake, J. A., Botstein, D., Butler, H., Cherry, J. M., et al. (2000). Gene ontology: Tool for the unification of biology. The gene ontology Consortium. *Nat. Genet.* 25, 25–29. doi:10.1038/75556

Audette, D. S., Anand, D., So, T., Rubenstein, T. B., Lachke, S. A., Lovicu, F. J., et al. (2016). Prox1 and fibroblast growth factor receptors form a novel regulatory loop controlling lens fiber differentiation and gene expression. *Development* 143, 318–328. doi:10.1242/dev.127860

Barnum, C. E., Al Saai, S., Patel, S. D., Cheng, C., Anand, D., Xu, X., et al. (2020). The Tudor-domain protein TDRD7, mutated in congenital cataract, controls the heat shock protein HSPB1 (HSP27) and lens fiber cell morphology. *Hum. Mol. Genet.* 29, 2076–2097. doi:10.1093/hmg/ddaa096

Berry, V., Georgiou, M., Fujinami, K., Quinlan, R., Moore, A., and Michaelides, M. (2020). Inherited cataracts: Molecular genetics, clinical features, disease mechanisms and novel therapeutic approaches. *Br. J. Ophthalmol.* 104, 1331–1337. doi:10.1136/bjophthalmol-2019-315282

Biswas, S., Son, A., Yu, Q., Zhou, R., and Lo, W.-K. (2016). Breakdown of interlocking domains may contribute to formation of membranous globules and lens opacity in ephrin-A5(-/-) mice. *Exp. Eye Res.* 145, 130–139. doi:10.1016/j.exer.2015.11.017

Blank, V. (2008). Small Maf proteins in mammalian gene control: Mere dimerization partners or dynamic transcriptional regulators? *J. Mol. Biol.* 376, 913–925. doi:10.1016/j.jmb.2007.11.074

Cavalheiro, G. R., Matos-Rodrigues, G. E., Zhao, Y., Gomes, A. L., Anand, D., Predes, D., et al. (2017). N-myc regulates growth and fiber cell differentiation in lens development. *Dev. Biol.* 429, 105–117. doi:10.1016/j.ydbio.2017.07.002

Cheng, C., Ansari, M. M., Cooper, J. A., and Gong, X. (2013). EphA2 and Src regulate equatorial cell morphogenesis during lens development. *Development* 140, 4237–4245. doi:10.1242/dev.100727

Cheng, C., Fowler, V. M., and Gong, X. (2017). EphA2 and ephrin-A5 are not a receptor-ligand pair in the ocular lens. *Exp. Eye Res.* 162, 9–17. doi:10.1016/j.exer.2017.06.016

Cheng, C., and Gong, X. (2011). Diverse roles of eph/ephrin signaling in the mouse lens. *PLOS ONE* 6, e28147. doi:10.1371/journal.pone.0028147

Choquet, H., Melles, R. B., Anand, D., Yin, J., Cuellar-Partida, G., Wang, W., et al. (2021). A large multiethnic GWAS meta-analysis of cataract identifies new risk loci and sex-specific effects. *Nat. Commun.* 12, 3595. doi:10.1038/s41467-021-23873-8

Congdon, N., Broman, K. W., Lai, H., Munoz, B., Bowie, H., Gilbert, D., et al. (2005). Cortical, but not posterior subcapsular, cataract shows significant familial aggregation in an older population after adjustment for possible shared environmental factors. *Ophthalmology* 112, 73–77. doi:10.1016/j.ophtha.2004.07.012

Cooper, M. A., Son, A. I., Komlos, D., Sun, Y., Kleiman, N. J., and Zhou, R. (2008). Loss of ephrin-A5 function disrupts lens fiber cell packing and leads to cataract. *Proc. Natl. Acad. Sci. U. S. A.* 105, 16620–16625. doi:10.1073/pnas.0808987105

Cvekl, A., and Zhang, X. (2017). Signaling and gene regulatory networks in mammalian lens development. *Trends Genet.* 33, 677–702. doi:10.1016/j.tig.2017.08.001

Dash, S., Siddam, A. D., Barnum, C. E., Janga, S. C., and Lachke, S. A. (2016). RNA-Binding proteins in eye development and disease: Implication of conserved RNA granule components. *Wiley Interdiscip. Rev. RNA* 7, 527–557. doi:10.1002/wrna.1355

Daviau, A., Couture, J.-P., and Blouin, R. (2011). Loss of DLK expression in WI-38 human diploid fibroblasts induces a senescent-like proliferation arrest. *Biochem. Biophys. Res. Commun.* 413, 282–287. doi:10.1016/j.bbrc.2011.08.086

Gerdes, J., Lemke, H., Baisch, H., Wacker, H. H., Schwab, U., and Stein, H. (1984). Cell cycle analysis of a cell proliferation-associated human nuclear antigen defined by the monoclonal antibody Ki-67. *J. Immunol.* 133, 1710–1715.

Haargaard, B., Wohlfahrt, J., Fledelius, H. C., Rosenberg, T., and Melbye, M. (2004). Incidence and cumulative risk of childhood cataract in a cohort of 2.6 million Danish children. *Invest. Ophthalmol. Vis. Sci.* 45, 1316–1320. doi:10.1167/iovs.03-0635

Hammond, C. J., Duncan, D. D., Snieder, H., de Lange, M., West, S. K., Spector, T. D., et al. (2001). The heritability of age-related cortical cataract: The twin eye study. *Invest. Ophthalmol. Vis. Sci.* 42, 601–605.

Hammond, C. J., Snieder, H., Spector, T. D., and Gilbert, C. E. (2000). Genetic and environmental factors in age-related nuclear cataracts in monozygotic and dizygotic twins. *N. Engl. J. Med.* 342, 1786–1790. doi:10.1056/NEJM200006153422404

Hanmer, K. L., and Mavri-Damelin, D. (2018). Peroxidasin is a novel target of the redox-sensitive transcription factor Nrf2. *Gene* 674, 104–114. doi:10.1016/j.gene.2018.06.076

Huang, D. W., Sherman, B. T., and Lempicki, R. A. (2009). Systematic and integrative analysis of large gene lists using DAVID bioinformatics resources. *Nat. Protoc.* 4, 44–57. doi:10.1038/nprot.2008.211

Jamieson, R. V., Perveen, R., Kerr, B., Carette, M., Yardley, J., Heon, E., et al. (2002). Domain disruption and mutation of the bZIP transcription factor, MAF, associated with cataract, ocular anterior segment dysgenesis and coloboma. *Hum. Mol. Genet.* 11, 33–42. doi:10.1093/hmg/11.1.33

Jiang, K., Hua, S., Mohan, R., Grigoriev, I., Yau, K. W., Liu, Q., et al. (2014). Microtubule minus-end stabilization by polymerization-driven CAMSAP deposition. *Dev. Cell* 28, 295–309. doi:10.1016/j.devcel.2014.01.001

Jun, G., Guo, H., Klein, B. E. K., Klein, R., Wang, J. J., Mitchell, P., et al. (2009). EPHA2 is associated with age-related cortical cataract in mice and humans. *PLoS Genet.* 5, e1000584. doi:10.1371/journal.pgen.1000584

Kakrana, A., Yang, A., Anand, D., Djordjevic, D., Ramachandruni, D., Singh, A., et al. (2018). iSyTE 2.0: a database for expression-based gene discovery in the eye. *Nucleic Acids Res.* 46, D875–D885. doi:10.1093/nar/gkx837

Kanehisa, M., and Goto, S. (2000). Kegg: Kyoto encyclopedia of genes and genomes. *Nucleic Acids Res.* 28, 27–30. doi:10.1093/nar/28.1.27

Kannan, M. B., Solovieva, V., and Blank, V. (2012). The small MAF transcription factors MAFF, MAFG and MAFK: Current knowledge and perspectives. *Biochim. Biophys. Acta* 1823, 1841–1846. doi:10.1016/j.bbamcr.2012.06.012

Katsuoka, F., Motohashi, H., Engel, J. D., and Yamamoto, M. (2005). Nrf2 transcriptionally activates the mafG gene through an antioxidant response element. *J. Biol. Chem.* 280, 4483–4490. doi:10.1074/jbc.M411451200

Katsuoka, F., and Yamamoto, M. (2016). Small Maf proteins (MafF, MafG, MafK): History, structure and function. *Gene* 586, 197–205. doi:10.1016/j.gene.2016.03.058

Kawauchi, S., Takahashi, S., Nakajima, O., Ogino, H., Morita, M., Nishizawa, M., et al. (1999). Regulation of lens fiber cell differentiation by transcription factor c-Maf. *J. Biol. Chem.* 274, 19254–19260. doi:10.1074/jbc.274.27.19254

Khan, K., Rudkin, A., Parry, D. A., Burdon, K. P., McKibbin, M., Logan, C. V., et al. (2011). Homozygous mutations in PXDN cause congenital cataract, corneal opacity, and developmental glaucoma. *Am. J. Hum. Genet.* 89, 464–473. doi:10.1016/j.ajhg.2011.08.005

Kim, D., Langmead, B., and Salzberg, S. L. (2015). Hisat: A fast spliced aligner with low memory requirements. *Nat. Methods* 12, 357–360. doi:10.1038/nmeth.3317

Kim, J. I., Li, T., Ho, I. C., Grusby, M. J., and Glimcher, L. H. (1999). Requirement for the c-Maf transcription factor in crystallin gene regulation and lens development. *Proc. Natl. Acad. Sci. U. S. A.* 96, 3781–3785. doi:10.1073/pnas.96.7.3781

King, M. D. A., Phillips, G. W., Bignone, P. A., Hayes, N. V. L., Pinder, J. C., and Baines, A. J. (2014). A conserved sequence in calmodulin regulated spectrin-associated protein 1 links its interaction with spectrin and calmodulin to neurite outgrowth. *J. Neurochem.* 128, 391–402. doi:10.1111/jnc.12462

Krall, M., Htun, S., Anand, D., Hart, D., Lachke, S. A., and Slavotinek, A. M. (2018). A zebrafish model of foxe3 deficiency demonstrates lens and eye defects

with dysregulation of key genes involved in cataract formation in humans. *Hum. Genet.* 137, 315–328. doi:10.1007/s00439-018-1884-1

Kuivaniemi, H., and Tromp, G. (2019). Type III collagen (COL3A1): Gene and protein structure, tissue distribution, and associated diseases. *Gene* 707, 151–171. doi:10.1016/j.gene.2019.05.003

Lachke, S. A., Alkuraya, F. S., Kneeland, S. C., Ohn, T., Aboukhalil, A., Howell, G. R., et al. (2011). Mutations in the RNA granule component TDRD7 cause cataract and glaucoma. *Science* 331, 1571–1576. doi:10.1126/science.1195970

Lachke, S. A., Higgins, A. W., Inagaki, M., Saadi, I., Xi, Q., Long, M., et al. (2012a). The cell adhesion gene PVRL3 is associated with congenital ocular defects. *Hum. Genet.* 131, 235–250. doi:10.1007/s00439-011-1064-z

Lachke, S. A., Ho, J. W. K., Kryukov, G. V., O'Connell, D. J., Aboukhalil, A., Bulyk, M. L., et al. (2012b). iSyTE: integrated Systems Tool for Eye gene discovery. *Invest. Ophthalmol. Vis. Sci.* 53, 1617–1627. doi:10.1167/iovs.11-8839

Lachke, S. A., and Maas, R. L. (2010). Building the developmental oculome: Systems biology in vertebrate eye development and disease. *Wiley Interdiscip. Rev. Syst. Biol. Med.* 2, 305–323. doi:10.1002/wsbm.59

Lachke, S. A. (2022). RNA-binding proteins and post-transcriptional regulation in lens biology and cataract: Mediating spatiotemporal expression of key factors that control the cell cycle, transcription, cytoskeleton and transparency. *Exp. Eye Res.* 214, 108889. doi:10.1016/j.exer.2021.108889

Manthey, A. L., Lachke, S. A., FitzGerald, P. G., Mason, R. W., Scheiblin, D. A., McDonald, J. H., et al. (2014). Loss of Sip1 leads to migration defects and retention of ectodermal markers during lens development. *Mech. Dev.* 131, 86–110. doi:10.1016/j.mod.2013.09.005

Matsuura, K., Kobayashi, S., Konno, K., Yamasaki, M., Horiuchi, T., Senda, T., et al. (2021). SIPA1L1/SPAR1 is a non-PSD protein involved in GPCR signaling. *J. Neurosci.* 2021, 430872. doi:10.1101/2021.02.12.430872

Murugan, S., and Cheng, C. (2022). Roles of eph-ephrin signaling in the eye lens cataractogenesis, biomechanics, and homeostasis. *Front. Cell Dev. Biol.* 10, 852236. doi:10.3389/fcell.2022.852236

Onodera, K., Shavit, J. A., Motohashi, H., Yamamoto, M., and Engel, J. D. (2000). Perinatal synthetic lethality and hematopoietic defects in compound mafG::mafK mutant mice. *EMBO J.* 19, 1335–1345. doi:10.1093/emboj/19.6.1335

Padula, S. L., Anand, D., Hoang, T. V., Chaffee, B. R., Liu, L., Liang, C., et al. (2019). High-throughput transcriptome analysis reveals that the loss of Pten activates a novel NKX6-1/RASGRP1 regulatory module to rescue microphthalmia caused by Fgfr2-deficient lenses. *Hum. Genet.* 138, 1391–1407. doi:10.1007/s00439-019-02084-8

Pak, D. T., Yang, S., Rudolph-Correia, S., Kim, E., and Sheng, M. (2001). Regulation of dendritic spine morphology by SPAR, a PSD-95-associated RapGAP. *Neuron* 31, 289–303. doi:10.1016/s0896-6273(01)00355-5

Patel, N., Anand, D., Monies, D., Maddirevula, S., Khan, A. O., Algoufi, T., et al. (2017). Novel phenotypes and loci identified through clinical genomics approaches to pediatric cataract. *Hum. Genet.* 136, 205–225. doi:10.1007/s00439-016-1747-6

Pertea, M., Pertea, G. M., Antonescu, C. M., Chang, T.-C., Mendell, J. T., and Salzberg, S. L. (2015). StringTie enables improved reconstruction of a transcriptome from RNA-seq reads. *Nat. Biotechnol.* 33, 290–295. doi:10.1038/nbt.3122

Pierce, S. B., Gersak, K., Michaelson-Cohen, R., Walsh, T., Lee, M. K., Malach, D., et al. (2013). Mutations in LARS2, encoding mitochondrial leucyl-tRNA synthetase, lead to premature ovarian failure and hearing loss in perrault syndrome. *Am. J. Hum. Genet.* 92, 614–620. doi:10.1016/j.ajhg.2013.03.007

Ring, B. Z., Cordes, S. P., Overbeek, P. A., and Barsh, G. S. (2000). Regulation of mouse lens fiber cell development and differentiation by the Maf gene. *Development* 127, 307–317. doi:10.1242/dev.127.2.307

Robinson, M. D., McCarthy, D. J., and Smyth, G. K. (2010). edgeR: a Bioconductor package for differential expression analysis of digital gene expression data. *Bioinformatics* 26, 139–140. doi:10.1093/bioinformatics/btp616

Robitaille, H., Proulx, R., Robitaille, K., Blouin, R., and Germain, L. (2005). The mitogen-activated protein kinase kinase kinase dual leucine zipper-bearing kinase (DLK) acts as a key regulator of keratinocyte terminal differentiation. *J. Biol. Chem.* 280, 12732–12741. doi:10.1074/jbc.M411619200

Robitaille, H., Simard-Bisson, C., Larouche, D., Tanguay, R. M., Blouin, R., and Germain, L. (2010). The small heat-shock protein Hsp27 undergoes ERK-dependent phosphorylation and redistribution to the cytoskeleton in response to dual leucine zipper-bearing kinase expression. *J. Invest. Dermatol.* 130, 74–85. doi:10.1038/jid.2009.185

Rowan, S., Jiang, S., Francisco, S. G., Pomatto, L. C. D., Ma, Z., Jiao, X., et al. (2021). Aged nrf2-null mice develop all major types of age-related cataracts. *Invest. Ophthalmol. Vis. Sci.* 62, 10. doi:10.1167/iovs.62.15.10

Santamaría, D., Barrière, C., Cerqueira, A., Hunt, S., Tardy, C., Newton, K., et al. (2007). Cdk1 is sufficient to drive the mammalian cell cycle. *Nature* 448, 811–815. doi:10.1038/nature06046

Shavit, J. A., Motohashi, H., Onodera, K., Akasaka, J., Yamamoto, M., and Engel, J. D. (1998). Impaired megakaryopoiesis and behavioral defects in mafG-null mutant mice. *Genes Dev.* 12, 2164–2174. doi:10.1101/gad.12.14.2164

Shi, Y., De Maria, A., Bennett, T., Shiels, A., and Bassnett, S. (2012). A role for epha2 in cell migration and refractive organization of the ocular lens. *Invest. Ophthalmol. Vis. Sci.* 53, 551–559. doi:10.1167/iovs.11-8568

Shiels, A., Bennett, T. M., Knopf, H. L. S., Maraini, G., Li, A., Jiao, X., et al. (2008). The EPHA2 gene is associated with cataracts linked to chromosome 1p. *Mol. Vis.* 14, 2042–2055.

Shiels, A., and Hejtmancik, J. F. (2019). Biology of inherited cataracts and opportunities for treatment. *Annu. Rev. Vis. Sci.* 5, 123–149. doi:10.1146/annurev-vision-091517-034346

Shiels, A., and Hejtmancik, J. F. (2021). Inherited cataracts: Genetic mechanisms and pathways new and old. *Exp. Eye Res.* 209, 108662. doi:10.1016/j.exer.2021.108662

Shihan, M. H., Novo, S. G., Le Marchand, S. J., Wang, Y., and Duncan, M. K. (2021). A simple method for quantitating confocal fluorescent images. *Biochem. Biophys. Rep.* 25, 100916. doi:10.1016/j.bbrep.2021.100916

Siddam, A. D., Gautier-Courteille, C., Perez-Campos, L., Anand, D., Kakrana, A., Dang, C. A., et al. (2018). The RNA-binding protein Celf1 post-transcriptionally regulates p27Kip1 and Dnase2b to control fiber cell nuclear degradation in lens development. *PLoS Genet.* 14, e1007278. doi:10.1371/journal.pgen.1007278

Son, A. I., Cooper, M. A., Sheleg, M., Sun, Y., Kleiman, N. J., and Zhou, R. (2013). Further analysis of the lens of ephrin-A5-/- mice: Development of postnatal defects. *Mol. Vis.* 19, 254–266.

Sugiyama, Y., Akimoto, K., Robinson, M. L., Ohno, S., and Quinlan, R. A. (2009). A cell polarity protein aPKClambda is required for eye lens formation and growth. *Dev. Biol.* 336, 246–256. doi:10.1016/j.ydbio.2009.10.010

Tauber, S., Jais, A., Jeitler, M., Haider, S., Husa, J., Lindroos, J., et al. (2010). Transcriptome analysis of human cancer reveals a functional role of heme oxygenase-1 in tumor cell adhesion. *Mol. Cancer* 9, 200. doi:10.1186/1476-4598-9-200

Wolf, L., Harrison, W., Huang, J., Xie, Q., Xiao, N., Sun, J., et al. (2013). Histone posttranslational modifications and cell fate determination: Lens induction requires the lysine acetyltransferases CBP and p300. *Nucleic Acids Res.* 41, 10199–10214. doi:10.1093/nar/gkt824

Xiang, W., Lin, H., Wang, Q., Chen, W., Liu, Z., Chen, H., et al. (2016). miR-34a suppresses proliferation and induces apoptosis of human lens epithelial cells by targeting E2F3. *Mol. Med. Rep.* 14, 5049–5056. doi:10.3892/mmr.2016.5901

Yan, X., Sabrautzki, S., Horsch, M., Fuchs, H., Gailus-Durner, V., Beckers, J., et al. (2014). Peroxidasin is essential for eye development in the mouse. *Hum. Mol. Genet.* 23, 5597–5614. doi:10.1093/hmg/ddu274

Yang, Y.-G., Lindahl, T., and Barnes, D. E. (2007). Trex1 exonuclease degrades ssDNA to prevent chronic checkpoint activation and autoimmune disease. *Cell* 131, 873–886. doi:10.1016/j.cell.2007.10.017

Yi, J., Yun, J., Li, Z.-K., Xu, C.-T., and Pan, B.-R. (2011). Epidemiology and molecular genetics of congenital cataracts. *Int. J. Ophthalmol.* 4, 422–432. doi:10.3980/j.issn.2222-3959.2011.04.20

Zampighi, G. A., Eskandari, S., and Kreman, M. (2000). Epithelial organization of the mammalian lens. *Exp. Eye Res.* 71, 415–435. doi:10.1006/exer.2000.0895

Zhang, P., Wong, C., DePinho, R. A., Harper, J. W., and Elledge, S. J. (1998). Cooperation between the Cdk inhibitors p27(KIP1) and p57(KIP2) in the control of tissue growth and development. *Genes Dev.* 12, 3162–3167. doi:10.1101/gad.12.20.3162

Zhao, Y., Zheng, D., and Cvekl, A. (2018). A comprehensive spatial-temporal transcriptomic analysis of differentiating nascent mouse lens epithelial and fiber cells. *Exp. Eye Res.* 175, 56–72. doi:10.1016/j.exer.2018.06.004

Zheng, Y.-Z., and Liang, L. (2018). High expression of PXDN is associated with poor prognosis and promotes proliferation, invasion as well as migration in ovarian cancer. *Ann. Diagn. Pathol.* 34, 161–165. doi:10.1016/j.anndiagpath.2018.03.002

Zheng, Y., Liu, Y., Ge, J., Wang, X., Liu, L., Bu, Z., et al. (2010). Resveratrol protects human lens epithelial cells against H2O2-induced oxidative stress by increasing catalase, SOD-1, and HO-1 expression. *Mol. Vis.* 16, 1467–1474.

Zhou, Y., and Shiels, A. (2018). Epha2 and Efna5 participate in lens cell pattern-formation. *Differentiation.* 102, 1–9. doi:10.1016/j.diff.2018.05.002

frontiers | Frontiers in Cell and Developmental Biology

TYPE Review
PUBLISHED 30 August 2022
DOI 10.3389/fcell.2022.963615



OPEN ACCESS

EDITED BY
Daisy Y. Shu,
Schepens Eye Research Institute and Harvard Medical School, United States

REVIEWED BY
William Miller,
Schepens Eye Research Institute and Harvard Medical School, United States
Karis Little,
Queen's University Belfast, United Kingdom

*CORRESPONDENCE
Hongsong Yu,
yuhongsong@163.com

SPECIALTY SECTION
This article was submitted to Molecular and Cellular Pathology, a section of the journal Frontiers in Cell and Developmental Biology

RECEIVED 07 June 2022
ACCEPTED 12 August 2022
PUBLISHED 30 August 2022

CITATION
Wei L, Sun X, Fan C, Li R, Zhou S and Yu H (2022), The pathophysiological mechanisms underlying diabetic retinopathy.
*Front. Cell Dev. Biol.* 10:963615.
doi: 10.3389/fcell.2022.963615



# The pathophysiological mechanisms underlying diabetic retinopathy

Lindan Wei[1], Xin Sun[2], Chenxi Fan[1], Rongli Li[1], Shuanglong Zhou[1] and Hongsong Yu[1]*

[1]Special Key Laboratory of Ocular Diseases of Guizhou Province, Department of Immunology, Zunyi Medical University, Zunyi, China, [2]Special Key Laboratory of Gene Detection and Therapy of Guizhou Province, School of Basic Medical Sciences, Zunyi Medical University, Zunyi, China

Diabetic retinopathy (DR) is the most common complication of diabetes mellitus (DM), which can lead to visual impairment and even blindness in severe cases. DR is generally considered to be a microvascular disease but its pathogenesis is still unclear. A large body of evidence shows that the development of DR is not determined by a single factor but rather by multiple related mechanisms that lead to different degrees of retinal damage in DR patients. Therefore, this article briefly reviews the pathophysiological changes in DR, and discusses the occurrence and development of DR resulting from different factors such as oxidative stress, inflammation, neovascularization, neurodegeneration, the neurovascular unit, and gut microbiota, to provide a theoretical reference for the development of new DR treatment strategies.

KEYWORDS

**diabetic retinopathy, oxidative stress, inflammation, neovascularization, neurodegeneration, neurovascular unit, gut microbiota**

## Introduction

Diabetic retinopathy (DR) is the most common complication of diabetes mellitus (DM) (Whitehead et al., 2018). It is an irreversible blinding eye disease that imposes a severe burden on patients, healthcare systems, and society throughout the world (Simó et al., 2020; Antonetti et al., 2021). The International Diabetes Federation has estimated that the number of DM patients worldwide will increase from 463 million in 2019 to 700 million by 2045 (Saeedi et al., 2019). Teo et al. estimated that, as 22.27% of DM patients develop DR, the global prevalence of DR will increase from 103.12 million in 2020 to 160.5 million by 2045 (Teo et al., 2021). DR can be classified into non-proliferative diabetic retinopathy (NPDR) and proliferative diabetic retinopathy (PDR) according to the disease process. NPDR, known as early DR, is characterized by clinical manifestations such as retinal microaneurysms, cotton wool spots, hemorrhages, and exudates, of which the patient may not be aware. NPDR progresses to a more severe disease over time. PDR, also known as late DR, is typically characterized by the formation of new blood vessels that are very fragile and can thus rupture and bleed profusely (Solomon et al., 2017). The proliferation and migration of retinal pigment epithelial (RPE) cells, together with the

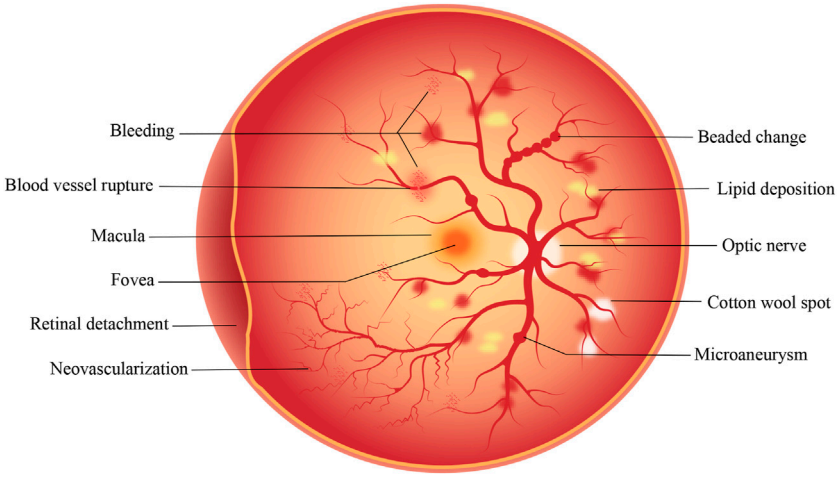


FIGURE 1
Pathological changes that occur on the retina in DR. The development of DR is a gradual process. In the early stage of NPDR, microaneurysm, cotton wool spots and minor bleeding may occur. In the later stage of PDR, serious conditions such as vascular rupture, severe bleeding, retinal detachment and neovascularization may occur.

secretion of extracellular matrix components by the cells, contribute to the distinctive fibrotic membranes formed at the vitreoretinal interface in PDR. Vascular endothelial growth factor (VEGF) and connective tissue growth factor (CCN2/CTGF) contribute to blindness through their promotion of neovascularization and subsequent fibrosis. It has been reported that CCN2 and the CCN2/VEGF ratio are the most powerful predictors of the extent of fibrosis (Kuiper et al., 2008). As DR progresses, retinal detachment, hemorrhage, and irreversible visual impairment occur. Figure 1 shows the pathological changes in the retina that occur in DR. Despite significant progress in the recognition and treatment of DR, its pathogenesis remains understudied, and the prevalence of DM, as well as DR, is still increasing. Therefore, it is crucial to study the specific pathogenesis of DR to develop new therapeutic strategies.

## DR and oxidative stress

DR is associated with a variety of stress mechanisms, among which the role of oxidative stress is crucial. In the early stage of DR, hyperglycemia leads to the formation of reactive oxygen species (ROS), composed of superoxide ions, hydrogen peroxide, and hydroxyl radicals. ROS are by-products of cellular metabolism, mainly derived from macrophages, mitochondrial electron transport chain, and mitochondrial lipid peroxidation. There are, however, antioxidants that actively scavenge ROS. In situations of excessive formation and reduced clearance of ROS, ROS accumulation in vascular endothelial cells leads to adverse effects mediated by activation of the polyol, protein kinase C (PKC), and hexosamine pathways, as well as the presence of increased amounts of advanced glycation end products (AGEs) and increased expression of AGE receptors together with their activating ligands (Kowluru et al., 2015; Kang and Yang, 2020). This leads to oxidative stress *in vivo*, which can result in pyroptosis, apoptosis, and autophagy (Lin and Kuang, 2014), promoting inflammation, vascular degeneration, neurodegeneration, and neovascularization (Rodríguez et al., 2019).

In addition to the well-known mechanisms described above, other mechanisms, including mitochondrial dysfunction (Ravikumar et al., 2004), decreased Nrf2 activity (Boland et al., 2008), epigenetic modification (Kowluru, 2020), and the activation or inhibition of multiple signaling pathways, have also been implicated in oxidative stress. The mitochondria in cells function as energy manufacturing factories. During adenosine triphosphate (ATP) synthesis and oxidative phosphorylation, the electron transport chain generates ROS (Dan Dunn et al., 2015), and the increase in ROS further damages mitochondrial DNA, resulting in abnormal mitochondrial function and reduced retinal function, ultimately leading to retinal damage produced by oxidative stress (Garcia Soriano et al., 2001; Madsen-Bouterse et al., 2010). It can be seen that the relationship between the mitochondria and ROS is both iterative and bidirectional. Nuclear factor E2-related factor 2 (Nrf2) is a redox-sensitive transcription factor. Wang et al. reported that silencing of Nrf2 led to increased ROS production and apoptosis in rat retinal pericytes (RRPs), a decreased B-cell lymphoma-2 (Bcl-2) to Bcl-2-associated X (BAX) ratio, and increased expression of heme oxygenase, nicotinamide adenine dinucleotide phosphate (NADP)

quinone redox reductase, superoxide dismutase 2 (SOD2), catalase, and glutamate-cysteine-ligase catalytic and modification subunits. The oxidative stress sensor DJ-1 is encoded by the *PARK7* gene and belongs to the C56 peptidase family. Overexpression of DJ-1 was found to induce Nrf2 expression leading to the controversial result (Wang et al., 2020). Zhou et al. found that forkhead box O6 (*FOXO6*) was overexpressed in vitreous samples from DR patients and a high-glucose (HG)-induced human RPE cell line (ARPE-19) and that *FOXO6* knockdown activated the Akt/Nrf2 signaling pathway (Zhou et al., 2019). These findings suggest that reductions in Nrf2 activity lead to increased oxidative stress and that Nrf2 activation may be a key strategy for the prevention of oxidative stress. However, we consider that H-RPE primary cells should also be included in investigations with these cellular models, as H-RPE primary cells maintain many important signs and functions *in vivo*. Both ARPE19 cells and H-RPE primary cells have been used as cell culture models, with H-RPE primary cells accepted as an effective primary cell culture model in recent years (Hwang et al., 2019; Udsen et al., 2022; Yang et al., 2022).

Epigenetic modifications, such as DNA methylation, histone methylation, histone acetylation, dysregulated miRNA, and lncRNA expression, mediate changes in the expression of genes associated with key regulatory pathways. Epigenetic modifications have been reported in a variety of cells in DR, together with observations of metabolic memory (Kato and Natarajan, 2019; Gao et al., 2021). Kowluru et al. demonstrated that methylation of Lysine9 on histone H3 (H3K9me3) on the Ras-related C3 botulinum toxin substrate 1 (Rac1) promoter activated Rac1 transcription, and regulation of Suv39H1-H3K9 trimethylation prevents further epigenetic modifications as well as the occurrence and development of DR (Kowluru et al., 2021).

It is well-known that high glucose levels increase the expression of lncRNA MALAT1 by increasing the binding of the Sp1 transcription factor to its promoter region, and a recent study identified a role of lncRNA MALAT1 in the regulation of the Keap1-Nrf2-antioxidant defense system in DR (Radhakrishnan and Kowluru, 2021). These authors found that retinal microvessels from STZ-induced diabetic mice and DR patients showed similar increases in lncRNA MALAT1, as well as confirming its interaction with Keap1 and decreased expression of Nrf2-mediated antioxidant defense genes. It can thus be seen that lncRNA MALAT1 can regulate the antioxidant defense system in DR through Keap1-Nrf2, suggesting that inhibition of the antioxidant defense system contributes significantly to DR pathogenesis, as has also been proposed by other authors (Kang and Yang, 2020; Saddala et al., 2020). Oxidative stress can also exert its effects through multiple signaling pathways, including the AMPK/TSC1/TSC2/RHEB pathway. AMPK can regulate the glucose metabolism pathway and can also inhibit the mTOR signaling pathway, ultimately leading to the induction of autophagy (Zhao et al., 2019).

The significance of oxidative stress is thus self-evident. It is the central link in the pathophysiology of DR and has a connecting role. Several studies support that oxidative stress should be considered a "unifying mechanism" in DR pathogenesis (Brownlee, 2005; Li et al., 2017). This suggests that antioxidant therapy would be a useful early adjuvant treatment for DR.

## DR and inflammation

In addition to the oxidative stress seen in early DR, chronic low-titer inflammation of the retina may also occur. As early as 1948, DR was known as "diabetic retinitis" (RODRIGUEZ and ROOT, 1948), and the role of pro-inflammatory mechanisms in DR has received considerable attention. Early-stage DR is characterized by various inflammation-associated features, including increased vascular permeability, increased retinal blood flow, neutrophil infiltration, macrophage infiltration, glial activation, complement activation, and tissue edema (Forrester et al., 2020). Several clinical studies have shown that the use of anti-inflammatory drugs can reduce both vascular permeability and VEGF expression, preventing cell death (Semeraro et al., 2019). This suggests that anti-inflammatory treatment is beneficial for DR.

DR-associated inflammation has been found to be mediated by factors such as leukocyte arrest, inflammation-related cytokines (such as interleukin-1β), miRNA regulation, and the activation or inhibition of signaling pathways. Studies using mice deficient in the genes encoding the cluster of differentiation 18 (CD18) and intercellular adhesion molecule 1 (ICAM-1) showed that leukocyte stasis increased within a few days after the onset of diabetes and was associated with increased expression of CD18 and ICAM-1 in the retina (Joussen et al., 2004). Despite its early onset and short duration, leukocyte stasis is considered to be a central event in inflammation (Joussen et al., 2004). However, Van et al. considered that leukocyte stasis is merely an incidental phenomenon occurring during DR (van der Wijk et al., 2017). Is leukocyte stasis associated with DR? Although this issue remains controversial, the centrality of inflammation in DR is clear. Feng et al. investigated the overexpression of high mobility group box-1 (HMGB1) resulting from exposure to high glucose, and found that overexpression of HMGB1 led to lysosomal membrane permeability (LMP) by upregulating the expression of lysosomal enzyme B; conversely, inhibition of HMGB1 expression could rescue LMP, restore autophagy-mediated degradation, reduce the expression of inflammatory factors and VEGF, and have a protective effect on apoptosis in RPE cells in the early stages of DR (Feng et al., 2022). The involvement of multiple inflammatory-associated factors has been reported in DR, including ICAM-1, CD18, IL-1β, IL-3, IL-6, IL-8, tumor necrosis factor-α (TNF-α), monocyte

chemotactic protein 1 (MCP-1), macrophage inflammatory protein 1 (MIP-1), CCL3, CCL15, and CCL21. Interestingly, some studies have found that CCL3 may be involved in the development of early DR, and CCL15 and CCL21 may be closely related to the formation of fibrovascular membranes and the progression to end-stage DR (Zeng et al., 2019), suggesting that the inflammatory response runs through DR development. Although inflammatory factors may have some protective effects in early-stage DR, the persistence of inflammation can cause cytotoxic damage. For example, the barrier effect of vascular wall pericytes caused by inflammation disappears (Ogura et al., 2017). Damage to the blood-retinal barrier accelerates the progression of DR. IL-1β is an essential inflammatory mediator derived from endothelial cells and microglia. IL-1β can be activated by nuclear factor-κB (NF-κB) to induce pericyte apoptosis, and it can also reduce the numbers of tight junction proteins in endothelial cells, ultimately enhancing endothelial cell permeability (Yun, 2021).

The regulatory mechanisms of miRNAs in DR have recently become a research hotspot. Several miRNAs have been found to influence biological processes in the retina by regulating gene expression (Bao and Cao, 2019). MiRNAs are found in adipose tissue and obesity is closely associated with chronic low-degree inflammation. Furthermore, miRNAs can directly influence the expression of inflammation-associated proteins and can also alleviate the development of DR by agonists, targeted inhibition of transcription, and other methods (Yang et al., 2020). MiRNAs are thus worthy of in-depth study and may be effective targets or biomarkers of DR treatment. Several inflammation-related signaling pathways are also activated in early-stage DR, such as the JAK-2/STAT3, PI3K/AKT, and MAPK signaling pathways; these pathways are also linked by common enzymatic reactions that are similar to signaling networks promoting the development of DR. The most-studied pathway is the PI3K/AKT signaling pathway, downstream components of which are associated with VEGF signaling, with the combined cascade of these signaling pathways ultimately driving VEGF expression and leading to vascular degeneration.

The most commonly used anti-inflammatory drugs are corticosteroids and non-steroidal anti-inflammatory drugs. The advantages of corticosteroids are the need for less frequent intraocular injections and their lower cost. However, adverse effects are common, and the overall efficacy of corticosteroids for treating PDR remains uncertain, and corticosteroids are thus not recommended for patients with PDR. IL-6 is one of the most important pro-inflammatory cytokines present in the vitreous of DR patients, Inhibition of IL-6 trans-signaling can significantly reduce oxidative stress in retinal endothelial cells and prevent retinal oxidative damage. Antibodies against IL-6 and IL-6 receptors have been developed and are currently undergoing clinical trials (Robinson et al., 2020).

## DR and neovascularization

Neovascularization develops gradually over time, starting with the destruction of the basement membrane surrounding the microvascular endothelial cells, thus allowing movement of the endothelial cells in the direction of chemokines. These migrating endothelial cells elongate, divide and eventually form tubular structures that gradually fuse over time, leading to the formation of new mature capillaries. It is well known that neovascularization plays an important role in DR pathogenesis. A summary of this pathological process is as follows: elevated blood glucose → retinal ischemia and hypoxia → capillary endothelial cell damage → capillary endothelial cell repair → capillary basement membrane hyperplasia and thickening → capillary lumen narrowing → aggravation of retinal ischemia and hypoxia → aggravation of capillary endothelial cell damage → microaneurysm formation → capillary occlusion → complete tissue hypoxia → capillary necrosis → neovascularization (Heitzig et al., 2017; Lechner et al., 2017; Scanlon, 2017). In terms of the timeline of DR development, it is apparent that early DR (NPDR) does not have any clinical symptoms, although obvious clinical discomfort may appear in late DR (PDR). In the final stages of the disease, the retina is characterized by neovascularization or hemorrhage.

Pericyte apoptosis, activation and inhibition of signaling pathways by multiple key factors, and increased VEGF all play crucial roles in neovascularization. Pericytes are important components of retinal blood vessels and their apoptosis can lead to increased vascular permeability, vascular occlusion, and microaneurysm formation. Mizutani et al. found that pericyte apoptosis in the retinas of DM patients was significantly accelerated compared with the control group (Mizutani et al., 1996). Of the various degenerative changes seen in DR microvessels, pericyte apoptosis and the presence of “pericyte ghosts” are the key histopathological hallmarks of DR. Cheng et al. reported that prostaglandin F2α (PGF2α) can reduce pericyte apoptosis by inhibiting the PI3K/Akt/GSK3β/β-catenin signaling pathway (Cheng et al., 2021). NEAT1 is a long non-coding RNA discovered in recent years. NEAT1 silencing can inhibit oxidative stress in human retinal endothelial cells, inhibit pro-inflammatory signaling, and also reduce the expression of VEGF (Shao et al., 2020). Gong et al. suggested that Roundabout 4 (ROBO4) was involved in neovascularization and that its expression varies with DR severity, and they found that targeting HIF-1α/SP1-dependent ROBO4 expression by miR-125b-5p/miR-146a-5p could delay DR progression (Gong et al., 2019). There are still many signaling pathway regulatory mechanisms to be explored, and the in-depth study of signaling pathways has become a fundamental way to explain disease mechanisms. The angiopoietin (Ang)/Tie2 signaling axis is a key regulator of neovascularization. The combination of Ang-2 and Tie2 destroys the stability of local blood vessels, causes vascular leakage, promotes vascular endothelial cell migration,

and ultimately leads to pathological neovascularization. Ang plays an important role in regulating vascular remodeling and maturation in the later stages of neovascularization. It has been proposed that inhibition of Ang-2 expression through regulation of the Ang/Tie2 signaling axis may be a potential therapeutic strategy for DR patients (Brkovic et al., 2007; Campochiaro and Peters, 2016). Currently, in addition to anti-VEGF drugs, several anti-angiogenic drugs are in clinical trials, including squalamine, AKB-9778 (Tie2 activator), Nesvacumab (anti-Ang-2), and RO6867461 (bispecific antibody: anti-Ang-2 + anti-VEGF). The discovery of these drugs is based on in-depth research into the mechanism of DR (Wang and Lo, 2018).

The growth factors closely related to DR include VEGF, erythropoietin (EPO), insulin-like growth factor (IGF), transforming growth factor-β (TGF-β), basic fibroblast growth factor (BFGF), CCN2/CTGF, hematopoietic growth factor (HGF), platelet-derived growth factor (PDGF), and epidermal growth factor (EGF). Although these growth factors have all been shown to be associated with DR, it was recently found that EPO can maintain the internal blood-retinal barrier (IBRB) by activating Src/Akt/cofilin signaling in microglia and inhibiting microglial phagocytosis. Although these data support the potential of EPO in the treatment of DR, VEGF still remains the research hotspot (Xie et al., 2021). VEGF is an angiogenic factor and it is the strongest selective mitogenic factor for endothelial cells. VEGF-A is the most important member of the VEGF family, and binds to the key receptor VEGFR2, stimulating the proliferation, migration, survival, and increased permeability of vascular endothelial cells, ultimately leading to neovascularization (Ferrão et al., 2019). Although VEGF is a causative factor for PDR, it is also required for normal vascular growth and plays a crucial role in maintaining endothelial cell integrity. Mima et al. found that while inflammation and oxidative stress can induce VEGF expression, they also suggested that, in addition to inflammation and oxidative stress, factors such as persistent hyperglycemia may induce VEGF expression (Mima et al., 2012). Excessive VEGF expression can disrupt the intracellular barrier, increase leakage of the choroid plexus endothelium, cause edema, and activate inflammatory signaling pathways (Kinoshita et al., 2016). Recently, Hachana et al. found that the anti-VEGF and B1 receptor antagonist (R-954) reduced the levels of B1 and B2 receptors, TNF-α, and ICAM-1 in choroidal neovascularization, and also downregulated the expression of VEGF-A, VEGF-R2, HIF-1α, CCL2, and VCAM-1 (Hachana et al., 2020). These findings indicate both the complexity of DR pathogenesis and the close relationships between the responsible mechanisms. Clinically, the most commonly used drugs for treating DR are anti-VEGF substances that can protect the function of the vascular wall, reduce retinal microvascular leakage, alleviate local ischemia and hypoxia, and inhibit neovascularization (Bressler et al., 2017). These anti-VEGF drugs include pegaptanib, ranibizumab, aflibercept, and bevacizumab. Intravitreal ranibizumab has been shown to benefit patients more than laser therapy (Massin et al., 2010) while aflibercept was found to be superior to ranibizumab and bevacizumab in improving vision in patients with moderate or severe vision loss (Wells et al., 2015). The method of injecting anti-VEGF drugs directly into the eyes of patients has been widely used in the treatment of DR. Although this invasive approach cannot completely cure DR, anti-VEGF drugs are still the first choice of first-line treatment.

## DR and neurodegeneration

Although the clinical classification of DR is based on the degree of neovascularization in patients, several studies have reported the presence of neuronal and glial changes in the retina before neovascularization (Carpineto et al., 2016). From another perspective, DR can also be regarded as a neurodegenerative disease. Neurodegeneration is often associated with mechanisms such as oxidative stress, impaired antioxidant defense mechanisms, imbalance of neuroprotective factors, glutamate excitotoxicity, mitochondrial dysfunction, activation of the renin-angiotensin system, and phosphorylation of the microtubule-associated protein tau (Masser et al., 2017; Sinclair and Schwartz, 2019; Pillar et al., 2020). The roles of oxidative stress and neovascularization in DR have also been extensively studied. Studies have found that in the retinas of diabetic mice, inhibition of ROS production can effectively block DR development and the caspase-3-mediated apoptosis of retinal neurons. It is apparent that these roles do not exist independently but are interrelated (Sasaki et al., 2010). Studies have shown that compared with non-diabetic patients, the retinas of diabetic patients have reduced levels of a variety of neuroprotective factors, such as pigment epithelium-derived growth factor (PEDF), somatostatin (SST), and interstitial retinol-binding protein (IRBP). Reduced expression of IRBP is observed in the very early stages of DR and has also been associated with retinal neurodegeneration. In addition to the down-regulation of neuroprotective factors and up-regulation of neurotrophic and survival factors, VEGF and EPO have been found to be overexpressed in patients with early DR. As mentioned earlier, neurodegeneration is thought to occur before vascular degeneration, suggesting the possibility that factors that have been linked to early-stage DR may be more closely associated with neurodegeneration than with blood vessels. This deserves attention. In a recent American Diabetes Association statement, DR was defined as a highly tissue-specific neurovascular complication, and it can be observed that the analysis of nerves or blood vessels alone is becoming less and less meaningful. Thus, blood vessels and nerves are inextricably linked. We should thus not define DR from a single perspective but should consider the interrelationships between multiple factors for a full understanding of the complexity of this disease (Oshitari, 2021).

When we realize that neurodegeneration is an early event in DR, therapeutic drugs based on neuroprotection become meaningful. Such drugs include somatostatin, nerve growth factor (NGF) and brain-derived neurotrophic factor (BDNF) (Simó and Hernández, 2014). In addition to confining the therapeutic targets to neurons, we should aim to restore the functions of damaged Müller cells and microglia. We should no longer limit DR treatment to one method only but should instead adopt a comprehensive treatment strategy, such as focusing on preventing the leakage of blood vessels, inhibiting the formation of new blood vessels, rebuilding the blood supply of the retina, and strengthening protection of the nerves, representing the ultimate goal for treating DR. It is important to realize that DR is a disease characterized by cross-links and interrelationships between nerves and blood vessels, and retinal dysfunction is the product of a complex array involving multiple inter-dependent mechanisms.

## DR and NVU

The concept of the neurovascular unit (NVU) was first formalized at the 2001 National Institute of Neurological Disorders and Stroke's Stroke Progress Review Group meeting and has since been applied to the retina (Iadecola, 2017). The NVU includes neurons, glia, immune cells, and vascular cells; however, both the functional coupling and interdependence among these cells are important for maintaining hemostatic function and regulating neuronal activity (Liu et al., 2019). All the constituent cells of the NVU are integrated to maintain the integrity of the inner blood-retinal barrier and to dynamically regulate local blood flow (Simó and Hernández, 2014). Disruption of the NVU may lead to the structural or functional impairment of both microvessels and neurons. NVU lesions can be caused by a variety of factors, such as neuronal loss, glial cell loss, and changes in the vasculature (Xia et al., 2021). There are several very interesting points concerning our knowledge of the NVU, namely, the influence of changes in associated factors and signal transmission, and the influence of Müller cells. Active neurotrophic factors are essential for retinal homeostasis, and when these factors are up-regulated, they produce strong angiogenic results in addition to their neuroprotective effects (Simó et al., 2014). Among them, VEGF, IGF-1, EPO, and secretogranin III (SCGIII) are the most important. Hernandez et al. showed that the pro-angiogenic effect of VEGF was weak during early-stage DR where the expression and release of VEGF functioned only to protect retinal neurons (Hernández et al., 2016). Hombrebueno et al. found that low levels of amacrine and ganglion cell death and albumin leakage occurred after continuous injection of anti-VEGF drugs in Akita mice (Hombrebueno et al., 2015). These results show that reducing VEGF levels can aggravate retinal neurodegeneration. In contrast, Rojo Arias et al. found that applying aflibercept (VEGF-Trap) to OIR mice not only alleviated retinal microvascular aberrations but also significantly improved the neural function of the retina (Rojo Arias et al., 2020). The reason for the discrepancies in these findings may be due to different drug dosages, different methods of drug use, and the different time nodes of onset. However, the findings indicate that these neuroprotective effects require further study. IGF-1 is considered to be a pleiotropic factor, mainly produced by endothelial cells, pericytes, and RPE cells. It acts as a survival factor for retinal microvascular endothelial cells and nerve cells and can play a key role in retinal immune regulation (García-Ramírez et al., 2008; Arroba et al., 2018). EPO overexpression is an early event in the retina of diabetic patients, and EPO is a potential neuroprotective factor that can mobilize endothelial progenitor cells to damaged retinal sites and is involved in the reconstruction of tissue injury (Chen et al., 2008). Similar to VEGF, SCGIII is also a pro-angiogenic factor similar to VEGF but, while VEGF is expressed in both normal and abnormal blood vessels, leading to potential drawbacks associated with anti-VEGF therapy, the expression of SCGIII is very specific. Li et al. found that the specific expression of SCGIII in retinal blood vessels of diabetic patients was as high as 97.69% with no specific expression in normal peripheral capillaries, and that expression of the SCGIII receptor was significantly increased in diabetic neonatal retinal vascular endothelial cells (Li et al., 2018). LeBlanc et al. observed that anti-SCGIII agents could prevent retinal neovascularization in mice with hypoxia-induced retinopathy, and suggested that SCGIII had great potential as a novel target for DR therapy (LeBlanc et al., 2017).

The NVU includes Müller cells, astrocytes, ganglion cells, amacrine cells, horizontal cells, bipolar cells, endothelial cells, pericytes, microglia, macrophages, and basement membrane. Recently, Alarcon-Martinez found that interpericyte tunneling nanotubes (IP-TNTs) can mediate signal transmission between pericytes, and that the NVU can also maintain homeostasis by regulating blood flow, vascular density, and vascular permeability (Alarcon-Martinez et al., 2020). In the NVU, neurons receive nutrients and eliminate metabolic wastes by regulating vascular activity (Nian et al., 2021), and glial cells play a synergistic role in blood vessels to eliminate metabolites, transmit neurotransmitters, maintain homeostasis, and transduce signals (Filosa et al., 2016). A characteristic change seen in DR is the increased expression of glial fiber acidic protein in the Müller cells. Furthermore, while activation of Müller cells is not the cause of neurodegeneration, it promotes neuroprotection through the activation of extracellular signal-regulated kinase 1/2 (ERK1/2) (Matteucci et al., 2014). Müller cells are closely connected with both retinal blood vessels and neurons, and Müller cells play important roles in glutamate metabolism, extracellular ion homeostasis, and neuronal function. Both Müller cells and ganglion cells secrete BDNF, and it has been found that down-regulation of BDNF expression in the diabetic

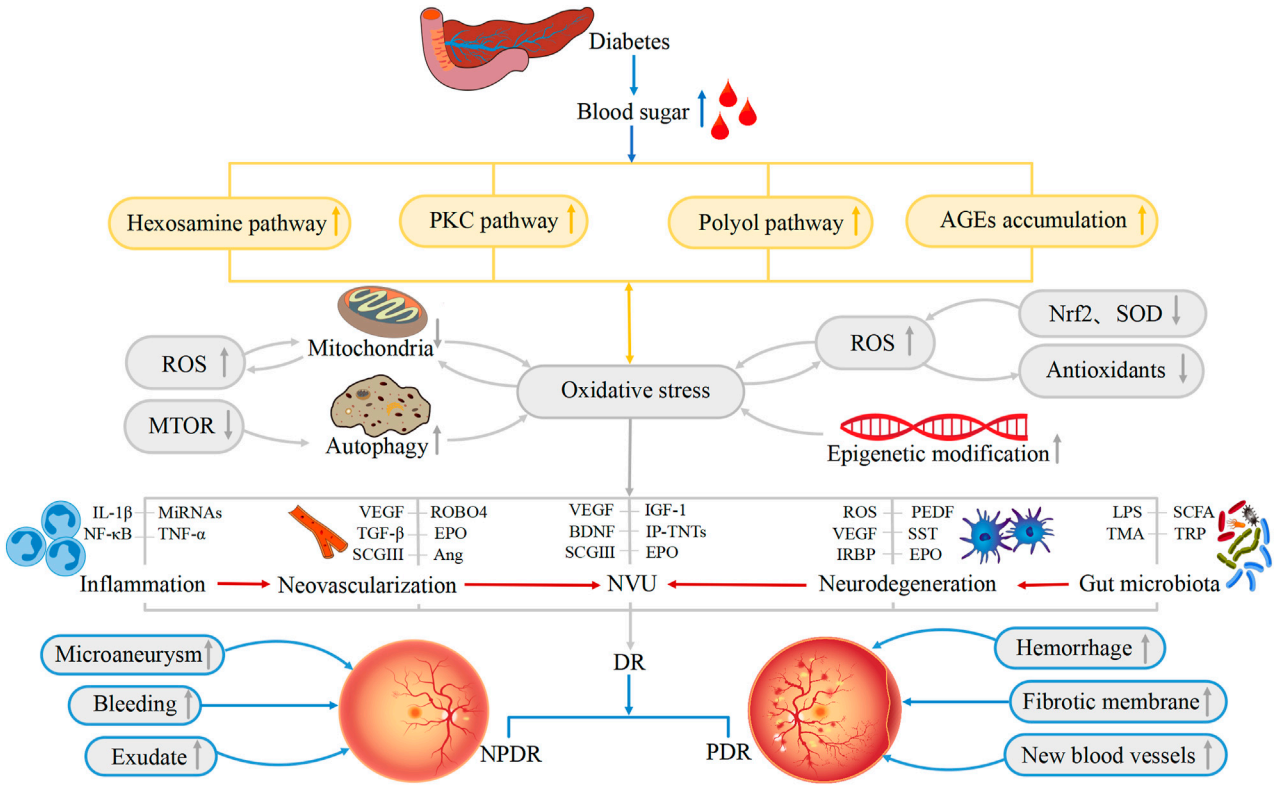


FIGURE 2
Physiological changes associated with the development of DR. Hexosamine pathway, polyol pathway, PKC pathway and AGEs accumulation lead to the occurrence of oxidative stress. Oxidative stress, inflammation, neovascularization, neurodegeneration, NVU, and gut microbiota are all involved in the pathogenesis of DR. ROS, Nrf2, SOD, IL-1β, VEGF, CSGIII, LPS and other substances also directly or indirectly lead to the occurrence of DR, resulting in the appearance of Microaneurysm, Fibrotic membrane, and New blood vessels and so on in the retina. These factors are interrelated and thus contribute to the development of DR.

retina can protect retinal neurons through the TrkB/ERK/MAPK signaling pathway (Liu et al., 2013; Le et al., 2021). These findings suggest that appropriate supplementation of neurotrophic factors could improve DR.

As hyperglycemia can cause changes in all the cells within the retinal NVU, the NVU could be used as one of the early therapeutic targets for DR (Gardner and Davila, 2017; Kugler et al., 2021; Simó et al., 2021). The same strategies for treating neovascularization and neurodegeneration apply to the NVU. In general, rather than studying the roles of the neurovascular cells only, we would recommend studying the NVU as a whole, especially as an early warning of DR, which would be helpful for the early prevention and early treatment of DR.

## DR and gut microbiota

Evidence suggests that the composition, modification, and disturbance of the gut microbiota can affect important physiological processes *in vivo* and that the gut microbiota may contribute to diseases including chronic inflammation, immune system imbalances, type 2 diabetes, chronic kidney disease, and rheumatoid arthritis (Scirocco et al., 2016; Schoeler and Caesar, 2019; Yang C Y et al., 2021). Similarly, the close relationship between the gut microbiota and uveitis and glaucoma, as well as age-related macular degeneration, illustrates the significance of the gut microbiota to disease susceptibility and development (Jiao et al., 2021). The gut microbiota forms a crucial part of the body and plays a powerful role in the maintenance of normal metabolism and immune regulation. Changes in environmental, immune, genetic, or host factors can disrupt the balance of the gut microbiota. Such disturbance in association with hyperglycemia can lead to disruption of the gut barrier, resulting in damage to multiple organs. Dysregulation of the gut microbiota by hyperglycemia in patients with type 2 diabetes leads to bacterial translocation and intestinal endotoxin accumulation, resulting in intestinal inflammation (Yang G et al., 2021). Lipopolysaccharide (LPS)

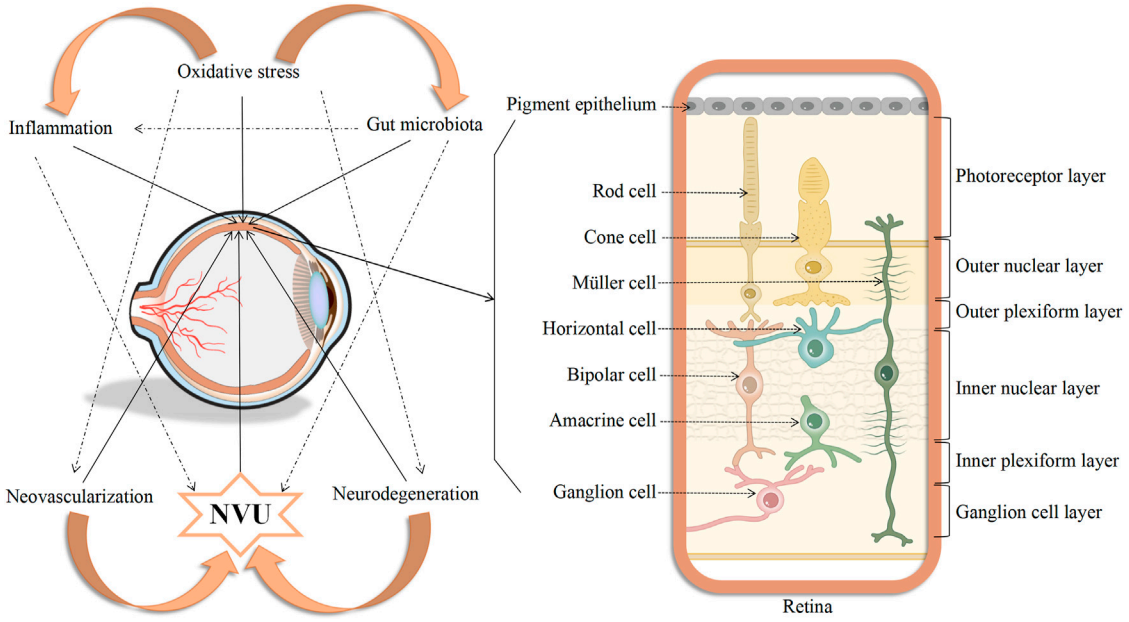


FIGURE 3
Diagram showing the interconnectedness between oxidative stress, inflammation, neovascularization, neurodegeneration, neurovascular unit, and gut microbiota, as well as the simulated picture of cells affected in the retina of DR.

derived from *Bacteroides* and Desulfobacteria in the gut is a major substance associated with microbial translocation during chronic inflammation, and LPS can accumulate in the gut and enter the bloodstream, causing metabolic endotoxemia. Vagaja et al. found that systemic exposure to LPS in Ins2 Akita mice may accelerate retinal capillary endothelial cell damage, suggesting that endotoxin-mediated retinal inflammation may affect the DR phenotype (Vagaja et al., 2013). Gut microbes are not only associated with inflammation but also with neurodegeneration. High glucose levels in the body can induce the expression of Toll-like receptor (TLR-4) in retinal ganglion cells, resulting in the expression of TNF-α, IL-8, and NF-κB and promoting activation of microglial glycosylase, as well as increased vascular permeability, ultimately resulting in neuronal damage (Campo et al., 2010). The composition of the gut microbiota can affect the levels of LPS, short-chain fatty acids (SCFA), bile acids, trimethylamine (TMA), and tryptophan (TRP) in the blood circulation. DM complications have been reported to be associated with the gut microbiota, leading to insulin resistance, chronic inflammation, and imbalances in immune regulation (Huang et al., 2021). It has been found that tryptophan, serotonin, and canine uric acid are closely related, and they can reflect the functioning of the "intestinal-brain axis" (Yano et al., 2015).

It is well known that there is a close relationship between retinal and brain microvessels. Several recent studies have proposed the concept of a "gut-retinal axis" and have investigated the relationships between the gut microbiota, DM, and DR. Rowan et al. found that the gut microbiota and its metabolites (tryptophan, serotonin, and maluric acid) can act within the "gut-retinal axis" (Rowan et al., 2017). Huang et al. investigated the changes in the composition of the gut microbiota in DM and DR and constructed a microbiota-based model that could effectively distinguish between DR and DM patients, as well as identify potential therapeutic targets for DR (Huang et al., 2021). Andriessen et al. demonstrated that high-fat diet-induced obesity leads to gut microbiota dysbiosis, which was found to drive retinal inflammation and pathological neovascularization in a mouse model of laser photocoagulation-induced choroidal neovascularization (CNV) (Andriessen et al., 2016). This series of studies have suggested potential mechanisms through which the gut microbiota affects the pathophysiology of ocular diseases. Therefore, we can boldly speculate that there is a strong association between both the gut microbiota and its metabolites, suggesting potential as future biomarkers for the clinical diagnosis and treatment of DR.

All in all, the gut microbiota is now considered to represent an additional human organ that has co-evolved with the host. Growing evidence suggests the crucial role played by the microbiota in the development of T2DM. Dysregulation of the gut microbiota leads to persistent inflammation and immunosenescence, both of which may be involved in the pathogenesis of DR. Beli et al. found that INT-767

prevented DR in a mouse model of diabetes. Notably, INT-767 is a potent and selective agonist and modulator of the farnesoid X receptor (FXR) and bile acid G protein-coupled membrane receptor 5 (TGR5) (Beli et al., 2018). Tauroursodeoxycholate (TUDCA) is an endoplasmic reticulum stress inhibitor and a neuroprotective secondary bile acid. TUDCA can affect glucose and lipid metabolism by regulating FXR and TGR5. Overall, changes in the gut microbiota lead to the production of TUDCA, which promotes TGR5 activation in retinal neurons to prevent DR. At present, there is insufficient research on the "gut-retinal axis" and there has been no dynamic monitoring of the gut microbiota. It is thus necessary to conduct longer-term and sustained research observations, and to further study the role of gut microbiota in DR from the cellular and molecular levels through multi-omics approaches, which will help us understand the underlying mechanism of the "gut-retinal axis". At present, there is no specific drug for the treatment of DR, and it may be possible to use the gut microbiota as an interventional measure for DR by adjusting the types, quantity, and microenvironments of the gut microbiota, and to predict the risk of DR.

## Conclusion

In summary, the pathophysiological mechanisms underlying DR are complex and include a variety of contributory factors, such as oxidative stress, inflammation, neovascularization, neurodegeneration, the NVU, and the gut microbiota. Oxidative stress is one of the primary triggers of inflammatory cascades and, in addition, both oxidative stress and inflammation increase the levels of retinal autophagy, leading to cellular dysfunction, necrosis, apoptosis, and death. The affected cells may be nerve cells, endothelial cells, pericytes, RPE cells, and glial cells which, in turn, lead to further abnormalities in neovascularization, neurodegeneration, and the NVU. All these factors may have subtle interactions with each other, ultimately contributing to the development of DR (Figure 2). However, more evidence is required on the factors controlling DR progression. Therefore, the integration of knowledge on these mechanisms allowing the construction of a complete network of factors contributing to the disease will surely provide sufficient theoretical basis for formulating new treatment strategies based on current clinical diagnosis and treatment (Figure 3).

Although the etiology and pathology of DR has been extensively studied for half a century, its treatment still presents great challenges. Conventional drugs can be used to control hyperglycemia, hypertension, and hyperlipidemia. However, the effects of these basic treatment methods are limited. There are also some targeted treatments for DR, such as topical surgery, topical laser therapy, and single-component drugs (anti-VEGF or steroid drugs). However, surgical treatment is only indicated for PDR cases with non-clearing vitreous hemorrhage or traction retinal detachment. Some new methods are replacing traditional laser treatment methods, including pattern scanning laser (PASCAL), micropulse technology, and the navigation laser system (NAVILAS). Although anti-VEGF drugs are the first-line treatment strategy, there are still many limitations associated with the use of a single treatment strategy. It is possible that as more therapeutic strategies and critical molecules are discovered that anti-VEGF drugs may cease to be first-line drugs for the treatment of DR and VEGF may be supplanted as the star molecule of DR. As mentioned above, there are several factors that have great potential to be new targets for DR therapy, including SCGIII, miRNAs, and the gut microbiota. In addition, new therapeutic drugs are also being developed, such as cardiolipin targeting peptide (MTP-131), lipoic acid, lutein, ARA290, and dalapradib (Wang and Lo, 2018). Unfortunately, there are currently no therapeutic strategies that can fully reverse the retinal damage caused by DR. Proposed new treatment strategies include traditional Chinese medicine treatment, targeted therapy, gene therapy, stem cells therapy, and nanotechnology. Although most of these have not yet entered clinical trials, it is likely that there will be earlier and faster detection of the pathophysiological changes in DR in the future. We hope to observe the progression of a patient's disease in a more individualized and longitudinal manner to avoid the occurrence and development of DR.

## Author contributions

LW, HY, and XS wrote the manuscript. LW helped drew the figures. CF, RL, and SZ revised the manuscript. All authors contributed to the article and approved the submitted version.

## Funding

This work was supported by National Key R & D Program of China (Grant Number: 2018YFC1004300), National Natural Science Foundation Project of China (Grant Number: 82160154), the Key Project of Guizhou Provincial Science and Technology Department (Grant Number: QKH-JC-2019-1464), the Excellent Talent Support Program of Guizhou Provincial Education Department (Grant Number: QJH-KY-2017-077), the Science and Technology Foundation of Guizhou Province (QKH-PTRC-2018-5772-042), the Science and Technology Foundation of Guizhou Provincial Health Commission (grant number: gzwkj2022-268), the Project of Development Research Center of Guizhou Provincial Dendrobium Industry (grant number: QSKH [2019003013]), the Program for Excellent Young Talents of Zunyi

Medical University (18-ZY-001), and the Science and Technology Program Project of Zunyi (ZSKH-HZ -2020-35).

## Conflict of interest

The authors declare that the research was conducted in the absence of any commercial or financial relationships that could be construed as a potential conflict of interest.

## Publisher's note



## References

Alarcon-Martinez, L., Villafranca-Baughman, D., Quintero, H., Kacerovsky, J. B., Dotigny, F., Murai, K. K., et al. (2020). Interpericyte tunnelling nanotubes regulate neurovascular coupling. *Nature* 585 (7823), 91–95. doi:10.1038/s41586-020-2589-x

Andriessen, E. M., Wilson, A. M., Mawambo, G., Dejda, A., Miloudi, K., Sennlaub, F., et al. (2016). Gut microbiota influences pathological angiogenesis in obesity-driven choroidal neovascularization. *EMBO Mol. Med.* 8, 1366–1379. doi:10.15252/emmm.201606531

Antonetti, D. A., Silva, P. S., and Stitt, A. W. (2021). Current understanding of the molecular and cellular pathology of diabetic retinopathy. *Nat. Rev. Endocrinol.* 17 (4), 195–206. doi:10.1038/s41574-020-00451-4

Arroba, A. I., Campos-Caro, A., Aguilar-Diosdado, M., and Valverde, Á. M. (2018). IGF-1, inflammation and retinal degeneration: A close network. *Front. Aging Neurosci.* 10, 203. doi:10.3389/fnagi.2018.00203

Bao, X. Y., and Cao, J. (2019). MiRNA-138-5p protects the early diabetic retinopathy by regulating NOVA1. *Eur. Rev. Med. Pharmacol. Sci.* 23 (18), 7749–7756. doi:10.26355/eurrev_201909_18984

Beli, E., Yan, Y., Moldovan, L., Vieira, C. P., Gao, R., Duan, Y., et al. (2018). Restructuring of the gut microbiome by intermittent fasting prevents retinopathy and prolongs survival in db/db Mice. *Diabetes* 67, 1867–1879. doi:10.2337/db18-0158

Boland, B., Kumar, A., Lee, S., Platt, F. M., Wegiel, J., Yu, W. H., et al. (2008). Autophagy induction and autophagosome clearance in neurons: Relationship to autophagic pathology in alzheimer's disease. *J. Neurosci.* 28 (27), 6926–6937. doi:10.1523/JNEUROSCI.0800-08.2008

Bressler, S. B., Liu, D., Glassman, A. R., Blodi, B. A., Castellarin, A. A., Jampol, L. M., et al. (2017). Change in diabetic retinopathy through 2 Years: Secondary analysis of a randomized clinical trial comparing aflibercept, bevacizumab, and ranibizumab. *JAMA Ophthalmol.* 135 (6), 558–568. doi:10.1001/jamaophthalmol.2017.0821

Brkovic, A., Pelletier, M., Girard, D., and Sirois, M. G. (2007). Angiopoietin chemotactic activities on neutrophils are regulated by PI-3K activation. *J. Leukoc. Biol.* 81, 1093–1101. doi:10.1189/jlb.0906580

Brownlee, M. (2005). The pathobiology of diabetic complications: A unifying mechanism. *Diabetes* 54, 1615–1625. doi:10.2337/diabetes.54.6.1615

Campo, G. M., Avenoso, A., Campo, S., D'Ascola, A., Nastasi, G., and Calatroni, A. (2010). Molecular size hyaluronan differently modulates toll-like receptor-4 in LPS-induced inflammation in mouse chondrocytes. *Biochimie* 92, 204–215. doi:10.1016/j.biochi.2009.10.006

Campochiaro, P. A., and Peters, K. G. (2016). Targeting Tie2 for treatment of diabetic retinopathy and diabetic macular edema. *Curr. Diab. Rep.* 16, 126. doi:10.1007/s11892-016-0816-5

Carpineto, P., Toto, L., Aloia, R., Ciciarelli, V., BorrElli, E., Vitacolonna, E., et al. (2016). Neuroretinal alterations in the early stages of diabetic retinopathy in patients with type 2 diabetes mellitus. *Eye* 30 (5), 673–679. doi:10.1038/eye.2016.13

Chen, J., Connor, K. M., Aderman, C. M., and Smith, L. E. (2008). Erythropoietin deficiency decreases vascular stability in mice. *J. Clin. Invest.* 118 (2), 526–533. doi:10.1172/JCI33813

Cheng, Y., Peng, L., Deng, X., Li, T., Guo, H., Xu, C., et al. (2021). Prostaglandin F2α protects against pericyte apoptosis by inhibiting the PI3K/Akt/GSK3β/β-catenin signaling pathway. *Ann. Transl. Med.* 9 (12), 1021. doi:10.21037/atm-21-2717

Dan Dunn, J., Alvarez, L. A., Zhang, X., and Soldati, T. (2015). Reactive oxygen species and mitochondria: A nexus of cellular homeostasis. *Redox Biol.* 6, 472–485. doi:10.1016/j.redox.2015.09.005

Feng, L., Liang, L., Zhang, S., Yang, J., Yue, Y., and Zhang, X. (2022). HMGB1 downregulation in retinal pigment epithelial cells protects against diabetic retinopathy through the autophagy-lysosome pathway. *Autophagy* 18 (2), 320–339. doi:10.1080/15548627.2021.1926655

Ferrão, J., Bonfim Neto, A. P., da Fonseca, V. U., Sousa, L., and Papa, P. C. (2019). Vascular endothelial growth factor C treatment for mouse hind limb lymphatic revascularization. *Vet. Med. Sci.* 5 (2), 249–259. doi:10.1002/vms3.151

Filosa, J. A., Morrison, H. W., Iddings, J. A., Du, W., and Kim, K. J. (2016). Beyond neurovascular coupling, role of astrocytes in the regulation of vascular tone. *Neuroscience* 323, 96–109. doi:10.1016/j.neuroscience.2015.03.064

Forrester, J. V., Kuffova, L., and Delibegovic, M. (2020). The role of inflammation in diabetic retinopathy. *Front. Immunol.* 11, 583687. doi:10.3389/fimmu.2020.583687

Gao, L. M., Fu, S., Liu, F., Wu, H. B., and Li, W. J. (2021). Astragalus polysaccharide regulates miR-182/bcl-2 Axis to relieve metabolic memory through suppressing mitochondrial damage-mediated apoptosis in retinal pigment epithelial cells. *Pharmacology* 106 (9-10), 520–533. doi:10.1159/000515901

Garcia Soriano, F., Virág, L., Jagtap, P., Szabo, E., Mabley, J. G., Liaudet, L., et al. (2001). Diabetic endothelial dysfunction: The role of poly(ADP-ribose) polymerase activation. *Nat. Med.* 7 (1), 108–113. doi:10.1038/83241

García-Ramírez, M., Hernández, C., and Simó, R. (2008). Expression of erythropoietin and its receptor in the human retina: A comparative study of diabetic and nondiabetic subjects. *Diabetes Care* 31 (6), 1189–1194. doi:10.2337/dc07-2075

Gardner, T. W., and Davila, J. R. (2017). The neurovascular unit and the pathophysiologic basis of diabetic retinopathy. *Graefes Arch. Clin. Exp. Ophthalmol.* 255 (1), 1–6. doi:10.1007/s00417-016-3548-y

Gong, Q., Xie, J., Li, Y., Liu, Y., and Su, G. (2019). Enhanced ROBO4 is mediated by up-regulation of HIF-1α/SP1 or reduction in miR-125b-5p/miR-146a-5p in diabetic retinopathy. *J. Cell. Mol. Med.* 23 (7), 4723–4737. doi:10.1111/jcmm.14369

Hachana, S., Fontaine, O., Sapieha, P., Lesk, M., Couture, R., and Vaucher, E. (2020). The effects of anti-VEGF and kinin B(1) receptor blockade on retinal inflammation in laser-induced choroidal neovascularization. *Br. J. Pharmacol.* 177 (9), 1949–1966. doi:10.1111/bph.14962

Heitzig, N., Brinkmann, B. F., Koerdt, S. N., Rosso, G., Shahin, V., and Rescher, U. (2017). Annexin A8 promotes VEGF-A driven endothelial cell sprouting. *Cell adh. Migr.* 11 (3), 275–287. doi:10.1080/19336918.2016.1264559

Hernández, C., Dal Monte, M., Simó, R., and Casini, G. (2016). Neuroprotection as a therapeutic target for diabetic retinopathy. *J. Diabetes Res.* 2016, 9508541. doi:10.1155/2016/9508541

Hombrebueno, J. R., Ali, I. H., Xu, H., and Chen, M. (2015). Sustained intraocular VEGF neutralization results in retinal neurodegeneration in the Ins2(Akita) diabetic mouse. *Sci. Rep.* 5, 18316. doi:10.1038/srep18316

Huang, Y., Wang, Z., Ma, H., Ji, S., Chen, Z., Cui, Z., et al. (2021). Dysbiosis and implication of the gut microbiota in diabetic retinopathy. *Front. Cell. Infect. Microbiol.* 11, 646348. doi:10.3389/fcimb.2021.646348

Hwang, N., Kwon, M. Y., Woo, J. M., and Chung, S. W. (2019). Oxidative stress-induced pentraxin 3 expression human retinal pigment epithelial cells is involved in the pathogenesis of age-related macular degeneration. *Int. J. Mol. Sci.* 20, E6028. doi:10.3390/ijms20236028

Iadecola, C. (2017). The neurovascular unit coming of age: A journey through neurovascular coupling in health and disease. *Neuron* 96, 17–42. doi:10.1016/j.neuron.2017.07.030

Jiao, J., Yu, H., Yao, L., Li, L., Yang, X., and Liu, L. (2021). Recent insights into the role of gut microbiota in diabetic retinopathy. *J. Inflamm. Res.* 14, 6929–6938. doi:10.2147/JIR.S336148

Joussen, A. M., Poulaki, V., Le, M. L., Koizumi, K., Esser, C., Janicki, H., et al. (2004). A central role for inflammation in the pathogenesis of diabetic retinopathy. *FASEB J.* 18 (12), 1450–1452. doi:10.1096/fj.03-1476fje

Kang, Q., and Yang, C. (2020). Oxidative stress and diabetic retinopathy: Molecular mechanisms, pathogenetic role and therapeutic implications. *Redox Biol.* 37, 101799. doi:10.1016/j.redox.2020.101799

Kato, M., and Natarajan, R. (2019). Epigenetics and epigenomics in diabetic kidney disease and metabolic memory. *Nat. Rev. Nephrol.* 15 (6), 327–345. doi:10.1038/s41581-019-0135-6

Kinoshita, S., Noda, K., Saito, W., Kanda, A., and Ishida, S. (2016). Vitreous levels of vascular endothelial growth factor-B in proliferative diabetic retinopathy. *Acta Ophthalmol.* 94 (6), e521–3. doi:10.1111/aos.12969

Kowluru, R. A., Kowluru, A., Mishra, M., and Kumar, B. (2015). Oxidative stress and epigenetic modifications in the pathogenesis of diabetic retinopathy. *Prog. Retin. Eye Res.* 48, 40–61. doi:10.1016/j.preteyeres.2015.05.001

Kowluru, R. A., Radhakrishnan, R., and Mohammad, G. (2021). Regulation of Rac1 transcription by histone and DNA methylation in diabetic retinopathy. *Sci. Rep.* 11 (1), 14097. doi:10.1038/s41598-021-93420-4

Kowluru, R. A. (2020). Retinopathy in a diet-induced type 2 diabetic rat model and role of epigenetic modifications. *Diabetes* 69 (4), 689–698. doi:10.2337/db19-1009

Kugler, E. C., Greenwood, J., and MacDonald, R. B. (2021). The "Neuro-Glial-Vascular" unit: The role of glia in neurovascular unit formation and dysfunction. *Front. Cell Dev. Biol.* 9, 732820. doi:10.3389/fcell.2021.732820

Kuiper, E. J., Van Nieuwenhoven, F. A., de Smet, M. D., van Meurs, J. C., Tanck, M. W., Oliver, N., et al. (2008). The angio-fibrotic switch of VEGF and CTGF in proliferative diabetic retinopathy. *PLoS ONE* 3, e2675. doi:10.1371/journal.pone.0002675

Le, Y. Z., Xu, B., Chucair-Elliott, A. J., Zhang, H., and Zhu, M. (2021). VEGF mediates retinal müller cell viability and neuroprotection through BDNF in diabetes. *Biomolecules* 11 (5), 712. doi:10.3390/biom11050712

LeBlanc, M. E., Wang, W., Chen, X., Caberoy, N. B., Guo, F., Shen, C., et al. (2017). Secretogranin III as a disease-associated ligand for antiangiogenic therapy of diabetic retinopathy. *J. Exp. Med.* 214 (4), 1029–1047. doi:10.1084/jem.20161802

Lechner, J., O'Leary, O. E., and Stitt, A. W. (2017). The pathology associated with diabetic retinopathy. *Vis. Res.* 139, 7–14. doi:10.1016/j.visres.2017.04.003

Li, C., Miao, X., Li, F., Wang, S., Liu, Q., Wang, Y., et al. (2017). Oxidative stress-related mechanisms and antioxidant therapy in diabetic retinopathy. *Oxid. Med. Cell. Longev.* 2017, 9702820. doi:10.1155/2017/9702820

Li, W., Webster, K. A., LeBlanc, M. E., and Tian, H. (2018). Secretogranin III: A diabetic retinopathy-selective angiogenic factor. *Cell. Mol. Life Sci.* 75 (4), 635–647. doi:10.1007/s00018-017-2635-5

Lin, W. J., and Kuang, H. Y. (2014). Oxidative stress induces autophagy in response to multiple noxious stimuli in retinal ganglion cells. *Autophagy* 10 (10), 1692–1701. doi:10.4161/auto.36076

Liu, J., Wang, Y. H., Li, W., Liu, L., Yang, H., Meng, P., et al. (2019). Structural and functional damage to the hippocampal neurovascular unit in diabetes-related depression. *Neural Regen. Res.* 14, 289–297. doi:10.4103/1673-5374.244794

Liu, Y., Tao, L., Fu, X., Zhao, Y., and Xu, X. (2013). BDNF protects retinal neurons from hyperglycemia through the TrkB/ERK/MAPK pathway. *Mol. Med. Rep.* 7 (6), 1773–1778. doi:10.3892/mmr.2013.1433

Madsen-Bouterse, S. A., Zhong, Q., Mohammad, G., Ho, Y. S., and Kowluru, R. A. (2010). Oxidative damage of mitochondrial DNA in diabetes and its protection by manganese superoxide dismutase. *Free Radic. Res.* 44 (3), 313–321. doi:10.3109/10715760903494168

Masser, D. R., Otalora, L., Clark, N. W., Kinter, M. T., Elliott, M. H., and Freeman, W. M. (2017). Functional changes in the neural retina occur in the absence of mitochondrial dysfunction in a rodent model of diabetic retinopathy. *J. Neurochem.* 143 (5), 595–608. doi:10.1111/jnc.14216

Massin, P., Bandello, F., Garweg, J. G., Hansen, L. L., Harding, S. P., Larsen, M., et al. (2010). Safety and efficacy of ranibizumab in diabetic macular edema (RESOLVE study): A 12-month, randomized, controlled, double-masked, multicenter phase II study. *Diabetes Care* 33, 2399–2405. doi:10.2337/dc10-0493

Matteucci, A., Gaddini, L., Villa, M., Varano, M., Parravano, M., Monteleone, V., et al. (2014). Neuroprotection by rat Müller glia against high glucose-induced neurodegeneration through a mechanism involving ERK1/2 activation. *Exp. Eye Res.* 125, 20–29. doi:10.1016/j.exer.2014.05.011

Mima, A., Qi, W., Hiraoka-Yamomoto, J., Park, K., Matsumoto, M., Kitada, M., et al. (2012). Retinal not systemic oxidative and inflammatory stress correlated with VEGF expression in rodent models of insulin resistance and diabetes. *Invest. Ophthalmol. Vis. Sci.* 53 (13), 8424–8432. doi:10.1167/iovs.12-10207

Mizutani, M., Kern, T. S., and Lorenzi, M. (1996). Accelerated death of retinal microvascular cells in human and experimental diabetic retinopathy. *J. Clin. Invest.* 97 (12), 2883–2890. doi:10.1172/JCI118746

Nian, S., Lo, A., Mi, Y., Ren, K., and Yang, D. (2021). Neurovascular unit in diabetic retinopathy: Pathophysiological roles and potential therapeutical targets. *Eye Vis. (Lond).* 8 (1), 15. doi:10.1186/s40662-021-00239-1

Ogura, S., Kurata, K., Hattori, Y., Takase, H., Ishiguro-Oonuma, T., Hwang, Y., et al. (2017). Sustained inflammation after pericyte depletion induces irreversible blood-retina barrier breakdown. *JCI Insight* 2 (3), e90905. doi:10.1172/jci.insight.90905

Oshitari, T. (2021). The pathogenesis and therapeutic approaches of diabetic neuropathy in the retina. *Int. J. Mol. Sci.* 22 (16), 9050. doi:10.3390/ijms22169050

Pillar, S., Moisseiev, E., Sokolovska, J., and Grzybowski, A. (2020). Recent developments in diabetic retinal neurodegeneration: A literature review. *J. Diabetes Res.* 2020, 5728674. doi:10.1155/2020/5728674

Radhakrishnan, R., and Kowluru, R. A. (2021). Long noncoding RNA MALAT1 and regulation of the antioxidant defense system in diabetic retinopathy. *Diabetes* 70, 227–239. doi:10.2337/db20-0375

Ravikumar, B., Vacher, C., Berger, Z., Davies, J. E., Luo, S., Oroz, L. G., et al. (2004). Inhibition of mTOR induces autophagy and reduces toxicity of polyglutamine expansions in fly and mouse models of Huntington disease. *Nat. Genet.* 36 (6), 585–595. doi:10.1038/ng1362

Robinson, R., Srinivasan, M., Shanmugam, A., Ward, A., Ganapathy, V., Bloom, J., et al. (2020). Interleukin-6 trans-signaling inhibition prevents oxidative stress in a mouse model of early diabetic retinopathy. *Redox Biol.* 34, 101574. doi:10.1016/j.redox.2020.101574

Rodríguez, M. L., Pérez, S., Mena-Mollá, S., Desco, M. C., and Ortega, Á. L. (2019). Oxidative stress and microvascular alterations in diabetic retinopathy: Future therapies. *Oxid. Med. Cell. Longev.* 2019, 4940825. doi:10.1155/2019/4940825

Rodriguez, R., and Root, H. F. (1948). Capillary fragility and diabetic retinitis; with a note on the use of rutin. *N. Engl. J. Med.* 238 (12), 391–397. doi:10.1056/NEJM194803182381202

Rojo Arias, J. E., Economopoulou, M., Juárez López, D. A., Kurzbach, A., Au Yeung, K. H., Englmaier, V., et al. (2020). VEGF-Trap is a potent modulator of vasoregenerative responses and protects dopaminergic amacrine network integrity in degenerative ischemic neovascular retinopathy. *J. Neurochem.* 153 (3), 390–412. doi:10.1111/jnc.14875

Rowan, S., Jiang, S., Korem, T., Szymanski, J., Chang, M. L., Szelog, J., et al. (2017). Involvement of a gut-retina axis in protection against dietary glycemia-induced age-related macular degeneration. *Proc. Natl. Acad. Sci. U. S. A.* 114 (22), E4472–E4481. doi:10.1073/pnas.1702302114

Saddala, M. S., Lennikov, A., and Huang, H. (2020). Placental growth factor regulates the pentose phosphate pathway and antioxidant defense systems in human retinal endothelial cells. *J. Proteomics* 217, 103682. doi:10.1016/j.jprot.2020.103682

Saeedi, P., Petersohn, I., Salpea, P., Malanda, B., Karuranga, S., Unwin, N., et al. (2019). Global and regional diabetes prevalence estimates for 2019 and projections for 2030 and 2045: Results from the international diabetes federation diabetes atlas, 9th edition. *Diabetes Res. Clin. Pract.* 9157, 107843. doi:10.1016/j.diabres.2019.107843

Sasaki, M., Ozawa, Y., Kurihara, T., Kubota, S., Yuki, K., Noda, K., et al. (2010). Neurodegenerative influence of oxidative stress in the retina of a murine model of diabetes. *Diabetologia* 53, 971–979. doi:10.1007/s00125-009-1655-6

Scanlon, P. H. (2017). The English national screening programme for diabetic retinopathy 2003-2016. *Acta Diabetol.* 54 (6), 515–525. doi:10.1007/s00592-017-0974-1

Schoeler, M., and Caesar, R. (2019). Dietary lipids, gut microbiota and lipid metabolism. *Rev. Endocr. Metab. Disord.* 20, 461–472. doi:10.1007/s11154-019-09512-0

Scirocco, A., Matarrese, P., Carabotti, M., Ascione, B., Malorni, W., and Severi, C. (2016). Cellular and molecular mechanisms of phenotypic switch in gastrointestinal smooth muscle. *J. Cell. Physiol.* 231, 295–302. doi:10.1002/jcp.25105

Semeraro, F., Morescalchi, F., Cancarini, A., Russo, A., Rezzola, S., and Costagliola, C. (2019). Diabetic retinopathy, a vascular and inflammatory disease: Therapeutic implications. *Diabetes Metab.* 45 (6), 517–527. doi:10.1016/j.diabet.2019.04.002

Shao, K., Xi, L., Cang, Z., Chen, C., and Huang, S. (2020). Knockdown of NEAT1 exerts suppressive effects on diabetic retinopathy progression via

inactivating TGF-β1 and VEGF signaling pathways. *J. Cell. Physiol.* 235 (12), 9361–9369. doi:10.1002/jcp.29740

Simó, R., Simó-Servat, O., Bogdanov, P., and Hernández, C. (2021). Neurovascular unit: A new target for treating early stages of diabetic retinopathy. *Pharmaceutics* 13 (8), 1320. doi:10.3390/pharmaceutics13081320

Simó, R., Stehouwer, C., and Avogaro, A. (2020). Diabetic retinopathy: Looking beyond the eyes. *Diabetologia* 63 (8), 1662–1664. doi:10.1007/s00125-020-05195-4

Simó, R., Sundstrom, J. M., and Antonetti, D. A. (2014). Ocular anti-VEGF therapy for diabetic retinopathy: The role of VEGF in the pathogenesis of diabetic retinopathy. *Diabetes Care* 37 (4), 893–899. doi:10.2337/dc13-2002

Simó, R., and Hernández, C. (2014). Neurodegeneration in the diabetic eye: New insights and therapeutic perspectives. *Trends Endocrinol. Metab.* 25, 23–33. doi:10.1016/j.tem.2013.09.005

Sinclair, S. H., and Schwartz, S. S. (2019). Diabetic retinopathy-an underdiagnosed and undertreated inflammatory, neuro-vascular complication of diabetes. *Front. Endocrinol.* 10, 843. doi:10.3389/fendo.2019.00843

Solomon, S. D., Chew, E., Duh, E. J., Sobrin, L., Sun, J. K., VanderBeek, B. L., et al. (2017). Diabetic retinopathy: A position statement by the American diabetes association. *Diabetes Care* 40 (3), 412–418. doi:10.2337/dc16-2641

Teo, Z. L., Tham, Y. C., Yu, M., Chee, M. L., Rim, T. H., Cheung, N., et al. (2021). Global prevalence of diabetic retinopathy and projection of burden through 2045: Systematic review and meta-analysis. *Ophthalmology* 128 (11), 1580–1591. doi:10.1016/j.ophtha.2021.04.027

Udsen, M., Tagmose, C., Garred, P., Nissen, M. H., and Faber, C. (2022). Complement activation by RPE cells preexposed to TNFα and IFNγ. *Exp. Eye Res.* 218, 108982. doi:10.1016/j.exer.2022.108982

Vagaja, N. N., Binz, N., McLenachan, S., Rakoczy, E. P., and McMenamin, P. G. (2013). Influence of endotoxin-mediated retinal inflammation on phenotype of diabetic retinopathy in Ins2 Akita mice. *Br. J. Ophthalmol.* 97, 1343–1350. doi:10.1136/bjophthalmol-2013-303201

van der Wijk, A. E., Hughes, J. M., Klaassen, I., Van Noorden, C., and Schlingemann, R. O. (2017). Is leukostasis a crucial step or epiphenomenon in the pathogenesis of diabetic retinopathy. *J. Leukoc. Biol.* 102 (4), 993–1001. doi:10.1189/jlb.3RU0417-139

Wang, W., Zhao, H., and Chen, B. (2020). DJ-1 protects retinal pericytes against high glucose-induced oxidative stress through the Nrf2 signaling pathway. *Sci. Rep.* 10 (1), 2477. doi:10.1038/s41598-020-59408-2

Wang, W., and Lo, A. (2018). Diabetic retinopathy: Pathophysiology and treatments. *Int. J. Mol. Sci.* 19, E1816. doi:10.3390/ijms19061816

Wells, J. A., Glassman, A. R., Ayala, A. R., Jampol, L. M., Aiello, L. P., Antoszyk, A. N., et al. (2015). Aflibercept, bevacizumab, or ranibizumab for diabetic macular edema. *N. Engl. J. Med.* 372, 1193–1203. doi:10.1056/NEJMoa1414264

Whitehead, M., Wickremasinghe, S., Osborne, A., Van Wijngaarden, P., and Martin, K. R. (2018). Diabetic retinopathy: A complex pathophysiology requiring novel therapeutic strategies. *Expert Opin. Biol. Ther.* 18 (12), 1257–1270. doi:10.1080/14712598.2018.1545836

Xia, F., Ha, Y., Shi, S., Li, Y., Li, S., Luisi, J., et al. (2021). Early alterations of neurovascular unit in the retina in mouse models of tauopathy. *Acta Neuropathol. Commun.* 9 (1), 51. doi:10.1186/s40478-021-01149-y

Xie, H., Zhang, C., Liu, D., Yang, Q., Tang, L., Wang, T., et al. (2021). Erythropoietin protects the inner blood-retinal barrier by inhibiting microglia phagocytosis via Src/Akt/cofilin signalling in experimental diabetic retinopathy. *Diabetologia* 64, 211–225. doi:10.1007/s00125-020-05299-x

Yang C Y, C. Y., Chen, T. W., Lu, W. L., Liang, S. S., Huang, H. D., Tseng, C. P., et al. (2021). Synbiotics alleviate the gut indole load and dysbiosis in chronic kidney disease. *Cells* 10. doi:10.3390/cells10010114

Yang G, G., Wei, J., Liu, P., Zhang, Q., Tian, Y., Hou, G., et al. (2021). Role of the gut microbiota in type 2 diabetes and related diseases. *Metabolism.* 117, 154712. doi:10.1016/j.metabol.2021.154712

Yang, L., Yu, P., Chen, M., and Lei, B. (2022). Mammalian target of rapamycin inhibitor rapamycin alleviates 7-ketocholesterol induced inflammatory responses and vascular endothelial growth factor elevation by regulating MAPK pathway in human retinal pigment epithelium cells. *J. Ocul. Pharmacol. Ther.* 38, 189–200. doi:10.1089/jop.2021.0082

Yang, Y., Liu, Y., Li, Y., Chen, Z., Xiong, Y., Zhou, T., et al. (2020). MicroRNA-15b targets VEGF and inhibits angiogenesis in proliferative diabetic retinopathy. *J. Clin. Endocrinol. Metab.* 105 (11), dgaa538–15. doi:10.1210/clinem/dgaa538

Yano, J. M., Yu, K., Donaldson, G. P., Shastri, G. G., Ann, P., Ma, L., et al. (2015). Indigenous bacteria from the gut microbiota regulate host serotonin biosynthesis. *Cell* 161 (2), 264–276. doi:10.1016/j.cell.2015.02.047

Yun, J. H. (2021). Interleukin-1β induces pericyte apoptosis via the NF-κB pathway in diabetic retinopathy. *Biochem. Biophys. Res. Commun.* 546, 46–53. doi:10.1016/j.bbrc.2021.01.108

Zeng, Y., Cao, D., Yu, H., Hu, Y., He, M., Yang, D., et al. (2019). Comprehensive analysis of vitreous humor chemokines in type 2 diabetic patients with and without diabetic retinopathy. *Acta Diabetol.* 56 (7), 797–805. doi:10.1007/s00592-019-01317-6

Zhao, B. W., Dai, H. Y., Hao, L. N., and Liu, Y. W. (2019). MiR-29 regulates retinopathy in diabetic mice via the AMPK signaling pathway. *Eur. Rev. Med. Pharmacol. Sci.* 23 (9), 3569–3574. doi:10.26355/eurrev_201905_17778

Zhou, Z., Liu, J., Bi, C., Chen, L., Jiao, Y., and Cui, L. (2019). Knockdown of FOXO6 inhibits high glucose-induced oxidative stress and apoptosis in retinal pigment epithelial cells. *J. Cell. Biochem.* 120 (6), 9716–9723. doi:10.1002/jcb.28252

frontiers | Frontiers in Cell and Developmental Biology

TYPE Review
PUBLISHED 07 September 2022
DOI 10.3389/fcell.2022.982564



OPEN ACCESS

EDITED BY
Rajalekshmy Shyam,
Indiana University Bloomington,
United States

REVIEWED BY
Yukio Fujiki,
Kyushu University Graduate School,
Japan
Maki Kamoshita,
Osaka University, Japan
Francesca Di Cara,
Dalhousie University, Canada
Anyuan He,
Anhui Medical University, China

*CORRESPONDENCE
Zhongjie Fu,
zhongjie.fu@childrens.harvard.edu

†These authors have contributed equally to this work and share first authorship

SPECIALTY SECTION
This article was submitted to Molecular and Cellular Pathology, a section of the journal Frontiers in Cell and Developmental Biology

RECEIVED 30 June 2022
ACCEPTED 17 August 2022
PUBLISHED 07 September 2022

CITATION
Chen CT, Shao Z and Fu Z (2022), Dysfunctional peroxisomal lipid metabolisms and their ocular manifestations.
*Front. Cell Dev. Biol.* 10:982564.
doi: 10.3389/fcell.2022.982564



# Dysfunctional peroxisomal lipid metabolisms and their ocular manifestations

Chuck T. Chen[1†], Zhuo Shao[2,3,4†] and Zhongjie Fu[5*]

[1]Department of Nutritional Sciences, Temerty Faculty of Medicine, University of Toronto, Toronto, ON, Canada, [2]Post-Graduate Medical Education, University of Toronto, Toronto, ON, Canada, [3]Division of Clinical and Metabolic Genetics, the Hospital for Sick Children, University of Toronto, Toronto, ON, Canada, [4]The Genetics Program, North York General Hospital, University of Toronto, Toronto, ON, Canada, [5]Department of Ophthalmology, Boston Children's Hospital, Harvard Medical School, Boston, MA, United States

Retina is rich in lipids and dyslipidemia causes retinal dysfunction and eye diseases. In retina, lipids are not only important membrane component in cells and organelles but also fuel substrates for energy production. However, our current knowledge of lipid processing in the retina are very limited. Peroxisomes play a critical role in lipid homeostasis and genetic disorders with peroxisomal dysfunction have different types of ocular complications. In this review, we focus on the role of peroxisomes in lipid metabolism, including degradation and detoxification of very-long-chain fatty acids, branched-chain fatty acids, dicarboxylic acids, reactive oxygen/nitrogen species, glyoxylate, and amino acids, as well as biosynthesis of docosahexaenoic acid, plasmalogen and bile acids. We also discuss the potential contributions of peroxisomal pathways to eye health and summarize the reported cases of ocular symptoms in patients with peroxisomal disorders, corresponding to each disrupted peroxisomal pathway. We also review the cross-talk between peroxisomes and other organelles such as lysosomes, endoplasmic reticulum and mitochondria.

KEYWORDS

**peroxisome, retinal lipids, fatty acid oxidation, retinal dystrophy, retinopathy**

## 1 Introduction

Peroxisomes are membrane bound organelles found in all eukaryotic cells and heavily involved in α and β-oxidation of lipids, glyoxylate detoxification, amino acid degradation, as well as reactive oxygen species (ROS) and reactive nitrogen species (RNS) metabolism. Peroxisomes are also essential in plasmalogen, docosahexaenoic acid (DHA) and bile acid synthesis. There are abundance of enzymes and transporter proteins associated with peroxisomes that are responsible for peroxisome biogenesis, transportation across peroxisomal membrane, and metabolism. Loss of function in various proteins due to pathogenic genetic variants lead to multisystem disorders in human. As these mutations cause the potential for severe and early onset neurological, ophthalmological, craniofacial, musculoskeletal, and hepatorenal damages, they pose significant health risks and burden on patients and their families (Steinberg et al., 1993). Recent studies have also suggested

that peroxisomes are involved in common neurodegenerative diseases such as Alzheimer's disease, Parkinson's disease, and multiple sclerosis (Lizard et al., 2012; Wojtowicz et al., 2020). Since neurodegeneration is associated with oxidative stress, lipid peroxidation, and cholesterol auto-oxidation, modifications of peroxisomal functions have been proposed as a potential mechanism for the altered metabolome. Retina is rich in lipids and highly metabolically demanding. Photoreceptors are very high in mitochondria, and nursed by retinal pigment epithelium (RPE) which uptakes nutrients from choroidal blood vessels and Müller glia which extends across the retinal layers and safeguards the blood-retinal barrier (Figure 1). This unique anatomical landscape and high metabolic demand made retina a vulnerable tissue prone to damage from metabolic insults such as peroxisomal disorders. In this review, we focus on the peroxisomal metabolism pathways that are involved in retinal health and the ocular dysfunction associated with peroxisomal disorders.

## 2 Peroxisome metabolic functions

Peroxisomes are essential for biosynthesis of DHA, plasmalogen and bile acids, as well as degradation and detoxification of very-long-chain fatty acids (VLCFAs), branched-chain fatty acids (BCFAs), dicarboxylic acids, reactive oxygen/nitrogen species (ROS/RNS), glyoxylate, and amino acids (Islinger et al., 2010; Islinger et al., 2018). In this section, we summarize the current updates on these pathways (Figure 2) and the eye diseases associated with gene mutation in these pathways (Table 1). The detailed eye symptoms are discussed in Section 3. The abbreviations are listed in Table 2.

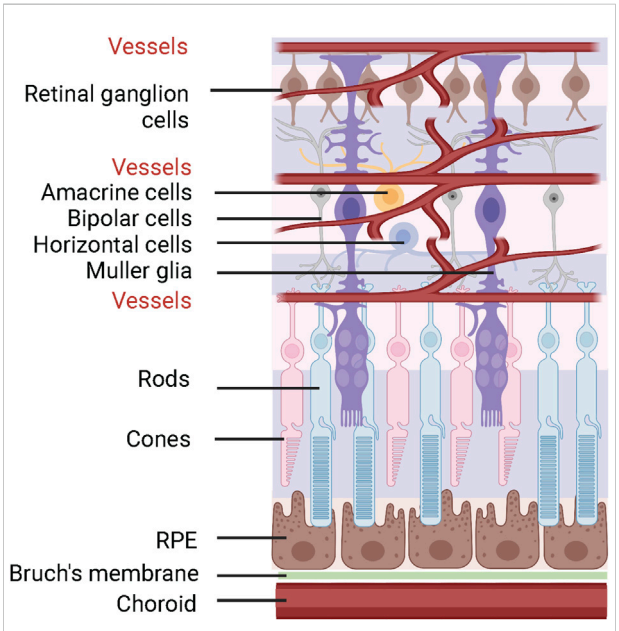


FIGURE 1
Schematics of retinal structure. The neural retina is supplied by retinal and choroidal vasculature. Photoreceptors (rods and cones) are supported by RPE and Müller glia cells. The figure was generated using Biorender (license # LX24BJEUXV).

### 2.1 Catabolic function: β-oxidation of monocarboxylic fatty acids and dicarboxylic acids

Peroxisomal β-oxidation of monocarboxylic fatty acids and dicarboxylic acids are ubiquitous within the animal kingdom (Ferdinandusse et al., 2004; Wanders, 2014). VLCFAs are a family of monocarboxylic fatty acids with greater than 22 carbons. These include saturated, monounsaturated, and polyunsaturated species of fatty acids such as behenic acid (22:0), lignoceric acid (24:0), cerotic acid (26:0), erucic acid (22:1n-9), nervonic acid (24:1n-9), adrenic acid (22:4n-6), docosapentaenoic acids (DPA; 22:5n-6 or 22:5n-3), DHA (22:6n-3), and nisinic acid/tetracosahexaenoic acid (THA; 24:6n-3). Since mitochondria lack expression of very long chain acyl-CoA synthetase (very long chain acyl-CoA synthetase/fatty acid transport protein, VLCS/FATP; bubblegum), and mitochondrial carnitine palmitoyltransferase I (CPTI) preferentially transports long-chain fatty acids (LCFA - 14–20 carbons), VLCFA are largely metabolized by the peroxisome (Gavino and Gavino, 1991; Lageweg et al., 1991; van den Bosch et al., 1992; Reddy and Mannaerts, 1994; Uchiyama et al., 1996; Coe et al., 1999; Smith et al., 1999; Steinberg et al., 1999b; Steinberg et al., 2000; Heinzer et al., 2003; Pridie et al., 2020) (Figure 3). Furthermore, peroxisomal ATP binding cassette sub family D members 1/2 (ABCD1/2) are essential for transport of VLCFA; though the exact mechanism is still debated (van Roermund et al., 2011; Kawaguchi et al., 2021). Long chain dicarboxylic acid are metabolites of monocarboxylic acid ω-oxidation by cytochrome P450 that are products of compromised β-oxidation (Grego and Mingrone, 1995). Dicarboxylic acids are transported to peroxisome via ABCD3 (van Roermund et al., 2014) (Figure 4).

Peroxisomal β-oxidation involves four sequential reactions: 1) dehydrogenation by ACOX, 2 + 3) hydration and dehydrogenation by multifunctional enzymes (MFE), and 4) thiolytic cleavage by 3-ketoacyl-CoA thiolases. The first step of peroxisomal β-oxidation involves ACOX catalyzed acyl-CoA and oxygen to 2E-enoyl-CoA and hydrogen peroxide. In rodents, there are three ACOX with different substrate specificity. Generally, ACOX1 (straight chain-CoA oxidase) has high affinity for CoA esters of medium chain fatty acids, LCFA, and VLCFA, whereas ACOX2 (pristanoyl-CoA oxidase)

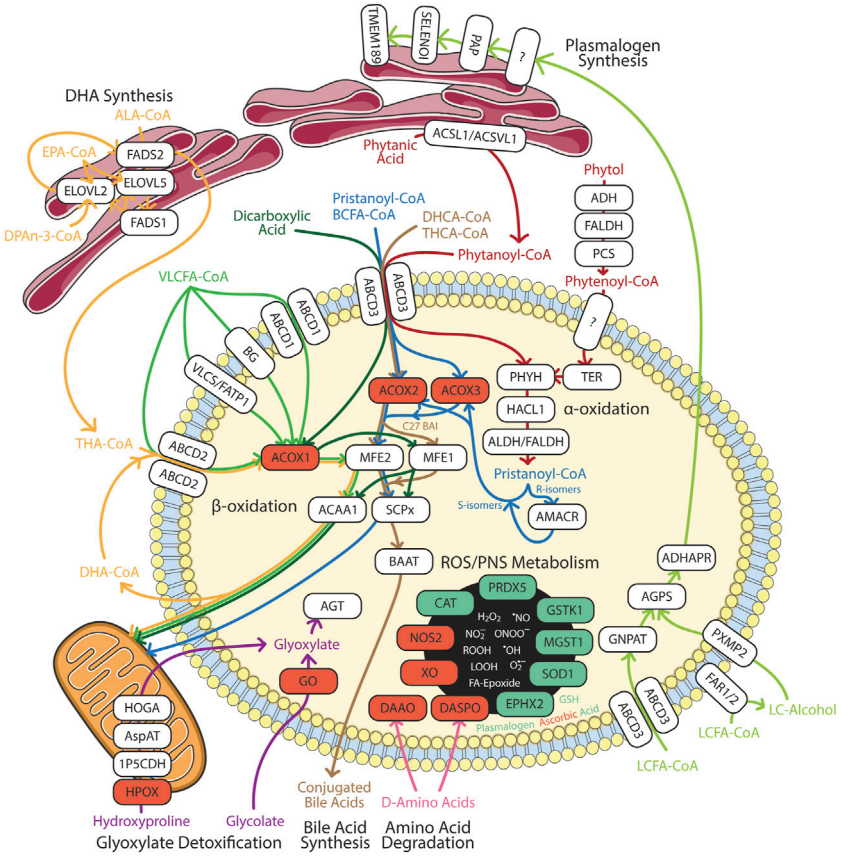


FIGURE 2
Summary of peroxisomal functions in humans. Enzymes involved in the catabolic and anabolic pathways in white boxes. Red box represents ROS/RNS producing enzymes. Green box represents anti-oxidation enzymes in redox homeostasis. 1P5CDH, $\Delta^1$-pyrroline-5-carboxylate dehydrogenase; ABCD, ATP-binding cassette sub-family D; ACAA, 3-oxoacyl thiolase; ACOX, acyl-CoA oxidase; ACSL, long chain acyl-CoA synthetase; ACSVL, very long chain acyl-CoA synthetase; ADH, alcohol dehydrogenase; ADHAPR, acyl/alkyl DHAP reductase; AGPS, alkyl-glycerone phosphate synthase; AGT, alanine:glyoxylate aminotransferase; ALA, α-linolenic acid; ALDH, aldehyde dehydrogenase; AMACR, α-methylacyl-CoA racemase; AspAT, aspartate aminotransferase; BAAT, bile acid-CoA:amino acid N-acyltransferase; BCFA, branched chain fatty acids; BG, bubblegum; CAT, catalase; DAAO, D-amino acid oxidase; DASPO, D-aspartate oxidase; DHA, docosahexaenoic acid; DHCA, 3α,7α-dihydroxy-5β-cholestanoic acid; DPAn-3, n-3 docosapentaenoic acid; ELOVL, fatty acid elongase; EPA, eicosapentaenoic acid; EPHX2, epoxide hydrolase 2; FADS, fatty acid desaturase; FALDH, fatty aldehyde dehydrogenase; FAR, fatty acyl-CoA reductase; FATP, fatty acid transport protein; GNPAT, glycerone-phosphate O-acyltransferase; GO, glycolate oxidase; GSH, glutathione; GSTK, glutathione transferase kappa; HACL, 2-hydroxyacyl-CoA lyase; HOGA, 4-hydroxy-2-oxoglutarate aldolase; HPOX, hydroxyproline oxidase; LCFA, long chain fatty acids; MFE, multifuctional enzyme; MGST, microsomal glutathione S-transferase; NOS2, inducible nitric oxide synthase; PAP, phosphatidic acid phosphatase; PCS, phytenoyl-CoA synthetase; PHYH, phytanoyl-CoA 2-hydroxylase; PRDX5, peroxiredoxin 5; PXMP2, peroxisomal membrane protein 2; SELENOI, selenoprotein 1 (ethanolamine phosphotransferase 1); SCPx, SCP-2/3-ketoacyl-CoA thiolase; SOD1, superoxide dismutase; TER, trans-2-enoyl-CoA reductase; THA, tetracosahexaenoic acid; THCA, 3α,7α, 12 α-trihydroxy-5β-cholestanoic acid; TMEM189, plasmanylethanolamine desaturase; VLCFA, very long chain fatty acids; VLCS, very long chain acyl-CoA synthetase; XO, xanthine oxidase. The Figure was partly generated using Servier Medical Art, provided by Servier, licensed under a Creative Commons Attribution 3.0 unported license.

and ACOX3 (cholestanoyl-CoA oxidase) prefer CoA esters of BCFA, 3α,7α-dihydroxy-5β-cholestanoic acid (DHCA), and 3α,7α, 12 α-trihydroxy-5β-cholestanoic acid (THCA), respectively (Bieber et al., 1981; Vamecq, 1987; Vanhove et al., 1993). In contrast, human ACOX2 dehydrogenate BCFA, DHCA and THCA while human ACOX3 metabolizes BCFA (Ferdinandusse et al., 2018).

Following ACOX, MFE catalyze the hydration and dehydrogenation of 2E-enoyl-CoA to chiral 3-hydroxy-acyl-CoA and 3-ketoacyl-CoA. In mammals, there are two MFE: 1) MFE-1 (L-bifunctional protein; LBP) and 2) MFE-2 (D-bifunctional protein; DBP). While MFE-1 has a broad substrate specificity which can bind CoA esters of fatty acids varying from short to long, hydroxylated C27 DHCA/THCA intermediates, and dicarboxylic acids, it predominantly catalyzes breakdown of medium and long chain dicarboxylic acids (Ferdinandusse et al., 2004; Houten et al., 2012). MFE-2 (coded by the *HSD17B4* gene in human) is essential for the

TABLE 1 Summary of common gene mutations and ocular symptoms in peroxisomal disorders.

| Gene | Function | Peroxisomal disorders | Ocular symptoms |
|---|---|---|---|
| ACOX1 | Peroxisomal β-oxidation | Single enzyme deficiency | Nystagmus, optic atrophy, tapetoretinal degeneration, pigmentary retinopathy, flattened or absent electroretinogram, and absence of flash-evoked visual responses |
| AGPS | Plasmalogen synthesis | RCDP | None reported |
| AGXT | Detoxification of glyoxylate | Single enzyme deficiency | Optic atrophy, choroidal neovascularization, and crystalline retinopathy |
| ALDH3A2/ FALDH | Phytenic acid production | Single enzyme deficiency | Photophobia, superficial corneal opacity, glistening white dots in fundus, central retinal thinning/macular degeneration, macular window defects without leakage, heterogeneous macular autofluorescence with crystals, and retinal pigment epithelial atrophy |
| AMACR | Bile acid synthesis/α-oxidation | Single enzyme deficiency | Variable pigmentary retinopathy |
| FAR1 | Plasmalogen synthesis | RCDP | Cataracts |
| GNPAT | Plasmalogen synthesis | RCDP | Cataract |
| HACL1 | Peroxisomal α-oxidation | No associated syndrome | Not reported |
| HSD17B4/ MFE2 | Peroxisomal β-oxidation multifunctional protein-2 (MFP2) | Single enzyme deficiency | Nystagmus, strabismus, abolished electroretinogram, and limited extraocular movements |
| PEX family genes | Peroxisomal biogenesis | PBD-ZSD | Nystagmus, glaucoma, corneal clouding, cataracts, pigmentary retinopathy, optic disc hypoplasia, abnormal electroretinogram, and macular dystrophy (rare) |
| PHYH | Peroxisomal α-oxidation | Single enzyme deficiency that mimics ZSD | Nystagmus, cataracts, retinitis pigmentosa, retinal degeneration, night blindness, constriction of visual fields, miosis, and poor pupillary reaction |
| SCPx/SCP2 | branched-chain fatty acids β-oxidation | Single enzyme deficiency | Pathologic saccadic eye movements |

breakdown of VLCFA, BCFA, DHCA, and THCA (Qi et al., 1999; Su et al., 2001; Huyghe et al., 2006).

In the final step of peroxisomal β-oxidation, 3-ketoacyl-CoA thiolases catalyze the cleavage of 3-ketoacyl-CoA to acetyl-CoA and shortened acyl-CoA. In rodents, there are three 3-ketoacyl-CoA thiolases: 1) thiolase A, 2) thiolase B, and 3) SCP-2/3-ketoacyl-CoA thiolase (SCPx). Thiolase A and B have similar profile in substrate specificity, where the preference is given to saturated fatty acid in various chain length. In addition to binding of saturated 3-ketoacyl-CoA esters, SCPx also binds BCFA CoA esters (Poirier et al., 2006). In contrast to rodents, human has two 3-ketoacyl-CoA thiolases: 1) 3-oxoacyl thiolase (ACAA1) and 2) sterol carrier protein X (SCPx—ortholog of rodent SCPx). ACAA1 ligand specificity is restricted to 3-ketoacyl-CoA esters of VLCFA, whereas SCPx prefers 3-oxoacyl-CoA esters of pristanic acid, and DHCA/THCA (Seedorf et al., 1994). ACAA1 is expressed equally or more in neural retina than RPE, while reversely, SCPx expression is more abundant in RPE as compared to neural retina (Das et al., 2019).

## 2.2 Catabolic function: α-oxidation of branched chain fatty acids

BCFAs are a specialized group of saturated fatty acids with mono- or poly-methyl branches on the carbon chain. Monomethyl BCFA are subdivided into iso and anteiso structure. Iso-BCFA have methyl branch on the penultimate carbon which is one carbon from the methyl end; meanwhile anteiso-BCFA have methyl branch on the antepenultimate carbon that is two carbons from the methyl end. Enriched sources of BCFA include ruminant-derived and fermented foods (Taormina et al., 2020). Phytanic acid and its metabolite pristanic acid are common 3-methyl BCFA synthesized in ruminant or derived from phytol that are bioaccumulated in the marine system from phytoplankton chlorophyll (Wanders et al., 2011a; Taormina et al., 2020). In humans, tissue phytanic acid levels are strictly derived from dietary sources as endogenous synthesis are limited (Steinberg et al., 1965).

Dietary phytol is oxidized to phytenal by alcohol dehydrogenase, then converted into phytenic acid by fatty aldehyde dehydrogenase (FALDH) (Rizzo et al., 1999) (Figure 4). Phytenic acid is activated by esterification of CoA to phytenoyl-CoA by phytenoyl-CoA synthetase (PCS) after which it can bind peroxisomal trans-2-enoyl-CoA reductase (TER) and reduced to produce phytanoyl-CoA for subsequent peroxisomal phytanoyl-CoA α-oxidation and pristanoyl-CoA β-oxidation (van den Brink et al., 2005; Gloerich et al., 2006). Reduction of phytenoyl-CoA to phytanoyl-CoA is localized to peroxisome for two reasons: 1) TER is targeted to peroxisome due to attached peroxisomal targeting signal type 1 (PTS1) peptide on the enzyme and 2) mitochondrial CPTI does not catalyze carnitine esterification to phytenoyl-CoA (Wanders et al., 2011a). Though the degradation pathways are characterized, only two enzymes have been identified, FALDH and TER. Further research is required to identify enzymes

TABLE 2 Abbreviations.

| Abbreviation | Full name |
|---|---|
| ABCD1/2 | ATP binding cassette sub family D members 1/2 |
| ACBD5 | acyl-CoA binding domain containing protein 5 |
| ACOX | acyl-CoA oxidase |
| AGPS | alkyl-glycerone phosphate synthase |
| AMD | age-related macular degeneration |
| ARA | arachidonic acid |
| BCFA | branched-chain fatty acids |
| CA | cholic acid |
| CAT | Catalase |
| CDCA | chenodeoxycholic acid |
| CNS | central nervous system |
| CPTI | carnitine palmitoyltransferase I |
| CYP | cytochrome P450 |
| DHA | docosahexaenoic acid |
| DHAP | dihydroxyacetone-phosphate |
| DHCA | 3α,7α-dihydroxy-5β-cholestanoic acid |
| DPA | docosapentaenoic acids |
| EPA | eicosapentaenoic acid |
| ER | endoplasmic reticulum |
| ERG | electroretinogram |
| FALDH | fatty aldehyde dehydrogenase |
| FAR | fatty acyl-CoA reductase |
| GNPAT | glycerone-phosphate O-acyltransferase |
| HACL1 | 2-hydroxyacyl-CoA lyase |
| HOGA | 4-hydroxy-2-oxoglutarate aldolase |
| MFE | multifunctional enzymes |
| PBD | peroxisomal biogenesis disorders |
| PHYH | phytanoyl-CoA 2-hydroxylase |
| Pls | plasmalogen |
| PTS1 | peroxisomal targeting signal type 1 |
| RCDP | rhizomelic chondrodysplasia punctata |
| ROP | retinopathy of prematurity |
| ROS/RNS | reactive oxygen/nitrogen species |
| RPE | retinal pigment epithelium |
| SCPx | SCP-2/3-ketoacyl-CoA thiolase |
| THCA | 3α,7α, 12 α-trihydroxy-5β-cholestanoic acid |
| VLCFA | very-long-chain fatty acids |
| X-ALD | X-linked adrenoleukodystrophy |
| ZSD | Zellweger Spectrum Disorder |

catalyzing the initial conversion to phytenal and CoA esterification to phytenoyl-CoA.

Like VLCFA, phytanic acid and pristanic acid are ligands for PPARα resulting in upregulation of peroxisomal β-oxidation enzymes and cytochrome P450 4A (CYP4A) enzymes facilitated ω-oxidation of phytanic acid in endoplasmic reticulum (ER) and microsome (Zomer et al., 2000; Wanders et al., 2011b; Kersten, 2014). Under normal conditions, phytanic acid is preferentially catabolized by α-oxidation (Wanders et al., 2011a). Degradation of dietary phytanic acid begins with activation of CoA esterification by phytanoyl-CoA synthetase, ACSL1 and ACSVL1 (Watkins et al., 1994). Phytanoyl-CoA is transported into peroxisome by ABCD3 (Morita and Imanaka, 2012). Hydroxylation of phytanoyl-CoA to 2-hydroxyphytanoyl-CoA is catalyzed by peroxisomal phytanoyl-CoA 2-hydroxylase (PHYH). Similar to TER, PHYH protein sequence includes PTS2; hence after is shuttled to peroxisome (Jansen et al., 1999a). 2-hydroxyphytanoyl-CoA is then cleaved by peroxisomal 2-hydroxyacyl-CoA lyase (HACL1) to pristanal and formyl-CoA (Jansen et al., 1999b; Foulon et al., 1999). Lastly, pristanal is oxidized to pristanic acid by unknown peroxisomal aldehyde dehydrogenase (potential candidate includes FALDH). In contrast to PHYH and HACL1, which are ubiquitously expressed in RPE and neural retina, ABCD3 is more abundantly found in RPE (Das et al., 2019). This suggests that phytanoyl-CoA and pristanoyl-CoA may have alternative route of entry in neural retina as compared to RPE.

Pristanic acid is activated to pristanoyl-CoA by ACSVL1 (Steinberg et al., 1999a). α-oxidation of phytanic acid may produce pristanoyl-CoA enantiomers; therefore, R-isomers are converted to S-isomer by α-methylacyl-CoA racemase (AMACR) in order to continue peroxisomal β-oxidation cycle due to stereospecificity of ACOX2 and ACOX3 (Van Veldhoven et al., 1996). Pristanoyl-CoA is catabolized by ACOX2/3, MFE-2, and SCPx in three rounds of peroxisomal β-oxidation (Verhoeven et al., 1998; Atshaves et al., 2007). Furthermore, recent report found that PMP34 are important in the peroxisomal oxidation of pristanic acid and the export of its metabolites (Van Veldhoven et al., 2020). However, the exact mechanistic details of PMP34's contribution to pristanic acid degradation requires further examination. AMACR deficiency results in increased plasma pristanic acid levels (Ferdinandusse et al., 2000; Thompson et al., 2009).

## 2.3 Catabolic function: Glyoxylate detoxification and amino acid degradation

Glyoxylate is a highly reactive two carbon aldehyde form primarily from metabolisms of plant-source glycolate by peroxisomal glycolate oxidase (GO) and animal-source hydroxyproline by sequential breakdown via hydroxyproline oxidase (HPOX), $\Delta^1$-pyrroline-5-carboxylate dehydrogenase (1P5CDH), aspartate aminotransferase (AspAT), and 4-hydroxy-2-oxoglutarate aldolase (HOGA) (Li et al., 2016; Wang et al., 2020). Glyoxylate is readily metabolized by dehydrogenase and oxidases to oxalate which then crystalizes with calcium to

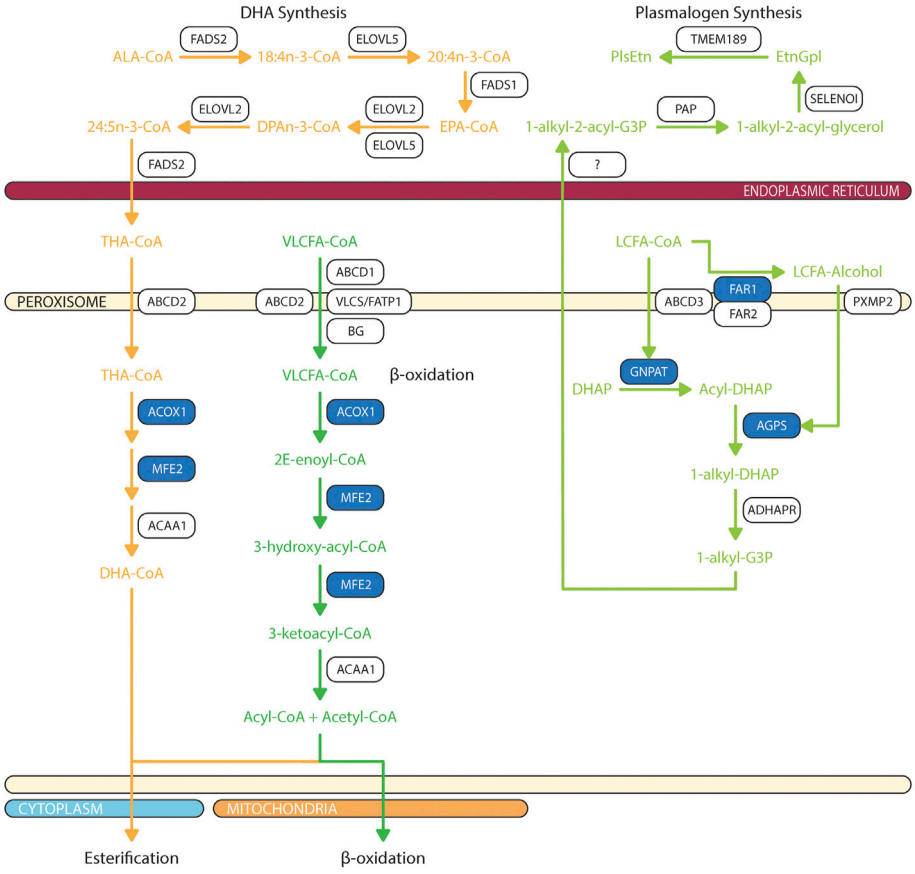


FIGURE 3
Biochemical pathways of peroxisomal lipid synthesis and degradation. Blue box represents enzymes with published pathogenic variants resulting in ocular manifestations in humans. ABCD, ATP-binding cassette sub-family D; ACAA, 3-oxoacyl thiolase; ACOX, acyl-CoA oxidase; ADHAPR, acyl/alkyl DHAP reductase; AGPS, alkyl-glycerone phosphate synthase; ALA, α-linolenic acid; BG, bubblegum; DHA, docosahexaenoic acid; DHAP, dihydroxyacetone phosphate; DPAn-3, n-3 docosapentaenoic acid; ELOVL, fatty acid elongase; EPA, eicosapentaenoic acid; EtnGpl, ethanolamine glycerophospholipids; FADS, fatty acid desaturase; FAR, fatty acyl-CoA reductase; FATP, fatty acid transport protein; G3P, glycerol-3-phosphate; GNPAT, glycerone-phosphate O-acyltransferase; LCFA, long chain fatty acids; MFE, multifuctional enzyme; PAP, phosphatidic acid phosphatase; PlsEtn, ethanolamine plasmalogens; PXMP2, peroxisomal membrane protein 2; SELENOI, selenoprotein 1 (ethanolamine phosphotransferase 1); THA, tetracosahexaenoic acid; TMEM189, plasmanylethanolamine desaturase; VLCFA, very long chain fatty acids; VLCS, very long chain acyl-CoA synthetase. The figure was partly generated using Servier Medical Art.

form calcium oxalate stone, a common source of kidney stones (Tsujihata, 2008). Since glyoxylate accumulation is correlated with dietary sources and intake, multiple detoxification mechanisms involving peroxisome and/or mitochondria are evolved depending on the food sources of the organisms (Danpure, 1997; Birdsey et al., 2005; Martin, 2010). Three enzymes are involved in the detoxification of glyoxylate: 1) peroxisomal and mitochondrial alanine:glyoxylate aminotransferase (AGT, encoded by the gene *AGXT*), 2) mitochondrial and cytosolic glyoxylate reductase/hydroxypyruvate reductase (GRHPR), and 3) cytosolic lactate dehydrogenase (LDH) (Figure 5). In contrast to rat where AGT is localized to both peroxisome and mitochondria, human AGT is exclusively expressed in peroxisome (Danpure, 1997). AGT catalyzes the transamination of glyoxylate and L-alanine to form pyruvate and glycine (Cellini et al., 2007). Cellular expressions of AGT in retina and RPE has not been elucidated.

Peroxisomes is also engaged in the catabolism of D-amino acids (Figure 5). Two stereospecific enzymes are localized to peroxisomes: 1) D-amino acid oxidase (DAAO/DAO) and 2) D-aspartate oxidase (DASPO/DDO) (Van Veldhoven et al., 1991; Pollegioni et al., 2018). DAAO have a wide substrate specificity; however, it prefers bulky hydrophobic D-amino acids (D-DOPA, D-Tyr, D-Phe, D-Trp) while having limited catalytic activity for small uncharged D-amino acids (D-Cys, D-Ala, D-Pro, D-Ser) (Kawazoe et al., 2007; Frattini et al., 2011; Shibuya et al., 2013; Murtas et al., 2017). DAAO does not actively metabolize glycine which explain the negligible contribution of glyoxylate from DAAO-mediated glycine degradation (Thureen

et al., 1995; Molla et al., 2006; Murtas et al., 2017). DASPO have high affinity for acidic D-amino acids (D-Asp, NMDA, D-Glu) followed by polar D-amino acids (D-Gln, D-Asn) (Pollegioni et al., 2021). DAAO is expressed in RPE and Müller cells (Beard et al., 1988); whereas DASPO retinal cell expression is unknown.

## 2.4 Anabolic and catabolic function: ROS/RNS metabolism

As its name defined, the core feature of peroxisome is the production of reactive oxygen species (ROS) and reactive nitrogen species (RNS) (De Duve and Baudhuin, 1966), which may cause biomolecular damage and cell death. As an organelle with high productions of ROS/RNS species, naturally, peroxisomes are equipped with an arsenal of antioxidant enzymes and non-enzymatic free radical scavengers (Figure 5). To-date, there is no consensus regarding peroxisome's overall contribution as a net source of cellular ROS/RNS or sink for ROS/RNS detoxification (Fransen et al., 2013). Cellular reduction-oxidation (redox) state is dependent on several factors including the type, concentration, localization, synthetic rate, and degradation rate of oxidants formed (Trachootham et al., 2008; Forman et al., 2010). The magnitude of oxidative stress can have divergent effects on cellular fates where at high levels can induced irreversible damage to lipids, protein, and DNA resulting in apoptosis, but at low levels oxidants act as signaling messengers to promote cell survival and proliferation (Jones and Go, 2010; Holmstrom and Finkel, 2014).

The most abundant oxidants produced in peroxisomes is hydrogen peroxide ($H_2O_2$) because of flavin-containing oxidases that reduce molecular oxygen ($O_2$) to $H_2O_2$ (Antonenkov et al., 2010). Peroxisomes account up to 35% of total hydrogen peroxide generation in the mammalian tissues and 20% of total cellular oxygen consumption (Cipolla and Lodhi, 2017). In human peroxisomes, $H_2O_2$ is degraded by catalase (CAT) and peroxiredoxin 5 (PRDX5).

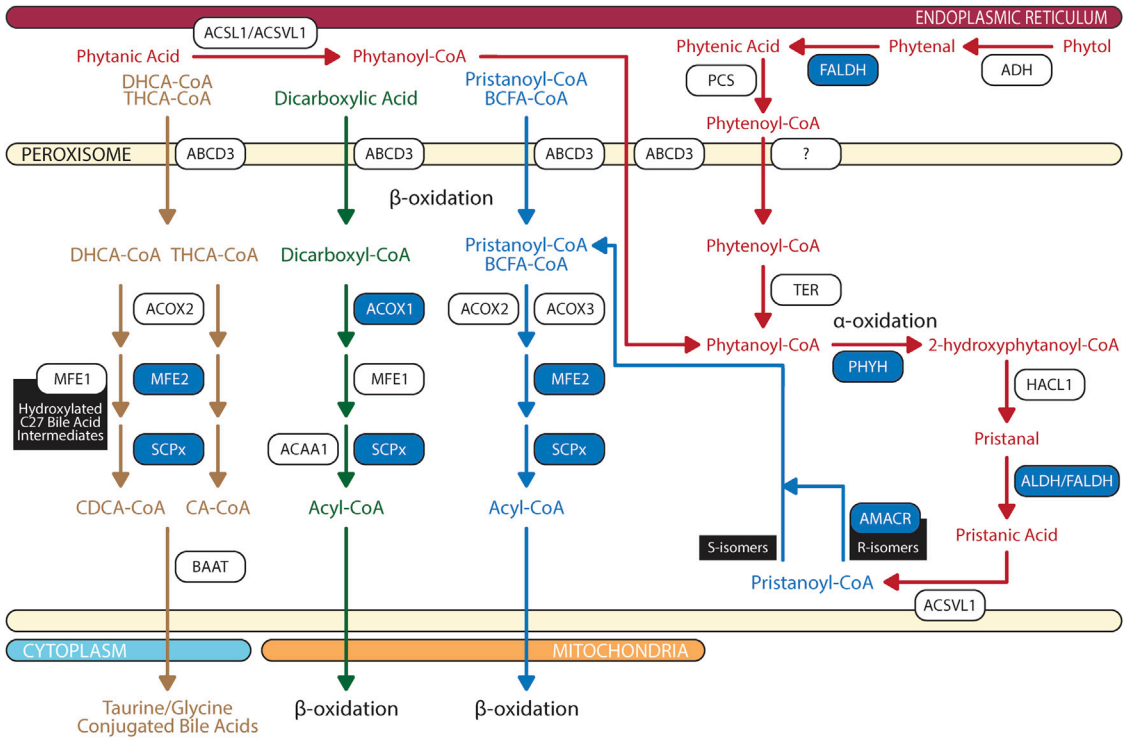


FIGURE 4
Biochemical pathways of peroxisomal branched chain fatty acid, dicarboxylic acid, and bile acid degradations. Blue box represents enzymes with published pathogenic variants resulting in ocular manifestations in humans. ABCD, ATP-binding cassette sub-family D; ACAA, 3-oxoacyl thiolase; ACOX, acyl-CoA oxidase; ADH, alcohol dehydrogenase; ALDH, aldehyde dehydrogenase; AMACR, α-methylacyl-CoA racemase; AspAT, aspartate aminotransferase; BAAT, bile acid-CoA:amino acid N-acyltransferase; BCFA, branched chain fatty acids; CA, cholic acid; CDCA, chenodeoxycholic acid; DHCA, 3α,7α-dihydroxy-5β-cholestanoic acid; FALDH, fatty aldehyde dehydrogenase; HACL, 2-hydroxyacyl-CoA lyase; MFE, multifuctional enzyme; PCS, phytenoyl-CoA synthetase; PHYH, phytanoyl-CoA 2-hydroxylase; SCPx, SCP-2/3-ketoacyl-CoA thiolase; TER, trans-2-enoyl-CoA reductase; THCA, 3α,7α, 12 α-trihydroxy-5β-cholestanoic acid. The figure was partly generated using Servier Medical Art.

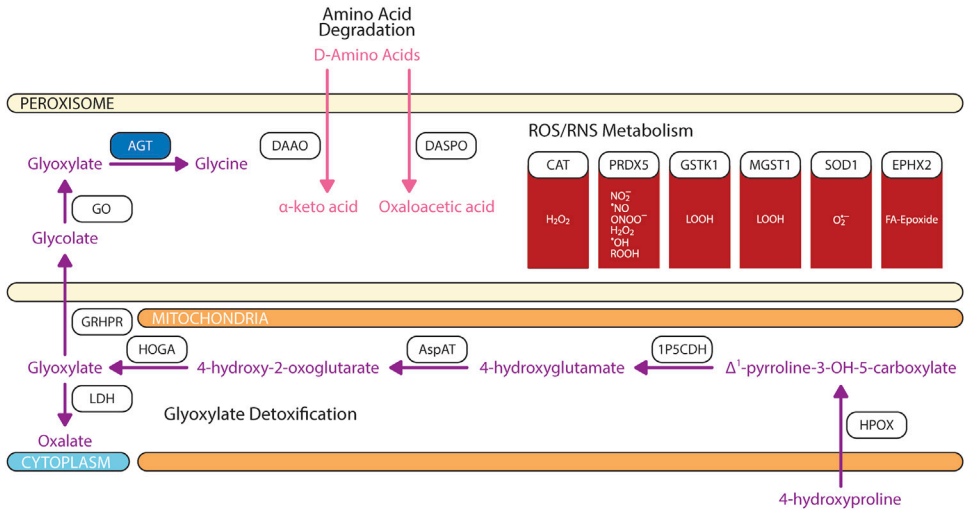


FIGURE 5
Biochemical pathways of glyoxylate, amino acids, and reactive oxygen/nitrogen species degradations. Blue box represents enzymes with published pathogenic variants resulting in ocular manifestations in humans. 1P5CDH, $\Delta^1$-pyrroline-5-carboxylate dehydrogenase; AGT, alanine: glyoxylate aminotransferase; AspAT, aspartate aminotransferase; CAT, catalase; DAAO, D-amino acid oxidase; DASPO, D-aspartate oxidase; EPHX2, epoxide hydrolase 2; GO, glycolate oxidase; GRHPR, glyoxylate and hydroxypyruvate reductase; GSH, glutathione; GSTK, glutathione transferase kappa; HOGA, 4-hydroxy-2-oxoglutarate aldolase; HPOX, hydroxyproline oxidase; LDH, lactate dehydrogenase; MGST, microsomal glutathione S-transferase; PRDX5, peroxiredoxin 5; SOD1, superoxide dismutase. The figure was partly generated using Servier Medical Art.

CAT is the most abundant peroxisomal antioxidant enzyme that is highly expressed in RPE as compared to neural retina. CAT activity exhibits a diurnal pattern where post-translational modification of CAT increases antioxidant activity in the morning during peak VLCFA β-oxidation. While PRDX5 can assist in $H_2O_2$ degradation, it is limited due to the small rate constant (Knoops et al., 2011). Superoxide anion radical ($O_2^{\bullet-}$) and nitric oxide radical ($^{\bullet}NO$) are produced by xanthine oxidase and the inducible form of nitric oxide synthase. While superoxide is degraded by superoxide dismutase 1 (SOD1), $^{\bullet}NO$ is thermodynamically favored to form peroxynitrite ($ONOO^-$) with superoxide anion radical after which $ONOO^-$is predominantly degraded by PRDX5 (Pacher et al., 2007; Trujillo et al., 2007; Antonenkov et al., 2010). Hydroxyl radical ($^{\bullet}OH$) are produced from $H_2O_2$ through Fenton reactions (Winterbourn, 1995). $^{\bullet}OH$ and $^{\bullet}NO$ may target protein cysteine thiol and unsaturated lipids causing cysteine oxidation and lipid peroxidation (Lismont et al., 2015). PRDX5 also degrades alkyl hydroperoxides (ROOH); whereas LOOH and fatty acid epoxides are detoxified by glutathione transferase kappa (GSTK1)/microsomal glutathione S-transferase 1 (MGST1) and epoxide hydrolase 2 (EPHX2) (Summerer et al., 2002; Sala et al., 2003; Knoops et al., 2011). Free radicals may also be non-enzymatically scavenged by glutathione (GSH), ascorbic acid (vitamin C), and plasmalogens (Circu and Aw, 2010; Ivashchenko et al., 2011). While the mechanisms by which GSH and ascorbic acid modulate oxidative stress are debated, plasmalogen quenches lipid peroxidation and protects unsaturated fatty acid from oxidation in the membrane because the vinyl-ether bond of plasmalogen interact faster with singlet oxygen and free radicals than other fatty acids (Broniec et al., 2011; Wallner and Schmitz, 2011).

Redox imbalance is a significant contributor to multiple retinal metabolic diseases (Kowluru and Chan, 2007; Bellezza, 2018; Trachsel-Moncho et al., 2018; Graziosi et al., 2020). Restoring the redox homeostasis preserves retinal neuronal and vascular stability. However, the role of peroxisomal redox contribution to retinopathy is understudied. A recent report has shown that overactivation of peroxisomal oxidation with a gain function of ACOX1 ($ACOX1^{N237S}$) causes elevated ROS and retinal glial loss (Chung et al., 2020). Further exploration of peroxisomal redox balance in retinal function is needed.

## 2.5 Anabolic function: Plasmalogen synthesis

Plasmalogen (Pls) are a subclass of glycerophospholipids defined by a vinyl-ether bond at *sn*-1 position of glycerol

backbone. Dependent on the polar head group at *sn*-3 position, compositions of fatty acids at the *sn*-1 ether-linkage and *sn*-2 ester-linkage differs. Plasmalogen ethanolamine (PlsEtn) is the predominant subclass in photoreceptor rod inner segment and RPE (Acar et al., 2007; Bretillon et al., 2008; Acar et al., 2012). In the retina and RPE, PlsEtn accounts for 20–40 and 30% of ethanolamine glycerophospholipids, respectively (Heymans et al., 1983; Acar et al., 2007; Acar et al., 2012). PlsEtn is composed of ether-linked saturated fatty acid (16:0/18:0) or monounsaturated fatty acid (18:1n-9/18:1n-7) at sn-1 position and ester-linked PUFA (DHA/20:4n-6—arachidonic acid, ARA) at *sn*-2 position (Acar et al., 2012). Plasmalogen choline (PlsCho) is the predominant subclass in white matter and optic nerve where it accounts for 76 and 36% of total glycerophospholipids, respectively (Han et al., 2001; Acar et al., 2012). PlsCho is composed of ether-linked saturated fatty acid (16:0/18:0) or monounsaturated fatty acid (18:1n-9/18:1n-7) at sn-1 position and ester-linked saturated fatty acid (18:0) at *sn*-2 position (Han et al., 2001; Acar et al., 2012). The concentrated Pls level in RPE is likely to protect against elevated oxidative stress as discussed in previous section.

Peroxisome is critical for initiation of ether phospholipid synthesis as the initial two enzymes in a complex, glycerone-phosphate O-acyltransferase (GNPAT) and alkyl-glyceronephosphate synthase (AGPS) are targeted to inner peroxisomal membrane via PTS2 and PTS1 signal peptide, respectively (Hasan et al., 2013; Fujiki et al., 2014) (Figure 3). Dihydroxyacetone-phosphate (DHAP) is esterified to a long chain fatty acyl-CoA at *sn*-1 position by GNPAT, then AGPS catalyzes the exchange of 1-acyl-DHAP and long chain alcohol to produce 1-alkyl-DHAP. This exchange is essential to ensure synthesis of alk-1′-enyl ether bond by plasmanylethanolamine desaturate (encoded by TMEM189 gene) in ER (Gallego-Garcia et al., 2019; Werner et al., 2020). Long chain alcohol is synthesized by two peroxisomal acyl-CoA reductases: fatty acyl-CoA reductase 1 (FAR1) and fatty acyl-CoA reductase 2 (FAR2) (Cheng and Russell, 2004). FAR1 have high affinity for palmitoyl-CoA (16:0-CoA), stearoyl-CoA (18:0-CoA), and oleoyl-CoA (18:1n-9-CoA); thereby explaining unique composition of saturated and monounsaturated fatty acids at *sn*-1 ether linkage (Bishop and Hajra, 1981). In contrast, FAR2 catalyzes synthesis of long chain fatty alcohol by binding fatty acyl-CoA with >20 carbons (Otsuka et al., 2022). Finally, 1-alkyl-DHAP is reduced by peroxisomal acyl/alkyl DHAP reductase (ADHAPR—encoded by *Dhrs7b*) (Honsho et al., 2020). GNPAT is ubiquitously expressed in neural retina and RPE (Acar et al., 2007; Das et al., 2019). Retinal distributions of AGPS, FAR1, FAR2, and ADHAPR have not yet been characterized.

## 2.6 Anabolic function: Docosahexaenoic acid (DHA) synthesis

DHA is the predominant omega-3 polyunsaturated fatty acids (n-3 PUFA) in retinal phospholipid membrane and its accretion may modulate membrane fluidity which affects assemblies of protein complexes and their retinal activity (Fliesler and Anderson, 1983; Treen et al., 1992; Litman and Mitchell, 1996). In human, DHA accounts for 15.3% of total fatty acids in photoreceptor rod cell outer segments as compared to 1–4% in other tissues (Fliesler and Anderson, 1983; Acar et al., 2012). In contrast to photoreceptor rod cells, the compositions of total DHA and diDHA (unique phospholipids with two ester-linked DHA) species in phosphatidylcholine, phosphatidylethanolamine and phosphatidylserine were approximately 2-fold lower in cone-dominant retinas (Agbaga et al., 2018). The unique DHA accretion in the retina is maintained by three mechanisms: 1) dietary uptake of DHA (Young, 1976; Wang and Anderson, 1993b; Pifferi et al., 2012), 2) recycling of phospholipid DHA in rod outer segments via phagocytosis (Young, 1976; Stinson et al., 1991b; Gordon et al., 1992; Gordon and Bazan, 1993), and 3) synthesis of DHA from dietary precursors including α-linolenic acid (ALA, 18:3n-3), eicosapentaenoic acid (EPA, 20:5n-3), and DPAn-3 (22:5n-3) (Anderson et al., 1990; Wang and Anderson, 1993a; Alvarez et al., 1994; Delton-Vandenbroucke et al., 1997). Although biosynthesis of DHA from dietary n-3 PUFA precursor in retina and RPE is limited, impairment in peroxisomal β-oxidation of THA to DHA was observed in patients with X-linked retinitis pigmentosa (Wetzel et al., 1991; Hoffman et al., 2001).

DHA synthesis was first described to be solely localized to the ER where a series of alternating elongation by ELOVL5/2 and desaturation by FADS1/2 to produce DPAn-3. DPAn-3 is subsequently desaturated to DHA by Δ4-desaturase. However, the presence of Δ4-desaturase in retina is still heavily debated (Metherel and Bazinet, 2019). Since the publication of Voss et al., in 1991, the dogma of DHA synthesis shifted from a localized ER pathway to concerted efforts between ER and peroxisome which is later termed the Sprecher Pathway (Voss et al., 1991; Sprecher et al., 1995) (Figure 3). From fibroblasts of patients with Zellweger and Refsum disease, the final steps of DHA synthesis were characterized as such that DPAn-3 is elongated to tetrapentaenoic acid (TPA, 24:5n-3) by ELOVL2 and desaturated to THA by FADS2 in ER, then transported to peroxisome via ABCD2, where peroxisomal β-oxidation retroconvert THA to DHA for export (Moore et al., 1995; Morita and Imanaka, 2012). The other possibility is that peroxisomal dysfunction also affect the DHA recycling from photoreceptor outer segment shedding, which will be further discussed in Session 3.

Peroxisomal dysfunction in patients causes DHA deficiency in the brain and retina (Martinez, 1992). Lack of DHA contribute to the pathophysiology of multiple retinal disorders (Fu et al., 2019). In retinal diseases including diabetic retinopathy, retinopathy of prematurity (ROP), age-related macular degeneration (AMD) and inherited retinal degenerative diseases, DHA deficiency is observed. However, DHA supplementation shows positive impacts in some but not all studies (Fu et al., 2019).

## 2.7 Anabolic function: Bile acid synthesis

Bile acids, cholic acid (CA) and chenodeoxycholic acid (CDCA), play an important role in homeostasis of cholesterol metabolism in the retina. Unconjugated and taurine-conjugated metabolites of CDCA, ursodeoxycholic acid and tauroursodeoxycholic acid, are neuroprotective of photoreceptors and ganglion cells (Daruich et al., 2019; Win et al., 2021). Classic bile acid synthesis commenced with conversion of cholesterol to 7α-hydroxycholesterol by 7α-hydroxylase (CYP7A1) leading to production of DHCA and THCA in mitochondria (Chiang, 2004). Then in the ER, CoA activation of DHCA and THCA is catalyzed by bile acid-CoA ligase (BACL) (Wheeler et al., 1997; Falany et al., 2002). DHCA-CoA and THCA-CoA are then transported by ABCD3 into peroxisome where β-oxidation chain shortening produce chenodeoxycholoyl-CoA and choloyl-CoA, respectively (Ferdinandusse et al., 2015) (Figure 4). In contrast to liver, retina predominantly relies on an alternative pathway for bile acid synthesis where mitochondrial CYP27A1 in rod inner segment and ER CYP46A1 in retinal ganglion cells convert cholesterol to 27-hydroxycholesterol and 24-hydroxycholesterol, respectively (Lee et al., 2006; Ramirez et al., 2008; Ishikawa et al., 2016; Mertens et al., 2017). Hydroxylated cholesterol intermediates of CYP27A1 and CYP46A1 are then converted to DHCA and THCA at which classic pathway of CDCA and CA synthesis resume (Omarova et al., 2012; Saadane et al., 2014). Chenodeoxycholoyl-CoA and choloyl-CoA are then conjugated with taurine or glycine by peroxisomal bile acid-CoA:amino acid N-acyltransferase (BAAT) to produce tauro/glycochenodeoxycholate and tauro/glycocholate (Pellicoro et al., 2007).

# 3 Peroxisomal disorders and ocular symptoms

Based on the results of enzyme activity studies and biochemical markers, the peroxisomal disorders was historically divided into three groups: 1) peroxisomal biogenesis disorders (PBD); 2) multiple enzyme deficiencies; and 3) single enzyme/transporter deficiency disorders. With recent development in the understanding of the biochemical and molecular genetic bases of these conditions, a new system has been proposed to divide the PBD into two subtypes: Zellweger Spectrum Disorder (PBD-ZSD) and the rhizomelic chondrodysplasia punctata (RCDP) spectrum (previously known as the multiple enzyme deficiencies). Other conditions such as Heimler Syndrome (HS), which was previously classified as a distinct syndrome consists of sensorineural hearing loss, amelogenesis inperfecta (AI) and nail anomalies with or without visual defect, is now considered as part of the PBD-ZSD (Ratbi et al., 2015). Single enzyme/transporter deficiency disorders such as X-linked adrenoleukodystrophy (X-ALD) and peroxisomal acyl-CoA oxidase (ACOX) deficiency remains a separate entity.

## 3.1 Gene mutations in peroxisomal biogenesis

PBD-ZSD is a group of conditions with a very broad clinical spectrum ranging from neonatal lethal conditions with severe neurological presentation to adult-onset isolated visual impairment, sensorineural hearing loss, adrenal insufficiency, or liver disease. The incidence of PBD-ZSD was estimated to be around 1 per 50,000 births (Braverman et al., 2016). PBD-ZSD is characterized by biochemical findings of elevated plasma VLCFAs (C24 and C26), elevated plasma C24:C22 and C26:C22 ratio, elevated plasma phytanic acid, pristanic acid, pipecolic acid and bile acids concentrations, reduced erythrocyte plasmalogen level, and elevated urinary excretion of dicarboxylic acid (Steinberg et al., 2006; Braverman et al., 2016) (Figure 4). Patients with PBD-ZSD typically carry biallelic (homozygous or compound heterozygous) pathogenic variants in the PEX family genes, which encode proteins involved in peroxisome biogenesis and proliferation. A total of sixteen PEX genes have been identified in humans, and PBD-ZSD have been associated with PEX1, PEX2, PEX3, PEX5, PEX6, PEX10, PEX11β, PEX12, PEX13, PEX14, PEX16, PEX19, and PEX26 (Ebberink et al., 2009; Waterham and Ebberink, 2012; Krause et al., 2013; Fedick et al., 2014; Kettelhut and Thoms, 2014; Komatsuzaki et al., 2015; Konkolova et al., 2015; Renaud et al., 2016; Waterham et al., 2016; Bjorgo et al., 2017; Rydzanicz et al., 2017; Stowe and Agarwal, 2017; Kumar et al., 2018). Patients with loss-of-function PEX gene defects and abolished peroxin activity, are most severe in their clinical presentation. In contrast, variants with residual peroxin function, such as missense variants, result in a milder cellular and clinical phenotype. However, not all missense variants have residual activity, and the clinical course of a patient cannot be predicted by the genetic variants alone.

Diagnosing patients with mild presentation of PBD-ZSD has been challenging due to the diverse and non-specific nature of the symptoms (Enns et al., 2021). Nonetheless, recent expansion in

newborn screening programs have included screening of X-ALD using liquid chromatography tandem mass spectroscopy (LC-MS/MS) to detect VLCFA, C26:0-lysophosphatidyl choline (C26:0-LPC), from dried blood spots (Turk et al., 2020). First introduced in 2013, newborn screening for X-ALD is now carried out in 20 States and the District of Columbia with 2 additional states currently running pilot programs (*https://adrenoleukodystrophy.info/clinical-diagnosis/ald-newborn-screening*). Therefore, every newborn from these states will have C26:0-LPC testing at birth, which will identify all newborns with PBD-ZSD (Klemp et al., 2021). Concerns have been raised around the "incidental" identification of PBD-ZSD patients through the X-ALD screening due to lack of targeted treatment that modifies the course of PBD-ZSD. Therefore, development of targeted PBD-ZSD treatment is in dire need.

The central nerves system (CNS) manifestations of PBD-ZSD involves structural brain malformations, predominantly involve the neuronal migration defects such as polymicrogyria, heterotopia, agenesis/hypoplasia of the corpus callosum, pachygyria, and hypoplastic olfactory bulb. Cerebral ventricular abnormalities such as colpocephaly and progressive dilatation of the ventricles were also reported (Nakai et al., 1995). Demyelination and global cerebral atrophy have also been reported in both early and late onset cases (Renaud et al., 2016). Ocular phenotypes related to PBD-ZSD includes anterior changes of cornea clouding, cataracts, and Brushfield spots (small, white or greyish/brown spots on the periphery of the iris). Posterior ocular findings include Leber congenital amaurosis (LCA), pigmentary retinopathy, and optic nerve dysplasia (Lambert et al., 1989; Mechaussier et al., 2019). LCA is a severe form of early onset retinal dystrophy. Patients with LCA typically have visual impairment since infancy. Symptoms of LCA include photophobia, nystagmus, keratoconus, and behavior of eye poking and picking (oculo-digital signs). Retinal changes associated with PBD-ZSD involve all retinal layers from RPE to retinal ganglion cells (Haddad et al., 1976), with most severe loss in photoreceptors (Haddad et al., 1976; Kretzer et al., 1981; Garner et al., 1982). These changes are scattered from central to peripheral retina. The optic nerve of patients with PBD-ZSD can be profoundly demyelinated (Thomas et al., 1975). Fundoscopic changes in patients with PBD-ZSD can include retinal arteriolar attenuation, pale optic disc and loss of pigment epithelium most prevalent in the macular area (Folz and Trobe, 1991).

Heimler Syndrome is a condition found to be caused by pathogenic variants in PEX1 and PEX6 genes (Ratbi et al., 2015). It represents the mild end of PBD-ZSD. Long term follow-ups of index cases revealed "salt-and-pepper"-like mottling of RPE and abnormal electroretinogram (ERG) recording in young adulthood after complaints of decreased vision in a female patient. The patient also had cystoid macular edema in keeping with the diagnosis of macular dystrophy (Lima et al., 2011). After evaluating other patients with Heimler syndrome, three additional patients with PEX1 variants and one patient with PEX6 variants were also found to have retinal pigmentary changes (Heimler et al., 1991; Zaki et al., 2016). Given the rarity of these conditions, most literature is constituted with case studies describing the retinal phenotype of PBD-ZSD. Studies focusing on the natural history of retinal dystrophy in PBD-ZSD are required to understand its progressive impact on vision.

## 3.2 Gene mutations in peroxisomal β-oxidation

Peroxisomal acyl-CoA oxidase deficiency disorder caused by biallelic pathogenic variants in *ACOX1* gene and D-bifunctional protein (DBP) deficiency disorder caused by either or both MFE 2-enoyl-CoA hydratase and 3-hydroxyacyl-CoA dehydrogenase deficiency, are disorders of peroxisomal fatty acid β oxidation (Figure 3). They can present with neonatal onset severe neurological sequela with progressive white-matter demyelination, seizures, and cortical malformations. Both conditions were associated with visual impairment, abolished electroretinogram possibly related to retinal degeneration or subretinal pigmentary retinopathy (Suzuki et al., 2002; Kurian et al., 2004; Bae et al., 2020). ACOX1 is abundantly expressed in the RPE as compared to neural retina, whereas the distribution of ACOX2 and ACOX3 in RPE and retinal layers remains unclear (Das et al., 2019). ACOX1 deficiency results in premature death in adolescence and are associated with abnormal retinal pigmentation, retinal degeneration, and optic atrophy (Das et al., 2021). Patients with ACOX1 deficiency have elevated plasma and fibroblast saturated VLCFA and comparable saturated LCFA, BCFA (phytanic acid), and DHCA/THCA to control (Ferdinandusse et al., 2007). MFE-2 is equally or more expressed in the neural retina than RPE, whereas expressions of MFE-1 has yet to be elucidated in the eyes (Das et al., 2019). Severe MFE-2 deficiency may manifest symptoms comparable to that of PBD-ZSD; however milder juvenile onset deficiency may present with abnormal retinal pigmentation with normal visual acuity (Das et al., 2021). Patients with MFE-2 deficiency have elevated levels of saturated VLCFA, BCFA (pristanic acid), and DHCA/THCA and reduced levels of plasma and retinal DHA (Martinez, 1992; Ferdinandusse et al., 2006a). Patients with peroxisomal ACOX deficiency and MFE-2 deficiency show no accumulation of pipecolic acid, with no reduction in erythrocyte plasmalogens. MFE-2 deficiency is associated with increased plasma levels of bile acid intermediates, but ACOX deficiency is not (Ferdinandusse et al., 2007).

SCPx deficiency was first reported in 2006 in a patient with normal level of VLCFA but elevated level of pristanic acid (Ferdinandusse et al., 2006b). The only ocular finding

reported was pathological saccadic eye movements indicating potential pathology in the brain stem. Another patient with SCPx deficiency had mild symptoms of nyctalopia. This individual had normal visual acuity. Detailed ocular investigation revealed peripapillary atrophy, irregular autofluorescence associated with the major vascular arcades, with no peripheral pigmentary retinal changes (Horvath et al., 2015; Morarji et al., 2017). ACAA1 deficiency has yet to be associated with human disease.

## 3.3 Gene mutations in peroxisomal α-oxidation

FALDH deficiency leads to Sjögren-Larsson Syndrome, a condition associated with accumulation of phytol. Sjögren-Larsson Syndrome is associated with reduced visual acuity, degeneration of Müller cells in the inner retina, retinal thinning, RPE atrophy, and photoreceptor dysfunction (van den Brink et al., 2004; Nanda and Kovach, 2019). PHYH deficiency is one of the primary causes of Refsum disease (Jansen et al., 1997) (Figure 4). Patient with Refsum disease have elevated levels of phytanic acid in blood and tissues. Clinical symptoms of Refsum disease includes retinitis pigmentosa, miosis with attenuated pupillary light response, iris atrophy, and cataract (Ruether et al., 2010). Phytanic acid exposure cause morphological changes in both fetal bovine and human RPE *in vitro*, mimicking the RPE pathology observed in patients with Refsum's disease (Bernstein et al., 1992). HACL1 deficiency has yet to be reported in humans; however, animal model suggests that dietary intake of phytol in *Hacl1*$^{-/+}$ mice exhibited elevated levels of phytanic acid in blood and tissues similar to the biochemical profile of patients with Refsum disease (Mezzar et al., 2017). Interestingly, the human HACL1 is only three amino acids different from its mouse analog. Clinical phenotypes of AMACR deficiency include retinitis pigmentosa and decreased visual acuity (Thompson et al., 2009; Stewart et al., 2011).

## 3.4 Gene mutations in glyoxylate detoxification

Defects in *AGXT* gene results in primary hyperoxaluria type 1, which is an inborn error of metabolism characterized by accumulation of calcium oxalate (Figure 5). This process leads to calcinosis cutis metastatica of the skin, tooth mobility, vascular spasm/occlusion, and nephrocalcinosis. Retinal complications include optic atrophy, retinopathy and choroidal neovascularization (Leumann and Hoppe, 2001; Cochat et al., 2006; Lorenzo et al., 2006). Patients with primary hyperoxaluria type 1 also exhibit crystalline deposit in RPE leading to bilateral vision loss (Roth et al., 2012; Kourti et al., 2020).

## 3.5 Gene mutations in plasmalogen synthesis

GNPAT deficiency results in RCDP type 2 (Wanders et al., 1992) (Figure 3). Patients with GNPAT deficiency have low plasmalogen levels in erythrocytes. They typically have a shortened life expectancy not exceeding a decade (Itzkovitz et al., 2012). Congenital cataracts have been reported (Wanders et al., 1992). AGPS deficiency results in RCDP type 3 and patients exhibited lower levels of plasmalogen in erythrocytes (Wanders et al., 1994). FAR1 deficiency results in autosomal recessive RCDP type 4 (Buchert et al., 2014). FAR1-deficient patients have markedly lower levels of plasmalogens, and congenital cataracts is a cardinal symptom (Buchert et al., 2014). Interestingly, patients with autosomal dominant FAR1 *de novo* variants also shares similar clinical phenotypes including congenital and juvenile cataracts, but a divergent biochemical phenotype of elevated plasmalogens in fibroblasts (Ferdinandusse et al., 2021). FAR1 *de novo* variant disrupted negative feedback regulation leading to un-inhibited biosynthesis of plasmalogen (Ferdinandusse et al., 2021). Deficiency in FAR2 has yet to be associated with human diseases.

## 3.6 Gene mutations in peroxisomal membrane transporter

Although, ABCD1 was shown to be expressed ubiquitously between RPE and neural retina in rodent model (Das et al., 2019), patients with X-ALD do not exhibit direct retinal pathology. The visual impairment in X-ALD patients are caused by two mechanisms: 1) the loss of color vision in a subgroup of X-ALD patients are caused by continuous gene deletions in X chromosome where *ABCD1* gene and red pigment gene are in close proximity (Sack et al., 1989) or by chromosome rearrangements (Alpern et al., 1993), 2) the cortical blindness associated with X-ALD is caused by visual track demyelination, which can subsequently lead to retrograde degeneration of ganglion cells (Kaplan et al., 1995; Ohkuma et al., 2014).

Patients with ABCD3 deficiency have elevated levels of DHCA and THCA, but ocular abnormalities have not yet been identified (Ferdinandusse et al., 2015). Patients with BAAT deficiency exhibited elevated levels of unconjugated bile acids (Carlton et al., 2003). BAAT expression in retinal cells are unknown and patients with BAAT deficiency has no reported ocular abnormalities.

Recently, patients with biallelic pathogenic variants in acyl-CoA binding domain containing protein 5 (ACBD5) gene have been reported (Abu-Safieh et al., 2013; Ferdinandusse et al., 2017; Bartlett et al., 2021). These patients demonstrated progressive neurological deterioration, nystagmus, optic atrophy, cone-rod dystrophy, early onset retinal dystrophy, attenuation of eye vessels, and diffuse granularity of RPE.

## 3.7 Current therapy

Currently, there is no curative or targeted disease modifying treatment for PBD-ZSD. Cholic acid (CA) therapy was approved by Food and Drug Administration (FDA) in March 2015 to treat liver disease in patients with PBD-ZSD. CA has been shown to decrease toxic bile acid intermediates, improve transaminase levels, and reduce liver inflammation, with improvement in growth parameters in pediatric populations (Anderson et al., 2021). Since PBD-ZSD patients have markedly low level of DHA (Janssen et al., 2000), trials of DHA supplementation were made as an attempt to restore the neurological, ocular and hepatic function in PBD-ZSD patients. M. Martinez conducted a cohort study in the 1990s treating 20 PBD-ZSD patients with DHA supplementation. Patients were treated with variable doses of DHA ethyl ether (depends on age and blood DHA level) between 9 months and 9 years and more than half of the patients not only had improved biochemical markers such as reduced VLCFA and increased erythrocyte plasmalogen level, but also improved brain and retinal function compared to pre-treatment (Martinez, 2001). Nonetheless, the clinical improvement was not subjectively quantified. A follow up study focusing on the visual function of this cohort demonstrated resolution of nystagmus, improvement of ERG recording, and amelioration of visual behaviors in some cases and stabilization in the rest. The improvement was better appreciated in patients who had baseline ophthalmological assessment (Noguer and Martinez, 2010). Based on this preliminary work, a randomized double-blind case control trial was conducted supplementing a fixed dose (100 mg/kg/d) of DHA triglyceride (47% DHA) and arachidonic acid (ARA; 20:4n-6) triglyceride (46% ARA) (Paker et al., 2010). This is a short-term study in 50 patients (25 in treatment group and 25 in control) with follow ups in 1 year. The study also focused exclusively on quantitative biometrics of patients such as ERG changes, weight, height and biochemical markers such as VLCFA, plasmalogen and liver enzymes. Given the short-term intervention and the broad spectrum of clinical variability of PBD-ZSD patients, it was not surprising that no statistically significant changes were obtained between the two groups. At this time, there is very limited evidence supporting the efficacy of clinical use of DHA in patients with PBD-ZSD.

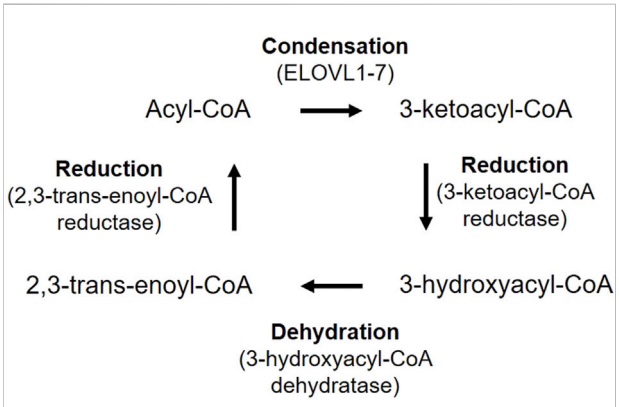


FIGURE 6
VLCFA biosynthesis in mammalians. Acyl-CoA is first condensed with malonyl-CoA to produce 3-ketoacyl-CoA, catalyzed by fatty acid elongase (ELOVL1-7). 3-ketoacyl-CoA is reduced to 3-hydroxyacyl-CoA by 3-ketoacyl-CoA reductase. 3-Hydroxyacyl-CoA is then dehydrated by 3-hydroxyacyl-CoA dehydratase and generate 2,3-trans-enoyl-CoA. Finally, 2,3-hydroxyacyl-CoA is reduced to an acyl-CoA by 2,3-trans-enoyl-CoA reductase, with two more carbon chain units than the original acyl-CoA.

# 4 Peroxisomes and other cell organelles

Peroxisomes are highly dependent on the interaction with other organelles (ER, mitochondria and lysosomes) in order to perform proper metabolism. For example, some of the peroxisomal substrates (e.g., VLCFAs) are synthesized and elongated from shorter chain fatty acids (SCFAs) in ER. In addition, the end products of peroxisomal β-oxidation subsequently enter mitochondria for metabolism and energy production.

## 4.1 Peroxisomes and ER

Most of VLCFAs are not derived from dietary source, instead, FAs are elongated in ER by cycling through a four-step process (condensation, reduction, dehydration and reduction) (Figure 6) (Kihara, 2012). Acyl-CoA is elongated to have two more carbon units in each cycle. The FA elongases ELOVL1-7 have characteristic substrate specificity (Kihara, 2012). ELOVL1,3,4,6 and 7 elongate SFAs and MUFAs, while ELOLV2 and 5 are strictly PUFA-specific. VLCPUFAs uniquely exist in mammalian retina, brain, and sperm (Kihara, 2012). ELOLV4 is critical for the synthesis of VLCFAs and expressed highest in the retina (Agbaga et al., 2010; Kihara, 2012). Mutations in the *ELOVL4* gene leads to Stargardt disease type 3 that causes vision loss starting around 14 years old (Edwards et al., 1999; Agbaga et al., 2010). Loss of photoreceptor ELOLV4 in mice causes significant decrease in retinal glycero-phospholipids containing VLCPUFAs, abnormal accumulation of lipid droplets and lipofuscin-like granules, as well as decreased retinal neuronal responses by ERG (Harkewicz et al., 2012). In addition, adiponectin receptor 1 (ADIPOR1), which is predominantly expressed in photoreceptors (Fu et al., 2017), may recycle VLCPUFAs (containing DHA C22:6) from shed photoreceptor apical disk membrane back to photoreceptor inner segments and further elongate in ER, thus preserves photoreceptor cell survival (Rice et al., 2015). The VAMP-associated proteins (VAP)-ACBD5 complex acts as the

primary ER-peroxisome tether, and loss of VAP or ACBD5 increases peroxisome mobility. VAP-ACBD5-mediated contact between the ER and peroxisomes is also important for peroxisome growth and lipid homeostasis (Costello et al., 2017; Hua et al., 2017).

In addition, plasmalogen synthesis starts in peroxisomes and completes in ER (Nagan and Zoeller, 2001; Braverman and Moser, 2012). The initial two steps are catalyzed by peroxisomal matrix enzymes dihydroxyacetone phosphate acyltransferase (DHAPAT/GNPAT) for transfer of acyl-DHAP across the enzyme active sites, and AGPS for the exchange of the acyl group (fatty acid) for an alkyl group (fatty alcohol, supplied by FAR1). Alkyl-DHAP is further reduced and plasmalogen synthesis proceeds in the ER (Figure 2).

Moreover, ER is involved in peroxisome biogenesis. Peroxisomal membrane proteins (PMP) are thought to be first inserted in ER and subsequently exit from ER to peroxisomes (Dimitrov et al., 2013). It has also been proposed that peroxisomes originate from ER and the avoidance of toxic lipid by-products is the driving force for the separation of the peroxisomes (Gabaldon, 2014). In mammalian cells, PEX16 with an appended $NH_2$-terminal type I signal anchor sequence moves to peroxisomes after being cotranslationally synthesized in the ER (Kim et al., 2006). In mouse dendritic cells, PEX13 and PMP70 are present in the ER domain with a peroxisomal reticulum from which mature peroxisomes are derived (Geuze et al., 2003). Meanwhile, the peroxisome biogenesis factors PEX19 and PEX3 cooperate and mediates the posttranslational targeting of proteins such as UBXD8, a lipid droplet-destined membrane protein and reticulon homology domain-containing protein to ER (Schrul and Kopito, 2016; Yamamoto and Sakisaka, 2018). Therefore, the close connection between peroxisome and ER is evident.

## 4.2 Peroxisomes and lysosomes

Peroxisomal substrates such as VLCFAs can also be generated from lysosomal degradation of different lipid species. Rod photoreceptor outer segment is rich in VLCPUFA and LCPUFA (DHA and ARA), which comprise ~60% of total phospholipids (Stinson et al., 1991a). To maintain normal retinal function, there is a continuous shedding of photoreceptor outer segment on daily basis (Fliesler & Anderson, 1983). The sheded outer segments are ingested by RPE via phagocytosis and packaged into membrane-bound phagosomes, which are then fused with lysosomes for subsequent degradation (Bosch et al., 1993; Ferrington et al., 2016). It has been reported that there is a dynamic membrane contact between peroxisomes and lysosomes mediated by lysosomal Synaptotagmin VII (Syt7) binding to the lipid $PI(4,5)P_2$ on peroxisomal membrane, and the organelle contact facilitates the transport of cholesterol from lysosomes to peroxisomes (Chu et al., 2015). Cholesterol is accumulated in cells and animal models of peroxisomal disorders (Chu et al., 2015). These findings suggest the potential involvement of peroxisomes in VLCFAs recycling during photoreceptor outer segment shedding. Although RPE immediately recycles DHA released from the disc membrane during degradation back to photoreceptors for disc membrane synthesis (Bazan et al., 1992), the involvement of peroxisome in this process is yet to be characterized. Moreover, compromised lysosomes with impaired degradative enzyme activity leads to lipofuscin-like autofluorescence in RPE (Guha et al., 2014). Understanding of the interactions between peroxisome and lysosome will uncover the basic lipid biology and balance in retina.

## 4.3 Peroxisomes and mitochondria

Peroxisomes and mitochondria tightly interact with each other in fatty acid metabolism and undergo close communication through three major pathways: 1) there is a physical association between these two organelles, and the degree of contact changes dynamically with the cell types and microenvironment (Fransen et al., 2017). For example, the peroxisomal membrane protein PEX34 (conserved to humans) and the outer mitochondrial membrane protein FZO1 (mammalian homologue Mitofusin 2) tether the peroxisome and mitochondria in the yeast (Shai et al., 2018). 2) mitochondria-derived vesicles containing mitochondria-anchored protein ligase that can fuse with a subset of peroxisomes (Neuspiel et al., 2008); 3) peroxisomes and mitochondria communicates through releasing of biological messengers such as ROS, lipids and $NAD^+$ etc.

VLCFAs, which cannot be degraded in mitochondria, need to be shortened by peroxisome β-oxidation. Shortened VLCFAs are further oxidized in mitochondria for energy production. Peroxisomal β-oxidation can also compensate defective mitochondrial fatty oxidation by breaking down medium-chain and long-chain fatty acids (Violante et al., 2019; Ranea-Robles et al., 2021). Studies of RPE from AMD vs control patients indicated that proliferation of peroxisomes is accompanied with mitochondrial abnormalities (Feher et al., 2006). Abnormal peroxisomal metabolism and redox status can rapidly disturb mitochondrial redox state. The antioxidant enzyme CAT is mainly localized in peroxisomes. Deficiency of CAT increases redox state of mitochondria and peroxisome-derived oxidative stress causes mitochondrial redox imbalance (Ivashchenko et al., 2011). Retinal transfection of AAV-expressing CAT and superoxide dismutases 2 (SOD2) prolonged cone photoreceptor survival in mice during retinal degeneration (Xiong et al., 2015), and AAV-CAT also exerts

neuroprotective effects on retinal ganglion cells in ischemia-induced retinal injury in rats (Chen and Tang, 2011).

In addition, peroxisomal oxidation also regulates lipid composition in mitochondria membrane, which in turn regulates mitochondrial dynamics and ATP production (Petrushka et al., 1959; Hatch, 2004). Oxidative stress induces release of cytochrome *c* from mitochondria, and cytochrome *c* cleaves plasmenylcholine (plasmalogens of the phosphocholine head group class) in membrane bilayers (Jenkins et al., 2018). Loss of plasmalogens in mitochondrial membrane causes inefficient respiration (Kimura et al., 2019). As VLCPUFAs are recycled back to the retina during photoreceptor outer segment renewal (Bazan et al., 1992; Gordon et al., 1992), mitochondrial DHA and ARA content could also be potentially modulated by peroxisomal oxidation. Both dietary DHA (no ARA) and ARA (no DHA) in rats profoundly alters cardiac mitochondrial phospholipid fatty acid compositions, and suppresses $Ca^{2+}$-induced opening of the mitochondrial permeability transition pore (MPTP), which causes cell death (Khairallah et al., 2010; Khairallah et al., 2012); dietary DHA (no ARA) also depletes cardiac mitochondrial ARA content (Khairallah et al., 2012). These findings suggest that peroxisomal oxidation may control mitochondrial membrane composition and activity via VLCPUFA recycling. More recently, it has been reported that adipose specific knockout of the peroxisomal biogenesis factor PEX16 or the plasmalogen synthetic enzyme GNPAT blocks cold-induced mitochondrial fission, decreases mitochondrial copy number and causes abnormal mitochondrial function. Dietary plasmalogen increases mitochondrial copy number, improves mitochondria function in mice with *Pex16* deficiency (Park et al., 2019). This work provides direct evidence of peroxisome-derived ether lipid regulating mitochondrial activity.

Moreover, mitochondrial respiration is also critical to reoxidize NADH formed in peroxisomes and maintain peroxisomal β-oxidation (Wanders et al., 2015). Altered NAD (+)/NADH redox state with age-dependent increases in intracellular NADH and decreases in NAD (+) content is shown in human brain (Zhu et al., 2015), reflecting declined mitochondrial function. NAD (+) levels also decrease in mouse RPE cells with aging (Jadeja et al., 2018). Mutations of gene encoding nicotinamide mononucleotide adenylyltransferase 1 involved in NAD (+) biosynthesis reduce the enzymatic activity and causes blindness within the first year after birth (Koenekoop et al., 2012). Taken together, peroxisomal metabolic and redox homeostasis is important to maintain mitochondrial function. Further understanding of peroxisomal and mitochondrial interaction will provide more clues to understand cellular activity in healthy and diseased retinas.

## 5 Knowledge from the brain

Although there are limited studies regarding the disease pathogenesis of peroxisome-related retinal dysfunction, we could gain some knowledge from the brain investigations as retina is part of the CNS (London et al., 2013). Peroxisomal dysfunction leads to compromised antioxidant defense with decreased CAT expression, attenuated D-serine degradation, disrupted lipid composition in myelin sheath and cellular membranes in the CNS (Uzor et al., 2020), which in turn cause abnormalities in the myelinated axons and synaptic transmission (Berger et al., 2016). Accumulated VLCFAs and decreased plasmalogen ethanolamine levels are observed in the brain of patients with Alzheimer's disease (Ginsberg et al., 1995; Kou et al., 2011). Reduced DHA, ARA and plasmalogen ethanolamine levels are found in the brain of patients with Parkinson's disease, and supplementation of DHA-containing plasmalogen precursor protects against striatal dopamine loss in mice modeling Parkinson's disease (Fabelo et al., 2011; Miville-Godbout et al., 2017). These findings suggest an essential role of peroxisomes and the related lipid metabolism in maintaining brain health.

The contribution of peroxisomes to brain function could be cell-dependent. In mice, dysfunction of peroxisome in neural cells leads to abnormal cortical neuronal migration and maturation of the cerebellum (Janssen et al., 2003; Krysko et al., 2007; Muller et al., 2011). Peroxisome deficiency in astrocytes disturbs brain-derived neurotrophic factor levels and dysregulates axogenesis of the hippocampus neurons (Abe et al., 2020), suggesting that astrocytic peroxisomes modulate neuronal integrity. Moreover, microglial peroxisomal dysfunction induces an inflammatory activated and proliferative state in the mouse brain, but does not affect neuronal health up to one-year old and the long-term impacts is yet to be evaluated (Beckers et al., 2019). Therefore, it would be important to uncover the contribution of neuronal and glial peroxisomal activity to neuronal function in the CNS.

## 6 Future perspectives

Defective peroxisomal function causes disturbed retinal homeostasis and retinal degeneration. However, the mechanisms behind are largely unknown. We speculate that the disrupted lipid metabolism and redox balance typically regulated through the interaction between peroxisomes, lysosomes, mitochondria and ER may contribute to the disease development and progression. Further investigations in the pathophysiology and natural history of peroxisomeal disorder associated retinal dystrophy will greatly advance the potential for therapeutic development.

## 6.1 Retinal lipid homeostasis and alterations

The retinal lipid homeostasis is essential in maintaining normal retinal neuronal and vascular function (Fu et al., 2019; Fliesler, 2021). As there are extensive lipid alterations accompanied with peroxisomal dysfunction, it is important to know that whether all or certain altered lipids are the significant contributors to the development of retinal diseases. Lipids are important membrane components of cells and organelles. Change in lipid composition alters organelle function and cell status. In addition, lipids and their downstream lipid metabolites can function as signaling molecules to induce various cellular responses in metabolism, inflammation, cell survival and apoptosis. Moreover, fatty acids such as palmitate are also possible fuel substrates for photoreceptor, but other type and source of fatty acids are understudied (Joyal et al., 2016). Supplementation of specific deficient lipids and modulating the downstream targeting pathways may be protective against retinal degeneration.

Furthermore, the interaction between RPE, Müller glia, and neuronal cells in retina is also important for the modulation of lipid availability and clearance of neighboring photoreceptors (Fu et al., 2021). For example, disrupted lipid homeostasis in RPE causes lipid droplet formation and RPE dysfunction with aging (Yako et al., 2022). Interestingly, peroxisomes and lipid droplets have physical interaction within cells. Peroxisomal β-oxidation-derived ROS regulate the levels of adipose triglyceride lipase, which control lipolysis of intracellular lipids (Ding et al., 2021). Therefore, increasing peroxisomal activity may decrease lipid droplets in RPE, preserve RPE function and in turn photoreceptor health. Fatty acid profiling focuses on the entire tissue and radiolabeled lipid tracing aids the understanding of the kinetic incorporation, turnover and loss of fatty acids in the retina (Rodriguez de Turco et al., 1990; Gordon and Bazan, 1993; Santos et al., 1995). However, the knowledge of cell-specific uses of lipids and the interactions among different lipid metabolic pathways are limited. The feasibility of single-cell transcriptomics and cell-specific lipidomics in retinal research may provide insight to the cell specific lipid and fatty acid metabolism. Furthermore, progress in characterizing dynamic processing of fatty acids in retina is often limited by the high cost of radiotracer and retinal tissue size. Recently, a cost-effective, tracer-free novel methods using compound-specific isotope analysis (CSIA) has been established to trace fatty acid metabolism by utilizing food sources differing in natural carbon isotope abundance. Briefly, because the carbon isotopic composition of a molecule is conserved following dietary intake, highly precise measurement of carbon 13 ($^{13}C$) abundance can provide insights to the dietary source that contributed to the incorporation of $^{13}C$ to an endogenous molecule. Therefore, by designing well-controlled dietary switch experiments that switches diets made from foods less enriched in $^{13}C$ foods (C3 plants) to foods more enriched in $^{13}C$ (C4 plants), fatty acid incorporation, turnover, and synthesis can be measured as effectively as radiotracer experiments (Lacombe et al., 2020; Lacombe and Bazinet, 2021). Moreover, due to the high precision of $^{13}C$ measurements by gas chromatography-isotope ratio mass spectrometry (GC-IRMS), cell-specific retinal extract can be quantified.

## 6.2 Implications of peroxisomes on other retinal disorders

Altered peroxisomal function has been implicated in age-related neurodegenerative diseases and diabetes-related complications (Cipolla and Lodhi, 2017). In RPE from AMD vs control patients, mitochondrial changes are associated with proliferation of peroxisomes (Feher et al., 2006). However, it is unclear that whether this mitochondrial response is protective or detrimental. Further investigation is required.

Furthermore, the knowledge of DHA metabolism and the application of dietary DHA for prevention of retinal dysfunction is translatable to a number of retinal diseases. Some (but not all) clinical trials showed that fish oil (rich in DHA and EPA) supplementation reduces risk for severe ROP (Pawlik et al., 2011; Beken et al., 2014; Pawlik et al., 2014; Molloy et al., 2016; Najm et al., 2017). Fish oil supplementation or dietary intake of food rich in DHA decreased the risk for AMD in a number of trials (Sangiovanni et al., 2009; Tan et al., 2009; Christen et al., 2011; Ho et al., 2011). However, dietary supplementation of DHA (350 mg/day) and EPA (650 mg/day) did not reduce the risk of advanced AMD in Age-Related Eye Disease Studies (AREDS/AREDS2) (Age-Related Eye Disease Study 2 Research Group, 2013). The reasons for the inconsistent observations are unclear. It has been noted that DHA and EPA supplements may lower circulating ARA levels (D'ascenzo et al., 2014; Zhao et al., 2015) and decrease the ARA/DHA ratio in preterm infants (Najm et al., 2017). Low serum ARA level in the postnatal period is strongly associated with development of clinically significant ROP (Lofqvist et al., 2018) and sufficient ARA is required for DHA to protect against severe ROP (Hellstrom et al., 2021). In addition, DHA- and ARA-oxylipins generated via cytochrome P450 oxidases exaggerates while DHA- and ARA-derived oxylipins via lipoxygenases inhibit pathological retinal neovascularization (Sapieha et al., 2011; Gong et al., 2016; Gong et al., 2017). Therefore, metabolic imbalance among these pathways may also contribute to the inconsistent observations among different trials.

In conclusion, understanding of retinal cell-specific peroxisomal function, VLCFA metabolism and natural history of retinal dysfunction in peroxisomal disorders is a key to development of disease modifying therapeutics. Given the involvement of peroxisomal dysfunction in various retinal pathophysiology, this therapeutic intervention is likely to

benefit common multifactorial retinal degenerative disorders as well.

## Author contributions

All authors listed have made a substantial, direct, and intellectual contribution to the work and approved it for publication.

## Funding

ZF is supported by NIH R01EY032492, NIH R01EY017017, Boston Children's Hospital (OFD/BTREC/CTREC Faculty Career Development Grant 97906, Pilot Grant 92214, and Ophthalmology Foundation 85010), Mass Lions Eye Foundation 87820.

## Conflict of interest

The authors declare that the research was conducted in the absence of any commercial or financial relationships that could be construed as a potential conflict of interest.

## Publisher's note

All claims expressed in this article are solely those of the authors and do not necessarily represent those of their affiliated organizations, or those of the publisher, the editors and the reviewers. Any product that may be evaluated in this article, or claim that may be made by its manufacturer, is not guaranteed or endorsed by the publisher.

## References

Abe, Y., Honsho, M., Kawaguchi, R., Matsuzaki, T., Ichiki, Y., Fujitani, M., et al. (2020). A peroxisome deficiency-induced reductive cytosol state up-regulates the brain-derived neurotrophic factor pathway. *J. Biol. Chem.* 295, 5321–5334. doi:10.1074/jbc.RA119.011989

Abu-Safieh, L., Alrashed, M., Anazi, S., Alkuraya, H., Khan, A. O., Al-Owain, M., et al. (2013). Autozygome-guided exome sequencing in retinal dystrophy patients reveals pathogenetic mutations and novel candidate disease genes. *Genome Res.* 23, 236–247. doi:10.1101/gr.144105.112

Acar, N., Berdeaux, O., Gregoire, S., Cabaret, S., Martine, L., Gain, P., et al. (2012). Lipid composition of the human eye: Are red blood cells a good mirror of retinal and optic nerve fatty acids? *PLoS One* 7, e35102. doi:10.1371/journal.pone.0035102

Acar, N., Gregoire, S., Andre, A., Juaneda, P., Joffre, C., Bron, A. M., et al. (2007). Plasmalogens in the retina: *In situ* hybridization of dihydroxyacetone phosphate acyltransferase (DHAP-AT)--the first enzyme involved in their biosynthesis--and comparative study of retinal and retinal pigment epithelial lipid composition. *Exp. Eye Res.* 84, 143–151. doi:10.1016/j.exer.2006.09.009

Agbaga, M. P., Mandal, M. N., and Anderson, R. E. (2010). Retinal very long-chain PUFAs: New insights from studies on ELOVL4 protein. *J. Lipid Res.* 51, 1624–1642. doi:10.1194/jlr.R005025

Agbaga, M. P., Merriman, D. K., Brush, R. S., Lydic, T. A., Conley, S. M., Naash, M. I., et al. (2018). Differential composition of DHA and very-long-chain PUFAs in rod and cone photoreceptors. *J. Lipid Res.* 59, 1586–1596. doi:10.1194/jlr.M082495

Age-Related Eye Disease Study 2 Research Group (2013). Lutein + zeaxanthin and omega-3 fatty acids for age-related macular degeneration: The age-related eye disease study 2 (AREDS2) randomized clinical trial. *JAMA* 309, 2005–2015. doi:10.1001/jama.2013.4997

Alpern, M., Sack, G. H., Krantz, D. H., Jenness, J., Zhang, H., and Moser, H. W. (1993). Chromosomal rearrangement segregating with adrenoleukodystrophy: Associated changes in color vision. *Proc. Natl. Acad. Sci. U. S. A.* 90, 9494–9498. doi:10.1073/pnas.90.20.9494

Alvarez, R. A., Aguirre, G. D., Acland, G. M., and Anderson, R. E. (1994). Docosapentaenoic acid is converted to docosahexaenoic acid in the retinas of normal and prcd-affected miniature poodle dogs. *Invest. Ophthalmol. Vis. Sci.* 35, 402–408.

Anderson, G. J., Connor, W. E., and Corliss, J. D. (1990). Docosahexaenoic acid is the preferred dietary n-3 fatty acid for the development of the brain and retina. *Pediatr. Res.* 27, 89–97. doi:10.1203/00006450-199001000-00023

Anderson, J. N., Ammous, Z., Eroglu, Y., Hernandez, E., Heubi, J., Himes, R., et al. (2021). Cholbam® and zellweger spectrum disorders: Treatment implementation and management. *Orphanet J. Rare Dis.* 16, 388. doi:10.1186/s13023-021-01940-z

Antonenkov, V. D., Grunau, S., Ohlmeier, S., and Hiltunen, J. K. (2010). Peroxisomes are oxidative organelles. *Antioxid. Redox Signal.* 13, 525–537. doi:10.1089/ars.2009.2996

Atshaves, B. P., Mcintosh, A. L., Landrock, D., Payne, H. R., Mackie, J. T., Maeda, N., et al. (2007). Effect of SCP-x gene ablation on branched-chain fatty acid metabolism. *Am. J. Physiol. Gastrointest. Liver Physiol.* 292, G939–G951. doi:10.1152/ajpgi.00308.2006

Bae, E. Y., Yi, Y., Lim, H. H., Lee, J. M., Lee, B., Kim, S. Y., et al. (2020). First case of peroxisomal D-bifunctional protein deficiency with novel HSD17B4 mutations and progressive neuropathy in korea. *J. Korean Med. Sci.* 35, e357. doi:10.3346/jkms.2020.35.e357

Bartlett, M., Nasiri, N., Pressman, R., Bademci, G., and Forghani, I. (2021). First reported adult patient with retinal dystrophy and leukodystrophy caused by a novel ACBD5 variant: A case report and review of literature. *Am. J. Med. Genet. A* 185, 1236–1241. doi:10.1002/ajmg.a.62073

Bazan, N. G., Gordon, W. C., and Rodriguez De Turco, E. B. (1992). Docosahexaenoic acid uptake and metabolism in photoreceptors: Retinal conservation by an efficient retinal pigment epithelial cell-mediated recycling process. *Adv. Exp. Med. Biol.* 318, 295–306. doi:10.1007/978-1-4615-3426-6_26

Beard, M. E., Davies, T., Holloway, M., and Holtzman, E. (1988). Peroxisomes in pigment epithelium and Muller cells of amphibian retina possess D-amino acid oxidase as well as catalase. *Exp. Eye Res.* 47, 795–806. doi:10.1016/0014-4835(88)90063-2

Beckers, L., Geric, I., Stroobants, S., Beel, S., Van Damme, P., D'hooge, R., et al. (2019). Microglia lacking a peroxisomal beta-oxidation enzyme chronically alter their inflammatory profile without evoking neuronal and behavioral deficits. *J. Neuroinflammation* 16, 61. doi:10.1186/s12974-019-1442-3

Beken, S., Dilli, D., Fettah, N. D., Kabatas, E. U., Zenciroglu, A., and Okumus, N. (2014). The influence of fish-oil lipid emulsions on retinopathy of prematurity in very low birth weight infants: A randomized controlled trial. *Early Hum. Dev.* 90, 27–31. doi:10.1016/j.earlhumdev.2013.11.002

Bellezza, I. (2018). Oxidative stress in age-related macular degeneration: Nrf2 as therapeutic target. *Front. Pharmacol.* 9, 1280. doi:10.3389/fphar.2018.01280

Berger, J., Dorninger, F., Forss-Petter, S., and Kunze, M. (2016). Peroxisomes in brain development and function. *Biochim. Biophys. Acta* 1863, 934–955. doi:10.1016/j.bbamcr.2015.12.005

Bernstein, P. S., Lloyd, M. B., O'day, W. T., and Bok, D. (1992). Effect of phytanic acid on cultured retinal pigment epithelium: An *in vitro* model for refsum's disease. *Exp. Eye Res.* 55, 869–878. doi:10.1016/0014-4835(92)90013-i

Bieber, L. L., Krahling, J. B., Clarke, P. R., Valkner, K. J., and Tolbert, N. E. (1981). Carnitine acyltransferases in rat liver peroxisomes. *Arch. Biochem. Biophys.* 211, 599–604. doi:10.1016/0003-9861(81)90494-x

Birdsey, G. M., Lewin, J., Holbrook, J. D., Simpson, V. R., Cunningham, A. A., and Danpure, C. J. (2005). A comparative analysis of the evolutionary relationship between diet and enzyme targeting in bats, marsupials and other mammals. *Proc. Biol. Sci.* 272, 833–840. doi:10.1098/rspb.2004.3011

Bishop, J. E., and Hajra, A. K. (1981). Mechanism and specificity of formation of long chain alcohols by developing rat brain. *J. Biol. Chem.* 256, 9542–9550. doi:10.1016/s0021-9258(19)68796-x

Bjorgo, K., Fjaer, R., Mork, H. H., Ferdinandusse, S., Falkenberg, K. D., Waterham, H. R., et al. (2017). Biochemical and genetic characterization of an unusual mild PEX3-related Zellweger spectrum disorder. *Mol. Genet. Metab.* 121, 325–328. doi:10.1016/j.ymgme.2017.06.004

Bosch, E., Horwitz, J., and Bok, D. (1993). Phagocytosis of outer segments by retinal pigment epithelium: Phagosome-lysosome interaction. *J. Histochem. Cytochem.* 41, 253–263. doi:10.1177/41.2.8419462

Braverman, N. E., and Moser, A. B. (2012). Functions of plasmalogen lipids in health and disease. *Biochim. Biophys. Acta* 1822, 1442–1452. doi:10.1016/j.bbadis.2012.05.008

Braverman, N. E., Raymond, G. V., Rizzo, W. B., Moser, A. B., Wilkinson, M. E., Stone, E. M., et al. (2016). Peroxisome biogenesis disorders in the Zellweger spectrum: An overview of current diagnosis, clinical manifestations, and treatment guidelines. *Mol. Genet. Metab.* 117, 313–321. doi:10.1016/j.ymgme.2015.12.009

Bretillon, L., Thuret, G., Gregoire, S., Acar, N., Joffre, C., Bron, A. M., et al. (2008). Lipid and fatty acid profile of the retina, retinal pigment epithelium/choroid, and the lacrimal gland, and associations with adipose tissue fatty acids in human subjects. *Exp. Eye Res.* 87, 521–528. doi:10.1016/j.exer.2008.08.010

Broniec, A., Klosinski, R., Pawlak, A., Wrona-Krol, M., Thompson, D., and Sarna, T. (2011). Interactions of plasmalogens and their diacyl analogs with singlet oxygen in selected model systems. *Free Radic. Biol. Med.* 50, 892–898. doi:10.1016/j.freeradbiomed.2011.01.002

Buchert, R., Tawamie, H., Smith, C., Uebe, S., Innes, A. M., Al Hallak, B., et al. (2014). A peroxisomal disorder of severe intellectual disability, epilepsy, and cataracts due to fatty acyl-CoA reductase 1 deficiency. *Am. J. Hum. Genet.* 95, 602–610. doi:10.1016/j.ajhg.2014.10.003

Carlton, V. E., Harris, B. Z., Puffenberger, E. G., Batta, A. K., Knisely, A. S., Robinson, D. L., et al. (2003). Complex inheritance of familial hypercholanemia with associated mutations in TJP2 and BAAT. *Nat. Genet.* 34, 91–96. doi:10.1038/ng1147

Cellini, B., Bertoldi, M., Montioli, R., Paiardini, A., and Borri Voltattorni, C. (2007). Human wild-type alanine:glyoxylate aminotransferase and its naturally occurring G82E variant: Functional properties and physiological implications. *Biochem. J.* 408, 39–50. doi:10.1042/BJ20070637

Chen, B., and Tang, L. (2011). Protective effects of catalase on retinal ischemia/reperfusion injury in rats. *Exp. Eye Res.* 93, 599–606. doi:10.1016/j.exer.2011.07.007

Cheng, J. B., and Russell, D. W. (2004). Mammalian wax biosynthesis. I. Identification of two fatty acyl-Coenzyme A reductases with different substrate specificities and tissue distributions. *J. Biol. Chem.* 279, 37789–37797. doi:10.1074/jbc.M406225200

Chiang, J. Y. (2004). Regulation of bile acid synthesis: Pathways, nuclear receptors, and mechanisms. *J. Hepatol.* 40, 539–551. doi:10.1016/j.jhep.2003.11.006

Christen, W. G., Schaumberg, D. A., Glynn, R. J., and Buring, J. E. (2011). Dietary omega-3 fatty acid and fish intake and incident age-related macular degeneration in women. *Arch. Ophthalmol.* 129, 921–929. doi:10.1001/archophthalmol.2011.34

Chu, B. B., Liao, Y. C., Qi, W., Xie, C., Du, X., Wang, J., et al. (2015). Cholesterol transport through lysosome-peroxisome membrane contacts. *Cell* 161, 291–306. doi:10.1016/j.cell.2015.02.019

Chung, H. L., Wangler, M. F., Marcogliese, P. C., Jo, J., Ravenscroft, T. A., Zuo, Z., et al. (2020). Loss- or gain-of-function mutations in ACOX1 cause axonal loss via different mechanisms. *Neuron* 106, 589–606. e586. doi:10.1016/j.neuron.2020.02.021

Cipolla, C. M., and Lodhi, I. J. (2017). Peroxisomal dysfunction in age-related diseases. *Trends Endocrinol. Metab.* 28, 297–308. doi:10.1016/j.tem.2016.12.003

Circu, M. L., and Aw, T. Y. (2010). Reactive oxygen species, cellular redox systems, and apoptosis. *Free Radic. Biol. Med.* 48, 749–762. doi:10.1016/j.freeradbiomed.2009.12.022

Cochat, P., Liutkus, A., Fargue, S., Basmaison, O., Ranchin, B., and Rolland, M. O. (2006). Primary hyperoxaluria type 1: Still challenging. *Pediatr. Nephrol.* 21, 1075–1081. doi:10.1007/s00467-006-0124-4

Coe, N. R., Smith, A. J., Frohnert, B. I., Watkins, P. A., and Bernlohr, D. A. (1999). The fatty acid transport protein (FATP1) is a very long chain acyl-CoA synthetase. *J. Biol. Chem.* 274, 36300–36304. doi:10.1074/jbc.274.51.36300

Costello, J. L., Castro, I. G., Hacker, C., Schrader, T. A., Metz, J., Zeuschner, D., et al. (2017). ACBD5 and VAPB mediate membrane associations between peroxisomes and the ER. *J. Cell Biol.* 216, 331–342. doi:10.1083/jcb.201607055

D'ascenzo, R., Savini, S., Biagetti, C., Bellagamba, M. P., Marchionni, P., Pompilio, A., et al. (2014). Higher docosahexaenoic acid, lower arachidonic acid and reduced lipid tolerance with high doses of a lipid emulsion containing 15% fish oil: A randomized clinical trial. *Clin. Nutr.* 33, 1002–1009. doi:10.1016/j.clnu.2014.01.009

Danpure, C. J. (1997). Variable peroxisomal and mitochondrial targeting of alanine: Glyoxylate aminotransferase in mammalian evolution and disease. *Bioessays* 19, 317–326. doi:10.1002/bies.950190409

Daruich, A., Picard, E., Boatright, J. H., and Behar-Cohen, F. (2019). Review: The bile acids urso- and tauroursodeoxycholic acid as neuroprotective therapies in retinal disease. *Mol. Vis.* 25, 610–624.

Das, Y., Roose, N., De Groef, L., Fransen, M., Moons, L., Van Veldhoven, P. P., et al. (2019). Differential distribution of peroxisomal proteins points to specific roles of peroxisomes in the murine retina. *Mol. Cell. Biochem.* 456, 53–62. doi:10.1007/s11010-018-3489-3

Das, Y., Swinkels, D., and Baes, M. (2021). Peroxisomal disorders and their mouse models point to essential roles of peroxisomes for retinal integrity. *Int. J. Mol. Sci.* 22, 4101. doi:10.3390/ijms22084101

De Duve, C., and Baudhuin, P. (1966). Peroxisomes (microbodies and related particles). *Physiol. Rev.* 46, 323–357. doi:10.1152/physrev.1966.46.2.323

Delton-Vandenbroucke, I., Grammas, P., and Anderson, R. E. (1997). Polyunsaturated fatty acid metabolism in retinal and cerebral microvascular endothelial cells. *J. Lipid Res.* 38, 147–159. doi:10.1016/s0022-2275(20)37284-9

Dimitrov, L., Lam, S. K., and Schekman, R. (2013). The role of the endoplasmic reticulum in peroxisome biogenesis. *Cold Spring Harb. Perspect. Biol.* 5, a013243. doi:10.1101/cshperspect.a013243

Ding, L., Sun, W., Balaz, M., He, A., Klug, M., Wieland, S., et al. (2021). Peroxisomal beta-oxidation acts as a sensor for intracellular fatty acids and regulates lipolysis. *Nat. Metab.* 3, 1648–1661. doi:10.1038/s42255-021-00489-2

Ebberink, M. S., Mooyer, P. A., Koster, J., Dekker, C. J., Eyskens, F. J., Dionisi-Vici, C., et al. (2009). Genotype-phenotype correlation in PEX5-deficient peroxisome biogenesis defective cell lines. *Hum. Mutat.* 30, 93–98. doi:10.1002/humu.20833

Edwards, A. O., Miedziak, A., Vrabec, T., Verhoeven, J., Acott, T. S., Weleber, R. G., et al. (1999). Autosomal dominant stargardt-like macular dystrophy: I. Clinical characterization, longitudinal follow-up, and evidence for a common ancestry in families linked to chromosome 6q14. *Am. J. Ophthalmol.* 127, 426–435. doi:10.1016/s0002-9394(98)00331-6

Enns, G. M., Ammous, Z., Himes, R. W., Nogueira, J., Palle, S., Sullivan, M., et al. (2021). Diagnostic challenges and disease management in patients with a mild Zellweger spectrum disorder phenotype. *Mol. Genet. Metab.* 134, 217–222. doi:10.1016/j.ymgme.2021.09.007

Fabelo, N., Martin, V., Santpere, G., Marin, R., Torrent, L., Ferrer, I., et al. (2011). Severe alterations in lipid composition of frontal cortex lipid rafts from Parkinson's disease and incidental Parkinson's disease. *Mol. Med.* 17, 1107–1118. doi:10.2119/molmed.2011.00119

Falany, C. N., Xie, X., Wheeler, J. B., Wang, J., Smith, M., He, D., et al. (2002). Molecular cloning and expression of rat liver bile acid CoA ligase. *J. Lipid Res.* 43, 2062–2071. doi:10.1194/jlr.m200260-jlr200

Fedick, A., Jalas, C., and Treff, N. R. (2014). A deleterious mutation in the PEX2 gene causes Zellweger syndrome in individuals of Ashkenazi Jewish descent. *Clin. Genet.* 85, 343–346. doi:10.1111/cge.12170

Feher, J., Kovacs, I., Artico, M., Cavallotti, C., Papale, A., and Balacco Gabrieli, C. (2006). Mitochondrial alterations of retinal pigment epithelium in age-related macular degeneration. *Neurobiol. Aging* 27, 983–993. doi:10.1016/j.neurobiolaging.2005.05.012

Ferdinandusse, S., Denis, S., Clayton, P. T., Graham, A., Rees, J. E., Allen, J. T., et al. (2000). Mutations in the gene encoding peroxisomal alpha-methylacyl-CoA racemase cause adult-onset sensory motor neuropathy. *Nat. Genet.* 24, 188–191. doi:10.1038/72861

Ferdinandusse, S., Denis, S., Hogenhout, E. M., Koster, J., Van Roermund, C. W., Moser, A. B., et al. (2007). Clinical, biochemical, and mutational spectrum of peroxisomal acyl-coenzyme A oxidase deficiency. *Hum. Mutat.* 28, 904–912. doi:10.1002/humu.20535

Ferdinandusse, S., Denis, S., Mooyer, P. A., Dekker, C., Duran, M., Soorani-Lunsing, R. J., et al. (2006a). Clinical and biochemical spectrum of D-bifunctional protein deficiency. *Ann. Neurol.* 59, 92–104. doi:10.1002/ana.20702

Ferdinandusse, S., Denis, S., Van Roermund, C. W. T., Preece, M. A., Koster, J., Ebberink, M. S., et al. (2018). A novel case of ACOX2 deficiency leads to recognition of a third human peroxisomal acyl-CoA oxidase. *Biochim. Biophys. Acta. Mol. Basis Dis.* 1864, 952–958. doi:10.1016/j.bbadis.2017.12.032

Ferdinandusse, S., Denis, S., Van Roermund, C. W., Wanders, R. J., and Dacremont, G. (2004). Identification of the peroxisomal beta-oxidation enzymes involved in the degradation of long-chain dicarboxylic acids. *J. Lipid Res.* 45, 1104–1111. doi:10.1194/jlr.M300512-JLR200

Ferdinandusse, S., Falkenberg, K. D., Koster, J., Mooyer, P. A., Jones, R., Van Roermund, C. W. T., et al. (2017). ACBD5 deficiency causes a defect in peroxisomal

very long-chain fatty acid metabolism. *J. Med. Genet.* 54, 330–337. doi:10.1136/jmedgenet-2016-104132

Ferdinandusse, S., Jimenez-Sanchez, G., Koster, J., Denis, S., Van Roermund, C. W., Silva-Zolezzi, I., et al. (2015). A novel bile acid biosynthesis defect due to a deficiency of peroxisomal ABCD3. *Hum. Mol. Genet.* 24, 361–370. doi:10.1093/hmg/ddu448

Ferdinandusse, S., Kostopoulos, P., Denis, S., Rusch, H., Overmars, H., Dillmann, U., et al. (2006b). Mutations in the gene encoding peroxisomal sterol carrier protein X (SCPx) cause leukencephalopathy with dystonia and motor neuropathy. *Am. J. Hum. Genet.* 78, 1046–1052. doi:10.1086/503921

Ferdinandusse, S., Mcwalter, K., Te Brinke, H., Mooijer, P. M., Ruiter, J. P. N., Van Lint, A. E. M., et al. (2021). An autosomal dominant neurological disorder caused by de novo variants in FAR1 resulting in uncontrolled synthesis of ether lipids. *Genet. Med.* 23, 740–750. doi:10.1038/s41436-020-01027-3

Ferrington, D. A., Sinha, D., and Kaarniranta, K. (2016). Defects in retinal pigment epithelial cell proteolysis and the pathology associated with age-related macular degeneration. *Prog. Retin. Eye Res.* 51, 69–89. doi:10.1016/j.preteyeres.2015.09.002

Fliesler, S. J., and Anderson, R. E. (1983). Chemistry and metabolism of lipids in the vertebrate retina. *Prog. Lipid Res.* 22, 79–131. doi:10.1016/0163-7827(83)90004-8

Fliesler, S. J. (2021). Introduction to the thematic review series: Seeing 2020: Lipids and lipid-soluble molecules in the eye. *J. Lipid Res.* 62, 100007. doi:10.1016/j.jlr.2020.100007

Folz, S. J., and Trobe, J. D. (1991). The peroxisome and the eye. *Surv. Ophthalmol.* 35, 353–368. doi:10.1016/0039-6257(91)90185-i

Forman, H. J., Maiorino, M., and Ursini, F. (2010). Signaling functions of reactive oxygen species. *Biochemistry* 49, 835–842. doi:10.1021/bi9020378

Foulon, V., Antonenkov, V. D., Croes, K., Waelkens, E., Mannaerts, G. P., Van Veldhoven, P. P., et al. (1999). Purification, molecular cloning, and expression of 2-hydroxyphytanoyl-CoA lyase, a peroxisomal thiamine pyrophosphate-dependent enzyme that catalyzes the carbon-carbon bond cleavage during alpha-oxidation of 3-methyl-branched fatty acids. *Proc. Natl. Acad. Sci. U. S. A.* 96, 10039–10044. doi:10.1073/pnas.96.18.10039

Fransen, M., Lismont, C., and Walton, P. (2017). The peroxisome-mitochondria connection: How and why? *Int. J. Mol. Sci.* 18, E1126. doi:10.3390/ijms18061126

Fransen, M., Nordgren, M., Wang, B., Apanasets, O., and Van Veldhoven, P. P. (2013). Aging, age-related diseases and peroxisomes. *Subcell. Biochem.* 69, 45–65. doi:10.1007/978-94-007-6889-5_3

Frattini, L. F., Piubelli, L., Sacchi, S., Molla, G., and Pollegioni, L. (2011). Is rat an appropriate animal model to study the involvement of D-serine catabolism in schizophrenia? Insights from characterization of D-amino acid oxidase. *FEBS J.* 278, 4362–4373. doi:10.1111/j.1742-4658.2011.08354.x

Fu, Z., Chen, C. T., Cagnone, G., Heckel, E., Sun, Y., Cakir, B., et al. (2019). Dyslipidemia in retinal metabolic disorders. *EMBO Mol. Med.* 11, e10473. doi:10.15252/emmm.201910473

Fu, Z., Kern, T. S., Hellstrom, A., and Smith, L. E. H. (2021). Fatty acid oxidation and photoreceptor metabolic needs. *J. Lipid Res.* 62, 100035. doi:10.1194/jlr.TR120000618

Fu, Z., Lofqvist, C. A., Liegl, R., Wang, Z., Sun, Y., Gong, Y., et al. (2017). Photoreceptor glucose metabolism determines normal retinal vascular growth. *EMBO Mol. Med.* 10, 76–90. doi:10.15252/emmm.201707966

Fujiki, Y., Okumoto, K., Mukai, S., Honsho, M., and Tamura, S. (2014). Peroxisome biogenesis in mammalian cells. *Front. Physiol.* 5, 307. doi:10.3389/fphys.2014.00307

Gabaldon, T. (2014). A metabolic scenario for the evolutionary origin of peroxisomes from the endomembranous system. *Cell. Mol. Life Sci.* 71, 2373–2376. doi:10.1007/s00018-013-1424-z

Gallego-Garcia, A., Monera-Girona, A. J., Pajares-Martinez, E., Bastida-Martinez, E., Perez-Castano, R., Iniesta, A. A., et al. (2019). A bacterial light response reveals an orphan desaturase for human plasmalogen synthesis. *Science* 366, 128–132. doi:10.1126/science.aay1436

Garner, A., Fielder, A. R., Primavesi, R., and Stevens, A. (1982). Tapetoretinal degeneration in the cerebro-hepato-renal (Zellweger's) syndrome. *Br. J. Ophthalmol.* 66, 422–431. doi:10.1136/bjo.66.7.422

Gavino, G. R., and Gavino, V. C. (1991). Rat liver outer mitochondrial carnitine palmitoyltransferase activity towards long-chain polyunsaturated fatty acids and their CoA esters. *Lipids* 26, 266–270. doi:10.1007/BF02537135

Geuze, H. J., Murk, J. L., Stroobants, A. K., Griffith, J. M., Kleijmeer, M. J., Koster, A. J., et al. (2003). Involvement of the endoplasmic reticulum in peroxisome formation. *Mol. Biol. Cell* 14, 2900–2907. doi:10.1091/mbc.e02-11-0734

Ginsberg, L., Rafique, S., Xuereb, J. H., Rapoport, S. I., and Gershfeld, N. L. (1995). Disease and anatomic specificity of ethanolamine plasmalogen deficiency in Alzheimer's disease brain. *Brain Res.* 698, 223–226. doi:10.1016/0006-8993(95)00931-f

Gloerich, J., Ruiter, J. P., Van Den Brink, D. M., Ofman, R., Ferdinandusse, S., and Wanders, R. J. (2006). Peroxisomal trans-2-enoyl-CoA reductase is involved in phytol degradation. *FEBS Lett.* 580, 2092–2096. doi:10.1016/j.febslet.2006.03.011

Gong, Y., Fu, Z., Edin, M. L., Liu, C. H., Wang, Z., Shao, Z., et al. (2016). Cytochrome P450 oxidase 2C inhibition adds to omega-3 long-chain polyunsaturated fatty acids protection against retinal and choroidal neovascularization. *Arterioscler. Thromb. Vasc. Biol.* 36, 1919–1927. doi:10.1161/ATVBAHA.116.307558

Gong, Y., Fu, Z., Liegl, R., Chen, J., Hellstrom, A., and Smith, L. E. (2017). ω-3 and ω-6 long-chain PUFAs and their enzymatic metabolites in neovascular eye diseases. *Am. J. Clin. Nutr.* 106, 16–26. doi:10.3945/ajcn.117.153825

Gordon, W. C., and Bazan, N. G. (1993). Visualization of [3H]docosahexaenoic acid trafficking through photoreceptors and retinal pigment epithelium by electron microscopic autoradiography. *Invest. Ophthalmol. Vis. Sci.* 34, 2402–2411.

Gordon, W. C., Rodriguez De Turco, E. B., and Bazan, N. G. (1992). Retinal pigment epithelial cells play a central role in the conservation of docosahexaenoic acid by photoreceptor cells after shedding and phagocytosis. *Curr. Eye Res.* 11, 73–83. doi:10.3109/02713689209069169

Graziosi, A., Perrotta, M., Russo, D., Gasparroni, G., D'egidio, C., Marinelli, B., et al. (2020). Oxidative stress markers and the retinopathy of prematurity. *J. Clin. Med.* 9, E2711. doi:10.3390/jcm9092711

Grego, A. V., and Mingrone, G. (1995). Dicarboxylic acids, an alternate fuel substrate in parenteral nutrition: An update. *Clin. Nutr.* 14, 143–148. doi:10.1016/s0261-5614(95)80011-5

Guha, S., Liu, J., Baltazar, G., Laties, A. M., and Mitchell, C. H. (2014). Rescue of compromised lysosomes enhances degradation of photoreceptor outer segments and reduces lipofuscin-like autofluorescence in retinal pigmented epithelial cells. *Adv. Exp. Med. Biol.* 801, 105–111. doi:10.1007/978-1-4614-3209-8_14

Haddad, R., Font, R. L., and Friendly, D. S. (1976). Cerebro-hepato-renal syndrome of Zellweger. Ocular histopathologic findings. *Arch. Ophthalmol.* 94, 1927–1930. doi:10.1001/archopht.1976.03910040633011

Han, X., Holtzman, D. M., and Mckeel, D. W., Jr. (2001). Plasmalogen deficiency in early alzheimer's disease subjects and in animal models: Molecular characterization using electrospray ionization mass spectrometry. *J. Neurochem.* 77, 1168–1180. doi:10.1046/j.1471-4159.2001.00332.x

Harkewicz, R., Du, H., Tong, Z., Alkuraya, H., Bedell, M., Sun, W., et al. (2012). Essential role of ELOVL4 protein in very long chain fatty acid synthesis and retinal function. *J. Biol. Chem.* 287, 11469–11480. doi:10.1074/jbc.M111.256073

Hasan, S., Platta, H. W., and Erdmann, R. (2013). Import of proteins into the peroxisomal matrix. *Front. Physiol.* 4, 261. doi:10.3389/fphys.2013.00261

Hatch, G. M. (2004). Cell biology of cardiac mitochondrial phospholipids. *Biochem. Cell Biol.* 82, 99–112. doi:10.1139/o03-074

Heimler, A., Fox, J. E., Hershey, J. E., and Crespi, P. (1991). Sensorineural hearing loss, enamel hypoplasia, and nail abnormalities in sibs. *Am. J. Med. Genet.* 39, 192–195. doi:10.1002/ajmg.1320390214

Heinzer, A. K., Watkins, P. A., Lu, J. F., Kemp, S., Moser, A. B., Li, Y. Y., et al. (2003). A very long-chain acyl-CoA synthetase-deficient mouse and its relevance to X-linked adrenoleukodystrophy. *Hum. Mol. Genet.* 12, 1145–1154. doi:10.1093/hmg/ddg126

Hellstrom, A., Pivodic, A., Granse, L., Lundgren, P., Sjobom, U., Nilsson, A. K., et al. (2021). Association of docosahexaenoic acid and arachidonic acid serum levels with retinopathy of prematurity in preterm infants. *JAMA Netw. Open* 4, e2128771. doi:10.1001/jamanetworkopen.2021.28771

Heymans, H. S., Schutgens, R. B., Tan, R., Van Den Bosch, H., and Borst, P. (1983). Severe plasmalogen deficiency in tissues of infants without peroxisomes (Zellweger syndrome). *Nature* 306, 69–70. doi:10.1038/306069a0

Ho, L., Van Leeuwen, R., Witteman, J. C., Van Duijn, C. M., Uitterlinden, A. G., Hofman, A., et al. (2011). Reducing the genetic risk of age-related macular degeneration with dietary antioxidants, zinc, and omega-3 fatty acids: The rotterdam study. *Arch. Ophthalmol.* 129, 758–766. doi:10.1001/archophthalmol.2011.141

Hoffman, D. R., Demar, J. C., Heird, W. C., Birch, D. G., and Anderson, R. E. (2001). Impaired synthesis of DHA in patients with X-linked retinitis pigmentosa. *J. Lipid Res.* 42, 1395–1401. doi:10.1016/s0022-2275(20)30271-6

Holmstrom, K. M., and Finkel, T. (2014). Cellular mechanisms and physiological consequences of redox-dependent signalling. *Nat. Rev. Mol. Cell Biol.* 15, 411–421. doi:10.1038/nrm3801

Honsho, M., Tanaka, M., Zoeller, R. A., and Fujiki, Y. (2020). Distinct functions of acyl/alkyl dihydroxyacetonephosphate reductase in peroxisomes and endoplasmic reticulum. *Front. Cell Dev. Biol.* 8, 855. doi:10.3389/fcell.2020.00855

Horvath, R., Lewis-Smith, D., Douroudis, K., Duff, J., Keogh, M., Pyle, A., et al. (2015). SCP2 mutations and neurodegeneration with brain iron accumulation. *Neurology* 85, 1909–1911. doi:10.1212/WNL.0000000000002157

Houten, S. M., Denis, S., Argmann, C. A., Jia, Y., Ferdinandusse, S., Reddy, J. K., et al. (2012). Peroxisomal L-bifunctional enzyme (Ehhadh) is essential for the production of medium-chain dicarboxylic acids. *J. Lipid Res.* 53, 1296–1303. doi:10.1194/jlr.M024463

Hua, R., Cheng, D., Coyaud, E., Freeman, S., Di Pietro, E., Wang, Y., et al. (2017). VAPs and ACBD5 tether peroxisomes to the ER for peroxisome maintenance and lipid homeostasis. *J. Cell Biol.* 216, 367–377. doi:10.1083/jcb.201608128

Huyghe, S., Mannaerts, G. P., Baes, M., and Van Veldhoven, P. P. (2006). Peroxisomal multifunctional protein-2: The enzyme, the patients and the knockout mouse model. *Biochim. Biophys. Acta* 1761, 973–994. doi:10.1016/j.bbalip.2006.04.006

Ishikawa, M., Yoshitomi, T., Zorumski, C. F., and Izumi, Y. (2016). 24(S)-Hydroxycholesterol protects the *ex vivo* rat retina from injury by elevated hydrostatic pressure. *Sci. Rep.* 6, 33886. doi:10.1038/srep33886

Islinger, M., Cardoso, M. J., and Schrader, M. (2010). Be different--the diversity of peroxisomes in the animal kingdom. *Biochim. Biophys. Acta* 1803, 881–897. doi:10.1016/j.bbamcr.2010.03.013

Islinger, M., Voelkl, A., Fahimi, H. D., and Schrader, M. (2018). The peroxisome: An update on mysteries 2.0. *Histochem. Cell Biol.* 150, 443–471. doi:10.1007/s00418-018-1722-5

Itzkovitz, B., Jiralerspong, S., Nimmo, G., Loscalzo, M., Horovitz, D. D., Snowden, A., et al. (2012). Functional characterization of novel mutations in GNPAT and AGPS, causing rhizomelic chondrodysplasia punctata (RCDP) types 2 and 3. *Hum. Mutat.* 33, 189–197. doi:10.1002/humu.21623

Ivashchenko, O., Van Veldhoven, P. P., Brees, C., Ho, Y. S., Terlecky, S. R., and Fransen, M. (2011). Intraperoxisomal redox balance in mammalian cells: Oxidative stress and interorganellar cross-talk. *Mol. Biol. Cell* 22, 1440–1451. doi:10.1091/mbc.E10-11-0919

Jadeja, R. N., Powell, F. L., Jones, M. A., Fuller, J., Joseph, E., Thounaojam, M. C., et al. (2018). Loss of NAMPT in aging retinal pigment epithelium reduces NAD(+) availability and promotes cellular senescence. *Aging (Albany NY)* 10, 1306–1323. doi:10.18632/aging.101469

Jansen, G. A., Ofman, R., Denis, S., Ferdinandusse, S., Hogenhout, E. M., Jakobs, C., et al. (1999a). Phytanoyl-CoA hydroxylase from rat liver. Protein purification and cDNA cloning with implications for the subcellular localization of phytanic acid alpha-oxidation. *J. Lipid Res.* 40, 2244–2254. doi:10.1016/s0022-2275(20)32099-x

Jansen, G. A., Ofman, R., Ferdinandusse, S., Ijlst, L., Muijsers, A. O., Skjeldal, O. H., et al. (1997). Refsum disease is caused by mutations in the phytanoyl-CoA hydroxylase gene. *Nat. Genet.* 17, 190–193. doi:10.1038/ng1097-190

Jansen, G. A., Verhoeven, N. M., Denis, S., Romeijn, G., Jakobs, C., Ten Brink, H. J., et al. (1999b). Phytanic acid alpha-oxidation: Identification of 2-hydroxyphytanoyl-CoA lyase in rat liver and its localisation in peroxisomes. *Biochim. Biophys. Acta* 1440, 176–182. doi:10.1016/s1388-1981(99)00126-2

Janssen, A., Baes, M., Gressens, P., Mannaerts, G. P., Declercq, P., and Van Veldhoven, P. P. (2000). Docosahexaenoic acid deficit is not a major pathogenic factor in peroxisome-deficient mice. *Lab. Invest.* 80, 31–35. doi:10.1038/labinvest.3780005

Janssen, A., Gressens, P., Grabenbauer, M., Baumgart, E., Schad, A., Vanhorebeek, I., et al. (2003). Neuronal migration depends on intact peroxisomal function in brain and in extraneuronal tissues. *J. Neurosci.* 23, 9732–9741. doi:10.1523/jneurosci.23-30-09732.2003

Jenkins, C. M., Yang, K., Liu, G., Moon, S. H., Dilthey, B. G., and Gross, R. W. (2018). Cytochrome c is an oxidative stress-activated plasmalogenase that cleaves plasmenylcholine and plasmenylethanolamine at the sn-1 vinyl ether linkage. *J. Biol. Chem.* 293, 8693–8709. doi:10.1074/jbc.RA117.001629

Jones, D. P., and Go, Y. M. (2010). Redox compartmentalization and cellular stress. *Diabetes Obes. Metab.* 12 (2), 116–125. doi:10.1111/j.1463-1326.2010.01266.x

Joyal, J. S., Sun, Y., Gantner, M. L., Shao, Z., Evans, L. P., Saba, N., et al. (2016). Retinal lipid and glucose metabolism dictates angiogenesis through the lipid sensor Ffar1. *Nat. Med.* 22, 439–445. doi:10.1038/nm.4059

Kaplan, P. W., Kruse, B., Tusa, R. J., Shankroff, J., Rignani, J., and Moser, H. W. (1995). Visual system abnormalities in adrenomyeloneuropathy. *Ann. Neurol.* 37, 550–552. doi:10.1002/ana.410370419

Kawaguchi, K., Mukai, E., Watanabe, S., Yamashita, A., Morita, M., So, T., et al. (2021). Acyl-CoA thioesterase activity of peroxisomal ABC protein ABCD1 is required for the transport of very long-chain acyl-CoA into peroxisomes. *Sci. Rep.* 11, 2192. doi:10.1038/s41598-021-81949-3

Kawazoe, T., Park, H. K., Iwana, S., Tsuge, H., and Fukui, K. (2007). Human D-amino acid oxidase: An update and review. *Chem. Rec.* 7, 305–315. doi:10.1002/tcr.20129

Kersten, S. (2014). Integrated physiology and systems biology of PPARα. *Mol. Metab.* 3, 354–371. doi:10.1016/j.molmet.2014.02.002

Kettelhut, T., and Thoms, S. (2014). *Molecular machines involved in peroxisome biogenesis and maintenance*. Vienna: Springer.

Khairallah, R. J., Kim, J., O'shea, K. M., O'connell, K. A., Brown, B. H., Galvao, T., et al. (2012). Improved mitochondrial function with diet-induced increase in either docosahexaenoic acid or arachidonic acid in membrane phospholipids. *PLoS One* 7, e34402. doi:10.1371/journal.pone.0034402

Khairallah, R. J., Sparagna, G. C., Khanna, N., O'shea, K. M., Hecker, P. A., Kristian, T., et al. (2010). Dietary supplementation with docosahexaenoic acid, but not eicosapentaenoic acid, dramatically alters cardiac mitochondrial phospholipid fatty acid composition and prevents permeability transition. *Biochim. Biophys. Acta* 1797, 1555–1562. doi:10.1016/j.bbabio.2010.05.007

Kihara, A. (2012). Very long-chain fatty acids: Elongation, physiology and related disorders. *J. Biochem.* 152, 387–395. doi:10.1093/jb/mvs105

Kim, P. K., Mullen, R. T., Schumann, U., and Lippincott-Schwartz, J. (2006). The origin and maintenance of mammalian peroxisomes involves a de novo PEX16-dependent pathway from the ER. *J. Cell Biol.* 173, 521–532. doi:10.1083/jcb.200601036

Kimura, T., Kimura, A. K., Ren, M., Monteiro, V., Xu, Y., Berno, B., et al. (2019). Plasmalogen loss caused by remodeling deficiency in mitochondria. *Life Sci. Alliance* 2, e201900348. doi:10.26508/lsa.201900348

Klemp, H. G., Kettwig, M., Streit, F., Gartner, J., Rosewich, H., and Kratzner, R. (2021). LC-MS based platform simplifies access to metabolomics for peroxisomal disorders. *Metabolites* 11, 347. doi:10.3390/metabo11060347

Knoops, B., Goemaere, J., Van Der Eecken, V., and Declercq, J. P. (2011). Peroxiredoxin 5: Structure, mechanism, and function of the mammalian atypical 2-cys peroxiredoxin. *Antioxid. Redox Signal.* 15, 817–829. doi:10.1089/ars.2010.3584

Koenekoop, R. K., Wang, H., Majewski, J., Wang, X., Lopez, I., Ren, H., et al. (2012). Mutations in NMNAT1 cause Leber congenital amaurosis and identify a new disease pathway for retinal degeneration. *Nat. Genet.* 44, 1035–1039. doi:10.1038/ng.2356

Komatsuzaki, S., Ogawa, E., Shimozawa, N., Sakamoto, O., Haginoya, K., Uematsu, M., et al. (2015). First Japanese case of Zellweger syndrome with a mutation in PEX14. *Pediatr. Int.* 57, 1189–1192. doi:10.1111/ped.12713

Konkolova, J., Petrovic, R., Chandoga, J., Halasova, E., Jungova, P., and Bohmer, D. (2015). A novel mutation in the PEX12 gene causing a peroxisomal biogenesis disorder. *Mol. Biol. Rep.* 42, 1359–1363. doi:10.1007/s11033-015-3885-7

Kou, J., Kovacs, G. G., Hoftberger, R., Kulik, W., Brodde, A., Forss-Petter, S., et al. (2011). Peroxisomal alterations in Alzheimer's disease. *Acta Neuropathol.* 122, 271–283. doi:10.1007/s00401-011-0836-9

Kourti, P., Gonzalez-Martin, J., and Yeo, D. C. M. (2020). Oxalate maculopathy. *Ophthalmol. Retina* 4, 898. doi:10.1016/j.oret.2020.04.008

Kowluru, R. A., and Chan, P. S. (2007). Oxidative stress and diabetic retinopathy. *Exp. Diabetes Res.* 2007, 43603. doi:10.1155/2007/43603

Krause, C., Rosewich, H., Woehler, A., and Gartner, J. (2013). Functional analysis of PEX13 mutation in a Zellweger syndrome spectrum patient reveals novel homooligomerization of PEX13 and its role in human peroxisome biogenesis. *Hum. Mol. Genet.* 22, 3844–3857. doi:10.1093/hmg/ddt238

Kretzer, F. L., Hittner, H. M., and Mehta, R. (1981). Ocular manifestations of conradi and zellweger syndromes. *Metab. Pediatr. Ophthalmol.* 5, 1–11.

Krysko, O., Hulshagen, L., Janssen, A., Schutz, G., Klein, R., De Bruycker, M., et al. (2007). Neocortical and cerebellar developmental abnormalities in conditions of selective elimination of peroxisomes from brain or from liver. *J. Neurosci. Res.* 85, 58–72. doi:10.1002/jnr.21097

Kumar, K. R., Wali, G., Davis, R. L., Mallawaarachchi, A. C., Palmer, E. E., Gayevskiy, V., et al. (2018). Expanding the spectrum of PEX16 mutations and novel insights into disease mechanisms. *Mol. Genet. Metab. Rep.* 16, 46–51. doi:10.1016/j.ymgmr.2018.07.003

Kurian, M. A., Ryan, S., Besley, G. T., Wanders, R. J., and King, M. D. (2004). Straight-chain acyl-CoA oxidase deficiency presenting with dysmorphia, neurodevelopmental autistic-type regression and a selective pattern of leukodystrophy. *J. Inherit. Metab. Dis.* 27, 105–108. doi:10.1023/b:boli.0000016687.88818.6d

Lacombe, R. J. S., and Bazinet, R. P. (2021). Natural abundance carbon isotope ratio analysis and its application in the study of diet and metabolism. *Nutr. Rev.* 79, 869–888. doi:10.1093/nutrit/nuaa109

Lacombe, R. J. S., Lee, C. C., and Bazinet, R. P. (2020). Turnover of brain DHA in mice is accurately determined by tracer-free natural abundance carbon isotope ratio analysis. *J. Lipid Res.* 61, 116–126. doi:10.1194/jlr.D119000518

Lageweg, W., Sykes, J. E., Lopes-Cardozo, M., and Wanders, R. J. (1991). Oxidation of very-long-chain fatty acids in rat brain: Cerotic acid is beta-oxidized exclusively in rat brain peroxisomes. *Biochim. Biophys. Acta* 1085, 381–384. doi:10.1016/0005-2760(91)90144-7

Lambert, S. R., Kriss, A., Taylor, D., Coffey, R., and Pembrey, M. (1989). Follow-up and diagnostic reappraisal of 75 patients with Leber's congenital amaurosis. *Am. J. Ophthalmol.* 107, 624–631. doi:10.1016/0002-9394(89)90259-6

Lee, J. W., Fuda, H., Javitt, N. B., Strott, C. A., and Rodriguez, I. R. (2006). Expression and localization of sterol 27-hydroxylase (CYP27A1) in monkey retina. *Exp. Eye Res.* 83, 465–469. doi:10.1016/j.exer.2005.11.018

Leumann, E., and Hoppe, B. (2001). The primary hyperoxalurias. *J. Am. Soc. Nephrol.* 12, 1986–1993. doi:10.1681/ASN.V1291986

Li, X., Knight, J., Fargue, S., Buchalski, B., Guan, Z., Inscho, E. W., et al. (2016). Metabolism of (13)C5-hydroxyproline in mouse models of Primary Hyperoxaluria and its inhibition by RNAi therapeutics targeting liver glycolate oxidase and hydroxyproline dehydrogenase. *Biochim. Biophys. Acta* 1862, 233–239. doi:10.1016/j.bbadis.2015.12.001

Lima, L. H., Barbazetto, I. A., Chen, R., Yannuzzi, L. A., Tsang, S. H., and Spaide, R. F. (2011). Macular dystrophy in Heimler syndrome. *Ophthalmic Genet.* 32, 97–100. doi:10.3109/13816810.2010.551797

Lismont, C., Nordgren, M., Van Veldhoven, P. P., and Fransen, M. (2015). Redox interplay between mitochondria and peroxisomes. *Front. Cell Dev. Biol.* 3, 35. doi:10.3389/fcell.2015.00035

Litman, B. J., and Mitchell, D. C. (1996). A role for phospholipid polyunsaturation in modulating membrane protein function. *Lipids* 31 (1), S193–S197. doi:10.1007/BF02637075

Lizard, G., Rouaud, O., Demarquoy, J., Cherkaoui-Malki, M., and Iuliano, L. (2012). Potential roles of peroxisomes in Alzheimer's disease and in dementia of the Alzheimer's type. *J. Alzheimers Dis.* 29, 241–254. doi:10.3233/JAD-2011-111163

Lofqvist, C. A., Najm, S., Hellgren, G., Engstrom, E., Savman, K., Nilsson, A. K., et al. (2018). Association of retinopathy of prematurity with low levels of arachidonic acid: A secondary analysis of a randomized clinical trial. *JAMA Ophthalmol.* 136, 271–277. doi:10.1001/jamaophthalmol.2017.6658

London, A., Benhar, I., and Schwartz, M. (2013). The retina as a window to the brain-from eye research to CNS disorders. *Nat. Rev. Neurol.* 9, 44–53. doi:10.1038/nrneurol.2012.227

Lorenzo, V., Alvarez, A., Torres, A., Torregrosa, V., Hernandez, D., and Salido, E. (2006). Presentation and role of transplantation in adult patients with type 1 primary hyperoxaluria and the I244T AGXT mutation: Single-center experience. *Kidney Int.* 70, 1115–1119. doi:10.1038/sj.ki.5001758

Martin, W. (2010). Evolutionary origins of metabolic compartmentalization in eukaryotes. *Philos. Trans. R. Soc. Lond. B Biol. Sci.* 365, 847–855. doi:10.1098/rstb.2009.0252

Martinez, M. (1992). Abnormal profiles of polyunsaturated fatty acids in the brain, liver, kidney and retina of patients with peroxisomal disorders. *Brain Res.* 583, 171–182. doi:10.1016/s0006-8993(10)80021-6

Martinez, M. (2001). Restoring the DHA levels in the brains of Zellweger patients. *J. Mol. Neurosci.* 16, 309–316. doi:10.1385/JMN:16:2-3:309

Mechaussier, S., Marlin, S., Kaplan, J., Rozet, J. M., and Perrault, I. (2019). Genetic deciphering of early-onset and severe retinal dystrophy associated with sensorineural hearing loss. *Adv. Exp. Med. Biol.* 1185, 233–238. doi:10.1007/978-3-030-27378-1_38

Mertens, K. L., Kalsbeek, A., Soeters, M. R., and Eggink, H. M. (2017). Bile acid signaling pathways from the enterohepatic circulation to the central nervous system. *Front. Neurosci.* 11, 617. doi:10.3389/fnins.2017.00617

Metherel, A. H., and Bazinet, R. P. (2019). Updates to the n-3 polyunsaturated fatty acid biosynthesis pathway: DHA synthesis rates, tetracosahexaenoic acid and (minimal) retroconversion. *Prog. Lipid Res.* 76, 101008. doi:10.1016/j.plipres.2019.101008

Mezzar, S., De Schryver, E., Asselberghs, S., Meyhi, E., Morvay, P. L., Baes, M., et al. (2017). Phytol-induced pathology in 2-hydroxyacyl-CoA lyase (HACL1) deficient mice. Evidence for a second non-HACL1-related lyase. *Biochim. Biophys. Acta. Mol. Cell Biol. Lipids* 1862, 972–990. doi:10.1016/j.bbalip.2017.06.004

Miville-Godbout, E., Bourque, M., Morissette, M., Al-Sweidi, S., Smith, T., Jayasinghe, D., et al. (2017). Plasmalogen precursor mitigates striatal dopamine loss in MPTP mice. *Brain Res.* 1674, 70–76. doi:10.1016/j.brainres.2017.08.020

Molla, G., Sacchi, S., Bernasconi, M., Pilone, M. S., Fukui, K., and Polegioni, L. (2006). Characterization of human D-amino acid oxidase. *FEBS Lett.* 580, 2358–2364. doi:10.1016/j.febslet.2006.03.045

Molloy, C. S., Stokes, S., Makrides, M., Collins, C. T., Anderson, P. J., and Doyle, L. W. (2016). Long-term effect of high-dose supplementation with DHA on visual function at school age in children born at <33 wk gestational age: Results from a follow-up of a randomized controlled trial. *Am. J. Clin. Nutr.* 103, 268–275. doi:10.3945/ajcn.115.114710

Moore, S. A., Hurt, E., Yoder, E., Sprecher, H., and Spector, A. A. (1995). Docosahexaenoic acid synthesis in human skin fibroblasts involves peroxisomal retroconversion of tetracosahexaenoic acid. *J. Lipid Res.* 36, 2433–2443. doi:10.1016/s0022-2275(20)39724-8

Morarji, J., Gillespie, R., Sergouniotis, P. I., Horvath, R., and Black, G. C. M. (2017). An unusual retinal phenotype Associated with a mutation in sterol carrier protein SCP2. *JAMA Ophthalmol.* 135, 167–169. doi:10.1001/jamaophthalmol.2016.4985

Morita, M., and Imanaka, T. (2012). Peroxisomal ABC transporters: Structure, function and role in disease. *Biochim. Biophys. Acta* 1822, 1387–1396. doi:10.1016/j.bbadis.2012.02.009

Muller, C. C., Nguyen, T. H., Ahlemeyer, B., Meshram, M., Santrampurwala, N., Cao, S., et al. (2011). PEX13 deficiency in mouse brain as a model of zellweger syndrome: Abnormal cerebellum formation, reactive gliosis and oxidative stress. *Dis. Model. Mech.* 4, 104–119. doi:10.1242/dmm.004622

Murtas, G., Sacchi, S., Valentino, M., and Pollegioni, L. (2017). Biochemical properties of human D-amino acid oxidase. *Front. Mol. Biosci.* 4, 88. doi:10.3389/fmolb.2017.00088

Nagan, N., and Zoeller, R. A. (2001). Plasmalogens: Biosynthesis and functions. *Prog. Lipid Res.* 40, 199–229. doi:10.1016/s0163-7827(01)00003-0

Najm, S., Lofqvist, C., Hellgren, G., Engstrom, E., Lundgren, P., Hard, A. L., et al. (2017). Effects of a lipid emulsion containing fish oil on polyunsaturated fatty acid profiles, growth and morbidities in extremely premature infants: A randomized controlled trial. *Clin. Nutr. ESPEN* 20, 17–23. doi:10.1016/j.clnesp.2017.04.004

Nakai, A., Shigematsu, Y., Nishida, K., Kikawa, Y., and Konishi, Y. (1995). MRI findings of Zellweger syndrome. *Pediatr. Neurol.* 13, 346–348. doi:10.1016/0887-8994(95)00215-4

Nanda, T., and Kovach, J. L. (2019). Ophthalmic findings in late stage sjogren-larsson syndrome. *Retin. Cases Brief. Rep.* 13, 251–254. doi:10.1097/ICB.0000000000000583

Neuspiel, M., Schauss, A. C., Braschi, E., Zunino, R., Rippstein, P., Rachubinski, R. A., et al. (2008). Cargo-selected transport from the mitochondria to peroxisomes is mediated by vesicular carriers. *Curr. Biol.* 18, 102–108. doi:10.1016/j.cub.2007.12.038

Noguer, M. T., and Martinez, M. (2010). Visual follow-up in peroxisomal-disorder patients treated with docosahexaenoic Acid ethyl ester. *Invest. Ophthalmol. Vis. Sci.* 51, 2277–2285. doi:10.1167/iovs.09-4020

Ohkuma, Y., Hayashi, T., Yoshimine, S., Tsuneoka, H., Terao, Y., Akiyama, M., et al. (2014). Retinal ganglion cell loss in X-linked adrenoleukodystrophy with an ABCD1 mutation (Gly266Arg). *Neuroophthalmology.* 38, 331–335. doi:10.3109/01658107.2014.950430

Omarova, S., Charvet, C. D., Reem, R. E., Mast, N., Zheng, W., Huang, S., et al. (2012). Abnormal vascularization in mouse retina with dysregulated retinal cholesterol homeostasis. *J. Clin. Invest.* 122, 3012–3023. doi:10.1172/JCI63816

Otsuka, K., Sawai-Ogawa, M., and Kihara, A. (2022). Formation of fatty alcohols-components of meibum lipids-by the fatty acyl-CoA reductase FAR2 is essential for dry eye prevention. *FASEB J.* 36, e22216. doi:10.1096/fj.202101733R

Pacher, P., Beckman, J. S., and Liaudet, L. (2007). Nitric oxide and peroxynitrite in health and disease. *Physiol. Rev.* 87, 315–424. doi:10.1152/physrev.00029.2006

Paker, A. M., Sunness, J. S., Brereton, N. H., Speedie, L. J., Albanna, L., Dharmaraj, S., et al. (2010). Docosahexaenoic acid therapy in peroxisomal diseases: Results of a double-blind, randomized trial. *Neurology* 75, 826–830. doi:10.1212/WNL.0b013e3181f07061

Park, H., He, A., Tan, M., Johnson, J. M., Dean, J. M., Pietka, T. A., et al. (2019). Peroxisome-derived lipids regulate adipose thermogenesis by mediating cold-induced mitochondrial fission. *J. Clin. Invest.* 129, 694–711. doi:10.1172/JCI120606

Pawlik, D., Lauterbach, R., and Turyk, E. (2011). Fish-oil fat emulsion supplementation may reduce the risk of severe retinopathy in VLBW infants. *Pediatrics* 127, 223–228. doi:10.1542/peds.2010-2427

Pawlik, D., Lauterbach, R., Walczak, M., Hurkala, J., and Sherman, M. P. (2014). Fish-oil fat emulsion supplementation reduces the risk of retinopathy in very low birth weight infants: A prospective, randomized study. *JPEN. J. Parenter. Enter. Nutr.* 38, 711–716. doi:10.1177/0148607113499373

Pellicoro, A., Van Den Heuvel, F. A., Geuken, M., Moshage, H., Jansen, P. L., and Faber, K. N. (2007). Human and rat bile acid-CoA:amino acid N-acyltransferase are liver-specific peroxisomal enzymes: Implications for intracellular bile salt transport. *Hepatology* 45, 340–348. doi:10.1002/hep.21528

Petrushka, E., Quastel, J. H., and Scholefield, P. G. (1959). Role of phospholipids in oxidative phosphorylation and mitochondrial structure. *Can. J. Biochem. Physiol.* 37, 989–998. doi:10.1139/y59-108

Pifferi, F., Perret, M., Guesnet, P., Aujard, F., and Alessandri, J. M. (2012). Fatty acid composition of the brain, retina, liver and adipose tissue of the grey mouse lemur (*Microcebus murinus*, primate). *Lipids* 47, 793–801. doi:10.1007/s11745-012-3686-x

Poirier, Y., Antonenkov, V. D., Glumoff, T., and Hiltunen, J. K. (2006). Peroxisomal beta-oxidation--a metabolic pathway with multiple functions. *Biochim. Biophys. Acta* 1763, 1413–1426. doi:10.1016/j.bbamcr.2006.08.034

Pollegioni, L., Molla, G., Sacchi, S., and Murtas, G. (2021). Human D-aspartate oxidase: A key player in D-aspartate metabolism. *Front. Mol. Biosci.* 8, 689719. doi:10.3389/fmolb.2021.689719

Pollegioni, L., Sacchi, S., and Murtas, G. (2018). Human D-amino acid oxidase: Structure, function, and regulation. *Front. Mol. Biosci.* 5, 107. doi:10.3389/fmolb.2018.00107

Pridie, C., Ueda, K., and Simmonds, A. J. (2020). Rosy beginnings: Studying peroxisomes in Drosophila. *Front. Cell Dev. Biol.* 8, 835. doi:10.3389/fcell.2020.00835

Qi, C., Zhu, Y., Pan, J., Usuda, N., Maeda, N., Yeldandi, A. V., et al. (1999). Absence of spontaneous peroxisome proliferation in enoyl-CoA Hydratase/L-3-hydroxyacyl-CoA dehydrogenase-deficient mouse liver. Further support for the role of fatty acyl CoA oxidase in PPARalpha ligand metabolism. *J. Biol. Chem.* 274, 15775–15780. doi:10.1074/jbc.274.22.15775

Ramirez, D. M., Andersson, S., and Russell, D. W. (2008). Neuronal expression and subcellular localization of cholesterol 24-hydroxylase in the mouse brain. *J. Comp. Neurol.* 507, 1676–1693. doi:10.1002/cne.21605

Ranea-Robles, P., Violante, S., Argmann, C., Dodatko, T., Bhattacharya, D., Chen, H., et al. (2021). Murine deficiency of peroxisomal L-bifunctional protein (EHHADH) causes medium-chain 3-hydroxydicarboxylic aciduria and perturbs hepatic cholesterol homeostasis. *Cell. Mol. Life Sci.* 78, 5631–5646. doi:10.1007/s00018-021-03869-9

Ratbi, I., Falkenberg, K. D., Sommen, M., Al-Sheqaih, N., Guaoua, S., Vandeweyer, G., et al. (2015). Heimler syndrome is caused by hypomorphic mutations in the peroxisome-biogenesis genes PEX1 and PEX6. *Am. J. Hum. Genet.* 97, 535–545. doi:10.1016/j.ajhg.2015.08.011

Reddy, J. K., and Mannaerts, G. P. (1994). Peroxisomal lipid metabolism. *Annu. Rev. Nutr.* 14, 343–370. doi:10.1146/annurev.nu.14.070194.002015

Renaud, M., Guissart, C., Mallaret, M., Ferdinandusse, S., Cheillan, D., Drouot, N., et al. (2016). Expanding the spectrum of PEX10-related peroxisomal biogenesis disorders: Slowly progressive recessive ataxia. *J. Neurol.* 263, 1552–1558. doi:10.1007/s00415-016-8167-3

Rice, D. S., Calandria, J. M., Gordon, W. C., Jun, B., Zhou, Y., Gelfman, C. M., et al. (2015). Corrigendum: Adiponectin receptor 1 conserves docosahexaenoic acid and promotes photoreceptor cell surviva.. *Nat. Commun.* 6, 7225. doi:10.1038/ncomms8225

Rizzo, W. B., Carney, G., and Lin, Z. (1999). The molecular basis of sjogren-larsson syndrome: Mutation analysis of the fatty aldehyde dehydrogenase gene. *Am. J. Hum. Genet.* 65, 1547–1560. doi:10.1086/302681

Rodriguez De Turco, E. B., Gordon, W. C., Peyman, G. A., and Bazan, N. G. (1990). Preferential uptake and metabolism of docosahexaenoic acid in membrane phospholipids from rod and cone photoreceptor cells of human and monkey retinas. *J. Neurosci. Res.* 27, 522–532. doi:10.1002/jnr.490270413

Roth, B. M., Yuan, A., and Ehlers, J. P. (2012). Retinal and choroidal findings in oxalate retinopathy using EDI-OCT. *Ophthalmic Surg. Lasers Imaging* 43, S142–S144. doi:10.3928/15428877-20121001-05

Ruether, K., Baldwin, E., Casteels, M., Feher, M. D., Horn, M., Kuranoff, S., et al. (2010). Adult Refsum disease: A form of tapetoretinal dystrophy accessible to therapy. *Surv. Ophthalmol.* 55, 531–538. doi:10.1016/j.survophthal.2010.03.007

Rydzanicz, M., Stradomska, T. J., Jurkiewicz, E., Jamroz, E., Gasperowicz, P., Kostrzewa, G., et al. (2017). Mild zellweger syndrome due to a novel PEX6 mutation: Correlation between clinical phenotype and *in silico* prediction of variant pathogenicity. *J. Appl. Genet.* 58, 475–480. doi:10.1007/s13353-017-0414-5

Saadane, A., Mast, N., Charvet, C. D., Omarova, S., Zheng, W., Huang, S. S., et al. (2014). Retinal and nonocular abnormalities in Cyp27a1(-/-)Cyp46a1(-/-) mice with dysfunctional metabolism of cholesterol. *Am. J. Pathol.* 184, 2403–2419. doi:10.1016/j.ajpath.2014.05.024

Sack, G. H., Jr., Raven, M. B., and Moser, H. W. (1989). Color vision defects in adrenomyeloneuropathy. *Am. J. Hum. Genet.* 44, 794–798.

Sala, A., Lanciotti, M., Valsecchi, M. G., Di Michele, P., Dufour, C., Haupt, R., et al. (2003). Genotypes of the glutathione S-transferase superfamily do not correlate with outcome of childhood acute lymphoblastic leukemia. *Leukemia* 17, 981–983. doi:10.1038/sj.leu.2402888

Sangiovanni, J. P., Agron, E., Meleth, A. D., Reed, G. F., Sperduto, R. D., Clemons, T. E., et al. (2009). Age-related eye disease study research, G{omega}-3 long-chain polyunsaturated fatty acid intake and 12-y incidence of neovascular age-related macular degeneration and central geographic atrophy: AREDS report 30, a prospective cohort study from the age-related eye disease study. *Am. J. Clin. Nutr.* 90, 1601–1607. doi:10.3945/ajcn.2009.27594

Santos, F. F., De Turco, E. B., Gordon, W. C., Peyman, G. A., and Bazan, N. G. (1995). Alterations in rabbit retina lipid metabolism induced by detachment. Decreased incorporation of [3H]DHA into phospholipids. *Int. Ophthalmol.* 19, 149–159. doi:10.1007/BF00133731

Sapieha, P., Stahl, A., Chen, J., Seaward, M. R., Willett, K. L., Krah, N. M., et al. (2011). 5-Lipoxygenase metabolite 4-HDHA is a mediator of the antiangiogenic effect of omega-3 polyunsaturated fatty acids. *Sci. Transl. Med.* 3, 69ra12. doi:10.1126/scitranslmed.3001571

Schrul, B., and Kopito, R. R. (2016). Peroxin-dependent targeting of a lipid-droplet-destined membrane protein to ER subdomains. *Nat. Cell Biol.* 18, 740–751. doi:10.1038/ncb3373

Seedorf, U., Brysch, P., Engel, T., Schrage, K., and Assmann, G. (1994). Sterol carrier protein X is peroxisomal 3-oxoacyl coenzyme A thiolase with intrinsic sterol carrier and lipid transfer activity. *J. Biol. Chem.* 269, 21277–21283. doi:10.1016/s0021-9258(17)31960-9

Shai, N., Yifrach, E., Van Roermund, C. W. T., Cohen, N., Bibi, C., Cavellini, L., et al. (2018). Systematic mapping of contact sites reveals tethers and a function for the peroxisome-mitochondria contact. *Nat. Commun.* 9, 1761. doi:10.1038/s41467-018-03957-8

Shibuya, N., Koike, S., Tanaka, M., Ishigami-Yuasa, M., Kimura, Y., Ogasawara, Y., et al. (2013). A novel pathway for the production of hydrogen sulfide from D-cysteine in mammalian cells. *Nat. Commun.* 4, 1366. doi:10.1038/ncomms2371

Smith, K. D., Kemp, S., Braiterman, L. T., Lu, J. F., Wei, H. M., Geraghty, M., et al. (1999). X-Linked adrenoleukodystrophy: Genes, mutations, and phenotypes. *Neurochem. Res.* 24, 521–535. doi:10.1023/a:1022535930009

Sprecher, H., Luthria, D. L., Mohammed, B. S., and Baykousheva, S. P. (1995). Reevaluation of the pathways for the biosynthesis of polyunsaturated fatty acids. *J. Lipid Res.* 36, 2471–2477. doi:10.1016/s0022-2275(20)41084-3

Steinberg, D., Avigan, J., Mize, C., Eldjarn, L., Try, K., and Refsum, S. (1965). Conversion of U-C14-phytol to phytanic acid and its oxidation in heredopathia atactica polyneuritiformis. *Biochem. Biophys. Res. Commun.* 19, 783–789. doi:10.1016/0006-291x(65)90328-1

Steinberg, S. J., Dodt, G., Raymond, G. V., Braverman, N. E., Moser, A. B., and Moser, H. W. (2006). Peroxisome biogenesis disorders. *Biochim. Biophys. Acta* 1763, 1733–1748. doi:10.1016/j.bbamcr.2006.09.010

Steinberg, S. J., Morgenthaler, J., Heinzer, A. K., Smith, K. D., and Watkins, P. A. (2000). Very long-chain acyl-CoA synthetases. Human "bubblegum" represents a new family of proteins capable of activating very long-chain fatty acids. *J. Biol. Chem.* 275, 35162–35169. doi:10.1074/jbc.M006403200

Steinberg, S. J., Raymond, G. V., Braverman, N. E., and Moser, A. B. (1993). "Zellweger spectrum disorder," in *GeneReviews*. Editors M. P. Adam, G. M. Mirzaa, R. A. Pagon, S. E. Wallace, L. J. H. Bean, K. W. Gripp, et al. (Seattle (WA): University of Washington).

Steinberg, S. J., Wang, S. J., Kim, D. G., Mihalik, S. J., and Watkins, P. A. (1999a). Human very-long-chain acyl-CoA synthetase: Cloning, topography, and relevance to branched-chain fatty acid metabolism. *Biochem. Biophys. Res. Commun.* 257, 615–621. doi:10.1006/bbrc.1999.0510

Steinberg, S. J., Wang, S. J., Mcguinness, M. C., and Watkins, P. A. (1999b). Human liver-specific very-long-chain acyl-coenzyme A synthetase: cDNA cloning and characterization of a second enzymatically active protein. *Mol. Genet. Metab.* 68, 32–42. doi:10.1006/mgme.1999.2883

Stewart, M. W., Vavra, M. W., and Whaley, N. R. (2011). Fundus findings in A patient with alpha-methlyacyl-coa racemase deficiency. *Retin. Cases Brief. Rep.* 5, 262–266. doi:10.1097/ICB.0b013e3181f047dd

Stinson, A. M., Wiegand, R. D., and Anderson, R. E. (1991a). Fatty acid and molecular species compositions of phospholipids and diacylglycerols from rat retinal membranes. *Exp. Eye Res.* 52, 213–218. doi:10.1016/0014-4835(91)90261-c

Stinson, A. M., Wiegand, R. D., and Anderson, R. E. (1991b). Recycling of docosahexaenoic acid in rat retinas during n-3 fatty acid deficiency. *J. Lipid Res.* 32, 2009–2017. doi:10.1016/s0022-2275(20)41904-2

Stowe, R. C., and Agarwal, S. (2017). Novel PEX26 mutation causing zellweger syndrome presenting as feeding intolerance and hypotonia. *Pediatr. Neurol.* 75, 96–97. doi:10.1016/j.pediatrneurol.2017.06.012

Su, H. M., Moser, A. B., Moser, H. W., and Watkins, P. A. (2001). Peroxisomal straight-chain Acyl-CoA oxidase and D-bifunctional protein are essential for the retroconversion step in docosahexaenoic acid synthesis. *J. Biol. Chem.* 276, 38115–38120. doi:10.1074/jbc.M106326200

Summerer, S., Hanano, A., Utsumi, S., Arand, M., Schuber, F., and Blee, E. (2002). Stereochemical features of the hydrolysis of 9, 10-epoxystearic acid catalysed by plant and mammalian epoxide hydrolases. *Biochem. J.* 366, 471–480. doi:10.1042/BJ20011778

Suzuki, Y., Iai, M., Kamei, A., Tanabe, Y., Chida, S., Yamaguchi, S., et al. (2002). Peroxisomal acyl CoA oxidase deficiency. *J. Pediatr.* 140, 128–130. doi:10.1067/mpd.2002.120511

Tan, J. S., Wang, J. J., Flood, V., and Mitchell, P. (2009). Dietary fatty acids and the 10-year incidence of age-related macular degeneration: The blue mountains eye study. *Arch. Ophthalmol.* 127, 656–665. doi:10.1001/archophthalmol.2009.76

Taormina, V. M., Unger, A. L., Schiksnis, M. R., Torres-Gonzalez, M., and Kraft, J. (2020). Branched-chain fatty acids-an underexplored class of dairy-derived fatty acids. *Nutrients* 12, E2875. doi:10.3390/nu12092875

Thomas, G. H., Haslam, R. H., Batshaw, M. L., Capute, A. J., Neidengard, L., and Ransom, J. L. (1975). Hyperpipecolic acidemia associated with hepatomegaly, mental retardation, optic nerve dysplasia and progressive neurological disease. *Clin. Genet.* 8, 376–382. doi:10.1111/j.1399-0004.1975.tb01517.x

Thompson, S. A., Calvin, J., Hogg, S., Ferdinandusse, S., Wanders, R. J., and Barker, R. A. (2009). Relapsing encephalopathy in a patient with alpha-methylacyl-CoA racemase deficiency. *BMJ Case Rep.* 2009, bcr08. doi:10.1136/bcr.08.2008.0814

Thureen, P. J., Narkewicz, M. R., Battaglia, F. C., Tjoa, S., and Fennessey, P. V. (1995). Pathways of serine and glycine metabolism in primary culture of ovine fetal hepatocytes. *Pediatr. Res.* 38, 775–782. doi:10.1203/00006450-199511000-00023

Trachootham, D., Lu, W., Ogasawara, M. A., Nilsa, R. D., and Huang, P. (2008). Redox regulation of cell survival. *Antioxid. Redox Signal.* 10, 1343–1374. doi:10.1089/ars.2007.1957

Trachsel-Moncho, L., Benlloch-Navarro, S., Fernandez-Carbonell, A., Ramirez-Lamelas, D. T., Olivar, T., Silvestre, D., et al. (2018). Oxidative stress and autophagy-related changes during retinal degeneration and development. *Cell Death Dis.* 9, 812. doi:10.1038/s41419-018-0855-8

Treen, M., Uauy, R. D., Jameson, D. M., Thomas, V. L., and Hoffman, D. R. (1992). Effect of docosahexaenoic acid on membrane fluidity and function in intact cultured Y-79 retinoblastoma cells. *Arch. Biochem. Biophys.* 294, 564–570. doi:10.1016/0003-9861(92)90726-d

Trujillo, M., Clippe, A., Manta, B., Ferrer-Sueta, G., Smeets, A., Declercq, J. P., et al. (2007). Pre-steady state kinetic characterization of human peroxiredoxin 5: Taking advantage of Trp84 fluorescence increase upon oxidation. *Arch. Biochem. Biophys.* 467, 95–106. doi:10.1016/j.abb.2007.08.008

Tsujihata, M. (2008). Mechanism of calcium oxalate renal stone formation and renal tubular cell injury. *Int. J. Urol.* 15, 115–120. doi:10.1111/j.1442-2042.2007.01953.x

Turk, B. R., Theda, C., Fatemi, A., and Moser, A. B. (2020). X-linked adrenoleukodystrophy: Pathology, pathophysiology, diagnostic testing, newborn screening and therapies. *Int. J. Dev. Neurosci.* 80, 52–72. doi:10.1002/jdn.10003

Uchiyama, A., Aoyama, T., Kamijo, K., Uchida, Y., Kondo, N., Orii, T., et al. (1996). Molecular cloning of cDNA encoding rat very long-chain acyl-CoA synthetase. *J. Biol. Chem.* 271, 30360–30365. doi:10.1074/jbc.271.48.30360

Uzor, N. E., Mccullough, L. D., and Tsvetkov, A. S. (2020). Peroxisomal dysfunction in neurological diseases and brain aging. *Front. Cell. Neurosci.* 14, 44. doi:10.3389/fncel.2020.00044

Vamecq, J. (1987). Chlorpromazine and carnitine-dependency of rat liver peroxisomal beta-oxidation of long-chain fatty acids. *Biochem. J.* 241, 783–791. doi:10.1042/bj2410783

van den Bosch, H., Schutgens, R. B., Wanders, R. J., and Tager, J. M. (1992). Biochemistry of peroxisomes. *Annu. Rev. Biochem.* 61, 157–197. doi:10.1146/annurev.bi.61.070192.001105

van den Brink, D. M., Van Miert, J. N., Dacremont, G., Rontani, J. F., Jansen, G. A., and Wanders, R. J. (2004). Identification of fatty aldehyde dehydrogenase in the breakdown of phytol to phytanic acid. *Mol. Genet. Metab.* 82, 33–37. doi:10.1016/j.ymgme.2004.01.019

van den Brink, D. M., Van Miert, J. N., Dacremont, G., Rontani, J. F., and Wanders, R. J. (2005). Characterization of the final step in the conversion of phytol into phytanic acid. *J. Biol. Chem.* 280, 26838–26844. doi:10.1074/jbc.M501861200

van Roermund, C. W., Ijlst, L., Wagemans, T., Wanders, R. J., and Waterham, H. R. (2014). A role for the human peroxisomal half-transporter ABCD3 in the oxidation of dicarboxylic acids. *Biochim. Biophys. Acta* 1841, 563–568. doi:10.1016/j.bbalip.2013.12.001

van Roermund, C. W., Visser, W. F., Ijlst, L., Waterham, H. R., and Wanders, R. J. (2011). Differential substrate specificities of human ABCD1 and ABCD2 in peroxisomal fatty acid beta-oxidation. *Biochim. Biophys. Acta* 1811, 148–152. doi:10.1016/j.bbalip.2010.11.010

Van Veldhoven, P. P., Brees, C., and Mannaerts, G. P. (1991). D-aspartate oxidase, a peroxisomal enzyme in liver of rat and man. *Biochim. Biophys. Acta* 1073, 203–208. doi:10.1016/0304-4165(91)90203-s

Van Veldhoven, P. P., Croes, K., Asselberghs, S., Herdewijn, P., and Mannaerts, G. P. (1996). Peroxisomal beta-oxidation of 2-methyl-branched acyl-CoA esters: Stereospecific recognition of the 2S-methyl compounds by trihydroxycoprostanoyl-CoA oxidase and pristanoyl-CoA oxidase. *FEBS Lett.* 388, 80–84. doi:10.1016/0014-5793(96)00508-x

Van Veldhoven, P. P., De Schryver, E., Young, S. G., Zwijsen, A., Fransen, M., Espeel, M., et al. (2020). Slc25a17 gene trapped mice: PMP34 plays a role in the peroxisomal degradation of phytanic and pristanic acid. *Front. Cell Dev. Biol.* 8, 144. doi:10.3389/fcell.2020.00144

Vanhove, G. F., Van Veldhoven, P. P., Fransen, M., Denis, S., Eyssen, H. J., Wanders, R. J., et al. (1993). The CoA esters of 2-methyl-branched chain fatty acids and of the bile acid intermediates di- and trihydroxycoprostanic acids are oxidized by one single peroxisomal branched chain acyl-CoA oxidase in human liver and kidney. *J. Biol. Chem.* 268, 10335–10344. doi:10.1016/s0021-9258(18)82206-2

Verhoeven, N. M., Roe, D. S., Kok, R. M., Wanders, R. J., Jakobs, C., and Roe, C. R. (1998). Phytanic acid and pristanic acid are oxidized by sequential peroxisomal and mitochondrial reactions in cultured fibroblasts. *J. Lipid Res.* 39, 66–74. doi:10.1016/s0022-2275(20)34204-8

Violante, S., Achetib, N., Van Roermund, C. W. T., Hagen, J., Dodatko, T., Vaz, F. M., et al. (2019). Peroxisomes can oxidize medium- and long-chain fatty acids through a pathway involving ABCD3 and HSD17B4. *FASEB J.* 33, 4355–4364. doi:10.1096/fj.201801498R

Voss, A., Reinhart, M., Sankarappa, S., and Sprecher, H. (1991). The metabolism of 7, 10, 13, 16, 19-docosapentaenoic acid to 4, 7, 10, 13, 16, 19-docosahexaenoic acid in rat liver is independent of a 4-desaturase. *J. Biol. Chem.* 266, 19995–20000. doi:10.1016/s0021-9258(18)54882-1

Wallner, S., and Schmitz, G. (2011). Plasmalogens the neglected regulatory and scavenging lipid species. *Chem. Phys. Lipids* 164, 573–589. doi:10.1016/j.chemphyslip.2011.06.008

Wanders, R. J., Dekker, C., Hovarth, V. A., Schutgens, R. B., Tager, J. M., Van Laer, P., et al. (1994). Human alkyldihydroxyacetonephosphate synthase deficiency: A new peroxisomal disorder. *J. Inherit. Metab. Dis.* 17, 315–318. doi:10.1007/BF00711817

Wanders, R. J., Komen, J., and Ferdinandusse, S. (2011a). Phytanic acid metabolism in health and disease. *Biochim. Biophys. Acta* 1811, 498–507. doi:10.1016/j.bbalip.2011.06.006

Wanders, R. J., Komen, J., and Kemp, S. (2011b). Fatty acid omega-oxidation as a rescue pathway for fatty acid oxidation disorders in humans. *FEBS J.* 278, 182–194. doi:10.1111/j.1742-4658.2010.07947.x

Wanders, R. J. (2014). Metabolic functions of peroxisomes in health and disease. *Biochimie* 98, 36–44. doi:10.1016/j.biochi.2013.08.022

Wanders, R. J., Schumacher, H., Heikoop, J., Schutgens, R. B., and Tager, J. M. (1992). Human dihydroxyacetonephosphate acyltransferase deficiency: A new peroxisomal disorder. *J. Inherit. Metab. Dis.* 15, 389–391. doi:10.1007/BF02435984

Wanders, R. J., Waterham, H. R., and Ferdinandusse, S. (2015). Metabolic interplay between peroxisomes and other subcellular organelles including mitochondria and the endoplasmic reticulum. *Front. Cell Dev. Biol.* 3, 83. doi:10.3389/fcell.2015.00083

Wang, B. J., Xia, J. M., Wang, Q., Yu, J. L., Song, Z., and Zhao, H. (2020). Diet and adaptive evolution of alanine-glyoxylate aminotransferase mitochondrial targeting in birds. *Mol. Biol. Evol.* 37, 786–798. doi:10.1093/molbev/msz266

Wang, N., and Anderson, R. E. (1993a). Synthesis of docosahexaenoic acid by retina and retinal pigment epithelium. *Biochemistry* 32, 13703–13709. doi:10.1021/bi00212a040

Wang, N., and Anderson, R. E. (1993b). Transport of 22:6n-3 in the plasma and uptake into retinal pigment epithelium and retina. *Exp. Eye Res.* 57, 225–233. doi:10.1006/exer.1993.1118

Waterham, H. R., and Ebberink, M. S. (2012). Genetics and molecular basis of human peroxisome biogenesis disorders. *Biochim. Biophys. Acta* 1822, 1430–1441. doi:10.1016/j.bbadis.2012.04.006

Waterham, H. R., Ferdinandusse, S., and Wanders, R. J. (2016). Human disorders of peroxisome metabolism and biogenesis. *Biochim. Biophys. Acta* 1863, 922–933. doi:10.1016/j.bbamcr.2015.11.015

Watkins, P. A., Howard, A. E., and Mihalik, S. J. (1994). Phytanic acid must be activated to phytanoyl-CoA prior to its alpha-oxidation in rat liver peroxisomes. *Biochim. Biophys. Acta* 1214, 288–294. doi:10.1016/0005-2760(94)90075-2

Werner, E. R., Keller, M. A., Sailer, S., Lackner, K., Koch, J., Hermann, M., et al. (2020). The TMEM189 gene encodes plasmanylethanolamine desaturase which introduces the characteristic vinyl ether double bond into plasmalogens. *Proc. Natl. Acad. Sci. U. S. A.* 117, 7792–7798. doi:10.1073/pnas.1917461117

Wetzel, M. G., Li, J., Alvarez, R. A., Anderson, R. E., and O'brien, P. J. (1991). Metabolism of linolenic acid and docosahexaenoic acid in rat retinas and rod outer segments. *Exp. Eye Res.* 53, 437–446. doi:10.1016/0014-4835(91)90161-7

Wheeler, J. B., Shaw, D. R., and Barnes, S. (1997). Purification and characterization of a rat liver bile acid coenzyme A ligase from rat liver microsomes. *Arch. Biochem. Biophys.* 348, 15–24. doi:10.1006/abbi.1997.0391

Win, A., Delgado, A., Jadeja, R. N., Martin, P. M., Bartoli, M., and Thounaojam, M. C. (2021). Pharmacological and metabolic significance of bile acids in retinal diseases. *Biomolecules* 11, 292. doi:10.3390/biom11020292

Winterbourn, C. C. (1995). Toxicity of iron and hydrogen peroxide: The Fenton reaction. *Toxicol. Lett.* 82-83, 969–974. doi:10.1016/0378-4274(95)03532-x

Wojtowicz, S., Strosznajder, A. K., Jezyna, M., and Strosznajder, J. B. (2020). The novel role of PPAR alpha in the brain: Promising target in therapy of alzheimer's disease and other neurodegenerative disorders. *Neurochem. Res.* 45, 972–988. doi:10.1007/s11064-020-02993-5

Xiong, W., Maccoll Garfinkel, A. E., Li, Y., Benowitz, L. I., and Cepko, C. L. (2015). NRF2 promotes neuronal survival in neurodegeneration and acute nerve damage. *J. Clin. Invest.* 125, 1433–1445. doi:10.1172/JCI79735

Yako, T., Otsu, W., Nakamura, S., Shimazawa, M., and Hara, H. (2022). Lipid droplet accumulation promotes RPE dysfunction. *Int. J. Mol. Sci.* 23, 1790. doi:10.3390/ijms23031790

Yamamoto, Y., and Sakisaka, T. (2018). The peroxisome biogenesis factors posttranslationally target reticulon homology domain-containing proteins to the endoplasmic reticulum membrane. *Sci. Rep.* 8, 2322. doi:10.1038/s41598-018-20797-0

Young, R. W. (1976). Visual cells and the concept of renewal. *Invest. Ophthalmol. Vis. Sci.* 15, 700–725.

Zaki, M. S., Heller, R., Thoenes, M., Nurnberg, G., Stern-Schneider, G., Nurnberg, P., et al. (2016). PEX6 is expressed in photoreceptor cilia and mutated in deafblindness with enamel dysplasia and microcephaly. *Hum. Mutat.* 37, 170–174. doi:10.1002/humu.22934

Zhao, Y., Wu, Y., Pei, J., Chen, Z., Wang, Q., and Xiang, B. (2015). Safety and efficacy of parenteral fish oil-containing lipid emulsions in premature neonates. *J. Pediatr. Gastroenterol. Nutr.* 60, 708–716. doi:10.1097/MPG.0000000000000665

Zhu, X. H., Lu, M., Lee, B. Y., Ugurbil, K., and Chen, W. (2015). *In vivo* NAD assay reveals the intracellular NAD contents and redox state in healthy human brain and their age dependences. *Proc. Natl. Acad. Sci. U. S. A.* 112, 2876–2881. doi:10.1073/pnas.1417921112

Zomer, A. W., Van Der Burg, B., Jansen, G. A., Wanders, R. J., Poll-The, B. T., and Van Der Saag, P. T. (2000). Pristanic acid and phytanic acid: Naturally occurring ligands for the nuclear receptor peroxisome proliferator-activated receptor α. *J. Lipid Res.* 41, 1801–1807. doi:10.1016/s0022-2275(20)31973-8

frontiers | Frontiers in Cell and Developmental Biology

TYPE Review
PUBLISHED 08 September 2022
DOI 10.3389/fcell.2022.994412



OPEN ACCESS

EDITED BY
Rajalekshmy Shyam,
Indiana University Bloomington,
United States

REVIEWED BY
Robert Mullins,
The University of Iowa, United States
Chi Sun,
Washington University in St. Louis,
United States

*CORRESPONDENCE
Ann C. Morris,
ann.morris@uky.edu

SPECIALTY SECTION
This article was submitted to Morphogenesis and Patterning, a section of the journal Frontiers in Cell and Developmental Biology

RECEIVED 14 July 2022
ACCEPTED 19 August 2022
PUBLISHED 08 September 2022

CITATION
Krueger LA and Morris AC (2022), Eyes on CHARGE syndrome: Roles of CHD7 in ocular development. *Front. Cell Dev. Biol.* 10:994412. doi: 10.3389/fcell.2022.994412



# Eyes on CHARGE syndrome: Roles of CHD7 in ocular development

Laura A. Krueger and Ann C. Morris*

Department of Biology, University of Kentucky, Lexington, KY, United States

The development of the vertebrate visual system involves complex morphogenetic interactions of cells derived from multiple embryonic lineages. Disruptions in this process are associated with structural birth defects such as microphthalmia, anophthalmia, and coloboma (collectively referred to as MAC), and inherited retinal degenerative diseases such as retinitis pigmentosa and allied dystrophies. MAC and retinal degeneration are also observed in systemic congenital malformation syndromes. One important example is CHARGE syndrome, a genetic disorder characterized by coloboma, heart defects, choanal atresia, growth retardation, genital abnormalities, and ear abnormalities. Mutations in the gene encoding Chromodomain helicase DNA binding protein 7 (CHD7) cause the majority of CHARGE syndrome cases. However, the pathogenetic mechanisms that connect loss of CHD7 to the ocular complications observed in CHARGE syndrome have not been identified. In this review, we provide a general overview of ocular development and congenital disorders affecting the eye. This is followed by a comprehensive description of CHARGE syndrome, including discussion of the spectrum of ocular defects that have been described in this disorder. In addition, we discuss the current knowledge of CHD7 function and focus on its contributions to the development of ocular structures. Finally, we discuss outstanding gaps in our knowledge of the role of CHD7 in eye formation, and propose avenues of investigation to further our understanding of how CHD7 activity regulates ocular and retinal development.

KEYWORDS

**retina, eye, photoreceptors, CHD7, CHARGE syndrome, zebrafish**

## 1 Introduction

Vision, one of our major senses, is considered the largest contributor to perception of the world around us (Pike, 2012). The visual system requires signals to be received by the eye, processed through the retina, and interpreted by the brain. When development of the visual system or eye structures are disrupted, congenital eye defects and pediatric visual impairment may result. Pediatric visual impairment can be life altering, affecting motor, language, emotional, social, and cognitive development (Wilkinson and Trantham, 2004; West, 2002; Berit Augestad, 2007; Sabra et al., 2009; Rainey et al., 2016). Disruptions in eye development and congenital eye defects are often found as part of larger syndromic

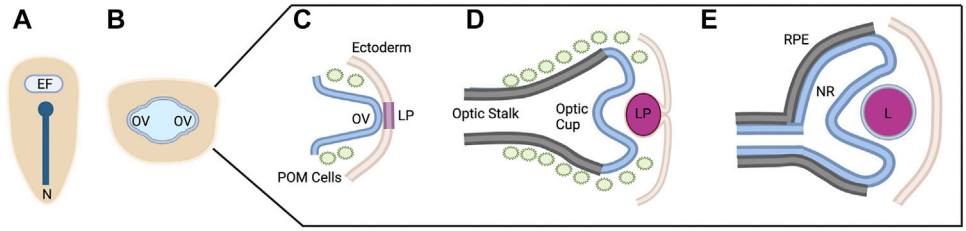


FIGURE 1
Vertebrate Ocular Development. Schematic representation of ocular development stages from eye field specification to bi-layered optic cup formation **(A–E)**. This process occurs between 12 and 24 hpf in zebrafish, E8-10 in mouse, and from ~4 to 7 weeks in human. See text for process details. EF, eye field; N, notochord; OV; optic vesicle; LP, lens placode/pit; POM, periocular mesenchyme; RPE, retinal pigment epithelium; NR, neural retina; L, lens. Figure created with Biorender.com.

disorders, including CHARGE syndrome, a genetic disorder characterized by coloboma, heart defects, choanal atresia, growth retardation, genital abnormalities, and ear abnormalities.

Development of the visual system is highly conserved among vertebrates (Stenkamp, 2015). A significant amount of work has been completed to better understand pathways involved in ocular morphogenesis and retinal development, however many questions remain about the role and mechanism of individual genes in these processes. In this review, we will provide an overview of the processes of vertebrate ocular morphogenesis, retinal development, and photoreceptor differentiation, and will compare these processes in zebrafish and mouse, two widely used animal models for development biology research, as well as humans to highlight similarities and differences across vertebrates. Next, we will describe some of the congenital disorders that result when these processes are disrupted, with a particular focus on CHARGE syndrome. We will discuss CHD7 function and its contributions to the development of ocular structures, and the potential roles of two of its downstream targets (Sox4 and Sox11) in visual system development. Finally, we will highlight outstanding gaps in our knowledge of CHD7 function, and avenues of investigation to further our understanding of how CHD7 activity regulates ocular and retinal development.

## 2 Vertebrate ocular development

Development of the vertebrate eye and ocular structures is a result of the organized interactions of neuroectoderm (forms the retina and retinal pigment epithelium), surface ectoderm (forms the lens), and periocular mesenchyme made up of mesoderm and cranial neural crest cells (form the ocular blood vessels and anterior ocular structures).

Briefly, early in vertebrate development, a single eye field is specified at the border of the anterior neural plate (Figure 1A) (Li et al., 1997). Cells within this eye field express known eye field transcription factors (EFTFs) including Pax6, Rax, Otx2, Six3, and Lhx2, among others; the eye field contains all necessary progenitor cells to form the neural portions of the eye (Zuber et al., 2003). Disruptions in the development of the eye field result in defects such as microphthalmia (small eye) or anophthalmia (single eye or no eyes) (Loosli et al., 2003; Voronina, 2003).

The eye field is subsequently separated into two domains through the action of Nodal/TGF-B and Sonic hedgehog (Shh) signaling as the midline of the embryo is established (Echelard et al., 1993; Zhang et al., 1998). Disruptions in these signaling pathways and/or abnormal segregation of the eye field result in holoprosencephaly and cyclopia (Belloni et al., 1996; Roessler et al., 1996; Maity et al., 2005). The two separate eye fields evaginate away from the midline, forming the optic vesicles (Figure 1B) (Svoboda and O'Shea, 1987; Rembold et al., 2006). During this evagination process, the neural retina, retinal pigment epithelium (RPE), and optic stalk begin to be specified. The distal portion of the optic vesicle forms the neural retina, expressing the homeobox gene Vsx2; the dorsal proximal portion forms the RPE, expressing the transcription factor Mitf; and the ventral proximal portion forms the optic stalk, expressing Pax2 (Svoboda and O'Shea, 1987; Schmitt and Dowling, 1994; Burmeister et al., 1996; Nguyen and Arnheiter, 2000; Kagiyama et al., 2005).

Evagination of the optic vesicle also allows for the interaction with the surface ectoderm. This interaction leads to the thickening of the surface ectoderm which eventually forms the lens placode and is the initial step in lens formation (Figure 1C) (Hendrix and Zwaan, 1975; Huang et al., 2011). At the same time, the optic vesicle invaginates, forming the bilayered optic cup (Figure 1D). This invagination is a result of distinct cellular events in each of the layers. The distal layer shapes the presumptive retina through cellular basal constriction and retinal rim involution (Martinez-Morales et al., 2009; Kwan et al., 2012; Nicolás-Pérez et al., 2016; Sidhaye and Norden, 2017). The RPE is shaped by flattening of cells in the medial layer that surround the outside and rim of the retina (Figure 1E) (Li et al., 2000; Miesfeld et al., 2015; Cechmanek and McFarlane, 2017).

Furthermore, the optic vesicle and optic cup are receiving extrinsic signals from the periocular mesenchyme. It has been shown that periocular mesenchyme, consisting of mesoderm and neural crest cells, begins to migrate with the optic structures at the stage of evagination of the optic vesicle (Gage et al., 2005; Langenberg et al., 2008; Bryan et al., 2020). These periocular mesenchyme cells supply the signals for the specification of the RPE and differentiation of the optic stalk, in addition to migrating into the optic cup to become anterior ocular structures such as iris stroma and corneal endothelium (Gage et al., 2005).

As optic cup invagination is occurring, at the ventral portion near and within the optic stalk, an opening known as the optic fissure forms. Fissure formation is the result of the ventral edges of the optic cup and optic stalk approaching each other during invagination but remaining separated. Control of fissure formation is both intrinsic to cells of the optic cup in addition to contributions from surrounding tissue by Hedgehog, retinoic acid, and Bmp signaling, among others (Bernstein et al., 2018; Gordon et al., 2018). This opening allows space for the entrance of developing hyaloid vasculature and exit of retinal ganglion cell axons that bundle together to form the optic nerve. The fissure eventually closes to encapsulate these structures. The underlying molecular events that mediate fissure closure are a strong area of current research, however the general sequence of events is widely accepted. The closure process includes apposition of the edges of the fissure, followed by basement membrane rearrangement then epithelial remodeling and tissue fusion, and finally intercalation of tissue (Bernstein et al., 2018). Additionally, periocular mesenchyme cells are required for fissure closure. Specifically, a subset of neural crest cells and endothelial cells seem to be necessary for basement membrane rearrangement (James et al., 2016; Cao et al., 2018; Gestri et al., 2018; Weaver et al., 2020). When optic fissure formation or closure is disrupted, the birth defect known as coloboma results (Chang et al., 2006). Coloboma can occur solely or as part of larger syndromic disorders and involves different portions of the eye, resulting in visual impairment of varying severity depending on its location and size; coloboma will be discussed further in a later section.

Finally, the anterior structures of the eye,—cornea, iris and ciliary body—are forming during and after optic cup completion. The cornea forms with interactions between the surface ectoderm and migrating periocular mesenchyme while the iris and ciliary body are formed at the edges of the optic cup from proliferating periocular mesenchyme cells (Cvekl and Tamm, 2004; Davis-Silberman and Ashery-Padan, 2008).

## 3 Vertebrate retinal development

As stated above, the inner layer of the of the optic cup forms the neural retina. The vertebrate neural retinal progenitor pool proliferates and differentiates into six neuronal cell types; retinal ganglion cells (RGCs), amacrine cells, horizontal cells, bipolar cells, and rod and cone photoreceptors; as well as one intrinsic glial cell type, the Müller glia. Within these broad cell categories, several subtypes have been described for some retinal cell types, the number of which can vary considerably among different vertebrate species. For example, at least 18 subtypes of RGCs have been described in the primate and human retina (Kim et al., 2021). Other cell types, such as astrocytes, microglia, and cells of the retinal vasculature, are generated outside the retina and subsequently migrate in. The retinal cells are organized in a conserved fashion across all vertebrates in three nuclear layers and two plexiform layers. The outer nuclear layer (ONL) contains the light sensitive rod and cone photoreceptors which then synapse with bipolar cells and horizontal cells in the outer plexiform layer (OPL). The inner nuclear layer (INL) contains the cell bodies of the bipolar, horizontal, amacrine, and Müller glial cells. The bipolar and amacrine cells synapse with retinal ganglion cells in the inner plexiform layer (IPL). The ganglion cell layer (GCL) contains the cell bodies of the retinal ganglion cells, whose axons then exit the retina and bundle together, forming the optic nerve, which transmits the visual signal to the brain. Müller glia span the entire retina and provide structural and functional support to the other retinal cells. This principal glial cell of the retina maintains architectural organization in addition to synthesizing and phagocytosing necessary products for retinal function and homeostasis (Figure 2A).

Decades of work in the retina have shown that all these retinal cell types differentiate from a single population of multipotent retinal progenitor cells (Turner and Cepko, 1987; Holt et al., 1988; Wetts and Fraser, 1988; Turner et al., 1990; Jensen and Raff, 1997). Furthermore, the spatiotemporal pattern of development and differentiation of the distinct retinal cells is largely conserved across vertebrates (Hu and Easter, 1999; Bassett and Wallace, 2012).

In zebrafish, formation of the bilayered optic cup is completed around 20 h post fertilization (hpf) and the inner neuroepithelial layer is the starting place for retinal cell differentiation (Schmitt and Dowling, 1994). Retinal neurogenesis begins in a small region of the ventronasal retinal neuroepithelium adjacent to the optic nerve (often referred to as the ventral patch). The ganglion cells are the first cell type to differentiate, exiting the cell cycle in a fan-shaped pattern that spreads from the ventral to dorsal retina (Schmitt and Dowling, 1999; Stenkamp, 2007). The cells of the INL follow the same fan-shaped pattern of differentiation between 36 hpf and 4 days post fertilization (dpf) for amacrine, horizontal, and bipolar cells (Schmitt and Dowling, 1999; Jusuf and Harris, 2009; Connaughton, 2011). Overlapping with this period, photoreceptors also begin to develop, with cone photoreceptors appearing first followed by rod photoceptors. Whereas cone photoreceptors differentiate in a pattern similar to

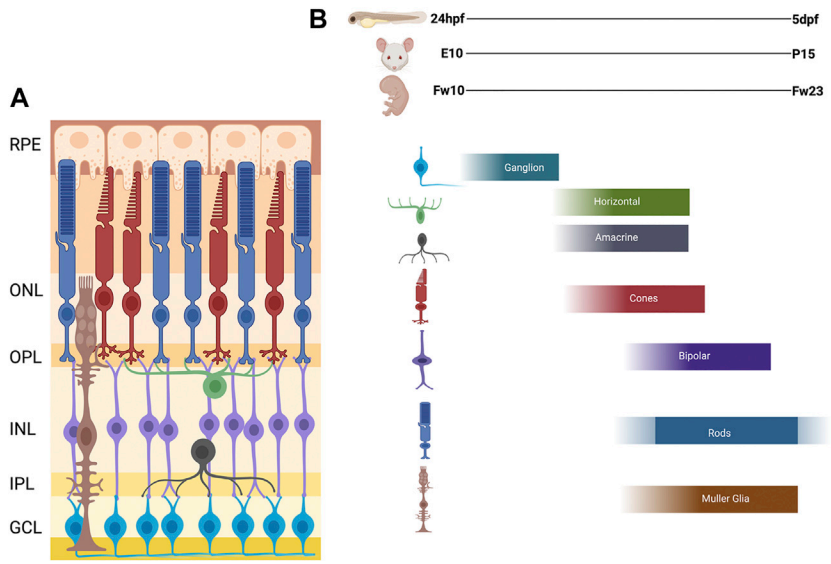


FIGURE 2
Schematic of Vertebrate Retina and Order of Retinal Cell Differentiation. **(A)** Diagram of vertebrate retina. The retina is composed of three nuclear layers: Outer Nuclear Layer (ONL), the Inner Nuclear Layer (INL), and the Ganglion Cell Layer (GCL), and two plexiform layers: Outer plexiform later (OPL) and Inner Plexiform Layer (IPL). The synapses for the photoreceptors, horizontal, bipolar are in the OPL and amacrine, bipolar, and ganglion are in the IPL. **(B)** The order of retinal cell differentiation is conserved across zebrafish, mouse and human. Most of this cell differentiation occurs between 24 h post fertilization (hpf) to 5 days post fertilization (dpf) in zebrafish, embryonic day 10 (E10) to post-natal day 15 (P15) in mouse, and fetal week 10 (Fw10) to fetal week 23 (Fw23) in humans. Figure created with Biorender.com.

the other retinal cell types (Suzuki et al., 2013), rod photoreceptor differentiation proceeds in an irregular pattern from the ventral patch to the dorsal and central retina (Raymond et al., 1995). In the post-embryonic retina, rods are primarily derived from a multipotent stem cell/Müller glia progenitor pool in the INL. These progenitors proliferate and migrate through the INL to ONL where they transition based on specific gene expression from progenitors to rod precursors, then to rod photoreceptors (Bernardos et al., 2007; Morris et al., 2008a, Morris et al., 2008b). The last cells to differentiate are the Müller glia (Turner and Cepko, 1987; Peterson et al., 2001).

The temporal progression of retinal neurogenesis is mostly conserved between mouse and zebrafish with specific timepoints of early born cells (ganglion cells, amacrine, horizontal and cone photoreceptors) developing between embryonic day 10 (E10) and postnatal day 1 (P1). The late born cells (rod photoreceptors, bipolar cells, and Müller glia) develop in the first 14 postnatal days (P0-P14) (Young, 1985; Marquardt and Gruss, 2002). In humans, this process occurs between fetal week 10–18 for the early born cells and fetal week 18–23 for the late born cells with some continued differentiation of photoreceptors occurring after birth (Figure 2B) (Aldiri et al., 2017; Hoshino et al., 2017).

While the cell type differentiation is complete in the mouse by 14 days after birth and in humans several months after birth, the zebrafish retina displays continual growth, which occurs from a persistently neurogenic area at the retinal periphery. This area, the ciliary marginal zone (CMZ), contains a pool of stem cells that allow for the continual addition of retinal cells as the zebrafish grows, enabling the retina to maintain appropriate cell density as the eye cup expands along with the body of the zebrafish (Stenkamp, 2007; Reinhardt et al., 2015). Furthermore, the zebrafish has the unique ability to respond to retinal damage with regeneration of retinal cells. In this case, Müller glia respond to damage by de-differentiating and asymmetrically dividing to produce multipotent stem cells that can regenerate all the lost retinal cell types (Yurco and Cameron, 2005; Sherpa et al., 2008, 2014).

## 4 Photoreceptor development

Vision requires that light be captured from the world around us. This process entails anterior structures of the eye (cornea, pupil, iris, and lens) to allow for light to enter, pass through, and focus correctly on the retina. Light hitting the retina must then be captured by the light sensitive cells, the photoreceptors. Photoreceptors can be broadly divided into two subtypes—the rods and cones. Rods are highly sensitive (able to detect a single photon of light) and mediate dim light vision (and peripheral vision in humans), whereas cones mediate daytime and color vision. Most mammals have two cone subtypes which are maximally sensitive to medium and long wavelenths of light.

Humans possess three cone subtypes (short-, medium-, and long-wavelength sensitive cones). Zebrafish possess four cone subtypes (short-, medium-, long- and UV-sensitive cones). Photoreceptors have a distinct morphology to allow for this light sensitivity (Lamb et al., 2007; Molday and Moritz, 2015). Rod and cone photoreceptor cells have five main regions: the outer segment, connecting cilium, inner segment, nuclear body, and axonal and synaptic region. Outer segments contain membranous disks (rods) or folds (cones) which enclose opsins, the light-sensitive G-protein coupled receptor proteins responsible for the detection of light. The photopigment molecule of rods, rhodopsin, allows for the detection of dim light while the opsins of cones (red, green, and blue) allow for color vison and higher visual acuity. The outer segments of rods have a long cylindrical shape whereas cones have a shorter conical shape. Capturing of light in these photopigment molecules of the outer segment initiates the phototransduction pathway allowing for light to be converted to an electrical signal that is transmitted to the second-order neurons of the retina. The connecting cilium connects the outer and inner segments and provides a channel to allow for important proteins to pass from the cell body and nuclear region to and from the outer segment. The synaptic region is the site of transfer of neurotransmitters to retinal bipolar cells and the horizontal neurons.

The development of the outer segments of photoreceptors and their contained structures and proteins are essential for visual function. The outer segment resembles the structure of a primary sensory cilia and develops in a similar manner. First, during initial photoreceptor development, the axoneme/cilium projects from its basal body located in the inner segment. This primitive cilium contains vesicles and tubules of "morphogenetic material" that will establish other structures of the outer segments. Second, the apical region of the cilium enlarges as the material is used to form beginnings of disks. Third, these primitive disks are then remodeled and reoriented to their final transverse position. Recent work suggests that the nascent photoreceptor outer segment disks are similar in composition to ciliary ectosomes (small membranous vesicles that bud off from a cell's primary cilium); these ecotomal structures form at the base of the photoreceptor cilium and are retained by structural proteins at the disk rim rather than being released into the extracellular space (Spencer et al., 2020). As a result of these steps the outer segment is formed by morphogenetic and differentiation events of the distal region of the primitive cilia. The undifferentiated basal portion remains continuous with the basal body and becomes the connecting cilium (de Robertis, 1956; Horst et al., 1990). Outer segment morphogenesis has been detected starting at 60–63 hpf in zebrafish and P8-9 in mice and continues until adult dimensions are met (de Robertis, 1956; Branchek and Bremiller, 1984; Obata and Usukura, 1992; Crespo and Knust, 2018). Outer segments are further maintained throughout life by undergoing constant renewal. New disks are continually being synthesized at the base of outer segments which leads to elongation of the outer segment. At the distal outer segment of the photoreceptor, the oldest disks are then shed and are phagocytosed by the RPE (Young, 1967).

Although photoreceptor function is conserved across species, the spatial organization and distribution of rods and cones varies based on evolutionary strategies. In humans, this means a peripheral retina that is rod dominant with a central region, the macula, which has a higher density of cones and a fovea with only cones allowing for our high visual acuity (Ahnelt, 1998). In contrast, nocturnal mice are rod dominant throughout their retina and only contain two types of cones, short and medium wavelength (Carter-Dawson and Lavail, 1979). The zebrafish has a cone-rich retina, possessing 60% cones, similar to the macula of humans and reflecting their diurnal lifestyle (Fadool, 2003; Allison et al., 2010; Zimmermann et al., 2018). In addition, zebrafish contain a fourth cone subtype that is sensitive to ultraviolet light. The four cones in zebrafish are arranged in a unique geometric mosaic pattern in which red/green double cones are always located next to blue cones on the red cone side and UV cones on the green cone side. Furthermore, in adult zebrafish, four rods form a square surrounding the UV cones (Fadool, 2003).

Much work has been done to investigate the many different signals and pathways involved in the process of photoreceptor development. This work has shown that progenitor cells are not limited to a specific path but instead during proliferation or post mitotically, precursors encounter different specification events leading to their fate. Furthermore, the pathway and sequence of events are generally conserved among vertebrates (Cepko et al., 1996; Wong and Rapaport, 2009). These events that control specification are from intrinsic gene expression programs as well as extrinsic signals and can be both positive (acquiring an event/signal) or negative (restricting another event/signal).

Briefly, the photoreceptor progenitor pool is fist specified by the expression of the transcription factors Otx2 and Crx. When Otx2 is absent, photoreceptors do not develop and instead there is an increase in amacrine like cells (Chen et al., 1997; Furukawa et al., 1997; Nishida et al., 2003) while defective photoreceptor development and degeneration occurs when Crx is absent (Furukawa et al., 1999). Additionally, NeuroD, a bHLH transcription factor, is present in the rod progenitor pool of the inner nuclear layer as well as cone progenitor pool and has been implicated in controlling cell cycle regulation and cellular proliferation of precursors (Ochocinska and Hitchcock, 2007; Nelson et al., 2008). This photoreceptor precursor pool is then further specified into rod and cone subtypes.

Expression of the transcription factor Nrl is required for the rod photoreceptor fate (Mears et al., 2001). Nrl, a basic

leucine zipper transcription factor, promotes the expression of important downstream rod photoreceptor genes including the orphan nuclear receptor Nr2e3, which is responsible for activating other rod specific genes as well as repressing cone specific genes like S-opsin (Kumar et al., 1996; Cheng et al., 2011; Kautzmann et al., 2011). Defects in both Nrl and Nr2e3 lead to non-functional rods in mice and the genetic disorder of S-cone syndrome is attributed to loss of Nr2e3 in humans and results in a fate switch from rods to S-cones (Haider et al., 2000; Mears et al., 2001).

For cones, subtype specification is somewhat more complicated. In zebrafish, two progenitor cone populations form. One population expresses the homeobox transcription factor Six7 and can only form green cones. A second population expresses the bone morphogenetic protein (BMP) ligand Gdf6a and differentiates into three distinct subtypes of cones based on additional expression of downstream genes (Ogawa et al., 2015). If Gdf6a is solely expressed, the cells become blue cones; if Gdf6a and thyroid hormone receptor beta (Thrb) are expressed the population becomes red cones. Finally, if Gdf6a and T-box transcription factor 2b (Tbx2b) are co-expressed the population differentiates into UV cones (DuVal and Allison, 2018). In mice, which only have short- and medium-wavelength cones, disruption of Thrb results in mice deficient for M-opsin and an overabundance of S-opsin (Ng et al., 2001; Roberts et al., 2006).

Several extrinsic signaling pathways have also been shown to have a role in photoreceptor development and specific opsin expression. These factors include (but are not limited to) Fgfs, Wnts, Shh, retinoic acid (RA), Notch and thyroid hormone (T3) and changes in their morphogen concentration gradients lead to loss of photoreceptors and differential opsin expression patterns (Roberts et al., 2006; Stevens et al., 2011). Briefly, in zebrafish, Hedgehog signaling from the RPE is associated with the wave-like differentiation of photoreceptors and when disrupted, differentiation is halted resulting in a decrease in photoreceptors (Stenkamp et al., 2000). In chick and rat *in vitro* experiments, retinoic acid was shown to be essential for differentiation and survival of photoreceptors and recently has been shown to accelerate photoreceptor development in retinal organoids (Stenkamp et al., 1993; Kelley et al., 1999; Zerti et al., 2020). Furthermore, retinoic acid-treated zebrafish showed altered photoreceptor differentiation, resulting in an increased number of rod photoreceptors and red cones, and a decrease in number of blue and UV cone photoreceptors (Hyatt et al., 1996; Prabhudesai et al., 2005). Finally, Notch signaling has been shown to maintain proliferative potential of retinal progenitors and the transition to photoreceptor precursors. An early loss of Notch signaling has been shown to lead to an increase in the number of cones and later loss of signaling leads to an increased number of rods (Jadhav et al., 2006).

In summary, while much has been learned about the intrinsic transcription factors and the external signaling that influences photoreceptor development, gaps in our knowledge about the contribution and timing of these genes and factors, as well as additional photoreceptor genes that participate in this process, still remain to be addressed.

## 5 Congenital ocular defects and syndromic disorders

Development of ocular structures and retinal cells require precise spatial and temporal organization. When these spatial or temporal dynamics are disrupted, congenital ocular and retinal defects can lead to visual impairment. These defects include three main groups: optic cup, anterior segment, and retinal disorders (Table 1). Optic cup abnormalities are present when formation of the eye field, and/or proper bilateralization and evagination are disrupted leading to anophthalmia (absence of the eye), or microphthalmia (smaller than normal eye) (Mathers et al., 1997; Fantes et al., 2003). Coloboma is also a part of this group and is a consequence of the optic fissure not closing properly, which affects the iris, choroid, retina, and optic nerve (Skalicky et al., 2013). Anterior segment deficits involve the structures of the cornea, iris, ciliary body, and lens leading to aniridia, anterior segment dysgenesis, Axenfeld-Rieger anomaly, and Peters Anomaly (Smith, 2000; Semina, 2001; Komatireddy et al., 2003). Retinal disorders are those that effect the neurons of the retina and most commonly the photoreceptors. These defects include cone-rod dystrophy, Leber congenital amaurosis, and retinitis pigmentosa and result when the genes responsible for function and maintenance of the photoreceptors are disrupted leading to photoreceptor degeneration, or when the photoreceptors don't form normally during development (Morimura et al., 1998; Sohocki et al., 1998; Lotery, 2001; Fazzi et al., 2003).

While some of these defects are rare, a child's vision and their future development can be strongly impacted. In fact, coloboma accounts for up to 10% of pediatric blindness (Chang et al., 2006). In addition, these congenital defects may present as the sole developmental defect or as part of a larger syndromic disorder. Axenfeld-Rieger anomaly and Peters Anomaly can be part of larger syndromes (Axenfeld-Rieger syndrome and Peters plus syndrome), in which affected individuals have both eye anterior segment defects in addition to craniofacial defects, dental anomalies, short stature, and intellectual disability (de Almeida and Llerena, 1993; Chang et al., 2012). Retinal cell defects are present in syndromic disorders such as Usher syndrome, Bardet-Biedl, Joubert, and Senior-Løken syndrome. In Usher syndrome, the affected individual has retinitis pigmentosa and faces a range of hearing loss and balance concerns that

TABLE 1 Congenital ocular defects.

| | Major characteristics | Additional ocular characteristics | Major genes | Frequency |
|---|---|---|---|---|
| Anterior segment defects | | | | |
| Aniridia | Loss of Iris | Misshapen pupil, glaucoma, cataracts | *PAX6, FOXC1, CYP1B1* | 1 in 50,000 to 100,000 |
| Anterior segment dysgenesis | Underdeveloped iris, cornea defects, ciliary body defects, lens defects | Glaucoma, cataracts | More than 15 genes; *PITX2, FOXC1, PITX3* | Varies |
| Axenfeld-Rieger anomaly | Defects in iris and pupil | Glaucoma, cataracts | *PITX2* and *FOXC1* | 1 in 200,000 |
| Peters anomaly | Opaque cornea | Amblyopia, glaucoma, cataracts | *FOXC1, PAX6, PITX2, CYP1B1* | 3 to 6 in 100,000 |
| Optic cup defects | | | | |
| Anophthalmia | Loss of one or both eyes | n/a | More than 75 genes; *SOX2, RAX, OTX2, PAX6* | 1 in 20,000 |
| Coloboma | Lack of optic fissure closure | Cataracts, glaucoma, myopia, nystagmus, retinal detachments | More than 50 genes; *SHH, PAX6, GDF3, VAX2* | 1 in 10,000 |
| Microphthalmia | Small eye | Cataracts, microcornea | More than 50 genes; *RAX, SIX6, OTX2, SHH, SOX2* | 1 in 10,000 |
| Retinal cell defects | | | | |
| Cone—rod dystrophy | Loss of cones then rod photoreceptors | Nystagmus | More than 30 genes; *ABCA4* | 1 in 30,000 to 40,000 |
| Leber congenital amaurosis | Loss of photoreceptors | Nystagmus, keratoconus, poor pupillary reflex | More than 15 genes; *CEP290, CRB1, RPE65* | 2 to 3 in 100,000 |
| Retinitis pigmentosa | Loss of rods then cone photoreceptors | n/a | More than 60 genes; *RHO, USH2A* | 1in 3,000 to 4,000 |
| Usher syndrome | Loss of rods then cone photoreceptors | n/a | *MYO7A, CDH23,CLRN, USH2A* | 4 to 17 in 100,000 people |
| Bardet-Biedl syndrome | Loss of cones then rod photoreceptors | n/a | More than 15 genes; BBS1, BBS10, | 1 in 140,000 to 1 in 160,000 |
| Joubert syndrome | Loss of rods then cone photoreceptors | Coloboma | More than 30 genes; *CEP290, KIF7, NPHP1* | 1 in 80,000 to 1 in 100,000 |
| Senior-Løken syndrome | Loss of photoreceptors | Nystagmus, keratoconus, poor pupillary reflex | *CEP290, NPHP1,WDR19,NPHP4* | 1 in 1,000,000 |

vary in severity depending on the affected gene (Bonnet and El-Amraoui, 2012). In Bardet-Biedl syndrome, most affected individuals have cone-rod dystrophy and are legally blind by adolescence, in addition to other characteristics such as obesity, polydactyly (extra fingers and toes), intellectual disability, and genital abnormalities (Beales, 2005). Individuals with Joubert syndrome can display brain abnormalities along with muscle, skeletal, kidney, liver and retinal dystrophy (Parisi, 2009). Senior-Løken syndrome is characterized by the combination of Leber congenital amaurosis and loss of photoreceptors with the kidney condition of nephronophthisis (Ronquillo et al., 2012). Finally, microphthalmia, anophthalmia, and coloboma, collectively referred to as MAC, can occur in isolation or alongside those of brain and craniofacial defects, signifying the similar signaling pathways responsible for the formation of head structures. One example is CHARGE syndrome, a genetic neurocristopathy characterized by coloboma, heart defects, choanal atresia, growth retardation, genital abnormalities, and ear abnormalities (Hsu et al., 2014).

## 6 Clinical presentation of CHARGE syndrome

The syndrome now known as CHARGE was first described in 1979 through two different cohorts of individuals with ear, ocular, cardiac, craniofacial anomalies, and intellectual disability (Hall, 1979; Hittner

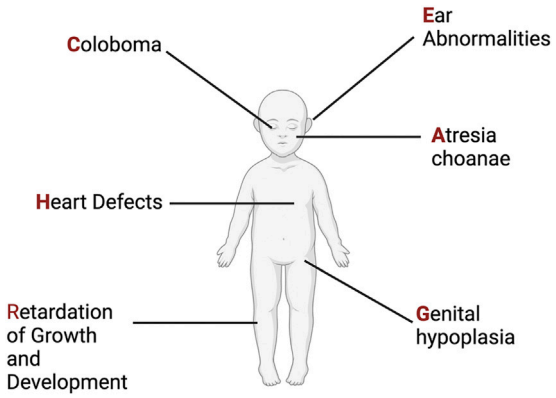


FIGURE 3
CHARGE Syndrome. Original phenotypic description leading to the acronym for CHARGE Syndrome. See text for more details. Figure created with Biorender.com.

et al., 1979; Issekutz et al., 2005; Janssen et al., 2012). Two years later another cohort of individuals was described, and the publishing group proposed the acronym CHARGE: C-coloboma, H-heart disorders A-atresia choanae, R-retarded growth and retarded development and/or CNS anomalies, G-genital hypoplasia, and E-ear anomalies and/or deafness (Pagon et al., 1981) (Figure 3). The prevalence of CHARGE syndrome is estimated to be between 1 in 10,000 to 1 in 15,000 live births.

Since first described, phenotypic reports have expanded, resulting in more detail and a wider range of possible phenotypic presentations. Some of the clinical manifestations of CHARGE syndrome are present at birth, whereas others become apparent later in life or upon more in-depth examination and testing. Ocular defects include coloboma and microphthalmia and will be discussed in more detail in Section 8 (Nishina et al., 2012). Heart defects include a wide spectrum of congenital abnormalities including aortic arch interruption, tetralogy of Fallot, double outlet right ventricle, arch vessel anomalies, and atrioventricular septal defects (Corsten-Janssen et al., 2013). Craniofacial and upper respiratory malformations include choanal atresia (narrowing of nasal cavity), orofacial clefts, tracheoesophageal fistulas along with characteristic facial features of prominent foreheads and nasal bridges (Inchingolo et al., 2014). Growth and developmental anomalies involve central nervous defects, cranial nerve abnormalities, short stature, and intellectual delays (Graham et al., 2005; Blake et al., 2008; Dörr et al., 2015; Hoch et al., 2017). Genital abnormalities include genital hypoplasia and late puberty (Ragan et al., 1999). Ear abnormalities involve cup shaped outer ear, triangular concha, ossicular malformations, absence or hypoplasia of semicircular canals and sensory hearing deficits (Morimoto et al., 2006; Holcomb et al., 2013; Ha et al., 2016; Wineland et al., 2017).

TABLE 2 CHARGE syndrome diagnostic criteria.

| CHARGE syndrome diagnostic criteria | |
|---|---|
| Major (2 or More) | Minor |
| Coloboma | Cranial nerve dysfunction |
| Choanal atresia or cleft palate | Dysphagia/feeding difficulties |
| Abnormal external, middle, or inner ears | Structural brain anomalies |
| Pathogenic *CHD7* variant | Developmental delay |
| | Hypothalamo-hypophyseal dysfunction (gonadotropin or growth hormone deficiency) and genital anomalies |
| | Heart or esophagus malformation |
| | Renal anomalies |
| | Skeletal and limb anomalies |

The expansion of the phenotypes described can be partially attributed to the identification in 2004 of the major causative gene, *CHD7*, which is reported to be mutant in 70%–90% of CHARGE syndrome cases (Vissers et al., 2004; Jongmans et al., 2006; Zentner et al., 2010). While molecular diagnosis was initially performed via traditional Sanger sequencing of *CHD7*, the recent application of whole exome sequencing in individuals suspected of having CHARGE syndrome has provided an opportunity to expand the number of pathogenic variants that have been detected in *CHD7*, as well as identifying additional genes associated with this disorder. The wide spectrum of phenotypes that have now been described for individuals with *CHD7*-associated CHARGE syndrome has resulted in several different published clinical diagnostic criteria centered on major and minor characteristics (Blake et al., 1998; Verloes, 2005; Blake and Prasad, 2006). The latest proposed criteria suggest a CHARGE diagnosis based on 2 major and any number of minor characteristics (Hale et al., 2016) (Table 2). One of the major characteristics is a pathogenic variant in *CHD7*, which has been the focus of CHARGE Syndrome research to further understand the diverse spectrum and mechanism of phenotypes observed and will be discussed more in Section 7.

## 7 Chromodomain helicase DNA binding protein 7 and CHARGE syndrome

CHD7 is a member of the chromodomain helicase-DNA binding domain (CHD) family of proteins. CHD members have specific non-redundant roles in the processes involved in

chromatin manipulation using ATP-hydrolysis (Woodage et al., 1997; Flaus and Owen-Hughes, 2011; Manning and Yusufzai, 2017). Members of this family have two conserved motifs: two chromodomains located in the N-terminal region, and the SNF2-like ATPase domains located in the central region, with other domains less well characterized at the C-terminus (Delmas et al., 1993). For a more in-depth discussion of CHD7 functional domains, we refer the reader to previously published reviews (Marfella and Imbalzano, 2007; Layman et al., 2010). In general, CHD7 has been shown to be responsible for nucleosome mobility, recognizing unique target sites to allow for the removal and sliding of the histone octamer thus leading to DNA access (Bouazoune and Kingston, 2012). This chromatin manipulation is essential for DNA transcription, replication, and repair, making CHD7 a vital gene for normal development (Ho and Crabtree, 2010). CHD7 has been shown to preferentially associate with H3Kme1, H3K4me3, and H3K27ac histone modifications, which mark poised and active promoters and enhancers (Reddy et al., 2021). ChIP experiments have shown that CHD7 occupies distinct sets of binding sites in different cell types, indicating that CHD7 regulates chromatin accessibility in a tissue-specific manner (Schnetz et al., 2009). CHD7 may control target gene expression by acting solely or as member of a complex with other transcription factors, such as PBAF and CHD8, which was shown to interact wth CHD7 via its conserved SANT domain (Bajpai et al., 2010; Batsukh et al., 2010). CHD7-mediated tissue-specific gene expression control has been found to be essential for cellular proliferation and differentiation in addition to maintenance of adult neural stem cell populations (Martin, 2010; Jones et al., 2015).

Heterozygous pathogenic variants in *CHD7* are identified in 70%–90% of clinically diagnosed individuals with CHARGE (Vissers et al., 2004; Jongmans et al., 2006; Zentner et al., 2010). With over 500 pathogenic variants spanning the entirety of the 38-exon gene (2997 amino acids, ~336 kD protein), 90% of the variants are nonsense, frameshift, and splice site variants resulting in a truncated protein (Bergman et al., 2011). In addition, pathogenic variants in *CHD7* have been reported in clinical cases of Kallmann syndrome, which is a disorder involving hypogonadotropic hypogonadism (deficit in gonadotropin-releasing hormone) and hyposmia or anosmia (diminished or lack of smell) (Jongmans et al., 2009). Interestingly, 70% of variants found in *CHD7* causing Kallmann syndrome are missense variants (Marcos et al., 2014). Since identification of *CHD7* as a causative gene in CHARGE syndrome, research has focused on understanding its role in the affected tissues. The following sections will focus on the ocular complications of CHARGE syndrome and the role that CHD7 plays in the development of the eye.

## 8 Ocular complications of CHARGE syndrome

Clinical reports indicate that coloboma is present in over 80% of clinically diagnosed individuals with CHARGE. The colobomas range in severity and involvement of the retina, choroid, lens, and iris. While the majority of the observed colobomas are bilateral, some individuals present with unilateral ocular defects. In addition to coloboma, other ocular complications including microphthalmia, optic nerve hypoplasia, nystagmus, cataracts, amblyopia, microcornea, strabismus and rarely angle closure defects and retinal detachment have been reported (Russell-Eggitt et al., 1990; Tellier et al., 1998; Guirgis and Lueder, 2003; Strömland et al., 2005; Aramaki et al., 2006; Lalani et al., 2006; Natung et al., 2014; Martin et al., 2020).

While ocular structural defects have been identified in different case reports and phenotype reviews of CHARGE syndrome, we lack an understanding of the correlation between the extent of ocular defects and an individual's visual impairment. This is partially due to the complex clinical presentation of CHARGE syndrome, which often imposes limits on performing normal vision assessment methods. Recently several groups have tried to address this lack of connection. First, the VISIOCHARGE questionnaire combined ophthalmological findings with a self- and/or guardian-administered questionnaire assessing distance-vision, near-vision, and overall vision. This group concluded that visual skills of everyday life were relatively good even in the presence of severe ocular structural defects, such as bilateral colobomas, and there was no association between visual ability and the severity of ocular malformation (Martin et al., 2020). However, this study has its limitations based on the small size of the cohort and the nature of self-administered questionnaires. More recently, the VISIOCHARGE questionnaire was combined with adapted visual behavior assessments and ophthalmic assessments to better fit the complexity of clinical findings in CHARGE syndrome (Onesimo et al., 2021). Visual behavior assessments were adapted to measure the ability to fix, track, perform saccades, and assess visual acuity and visual fields along with measuring contrast sensitivity, stereopsis, and strabismus. Overall, this systematic assessment resulted in categorizing 57% of the individuals with severe visual impairment. However, there was no correlation between the extent of visual impairment and the severity of the ocular structural abnormality. This study did identify a correlation between ocular abnormalities and the type of pathogenic variants in CHD7, suggesting that earlier truncating pathogenic variants resulted in more severe findings such as extensive colobomas. This study also has limitations due to size, but leads to questions about why there is a lack of correlation between ocular structural defects and assessed visual function. One possible explanation is that loss of CHD7 results in additional retinal abnormalities that are

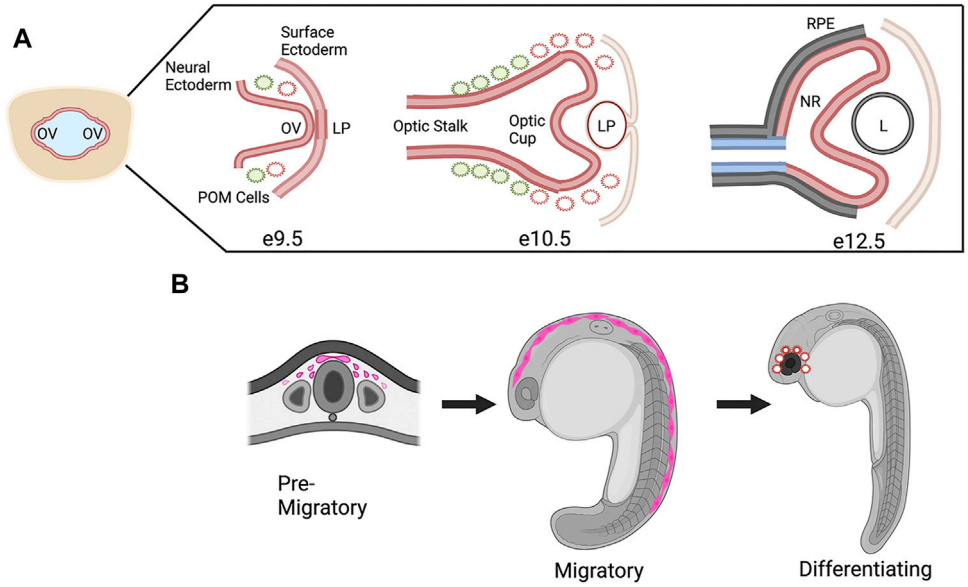


FIGURE 4
CHD7 Expression in Ocular Morphogenesis and Neural Crest Cell Development. **(A)** Schematic representation of ocular development stages in mouse from optic vesicle evagination at E9.9 to bi-layered optic cup at E12.5, CHD7 expression is colored in red. OV, optic vesicle; LP, lens placode/pit; POM, periocular mesenchyme; RPE, retinal pigment epithelium; NR, neural retina; L, lens. **(B)** Schematic representation of CHD7 expression in neural crest cell development, CHD7 expression is colored in pink. Figure created with Biorender.com.

currently underdiagnosed in CHARGE syndrome. To further understand the full extent of ocular complications of CHARGE syndrome, it is essential to better understand CHD7's role in eye development beyond the initial stage of ocular morphogenesis.

## 9 Role of CHD7 in development of ocular structures

Xenopus, Drosophila, zebrafish, and mouse models have been established to further study the development and mechanism of CHD7 and CHARGE syndrome (Bajpai et al., 2010; Melicharek et al., 2010; Patten et al., 2012). Homozygous loss-of-function mouse models are embryonic lethal at E10.5 while heterozygous mice display characteristics like those of individuals with CHARGE (Bosman et al., 2005; Hurd et al., 2007). These models have been used to extensively study brain, ear, heart, and craniofacial developmental phenotypes upon loss of CHD7 (Bosman et al., 2005; Melicharek et al., 2010; Ogier et al., 2014; Sperry et al., 2014; Whittaker et al., 2017a). However, less work has concentrated on eye development in these models, partially due to the complex contributions of multiple tissues in the eye.

One study that focused on CHD7 in mouse eye development used conditional knockouts to delete *Chd7* from various embryonic tissues that contribute to the eye, including the neural ectoderm (*Rx-Cre*), surface ectoderm (*Le-Cre*), and both surface and neural ectoderm (*Foxg1-Cre*) (Gage et al., 2015). This work was the first detailed expression study in the eye and CHD7 was shown to be widely expressed in early neural and surface ectoderm from E9.5-E12.5, the timing of which corresponds to optic vesicle evagination at E9.5 through formation of the optic cup and lens at E12.5 (Figure 4A). Furthermore, conditional knockouts of *Chd7* in surface ectoderm and/or neural ectoderm demonstrated that expression of CHD7 was required in the neural ectoderm for proper ocular morphogenesis of the optic cup and optic fissure closure. In addition, this work established and qualitatively described the presence of coloboma in the *Chd7* mutant mouse model which previously had not been addressed.

Ocular structural defects upon loss of Chd7 in other species have been broadly described but not rigorously investigated. Results of knockdown and knockout studies contain general descriptions of microphthalmia, coloboma, and anterior defects, but an in-depth understanding of mechanism or contribution of CHD7 to these defects is lacking (Jacobs-Mcdaniels and Albertson, 2011; Balow et al., 2013; Cloney et al., 2018; Liu et al., 2018; Liu and Liu, 2019; Breuer et al., 2020).

An area of focus for CHD7 research has been its role in neural crest cells, which contribute to many of the structures affected in CHARGE syndrome (Siebert et al., 1985). Neural crest cells are multipotent migratory cells that arise early in development and contribute to tissues and structures in the

TABLE 3 CHD7 and neurogenesis.

| System | Neurons affected | Potential downstream targets of CHD7 | Association with CHARGE phenotype |
|---|---|---|---|
| Cerebellum | Reduction in cerebellar granule neurons | *Reln, Fgf8* | Cerebellar hypoplasia leading to developmental delays |
| Global brain | Reduction in GABAergic neurons | *paqr3b* | Autism-like behavior, attention-deficit/ hyperactivity disorder, anxiety, aggressivity and seizures |
| Hippocampus | Decrease in adult neurogenesis from subventricular zone (SVZ) of the lateral ventricle and the subgranular zone (SGZ) of the dentate gyrus | *Sox4, Sox11* | Development delays |
| Hypothalamus | Reduced gonadotropin-releasing hormone (GnRH) neurons | *Fgfr1,Bmp4, Otx2* | Hypogonads, genital hypoplasia, and delayed puberty |
| Olfactory | Reduced olfactory bulb size and reduced olfactory neurons | *Mash1, NeuroD* | Hyposmia and Anosmia |
| Auditory and vestibular | Vestibulo-cochlear ganglion size and neuron number | *Ngn1, Otx2, Fgf10* | Hearing loss and balance disorders |

heart, craniofacial skeleton, ear, eye, and peripheral nervous system, among others (Pauli et al., 2017). It has been shown in mouse, zebrafish, and Xenopus models that Chd7 is expressed in pre-migratory neural crest cells and when Chd7 expression is altered there is a decrease and disruption of these cells (Fujita et al., 2014; Schulz et al., 2014). Expression continues during neural crest cell migration where in Xenopus and in human cells (including patient derived iPS cells) CHD7 has been shown to target downstream genes such as *Sox9*, *Twist*, and *Snail 1/2* (Bajpai et al., 2010; Sperry et al., 2014; Okuno et al., 2017). Furthermore, in mouse models CHD7 has been shown to work in conjunction with other transcription factors and chromatin remodeling complexes to direct neural crest cell differentiation and when CHD7 is absent neural crest cell fates are altered (Figure 4B) (Fan et al., 2021).

Concentrating on the eye, it is known that cranial neural crest cells contribute to the periocular mesenchyme, which forms anterior ocular structures including the cornea, ciliary body, iris, sclera, and aqueous humor outflow tract. Disruptions in neural crest cells result in defects of these structures and congenital disorders such as Axenfeld-Reiger syndrome and Peters Anomaly (Cvekl and Tamm, 2004; Gage et al., 2005). Neural crest cells also secondarily play a role in optic cup formation and optic fissure closure, interacting with the neural derived optic cup. Disruptions in this process result in microphthalmia and coloboma (Bassett et al., 2010; Bryan et al., 2020).

However, the exact role of CHD7 in the cranial neural crest cells that contribute to ocular development is still unknown, creating a need for more investigation and additional models. Anterior segment defects have been identified in individuals with CHARGE suggesting that CHD7 may contribute to neural crest cells in the periocular mesenchyme (McMain et al., 2008; Nishina et al., 2012; Dote et al., 2019). Models with live imaging and transgenic lines of zebrafish that have fluorescently labeled neural crest cells could help to delineate the exact role of Chd7 in cranial neural crest cells and periocular mesenchyme. Furthermore, based on CHD7's role in neural ectoderm and ocular structures, conditional knockout models will need to be established to determine the contribution from each cell type.

## 10 CHD7 in neurogenesis

In addition to the role of CHD7 in neural crest cell dynamics, CHD7 has strongly been associated with tissue-specific neurogenesis. These associations are evident in many of the systems affected in CHARGE syndrome which contain nervous tissue (Table 3). In the ear, CHD7 has been shown to act upstream of pro-neural genes in inner ear neuroblasts; mice lacking functional CHD7 have a smaller vestibulo-cochlear ganglion and decrease in neuron number (Hurd et al., 2010). In the olfactory system, CHD7 is expressed in the pro-neural basal cells during development and adulthood. When disrupted, there is disorganization and a decrease in olfactory sensory neurons (Layman et al., 2009). Gonadotropin-releasing hormone (GnRH) neurons are also reduced in the hypothalamus of haploinsufficient CHD7 mice (Layman et al., 2011). In other parts of the brain, there are examples of CHD7 controlling neurogenesis in both development and adulthood. The neurogenic areas of adult mammalian brain, the subventricular zone (SVZ) of the lateral ventricle and the subgranular zone (SGZ) of the dentate gyrus in the hippocampus, show expression of CHD7 in active neural stem cells and when inactivated there is a decrease in adult neurogenesis (Feng et al., 2013). During development, CHD7 is expressed in cerebellar granule cells and loss of CHD7 in subsets of these cells leads to a decrease of neurogenesis and eventual cerebellar hypoplasia

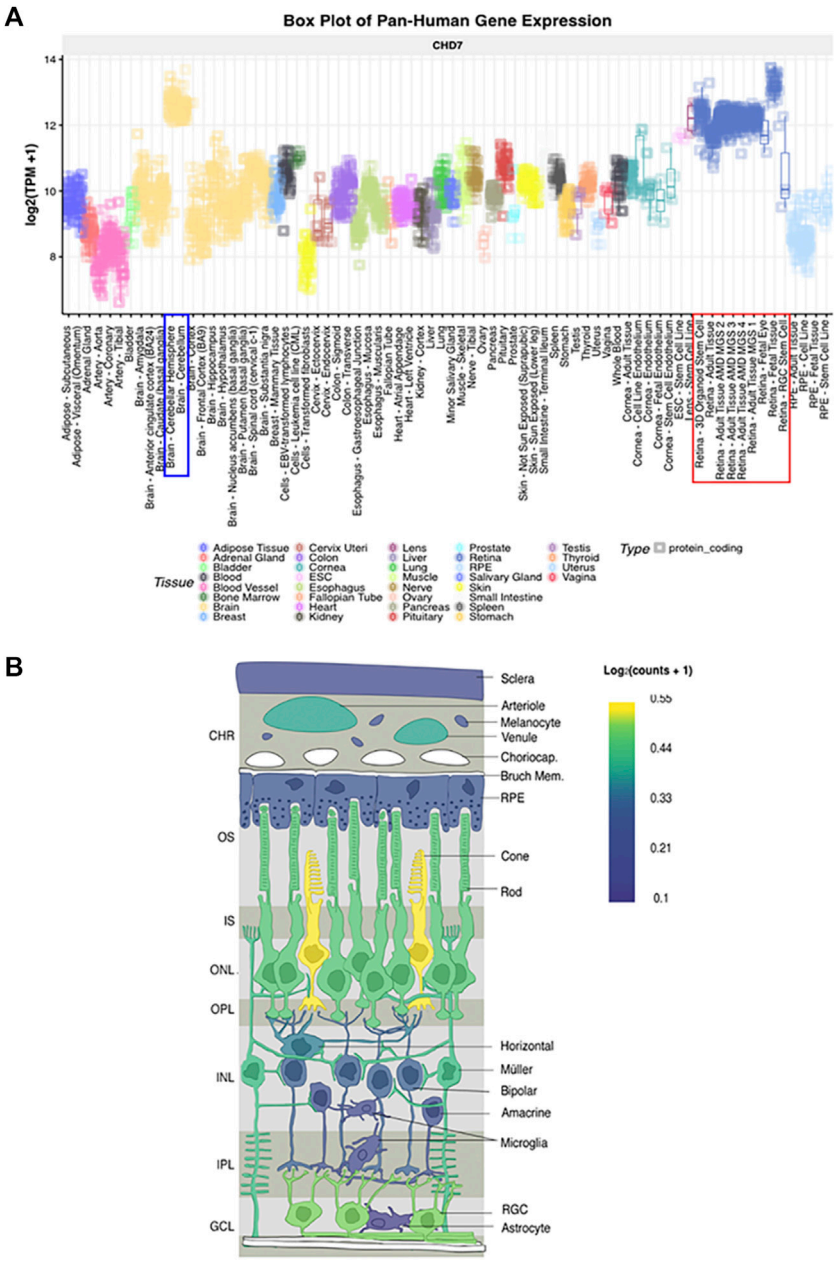


FIGURE 5
CHD7 expression in human retina **(A)** Box plot of pan-Human *CHD7* expression in fetal and adult retinal tissue (red outline) compared to other tissues, assembled with the eyeIntegration v1.05 platform (Bryan et al., 2018). **(B)** *In-situ* projection from published human single cell RNAseq datasets. Assembled with PLatform for Analysis of scEiad (Swamy et al., 2021). Expression is highest in cones, rods, and retinal ganglion cells with lower expression in Müller glia. Reprinted with permission from (Krueger et al., 2022).

(Whittaker et al., 2017b, 2017a; Donovan et al., 2017; Feng et al., 2017).

Globally, CHD7 has been found to be a co-factor of Sox2, which is essential for neural stem cell maintenance and neurogenesis in mouse. It also contributes to neural progenitor differentiation in mouse embryonic stem cells where the loss of CHD7 results in disruption of the number and complexity of new neurons (Engelen et al., 2011; Yao et al., 2020). In addition to mouse models, recent *chd7* mutant and morphant zebrafish models have shown a decrease in branchiomotor neurons of the hindbrain and GABAergic neurons in the brain (Patten et al., 2012; Jamadagni et al., 2021).

While the effects of *CHD7* pathogenic variants on neurogenesis have been studied for many regions of the central and peripheral nervous system, there is little data available on whether loss of CHD7 alters retinal neurogenesis. As described above, much of the focus of published literature has been on ocular morphogenesis and those studies did not examine later timepoints that are relevant for retinal neuron differentiation (Gage et al., 2015).

With the advancement of single-cell transcriptomics, large data meta-analysis platforms have become more accessible to analyze specific tissue transcriptomics. This is the case with the eye and the analysis platform eyeIntegration v1.05 from the National Eye Institute which collates human eye tissue RNA-seq data with other human body tissues (Bryan et al., 2018). When using this platform, Chd7 is shown to be globally expressed in fetal human retina and postnatal retina at levels equal to that of the cerebellum (Figure 5 and Krueger et al., 2022). These data suggest that CHD7 may have some functional role in both the developing and mature retina. Additional data supporting a role for CHD7 in the retina comes from GWAS studies, which have identified variants in *CHD7* that are significantly associated with myopia (Kiefer et al., 2013; Verhoeven et al., 2013; Tedja et al., 2018). Given that retinal signals drive eye growth (Brown et al., 2022), and abnormalities in the photoreceptor cell layer are associated with myopia development (Greenwald et al., 2017; Chakraborty et al., 2019), this suggests that altered CHD7 expression or function may contribute to a broader spectrum of retinal defects than has been previously appreciated.

Interestingly, morpholino-mediated knockdown of zebrafish *chd7* was associated with a decrease in retinal ganglion cells and photoreceptors in addition to global retinal disorganization and laminar defects (Patten et al., 2012). However, there have been no follow up studies to further characterize this phenotype or elucidate contributions of Chd7 to the retina. Taken together with the lack of correlation between the presence of ocular malformations and extent of visual impairment in individuals with CHARGE, this may point to retinal neuron deficits as an additional feature of CHARGE syndrome, and thus should be an avenue for future studies. Furthermore, recent work has shown that Chd7 plays a role in protecting hair cells of the ear from oxidative stress and loss of Chd7 leads to misregulation of stress response pathways resulting in degeneration (Ahmed et al., 2021). Given that photoreceptors are sensory neurons with a high metabolic demand, the role of Chd7 in their oxidative stress response also warrants investigation.

## 11 SoxC factors: Potential targets of CHD7 in eye development

The wide spectrum of phenotypes observed in CHARGE syndrome is not only a result of the broad expression of CHD7 in development but also the wide range of potential downstream targets of CHD7 transcriptional regulation. Generally, CHD7 has been shown to bind regions distal to transcription start sites in the genome marked by H3K4 methylation—the histone modification indicating active transcription. This epigenetic signature of histone methylation and correlation with CHD7 binding signifies the role CHD7 plays in modifying downstream gene expression (Schnetz et al., 2009). Two of these identified binding sites are in the promoters of *Sox11* and *Sox4*, which appears to be required during adult neurogenesis in the hippocampus. In CHD7 mutant mice, there is a decrease in the active histone marker H3K4 methylation at the *Sox11* and *Sox4* promoters in neural stem cells potentially as a direct result of the coordination of Chd7 with methyltransferase complexes (Yan et al., 2020) . *Sox4* and *Sox11* were also shown to be direct targets of CHD7 binding via chromatin immunoprecipitation (ChIP) assays in cultured neural stem cells. In *CHD7* mutants the chromatin structure at *Sox11* and *Sox4* loci remains closed, preventing the transcription of *Sox11* and *Sox4* and inhibiting neurogenesis (Feng et al., 2013).

SOX4 and SOX11 are members of the group C family of SOX transcriptional activators, whose name is derived from a shared DNA binding domain (the SRY-box) originally identified in the mammalian sex-determining gene SRY (Denny et al., 1992). SOX proteins encode a large family of transcription factors that are grouped into individual families, SOXA-SOXH, based on protein structure, expression, and conservation of amino acids. Within individual families there is homology among the N-terminal DNA binding high-mobility group (HMG) region, in addition to regions outside of this domain. The family of SOXC proteins also contains SOX12. All three genes are single exon genes that encode two highly conserved domains, the HMG domain and a C-terminal transactivation domain (TAD) (Bowles et al., 2000). The HMG domain enables specific DNA binding to the sequence (A/T A/T CAA A/T) as well as nonspecific binding in the minor groove of DNA, which induces DNA bending and makes regulatory regions such as promoters and enhancers more accessible to other proteins (Harley et al., 1994; Wegner, 1999; Kamachi et al., 2000). These domains allow for transcriptional control of downstream targets with the contribution of other regulatory proteins.

SOX proteins have been shown to regulate many developmental processes, including early control of the establishment of blastocyst, gastrulation, and germ layers as well as continued cellular pluripotency and cell fate and differentiation in tissue formation and organogenesis (Kamachi et al., 2000; Lefebvre et al., 2007; She and Yang, 2015). More specifically, SOXC proteins have been implicated in different aspects of neurogenesis including fate determination, specification, migration, tract formation, and plasticity (Bhattaram et al., 2010; Chen et al., 2015).

Interestingly, Sox4 and Sox11 are also expressed in neural crest cells during development and are strongly expressed in purified neural crest cells from zebrafish (Uy et al., 2015). Moreover, Sox4- and Sox11-deficient animal models display coloboma, cardiac malformations and brain defects like those seen in CHARGE syndrome (Wurm et al., 2008; Paul et al., 2014; Pillai-Kastoori et al., 2014; Schulz et al., 2014; Gnedeva and Hudspeth, 2015; Wen et al., 2015). In addition, our group has previously shown that Sox11 contributes to coloboma in zebrafish and humans and another group has identified an individual with CHARGE with a chromosomal duplication involving the SOX11 locus (Pillai-Kastoori et al., 2014; Sperry et al., 2016). To better understand the connection of CHD7 and Sox11 with respect to the ocular features of CHARGE syndrome, further characterization of the contribution of these specific genes to ocular development and retinal neurogenesis must be elucidated.

## 12 Conclusion

The intricate process of visual system development requires the coordination of numerous signaling pathways and gene expression programs across different embryonic tissues to achieve a fully functional ocular structure. Disruptions to this process can affect many parts of the developing eye, and several result in significant pediatric visual impairment. One example is CHARGE syndrome, a genetic disorder characterized by ocular coloboma, heart defects, choanal atresia, growth retardation, genital abnormalities, and ear abnormalities. Pathogenic variants in the chromatin remodeling factor CHD7 are the most common cause of CHARGE syndrome, accounting for approximately 70%–90% of CHARGE syndrome cases. Coloboma, which is present in over 80% of individuals with CHARGE syndrome, is generally thought to be the major ocular complication of CHARGE syndrome. However, CHARGE syndrome is also associated with other ocular complications, including microphthalmia, optic nerve hypoplasia, nystagmus, cataracts, amblyopia, microcornea, strabismus, angle closure defects, and retinal detachment. Moreover, the lack of correlation between the extent of visual impairment and the presence of structural ocular defects indicates that additional ophthalmic complications associated with CHARGE syndrome may be missed or overlooked. One defining feature of CHARGE syndrome is that it involves abnormal neural crest cell development: the structures affected in CHARGE syndrome—eyes, brain, heart, craniofacial structures, ear—are composed of neural crest cell derivatives; *CHD7* is expressed in neural crest cells; and neural crest cell progenitors are reduced and their migration is abnormal in animal models of CHARGE syndrome. Therefore, it is possible that some of the ocular defects associated with CHARGE syndrome are due to cell autonomous functions of CHD7 in retnal progenitor cells, whereas some ocular complications could result from non-cell autonomous mechanisms due to loss of CHD7 in cranial neural crest cells and/or the periocular mesenchyme, although the precise balance of mechanisms remain to be determined. Future studies could address this question using conditional knockout models and fluorescent transgenic reporter lines that label specific neural crest cell lineages. CHARGE syndrome also involves abnormal neurogenesis in the CNS (which includes the retina). Recent studies in animal models of CHD7 deficiency, as well as GWAS studies implicating CHD7 variants in myopia, point to a potential role for CHD7 in the developing retina and in retinal cell type differentiation or maintenance. Therefore, future studies should more closely investigate the function of CHD7 in specific subsets of retinal neurons, in particular the critical light-capturing photoreceptors. One promising approach to modeling the ocular complications of CHARGE syndrome would be to use patient-derived iPS cells to generate retinal organoids. A better understanding of the pathogenetic mechanisms underlying the ocular complications of CHARGE syndrome is critical, not only to improve patient care and to identify potential long-term disease sequelae, but also to inform the development of new therapeutic strategies.

## Author contributions

LK drafted the manuscript and prepared the figures. AM edited the manuscript and figures, and contributed to the writing.

## Funding

Research in the Morris lab is supported by grants from the NIH National Eye Institute (R01EY021769, to AM;

F30EY031545, to LK) and from the CHARGE Syndrome Foundation (to AM).

## Conflict of interest

The authors declare that the research was conducted in the absence of any commercial or financial relationships that could be construed as a potential conflict of interest.

## Publisher's note



## References

Ahmed, M., Moon, R., Prajapati, R. S., James, E., Albert Basson, M., and Streit, A. (2021). The chromatin remodelling factor Chd7 protects auditory neurons and sensory hair cells from stress-induced degeneration. *Commun. Biol.* 4, 1260. doi:10.1038/s42003-021-02788-6

Ahnelt, P. K. (1998). The photoreceptor mosaic. *Eye* 12, 531–540. doi:10.1038/eye.1998.142

Aldiri, I., Xu, B., Wang, L., Chen, X., Hiler, D., Griffiths, L., et al. (2017). The dynamic epigenetic landscape of the retina during development, reprogramming, and tumorigenesis. *Neuron* 94, 550–568. e10. doi:10.1016/j.neuron.2017.04.022

Allison, W. T., Barthel, L. K., Skebo, K. M., Takechi, M., Kawamura, S., and Raymond, P. A. (2010). Ontogeny of cone photoreceptor mosaics in zebrafish. *J. Comp. Neurol.* 518, 4182–4195. doi:10.1002/cne.22447

Aramaki, M., Udaka, T., Kosaki, R., Makita, Y., Okamoto, N., Yoshihashi, H., et al. (2006). Phenotypic spectrum of CHARGE syndrome with CHD7 mutations. *J. Pediatr.* 148, 410–414. doi:10.1016/j.jpeds.2005.10.044

Bajpai, R., Chen, D. A., Rada-Iglesias, A., Zhang, J., Xiong, Y., Helms, J., et al. (2010a). CHD7 cooperates with PBAF to control multipotent neural crest formation. *Nature* 463, 958–962. doi:10.1038/nature08733

Balow, S. A., Pierce, L. X., Zentner, G. E., Conrad, P. A., Davis, S., Sabaawy, H. E., et al. (2013). Knockdown of fbxl10/kdm2bb rescues chd7 morphant phenotype in a zebrafish model of CHARGE syndrome. *Dev. Biol.* 382, 57–69. doi:10.1016/j.ydbio.2013.07.026

Bassett, E. A., and Wallace, V. A. (2012). Cell fate determination in the vertebrate retina. *Trends Neurosci.* 35, 565–573. doi:10.1016/j.tins.2012.05.004

Bassett, E. A., Williams, T., Zacharias, A. L., Gage, P. J., Fuhrmann, S., and West-Mays, J. A. (2010). AP-2alpha knockout mice exhibit optic cup patterning defects and failure of optic stalk morphogenesis. *Hum. Mol. Genet.* 19, 1791–1804. doi:10.1093/hmg/ddq060

Batsukh, T., Pieper, L., Koszucka, A. M., von Velsen, N., Hoyer-Fender, S., Elbracht, M., et al. (2010). CHD8 interacts with CHD7, a protein which is mutated in CHARGE syndrome. *Hum. Mol. Genet.* 19, 2858–2866. doi:10.1093/hmg/ddq189

Beales, P. L. (2005). Lifting the lid on pandora's box: The bardet-biedl syndrome. *Curr. Opin. Genet. Dev.* 15, 315–323. doi:10.1016/j.gde.2005.04.006

Belloni, E., Muenke, M., Roessler, E., Traverse, G., Siegel-Bartelt, J., Frumkin, A., et al. (1996). Identification of Sonic hedgehog as a candidate gene responsible for holoprosencephaly. *Nat. Genet.* 14, 353–356. doi:10.1038/ng1196-353

Bergman, J. E. H., Janssen, N., Hoefsloot, L. H., Jongmans, M. C. J., Hofstra, R. M. W., and van Ravenswaaij-Arts, C. M. A. (2011). CHD7 mutations and CHARGE syndrome: The clinical implications of an expanding phenotype. *J. Med. Genet.* 48, 334–342. doi:10.1136/jmg.2010.087106

Berit Augestad, L. (2007). *Mental health among children and young adults with visual impairments: A systematic review*.

Bernardos, R. L., Barthel, L. K., Meyers, J. R., and Raymond, P. A. (2007). Late-stage neuronal progenitors in the retina are radial muller glia that function as retinal stem cells. *J. Neurosci.* 27, 7028–7040. doi:10.1523/JNEUROSCI.1624-07.2007

Bernstein, C. S., Anderson, M. T., Gohel, C., Slater, K., Gross, J. M., and Agarwala, S. (2018a). The cellular bases of choroid fissure formation and closure. *Dev. Biol.* 440, 137–151. doi:10.1016/j.ydbio.2018.05.010

Bhattaram, P., Penzo-Méndez, A., Sock, E., Colmenares, C., Kaneko, K. J., Vassilev, A., et al. (2010). Organogenesis relies on SoxC transcription factors for the survival of neural and mesenchymal progenitors. *Nat. Commun.* 1, 9. doi:10.1038/ncomms1008

Blake, K. D., Davenport, S. L. H., Hall, B. D., Hefner, M. A., Pagon, R. A., Williams, M. S., et al. (1998). CHARGE association: An update and review for the primary pediatrician. *Clin. Pediatr.* 37, 159–173. doi:10.1177/000992289803700302

Blake, K. D., Hartshorne, T. S., Lawand, C., Dailor, A. N., and Thelin, J. W. (2008). Cranial nerve manifestations in CHARGE syndrome. *Am. J. Med. Genet. A* 146A, 585–592. doi:10.1002/ajmg.a.32179

Blake, K. D., and Prasad, C. (2006). CHARGE syndrome. *Orphanet J. Rare Dis.* 1, 34. doi:10.1186/1750-1172-1-34

Bonnet, C., and El-Amraoui, A. (2012). Usher syndrome (sensorineural deafness and retinitis pigmentosa): Pathogenesis, molecular diagnosis and therapeutic approaches. *Curr. Opin. Neurol.* 25, 42–49. doi:10.1097/WCO.0b013e32834ef8b2

Bosman, E. A., Penn, A. C., Ambrose, J. C., Kettleborough, R., Stemple, D. L., and Steel, K. P. (2005). Multiple mutations in mouse Chd7 provide models for CHARGE syndrome. *Hum. Mol. Genet.* 14, 3463–3476. doi:10.1093/hmg/ddi375

Bouazoune, K., and Kingston, R. E. (2012). Chromatin remodeling by the CHD7 protein is impaired by mutations that cause human developmental disorders. *Proc. Natl. Acad. Sci. U. S. A.* 109, 19238–19243. doi:10.1073/pnas.1213825109

Bowles, J., Schepers, G., and Koopman, P. (2000). Phylogeny of the SOX family of developmental transcription factors based on sequence and structural indicators. *Dev. Biol.* 227, 239–255. doi:10.1006/dbio.2000.9883

Branchek, T., and Bremiller, R. (1984). The development of photoreceptors in the zebrafish, Brachydanio rerio. I. Structure. *J. Comp. Neurol.* 224, 107–115. doi:10.1002/cne.902240109

Breuer, M., Rummler, M., Zaouter, C., Willie, B. M., and Patten, S. A. (2020). Altered vertebrae morphology and bone mineralization in a zebrafish model of CHARGE syndrome. *bioRxiv*. doi:10.1101/2020.07.10.197533

Brown, D. M., Mazade, R., Clarkson-Townsend, D., Hogan, K., Datta Roy, P. M., and Pardue, M. T. (2022). Candidate pathways for retina to scleral signaling in refractive eye growth. *Exp. Eye Res.* 219, 109071. doi:10.1016/j.exer.2022.109071

Bryan, C. D., Casey, M. A., Pfeiffer, R. L., Jones, B. W., and Kwan, K. M. (2020). Optic cup morphogenesis requires neural crest-mediated basement membrane assembly. *Development* 147, dev181420. doi:10.1242/dev.181420

Bryan, J. M., Fufa, T. D., Bharti, K., Brooks, B. P., Hufnagel, R. B., and McGaughey, D. M. (2018). Identifying core biological processes distinguishing human eye tissues with precise systems-level gene expression analyses and weighted correlation networks. *Hum. Mol. Genet.* 27, 3325–3339. doi:10.1093/hmg/ddy239

Burmeister, M., Novak, J., Liang, M.-Y., Basu, S., Ploder, L., Hawes, N. L., et al. (1996). Ocular retardation mouse caused by Chx10 homeobox null allele: Impaired retinal progenitor proliferation and bipolar cell differentiation. *Nat. Genet.* 12, 376–384. doi:10.1038/ng0496-376

Cao, M., Ouyang, J., Guo, J., Lin, S., and Chen, S. (2018). Metalloproteinase *Adamts16* is required for proper closure of the optic fissure. *Investig. Ophthalmol. Vis. Sci.* 59, 1167–1177. doi:10.1167/iovs.17-22827

Carter-Dawson, L. D., and Lavail, M. M. (1979). Rods and cones in the mouse retina. I. Structural analysis using light and electron microscopy. *J. Comp. Neurol.* 188, 245–262. doi:10.1002/cne.901880204

Cechmanek, P. B., and McFarlane, S. (2017). Retinal pigment epithelium expansion around the neural retina occurs in two separate phases with distinct mechanisms. *Dev. Dyn.* 246, 598–609. doi:10.1002/dvdy.24525

Cepko, C. L., Austin, C. P., Yang, X., Alexiades, M., and Ezzeddine, D. (1996). Cell fate determination in the vertebrate retina. *Proc. Natl. Acad. Sci. U. S. A.* 93, 589–595. doi:10.1073/pnas.93.2.589

Chakraborty, R., Yang, V., Park, H. na, Landis, E. G., Dhakal, S., Motz, C. T., et al. (2019). Lack of cone mediated retinal function increases susceptibility to form-deprivation myopia in mice. *Exp. Eye Res.* 180, 226–230. doi:10.1016/j.exer.2018.12.021

Chang, L., Blain, D., Bertuzzi, S., and Brooks, B. P. (2006a). Uveal coloboma: Clinical and basic science update. *Curr. Opin. Ophthalmol.* 17, 447–470. doi:10.1097/01.icu.0000243020.82380.f6

Chang, T. C., Summers, C. G., Schimmenti, L. A., and Grajewski, A. L. (2012). Axenfeld-rieger syndrome: New perspectives. *Br. J. Ophthalmol.* 96, 318–322. doi:10.1136/bjophthalmol-2011-300801

Chen, C., Lee, G. A., Pourmorady, A., Sock, E., and Donoghue, M. J. (2015). Orchestration of neuronal differentiation and progenitor pool expansion in the developing cortex by SoxC genes. *J. Neurosci.* 35, 10629–10642. doi:10.1523/JNEUROSCI.1663-15.2015

Chen, S., Wang, Q.-L., Nie, Z., Sun, H., Lennon, G., Copeland, N. G., et al. (1997). Crx, a novel otx-like paired-homeodomain protein, binds to and transactivates photoreceptor cell-specific genes. *Neuron* 19, 1017–1030. doi:10.1016/S0896-6273(00)80394-3

Cheng, H., Khan, N. W., Roger, J. E., and Swaroop, A. (2011). Excess cones in the retinal degeneration rd7 mouse, caused by the loss of function of orphan nuclear receptor Nr2e3, originate from early-born photoreceptor precursors. *Hum. Mol. Genet.* 20, 4102–4115. doi:10.1093/hmg/ddr334

Cloney, K., Steele, S. L., Stoyek, M. R., Croll, R. P., Smith, F. M., Prykhozhij, S. v., et al. (2018). Etiology and functional validation of gastrointestinal motility dysfunction in a zebrafish model of CHARGE syndrome. *FEBS J.* 285, 2125–2140. doi:10.1111/febs.14473

Connaughton, V. P. (2011). Bipolar cells in the zebrafish retina. *Vis. Neurosci.* 28, 77–93. doi:10.1017/S0952523810000295

Corsten-Janssen, N., Kerstjens-Frederikse, W. S., du Marchie Sarvaas, G. J., Baardman, M. E., Bakker, M. K., Bergman, J. E. H., et al. (2013). The cardiac phenotype in patients with a *CHD7* mutation. *Circ. Cardiovasc. Genet.* 6, 248–254. doi:10.1161/CIRCGENETICS.113.000054

Crespo, C., and Knust, E. (2018). Characterisation of maturation of photoreceptor cell subtypes during zebrafish retinal development. *Biol. Open* 7, bio036632. doi:10.1242/bio.036632

Cvekl, A., and Tamm, E. R. (2004). Anterior eye development and ocular mesenchyme: New insights from mouse models and human diseases. *BioEssays* 26, 374–386. doi:10.1002/bies.20009

Davis-Silberman, N., and Ashery-Padan, R. (2008). Iris development in vertebrates; genetic and molecular considerations. *Brain Res.* 1192, 17–28. doi:10.1016/j.brainres.2007.03.043

de Almeida, J. C. C., and Llerena, J. C. (1993). Peters' plus syndrome. *Am. J. Med. Genet.* 47, 125. doi:10.1002/ajmg.1320470129

de Robertis, E. T. H. E. (1956). Retinal rods an electron microscope study. Available at: http://rupress.org/jcb/article-pdf/2/4/209/1383596/209.pdf.

Delmas, V., Stokes, D. G., and Perry, R. P. (1993). A mammalian DNA-binding protein that contains a chromodomain and an SNF2/SWI2-like helicase domain. *Proc. Natl. Acad. Sci. U. S. A.* 90, 2414–2418. doi:10.1073/pnas.90.6.2414

Denny, P., Swift, S., Brand, N., Dabhade, N., Barton, P., and Ashworth, A. (1992). A conserved family of genes related to the testis determining gene, SRY. *Nucleic Acids Res.* 20, 2887. doi:10.1093/nar/20.11.2887

Donovan, A. P. A., Yu, T., Ellegood, J., Riegman, K. L. H., de Geus, C., van Ravenswaaij-Arts, C., et al. (2017). Cerebellar vermis and midbrain hypoplasia upon conditional deletion of Chd7 from the embryonic mid-hindbrain region. *Front. Neuroanat.* 11, 86. doi:10.3389/fnana.2017.00086

Dörr, H. G., Madeja, J., and Junghans, C. (2015). Spontaneous postnatal growth is reduced in children with CHARGE syndrome. *Acta Paediatr.* 104, e314–e318. doi:10.1111/apa.12980

Dote, S., Nakakura, S., Tanabe, H., Terao, E., Nagata, Y., Tabuchi, H., et al. (2019). CHARGE syndrome associated with angle closure despite high myopia: A case report with structural suggestion. *Case Rep. Ophthalmol.* 11, 28–36. doi:10.1159/000505389

DuVal, M. G., and Allison, W. T. (2018). Photoreceptor progenitors depend upon coordination of *gdf6a* , *thrβ* , and *tbx2b* to generate precise populations of cone photoreceptor subtypes. *Investig. Ophthalmol. Vis. Sci.* 59, 6089–6101. doi:10.1167/iovs.18-24461

Echelard, Y., Epstein, D. J., St-Jacques, B., Shen, L., Mohler, J., McMahon, J. A., et al. (1993). Sonic hedgehog, a member of a family of putative signaling molecules, is implicated in the regulation of CNS polarity. *Cell.* 75, 1417–1430. doi:10.1016/0092-8674(93)90627-3

Engelen, E., Akinci, U., Bryne, J. C., Hou, J., Gontan, C., Moen, M., et al. (2011). Sox2 cooperates with Chd7 to regulate genes that are mutated in human syndromes. *Nat. Genet.* 43, 607–611. doi:10.1038/ng.825

Fadool, J. M. (2003). Development of a rod photoreceptor mosaic revealed in transgenic zebrafish. *Dev. Biol.* 258, 277–290. doi:10.1016/S0012-1606(03)00125-8

Fan, X., Masamsetti, V. P., Sun, J. Q., Engholm-Keller, K., Osteil, P., Studdert, J., et al. (2021). TWIST1 and chromatin regulatory proteins interact to guide neural crest cell differentiation. *Elife* 10, e62873. doi:10.7554/eLife.62873

Fantes, J., Ragge, N. K., Lynch, S.-A., McGill, N. I., Collin, J. R. O., Howard-Peebles, P. N., et al. (2003). Mutations in SOX2 cause anophthalmia. *Nat. Genet.* 33, 461–463. doi:10.1038/ng1120

Fazzi, E., Signorini, S. G., Scelsa, B., Bova, S. M., and Lanzi, G. (2003). Leber's congenital amaurosis: An update. *Eur. J. Paediatr. Neurol.* 7, 13–22. doi:10.1016/S1090-3798(02)00135-6

Feng, W., Kawauchi, D., Körkel-Qu, H., Deng, H., Serger, E., Sieber, L., et al. (2017). Chd7 is indispensable for mammalian brain development through activation of a neuronal differentiation programme. *Nat. Commun.* 8, 14758. doi:10.1038/ncomms14758

Feng, W., Khan, M. A., Bellvis, P., Zhu, Z., Bernhardt, O., Herold-Mende, C., et al. (2013). The chromatin remodeler CHD7 regulates adult neurogenesis via activation of soxc transcription factors. *Cell. Stem Cell.* 13, 62–72. doi:10.1016/j.stem.2013.05.002

Flaus, A., and Owen-Hughes, T. (2011). Mechanisms for ATP-dependent chromatin remodelling: The means to the end. *FEBS J.* 278, 3579–3595. doi:10.1111/j.1742-4658.2011.08281.x

Fujita, K., Ogawa, R., Kawawaki, S., and Ito, K. (2014). Roles of chromatin remodelers in maintenance mechanisms of multipotency of mouse trunk neural crest cells in the formation of neural crest-derived stem cells. *Mech. Dev.* 133, 126–145. doi:10.1016/j.mod.2014.05.001

Furukawa, T., Morrow, E. M., and Cepko, C. L. (1997). Crx, a novel otx-like homeobox gene, shows photoreceptor-specific expression and regulates photoreceptor differentiation. *Cell.* 91, 531–541. doi:10.1016/S0092-8674(00)80439-0

Furukawa, T., Morrow, E. M., Li, T., Davis, F. C., and Cepko, C. L. (1999). Retinopathy and attenuated circadian entrainment in Crx-deficient mice. *Nat. Genet.* 23, 466–470. doi:10.1038/70591

Gage, P. J., Hurd, E. A., and Martin, D. M. (2015). Mouse models for the dissection of CHD7 functions in eye development and the molecular basis for ocular defects in CHARGE syndrome. *Investig. Ophthalmol. Vis. Sci.* 56, 7923–7930. doi:10.1167/iovs.15-18069

Gage, P. J., Rhoades, W., Prucka, S. K., and Hjalt, T. (2005). Fate maps of neural crest and mesoderm in the mammalian eye. *Investig. Ophthalmol. Vis. Sci.* 46, 4200–4208. doi:10.1167/iovs.05-0691

Gestri, G., Bazin-Lopez, N., Scholes, C., and Wilson, S. W. (2018). Cell behaviors during closure of the choroid fissure in the developing eye. *Front. Cell. Neurosci.* 12, 42. doi:10.3389/fncel.2018.00042

Gnedeva, K., and Hudspeth, A. J. (2015). SoxC transcription factors are essential for the development of the inner ear. *Proc. Natl. Acad. Sci. U. S. A.* 112, 14066–14071. doi:10.1073/pnas.1517371112

Gordon, H. B., Lusk, S., Carney, K. R., Wirick, E. O., Murray, B. F., and Kwan, K. M. (2018). Hedgehog signaling regulates cell motility and optic fissure and stalk formation during vertebrate eye morphogenesis. *Development* 145, dev165068. doi:10.1242/dev.165068

Graham, J. M., Rosner, B., Dykens, E., and Visootsak, J. (2005). Behavioral features of CHARGE syndrome (Hall-Hittner syndrome) comparison with Down syndrome, Prader-Willi syndrome, and Williams syndrome. *Am. J. Med. Genet. A* 133A, 240–247. doi:10.1002/ajmg.a.30543

Greenwald, S. H., Kuchenbecker, J. A., Rowlan, J. S., Neitz, J., and Neitz, M. (2017). Role of a dual splicing and amino acid code in myopia, cone dysfunction and cone dystrophy associated with *L* / *M* opsin interchange mutations. *Transl. Vis. Sci. Technol.* 6, 2. doi:10.1167/tvst.6.3.2

Guirgis, M. F., and Lueder, G. T. (2003). Choroidal neovascular membrane associated with optic nerve coloboma in a patient with CHARGE association. *Am. J. Ophthalmol.* 135, 919–920. doi:10.1016/S0002-9394(02)02293-6

Ha, J., Ong, F., Wood, B., and Vijayasekaran, S. (2016). Radiologic and audiologic findings in the temporal bone of patients with CHARGE syndrome. *Ochsner J.* 16, 125–129.

Haider, N. B., Jacobson, S. G., Cideciyan, A. v., Swiderski, R., Streb, L. M., Searby, C., et al. (2000). Mutation of a nuclear receptor gene, NR2E3, causes enhanced S cone syndrome, a disorder of retinal cell fate. *Nat. Genet.* 24, 127–131. doi:10.1038/72777

Hale, C. L., Niederriter, A. N., Green, G. E., and Martin, D. M. (2016). Atypical phenotypes associated with pathogenic *CHD7* variants and a proposal for broadening CHARGE syndrome clinical diagnostic criteria. *Am. J. Med. Genet. A* 170, 344–354. doi:10.1002/ajmg.a.37435

Hall, B. D. (1979). Choanal atresia and associated multiple anomalies. *J. Pediatr.* 95, 395–398. doi:10.1016/S0022-3476(79)80513-2

Harley, V. R., Lovell-Badge, R., and Goodfellow, P. N. (1994). Definition of a consensus DNA binding site for SRY. *Nucleic Acids Res.* 22, 1500–1501. doi:10.1093/nar/22.8.1500

Hendrix, R. W., and Zwaan, J. (1975). The matrix of the optic vesicle-presumptive lens interface during induction of the lens in the chicken embryo. *Development* 33, 1023–1049. doi:10.1242/dev.33.4.1023

Hittner, H. M., Hirsch, N. J., Kreh, G. M., and Rudolph, A. J. (1979). Colobomatous microphthalmia, heart disease, hearing loss, and mental retardation-A syndrome. *J. Pediatr. Ophthalmol. Strabismus* 16, 122–128. doi:10.3928/0191-3913-19790301-10

Ho, L., and Crabtree, G. R. (2010). Chromatin remodelling during development. *Nature* 463, 474–484. doi:10.1038/nature08911

Hoch, M. J., Patel, S. H., Jethanamest, D., Win, W., Fatterpekar, G. M., Roland, J. T., et al. (2017). Head and neck MRI findings in CHARGE syndrome. *AJNR. Am. J. Neuroradiol.* 38, 2357–2363. doi:10.3174/ajnr.A5297

Holcomb, M. A., Rumboldt, Z., and White, D. R. (2013). Cochlear nerve deficiency in children with CHARGE syndrome. *Laryngoscope* 123, 793–796. doi:10.1002/lary.23682

Holt, C. E., Bertsch, T. W., Ellis, H. M., and Harris, W. A. (1988). Cellular determination in the xenopus retina is independent of lineage and birth date. *Neuron* 1, 15–26. doi:10.1016/0896-6273(88)90205-X

Horst, C. J., Johnson, L. v., and Besharse, J. C. (1990). Transmembrane assemblage of the photoreceptor connecting cilium and motile cilium transition zone contain a common immunologic epitope. *Cell. Motil. Cytoskelet.* 17, 329–344. doi:10.1002/cm.970170408

Hoshino, A., Ratnapriya, R., Brooks, M. J., Chaitankar, V., Wilken, M. S., Zhang, C., et al. (2017). Molecular anatomy of the developing human retina. *Dev. Cell.* 43, 763–779. e4. doi:10.1016/j.devcel.2017.10.029

Hsu, P., Ma, A., Wilson, M., Williams, G., Curotta, J., Munns, C. F., et al. (2014). CHARGE syndrome: A review. *J. Paediatr. Child. Health* 50, 504–511. doi:10.1111/jpc.12497

Hu, M., and Easter, S. S. (1999). Retinal neurogenesis: The formation of the initial central patch of postmitotic cells. *Dev. Biol.* 207, 309–321. doi:10.1006/dbio.1998.9031

Huang, J., Rajagopal, R., Liu, Y., Dattilo, L. K., Shaham, O., Ashery-Padan, R., et al. (2011). The mechanism of lens placode formation: A case of matrix-mediated morphogenesis. *Dev. Biol.* 355, 32–42. doi:10.1016/j.ydbio.2011.04.008

Hurd, E. A., Capers, P. L., Blauwkamp, M. N., Adams, M. E., Raphael, Y., Poucher, H. K., et al. (2007). Loss of Chd7 function in gene-trapped reporter mice is embryonic lethal and associated with severe defects in multiple developing tissues. *Mamm. Genome* 18, 94–104. doi:10.1007/s00335-006-0107-6

Hurd, E. A., Poucher, H. K., Cheng, K., Raphael, Y., and Martin, D. M. (2010). The ATP-dependent chromatin remodeling enzyme CHD7 regulates pro-neural gene expression and neurogenesis in the inner ear. *Development* 137, 3139–3150. doi:10.1242/dev.047894

Hyatt, G. A., Schmitt, E. A., Fadool, J. M., and Dowling, J. E. (1996). Retinoic acid alters photoreceptor development *in vivo*. *Proc. Natl. Acad. Sci. U. S. A.* 93, 13298–13303. doi:10.1073/pnas.93.23.13298

Inchingolo, F., Pacifici, A., Gargari, M., Acitores Garcia, J. I., Amantea, M., Marrelli, M., et al. (2014). CHARGE syndrome: An overview on dental and maxillofacial features. *Eur. Rev. Med. Pharmacol. Sci.* 18, 2089–2093.

Issekutz, K. A., Graham, J. M., Prasad, C., Smith, I. M., and Blake, K. D. (2005). An epidemiological analysis of CHARGE syndrome: Preliminary results from a Canadian study. *Am. J. Med. Genet. A* 133A, 309–317. doi:10.1002/ajmg.a.30560

Jacobs-Mcdaniels, N. L., and Albertson, R. C. (2011). Chd7 plays a critical role in controlling left-right symmetry during zebrafish somitogenesis. *Dev. Dyn.* 240, 2272–2280. doi:10.1002/dvdy.22722

Jadhav, A. P., Mason, H. A., and Cepko, C. L. (2006). Notch 1 inhibits photoreceptor production in the developing mammalian retina. *Development* 133, 913–923. doi:10.1242/dev.02245

Jamadagni, P., Breuer, M., Schmeisser, K., Cardinal, T., Kassa, B., Parker, J. A., et al. (2021). Chromatin remodeller CHD7 is required for GABAergic neuron development by promoting PAQR3 expression. *EMBO Rep.* 22, e50958. doi:10.15252/embr.202050958

James, A., Lee, C., Williams, A. M., Angileri, K., Lathrop, K. L., and Gross, J. M. (2016). The hyaloid vasculature facilitates basement membrane breakdown during choroid fissure closure in the zebrafish eye. *Dev. Biol.* 419, 262–272. doi:10.1016/j.ydbio.2016.09.008

Janssen, N., Bergman, J. E. H., Swertz, M. A., Tranebjaerg, L., Lodahl, M., Schoots, J., et al. (2012). Mutation update on the CHD7 gene involved in CHARGE syndrome. *Hum. Mutat.* 33, 1149–1160. doi:10.1002/humu.22086

Jensen, A. M., and Raff, M. C. (1997). Continuous observation of multipotential retinal progenitor cells in clonal density culture. *Dev. Biol.* 188, 267–279. doi:10.1006/dbio.1997.8645

Jones, K. M., Sarić, N., Russell, J. P., Andoniadou, C. L., Scambler, P. J., and Basson, M. A. (2015). CHD7 maintains neural stem cell quiescence and prevents premature stem cell depletion in the adult Hippocampus. *Stem Cells* 33, 196–210. doi:10.1002/stem.1822

Jongmans, M. C. J., Admiraal, R. J., van der Donk, K. P., Vissers, L. E. L. M., Baas, A. F., Kapusta, L., et al. (2006). CHARGE syndrome: The phenotypic spectrum of mutations in the CHD7 gene. *J. Med. Genet.* 43, 306–314. doi:10.1136/jmg.2005.036061

Jongmans, M. C. J., van Ravenswaaij-Arts, C. M. A., Pitteloud, N., Ogata, T., Sato, N., Claahsen-van der Grinten, H. L., et al. (2009). CHD7 mutations in patients initially diagnosed with Kallmann syndrome--the clinical overlap with CHARGE syndrome. *Clin. Genet.* 75, 65–71. doi:10.1111/j.1399-0004.2008.01107.x

Jusuf, P. R., and Harris, W. A. (2009). Ptf1a is expressed transiently in all types of amacrine cells in the embryonic zebrafish retina. *Neural Dev.* 4, 34. doi:10.1186/1749-8104-4-34

Kagiyama, Y., Gotouda, N., Sakagami, K., Yasuda, K., Mochii, M., and Araki, M. (2005). Extraocular dorsal signal affects the developmental fate of the optic vesicle and patterns the optic neuroepithelium. *Dev. Growth Differ.* 47, 523–536. doi:10.1111/j.1440-169X.2005.00828.x

Kamachi, Y., Uchikawa, M., and Kondoh, H. (2000). Pairing SOX off: With partners in the regulation of embryonic development. *Trends Genet.* 16, 182–187. doi:10.1016/S0168-9525(99)01955-1

Kautzmann, M.-A. I., Kim, D. S., Felder-Schmittbuhl, M.-P., and Swaroop, A. (2011). Combinatorial regulation of photoreceptor differentiation factor, neural retina leucine zipper gene Nrl, revealed by *in vivo* promoter analysis. *J. Biol. Chem.* 286, 28247–28255. doi:10.1074/jbc.M111.257246

Kelley, M. W., Williams, R. C., Turner, J. K., Creech-Kraft, J. M., and Reh, T. A. (1999). Retinoic acid promotes rod photoreceptor differentiation in rat retina *in vivo*. *NeuroReport* 10, 2389–2394. doi:10.1097/00001756-199908020-00031

Kiefer, A. K., Tung, J. Y., Do, C. B., Hinds, D. A., Mountain, J. L., Francke, U., et al. (2013). Genome-wide analysis points to roles for extracellular matrix remodeling, the visual cycle, and neuronal development in myopia. *PLoS Genet.* 9, e1003299. doi:10.1371/journal.pgen.1003299

Kim, U. S., Mahroo, O. A., Mollon, J. D., and Yu-Wai-Man, P. (2021). Retinal ganglion cells – diversity of cell types and clinical relevance. *Front. Neurol.* 12, 661938. doi:10.3389/fneur.2021.661938

Komatireddy, S., Chakrabarti, S., Mandal, A. K., Reddy, A. B. M., Sampath, S., Panicker, S. G., et al. (2003). Mutation spectrum of FOXC1 and clinical genetic heterogeneity of Axenfeld-Rieger anomaly in India. *Mol. Vis.* 9, 43–48.

Krueger, L. A., Bills, J. D., Lim, Z. Y., Skidmore, J. M., Martin, D. M., and Morris, A. C. (2022. *Chromatin remodeler Chd7 regulates photoreceptor development and outer segment length*. bioRxiv. doi:10.1101/2022.05.30.494019

Kumar, R., Chen, S., Scheurer, D., Wang, Q.-L., Duh, E., Sung, C.-H., et al. (1996). The bZIP transcription factor Nrl stimulates rhodopsin promoter activity in primary retinal cell cultures. *J. Biol. Chem.* 271, 29612–29618. doi:10.1074/jbc.271.47.29612

Kwan, K. M., Otsuna, H., Kidokoro, H., Carney, K. R., Saijoh, Y., and Chien, C.-B. (2012). A complex choreography of cell movements shapes the vertebrate eye. *Development* 139, 359–372. doi:10.1242/dev.071407

Lalani, S. R., Safiullah, A. M., Fernbach, S. D., Harutyunyan, K. G., Thaller, C., Peterson, L. E., et al. (2006). *Spectrum of CHD7 mutations in 110 individuals with CHARGE syndrome and genotype-phenotype correlation*. Available at: CHD7MutationsinCHARGESyndrome www.ajhg.orgLalanietal.

Lamb, T. D., Collin, S. P., and Pugh, E. N. (2007). Evolution of the vertebrate eye: Opsins, photoreceptors, retina and eye cup. *Nat. Rev. Neurosci.* 8, 960–976. doi:10.1038/nrn2283

Langenberg, T., Kahana, A., Wszalek, J. A., and Halloran, M. C. (2008). The eye organizes neural crest cell migration. *Dev. Dyn.* 237, 1645–1652. doi:10.1002/dvdy.21577

Layman, W. S., Hurd, E. A., and Martin, D. M. (2010). Chromodomain proteins in development: Lessons from CHARGE syndrome. *Clin. Genet.* 78, 11–20. doi:10.1111/j.1399-0004.2010.01446.x

Layman, W. S., Hurd, E. A., and Martin, D. M. (2011). Reproductive dysfunction and decreased GnRH neurogenesis in a mouse model of CHARGE syndrome. *Hum. Mol. Genet.* 20, 3138–3150. doi:10.1093/hmg/ddr216

Layman, W. S., McEwen, D. P., Beyer, L. A., Lalani, S. R., Fernbach, S. D., Oh, E., et al. (2009). Defects in neural stem cell proliferation and olfaction in Chd7 deficient mice indicate a mechanism for hyposmia in human CHARGE syndrome. *Hum. Mol. Genet.* 18, 1909–1923. doi:10.1093/hmg/ddp112

Lefebvre, V., Dumitriu, B., Penzo-Méndez, A., Han, Y., and Pallavi, B. (2007). Control of cell fate and differentiation by Sry-related high-mobility-group box (Sox) transcription factors. *Int. J. Biochem. Cell. Biol.* 39, 2195–2214. doi:10.1016/j.biocel.2007.05.019

Li, H., Tierney, C., Wen, L., Wu, J. Y., and Rao, Y. (1997). A single morphogenetic field gives rise to two retina primordia under the influence of the prechordal plate. *Development* 124, 603–615. doi:10.1242/dev.124.3.603

Li, Z., Joseph, N. M., and Easter, S. S. (2000)The morphogenesis of the zebrafish eye, including a fate map of the optic vesicle. *Dev. Dyn.* 218, 175–188. doi:10.1002/(SICI)1097-0177218:1<175::AID-DVDY15>3.0

Liu, H., and Liu, Z. Z. (2019). Aggressive-like behavior and increased glycine transporters in a zebrafish model of CHARGE syndrome. *Behav. Brain Res.* 378, 112293. doi:10.1016/j.bbr.2019.112293

Liu, Z. Z., Wang, Z. L., Choi, T. I., Huang, W. T., Wang, H. T., Han, Y. Y., et al. (2018). Chd7 is critical for early T-cell development and thymus organogenesis in zebrafish. *Am. J. Pathol.* 188, 1043–1058. doi:10.1016/j.ajpath.2017.12.005

Loosli, F., Staub, W., Finger-Baier, K. C., Ober, E. A., Verkade, H., Wittbrodt, J., et al. (2003). Loss of eyes in zebrafish caused by mutation of *chokh* / *rx3*. *EMBO Rep.* 4, 894–899. doi:10.1038/sj.embor.embor919

Lotery, A. J., Jacobson, S. G., Fishman, G. A., Weleber, R. G., Fulton, A. B., NamPerumalsamy, P., et al. (2001). Mutations in the CRB1 gene cause leber congenital amaurosis. *Arch. Ophthalmol.* 119, 415–420. doi:10.1001/archopht.119.3.415

Maity, T., Fuse, N., and Beachy, P. A. (2005). Molecular mechanisms of Sonic hedgehog mutant effects in holoprosencephaly. *Proc. Natl. Acad. Sci. U. S. A.* 102, 17026–17031. doi:10.1073/pnas.0507848102

Manning, B. J., and Yusufzai, T. (2017). The ATP-dependent chromatin remodeling enzymes CHD6, CHD7, and CHD8 exhibit distinct nucleosome binding and remodeling activities. *J. Biol. Chem.* 292, 11927–11936. doi:10.1074/jbc.M117.779470

Marcos, S., Sarfati, J., Leroy, C., Fouveaut, C., Parent, P., Metz, C., et al. (2014). The prevalence of *CHD7* missense versus truncating mutations is higher in patients with Kallmann syndrome than in typical CHARGE patients. *J. Clin. Endocrinol. Metab.* 99, E2138–E2143. doi:10.1210/jc.2014-2110

Marfella, C. G., and Imbalzano, A. N. (2007). The Chd family of chromatin remodelers. *Mutat. Res.* 618, 30–40. doi:10.1016/j.mrfmmm.2006.07.012

Marquardt, T., and Gruss, P. (2002). Generating neuronal diversity in the retina: One for nearly all. *Trends Neurosci.* 25, 32–38. doi:10.1016/S0166-2236(00)02028-2

Martin, D. M. (2010). Chromatin remodeling in development and disease: Focus on CHD7. *PLoS Genet.* 6, e1001010. doi:10.1371/journal.pgen.1001010

Martin, G. C., Robert, M. P., Challe, G., Trinh, N. T. H., Attié-Bitach, T., Brémond-Gignac, D., et al. (2020). Functional vision analysis in patients with CHARGE syndrome. *J. Pediatr. Ophthalmol. Strabismus* 57, 120–128. doi:10.3928/01913913-20200207-02

Martinez-Morales, J. R., Rembold, M., Greger, K., Simpson, J. C., Brown, K. E., Quiring, R., et al. (2009). *Ojoplano* -mediated basal constriction is essential for optic cup morphogenesis. *Development* 136, 2165–2175. doi:10.1242/dev.033563

Mathers, P. H., Grinberg, A., Mahon, K. A., and Jamrich, M. (1997). The Rx homeobox gene is essential for vertebrate eye development. *Nature* 387, 603–607. doi:10.1038/42475

McMain, K., Robitaille, J., Smith, I., Johnson, J., Wood, E., Tremblay, F., et al. (2008). Ocular features of CHARGE syndrome. *J. AAPOS* 12, 460–465. doi:10.1016/j.jaapos.2008.02.009

Mears, A. J., Kondo, M., Swain, P. K., Takada, Y., Bush, R. A., Saunders, T. L., et al. (2001). Nrl is required for rod photoreceptor development. *Nat. Genet.* 29, 447–452. doi:10.1038/ng774

Melicharek, D. J., Ramirez, L. C., Singh, S., Thompson, R., and Marenda, D. R. (2010). Kismet/CHD7 regulates axon morphology, memory and locomotion in a Drosophila model of CHARGE syndrome. *Hum. Mol. Genet.* 19, 4253–4264. doi:10.1093/hmg/ddq348

Miesfeld, J. B., Gestri, G., Clark, B. S., Flinn, M. A., Poole, R. J., Bader, J. R., et al. (2015). *Yap and Taz regulate retinal pigment epithelial cell fate*. Cambridge, UK: Development. doi:10.1242/dev.119008

Molday, R. S., and Moritz, O. L. (2015). Photoreceptors at a glance. *J. Cell. Sci.* 128, 4039–4045. doi:10.1242/jcs.175687

Morimoto, A. K., Wiggins, R. H., Hudgins, P. A., Hedlund, G. L., Hamilton, B., Mukherji, S. K., et al. (2006). Absent semicircular canals in CHARGE syndrome: Radiologic spectrum of findings. *AJNR. Am. J. Neuroradiol.* 27, 1663–1671.

Morimura, H., Fishman, G. A., Grover, S. A., Fulton, A. B., Berson, E. L., and Dryja, T. P. (1998). Mutations in the RPE65 gene in patients with autosomal recessive retinitis pigmentosa or Leber congenital amaurosis. *Proc. Natl. Acad. Sci. U. S. A.* 95, 3088–3093. doi:10.1073/pnas.95.6.3088

Morris, A. C., Scholz, T., and Fadool, J. M. (2008a). "Rod progenitor cells in the mature zebrafish retina," in, 361–368. doi:10.1007/978-0-387-74904-4_42

Morris, A. C., Scholz, T. L., Brockerhoff, S. E., and Fadool, J. M. (2008b). Genetic dissection reveals two separate pathways for rod and cone regeneration in the teleost retina. *Dev. Neurobiol.* 68, 605–619. doi:10.1002/dneu.20610

Natung, T., Goyal, A., Handique, A., and Kapoor, M. (2014). Symmetrical chorioretinal colobomata with craniovertebral junction anomalies in charge syndrome - a case report with review of literature. *J. Clin. Imaging Sci.* 4, 5. doi:10.4103/2156-7514.126046

Nelson, S. M., Frey, R. A., Wardwell, S. L., and Stenkamp, D. L. (2008). The developmental sequence of gene expression within the rod photoreceptor lineage in embryonic zebrafish. *Dev. Dyn.* 237, 2903–2917. doi:10.1002/dvdy.21721

Ng, L., Hurley, J. B., Dierks, B., Srinivas, M., Saltó, C., Vennström, B., et al. (2001). A thyroid hormone receptor that is required for the development of green cone photoreceptors. *Nat. Genet.* 27, 94–98. doi:10.1038/83829

Nguyen, M., and Arnheiter, H. (2000). Signaling and transcriptional regulation in early mammalian eye development: A link between FGF and MITF. *Development* 127, 3581–3591. doi:10.1242/dev.127.16.3581

Nicolás-Pérez, M., Kuchling, F., Letelier, J., Polvillo, R., Wittbrodt, J., and Martínez-Morales, J. R. (2016). Analysis of cellular behavior and cytoskeletal dynamics reveal a constriction mechanism driving optic cup morphogenesis. *Elife* 5, e15797. doi:10.7554/eLife.15797

Nishida, A., Furukawa, A., Koike, C., Tano, Y., Aizawa, S., Matsuo, I., et al. (2003). Otx2 homeobox gene controls retinal photoreceptor cell fate and pineal gland development. *Nat. Neurosci.* 6, 1255–1263. doi:10.1038/nn1155

Nishina, S., Kosaki, R., Yagihashi, T., Azuma, N., Okamoto, N., Hatsukawa, Y., et al. (2012). Ophthalmic features of CHARGE syndrome with CHD7 mutations. *Am. J. Med. Genet. A* 158A, 514–518. doi:10.1002/ajmg.a.34400

Obata, S., and Usukura, J. (1992). Morphogenesis of the photoreceptor outer segment during postnatal development in the mouse (BALB/c) retina. *Cell. Tissue Res.* 269, 39–48. doi:10.1007/BF00384724

Ochocinska, M. J., and Hitchcock, P. F. (2007). Dynamic expression of the basic helix-loop-helix transcription factor neuroD in the rod and cone photoreceptor lineages in the retina of the embryonic and larval zebrafish. *J. Comp. Neurol.* 501, 1–12. doi:10.1002/cne.21150

Ogawa, Y., Shiraki, T., Kojima, D., and Fukada, Y. (2015). Homeobox transcription factor Six7 governs expression of green opsin genes in zebrafish. *Proc. Biol. Sci.* 282, 20150659. doi:10.1098/rspb.2015.0659

Ogier, J. M., Carpinelli, M. R., Arhatari, B. D., Symons, R. C. A., Kile, B. T., and Burt, R. A. (2014). CHD7 deficiency in "Looper", a new mouse model of CHARGE syndrome, results in ossicle malformation, otosclerosis and hearing impairment a new mouse model of CHARGE syndrome, results in ossicle malformation, otosclerosis and hearing impairment. *PLoS ONE* 9, e97559. doi:10.1371/journal.pone.0097559

Okuno, H., Renault Mihara, F., Ohta, S., Fukuda, K., Kurosawa, K., Akamatsu, W., et al. (2017). CHARGE syndrome modeling using patient-iPSCs reveals defective migration of neural crest cells harboring CHD7 mutations. *Elife* 6, e21114. doi:10.7554/eLife.21114

Onesimo, R., Ricci, D., Agazzi, C., Leone, S., Petrianni, M., Orazi, L., et al. (2021). Visual function and ophthalmological findings in CHARGE syndrome: Revision of literature, definition of a new clinical spectrum and genotype phenotype correlation. *Genes. (Basel)* 12, 972. doi:10.3390/genes12070972

Pagon, R. A., Graham, J. M., Zonana, J., and Yong, S.-L. (1981). Coloboma, congenital heart disease, and choanal atresia with multiple anomalies: CHARGE association. *J. Pediatr.* 99, 223–227. doi:10.1016/S0022-3476(81)80454-4

Parisi, M. A. (2009). Clinical and molecular features of Joubert syndrome and related disorders. *Am. J. Med. Genet. C Semin. Med. Genet.* 151C, 326–340. doi:10.1002/ajmg.c.30229

Patten, S. A., Jacobs-McDaniels, N. L., Zaouter, C., Drapeau, P., Albertson, R. C., and Moldovan, F. (2012). Role of Chd7 in zebrafish: A model for CHARGE syndrome. *PLoS ONE* 7, e31650. doi:10.1371/journal.pone.0031650

Paul, M. H., Harvey, R. P., Wegner, M., and Sock, E. (2014). Cardiac outflow tract development relies on the complex function of Sox4 and Sox11 in multiple cell types. *Cell. Mol. Life Sci.* 71, 2931–2945. doi:10.1007/s00018-013-1523-x

Pauli, S., Bajpai, R., and Borchers, A. (2017). CHARGEd with neural crest defects. *Am. J. Med. Genet. C Semin. Med. Genet.* 175, 478–486. doi:10.1002/ajmg.c.31584

Peterson, R. E., Fadool, J. M., McClintock, J., and Linser, P. J. (2001). Müller cell differentiation in the zebrafish neural retina: Evidence of distinct early and late stages in cell maturation. *J. Comp. Neurol.* 429, 530–540. doi:10.1002/1096-9861(20010122)429:4<530:aid-cne2>3.0.co;2-c

Pike, G. E. G. (2012). "Perception," in *Cognitive psychology*. Editors N. Braisby and A. Gellatly (Oxford University Press), 65–99.

Pillai-Kastoori, L., Wen, W., Wilson, S. G., Strachan, E., Lo-Castro, A., Fichera, M., et al. (2014). Sox11 is required to maintain proper levels of hedgehog signaling during vertebrate ocular morphogenesis. *PLoS Genet.* 10, e1004491. doi:10.1371/journal.pgen.1004491

Prabhudesai, S. N., Cameron, D. A., and Stenkamp, D. L. (2005). Targeted effects of retinoic acid signaling upon photoreceptor development in zebrafish. *Dev. Biol.* 287, 157–167. doi:10.1016/j.ydbio.2005.08.045

Ragan, D. C., Casale, A. J., Rink, R. C., Cain, M. P., and Weaver, D. D. (1999). Genitourinary anomalies in the CHARGE association. *J. Urology* 161, 622–625. doi:10.1097/00005392-199902000-00089

Rainey, L., Elsman, E. B. M., van Nispen, R. M. A., van Leeuwen, L. M., and van Rens, G. H. M. B. (2016). Comprehending the impact of low vision on the lives of children and adolescents: A qualitative approach. *Qual. Life Res.* 25, 2633–2643. doi:10.1007/s11136-016-1292-8

Raymond, P. A., Barthel, L. K., and Curran, G. A. (1995). Developmental patterning of rod and cone photoreceptors in embryonic zebrafish. *J. Comp. Neurol.* 359, 537–550. doi:10.1002/cne.903590403

Reddy, N. C., Majidi, S. P., Kong, L., Nemera, M., Ferguson, C. J., Moore, M., et al. (2021). CHARGE syndrome protein CHD7 regulates epigenomic activation of enhancers in granule cell precursors and gyrification of the cerebellum. *Nat. Commun.* 12, 5702. doi:10.1038/s41467-021-25846-3

Reinhardt, R., Centanin, L., Tavhelidse, T., Inoue, D., Wittbrodt, B., Concordet, J., et al. (2015). Sox2, Tlx, Gli3, and Her9 converge on Rx2 to define retinal stem cells *in vivo*. *EMBO J.* 34, 1572–1588. doi:10.15252/embj.201490706

Rembold, M., Loosli, F., Adams, R. J., and Wittbrodt, J. (2006). Individual cell migration serves as the driving force for optic vesicle evagination. *Science* 313, 1130–1134. doi:10.1126/science.1127144

Roberts, M. R., Srinivas, M., Forrest, D., Morreale de Escobar, G., and Reh, T. A. (2006a). Making the gradient: Thyroid hormone regulates cone opsin expression in the developing mouse retina. *Proc. Natl. Acad. Sci. U. S. A.* 103, 6218–6223. doi:10.1073/pnas.0509981103

Roessler, E., Belloni, E., Gaudenz, K., Jay, P., Berta, P., Scherer, S. W., et al. (1996). Mutations in the human Sonic Hedgehog gene cause holoprosencephaly. *Nat. Genet.* 14, 357–360. doi:10.1038/ng1196-357

Ronquillo, C. C., Bernstein, P. S., and Baehr, W. (2012). Senior–løken syndrome: A syndromic form of retinal dystrophy associated with nephronophthisis. *Vis. Res.* 75, 88–97. doi:10.1016/j.visres.2012.07.003

Russell-Eggitt, I. M., Blake, K. D., Taylor, D. S., and Wyse, R. K. (1990). The eye in the CHARGE association. *Br. J. Ophthalmol.* 74, 421–426. doi:10.1136/bjo.74.7.421

Sabra, N., Abdel Aleem, H., Labib, T., el Sada, M., and Mohamed, B. (2009). Assessment and management of children with visual impairment. *Middle East Afr. J. Ophthalmol.* 16, 64–68. doi:10.4103/0974-9233.53863

Schmitt, E. A., and Dowling, J. E. (1999). Early retinal development in the zebrafish, *Danio rerio*: Light and electron microscopic analyses. *J. Comp. Neurol.* 404, 515–536. doi:10.1002/(sici)1096-9861(19990222)404:4<515:aid-cne8>3.0.co;2-a

Schmitt, E. A., and Dowling, J. E. (1994). Early-eye morphogenesis in the zebrafish, Brachydanio rerio. *J. Comp. Neurol.* 344, 532–542. doi:10.1002/cne.903440404

Schnetz, M. P., Bartels, C. F., Shastri, K., Balasubramanian, D., Zentner, G. E., Balaji, R., et al. (2009a). Genomic distribution of CHD7 on chromatin tracks H3K4 methylation patterns. *Genome Res.* 19, 590–601. doi:10.1101/gr.086983.108

Schulz, Y., Wehner, P., Opitz, L., Salinas-Riester, G., Bongers, E. M. H. F., van Ravenswaaij-Arts, C. M. A., et al. (2014a). CHD7, the gene mutated in CHARGE syndrome, regulates genes involved in neural crest cell guidance. *Hum. Genet.* 133, 997–1009. doi:10.1007/s00439-014-1444-2

Semina, E. v., Brownell, I., Mintz-Hittner, H. A., Murray, J. C., and JaMrichM. (2001). Mutations in the human forkhead transcription factor FOXE3 associated with anterior segment ocular dysgenesis and cataracts. *Hum. Mol. Genet.* 10, 231–236. doi:10.1093/hmg/10.3.231

She, Z.-Y., and Yang, W.-X. (2015). SOX family transcription factors involved in diverse cellular events during development. *Eur. J. Cell. Biol.* 94, 547–563. doi:10.1016/j.ejcb.2015.08.002

Sherpa, T., Fimbel, S. M., Mallory, D. E., Maaswinkel, H., Spritzer, S. D., Sand, J. A., et al. (2008). Ganglion cell regeneration following whole-retina destruction in zebrafish. *Dev. Neurobiol.* 68, 166–181. doi:10.1002/dneu.20568

Sherpa, T., Lankford, T., McGinn, T. E., Hunter, S. S., Frey, R. A., Sun, C., et al. (2014). Retinal regeneration is facilitated by the presence of surviving neurons. *Dev. Neurobiol.* 74, 851–876. doi:10.1002/dneu.22167

Sidhaye, J., and Norden, C. (2017). Concerted action of neuroepithelial basal shrinkage and active epithelial migration ensures efficient optic cup morphogenesis. *Elife* 6, e22689. doi:10.7554/eLife.22689

Siebert, J. R., Graham, J. M., and MacDonald, C. (1985). Pathologic features of the CHARGE association: Support for involvement of the neural crest. *Teratology* 31, 331–336. doi:10.1002/tera.1420310303

Skalicky, S. E., White, A. J. R., Grigg, J. R., Martin, F., Smith, J., Jones, M., et al. (2013). Microphthalmia, anophthalmia, and coloboma and associated ocular and systemic features: Understanding the spectrum. *JAMA Ophthalmol.* 131, 1517–1524. doi:10.1001/jamaophthalmol.2013.5305

Smith, R. S., ZAbAletA, A., Kume, T., Savinova, O. V., Kidson, S. H., Martin, J. E., et al. (2000). Haploinsufficiency of the transcription factors FOXC1 and FOXC2 results in aberrant ocular development. *Hum. Mol. Genet.* 9, 1021–1032. doi:10.1093/hmg/9.7.1021

Sohocki, M. M., Sullivan, L. S., Mintz-Hittner, H. A., Birch, D., Heckenlively, J. R., Freund, C. L., et al. (1998). A range of clinical phenotypes associated with mutations in CRX, a photoreceptor transcription-factor gene. *Am. J. Hum. Genet.* 63, 1307–1315. doi:10.1086/302101

Spencer, W. J., Lewis, T. R., Pearring, J. N., and Arshavsky, V. Y. (2020). Photoreceptor discs: Built like ectosomes. *Trends Cell. Biol.* 11, 904–915. doi:10.1016/j.tcb.2020.08.005

Sperry, E. D., Hurd, E. A., Durham, M. A., Reamer, E. N., Stein, A. B., and Martin, D. M. (2014). The chromatin remodeling protein CHD7, mutated in CHARGE syndrome, is necessary for proper craniofacial and tracheal development. *Dev. Dyn.* 243, 1055–1066. doi:10.1002/dvdy.24156

Sperry, E. D., Schuette, J. L., van Ravenswaaij-Arts, C. M. A., Green, G. E., and Martin, D. M. (2016). Duplication 2p25 in a child with clinical features of CHARGE syndrome. *Am. J. Med. Genet. A* 170, 1148–1154. doi:10.1002/ajmg.a.37592

Stenkamp, D. L. (2015). *Development of the vertebrate eye and retina*. doi:10.1016/bs.pmbts.2015.06.006

Stenkamp, D. L., Frey, R. A., Prabhudesai, S. N., and Raymond, P. A. (2000). Function for hedgehog genes in zebrafish retinal development. *Dev. Biol.* 220, 238–252. doi:10.1006/dbio.2000.9629

Stenkamp, D. L., Gregory, J. K., and Adler, R. (1993). Retinoid effects in purified cultures of chick embryo retina neurons and photoreceptors. *Investig. Ophthalmol. Vis. Sci.* 34, 2425–2436.

Stenkamp, D. L. (2007). *Neurogenesis in the fish retina*, 173–224. doi:10.1016/S0074-7696(06)59005-9

Stevens, C. B., Cameron, D. A., and Stenkamp, D. L. (2011). Plasticity of photoreceptor-generating retinal progenitors revealed by prolonged retinoic acid exposure. *BMC Dev. Biol.* 11, 51. doi:10.1186/1471-213X-11-51

Strömland, K., Sjögreen, L., Johansson, M., Joelsson, B. M. E., Miller, M., Danielsson, S., et al. (2005). CHARGE association in Sweden: Malformations and functional deficits. *Am. J. Med. Genet. A* 133 A, 331–339. doi:10.1002/ajmg.a.30563

Suzuki, S. C., Bleckert, A., Williams, P. R., Takechi, M., Kawamura, S., and Wong, R. O. L. (2013). Cone photoreceptor types in zebrafish are generated by symmetric terminal divisions of dedicated precursors. *Proc. Natl. Acad. Sci. U. S. A.* 110, 15109–15114. doi:10.1073/pnas.1303551110

Svoboda, K. K., and O'Shea, K. S. (1987). An analysis of cell shape and the neuroepithelial basal lamina during optic vesicle formation in the mouse embryo. *Development* 100, 185–200. doi:10.1242/dev.100.2.185

Swamy, V. S., Fufa, T. D., Hufnagel, R. B., and McGaughey, D. M. (2021). Building the mega single-cell transcriptome ocular meta-atlas. *Gigascience* 10, giab061. doi:10.1093/gigascience/giab061/gigascience/giab061

Tedja, M. S., Wojciechowski, R., Hysi, P. G., Eriksson, N., Furlotte, N. A., Verhoeven, V. J. M., et al. (2018). Genome-wide association meta-analysis highlights light-induced signaling as a driver for refractive error. *Nat. Genet.* 50, 834–848. doi:10.1038/s41588-018-0127-7

Tellier, A. L., Cormier-Daire, V., Abadie, V., Amiel, J., Sigaudy, S., Bonnet, D., et al. (1998). CHARGE syndrome: Report of 47 cases and review. *Am. J. Med. Genet.* 76, 402–409. doi:10.1002/(SICI)1096-8628(19980413)76:5<402:AID-AJMG7>3.0.CO;2-O

Turner, D. L., and Cepko, C. L. (1987). A common progenitor for neurons and glia persists in rat retina late in development. *Nature* 328, 131–136. doi:10.1038/328131a0

Turner, D. L., Snyder, E. Y., and Cepko, C. L. (1990). Lineage-independent determination of cell type in the embryonic mouse retina. *Neuron* 4, 833–845. doi:10.1016/0896-6273(90)90136-4

Uy, B. R., Simoes-Costa, M., Koo, D. E. S., Sauka-Spengler, T., and Bronner, M. E. (2015). Evolutionarily conserved role for SoxC genes in neural crest specification and neuronal differentiation. *Dev. Biol.* 397, 282–292. doi:10.1016/j.ydbio.2014.09.022

Verhoeven, V. J. M., Hysi, P. G., Wojciechowski, R., Fan, Q., Guggenheim, J. A., Höhn, R., et al. (2013). Genome-wide meta-analyses of multiancestry cohorts identify multiple new susceptibility loci for refractive error and myopia. *Nat. Genet.* 45, 314–318. doi:10.1038/ng.2554

Verloes, A. (2005). Updated diagnostic criteria for CHARGE syndrome: A proposal. *Am. J. Med. Genet. A* 133A, 306–308. doi:10.1002/ajmg.a.30559

Vissers, L. E. L. M., van Ravenswaaij, C. M. A., Admiraal, R., Hurst, J. A., de Vries, B. B. A., Janssen, I. M., et al. (2004). Mutations in a new member of the chromodomain gene family cause CHARGE syndrome. *Nat. Genet.* 36, 955–957. doi:10.1038/ng1407

Voronina, V. A., Kozhemyakina, E. A., O'Kernick, C. M., Kahn, N. D., Wenger, S. L., Linberg, J. V., et al. (2003). Mutations in the human RAX homeobox gene in a patient with anophthalmia and sclerocornea. *Hum. Mol. Genet.* 13, 315–322. doi:10.1093/hmg/ddh025

Weaver, M. L., Piedade, W. P., Meshram, N. N., and Famulski, J. K. (2020). Hyaloid vasculature and mmp2 activity play a role during optic fissure fusion in zebrafish. *Sci. Rep.* 10, 10136. doi:10.1038/s41598-020-66451-6

Wegner, M. (1999). From head to toes: The multiple facets of Sox proteins. *Nucleic Acids Res.* 27, 1409–1420. doi:10.1093/nar/27.6.1409

Wen, W., Pillai-Kastoori, L., Wilson, S. G., and Morris, A. C. (2015). Sox4 regulates choroid fissure closure by limiting Hedgehog signaling during ocular morphogenesis. *Dev. Biol.* 399, 139–153. doi:10.1016/j.ydbio.2014.12.026

West, S. K., Rubin, G. S., Broman, A. T., Munoz, B., Bandeen-Roche, K., and Turano, K. (2002). How does visual impairment affect performance on tasks of everyday life? *Arch. Ophthalmol.* 120, 774–780. doi:10.1001/archopht.120.6.774

Wetts, R., and Fraser, S. E. (1988). Multipotent precursors can give rise to all major cell types of the frog retina. *Science* 239, 1142–1145. doi:10.1126/science.2449732

Whittaker, D. E., Kasah, S., Donovan, A. P. A., Ellegood, J., Riegman, K. L. H., Volk, H. A., et al. (2017a). Distinct cerebellar foliation anomalies in a CHD7 haploinsufficient mouse model of CHARGE syndrome. *Am. J. Med. Genet.* 175. doi:10.1002/ajmg.c.31595

Whittaker, D. E., Riegman, K. L. H., Kasah, S., Mohan, C., Yu, T., Sala, B. P., et al. (2017b). The chromatin remodeling factor CHD7 controls cerebellar development by regulating reelin expression. *J. Clin. Investig.* 127, 874–887. doi:10.1172/JCI83408

Wilkinson, M. E., and Trantham, C. S. (2004). Characteristics of children evaluated at a pediatric low vision clinic: 1981–2003. *J. Vis. Impair. Blind.* 98 (11), 693–702. doi:10.1177/0145482X0409801104

Wineland, A., Menezes, M. D., Shimony, J. S., Shinawi, M. S., Hullar, T. E., and Hirose, K. (2017). Prevalence of semicircular canal hypoplasia in patients with CHARGE syndrome: 3C syndrome. *JAMA Otolaryngol. Head. Neck Surg.* 143, 168–177. doi:10.1001/jamaoto.2016.3175

Wong, L. L., and Rapaport, D. H. (2009). Defining retinal progenitor cell competence in *Xenopus laevis* by clonal analysis. *Development* 136, 1707–1715. doi:10.1242/dev.027607

Woodage, T., Basrai, M. A., Baxevanis, A. D., Hieter, P., and Collins, F. S. (1997). Characterization of the CHD family of proteins. *Proc. Natl. Acad. Sci. U. S. A.* 94, 11472–11477. doi:10.1073/pnas.94.21.11472

Wurm, A., Sock, E., Fuchshofer, R., Wegner, M., and Tamm, E. R. (2008). Anterior segment dysgenesis in the eyes of mice deficient for the high-mobility-group transcription factor Sox11. *Exp. Eye Res.* 86, 895–907. doi:10.1016/j.exer.2008.03.004

Yan, S., Thienthanasit, R., Chen, D., Engelen, E., Brühl, J., Crossman, D. K., et al. (2020). CHD7 regulates cardiovascular development through ATP-dependent and -independent activities. *Proc. Natl. Acad. Sci. U. S. A.* 117, 28847–28858. doi:10.1073/pnas.2005222117

Yao, H., Hannum, D. F., Zhai, Y., Hill, S. F., Albanus, R. D. 'Oliveira, Lou, W., et al. (2020). CHD7 promotes neural progenitor differentiation in embryonic stem cells via altered chromatin accessibility and nascent gene expression. *Sci. Rep.* 10, 17445. doi:10.1038/s41598-020-74537-4

Young, R. W. (1985). Cell differentiation in the retina of the mouse. *Anat. Rec.* 212, 199–205. doi:10.1002/ar.1092120215

Young, R. W. (1967). The renewal of photoreceptor cell outer segments. *J. Cell. Biol.* 33, 61–72. doi:10.1083/jcb.33.1.61

Yurco, P., and Cameron, D. A. (2005). Responses of Müller glia to retinal injury in adult zebrafish. *Vis. Res.* 45, 991–1002. doi:10.1016/j.visres.2004.10.022

Zentner, G. E., Layman, W. S., Martin, D. M., and Scacheri, P. C. (2010). Molecular and phenotypic aspects of CHD7 mutation in CHARGE syndrome. *Am. J. Med. Genet. A* 152A, 674–686. doi:10.1002/ajmg.a.33323

Zerti, D., Dorgau, B., Felemban, M., Ghareeb, A. E., Yu, M., Ding, Y., et al. (2020). Developing a simple method to enhance the generation of cone and rod photoreceptors in pluripotent stem cell-derived retinal organoids. *Stem Cells* 38, 45–51. doi:10.1002/stem.3082

Zhang, J., Talbot, W. S., and Schier, A. F. (1998). Positional cloning identifies zebrafish one-eyed pinhead as a permissive EGF-related ligand required during gastrulation. *Cell.* 92, 241–251. doi:10.1016/S0092-8674(00)80918-6

Zimmermann, M. J. Y., Nevala, N. E., Yoshimatsu, T., Osorio, D., Nilsson, D.-E., Berens, P., et al. (2018). Zebrafish differentially process color across visual space to match natural scenes. *Curr. Biol.* 28, 2018–2032. e5. doi:10.1016/j.cub.2018.04.075

Zuber, M. E., Gestri, G., Viczian, A. S., Barsacchi, G., and Harris, W. A. (2003). Specification of the vertebrate eye by a network of eye field transcription factors. *Development* 130, 5155–5167. doi:10.1242/dev.00723

frontiers | Frontiers in Cell and Developmental Biology

TYPE Methods
PUBLISHED 13 September 2022
DOI 10.3389/fcell.2022.983178



OPEN ACCESS

EDITED BY
Elizabeth Zuniga-Sanchez,
Baylor College of Medicine,
United States

REVIEWED BY
Lili Gong,
Zhongshan Ophthalmic Center, Sun Yat-sen University, China
Janice Walker,
Thomas Jefferson University,
United States
Daisy Y. Shu,
Schepens Eye Research Institute and Harvard Medical School, United States

*CORRESPONDENCE
Justin Parreno,
jparreno@udel.edu
Catherine Cheng,
ckcheng@iu.edu

SPECIALTY SECTION
This article was submitted to Molecular and Cellular Pathology, a section of the journal Frontiers in Cell and Developmental Biology

RECEIVED 30 June 2022
ACCEPTED 16 August 2022
PUBLISHED 13 September 2022

CITATION
Parreno J, Emin G, Vu MP, Clark JT, Aryal S, Patel SD and Cheng C (2022), Methodologies to unlock the molecular expression and cellular structure of ocular lens epithelial cells.
*Front. Cell Dev. Biol.* 10:983178.
doi: 10.3389/fcell.2022.983178



# Methodologies to unlock the molecular expression and cellular structure of ocular lens epithelial cells

Justin Parreno[1,2]*, Grace Emin[1], Michael P. Vu[3], Jackson T. Clark[3], Sandeep Aryal[1,4], Shaili D. Patel[1] and Catherine Cheng[3]*

[1]Department of Biological Sciences, University of Delaware, Newark, DE, United States, [2]Department of Biomedical Engineering, University of Delaware, Newark, DE, United States, [3]School of Optometry and Vision Science Program, Indiana University, Bloomington, IN, United States, [4]Department of Neurology, Massachusetts General Hospital and Harvard Medical School, Boston, MA, United States

The transparent ocular lens in the anterior chamber of the eye is responsible for fine focusing of light onto the retina. The lens is entirely cellular with bulk of the tissue composed of fiber cells, and the anterior hemisphere of the lens is covered by a monolayer of epithelial cells. Lens epithelial cells are important for maintaining fiber cell homeostasis and for continual growth of the lens tissue throughout life. Cataracts, defined as any opacity in the lens, remain the leading cause of blindness in the world. Following cataract surgery, lens epithelial cells can undergo a process of epithelial-to-mesenchymal transition (EMT), leading to secondary cataracts due to posterior capsular opacification (PCO). Since the epithelial cells make up only a small fraction of the lens, specialized techniques are required to study lens epithelial cell biology and pathology. Studies using native lens epithelial cells often require pooling of samples to obtain enough cells to make sufficient samples for traditional molecular biology techniques. Here, we provide detailed protocols that enable the study of native mouse lens epithelial cells, including immunostaining of the native lens epithelium in flat mounts, extraction of RNA and proteins from pairs of lens epithelial monolayers, and isolation of lens epithelial cells for primary culture. These protocols will enable researchers to gain better insight on representative molecular expression and cellular structure of lens epithelial cells. We also provide comparative data between native, primary culture, and immortalized lens epithelial cells and discuss the advantages and disadvantages of each technique presented.

KEYWORDS

**Western blot, flat mount, RNA, PCR, primary culture, immunostaining, whole mount**

## Introduction

The eye lens is an ellipsoid, transparent tissue in the anterior chamber of the eye that is responsible for fine focusing light onto the retina to create a clear image (Lovicu and Robinson, 2004). The bulk of the lens is composed of fiber cells, while a monolayer of the lens epithelium covers the anterior hemisphere of the lens (Piatigorsky, 1981). The entire tissue is encapsulated by a basement membrane, known as the lens capsule (Lovicu and Robinson, 2004). Lens epithelial cells are divided spatially into anterior epithelial cells that are quiescent and equatorial epithelial cells that continuously proliferate, migrate, elongate, and differentiate into new generations of lens fiber cells throughout life (Piatigorsky, 1981; Kuszak et al., 2004; Yamamoto et al., 2008). Anterior epithelial cells are cuboidal and cobblestone in cross-section, while equatorial epithelial cells transition to the organized hexagon-shaped cells at the region of epithelial-to-fiber cell differentiation (Bassnett et al., 1999; Zampighi et al., 2000; Cheng and Gong, 2011; Cheng et al., 2013).

Lens epithelial cells are oriented with their basal side toward the capsule. These cells have a strong attachment to the capsule, while the apical–apical junction with fiber cells is a relatively weaker adhesion (Wang et al., 2007). The interface between epithelial and fiber cells creates a rare apical–apical junction within the tissue (Zampighi et al., 2000). Fiber cells are continuously added to the lens in concentric shells with the newly formed cells on the periphery (Piatigorsky, 1981), similar to rings on a tree. As fiber cells mature and compact, they lose all of their cellular organelles to reduce light scattering (Bassnett et al., 2011). These cells become highly compact at the center of the lens, known as the lens nucleus. Anterior epithelial cells are thought to be important for cellular communication and maintenance of underlying mature fiber cells (Lovicu and Robinson, 2004). In rodent lenses, the nucleus is compact and can be separated from cortical fibers by dissection (Gong et al., 1997; De Maria et al., 2009), controlled lysis (Pierscionek and Augusteyn, 1988; De Maria et al., 2009; Cheng et al., 2022), or mechanical separation (Gokhin et al., 2012; Cheng et al., 2016; Cheng et al., 2018; Cheng et al., 2019; Cheng et al., 2022). Since cell proliferation is restricted to lens equatorial epithelial cells, continual differentiation of lens epithelial cells to fiber cells for lifelong lens growth is dependent on lens epithelial cells (Piatigorsky, 1981; Shi et al., 2014).

Specialized techniques are required to study the limited population of lens epithelium monolayer cells. Lens epithelial cell differentiation and behavior have been studied in many species using *in vitro* primary cell culture and immortalized cell lines (Kirby, 1927; Mann, 1948; Mamo and Leinfelder, 1958; Van Der Veen and Heyen, 1959; Okada et al., 1971; Creighton et al., 1976; Hamada and Okada, 1978; Reddan et al., 1980; Menko et al., 1984; FitzGerald and Goodenough, 1986; Reddan et al., 1989; Musil et al., 1990; Bermbach et al., 1991; Andley et al., 1998; Ibaraki et al., 1998; Ogiso et al., 1998; Wang et al., 2007; Bannik et al., 2013; Matsuyama et al., 2013; Sundelin et al., 2014; Terrell et al., 2015; Wang et al., 2017; Weatherbee et al., 2019). However, primary lens epithelial cells in culture often do not maintain native lens epithelial cell characteristics. Examining lens epithelial cell behavior in native lenses is challenging. Protein and nucleic acid isolation of whole lenses disproportionately reflect molecular expression from fiber cells, which make up the bulk of the lens. Separation of epithelial cells from fiber cells to enrich epithelial cell isolates is possible; however, traditional methods of RNA extraction and protein analysis (Western blotting) require the pooling of multiple lens epithelia to increase extraction yield. Additionally, the examination of lens tissue sections often focuses on fiber cells and does not reveal changes in the epithelial monolayer that is reduced to a 2D cross-section of the monolayer. Therefore, refined methods are required for in-depth study of lens epithelial cell changes due to aging, genetic manipulation, or diseases.

We describe in detail several methods to study the lens epithelial cells from mouse tissue, including 1) primary culture, 2) RNA isolation, 3) protein extraction, and 4) immunostaining of flat mounts of lens epithelial cell sheets and whole-mount lenses.

1) Primary culture isolation of epithelial cells has been performed by many other researchers from various animals, including mice (Mann, 1948; Reddan et al., 1989; Andley et al., 1998; Wang et al., 2007; Bannik et al., 2013; Wang et al., 2017). The detailed primary epithelial cell isolation method presented here is our modification of a previously published method (Wang et al., 2007).
2) The method for RNA isolation presented here is a novel protocol for lens epithelial cells. We present method validation data by comparing RNA expression levels for various epithelial and mesenchymal markers between native epithelial cells, primary culture cells, and immortalized cells.
3) We detail our previously published method for protein isolation from lens epithelial cells (Parreno et al., 2020; Cheng et al., 2022), cortical fiber cells, and nuclear fiber cells (Cheng et al., 2022), including homogenization buffer volumes and the expected protein yield for each fraction. We compare β-actin levels between the three protein fractions isolated from the lens.
4) To better visualize the lens epithelial cell monolayer, we also present a detailed protocol to immunostain lens capsule flat mounts with attached epithelial cells (Cheng and Gong, 2011; Cheng et al., 2013; Cheng et al., 2017). We include crucial details to distinguish the anterior and posterior poles of the lens and show continuous imaging of the epithelial monolayer from the anterior pole to the equator to compare cell arrangement and shape from distinct regions of the lens.

Our methods for protein and RNA extraction can be applied to single or pairs of lens epithelial monolayers, reducing the number of animals required for generating these samples and allowing researchers to produce more biological replicates for improved statistical analysis. In general, the procedures described here use common laboratory equipment. However, protein analysis of epithelial cell lysates requires a specialized instrument for capillary-based electrophoresis (Parreno et al., 2020; Cheng et al., 2022). Using capillary-based electrophoresis allows examination of protein expression from single or paired mouse lens epithelium. While the methods we present here were developed for mouse lenses, they could be adapted for lenses from larger animals or humans.

## Step-By-Step Procedures

All procedures were conducted in accordance with the approved animal protocols from the University of Delaware and Indiana University, Bloomington Institutional Animal Care and Use Committees (IACUC) and in accordance with the Use of Animals in Ophthalmic and Vision Research and the Guide for the Care and Use of Laboratory Animals by the National Institutes of Health. A video of, and a detailed protocol for, mouse lens dissection can be found in our previous work (Cheng et al., 2016). Dissection of freshly enucleated eyes was performed in 1X phosphate-buffered saline (PBS) in a dissection plate. PBS for dissection is maintained at room temperature, but for lenses from mice younger than postnatal day 14 (P14), PBS should be warmed to 37°C to avoid cold cataracts (Zigman and Lerman, 1964; Lo, 1989; Wang et al., 2007). A complete material list is provided in Supplementary Table S1.

### Lens epithelium and fiber mass separation for epithelial cell isolation for primary culture, RNA isolation, and protein extraction

1) For protein and RNA isolation, any tissue stuck to the outside of the dissected lens is removed by transferring the lens to a Kimwipe using curved forceps and gently rolling the lens along the Kimwipe. This will remove most/all small tissue bits that may be adhered to the lens capsule. This step may be repeated until the lens capsule is completely free of visible extraneous tissues.

It should be noted that after rolling on the Kimwipe, the capsule may become slightly hazy due to brief drying. The capsule should become clear again after the lens is rehydrated in the next step. For RNA isolation, spraying RNAse away on the Kimwipe will help reduce the RNA degradation caused by RNAse contamination.

2) The clean lens is transferred back to the dissection dish filled with 1X PBS. The lenses are weighed to obtain the whole lens wet weight if needed to determine the amount of buffer to be used in subsequent steps.
3) Using the fine straight forceps, the capsule is carefully punctured at the lens equator and the capsule is peeled off in one continuous sheet. The lens epithelial cells are firmly attached to the lens capsule. The mass of the lens fiber cells will remain intact. The capsule with the attached lens epithelial cells is transferred to the appropriate buffer for the next step of the specific experiment.

### Isolation of lens epithelial cells for primary culture

For this protocol (Figure 1), we suggest using lenses from P10 mice, which contain a substantial number of epithelial cells. This method is modified from a previous study (Wang et al., 2007). For this, we pool together 14 capsules. All solutions should be prepared under sterile conditions, and instruments should be autoclaved or brand new. Cultured cells should be cared for with regular medium changes. The cells will reach confluence in the center of the plate within about 14 days of culture and cannot be passaged. Instead of using a 35-mm dish, culture can also be carried out on chamber slides or in multi-well plates.

1) Place the dissected lenses in a 15-ml tube with 5 ml of 0.05% Trypsin-EDTA.

It should be noted that there is no need to remove small pieces of tissue attached to the capsule of the lens since the next step will remove any extraneous tissues. The blood vessels attached to the lenses from P14 or younger mice are difficult to remove by dissection without damaging the lens.

2) The lens is incubated in trypsin for 5–10 min at 37°C. Gently swirl the lenses in the trypsin solution every 1–2 min. Meanwhile, 0.4 ml of trypsin is prepared in another 1.5-ml microcentrifuge tube in sterile conditions for step 5.
3) 5 ml of Dulbecco's modified Eagle's medium (DMEM) containing 10% fetal bovine serum (FBS) is added to inactivate the trypsin.
4) The lenses are transferred to a clean plastic dish, and the lens capsule is dissected by puncturing the lens at the equator and using fine forceps to gently peel away the lens capsule with the attached lens epithelial cells.
5) The dissected lens capsules are placed in the 1.5-ml microcentrifuge tube with 0.4 ml of 0.05% Trypsin-EDTA.
6) The lens capsules are incubated in Trypsin-EDTA at 37°C for 10 min.
7) In a tissue culture hood, under sterile conditions, a cell strainer (100 μm) is added on top of a 50-ml tube. The lens capsule and trypsin mixture are passed through the cell strainer, collecting the cell sample at the bottom of the 50-ml

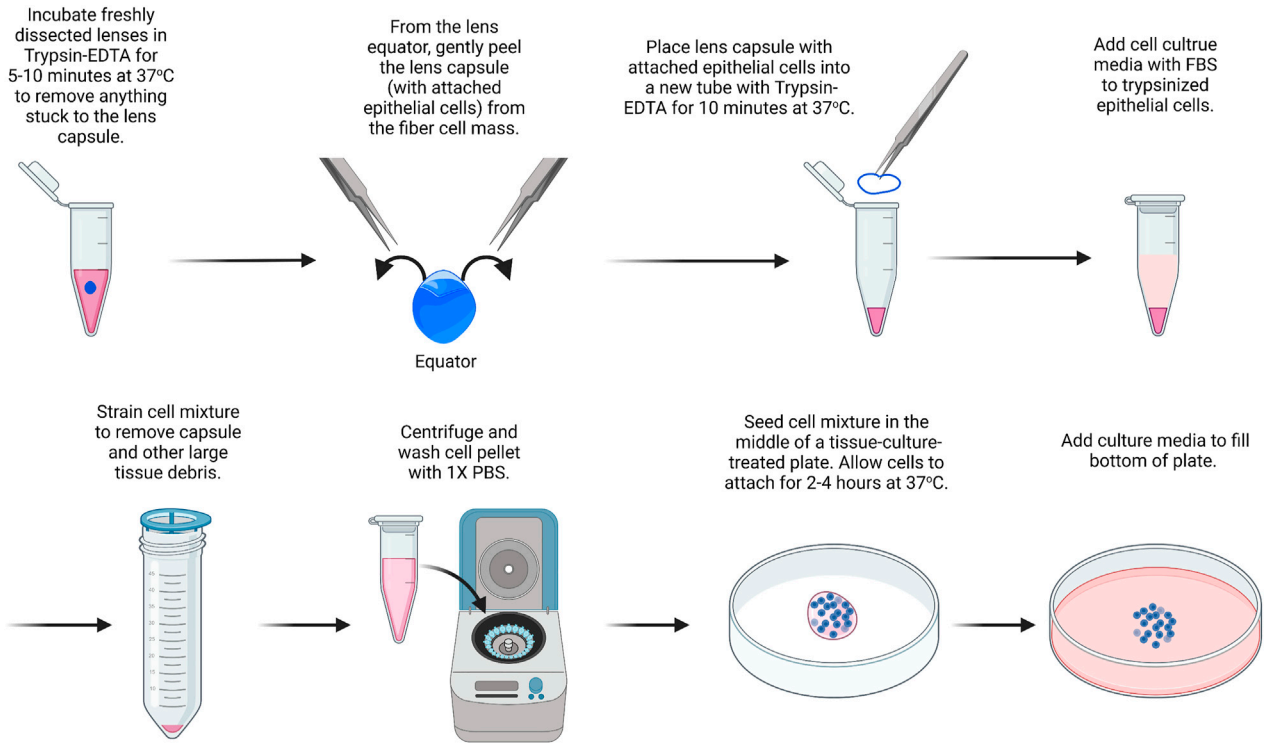


FIGURE 1
Primary lens epithelial cell isolation. Lenses are placed in trypsin/EDTA solution to remove extraneous materials that could stuck to the lenses during dissection. Capsules are then isolated and placed in trypsin/EDTA to liberate/dissociate cells. Cells are seeded onto the center of a culture dish and filled with media after they attach. The image was drawn using Biorender and not drawn to scale.

tube. The cell strainer will help remove debris from the lens capsule so that only epithelial cells are left behind in the sample after filtering.

8) The cell sample is centrifuged at 800 × g for 8 min.
9) The supernatant is removed without disturbing the cell pellet. The cell pellet is resuspended in 1 ml of PBS and centrifuged again. Repeat PBS wash and centrifugation two more times.
10) The cell pellet is resuspended in 50 µL of media and seeded in the middle of a 35-mm tissue-culture treated plastic or glass-bottom dish.
11) Let the cells sit undisturbed at 37°C to allow for cell attachment. After approximately 2–4 h, the dish is filled with 2 ml of DMEM containing 10% FBS and 1% antibiotic/antimycotic.

The media is changed every 2–3 days, and the cells at the center of the plate will reach confluence in ~7–10 days of culture.

## RNA isolation from epithelial cells

While it is possible to isolate RNA from a single-lens capsule with attached epithelial cells, the yield is low in our experience. We recommend using a pair of capsules from the same mouse as one biological replicate. Typically, the RNA yield from a pair of lens capsules is ~75–150 ng/µL (Figure 2). RNA from the fiber cell mass can also be isolated from the dissected lenses using a standard TRIzol–chloroform method. While we do not include that protocol here, we recommend using 20 µL of DEPC-treated water to dissolve the RNA pellets from pairs of fiber masses. Usually, the RNA yield from a pair of fiber masses is 500–800 ng/µL.

1) The lens capsule is placed immediately in 0.4 ml of cold TRIzol reagent to a 1.5-ml microcentrifuge tube. Tubes are inverted and ensure capsules are fully immersed in TRIzol.
2) Samples are incubated for 30 min at room temperature in a chemical fume hood for the lens capsule to fully dissolve.
3) For phase separation, 0.2 ml of chloroform is added per 0.4 ml of TRIzol added to act as a chemical cabinet. The tubes are shaken vigorously by hand for 15 s or vortexed lightly. Do not over vortex to avoid breaking up of RNA. Samples are incubated at room temperature for 10–15 min.
4) The sample is centrifuged at 14,000 x *g* for 15 min at 4°C. Transfer aqueous phase to a fresh tube using a P200 pipettor. Typically, there will be ~150 µL of the aqueous phase. Avoid capturing the white protein layer between the aqueous phase

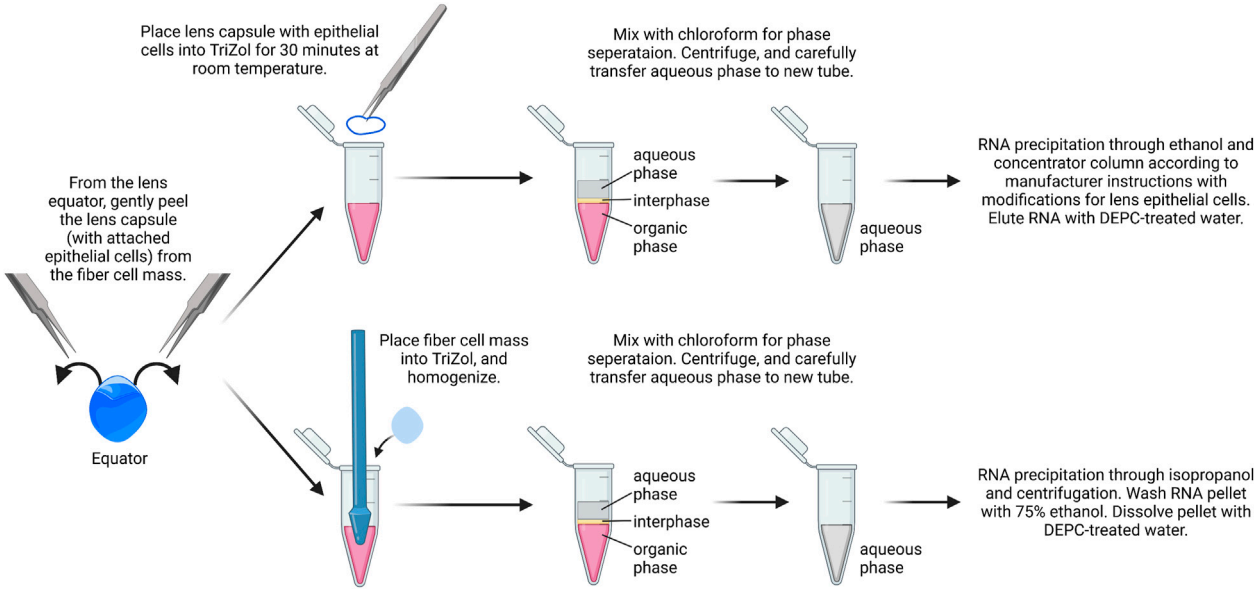


FIGURE 2
RNA isolation from lens epithelial cells. Capsules are isolated from lenses and placed in TRIzol. Chloroform is added for phase separation, and RNA is precipitated using ethanol followed by RNA clean up using spin columns. From the same samples, the fiber cell RNA can also be isolated with standard TRIzol/chloroform extraction, isopropanol precipitation, and ethanol wash. The image was drawn using Biorender and not drawn to scale.

and the pink TRIzol layer. Some of the aqueous layer will be left behind to avoid disturbing the white protein layer.

TRIzol and chloroform waste are collected in the phenol and the chloroform waste bottle. Leave them open in the fume hood overnight to allow for evaporation.

5) In a fresh tube with the aqueous layer only, an equal volume of 100% ethanol is added to the aqueous phase. The tube is gently inverted to gently mix the contents.

For steps 6–16, this protocol uses a ZYMO Research RNA extraction and a clean kit.

6) Transfer the entire volume of the sample to a new spin column with a collecting tube from the kit (e.g., if 150 µL of the top aqueous phase is collected, there will be a total of 300 µL of sample with an equal volume of ethanol added).
7) Centrifuge the column and collecting tube at 16,000 × g for 30 s at 4°C and remove the collected liquid from the collecting tube and dispose.

The RNA binds to the silica-based matrix at the bottom of the spin column tube, so pouring out the collected liquid does not remove the RNA.

8) Wash the RNA by adding 400 µL of RNA prep buffer into the spin column to remove impurities.
9) Centrifuge the column and collecting tube at 16,000 × g for 30 s at 4°C and discard the liquid from the collecting tube and dispose.
10) Add 700 µL of RNA wash buffer to the spin column tube.
11) Centrifuge the column and collecting tube at 16,000 × g for 30 s at 4°C and remove the collected liquid from the collecting tube and dispose.
12) Add 400 µL of RNA wash buffer to the spin column tube.
13) Centrifuge the column and collecting tube at 16,000 × g for 1 min at 4°C and discard the liquid from the collecting tube and dispose.
14) Centrifuge the column and collecting tube at 16,000 × g for 30 s at 4°C to remove any residual wash buffer and dispose the liquid from the collecting tube.
15) Replace the collecting tube with an RNAse-free 1.5-ml microcentrifuge tube and place the spin column on top of the new microcentrifuge tube.
16) Add 15 µL of DEPC-treated or molecular grade water directly onto the membrane of the spin column. Let water stand on the spin column membrane for 2 min, and then centrifuge the spin column and 1.5-ml microcentrifuge tube at 16,000 × g for 1 min at 4°C.
17) The collected ~15 µL of sample is in the 1.5-ml microcentrifuge tube. This is the RNA sample.

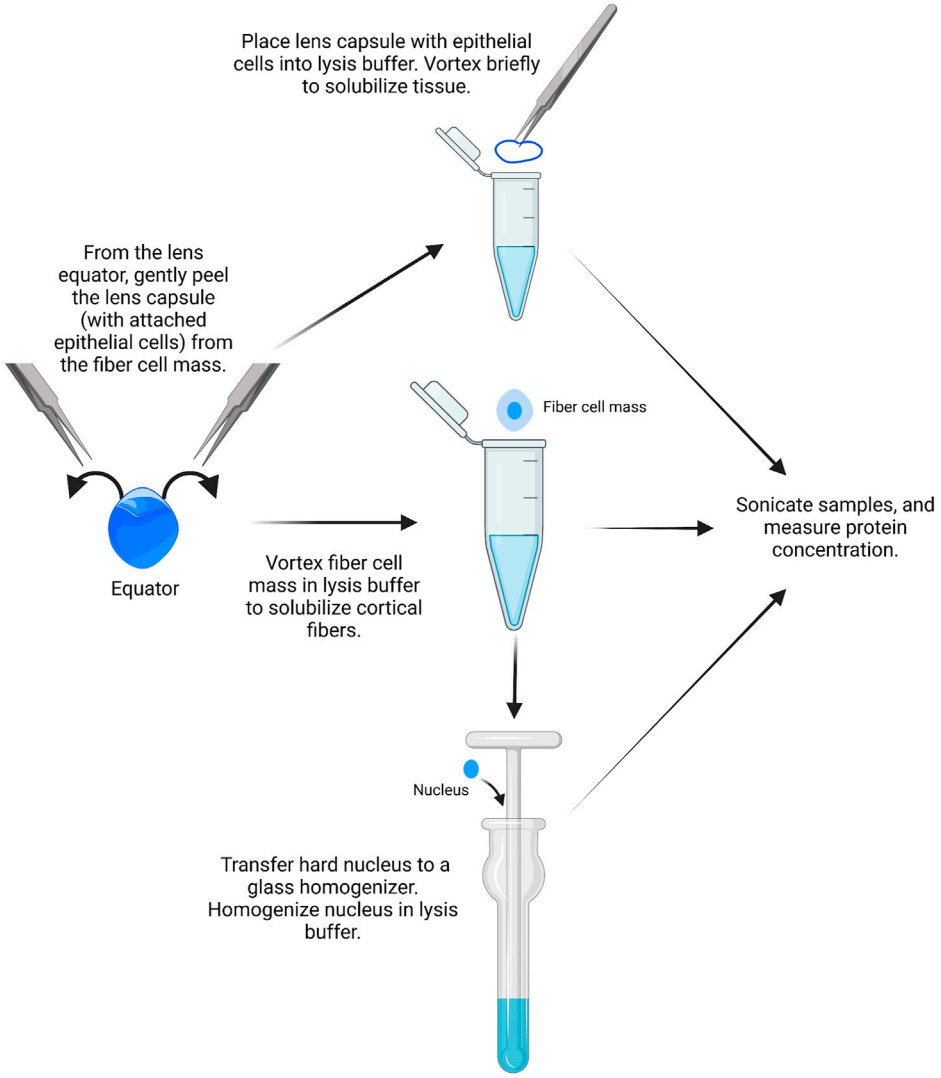


FIGURE 3
Epithelial, cortical fiber, and nuclear fiber protein sample isolation. Remove the lens capsule and isolate the protein sample from the lens epithelial cells. The fiber cell mass can then be vortexed to solubilize cortical fiber cells, leaving a hard lens nucleus. The hard lens nucleus can then be homogenized to create nuclear fiber protein lysates. The image was drawn using Biorender and not drawn to scale.

18) Before quantifying, the RNA sample tube is incubated at 55–65°C for 10 min to dissolve the RNA. After this, the tubes are immediately placed on ice.
19) The RNA samples are stored at −80°C for future work as RNA is less stable at higher temperatures and will degrade.

## Protein extraction from epithelial cells, cortical fibers, and nuclear fibers

Similar to RNA isolation, it is possible to isolate proteins from single-lens capsules with attached epithelial cells, but the yield is very low. We recommend using pairs of lens capsules from one mouse to prepare the epithelial cell samples (Figure 3).

1) A pair of lens capsules/epithelium is placed into a 1.5-ml microcentrifuge tube filled with 16 µL of homogenization buffer (e.g., ice-cold lens homogenization buffer (Nowak et al., 2009; Gokhin et al., 2012; Cheng et al., 2018; Cheng et al., 2022) or 1X RIPA buffer) with phosphatase and protease inhibitors.

Lens homogenization buffer requires the addition of fresh 1 mM DTT. For epithelial cell samples, 14.75 µL lens homogenization buffer is mixed with 1.25 µL lens homogenization buffer with 2X sample buffer without bromophenol blue (see references above or Supplementary Table S1 for buffer contents). For fiber cell lysates, tissues

should be homogenized in a 1:1 ratio of lens homogenization buffer and 2X sample buffer without bromophenol blue. 1X RIPA buffer and other commercial lysis buffers can also be used for homogenization. The ProteinSimple website should be referenced for buffer compatibility before starting. All homogenization buffers should be prepared fresh on the day of protein isolation.

2) The lens capsules are vortexed briefly in the homogenization buffer for two short pulses, and the tubes are centrifuged briefly in a mini table-top microcentrifuge.
3) Proteins from the lens cortex can be extracted from the lens fiber cell mass by placing a pair of dissected fiber masses into a 1.5-ml microcentrifuge tube filled with 250 µL of homogenization buffer per 10 mg of whole lens wet weight. The fiber cell masses are vortexed for 2–4 min in 30-second intervals until the ball of fiber cells does not become smaller in size with successive vortexing.

It should be noted that the leftover fiber cell mass is the compacted lens nucleus in mouse lenses.

4) Using clean, fine forceps, the pair of dense lens nuclei is transferred to a Dounce homogenizer (2 ml mortar, type B pestle) filled with 250 µL of homogenization buffer per 10 mg of the whole lens wet weight.
5) The lens nuclei are homogenized with the Dounce homogenizer until the solution is uniformly cloudy. Take caution to not get the lens tissue stuck at the bottom of the homogenizer to prevent loss of proteins.
6) The homogenized nuclear fiber cell lysates are transferred to microcentrifuge tubes using a gel-loading pipette tip. All samples are stored on ice before sonication.
7) The samples (QSonica Q55, 2 mm probe tip, amplitude 15) are sonicated in cycles of: 3 s of sonication and 10 s of cooling on ice. The epithelial samples are sonicated for one cycle, and the fiber cell samples are sonicated for three cycles.
8) The protein samples are stored at −80°C if not measuring the protein concentration immediately.
9) To determine the protein concentration, use the Bradford or bicinchoninic acid (BCA) assay as per the manufacturer's instructions.

It should be noted that after measuring the protein concentration of epithelial cell lysates once, we can approximate the concentration of this fraction to conserve the amount of the protein sample. The amount of protein in epithelial cell samples from a pair of capsules from 6–8-week-old mice is ~0.5 µg/µL. The amount of protein from cortical and nuclear fiber cells from a pair of lenses from 6–8-week-old mice is 6–10 µg µL and 4–6 µg/µL, respectively.

## Protein sample preparation for JESS/WES capillary electrophoresis

The detection of proteins from pairs of lens epithelial cell samples requires the ProteinSimple JESS or WES capillary electrophoresis machine (Parreno et al., 2020; Cheng et al., 2022). It should be noted that all antibodies and protein concentrations should be titrated as per the manufacturer's instructions prior to proceeding with actual experiments to determine the optimal conditions for antibody saturation and protein concentration. The following is a basic procedure for JESS/WES that does not cover the optimization protocol, assay setup, or data analyses. See discussion for more information on optimization, assay design, and data analysis.

1) The standard pack reagents are prepared as per the manufacturer's instructions.
2) JESS/WES can identify the target protein at concentrations as low as 0.1 µg/µL. The epithelial cell samples are prepared by diluting 15 µL of the sample with 11.25 µL of 0.1X sample buffer provided by the manufacturer. For fiber cell lysates, samples are diluted to the appropriate concentration based on titration experiments with 0.1X sample buffer provided by the manufacturer in 1.5-ml microcentrifuge tubes. The samples will be mixed with one-part fluorescent 5X master mix to four parts of the prepared lysates.
3) Ensure that the samples are mixed by brief vortexing and spin down the tubes in a mini table-top microcentrifuge. The samples are incubated at 95°C for 5 min.
4) After incubation, the samples are briefly vortexed and spun down before placing them on ice until use.
5) Primary antibodies are diluted as appropriate in the diluent buffer provided by the manufacturer. The antibody diluent that is used will depend on whether the run requires chemiluminescence or fluorescence detection. If running fluorescence, a milk-free antibody diluent must be used to reduce the amount of background signal. Otherwise, antibody diluent 2 can be used.
6) The secondary antibody is prepared as per the manufacturer's instructions. For chemiluminescence, the luminol-S and peroxide solutions are prepared as per the manufacturer's instructions, combining each in a 1:1 ratio.
7) For multiplexing on the JESS, the RePlex reagent is prepared as per the manufacturer's instructions.
8) For these assays, we suggest using the total protein detection kit as the loading control according to the manufacturer's instructions. This assay can be carried out using RePlex on the JESS or in separate wells on the WES. More details are provided in the discussion.
9) To load the capillary electrophoresis plate, the reagents are pipetted carefully according to Table 1. This is a generic example, so the plate assay design may vary depending on the experiment.

TABLE 1 JESS/WES plate loading guide.

| Well | | | |
|---|---|---|---|
| **One antibody only** | **w/total protein** | **Component** | **Volume** |
| A1 | A1 | Biotinylated ladder | 5 µL |
| A2–A25 | A2–A25 | Lens lysate samples | 3 µL |
| B1–B25, C1 | B1, C1–C25, D1 | Antibody diluent | 10 µL |
| | B2–B25 | Total protein labeling reagent | 10 µL |
| C2–C25 | D2–D25 | Primary antibody | 8.5 µL |
| D1 | E1 | Streptavidin-HRP | 10 µL |
| D2–D25 | E2–E25 | Secondary antibody | 10 µL |
| | F1–F25 | Total protein streptavidin-HRP | 8 µL |
| E2–E25 | Row J | Luminol–peroxide | 15 µL (immunoassay) |
| | | | 170 µL (total protein) |
| Rows G, H, and I | Row G, H, I | Wash buffer | 500 µL (load after step 10) |
| | Row K | RePlex reagent | 300 µL (load after step 10) |

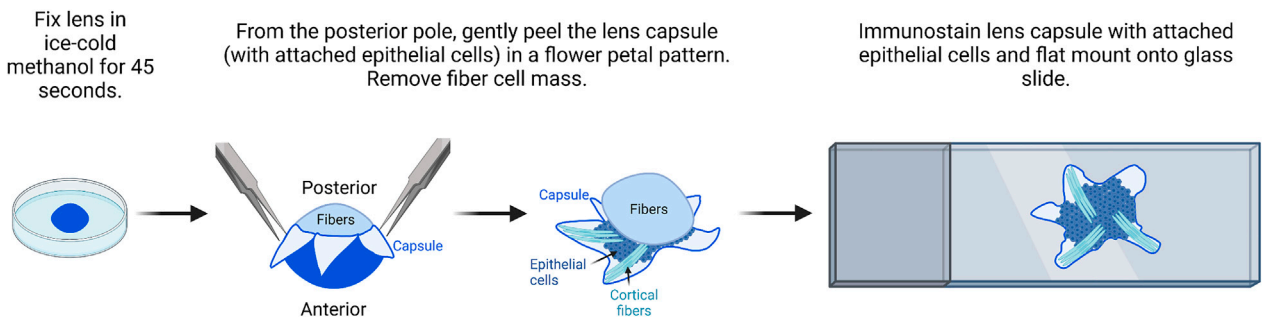


FIGURE 4
Flat mount imaging of lens epithelial cell monolayer. After methanol fixation of the lens, gently peel the lens capsule with attached epithelial cells from the posterior and remove the fiber cell mass. There will be a small amount of peripheral fiber cells attached to the flat mount sample. After immunostaining, flat mount the lens capsule onto a glass slide in mounting media and then cover and seal with a coverslip for imaging. The image was drawn using Biorender and not drawn to scale.

10) The plate is centrifuged at 1,000 × g for 5 min at room temperature before loading the wash buffer and RePlex buffer.

11) Set up the assay accordingly in the Compass for SW software. The plates take ~3 h to run for standard assays and ~5 h for RePlex assays.

## Lens epithelial cell flat mounts and immunostaining

Mouse lens capsule flat mounts (Figure 4) (Cheng and Gong, 2011; Cheng et al., 2013; Cheng et al., 2017) were prepared using a protocol previously described for rat lenses (Sugiyama et al., 2010).

1) Lenses are dissected from freshly enucleated eyes and immediately fixed for 45 s in ice-cold methanol.

It should be noted for this procedure, the lens does not have to be perfectly clean of all extraneous tissues, but all larger tissue bits should be removed during dissection.

2) The fixed lens is transferred back into the dissection plate with 1X PBS. The anterior capsule will be whiter than the posterior capsule for a few seconds. The lens is oriented with the anterior lens capsule down toward the bottom of the dish.
3) Two pairs of fine forceps or one pair of fine forceps and one pair of dissection scissors are used to make a cross-pattern radial cut into the posterior lens capsule.

4) Fine forceps are used to peel the capsule petals toward the lens equator. The capsule flat mounts will contain epithelial cells and some superficial fiber cells.
5) Place the lens capsule flat mounts into a blocking solution (3–5% normal serum (species depends on the secondary) and 0.3% Triton X-100) for 1 h at room temperature. The blocking and immunostaining steps can be carried out in multi-well plates or 1.5-ml microcentrifuge tubes.
6) The lens capsule flat mounts are transferred to the primary antibody solution and incubated overnight at 4°C with gentle rocking.

The primary and secondary antibody concentrations should be optimized by immunostaining with lens frozen tissue sections.

7) The lens capsule flat mounts are washed with 1X PBS three times for 5 min per wash with gentle rocking.
8) The lens capsule flat mounts with appropriate fluorescent secondary antibodies are incubated for 2 h at room temperature with gentle rocking.

It should be noted that due to the methanol fixation, phalloidin dyes that stain F-actin networks will not work on these flat mounts.

9) The lens capsule flat mounts are washed with 1X PBS four times for 5 min per wash with gentle rocking.
10) On a clean SuperFrost Plus glass slide, place one generous dot (~50 µL) of DAPI VectaShield mounting medium. Transfer one sample to the dot of the mounting media.
11) Two pairs of fine forceps are used to gently open up and flatten the lens capsules. If being imaged by confocal microscopy, since the tissue is not thick, any side can be facing up. If using a fluorescence microscope, the capsule should be side facing up. The sample does not have to be perfectly flat, but it should not be twisted or folded on itself.
12) A coverslip is placed on top of the flatten lens capsule. The weight of the coverslip will help the tissue become more flattened. For confocal microscopy, use 1.5-thickness coverslips.
13) Seal the coverslip with nail polish and allow it to dry overnight before imaging. Under the microscope, the epithelial cell side of the flat mount will usually have a few fiber cells stuck to it, while the capsule side will not.

# Method validation and discussion

## RNA isolation and primary culture epithelial cells

Extracting RNA from lens epithelium using TRIzol/chloroform-based precipitation requires pooling of multiple lens epithelial capsular peels for RNA processing. In our previous study, this required the pooling of at least six capsular peels (Parreno et al., 2020). Here we demonstrated, using a modified version of the TRIspin method previously developed for cartilage samples (Reno et al., 1997), that we are able to obtain enough RNA from just two lens capsules from 8–10-week old mice for real-time RT-PCR purposes. The RNA achieved A260/280 values of 1.875 with an average concentration of 131 ± 35.5 ng/µL (mean ± standard error; $n$ = 3). To determine the quality of the extracted RNA, we measured the RNA integrity value (RIN) (Schroeder et al., 2006). We determined that our RIN from the lens epithelial cell samples was 5.0 ± 0.5, which is consistent with values from other tissues (Fleige and Pfaffl, 2006). This RIN value has been shown to be suitable for analyzing gene expression by real-time RT-PCR (Fleige and Pfaffl, 2006).

This RNA isolation technique allows comparison of gene expression between mouse native lens epithelial cells, immortalized lens epithelial cell lines (imLEC and 21EM15), and embryonic fibroblast cells (NIH3T3) (Figure 5). Our PCR analysis reveals that immortalized lens epithelial cell mRNA expression of epithelial cell markers does not fully resemble that of native lens epithelial cells. 21EM15 cells express significantly lower levels of epithelial markers, Cdh1 and Pax6, while having elevated mRNA levels for mesenchymal cell markers, Fn, Col1, and αsma, more closely resembling mRNA levels of NIH3T3 fibroblasts. While the epithelial marker expression in imLECs is similar to native lens epithelial cells, the expression of mesenchymal/fibroblast markers is elevated, including Fn and Col1. Based on these gene expression findings, caution must be exercised when using immortalized cell lines for experiments as they no longer fully resemble the native lens epithelial cells and express mesenchymal/fibroblastic markers.

Primary culture of lens epithelial cells has been performed by many different protocols on lenses from many species of animals. It is known that the isolated lens epithelial cells often lose their normal cuboidal shape, polarity, and cytoskeletal network when plated on hard tissue-culture substrates with media supplemented by FBS. Several groups have developed methods for serum-free primary culture (Wunderlich et al., 1994; Musil, 2012) to avoid changes and inconsistencies due to serum supplementation related to the batch of serum and the manufacturer. While it may be possible to preserve the morphology of primary culture lens epithelial cells through ECM modifications, such as laminin- or fibronectin-coated plates (Long et al., 2008; VanSlyke et al., 2018) or cultures on the native lens capsule (Campbell and McAvoy, 1984; McAvoy and Fernon, 1984; Nagineni and Bhat, 1988; 1989b; a;Saika et al., 2002; Wernecke et al., 2018), and through TGFβ inhibition (Wang et al., 2017),

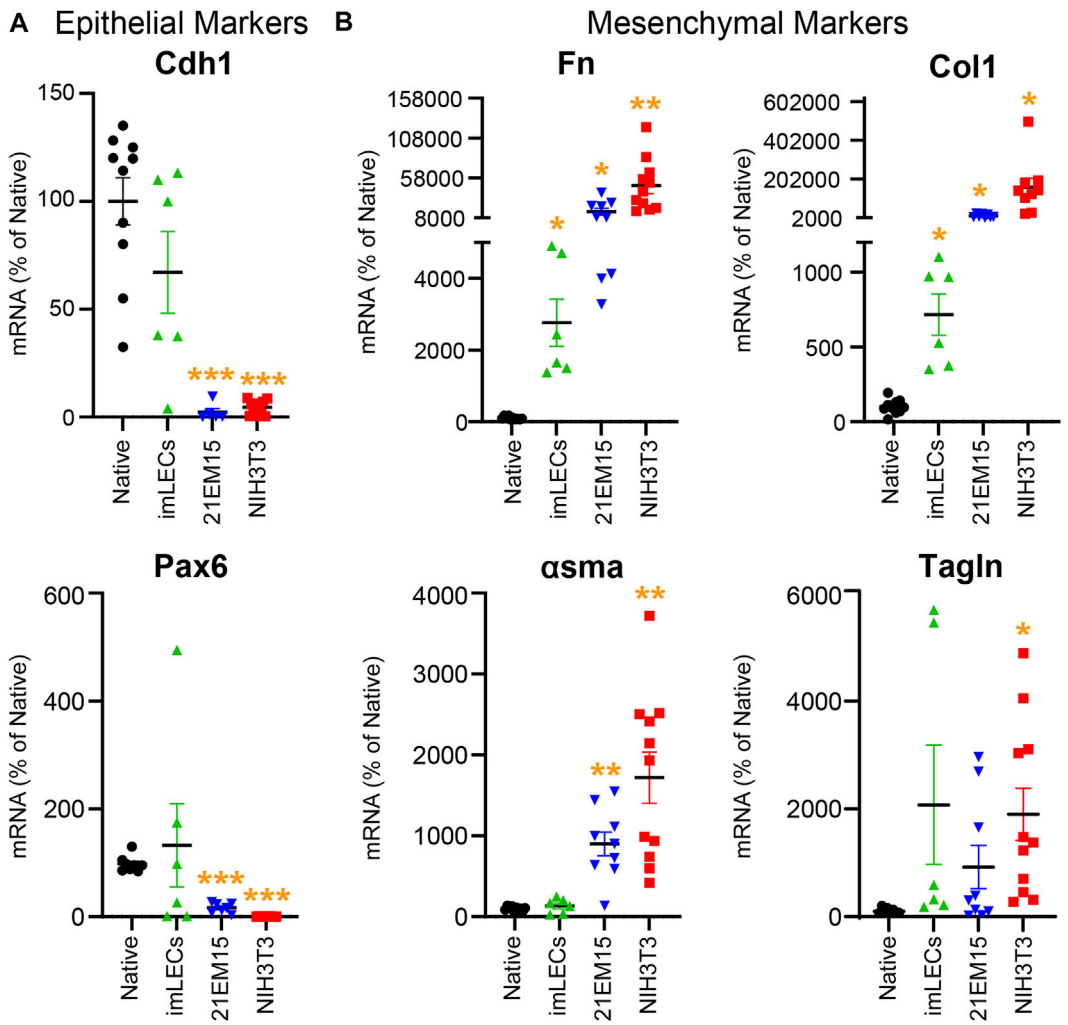


FIGURE 5
Analysis comparing the mRNA levels isolated from native mouse lens epithelial cells (Native), mouse immortalized lens epithelial cells (imLECs and 21EM15), and mouse fibroblasts (NIH3T3). **(A)** mRNA levels for the lens epithelial cell marker genes cadherin-1 (Cdh1) and paired box 6 (Pax6). While the imLEC cell line had no significant difference in the expression for epithelial cell markers compared to native cells, 21EM15 and NIH3T3 cells had significantly lower expression of epithelial cells markers than native lens epithelial cells. **(B)** mRNA levels for the mesenchymal/fibroblastic marker genes fibronectin (Fn), collagen-1 (Col1), α-smooth muscle actin (αsma), and transgelin (Tagln). The imLEC cell line had elevated expression for Fn and Col1 when compared to that of native lens epithelial cells. Both the 21EM15 and NIH3T3 cell lines had greater mesenchymal characteristics with substantially reduced epithelial marker mRNA levels and highly elevated mesenchymal/fibroblast marker mRNA levels. Dot plots show the average and standard error of mean. Individual genes were normalized to 18S. The mRNA levels were calculated using delta−delta Ct method and expressed as a percentage of native lens epithelial cell controls. *, $p < 0.05$; **, $p < 0.01$; ***, $p < 0.001$.

researchers should conduct a detailed study of RNA expression and cytoskeleton architecture, as we discuss below, before using cultured cells as models for native cells.

Though several issues make studying the primary culture or immortalized lens epithelial cells not an ideal representation for native lens epithelial cells, primary culture cells can be an excellent tool to understand the growth and behavior of transformed epithelial cells that occur during posterior capsular opacification (PCO) following cataract surgery. For PCO research, primary culture cells plated on various intraocular lens (IOL) materials could reveal methods to prevent unwanted cell adhesion onto the surface of IOLs that are inserted during cataract surgery to replace the native lens. Several groups have also cultured primary lens epithelial cells on the lens capsule to maintain a normal ECM environment and mimic the proliferation and migration of the epithelial cells after cataract surgery onto the posterior lens capsule (Liu et al., 1996; Wormstone et al., 1997; Saxby et al., 1998; Futter et al., 2005; Zelenka et al., 2009; Andjelic et al., 2014; Sundelin et al., 2014;

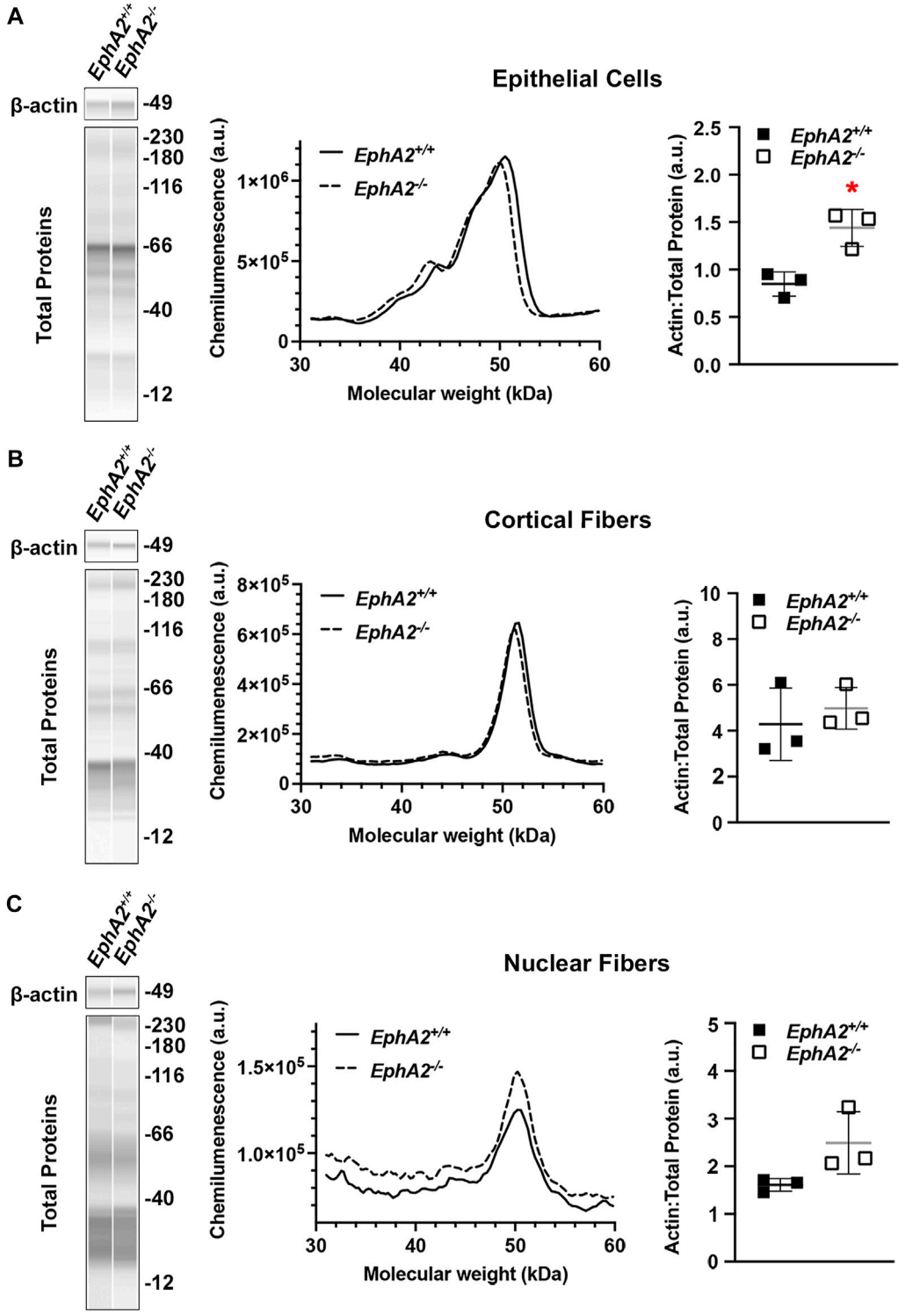


FIGURE 6
Analysis of epithelial, cortical fiber, and nuclear fiber protein samples by capillary electrophoresis. Representative gel bands for β-actin (~49 kDa) and total protein profiles (12–230 kDa) from each fraction are presented in pseudo-lane views. Normal wild-type (+/+) control lenses are compared to knockout (−/−) lenses. All mice were littermates and 4 months old. **(A)** Representative electropherogram of β-actin peaks from the epithelial cell fraction is plotted for control (+/+) and knockout (−/−) samples. The β-actin protein amount normalized to total protein is plotted on the dot plots with lines showing the average and standard deviation. The knockout samples showed increased amount of β-actin in the epithelial cells. *, $p < 0.05$. **(B,C)** Representative electropherograms of β-actin in cortical fibers and nuclear fibers from control and knockout lenses. Dot plots show the average and standard deviation for the normalized amount of β-actin in each sample. There is no difference in β-actin levels in control vs. knockout lenses in the cortical fiber and nuclear fiber fractions.

Luft et al., 2015; Recek et al., 2016). Thus, while the use of primary culture or immortalized epithelial cells is not an ideal model for native epithelial cells, the isolation of these cells can be used to advance our understanding of pathological changes that occur after cataract surgery and may be an appropriate model for testing new PCO treatments.

## Protein separation *via* capillary electrophoresis

Traditional methods for Western blotting using SDS-PAGE gels and membrane transfer require high protein concentrations (>15–20 μg/μL) and volume of sample (15–20 μL). The monolayers of lens epithelial cells yield relatively low protein concentration, and thus, excessive numbers of lens epithelial cell samples would need to be pooled together to run traditional Western blots. The capillary electrophoresis systems (JESS/WES) by ProteinSimple have made it possible to utilize a pair of lens epithelial cell samples to test several (3–5) antibodies (Parreno et al., 2020; Cheng et al., 2022). We recently published our results for detecting EphA2 in whole lenses, lens epithelial cells, cortical fiber cells, and the lens nucleus using this method (Cheng et al., 2022), and we demonstrate in Figure 6 that the same method can be applied to determine the levels of β-actin different compartments of the lens. Protein lysates from other monolayers of cells in the eye, including the corneal endothelium (Ogando et al., 2021; Shyam et al., 2021), retinal pigmented epithelial cells (Vessey et al., 2022), and from embryonic lens samples (Gheyas et al., 2022), can also be used on this platform.

In this protocol, we have also included the method to prepare the cortical fiber cell and nuclear fiber cell protein lysates (Figures 3, 6). For nuclear fiber lysates, pilot studies may be needed to determine the normal size of the lens nucleus to estimate the duration of vortexing to remove all cortical fiber cells. To serve as a guide, we have previously measured the lens nucleus size in C57BL/6 J wild-type lenses from mice of various ages (Cheng et al., 2019). The nucleus of rodent lenses is firm and can be easily removed by mechanical disruption (Cheng et al., 2016). For mutant lenses that may have compromised fiber cells, lens nucleus separation may be more challenging and require careful handling (Cheng et al., 2022). In those cases where the lens nucleus cannot be easily removed, the entire lens cell mass may be homogenized together in the Dounce homogenizer for a total fiber cell fraction.

Assay design and optimization of protein and antibody concentrations are required to produce the best results. ProteinSimple offers free video tutorials on assay design, plate loading, and detailed data analysis through the BioTechne Academy (https://academy.bio-techne.com/learn/signin). In general, we would recommend titration of every new antibody with appropriate negative control when possible and utilization of the total protein detection kits as the loading control. Using the total protein detection as the loading control avoids arbitrary designation of a housekeeping protein that may be inadvertently and/or unknowingly be altered between the test and control samples (Aldridge et al., 2008; Moritz, 2017; Wang et al., 2021). In the JESS system, RePlex allows for total protein to be detected after stripping and re-probing steps within the same capillary used for target detection. This allows for protein signal normalization within each capillary to minimize loading and sample preparation variability.

## Visualizing of lens epithelial cell structures in cell culture, flat, and whole mounts

Visualization of cell proteins/structure in primary and immortalized lens epithelial cells is possible using traditional fluorescence immunostaining techniques (Figure 7A). However, primary and immortalized lens epithelial cell shape and cytoskeletal structure are markedly different from native lens epithelial as visualized by flat (Figure 8) or whole mounting (Figure 7B). Unlike native lens epithelial cells, cultured primary and immortalized epithelial cells are no longer attached to one another. Furthermore, cultured epithelial cells contain F-actin organized into stress fibers unlike native lens epithelial cells, further supporting the notion that cultured lens epithelial cells have fibroblastic characteristics (Parreno et al., 2020).

The monolayer of lens epithelial cells is difficult to visualize in the lens tissue sections as we can only visualize a cross section of those cells. Lens capsule flat mounts with attached epithelial cells and a thin layer of peripheral lens fibers allow for examination of the entire monolayer of epithelial cells from different areas of the lens, anterior cells, proliferating equatorial cells, and differentiating equatorial cells that are packed into meridional rows (Figure 8). This method permits the study of the basal surface adjacent to the lens capsule, the lateral membrane between the epithelial cells, and the apical surface juxtaposed by the apical tips of newly formed lens fibers. The anterior epithelial cells are cobblestone in cross section, evenly spaced, and similar in size with oval nuclei. In contrast, cells closer to the lens equators are more closely packed and retain the cobblestone shape. As the equatorial epithelial cells start to differentiate, the cells become hexagon-shaped and organized into meridional rows. These cells are hexagonal on the basal lateral sides and narrow to the point at the apical surface and anchor at the fulcrum (Sugiyama et al., 2009) or modiolus (Zampighi et al., 2000) before continuing their elongation and differentiation programming to become lens fiber cells.

Flat mount preparations do not always have continuous and wrinkle-free regions, and thus, using the epithelial cell shape and arrangement as a guide is an important visual landmark to determine the approximate region of the epithelial monolayer being observed. A consideration when

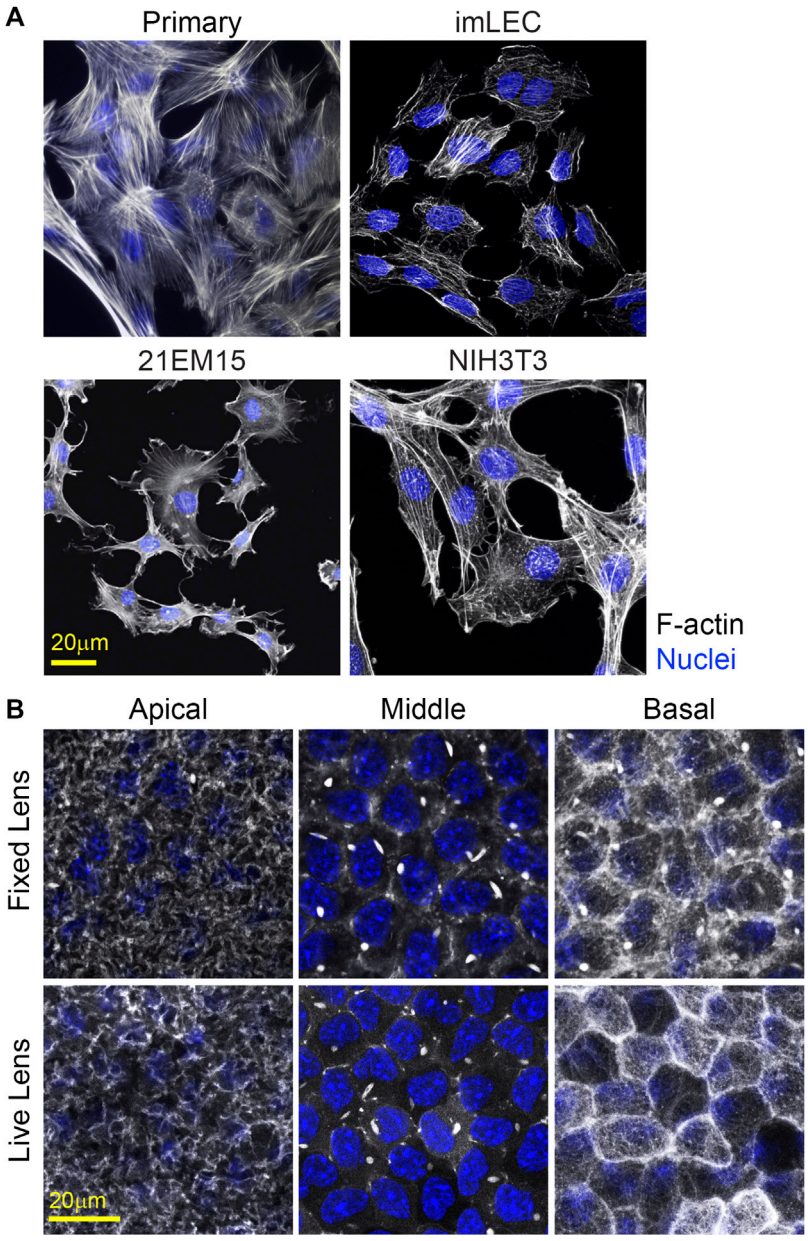


FIGURE 7
F-actin staining for cultured cells and in whole mount imaging of F-actin in fixed and unfixed lenses. **(A)** Cells were stained for F-actin (light gray) and nuclei (blue). Primary lens epithelial cells cultured after 7 days of initial seeding on glass dishes contain stress fibers similar to imLECS, 21EM15, and NIH3T3 cells in culture. **(B)** C57BL/6J wild-type fixed mouse lenses or LifeAct-GFP transgenic unfixed mouse lenses imaged for F-actin (light gray) and nuclei (blue). Fixed lenses (wild-type) were stained for F-actin using phalloidin, while unfixed lenses expressed LifeAct-GFP, allowing for visualization of F-actin directly. The epithelial cells nuclei in both fixed and unfixed lenses were stained with Hoechst. Images shown are of single optical slices. Both fixed and unfixed lens anterior epithelial cells had similar basal reticular F-actin organization with limited stress fibers. At the middle region in the lateral sides of these cuboidal cells, F-actin is at cell–cell junctions and within the bright structures called sequestered actin bundles (SABs). The basal region of fixed lens epithelial cells differed from that in unfixed lenses. In the unfixed lens, the basal region of lens epithelial cells had polygonal actin arrays, while, in the fixed lens, the polygonal arrays appear disrupted on the basal surface of these epithelial cells. Furthermore, SABs were present in the basal region of fixed lens epithelial cells. Scale bars, 20 μm.

collecting Z-stacks through epithelial cells is axial distortion (Smith et al., 2018). Oversampling in the *Z*-axis is needed to correct the stretch distortion for proper 3D reconstructions (Smith et al., 2018). Flat mount preparations from rat, pig, or human lenses have also been prepared by pinning the capsule with epithelial cells into a flat plate (Zelenka et al., 2009; Wu

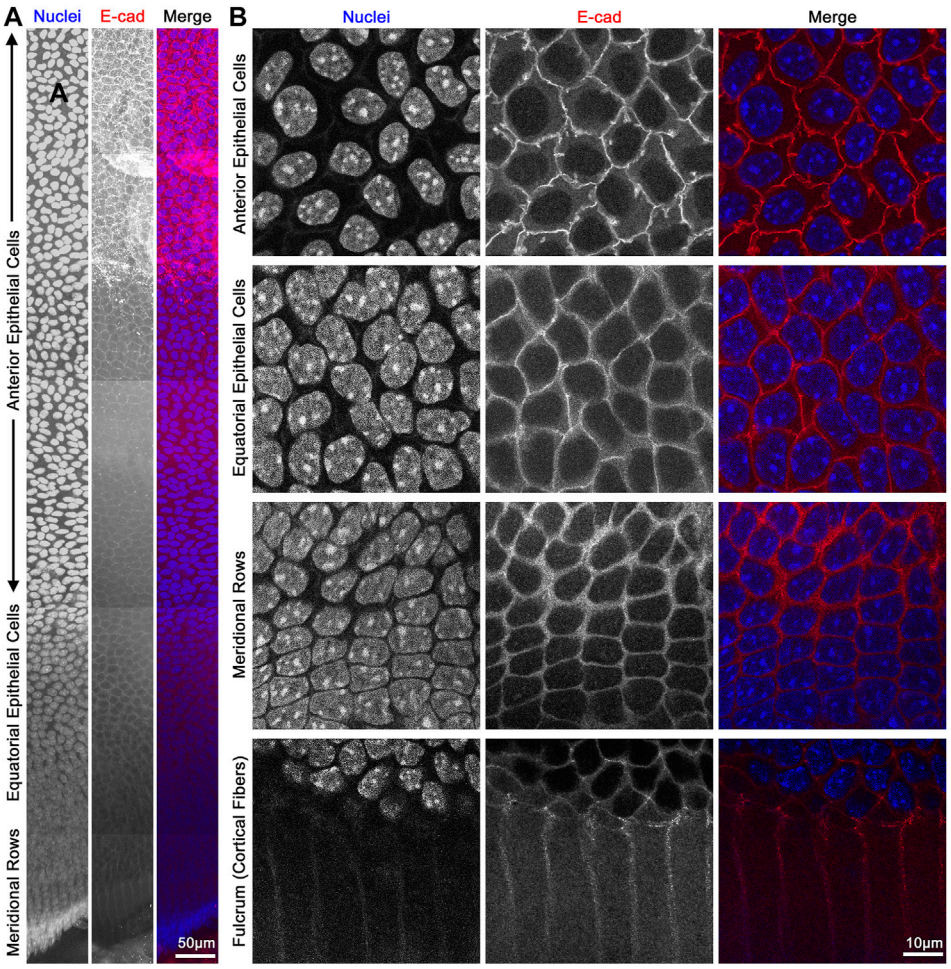


FIGURE 8
Flat mount of lens epithelial cell monolayer. **(A)** Lens capsule flat mount was stained for E-cadherin (red) and nuclei (blue). Tiled Z-stack scans from the anterior (top) to the meridional rows at the equator (bottom) were stitched, and this image is a maximum intensity projection of the stitched Z-stacks compressed into a 2D image. Scale bar, 50 μm. **(B)** Magnified images of epithelial cells from different regions of the lens. As expected, E-cadherin outlines the membrane of the epithelial cells and has reduced signals after epithelial cells differentiate into fiber cells at the lens fulcrum. It should be noted that the spacing of the nuclei changes slightly between anterior vs. equatorial epithelial cells. Scale bar, 10 μm.

et al., 2015; Kumar et al., 2019). But in our experience, it is difficult to pin the capsule to a plate with small mouse lenses, and fixation of mouse lenses with paraformaldehyde and then peeling the lens capsule result in thin and completely transparent samples that are fragile and easily damaged during the immunostaining process. There are examples of capsular preparation from mouse lenses where small pieces of the lens capsule are adhered to poly-lysine-coated slides (Liou and Rafferty, 1988; Rafferty and Scholz, 1989). These preparations, however, would only allow the study of small regions of the epithelial monolayer.

Drawbacks of flat mounts include the loss of 3D structure of the lens and the disruption of apical–apical epithelial-to-fiber cell connections due to mechanical dissection. An alternate method to visualize lens epithelial cell structures is to perform whole lens staining. Small dyes, including wheat germ agglutinin (WGA) or phalloidin, can penetrate the lens to stain cell membranes or F-actin network, respectively (Cheng et al., 2013; Parreno et al., 2018; Cheng et al., 2019). However, large antibodies do not readily penetrate the lens capsule. We have previously detailed a method to immunostain the whole lens after incubation in collagenase to partially digest the lens capsule and facilitate antibody penetration (Patel et al., 2021). Whole mount staining maintains the 3D structure of tissue, but imaging whole mount lenses requires repositioning of the lens to visualize the various regions of the epithelium. Excessive disruption of the lens capsule for antibody labeling may alter the basal surface of lens epithelial cells and lead to cellular disorganization (Patel et al., 2021).

An alternative to imaging of fixed and stained lenses is performing confocal imaging on unfixed lenses. Previously, we

examined the effect of whole lens compression on epithelial morphology using lenses from mice that express tdTomato, which localizes to cellular membranes (Parreno et al., 2018). In this study, we extend our unfixed lens imaging to visualization of cytoskeletal F-actin structures using lenses from LifeAct-GFP transgenic mice. F-actin networks in unfixed epithelial cells in transgenic LifeAct-GFP lenses resemble those of fixed whole lenses stained with phalloidin (Figure 7B). However, the fixation may affect cell structures and disrupt the F-actin network. For instance, in fixed whole lenses, the sequestered actin bundles (SABs) (Rafferty and Scholz, 1984; Rafferty, 1985; Rafferty and Scholz, 1985; Scholz and Rafferty, 1988; Rafferty and Scholz, 1989; Rafferty et al., 1990) are bright structures that appear at the basolateral regions of the lens epithelial cells. In contrast, SABs are only found in the lateral (middle) regions of the unfixed lenses. Thus, the fixation conditions for whole lens imaging may need to be optimized to best preserve the native cell morphology and cytoskeletal arrangements.

## Conclusion

Even though the monolayer of epithelial cells in the lens forms just a small fraction of the entire lens tissue, it plays a principal role in lifelong lens growth and pathological conditions (i.e., PCO formation after cataract surgery). The protocols described here can facilitate the enrichment of epithelial RNA and protein, allowing for the study of molecular expression without pooling of large numbers of lenses. The protocols will need further refinement to increase the RIN for RNA-seq experiments, and future developments in technology may allow proteomic analysis on low volume epithelial cell protein lysates. Furthermore, the imaging techniques will permit investigations of the lens epithelial cellular structure in flat mounts, fixed lenses, or unfixed lenses, which more faithfully retain the native lens epithelial cell structure. The development of new transgenic mouse lines with fluorescent markers may allow more detailed imaging of unfixed whole lenses. Future studies may also compare ultrastructure information from electron microscopy images with whole lens or flat mount staining. Our detailed protocols allow for the study of native epithelial cell biology and the mechanistic role(s) they play in pathologies.

## Data availability statement

The raw data supporting the conclusion of this article will be made available by the authors, without undue reservation.

## Ethics statement

The animal study was reviewed and approved by the University of Delaware/Indiana University IACUC.

## Author contributions

JTC, SA, and SDP conducted experiments, prepared figures, and read, edited, and approved the manuscript. JP, GE, MPV, and CC conducted experiments, prepared figures, and wrote and edited the manuscript.

## Funding

This work was supported by the National Eye Institute Grant R01 EY032056 to CC and R01 EY017724 (to VMF and co-investigator JP) as well as the National Institute of General Medical Sciences under grant number P20GM139760.

## Acknowledgments

The authors thank Subashree Murugan for assistance with illustrations and Rylee King for her critical reading of the manuscript. The authors also thank Drs. Velia M. Fowler and Xiaohua Gong for their input in the original development of these protocols.

## Conflict of interest

The authors declare that the research was conducted in the absence of any commercial or financial relationships that could be construed as a potential conflict of interest.

The reviewer DS declared a shared affiliation with the author SA to the handling editor at the time of review.

## Publisher's note



## Supplementary material

The Supplementary Material for this article can be found online at: https://www.frontiersin.org/articles/10.3389/fcell.2022.983178/full#supplementary-material

# References


Aldridge, G. M., Podrebarac, D. M., Greenough, W. T., and Weiler, I. J. (2008). The use of total protein stains as loading controls: an alternative to high-abundance single-protein controls in semi-quantitative immunoblotting. *J. Neurosci. Methods* 172, 250–254. doi:10.1016/j.jneumeth.2008.05.003

Andjelic, S., Lumi, X., Vereb, Z., Josifovska, N., Facsko, A., Hawlina, M., et al. (2014). A simple method for establishing adherent *ex vivo* explant cultures from human eye pathologies for use in subsequent calcium imaging and inflammatory studies. *J. Immunol. Res.* 2014, 232659. doi:10.1155/2014/232659

Andley, U. P., Song, Z., Wawrousek, E. F., and Bassnett, S. (1998). The molecular chaperone alphaA-crystallin enhances lens epithelial cell growth and resistance to UVA stress. *J. Biol. Chem.* 273, 31252–31261. doi:10.1074/jbc.273.47.31252

Bannik, K., Rossler, U., Faus-Kessler, T., Gomolka, M., Hornhardt, S., Dalke, C., et al. (2013). Are mouse lens epithelial cells more sensitive to gamma-irradiation than lymphocytes? *Radiat. Environ. Biophys.* 52, 279–286. doi:10.1007/s00411-012-0451-8

Bassnett, S., Missey, H., and Vucemilo, I. (1999). Molecular architecture of the lens fiber cell basal membrane complex. *J. Cell Sci.* 112 (13), 2155–2165. doi:10.1242/jcs.112.13.2155

Bassnett, S., Shi, Y., and Vrensen, G. F. (2011). Biological glass: structural determinants of eye lens transparency. *Philos. Trans. R. Soc. Lond. B Biol. Sci.* 366, 1250–1264. doi:10.1098/rstb.2010.0302

Bermbach, G., Mayer, U., and Naumann, G. O. (1991). Human lens epithelial cells in tissue culture. *Exp. Eye Res.* 52, 113–119. doi:10.1016/0014-4835(91)90251-9

Campbell, M. T., and Mcavoy, J. W. (1984). Onset of fibre differentiation in cultured rat lens epithelium under the influence of neural retina-conditioned medium. *Exp. Eye Res.* 39, 83–94. doi:10.1016/0014-4835(84)90117-9

Cheng, C., Ansari, M. M., Cooper, J. A., and Gong, X. (2013). EphA2 and Src regulate equatorial cell morphogenesis during lens development. *Development* 140, 4237–4245. doi:10.1242/dev.100727

Cheng, C., Fowler, V. M., and Gong, X. (2017). EphA2 and ephrin-A5 are not a receptor-ligand pair in the ocular lens. *Exp. Eye Res.* 162, 9–17. doi:10.1016/j.exer.2017.06.016

Cheng, C., Gokhin, D. S., Nowak, R. B., and Fowler, V. M. (2016). Sequential application of glass coverslips to assess the compressive stiffness of the mouse lens: Strain and morphometric analyses. *J. Vis. Exp.* (111), 53986. doi:10.3791/53986

Cheng, C., and Gong, X. (2011). Diverse roles of Eph/ephrin signaling in the mouse lens. *PLoS One* 6, e28147. doi:10.1371/journal.pone.0028147

Cheng, C., Nowak, R. B., Amadeo, M. B., Biswas, S. K., Lo, W. K., and Fowler, V. M. (2018). Tropomyosin 3.5 protects the F-actin networks required for tissue biomechanical properties. *J. Cell Sci.* 131, jcs222042. doi:10.1242/jcs.222042

Cheng, C., Parreno, J., Nowak, R. B., Biswas, S. K., Wang, K., Hoshino, M., et al. (2019). Age-related changes in eye lens biomechanics, morphology, refractive index and transparency. *Aging (Albany NY)* 11, 12497–12531. doi:10.18632/aging.102584

Cheng, C., Wang, K., Hoshino, M., Uesugi, K., Yagi, N., and Pierscionek, B. (2022). EphA2 affects development of the eye lens nucleus and the gradient of refractive index. *Invest. Ophthalmol. Vis. Sci.* 63, 2. doi:10.1167/iovs.63.1.2

Creighton, M. O., Mousa, G. Y., and Trevithick, J. R. (1976). Differentiation of rat lens epithelial cells in tissue culture. (I) Effects of cell density, medium and embryonic age of initial culture. *Differentiation.* 6, 155–167. doi:10.1111/j.1432-0436.1976.tb01482.x

De Maria, A., Shi, Y., Kumar, N. M., and Bassnett, S. (2009). Calpain expression and activity during lens fiber cell differentiation. *J. Biol. Chem.* 284, 13542–13550. doi:10.1074/jbc.M900561200

Fitzgerald, P. G., and Goodenough, D. A. (1986). Rat lens cultures: MIP expression and domains of intercellular coupling. *Invest. Ophthalmol. Vis. Sci.* 27, 755–771.

Fleige, S., and Pfaffl, M. W. (2006). RNA integrity and the effect on the real-time qRT-PCR performance. *Mol. Asp. Med.* 27, 126–139. doi:10.1016/j.mam.2005.12.003

Futter, C. E., Crowston, J. G., and Allan, B. D. (2005). Interaction with collagen IV protects lens epithelial cells from Fas-dependent apoptosis by stimulating the production of soluble survival factors. *Invest. Ophthalmol. Vis. Sci.* 46, 3256–3262. doi:10.1167/iovs.05-0086

Gheyas, R., Ortega-Alvarez, R., Chauss, D., Kantorow, M., and Menko, A. S. (2022). Suppression of PI3K signaling is linked to autophagy activation and the spatiotemporal induction of the lens organelle free zone. *Exp. Cell Res.* 412, 113043. doi:10.1016/j.yexcr.2022.113043

Gokhin, D. S., Nowak, R. B., Kim, N. E., Arnett, E. E., Chen, A. C., Sah, R. L., et al. (2012). Tmod1 and CP49 synergize to control the fiber cell geometry, transparency, and mechanical stiffness of the mouse lens. *PLoS One* 7, e48734. doi:10.1371/journal.pone.0048734

Gong, X., Li, E., Klier, G., Huang, Q., Wu, Y., Lei, H., et al. (1997). Disruption of alpha3 connexin gene leads to proteolysis and cataractogenesis in mice. *Cell* 91, 833–843. doi:10.1016/s0092-8674(00)80471-7

Hamada, Y., and Okada, T. S. (1978). *In vitro* differentiation of cells of the lens epithelium of human fetus. *Exp. Eye Res.* 26, 91–97. doi:10.1016/0014-4835(78)90156-2

Ibaraki, N., Chen, S. C., Lin, L. R., Okamoto, H., Pipas, J. M., and Reddy, V. N. (1998). Human lens epithelial cell line. *Exp. Eye Res.* 67, 577–585. doi:10.1006/exer.1998.0551

Kirby, D. B. (1927). The cultivation of lens epithelium *in vitro*. *J. Exp. Med.* 45, 1009–1016. doi:10.1084/jem.45.6.1009

Kumar, B., Chandler, H. L., Plageman, T., and Reilly, M. A. (2019). Lens stretching modulates lens epithelial cell proliferation via YAP regulation. *Invest. Ophthalmol. Vis. Sci.* 60, 3920–3929. doi:10.1167/iovs.19-26893

Kuszak, J. R., Zoltoski, R. K., and Sivertson, C. (2004). Fibre cell organization in crystalline lenses. *Exp. Eye Res.* 78, 673–687. doi:10.1016/j.exer.2003.09.016

Liou, W., and Rafferty, N. S. (1988). Actin filament patterns in mouse lens epithelium: a study of the effects of aging, injury, and genetics. *Cell Motil. Cytoskelet.* 9, 17–29. doi:10.1002/cm.970090104

Liu, C. S., Wormstone, I. M., Duncan, G., Marcantonio, J. M., Webb, S. F., and Davies, P. D. (1996). A study of human lens cell growth *in vitro*. A model for posterior capsule opacification. *Invest. Ophthalmol. Vis. Sci.* 37, 906–914.

Lo, W. K. (1989). Visualization of crystallin droplets associated with cold cataract formation in young intact rat lens. *Proc. Natl. Acad. Sci. U. S. A.* 86, 9926–9930. doi:10.1073/pnas.86.24.9926

Long, A. C., Agler, A., Colitz, C. M., Zhang, J., Hayek, M. G., Failla, M. L., et al. (2008). Isolation and characterization of primary canine lens epithelial cells. *Vet. Ophthalmol.* 11, 38–42. doi:10.1111/j.1463-5224.2007.00599.x

Lovicu, F. J., and Robinson, M. L. (2004). *Development of the ocular lens*. Cambridge, UK ; New York: Cambridge University Press.

Luft, N., Kreutzer, T. C., Dirisamer, M., Priglinger, C. S., Burger, J., Findl, O., et al. (2015). Evaluation of laser capsule polishing for prevention of posterior capsule opacification in a human *ex vivo* model. *J. Cataract. Refract. Surg.* 41, 2739–2745. doi:10.1016/j.jcrs.2015.06.039

Mamo, J. G., and Leinfelder, P. J. (1958). Growth of lens epithelium in culture. I. Characteristics of growth. *AMA. Arch. Ophthalmol.* 59, 417–419. doi:10.1001/archopht.1958.00940040123014

Mann, I. (1948). Tissue cultures of mouse lens epithelium. *Br. J. Ophthalmol.* 32, 591–596. doi:10.1136/bjo.32.9.591

Matsuyama, M., Tanaka, H., Inoko, A., Goto, H., Yonemura, S., Kobori, K., et al. (2013). Defect of mitotic vimentin phosphorylation causes microophthalmia and cataract via aneuploidy and senescence in lens epithelial cells. *J. Biol. Chem.* 288, 35626–35635. doi:10.1074/jbc.M113.514737

Mcavoy, J. W., and Fernon, V. T. (1984). Neural retinas promote cell division and fibre differentiation in lens epithelial explants. *Curr. Eye Res.* 3, 827–834. doi:10.3109/02713688409000795

Menko, A. S., Klukas, K. A., and Johnson, R. G. (1984). Chicken embryo lens cultures mimic differentiation in the lens. *Dev. Biol.* 103, 129–141. doi:10.1016/0012-1606(84)90014-9

Moritz, C. P. (2017). Tubulin or not tubulin: Heading toward total protein staining as loading control in western blots. *Proteomics* 17, 1600189. doi:10.1002/pmic.201600189

Musil, L. S., Beyer, E. C., and Goodenough, D. A. (1990). Expression of the gap junction protein connexin43 in embryonic chick lens: molecular cloning, ultrastructural localization, and post-translational phosphorylation. *J. Membr. Biol.* 116, 163–175. doi:10.1007/BF01868674

Musil, L. S. (2012). Primary cultures of embryonic chick lens cells as a model system to study lens gap junctions and fiber cell differentiation. *J. Membr. Biol.* 245, 357–368. doi:10.1007/s00232-012-9458-y

Nagineni, C. N., and Bhat, S. P. (1989a). Alpha B-crystallin is expressed in kidney epithelial cell lines and not in fibroblasts. *FEBS Lett.* 249, 89–94. doi:10.1016/0014-5793(89)80022-5

Nagineni, C. N., and Bhat, S. P. (1989b). Human fetal lens epithelial cells in culture: an *in vitro* model for the study of crystallin expression and lens differentiation. *Curr. Eye Res.* 8, 285–291. doi:10.3109/02713688908997570

Nagineni, C. N., and Bhat, S. P. (1988). Maintenance of the synthesis of alpha B-crystallin and progressive expression of beta Bp-crystallin in human fetal lens epithelial cells in culture. *Dev. Biol.* 130, 402–405. doi:10.1016/0012-1606(88)90446-0

Nowak, R. B., Fischer, R. S., Zoltoski, R. K., Kuszak, J. R., and Fowler, V. M. (2009). Tropomodulin1 is required for membrane skeleton organization and hexagonal geometry of fiber cells in the mouse lens. *J. Cell Biol.* 186, 915–928. doi:10.1083/jcb.200905065

Ogando, D. G., Shyam, R., Kim, E. T., Wang, Y. C., Liu, C. Y., and Bonanno, J. A. (2021). Inducible Slc4a11 knockout triggers corneal edema through perturbation of corneal endothelial pump. *Invest. Ophthalmol. Vis. Sci.* 62, 28. doi:10.1167/iovs.62.7.28

Ogiso, M., Takehana, M., Kobayashi, S., and Hoshi, M. (1998). Expression of sialylated Lewisx gangliosides in cultured lens epithelial cells from rhesus monkey. *Exp. Eye Res.* 66, 765–773. doi:10.1006/exer.1998.0489

Okada, T. S., Eguchi, G., and Takeichi, M. (1971). The expression of differentiation by chicken lens epithelium in *in vitro* cell culture. *Dev. Growth Differ.* 13, 323–336. doi:10.1111/j.1440-169x.1971.00323.x

Parreno, J., Amadeo, M. B., Kwon, E. H., and Fowler, V. M. (2020). Tropomyosin 3.1 association with actin stress fibers is required for lens epithelial to mesenchymal transition. *Invest. Ophthalmol. Vis. Sci.* 61, 2. doi:10.1167/iovs.61.6.2

Parreno, J., Cheng, C., Nowak, R. B., and Fowler, V. M. (2018). The effects of mechanical strain on mouse eye lens capsule and cellular microstructure. *Mol. Biol. Cell* 29, 1963–1974. doi:10.1091/mbc.E18-01-0035

Patel, S. D., Aryal, S., Mennetti, L. P., and Parreno, J. (2021). Whole mount staining of lenses for visualization of lens epithelial cell proteins. *MethodsX* 8, 101376. doi:10.1016/j.mex.2021.101376

Piatigorsky, J. (1981). Lens differentiation in vertebrates. A review of cellular and molecular features. *Differentiation.* 19, 134–153. doi:10.1111/j.1432-0436.1981.tb01141.x

Pierscionek, B., and Augusteyn, R. C. (1988). Protein distribution patterns in concentric layers from single bovine lenses: changes with development and ageing. *Curr. Eye Res.* 7, 11–23. doi:10.3109/02713688809047015

Rafferty, N. S. (1985). *Lens morphology*. New York: Dekker.

Rafferty, N. S., and Scholz, D. L. (1985). Actin in polygonal arrays of microfilaments and sequestered actin bundles (SABs) in lens epithelial cells of rabbits and mice. *Curr. Eye Res.* 4, 713–718. doi:10.3109/02713688509017667

Rafferty, N. S., and Scholz, D. L. (1989). Comparative study of actin filament patterns in lens epithelial cells. Are these determined by the mechanisms of lens accommodation? *Curr. Eye Res.* 8, 569–579. doi:10.3109/02713688908995756

Rafferty, N. S., Scholz, D. L., Goldberg, M., and Lewyckyj, M. (1990). Immunocytochemical evidence for an actin-myosin system in lens epithelial cells. *Exp. Eye Res.* 51, 591–600. doi:10.1016/0014-4835(90)90090-h

Rafferty, N. S., and Scholz, D. L. (1984). Polygonal arrays of microfilaments in epithelial cells of the intact lens. *Curr. Eye Res.* 3, 1141–1149. doi:10.3109/02713688409000814

Recek, N., Andjelic, S., Hojnik, N., Filipic, G., Lazovic, S., Vesel, A., et al. (2016). Microplasma induced cell morphological changes and apoptosis of *ex vivo* cultured human anterior lens epithelial cells - relevance to capsular opacification. *PLoS One* 11, e0165883. doi:10.1371/journal.pone.0165883

Reddan, J. R., Friedman, T. B., Mostafapour, M. K., Sutherland, S. H., Bondy, R. L., Mcgee, S. J., et al. (1980). Establishment of epithelial cell lines from individual rabbit lenses. *J. tissue Cult. methods* 6, 57–60. doi:10.1007/bf01666017

Reddan, J. R., Kuck, J. F., Dziedzic, D. C., Kuck, K. D., Reddan, P. R., and Wasielewski, P. (1989). Establishment of lens epithelial cell lines from Emory and cataract resistant mice and their response to hydrogen peroxide. *Lens Eye Toxic. Res.* 6, 687–701. doi:10.1007/BF01666017

Reno, C., Marchuk, L., Sciore, P., Frank, C., and Hart, D. A. (1997). Rapid isolation of total RNA from small samples of hypocellular, dense connective tissues. *Biotechniques* 22, 1082–1086. doi:10.2144/97226bm16

Saika, S., Miyamoto, T., Ishida, I., Shirai, K., Ohnishi, Y., Ooshima, A., et al. (2002). TGFbeta-Smad signalling in postoperative human lens epithelial cells. *Br. J. Ophthalmol.* 86, 1428–1433. doi:10.1136/bjo.86.12.1428

Saxby, L., Rosen, E., and Boulton, M. (1998). Lens epithelial cell proliferation, migration, and metaplasia following capsulorhexis. *Br. J. Ophthalmol.* 82, 945–952. doi:10.1136/bjo.82.8.945

Scholz, D. L., and Rafferty, N. S. (1988). Immunogold-EM localization of actin and vimentin filaments in relation to polygonal arrays in lens epithelium *in situ*. *Curr. Eye Res.* 7, 705–719. doi:10.3109/02713688809033200

Schroeder, A., Mueller, O., Stocker, S., Salowsky, R., Leiber, M., Gassmann, M., et al. (2006). The RIN: an RNA integrity number for assigning integrity values to RNA measurements. *BMC Mol. Biol.* 7, 3. doi:10.1186/1471-2199-7-3

Shi, Y., De Maria, A., Lubura, S., Sikic, H., and Bassnett, S. (2014). The penny pusher: a cellular model of lens growth. *Invest. Ophthalmol. Vis. Sci.* 56, 799–809. doi:10.1167/iovs.14-16028

Shyam, R., Ogando, D. G., Choi, M., Liton, P. B., and Bonanno, J. A. (2021). Mitochondrial ROS induced lysosomal dysfunction and autophagy impairment in an animal model of congenital hereditary endothelial dystrophy. *Invest. Ophthalmol. Vis. Sci.* 62, 15. doi:10.1167/iovs.62.12.15

Smith, A. S., Nowak, R. B., and Fowler, V. M. (2018). High-resolution fluorescence microscope imaging of erythroblast structure. *Methods Mol. Biol.* 1698, 205–228. doi:10.1007/978-1-4939-7428-3_12

Sugiyama, Y., Akimoto, K., Robinson, M. L., Ohno, S., and Quinlan, R. A. (2009). A cell polarity protein aPKClambda is required for eye lens formation and growth. *Dev. Biol.* 336, 246–256. doi:10.1016/j.ydbio.2009.10.010

Sugiyama, Y., Stump, R. J., Nguyen, A., Wen, L., Chen, Y., Wang, Y., et al. (2010). Secreted frizzled-related protein disrupts PCP in eye lens fiber cells that have polarised primary cilia. *Dev. Biol.* 338, 193–201. doi:10.1016/j.ydbio.2009.11.033

Sundelin, K., Petersen, A., Soltanpour, Y., and Zetterberg, M. (2014). *In vitro* growth of lens epithelial cells from cataract patients - association with possible risk factors for posterior capsule opacification. *Open Ophthalmol. J.* 8, 19–23. doi:10.2174/1874364101408010019

Terrell, A. M., Anand, D., Smith, S. F., Dang, C. A., Waters, S. M., Pathania, M., et al. (2015). Molecular characterization of mouse lens epithelial cell lines and their suitability to study RNA granules and cataract associated genes. *Exp. Eye Res.* 131, 42–55. doi:10.1016/j.exer.2014.12.011

Van Der Veen, J., and Heyen, C. F. (1959). Lens cells of the calf in continuous culture. *Nature* 183, 1137–1138. doi:10.1038/1831137a0

Vanslyke, J. K., Boswell, B. A., and Musil, L. S. (2018). Fibronectin regulates growth factor signaling and cell differentiation in primary lens cells. *J. Cell Sci.* 131, jcs217240. doi:10.1242/jcs.217240

Vessey, K. A., Jobling, A. I., Tran, M. X., Wang, A. Y., Greferath, U., and Fletcher, E. L. (2022). Treatments targeting autophagy ameliorate the age-related macular degeneration phenotype in mice lacking APOE (apolipoprotein E). *Autophagy*, 1–17. doi:10.1080/15548627.2022.2034131

Wang, D., Wang, E., Liu, K., Xia, C. H., Li, S., and Gong, X. (2017). Roles of TGFβ and FGF signals during growth and differentiation of mouse lens epithelial cell *in vitro*. *Sci. Rep.* 7, 7274. doi:10.1038/s41598-017-07619-5

Wang, J. L., Li, M. Q., Zhang, J. J., and Xu, C. J. (2021). Total protein staining with Congo red as an alternative loading control for Western blot analysis. *Biotech. Histochem* 97, 1–11. doi:10.1080/10520295.2021.2008008

Wang, K., Cheng, C., Li, L., Liu, H., Huang, Q., Xia, C. H., et al. (2007). GammaD-crystallin associated protein aggregation and lens fiber cell denucleation. *Invest. Ophthalmol. Vis. Sci.* 48, 3719–3728. doi:10.1167/iovs.06-1487

Weatherbee, B. a. T., Barton, J. R., Siddam, A. D., Anand, D., and Lachke, S. A. (2019). Molecular characterization of the human lens epithelium-derived cell line SRA01/04. *Exp. Eye Res.* 188, 107787. doi:10.1016/j.exer.2019.107787

Wernecke, L., Keckeis, S., Reichhart, N., Strauss, O., and Salchow, D. J. (2018). Epithelial-mesenchymal transdifferentiation in pediatric lens epithelial cells. *Invest. Ophthalmol. Vis. Sci.* 59, 5785–5794. doi:10.1167/iovs.18-23789

Wormstone, I. M., Liu, C. S., Rakic, J. M., Marcantonio, J. M., Vrensen, G. F., and Duncan, G. (1997). Human lens epithelial cell proliferation in a protein-free medium. *Invest. Ophthalmol. Vis. Sci.* 38, 396–404.

Wu, J. J., Wu, W., Tholozan, F. M., Saunter, C. D., Girkin, J. M., and Quinlan, R. A. (2015). A dimensionless ordered pull-through model of the mammalian lens epithelium evidences scaling across species and explains the age-dependent changes in cell density in the human lens. *J. R. Soc. Interface* 12, 20150391. doi:10.1098/rsif.2015.0391

Wunderlich, K., Knorr, M., and Dartsch, P. C. (1994). Serum-free cultivation of bovine lens epithelial cells. *Graefes Arch. Clin. Exp. Ophthalmol.* 232, 355–360. doi:10.1007/BF00175987

Yamamoto, N., Majima, K., and Marunouchi, T. (2008). A study of the proliferating activity in lens epithelium and the identification of tissue-type stem cells. *Med. Mol. Morphol.* 41, 83–91. doi:10.1007/s00795-008-0395-x

Zampighi, G. A., Eskandari, S., and Kreman, M. (2000). Epithelial organization of the mammalian lens. *Exp. Eye Res.* 71, 415–435. doi:10.1006/exer.2000.0895

Zelenka, P. S., Gao, C. Y., and Saravanamuthu, S. S. (2009). Preparation and culture of rat lens epithelial explants for studying terminal differentiation. *J. Vis. Exp.* (31), 1519. doi:10.3791/1519

Zigman, S., and Lerman, S. (1964). A cold precipitable protein in the lens. *Nature* 203, 662–663. doi:10.1038/203662a0

frontiers | Frontiers in Cell and Developmental Biology

TYPE Original Research
PUBLISHED 28 October 2022
DOI 10.3389/fcell.2022.1044672



OPEN ACCESS

EDITED BY
Rajalekshmy Shyam,
Indiana University Bloomington,
United States

REVIEWED BY
Hsuan-Yeh Pan,
Indiana University Bloomington,
United States
Daisy Y. Shu,
Harvard Medical School, United States
Michelle Grunin,
Case Western Reserve University,
United States

*CORRESPONDENCE
Aparna Lakkaraju,
Aparna.Lakkaraju@ucsf.edu

SPECIALTY SECTION
This article was submitted to Signaling, a section of the journal Frontiers in Cell and Developmental Biology

RECEIVED 14 September 2022
ACCEPTED 19 October 2022
PUBLISHED 28 October 2022

CITATION
Tan LX, Li J, Germer CJ and Lakkaraju A (2022), Analysis of mitochondrial dynamics and function in the retinal pigment epithelium by high-speed high-resolution live imaging.
*Front. Cell Dev. Biol.* 10:1044672.
doi: 10.3389/fcell.2022.1044672



# Analysis of mitochondrial dynamics and function in the retinal pigment epithelium by high-speed high-resolution live imaging

Li Xuan Tan[1], Jianlong Li[2], Colin J. Germer[1,3] and Aparna Lakkaraju[1,3,4]*

[1]Department of Ophthalmology, School of Medicine, University of California, San Francisco, CA, United States, [2]Department of Cell and Tissue Biology, School of Dentistry, University of California, San Francisco, CA, United States, [3]Pharmaceutical Sciences and Pharmacogenomics Graduate Program, University of California, San Francisco, CA, United States, [4]Department of Anatomy, School of Medicine, University of California, San Francisco, CA, United States

Mitochondrial dysfunction is strongly implicated in neurodegenerative diseases including age-related macular degeneration (AMD), which causes irreversible blindness in over 50 million older adults worldwide. A key site of insult in AMD is the retinal pigment epithelium (RPE), a monolayer of postmitotic polarized cells that performs essential functions for photoreceptor health and vision. Recent studies from our group and others have identified several features of mitochondrial dysfunction in AMD including mitochondrial fragmentation and bioenergetic defects. While these studies provide valuable insight at fixed points in time, high-resolution, high-speed live imaging is essential for following mitochondrial injury in real time and identifying disease mechanisms. Here, we demonstrate the advantages of live imaging to investigate RPE mitochondrial dynamics in cell-based and mouse models. We show that mitochondria in the RPE form extensive networks that are destroyed by fixation and discuss important live imaging considerations that can interfere with accurate evaluation of mitochondrial integrity such as RPE differentiation status and acquisition parameters. Our data demonstrate that RPE mitochondria show localized heterogeneities in membrane potential and ATP production that could reflect focal changes in metabolism and oxidative stress. Contacts between the mitochondria and organelles such as the ER and lysosomes mediate calcium flux and mitochondrial fission. Live imaging of mouse RPE flatmounts revealed a striking loss of mitochondrial integrity in albino mouse RPE compared to pigmented mice that could have significant functional consequences for cellular metabolism. Our studies lay a framework to guide experimental design and selection of model systems for evaluating mitochondrial health and function in the RPE.

KEYWORDS

**mitochondria, live imaging, retina, RPE, pigmented and albino mice**

# Introduction

Mitochondria are essential signaling platforms that regulate ATP generation, calcium homeostasis, and cell fate decisions. This functional versatility is made possible by the continuous remodeling of the mitochondrial network by fusion, fission, and mitophagy, and communication with other organelles *via* membrane contacts that help the cell adapt to diverse metabolic needs (Gordaliza-Alaguero et al., 2019; Giacomello et al., 2020). Mitochondrial fission generates reactive oxygen species (ROS) and activates mitophagy whereas mitochondrial fusion into tubular networks prevents mitochondrial DNA (mtDNA) damage, improves the efficiency of oxidative phosphorylation (OXPHOS), and enhances interactions with the endoplasmic reticulum (ER) necessary for $Ca^{2+}$ flux (Giacomello et al., 2020).

In the eye, mitochondrial dysfunction is strongly associated with several diseases including inherited and age-related macular degenerations (AMD), which cause irreversible vision loss in millions of people globally (Handa et al., 2019; Ferrington et al., 2021). A key site of insult in these diseases is the postmitotic retinal pigment epithelium (RPE), which sits between the photoreceptors and the choriocapillaris, and performs numerous functions essential for maintaining healthy vision (Caceres and Rodriguez-Boulan, 2020; Lakkaraju et al., 2020). Clinically, RPE abnormalities and the accumulation of lipid-protein aggregates called drusen above and beneath the RPE are associated with AMD progression.

The RPE is a highly metabolically active tissue that relies on mitochondrial OXPHOS for its energy needs. It shuttles glucose to the photoreceptors and muller glia, which rely on aerobic glycolysis, and uses metabolites from glycolysis and photoreceptor outer segment clearance as OXPHOS substrates (Hurley, 2021). In mice, disruption of this "metabolic ecosystem" (Du et al., 2016; Kanow et al., 2017; Reyes-Reveles et al., 2017) by RPE-specific deletion of mitochondrial genes causes a glycolytic shift in the RPE, which starves photoreceptors and eventually leads to retinal degeneration (Zhao et al., 2011; Brown et al., 2019). These studies highlight the central role of RPE mitochondria in regulating the health of the retina and suggest that RPE mitochondrial injury can trigger photoreceptor dysfunction and vision loss.

Increased mtDNA damage and OXPHOS defects (Ferrington et al., 2017; Zhang et al., 2020) have been documented in RPE cultures established from human donors with AMD. Using high-resolution imaging, we recently demonstrated that RPE mitochondria in retinal cryosections from AMD donors are highly fragmented, in contrast to the interconnected, healthy mitochondria seen in the RPE of unaffected donors (La Cunza et al., 2021). High-speed live imaging of cell-based and mouse model of macular degeneration helped us identify a novel biophysical mechanism that directly connects RPE mitochondrial dysfunction to drusen formation: redox state changes in fragmented mitochondria drive liquid-liquid phase separation of proteins with reactive cysteines, which nucleate drusen-like aggregates within the RPE (La Cunza et al., 2021). Thus, RPE mitochondrial deficits not only compromise RPE homeostasis but also initiate the development of AMD-associated pathologies.

These studies underscore the importance of analyzing mitochondrial form and function to better understand retinal biology and pathological mechanisms and to identify novel drug targets for diseases like AMD. Here, we demonstrate the power of high-speed, high-resolution live-cell imaging to evaluate mitochondrial dynamics in the RPE. We discuss important considerations when selecting imaging modalities and issues specific to the RPE that can interfere with mitochondrial imaging such as fixation, pigmentation, and lipofuscin accumulation. Lastly, by extending this technology to image mitochondrial dynamics in the living mouse RPE, we demonstrate that mitochondrial morphology, connectivity, and subcellular distribution are strikingly altered in albino mice RPE compared to that in pigmented mice, which could have significant functional consequences on cellular metabolism. Our studies lay a framework to guide experimental design and selection of model systems for evaluating mitochondrial health and function in the RPE.

# Materials and methods

## Primary RPE cultures and transfections

Primary RPE were harvested from porcine eyes as previously described (Toops et al., 2014), plated onto T25 flasks in DMEM with 10% FBS for the first week and 1% FBS for the second week (American Type Culture Collection, Manassas, VA). To generate polarized cultures, cells were plated at ~350,000 cells/$cm^2$ onto collagen-coated Transwell filters (Corning, Corning, NY) (Toops et al., 2014). Primary RPE were magnetofected with 0.5 µg mito-GCaMP5G plasmid (105,009, Addgene, Watertown, MA) for every ~3 × $10^5$ cells using LipoMag Transfection Kit (OZ Biosciences, San Diego, CA).

## Preparation of mouse RPE flatmounts for live imaging

All animal experiments were approved by the Institutional Animal Care and Use committee at the University of California, San Francisco. 3- to 5-months-old pigmented 129S1/SvlmJ (Jackson Laboratories), C57BL/6J (Jackson Laboratories), and albino BALB/c (Knox lab, UCSF) mice were raised under 12-h cyclic light with standard lab diet. We used 3 mice per strain, 1 eye of each mouse, therefore n = 3 biological replicates for each experiment. Mouse eyes were dissected immediately after $CO_2$

asphyxiation and enucleation. Extra-ocular tissues were removed under a dissection microscope, and a hole was made near the ora serrata with a 25G x 1 ½ BD PrecisionGlide (BD Biosciences, 305,127). A pair of curved spring micro-scissors and a tweezer was used to remove the anterior portion and the lens from the eye, leaving behind the eyecup. Four deep, perpendicular relaxing cuts were made. The retina was then peeled and removed by snipping it off at the optic nerve head. The perpendicular cuts were extended to obtain four RPE flatmount leaflets, which were then incubated in complete growth media (DMEM supplemented with 1% FBS, 1% NEAA, 1% penicillin/streptomycin) at 37°C in a cell culture incubator. Each leaflet was stained and imaged as described below. Dissection was performed in dim light for albino mice.

## High-speed high-resolution live imaging system

Mouse RPE flatmounts or primary RPE cultures were stained with Mitotracker (200 nM, 15 min), ERtracker (1 μM, 30 min), Biotracker ATPRed (10 μM, 15 min), or tetramethyl rhodamine (TMRE) (500 nM, 10 min) in recording media (1 x HBSS, 4.5 g/L glucose, 0.01 M HEPES), rinsed, and mounted onto a Warner chamber as previously described (Toops et al., 2014). Briefly, RPE grown on Transwell filters were excised using a scalpel blade and mounted cell-side down onto ~35 μL of recording medium between two coverslips. For RPE grown on glass-bottom dishes (Mattek), growth media was replaced with recording media immediately before imaging. Images were acquired at 37°C in Okolab humidified environmental chamber using CFI60 Apochromat TIRF ×100 oil immersion objective (1.49 NA). Live imaging was performed on the Nikon spinning disk confocal microscope equipped with: Yokogawa CSU-X1 confocal spinning disk head, Nikon Eclipse Ti2-E inverted microscope, Live-SR super-resolution module, Andor iXon Ultra 888 EMCCD camera, TI2-S-SE-E motorized stage with piezo-Z for rapid Z-stack acquisition, and a laser combiner with four solid-state lasers at 405, 488, 561, and 640 nm and the corresponding band-pass emission filter sets (Chroma) loaded on a FLI high speed filter wheel. The Live-SR is a super-resolution module that increases x-y resolution to ~ 120–140 nm, making it comparable to the resolution achieved by structured illumination microscopy (SIM). During image acquisition, care was taken to maintain the same laser power, exposure and electron-multiplying gain settings. Movies were acquired at the following rates: Supplementary Movies S1 (~2 s intervals for 2 min), Supplementary Movies S2 (~15 s intervals for 2 min), Supplementary Movies S3 (5 s intervals for 1 min), Supplementary Movies S4 (no delay (~3.7 s intervals for a z-stack) for 5 min), Supplementary Movies S5 (15 s intervals for 5 min), Supplementary Movies S9 (10 s intervals for 3 min).

## Image analysis

Images were subjected to Gaussian filtering and background subtraction prior to analysis using the same thresholds for all images. Imaris 9.9 (Bitplane) was used for surface rendering using the "Surfaces" module to determine parameters such as mean intensity, object volumes, and number of discrete objects. For quantification of mitochondrial volumes, thresholds for surface creation were guided by automatic thresholding. For timelapse analyses, tracking was enabled to track intensity changes with time, and intensity values were exported from the statistics tab. For ATP analysis, surfaces were created for the ATP channel as detailed above. The number of ATP puncta was exported from the statistics tab and normalized to Mitotracker intensity in Microsoft Excel. TMRE signals were pseudo-colored with the "Fire" look-up-table under the "Mapped Color" tab to visualize relative intensity. NIS Elements (Nikon) was used for automatic deconvolution of images, generation of kymographs, and line intensity profiles. Insets for kymographs and line intensity profiles were exported from NIS Elements using the "Create View Snapshot" function. All exported data were compiled on Microsoft Excel and plotted on Prism 8 (GraphPad).

## Immunostaining and imaging

Primary porcine RPE monolayers were fixed with 2% PFA for 10 min at room temperature. After brief rinses in 1x PBS, cells were incubated with blocking solution (1% BSA in PBS) for 30 min at room temperature, followed by 1 h incubation with CoraLite 488-conjugated TOM20 primary antibody (see Supplementary Table S1) diluted in 1% BSA in the presence of 0.1% saponin for permeabilization. Cells were then rinsed and mounted in Vectashield. For immunostaining mouse RPE flatmounts, retinas were removed and the flatmounts were fixed with 4% PFA for 1 h at room temperature, rinsed, and blocked for 1 h in 2% BSA in PBS in the presence of 0.1% Triton-X for permeabilization. Flatmounts were then stained with TOM20 primary antibody, followed by AlexaFluor secondary antibody, phalloidin, and DAPI (see Supplementary Table S1), sealed under no. 1.5 coverslips using Vectashield as a mounting medium. All images were captured on Nikon spinning disk confocal microscope using 100×/1.49 NA oil objective. Images were subjected to background subtraction and Gaussian smoothing in Imaris (Bitplane, South Windsor, CT).

## Statistical analysis

Data were analyzed by either unpaired two-tailed *t*-test with Welch's correction for testing effects between two experimental groups or one-way ANOVA with post-hoc analysis for

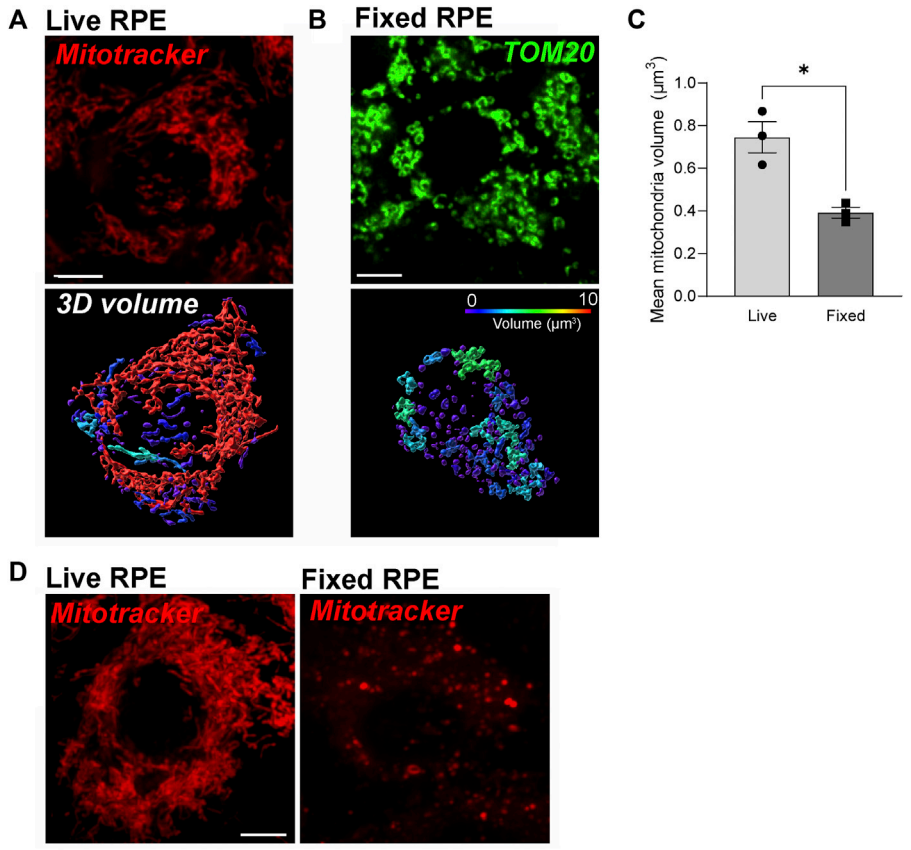


FIGURE 1
Dynamic RPE mitochondrial networks are best captured by high-speed live imaging and are destroyed by fixation. **(A)** Stills from high-speed high-resolution live imaging of primary RPE monolayers labeled with Mitotracker deep red (red). **(B)** Immunofluorescence imaging of paraformaldehyde-fixed primary RPE monolayers stained with an antibody to TOM20 (green). In A and B, top panel: single-plane view; Lower panel: 3D reconstructions. Warmer colors indicate larger volumes or integrated mitochondria, cooler colors indicate smaller volumes or fragmented mitochondria. **(C)** Quantification of mitochondrial volumes in A and **(B)**. Mean ± SEM. $n$ = 3 independent experiments, ~170 cells per condition. *$p$ = 0.0286 with Welch's t-test. **(D)** Comparison of Mitotracker deep red (red) fluorescence before and after fixation.

comparison between multiple groups (GraphPad Prism). Specific tests, sample sizes, and p-values are included in the legend of each figure.

# Results

## Dynamic RPE mitochondrial networks are best captured by high-speed live imaging and are destroyed by fixation

In all cells and tissues including the RPE, mitochondria undergo coordinated fusion and fission to establish extensive networks that span the volume of the cell. The integrity of the mitochondrial network is directly related to mitochondrial health and function. For instance, mutations in proteins that regulate fusion and fission cause diseases characterized by fragmentation of the mitochondrial network, loss of mitochondrial membrane potential, and OXPHOS defects (Giacomello et al., 2020). In the context of AMD, abnormal complement activation at the RPE cell surface leads to increased intracellular calcium that activates mitochondrial fission machinery resulting in mitochondrial fragmentation and production of reactive oxygen species in the RPE (Tan et al., 2016). Therefore, changes in mitochondrial morphology reflect changes in mitochondrial function.

Immunostaining for mitochondrial proteins is widely used to examine mitochondrial morphology in fixed tissues or cells. Chemical fixation using paraformaldehyde or other fixatives is known to alter the morphology of endosomes and lysosomes and destroy tubular endosomes (Murk et al., 2003). To investigate how fixation affects RPE mitochondria, we compared 3D reconstructions of mitochondrial networks in the RPE generated from live imaging with those from

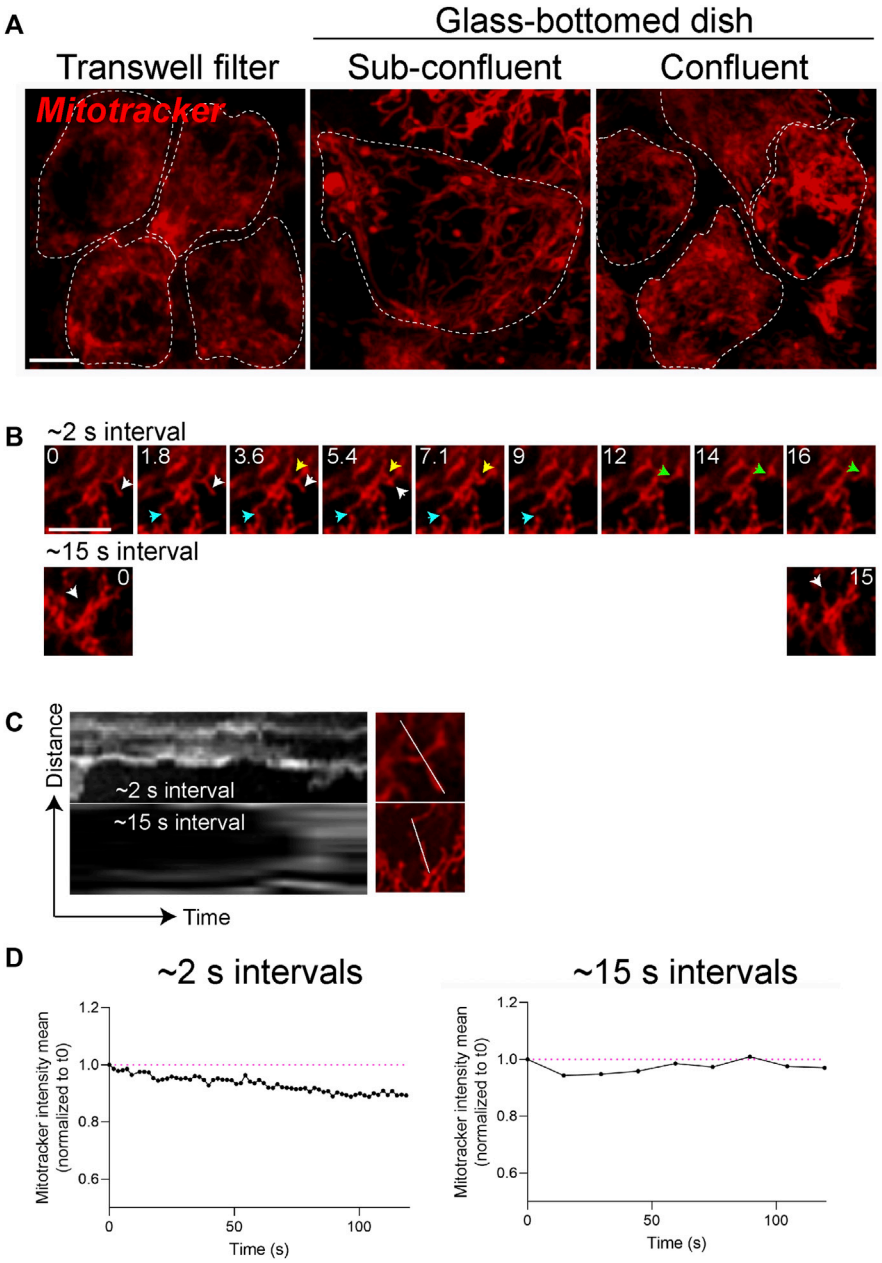


FIGURE 2
Mitochondrial integrity is coupled to RPE polarity and differentiation status. **(A)** Stills from live imaging of mitochondrial networks (Mitotracker, red) in primary RPE grown on Transwell filters to enable differentiation and establishment of polarity or on glass-bottomed dishes. Cell boundaries demarcated by white dotted lines show packing density or confluence of the monolayer. Scale bar = 5 μM. **(B)** High magnification stills from live imaging of mitochondria acquired with ~2 s intervals (top panel) or at 15 s intervals (bottom panel). Only the first ~16 s are shown. Blue, yellow, and white arrows depict distinct fusion or fission events. Scale bar = 5 μM. **(C)** Kymographs of mitochondrial movements along the indicated axis. Also see Supplementary Movies S1, S2. **(D)** Photobleaching and loss of signal intensity as a function of acquisition speeds. Magenta lines mark signal intensities at the start of imaging (t = 0).

immunofluorescence images of fixed RPE monolayers. Mitochondria in polarized primary RPE monolayers were labeled with Mitotracker Deep Red (Thermo Fisher) and imaged live using the Nikon spinning disk confocal microscope with a Live-SR module (See Materials and Methods for a detailed description of the imaging system and image analysis). Cells were then fixed and stained with an antibody to TOM20 and imaged using the same camera and

objective as for live imaging. Our live-cell imaging showed that the mitochondrial network in the RPE is filamentous and highly interconnected as has been reported in live imaging studies of other cell types (Rambold et al., 2011) (Figure 1A). However, we observed that even light fixation in 2% paraformaldehyde for 10 min almost completely dismantles this network, indicating that RPE mitochondria are highly susceptible to fixation-induced artifacts (Figures 1B,C). These data strongly suggest that immunostaining-based analysis of mitochondrial integrity in the RPE should be corroborated with live imaging studies whenever possible.

In our experience, dyes that emit at longer wavelengths such as Mitotracker Deep Red (Excitation 644 nm; Emission 665 nm) are best for imaging pigmented tissues like the RPE. This is because melanin quenches the fluorescence of shorter wavelength dyes, especially those that emit in the 420–520 nm range. Although Mitotracker Deep Red FM (Thermo Fisher) has been reported to be retained after fixation, we noticed a significant loss of fluorescence intensity after fixation (Figure 1D).

## Mitochondrial integrity is coupled to RPE polarity and differentiation status

The terminally differentiated polarized phenotype of the RPE–with a distinct repertoire of proteins on the apical and basolateral membranes (Caceres and Rodriguez-Boulan, 2020)—is central to its functional specializations. Recent studies suggest that mitochondrial metabolism helps maintain the differentiated status of the RPE (Hazim et al., 2022). To investigate if this is a bidirectional relationship - i.e., whether RPE polarity also modulates mitochondrial integrity - we compared mitochondrial networks in polarized adult primary RPE monolayers cultured on collagen-coated semipermeable polyester Transwell filters (Toops et al., 2014) with those in adult primary RPE cultured on glass coverslips. Live imaging showed that polarized RPE on filters have a more complex mitochondrial reticulum relative to those on glass. However, increasing the plating density of RPE on glass increases mitochondrial connectivity to a level comparable to RPE on filters (Figure 2A). This is because plating RPE at high density helps establish a confluent monolayer by preventing cell division and thereby promoting differentiation (Lane et al., 2014; Toops et al., 2014). These data support the hypothesis that organization of the mitochondrial network is tightly coupled to the differentiation status of the RPE. Collagen or other extracellular matrix components used to culture primary RPE could also contribute to mitochondrial integrity *via* integrins or by modulating the actin or microtubule cytoskeleton to regulate mitochondrial fission and fusion (Rizzuto, 2003).

One technical challenge in working with polarized RPE monolayers is their very low transfection efficiency and expression of exogenous genes. In addition to dyes such as Mitotracker, viral transduction using baculovirus to express fluorescently-tagged pyruvate dehydrogenase (CellLight Mitochondria, Thermo Fisher) can be used for live imaging (Table 1). Transducing primary polarized RPE with CellLight Mitochondria at ~14 virus particles/cell for 18 h yielded transduction efficiencies of ≥ 40% with no observed toxicity and labeled mitochondria comparable to that seen with Mitotracker probes (Tan et al., 2016; La Cunza et al., 2021). Compared to transgene expression, fluorescent probes that label the mitochondria uniformly label almost all the cells in the monolayer. However, genetic approaches yield longer-lasting labeling and are relatively non-toxic compared to fluorescent dyes. Studies in breast cancer cell lines found that Mitotracker deep red inhibits basal respiration and blocks ATP synthesis at concentrations at or above 500 nM (Sargiacomo et al., 2021). Although the toxicity of mitochondria dyes is likely cell-type dependent, care must be taken to avoid artifacts by using the lowest-possible concentration for labeling.

Because mitochondria are highly dynamic, capturing rapid fission and fusion events necessitates the use of microscopes with high spatial and temporal resolution. The acquisition speed of timelapse experiments needs to be optimized for imaging the trafficking and fission/fusion dynamics of mitochondria. Compared to the fission and fusion events captured with timelapse imaging acquired with ~2-second intervals, acquisitions at 15-second intervals captured significantly fewer movements (Figures 2B,C, Supplementary Movies S1, S2). Choosing the acquisition speed needs to be balanced with other experimental requirements such as imaging entire volume of the cell (z-stacks), single- or multi-channel imaging, and the susceptibility of the fluorescence probe to photobleaching. For instance, although not significant, acquiring images at 2-second intervals results in a slight loss of Mitotracker signal intensity after 2 min compared to when images are acquired at 15-second intervals (Figure 2D). Thus, RPE polarity, choice of reporter, and acquisition speed are important parameters that can impact live imaging of mitochondrial dynamics.

## Live imaging reveals morphological and functional heterogeneity of mitochondria in the RPE

Although Mitotracker and CellLight constructs are useful for examining the integrity and dynamics of the mitochondrial network, analysis of specific mitochondrial functions requires specialized tools to quantify ATP release, mitochondrial membrane potential, and calcium flux (Iannetti et al., 2019). Altered expression of the mitochondrial ATP synthase has been reported in neurodegenerative diseases including AMD (Nordgaard et al., 2008; Ebanks and Chakrabarti, 2022) but

TABLE 1 Tools to visualize mitochondria in polarized RPE monolayers.

| | Fluorescent probes | Transgenes |
|---|---|---|
| Ease of use | Very easy, ~15 min labeling time | Easy, overnight transfection/transduction |
| Efficiency of labeling | Very high, almost all cells labelled | ~30–50% depending on the constructs used |
| Stability of signal | High | High |
| Imaging window | Must be imaged immediately after labeling | Days |
| Toxicity | Reported to be toxic at high concentrations | Minimal observed or reported |

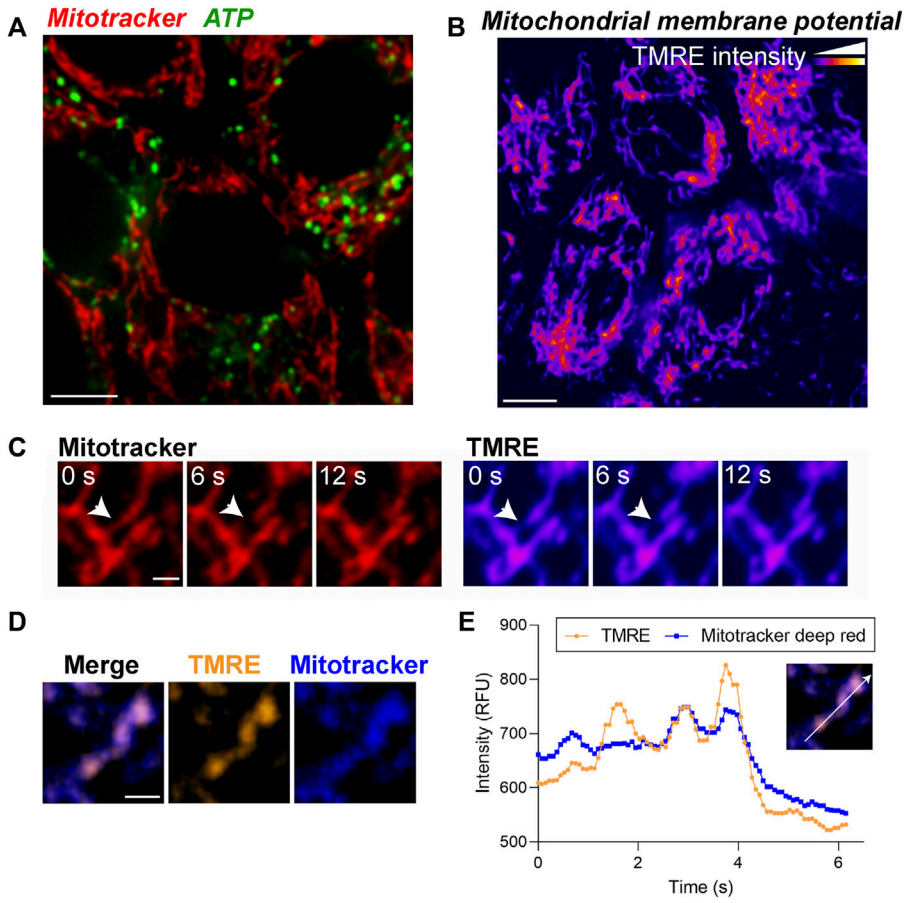


FIGURE 3
Live imaging of ATP and mitochondrial membrane potential demonstrates morphological and functional heterogeneity of mitochondria in the RPE. **(A)** Stills from live imaging of mitochondria (Mitotracker, red) and BioTracker-ATP (green) in primary RPE monolayers. **(B)** Mitochondrial membrane potential (MMP) measured by TMRE labeling in primary RPE monolayers. Color scale: warmer colors indicate higher TMRE intensities. **(C)** High magnification images showing local heterogeneity of MMP within a single mitochondrion. Note that areas of low TMRE intensity predict putative fission sites (arrow). Scale bar = 1 μM. Also see Supplementary Movies S3. **(D)** Overlay of TMRE (gold) and Mitotracker deep red (blue). Note that TMRE is more sensitive to local MMP heterogeneity within a single mitochondrion compared to Mitotracker deep red. Right panels show split channel views. Scale bar = 1 μM. **(E)** Intensity profile of TMRE and Mitotracker deep red along the axis indicated in the inset.

whether and to what extent these changes translate to impaired mitochondrial ATP production has yet to be established. To evaluate ATP generation in the RPE in realtime, we used BioTracker ATP-Red (Millipore). The probe forms a non-fluorescent closed-ring structure in the absence of ATP; however, the covalent bonds holding the ring are broken by

ATP, resulting in fluorescence unquenching (Wang et al., 2016). Primary RPE monolayers labeled with Mitotracker and BioTracker ATP showed ATP puncta along mitochondrial filaments (Figure 3A). Intra- and intercellular heterogeneity in ATP levels can be quantified by measuring the number and intensity of puncta and normalizing to either cell number or Mitotracker intensity (Rieger et al., 2021).

As mitochondrial ATP production is dependent on the electrochemical gradient generated by the mitochondrial membrane potential (ΔΨm), changes in ΔΨm are an important indicator of mitochondrial health and function. Tetramethylrhodamine ethyl ester (TMRE) is widely used to measure ΔΨm as changes in TMRE fluorescence positively correlate with ΔΨm. In primary RPE monolayers, on a cellular level, the TMRE fluorescence pattern was comparable to that of Mitotracker (Figure 3B). However, at a subcellular level, we observed local changes in TMRE fluorescence within a single mitochondrion that preceded mitochondrial scission (Figure 3C, Supplementary Movies S3), suggesting that changes in ΔΨm mark putative scission sites (Twig et al., 2008). Although the mitochondrial localization of Mitotracker Deep Red is also dependent on ΔΨm, our live imaging data show that in primary RPE monolayers, TMRE staining is more sensitive than Mitotracker Deep Red in capturing subtle changes in ΔΨm (Figures 3D,E).

## Functional relevance of mitochondria-ER and mitochondria-lysosome contacts in the RPE

Mitochondria form elaborate contacts with other organelles including the ER and lysosomes that act as conduits for exchanging calcium, lipids, and metabolites (Rieusset, 2018; Aoyama-Ishiwatari and Hirabayashi, 2021; Cisneros et al., 2022). The architecture and function of these contacts has been largely studied in cell lines, which has little relevance to the postmitotic RPE. As these contacts are continuously remodeled in response to the changing metabolic needs of the local environment within the cell, high-speed live imaging is essential to capture contact sites and follow their functions. Here, we took advantage of the availability of probes that selectively label the ER (ER-tracker), mitochondria (Mitotracker), and lysosomes (LysoTracker) and the high speed of acquisition of the spinning disc imaging system to capture ER-mitochondrial calcium transport and lysosome-mediated mitochondrial fission in polarized primary RPE monolayers.

Calcium transport from the ER to mitochondria regulates critical mitochondrial functions. The production of ATP in the mitochondria, for instance, is driven by calcium-sensitive mitochondrial enzymes (Griffiths and Rutter, 2009). However, mitochondrial calcium overload induces fragmentation by activating fission machinery including dynamin-related protein 1 (DRP1) (Horn et al., 2020) and can also lead to cell death by activating the mitochondrial permeability transition pore (Bauer and Murphy, 2020). To evaluate focal changes in mitochondrial calcium, we transfected the RPE with the mitochondria-targeted fluorescent calcium sensor (mito-GCaMP5G) (Kwon et al., 2016). Our live imaging data revealed a heterogeneous distribution of calcium within the mitochondrial network (Figure 4A) and mitochondria-ER contact sites mediating dynamic transport of calcium between mitochondria (Figure 4B, Supplementary Movies S4).

Apart from extensive contacts with the ER, mitochondria also interact dynamically with lysosomes. These mitochondria-lysosome interactions serve many important functions, including mediating substrate transfer and maintaining mitochondrial homeostasis through autophagic clearance (mitophagy) (Giacomello et al., 2020; Cisneros et al., 2022). Recruitment of mitochondrial fission machinery to mitochondria-lysosome contact sites has been shown to promote mitochondrial fission in several cell lines (Wong et al., 2018; Qiu et al., 2022). High resolution imaging of interactions between mitochondria and lysosomes in primary RPE monolayers revealed multiple dynamic interactions between the two organelles that precede mitochondrial fission events (Figure 4C, Supplementary Movies S5).

## Live imaging of mouse RPE flatmounts reveals an unexpected impact of genetic background on mitochondrial integrity and function

Investigating mitochondrial dynamics in the intact living mouse retina is essential for understanding how RPE mitochondrial function and dysfunction contributes to retinal disease. Mice, which are widely used to model and study retinal degenerations, are generated on different genetic backgrounds such as the pigmented 129S1/SvlmJ and C57BL/6J mice, the BALB/c albino mice, as well as mixed backgrounds (Zhao et al., 2011; Mao et al., 2014; Biswal et al., 2018; Brown et al., 2019; La Cunza et al., 2021). The RPE in its native state is pigmented due to the presence of melanosomes, which protect the RPE by scavenging free radicals (Rózanowski et al., 2008). Consequently, transgenic mice on the albino BALB/c background have been used to investigate mitochondrial dysfunction in the RPE as they are more susceptible to photo-oxidative stress (Biswal et al., 2018; Brown et al., 2019). However, to compare studies on mitochondrial proteins in the RPE of transgenic mice of different backgrounds, it is important to have comparative data on mitochondrial morphology and function in the RPE of wildtype pigmented and albino mouse strains.

To evaluate RPE mitochondrial structure and subcellular distribution as a function of mouse genetic background, we first performed live imaging of Mitotracker deep red in RPE

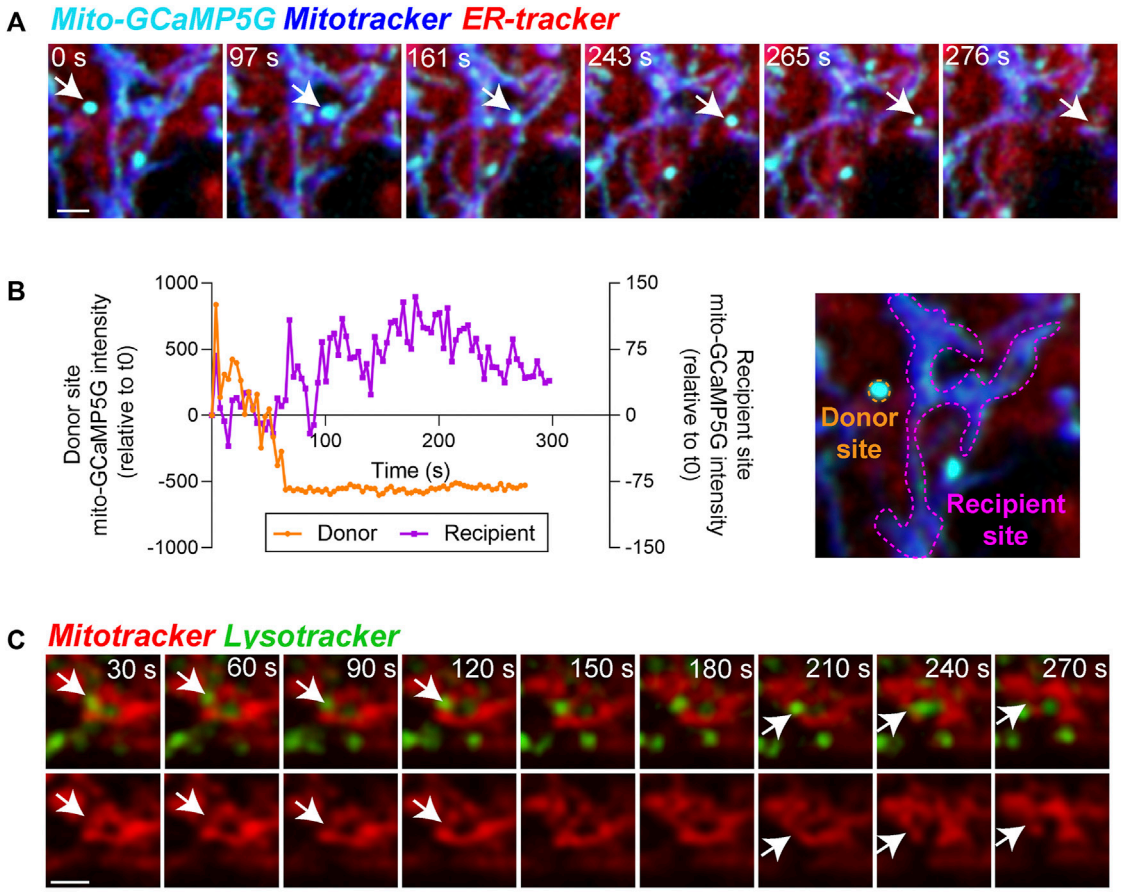


FIGURE 4
Functional relevance of mitochondria-ER and mitochondria-lysosome contacts in the RPE. **(A)** Stills from live imaging of interactions between mitochondrial calcium (mito-GCaMP5G, cyan), ER-tracker (red), and Mitotracker deep red (blue) in primary RPE monolayers showing heterogeneity of mitochondrial calcium within the cell. Arrow indicates one calcium transfer event. Note ER-mediated transfer of calcium to mitochondria in frames 243 s and 265 s. Images were deconvolved using Nikon NIS-Elements. Scale bar = 1 μM. Also see Supplementary Movies S4. **(B)** Changes in mean intensity of mito-GCaMP5G on the indicated donor and recipient sites. **(C)** Stills from live imaging of contacts between Mitotracker (red) and Lysotracker (green). Top panel shows merged view, bottom panel shows Mitotracker signal only. Arrows indicate mitochondrial fission events. Images were deconvolved using Nikon NIS-Elements. Scale bar = 1 μM. Also see Supplementary Movies S5.

flatmounts generated from wildtype pigmented C57BL/6J, pigmented 129S1/SvlmJ, and albino BALB/c mice. Our data show striking differences in mitochondrial morphology and distribution between pigmented and albino mice RPE. Whereas mitochondria in pigmented C57BL/6J and 129S1/SvlmJ RPE form interconnected networks along the cell periphery, mitochondria in albino BALB/c RPE mice were largely fragmented and appear as disconnected discrete structures (Figures 5A,B). To establish that this was not an artifact of live imaging, we immunostained RPE flatmounts for TOM20 and observed a similar pattern of smaller mitochondrial volumes in albino RPE compared to that of pigmented RPE (Figures 5C,D, Supplementary Movies S6-8). Comparison of live imaging and fixed imaging datasets revealed that although fixation resulted in decreased mean mitochondrial volumes in all three mouse strains (similar to that observed in primary RPE cultures in Figure 1), differences between mouse strains are conserved and correlate with live imaging data (Figure 5D). Analyses of mitochondrial distribution as a function of z-position within the RPE revealed another important difference between mouse strains: unlike mitochondria in pigmented RPE that are distributed throughout the volume of the cell, mitochondria in albino RPE are predominantly concentrated near the basal surface of the RPE (Figure 5E).

We then asked if the significant differences in RPE mitochondrial morphology and distribution translate to functional differences in albino and pigmented mice. We focused on mitochondrial ATP and $\Delta\Psi m$ as functional readouts of mitochondrial health and bioenergetics. Live

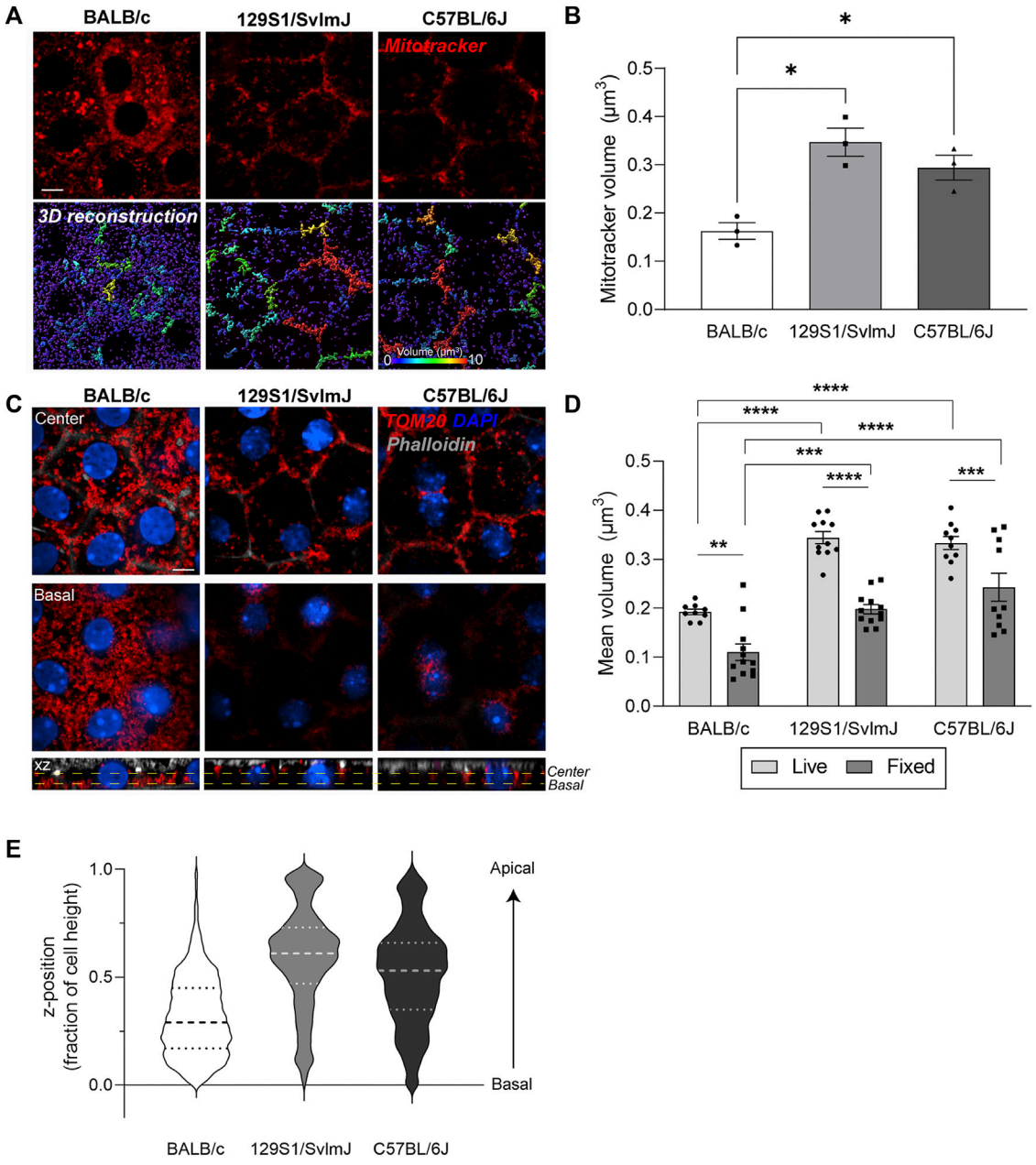


FIGURE 5
Live imaging of mouse RPE flatmounts reveals impaired mitochondrial integrity in albino mouse RPE. **(A)** Stills from live imaging of Mitotracker deep red (red) in RPE flatmounts from albino BALB/c, pigmented 129S1/SvImJ, and pigmented C57BL/6J mice. Lower panel: 3D reconstructions of mitochondria. Scale bar = 5 μM. Warmer colors indicate larger volumes or integrated mitochondria, cooler colors indicate smaller volumes or fragmented mitochondria. **(B)** Quantification of mitochondrial volumes in **(A)**. Mean ± SEM. $n$ = 3 mice per strain. *$p$ = 0.0215 between BALB/c and 129S1/SvImJ; $p$ = 0.0425 between BALB/c and C57BL/6J by one-way ANOVA. **(C)** Immunofluorescence images of paraformaldehyde-fixed mouse RPE flatmounts stained for TOM20 (red). Top: Single-plane view across the center of the RPE; Middle: Single-plane view across the basal side of the RPE; Lower panel: x-z view showing mitochondrial distribution along the height of the RPE. Phalloidin (grey) labels the actin cytoskeleton and microvilli at the apical surface of the RPE. Also see Supplementary Movies S6–8. **(D)** Quantification of mitochondrial volumes in RPE flatmounts from live and fixed imaging. Mean ± SEM., **, $p$ = 0.023; ***, $p$ = 0.0009; ****$p$ < 0.0001. Two-way ANOVA was used for comparison between live and fixed imaging, one-way ANOVA was used for comparison within live and fixed imaging respectively. Representative data from ~60 cells per mouse, data based on $n$ = 3 mice per strain. **(E)** Representative violin plot of individual mitochondria z-positions normalized to cell height (0 = bottom-most z-position, 1 = top-most z-position). Dashed lines represent quartiles and medians of the respective dataset.

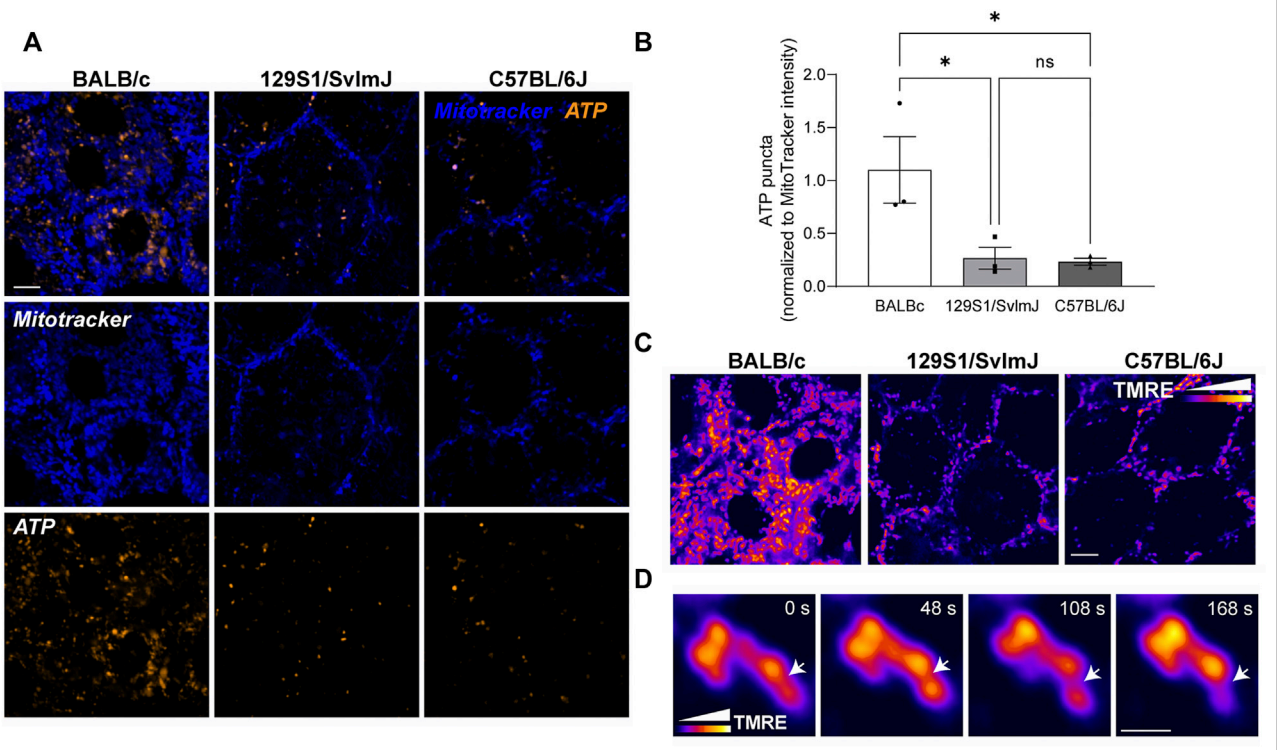


FIGURE 6
Genetic background of wildtype mice determines mitochondrial integrity and function in the RPE. **(A)** Stills from live imaging of mitochondria (Mitotracker, blue) and BioTracker-ATP (gold) in albino BALB/c, pigmented 129S1/SvlmJ, and pigmented C57BL/6J mouse RPE flatmounts. **(B)** Quantitation of ATP puncta normalized to Mitotracker intensity. Mean ± SEM. $n$ = 3 mice per strain. *$p$ = 0.0497 between BALB/c and 129S1/SvlmJ; $p$ = 0.0427 between BALB/c and C57BL/6J by one-way ANOVA. **(C)** Mitochondrial membrane potential (MMP) measured by TMRE labeling in mouse RPE flatmounts. Color scale depicts relative intensity of TMRE. Scale bar = 3 μM. **(D)** High magnification images showing local heterogeneity of MMP within a single mitochondrion. Note that areas of low TMRE intensity predict putative fission sites (arrow). Scale bar = 1 μM. Also see Supplementary Movies S9.

imaging showed higher BioTracker ATP signal in albino mouse RPE flatmounts compared to pigmented RPE (Figures 6A,B), suggesting that albino RPE have higher ATP content compared to pigmented RPE. Of note, although the BioTracker ATP signal was in close proximity to the mitochondria, it did not colocalize strongly with Mitotracker fluorescence (Figure 6A) unlike that reported in the oral squamous cell carcinoma cells in which the probe was first tested (Wang et al., 2016). This potentially reflects cell-type-specific differences in cellular bioenergetics. Because interconnected mitochondria are more efficient in oxidative phosphorylation compared to fragmented mitochondria (Chen et al., 2005; Gomes et al., 2011; Rambold et al., 2011), it is also plausible that the increased BioTracker ATP signals we observed in the albino RPE reflects ATP generated *via* glycolysis in the cytosol (Ozawa et al., 2015). Further studies are required to establish how functional mitochondria are in the albino RPE, and whether there is a shift from oxidative phosphorylation towards glycolysis in albino RPE due to increased oxidative stress and mitochondrial fragmentation.

Live imaging of TMRE staining in the RPE of albino and pigmented mice showed heterogeneity of ΔΨm within individual mitochondrial similar to our data in primary RPE monolayers (Figure 6C). High-speed live imaging allowed us to capture focal loss of ΔΨm preceding mitochondrial fission in 129S1/SvlmJ mouse RPE flatmounts (Figure 6D, Supplementary Movies S9), consistent with our observation in primary RPE cultures (Figure 3C).

## Discussion

The unique features of the RPE–a postmitotic, polarized tissue that deals with the immense metabolic burden of daily photoreceptor outer segment clearance in a highly oxidative environment–places unique stresses on its mitochondria. Recent studies show that mitochondrial function influences RPE cell fate (Hazim et al., 2022), and that AMD-associated stressors such as smoking and complement activation promote mitochondrial fragmentation and dysfunction (Woodell et al.,

2013; Tan et al., 2016; La Cunza et al., 2021). Given that RPE mitochondrial function directly impacts photoreceptor health and vision (Handa et al., 2019; Ferrington et al., 2021; Hurley, 2021), insight into mechanisms and machinery that maintain mitochondrial homeostasis in the RPE *in vivo* and how they are disrupted in disease is essential for developing sight-saving therapies.

Mitochondrial form is closely related to its function (Liesa and Shirihai, 2013; Giacomello et al., 2020). Early studies using two-dimensional electron microscopy showed mitochondria as discrete sausage-shaped structures in the cell. Over the last decade or so, advances in high-resolution and super-resolution microscopy have allowed imaging of organelles below the diffraction limit of light (250 nm laterally and 500 nm axially). These studies show that mitochondria form extensive networks that span the volume of the cell and dynamically interact with the ER, lysosomes, and other organelles (Murley and Nunnari, 2016; Iannetti et al., 2019; Lackner, 2019; Giacomello et al., 2020; Aoyama-Ishiwatari and Hirabayashi, 2021; Cisneros et al., 2022). Using these advanced imaging tools to investigate mitochondrial dynamics in the RPE is complicated by technical challenges in dealing with RPE polarity, pigmentation, and accumulation of lipofuscin. For instance, super-resolution techniques such as Structured Illumination Microscopy (SIM) is compatible with imaging pigmented cells, while Stimulated Emission Depletion (STED) or Stochastic Optical Reconstruction Microscopy (STORM) cannot be used to image pigmented RPE because melanin interferes with fluorophore quenching and photo-switching of the dyes. Imaging mitochondrial dynamics in living cells requires balancing image resolution with acquisition speed to capture fission, fusion, and contact sites. In this regard, capturing and processing multiple images per plane required for SIM, slows down the acquisition speed especially for multicolor imaging, which prevents accurate temporal analysis of mitochondrial dynamics.

Here, we used a spinning disc confocal microscope with an EMCCD camera engineered for very fast acquisition (26 fps) coupled with the Live-SR super-resolution module, which increases image resolution to ~120–140 nm laterally without any loss of acquisition speed. Imaging mitochondrial dynamics in polarized primary RPE cultures and mouse RPE flatmounts using this system showed that mitochondrial networks in the RPE reflect its differentiation status and are destroyed by fixation. Therefore, experiments on mitochondrial function in fixed non-polarized or poorly differentiated RPE cultures should be evaluated carefully. The increased resolution and acquisition speeds enabled by our system showed that RPE mitochondria show localized heterogeneities in membrane potential and ATP production that could reflect focal changes in metabolism and oxidative stress; that contacts between the mitochondria and ER modulate calcium flux; and that lysosomes remodel the mitochondrial network by mediating fission.

In comparing mitochondrial dynamics in RPE flatmounts from widely used mouse strains, we unexpectedly observed that in contrast to the highly interconnected mitochondria in the RPE of pigmented mouse strains, mitochondria in albino mouse RPE are highly fragmented and localized to the basal surface of the RPE. The difference in mitochondrial structure may contribute to the increased susceptibility of albino rodents to AMD-like pathology upon light damage, including changes in photoreceptor function, photoreceptor death, and accumulation of subretinal deposits (Montalbán-Soler et al., 2012; Polosa et al., 2016). Moreover, albino *Abca4*$^{-/-}$ mouse model of inherited macular degeneration exhibits progressive photoreceptor loss beginning at 8 months of age, whereas no photoreceptor death was observed up to 18 months of age in pigmented *Abca4*$^{-/-}$ mice (Radu et al., 2008; Charbel Issa et al., 2013; Wu et al., 2014). The link between albino RPE and mitochondrial dysfunction is likely mediated by several factors: First, melanosomes in pigmented RPE act as anti-oxidants to sequester reactive oxygen species, thereby protecting the RPE against mitochondrial DNA damage and disruption of mitochondrial respiratory chain activity (Seagle et al., 2005; Van Houten et al., 2006; Rózanowski et al., 2008; Voets et al., 2012). Secondly, light exposure promotes photodegradation of lipofuscin bisretinoids in the RPE resulting in increased RPE oxidative stress, that is, especially pronounced in albino mice (Ueda et al., 2016). Alteration in cellular redox state could also directly modulate mitochondrial integrity by promoting redox-sensitive post-translational modifications in proteins involved in mitochondrial fission and fusion (Willems et al., 2015).

Interconnected mitochondria are known to be more efficient at OXPHOS and ATP generation compared to fragmented mitochondria (Chen et al., 2005; Gomes et al., 2011; Rambold et al., 2011). However, we observed increased ATP fluorescence in albino mice RPE compared to pigmented RPE. Because the ATP signal did not colocalize with Mitotracker, we hypothesize that OXPHOS defects in fragmented mitochondria could lead to increased glycolysis in albino RPE resulting in ATP generation in the cytosol. Moreover, although fragmented mitochondria are defective in OXPHOS, this does not always translate to loss of ATP production, because these mitochondria can consume alternate fuel sources such as aspartate to generate ATP (Yao et al., 2019). Bioenergetic profiling of albino and pigmented mouse RPE using SeaHorse Flux Analyzer or commercially available kits to measure temporal changes in oxygen consumption rates (Hazim et al., 2022) will provide valuable insight into bioenergetic differences in these mice. While mechanisms responsible for the observed increased ATP production in albino RPE need further investigation, one negative consequence would be the accelerated generation of reactive oxygen species (ROS), which would exacerbate oxidative

stress in albino RPE (Rattner et al., 2008; Hunter et al., 2012; Mao et al., 2014; Brown et al., 2019). This is supported by an intriguing study showing that temporal RPE in pigmented C57BL/6J mice have fewer melanosomes and are more susceptible to oxidative stress (Dieguez et al., 2019). Since mitochondrial cristae harbor OXPHOS machinery, high-resolution live imaging of mitochondrial cristae organization (Segawa et al., 2020) and ROS generation (Chandrasekharan et al., 2019) in pigmented and albino mice is necessary for better insight into the mechanisms involved.

Based on electron microscopy studies of mouse, non-human primate, and human RPE, it has been widely thought that mitochondria are predominantly located basally where there is a large energy demand (Gouras et al., 2010; Williams et al., 2013; Gouras et al., 2016; Pollreisz et al., 2020). However, a recent serial block-face scanning EM analysis of a single human donor shows apical mitochondria (Pollreisz et al., 2020). As we show in this study, fixation can induce artifacts that can drastically alter mitochondrial morphology and distribution in the RPE. Our high-resolution live imaging of pigmented mouse RPE flatmounts now show that RPE mitochondria are spread throughout the volume of the cell with a band of highly integrated mitochondria near the circumferential actin ring below the junctional complexes, which has also been observed by others (McWilliams et al., 2019). These interconnected mitochondria could serve multiple functions for RPE homeostasis such as maintaining cell-cell junctions that depend on ATP (Hong et al., 2010); promoting ATP release from gap junctions to support development of the neural retina (Pearson et al., 2005); and providing ATP for the phagocytosis and degradation of photoreceptor outer segments, an energetically intensive function. In albino mice RPE, lack of this band of interconnected mitochondria could explain the observed gap junction and adherens junction abnormalities (Iwai-Takekoshi et al., 2016) and delayed retinal neurogenesis (Bhansali et al., 2014).

Currently, imaging mitochondrial dynamics in human RPE is limited by access to donor tissues soon after death and the presence of lipofuscin that can interfere with imaging. Autofluorescence quenching tools such as TrueBlack can be used for both fixed and live imaging human donor RPE (Kaur et al., 2018; La Cunza et al., 2021). Development of new imaging technologies such as three-photon microscopy that can image pigmented RPE or increased resolution of adaptive optics optical coherence tomography (AO-OCT) would allow monitoring mitochondrial dynamics in the living eye (Liu et al., 2016; Shirazi et al., 2020; Bower et al., 2021).

This study demonstrates the power of high-speed, high-resolution live imaging for evaluating the integrity, health, and function of mitochondria in fully differentiated RPE monolayers in culture and in mouse RPE flatmounts. We show that live imaging is essential for investigating spatiotemporal changes in mitochondrial fusion and fission, as well as changes in mitochondrial membrane potential and ATP generation that are not detectable in fixed tissues. A key finding from this study is the striking difference in mitochondrial integrity and localization between albino and pigmented mice RPE. Albino mice have been used to generate transgenic models of retinal disease because of the ease of imaging RPE without pigment and because their increased susceptibility to oxidative stress shortens the time to retinal degeneration compared to transgenic mice on a pigmented background (Ueda et al., 2016). Our data now show that it is important to compare mitochondrial integrity and dynamics in wildtype mice of different genetic strains to better understand the impact of the gene of interest in transgenic models. We anticipate that these studies will provide a framework to guide experimental design and selection of mouse models for evaluating RPE mitochondrial function in health and disease.

## Data availability statement

The original contributions presented in the study are included in the article/Supplementary Material, further inquiries can be directed to the corresponding author.

## Ethics statement

The animal study was reviewed and approved by the UCSF IACUC.

## Author contributions

LT and AL conceived the project. LT and AL designed the experiments. LT, JL, and CG performed experiments. LT and JL performed data analysis. LT and AL wrote the manuscript. All authors approved the final version of the paper.

## Funding

Supported by the NIH grants R01EY023299 (AL) and R01EY030668 (AL), P30 core grant EY002162 (UCSF Department of Ophthalmology), the Research to Prevent Blindness/AMDF Catalyst Award for novel approaches to AMD (AL), the BrightFocus Foundation Lorraine Maresca award for Innovative research in AMD M2021020I (AL), Reeves Foundation award for AMD (AL), and the All May See Foundation Postdoctoral Grant Award (LXT). We thank the Knox lab for the albino BALB/c mice.

## Conflict of interest

The authors declare that the research was conducted in the absence of any commercial or financial relationships that could be construed as a potential conflict of interest.

## Publisher's note

All claims expressed in this article are solely those of the authors and do not necessarily represent those of their affiliated organizations, or those of the publisher, the editors and the reviewers. Any product that may be evaluated in this article, or claim that may be made by its manufacturer, is not guaranteed or endorsed by the publisher.

## Supplementary material

The Supplementary Material for this article can be found online at: https://www.frontiersin.org/articles/10.3389/fcell.2022.1044672/full#supplementary-material

## References


Aoyama-Ishiwatari, S., and Hirabayashi, Y. (2021). Endoplasmic reticulum-mitochondria contact sites-emerging intracellular signaling hubs. *Front. Cell. Dev. Biol.* 9, 653828. doi:10.3389/fcell.2021.653828

Bauer, T. M., and Murphy, E. (2020). Role of mitochondrial calcium and the permeability transition pore in regulating cell death. *Circ. Res.* 126 (2), 280–293. doi:10.1161/CIRCRESAHA.119.316306

Bhansali, P., Rayport, I., Rebsam, A., and Mason, C. (2014). Delayed neurogenesis leads to altered specification of ventrotemporal retinal ganglion cells in albino mice. *Neural Dev.* 9, 11. doi:10.1186/1749-8104-9-11

Biswal, M. R., Justis, B. D., Han, P., Li, H., Gierhart, D., Dorey, C. K., et al. (2018). Daily zeaxanthin supplementation prevents atrophy of the retinal pigment epithelium (RPE) in a mouse model of mitochondrial oxidative stress. *PLoS One* 13 (9), e0203816. doi:10.1371/journal.pone.0203816

Bower, A. J., Liu, T., Aguilera, N., Li, J., Liu, J., Lu, R., et al. (2021). Integrating adaptive optics-SLO and OCT for multimodal visualization of the human retinal pigment epithelial mosaic. *Biomed. Opt. Express* 12 (3), 1449–1466. doi:10.1364/BOE.413438

Brown, E. E., DeWeerd, A. J., Ildefonso, C. J., Lewin, A. S., and Ash, J. D. (2019). Mitochondrial oxidative stress in the retinal pigment epithelium (RPE) led to metabolic dysfunction in both the RPE and retinal photoreceptors. *Redox Biol.* 24, 101201. doi:10.1016/j.redox.2019.101201

Caceres, P. S., and Rodriguez-Boulan, E. (2020). Retinal pigment epithelium polarity in health and blinding diseases. *Curr. Opin. Cell. Biol.* 62, 37–45. doi:10.1016/j.ceb.2019.08.001

Chandrasekharan, A., Varadarajan, S. N., Lekshmi, A., Lupitha, S. S., Darvin, P., Chandrasekhar, L., et al. (2019). A high-throughput real-time *in vitro* assay using mitochondrial targeted roGFP for screening of drugs targeting mitochondria. *Redox Biol.* 20, 379–389. doi:10.1016/j.redox.2018.10.013

Charbel Issa, P., Barnard, A. R., Singh, M. S., Carter, E., Jiang, Z., Radu, R. A., et al. (2013). Fundus autofluorescence in the Abca4(-/-) mouse model of Stargardt disease--correlation with accumulation of A2E, retinal function, and histology. *Investig. Ophthalmol. Vis. Sci.* 54 (8), 5602–5612. doi:10.1167/iovs.13-11688

Chen, H., Chomyn, A., and Chan, D. C. (2005). Disruption of fusion results in mitochondrial heterogeneity and dysfunction. *J. Biol. Chem.* 280 (28), 26185–26192. doi:10.1074/jbc.M503062200

Cisneros, J., Belton, T. B., Shum, G. C., Molakal, C. G., and Wong, Y. C. (2022). Mitochondria-lysosome contact site dynamics and misregulation in neurodegenerative diseases. *Trends Neurosci.* 45 (4), 312–322. doi:10.1016/j.tins.2022.01.005

Dieguez, H. H., Romeo, H. E., Alaimo, A., González Fleitas, M. F., Aranda, M. L., Rosenstein, R. E., et al. (2019). Oxidative stress damage circumscribed to the central temporal retinal pigment epithelium in early experimental non-exudative age-related macular degeneration. *Free Radic. Biol. Med.* 131, 72–80. doi:10.1016/j.freeradbiomed.2018.11.035

Du, J., Yanagida, A., Knight, K., Engel, A. L., Vo, A. H., Jankowski, C., et al. (2016). Reductive carboxylation is a major metabolic pathway in the retinal pigment epithelium. *Proc. Natl. Acad. Sci. U. S. A.* 113 (51), 14710–14715. doi:10.1073/pnas.1604572113

Ebanks, B., and Chakrabarti, L. (2022). Mitochondrial ATP synthase is a target of oxidative stress in neurodegenerative diseases. *Front. Mol. Biosci.* 9, 854321. doi:10.3389/fmolb.2022.854321

Ferrington, D. A., Ebeling, M. C., Kapphahn, R. J., Terluk, M. R., Fisher, C. R., Polanco, J. R., et al. (2017). Altered bioenergetics and enhanced resistance to oxidative stress in human retinal pigment epithelial cells from donors with age-related macular degeneration. *Redox Biol.* 13, 255–265. doi:10.1016/j.redox.2017.05.015

Ferrington, D. A., Kenney, M. C., Atilano, S. R., Hurley, J. B., Brown, E. E., and Ash, J. D. (2021). Mitochondria: The retina's achilles' heel in AMD. *Adv. Exp. Med. Biol.* 1256, 237–264. doi:10.1007/978-3-030-66014-7_10

Giacomello, M., Pyakurel, A., Glytsou, C., and Scorrano, L. (2020). The cell biology of mitochondrial membrane dynamics. *Nat. Rev. Mol. Cell. Biol.* 21 (4), 204–224. doi:10.1038/s41580-020-0210-7

Gomes, L. C., Di Benedetto, G., and Scorrano, L. (2011). During autophagy mitochondria elongate, are spared from degradation and sustain cell viability. *Nat. Cell. Biol.* 13 (5), 589–598. doi:10.1038/ncb2220

Gordaliza-Alaguero, I., Cantó, C., and Zorzano, A. (2019). Metabolic implications of organelle-mitochondria communication. *EMBO Rep.* 20 (9), e47928. doi:10.15252/embr.201947928

Gouras, P., Ivert, L., Neuringer, M., and Mattison, J. A. (2010). Topographic and age-related changes of the retinal epithelium and Bruch's membrane of rhesus monkeys. *Graefes Arch. Clin. Exp. Ophthalmol.* 248 (7), 973–984. doi:10.1007/s00417-010-1325-x

Gouras, P., Ivert, L., Neuringer, M., and Nagasaki, T. (2016). Mitochondrial elongation in the macular RPE of aging monkeys, evidence of metabolic stress. *Graefes Arch. Clin. Exp. Ophthalmol.* 254 (6), 1221–1227. doi:10.1007/s00417-016-3342-x

Griffiths, E. J., and Rutter, G. A. (2009). Mitochondrial calcium as a key regulator of mitochondrial ATP production in mammalian cells. *Biochim. Biophys. Acta* 1787 (11), 1324–1333. doi:10.1016/j.bbabio.2009.01.019

Handa, J. T., Bowes Rickman, C., Dick, A. D., Gorin, M. B., Miller, J. W., Toth, C. A., et al. (2019). A systems biology approach towards understanding and treating non-neovascular age-related macular degeneration. *Nat. Commun.* 10 (1), 3347. doi:10.1038/s41467-019-11262-1

Hazim, R. A., Paniagua, A. E., Tang, L., Yang, K., Kim, K. K. O., Stiles, L., et al. (2022). Vitamin B3, nicotinamide, enhances mitochondrial metabolism to promote differentiation of the retinal pigment epithelium. *J. Biol. Chem.* 298 (9), 102286. doi:10.1016/j.jbc.2022.102286

Hong, S., Troyanovsky, R. B., and Troyanovsky, S. M. (2010). Spontaneous assembly and active disassembly balance adherens junction homeostasis. *Proc. Natl. Acad. Sci. U. S. A.* 107 (8), 3528–3533. doi:10.1073/pnas.0911027107

Horn, A., Raavicharla, S., Shah, S., Cox, D., and Jaiswal, J. K. (2020). Mitochondrial fragmentation enables localized signaling required for cell repair. *J. Cell. Biol.* 219 (5), e201909154. doi:10.1083/jcb.201909154

Hunter, J. J., Morgan, J. I., Merigan, W. H., Sliney, D. H., Sparrow, J. R., and Williams, D. R. (2012). The susceptibility of the retina to photochemical damage from visible light. *Prog. Retin. Eye Res.* 31 (1), 28–42. doi:10.1016/j.preteyeres.2011.11.001

Hurley, J. B. (2021). Retina metabolism and metabolism in the pigmented epithelium: A busy intersection. *Annu. Rev. Vis. Sci.* 7, 665–692. doi:10.1146/annurev-vision-100419-115156

Iannetti, E. F., Prigione, A., Smeitink, J. A. M., Koopman, W. J. H., Beyrath, J., and Renkema, H. (2019). Live-imaging readouts and cell models for phenotypic profiling of mitochondrial function. *Front. Genet.* 10, 131. doi:10.3389/fgene.2019.00131

Iwai-Takekoshi, L., Ramos, A., Schaler, A., Weinreb, S., Blazeski, R., and Mason, C. (2016). Retinal pigment epithelial integrity is compromised in the developing albino mouse retina. *J. Comp. Neurol.* 524 (18), 3696–3716. doi:10.1002/cne.24025

Kanow, M. A., Giarmarco, M. M., Jankowski, C. S., Tsantilas, K., Engel, A. L., Du, J., et al. (2017). Biochemical adaptations of the retina and retinal pigment epithelium support a metabolic ecosystem in the vertebrate eye. *Elife* 6, e28899. doi:10.7554/eLife.28899

Kaur, G., Tan, L. X., Rathnasamy, G., La Cunza, N., Germer, C. J., Toops, K. A., et al. (2018). Aberrant early endosome biogenesis mediates complement activation in the retinal pigment epithelium in models of macular degeneration. *Proc. Natl. Acad. Sci. U. S. A.* 115 (36), 9014–9019. doi:10.1073/pnas.1805039115

Kwon, S. K., Sando, R., Lewis, T. L., Hirabayashi, Y., Maximov, A., and Polleux, F. (2016). LKB1 regulates mitochondria-dependent presynaptic calcium clearance and neurotransmitter release properties at excitatory synapses along cortical axons. *PLoS Biol.* 14 (7), e1002516. doi:10.1371/journal.pbio.1002516

La Cunza, N., Tan, L. X., Thamban, T., Germer, C. J., Rathnasamy, G., Toops, K. A., et al. (2021). Mitochondria-dependent phase separation of disease-relevant proteins drives pathological features of age-related macular degeneration. *JCI Insight* 6 (9), 142254. doi:10.1172/jci.insight.142254

Lackner, L. L. (2019). The expanding and unexpected functions of mitochondria contact sites. *Trends Cell. Biol.* 29 (7), 580–590. doi:10.1016/j.tcb.2019.02.009

Lakkaraju, A., Umapathy, A., Tan, L. X., Daniele, L., Philp, N. J., Boesze-Battaglia, K., et al. (2020). The cell biology of the retinal pigment epithelium. *Prog. Retin. Eye Res.* 78, 100846. doi:10.1016/j.preteyeres.2020.100846

Lane, A., Philip, L. R., Ruban, L., Fynes, K., Smart, M., Carr, A., et al. (2014). Engineering efficient retinal pigment epithelium differentiation from human pluripotent stem cells. *Stem Cells Transl. Med.* 3 (11), 1295–1304. doi:10.5966/sctm.2014-0094

Liesa, M., and Shirihai, O. S. (2013). Mitochondrial dynamics in the regulation of nutrient utilization and energy expenditure. *Cell. Metab.* 17 (4), 491–506. doi:10.1016/j.cmet.2013.03.002

Liu, Z., Kocaoglu, O. P., and Miller, D. T. (2016). 3D imaging of retinal pigment epithelial cells in the living human retina. *Investig. Ophthalmol. Vis. Sci.* 57 (9), OCT533–43. doi:10.1167/iovs.16-19106

Mao, H., Seo, S. J., Biswal, M. R., Li, H., Conners, M., Nandyala, A., et al. (2014). Mitochondrial oxidative stress in the retinal pigment epithelium leads to localized retinal degeneration. *Investig. Ophthalmol. Vis. Sci.* 55 (7), 4613–4627. doi:10.1167/iovs.14-14633

McWilliams, T. G., Prescott, A. R., Villarejo-Zori, B., Ball, G., Boya, P., and Ganley, I. G. (2019). A comparative map of macroautophagy and mitophagy in the vertebrate eye. *Autophagy* 15 (7), 1296–1308. doi:10.1080/15548627.2019.1580509

Montalbán-Soler, L., Alarcón-Martínez, L., Jiménez-López, M., Salinas-Navarro, M., Galindo-Romero, C., Bezerra de Sá, F., et al. (2012). Retinal compensatory changes after light damage in albino mice. *Mol. Vis.* 18, 675–693.

Murk, J. L., Posthuma, G., Koster, A. J., Geuze, H. J., Verkleij, A. J., Kleijmeer, M. J., et al. (2003). Influence of aldehyde fixation on the morphology of endosomes and lysosomes: Quantitative analysis and electron tomography. *J. Microsc.* 212 (1), 81–90. doi:10.1046/j.1365-2818.2003.01238.x

Murley, A., and Nunnari, J. (2016). The emerging network of mitochondria-organelle contacts. *Mol. Cell.* 61 (5), 648–653. doi:10.1016/j.molcel.2016.01.031

Nordgaard, C. L., Karunadharma, P. P., Feng, X., Olsen, T. W., and Ferrington, D. A. (2008). Mitochondrial proteomics of the retinal pigment epithelium at progressive stages of age-related macular degeneration. *Investig. Ophthalmol. Vis. Sci.* 49 (7), 2848–2855. doi:10.1167/iovs.07-1352

Ozawa, S., Ueda, S., Imamura, H., Mori, K., Asanuma, K., Yanagita, M., et al. (2015). Glycolysis, but not Mitochondria, responsible for intracellular ATP distribution in cortical area of podocytes. *Sci. Rep.* 5, 18575. doi:10.1038/srep18575

Pearson, R. A., Dale, N., Llaudet, E., and Mobbs, P. (2005). ATP released via gap junction hemichannels from the pigment epithelium regulates neural retinal progenitor proliferation. *Neuron* 46 (5), 731–744. doi:10.1016/j.neuron.2005.04.024

Pollreisz, A., Neschi, M., Sloan, K. R., Pircher, M., Mittermueller, T., Dacey, D. M., et al. (2020). Atlas of human retinal pigment epithelium organelles significant for clinical imaging. *Investig. Ophthalmol. Vis. Sci.* 61 (8), 13. doi:10.1167/iovs.61.8.13

Polosa, A., Bessaklia, H., and Lachapelle, P. (2016). Strain differences in light-induced retinopathy. *PLoS One* 11 (6), e0158082. doi:10.1371/journal.pone.0158082

Qiu, K., Zou, W., Fang, H., Hao, M., Mehta, K., Tian, Z., et al. (2022). Light-activated mitochondrial fission through optogenetic control of mitochondria-lysosome contacts. *Nat. Commun.* 13 (1), 4303. doi:10.1038/s41467-022-31970-5

Radu, R. A., Yuan, Q., Hu, J., Peng, J. H., Lloyd, M., Nusinowitz, S., et al. (2008). Accelerated accumulation of lipofuscin pigments in the RPE of a mouse model for ABCA4-mediated retinal dystrophies following Vitamin A supplementation. *Investig. Ophthalmol. Vis. Sci.* 49 (9), 3821–3829. doi:10.1167/iovs.07-1470

Rambold, A. S., Kostelecky, B., Elia, N., and Lippincott-Schwartz, J. (2011). Tubular network formation protects mitochondria from autophagosomal degradation during nutrient starvation. *Proc. Natl. Acad. Sci. U. S. A.* 108 (25), 10190–10195. doi:10.1073/pnas.1107402108

Rattner, A., Toulabi, L., Williams, J., Yu, H., and Nathans, J. (2008). The genomic response of the retinal pigment epithelium to light damage and retinal detachment. *J. Neurosci.* 28 (39), 9880–9889. doi:10.1523/JNEUROSCI.2401-08.2008

Reyes-Reveles, J., Dhingra, A., Alexander, D., Bragin, A., Philp, N. J., and Boesze-Battaglia, K. (2017). Phagocytosis-dependent ketogenesis in retinal pigment epithelium. *J. Biol. Chem.* 292 (19), 8038–8047. doi:10.1074/jbc.M116.770784

Rieger, B., Arroum, T., Borowski, M. T., Villalta, J., and Busch, K. B. (2021). Mitochondrial $F1_FO$ ATP synthase determines the local proton motive force at cristae rims. *EMBO Rep.* 22 (12), e52727. doi:10.15252/embr.202152727

Rieusset, J. (2018). The role of endoplasmic reticulum-mitochondria contact sites in the control of glucose homeostasis: An update. *Cell. Death Dis.* 9 (3), 388. doi:10.1038/s41419-018-0416-1

Rizzuto, R. (2003). The collagen-mitochondria connection. *Nat. Genet.* 35 (4), 300–301. doi:10.1038/ng1203-300

Rózanowski, B., Burke, J. M., Boulton, M. E., Sarna, T., and Rózanowska, M. (2008). Human RPE melanosomes protect from photosensitized and iron-mediated oxidation but become pro-oxidant in the presence of iron upon photodegradation. *Investig. Ophthalmol. Vis. Sci.* 49 (7), 2838–2847. doi:10.1167/iovs.08-1700

Sargiacomo, C., Stonehouse, S., Moftakhar, Z., Sotgia, F., and Lisanti, M. P. (2021). MitoTracker deep red (MTDR) is a metabolic inhibitor for targeting mitochondria and eradicating cancer stem cells (CSCs), with anti-tumor and anti-metastatic activity *in vivo*. *Front. Oncol.* 11, 678343. doi:10.3389/fonc.2021.678343

Seagle, B. L., Rezai, K. A., Kobori, Y., Gasyna, E. M., Rezaei, K. A., and Norris, J. R. (2005). Melanin photoprotection in the human retinal pigment epithelium and its correlation with light-induced cell apoptosis. *Proc. Natl. Acad. Sci. U. S. A.* 102 (25), 8978–8983. doi:10.1073/pnas.0501971102

Segawa, M., Wolf, D. M., Hultgren, N. W., Williams, D. S., van der Bliek, A. M., Shackelford, D. B., et al. (2020). Quantification of cristae architecture reveals time-dependent characteristics of individual mitochondria. *Life Sci. Alliance* 3 (7), e201900620. doi:10.26508/lsa.201900620

Shirazi, M. F., Brunner, E., Laslandes, M., Pollreisz, A., Hitzenberger, C. K., and Pircher, M. (2020). Visualizing human photoreceptor and retinal pigment epithelium cell mosaics in a single volume scan over an extended field of view with adaptive optics optical coherence tomography. *Biomed. Opt. Express* 11 (8), 4520–4535. doi:10.1364/BOE.393906

Tan, L. X., Toops, K. A., and Lakkaraju, A. (2016). Protective responses to sublytic complement in the retinal pigment epithelium. *Proc. Natl. Acad. Sci. U. S. A.* 113 (31), 8789–8794. doi:10.1073/pnas.1523061113

Toops, K. A., Tan, L. X., and Lakkaraju, A. (2014). A detailed three-step protocol for live imaging of intracellular traffic in polarized primary porcine RPE monolayers. *Exp. Eye Res.* 124, 74–85. doi:10.1016/j.exer.2014.05.003

Twig, G., Elorza, A., Molina, A. J., Mohamed, H., Wikstrom, J. D., Walzer, G., et al. (2008). Fission and selective fusion govern mitochondrial segregation and elimination by autophagy. *EMBO J.* 27 (2), 433–446. doi:10.1038/sj.emboj.7601963

Ueda, K., Zhao, J., Kim, H. J., and Sparrow, J. R. (2016). Photodegradation of retinal bisretinoids in mouse models and implications for macular degeneration. *Proc. Natl. Acad. Sci. U. S. A.* 113 (25), 6904–6909. doi:10.1073/pnas.1524774113

Van Houten, B., Woshner, V., and Santos, J. H. (2006). Role of mitochondrial DNA in toxic responses to oxidative stress. *DNA Repair (Amst)* 5 (2), 145–152. doi:10.1016/j.dnarep.2005.03.002

Voets, A. M., Huigsloot, M., Lindsey, P. J., Leenders, A. M., Koopman, W. J., Willems, P. H., et al. (2012). Transcriptional changes in OXPHOS complex I deficiency are related to anti-oxidant pathways and could explain the disturbed calcium homeostasis. *Biochim. Biophys. Acta* 1822 (7), 1161–1168. doi:10.1016/j.bbadis.2011.10.009

Wang, L., Yuan, L., Zeng, X., Peng, J., Ni, Y., Er, J. C., et al. (2016). A multisite-binding switchable fluorescent probe for monitoring mitochondrial ATP level fluctuation in live cells. *Angew. Chem. Int. Ed. Engl.* 55 (5), 1773–1776. doi:10.1002/anie.201510003

Willems, P. H., Rossignol, R., Dieteren, C. E., Murphy, M. P., and Koopman, W. J. (2015). Redox homeostasis and mitochondrial dynamics. *Cell. Metab.* 22 (2), 207–218. doi:10.1016/j.cmet.2015.06.006

Williams, J. A., Greenwood, J., and Moss, S. E. (2013). Retinal changes precede visual dysfunction in the complement factor H knockout mouse. *PLoS One* 8 (7), e68616. doi:10.1371/journal.pone.0068616

Wong, Y. C., Ysselstein, D., and Krainc, D. (2018). Mitochondria-lysosome contacts regulate mitochondrial fission via RAB7 GTP hydrolysis. *Nature* 554 (7692), 382–386. doi:10.1038/nature25486

Woodell, A., Coughlin, B., Kunchithapautham, K., Casey, S., Williamson, T., Ferrell, W. D., et al. (2013). Alternative complement pathway deficiency ameliorates chronic smoke-induced functional and morphological ocular injury. *PLoS One* 8 (6), e67894. doi:10.1371/journal.pone.0067894

Wu, L., Ueda, K., Nagasaki, T., and Sparrow, J. R. (2014). Light damage in Abca4 and Rpe65rd12 mice. *Investig. Ophthalmol. Vis. Sci.* 55 (3), 1910–1918. doi:10.1167/iovs.14-13867

Yao, C. H., Wang, R., Wang, Y., Kung, C. P., Weber, J. D., and Patti, G. J. (2019). Mitochondrial fusion supports increased oxidative phosphorylation during cell proliferation. *Elife* 8, e41351. doi:10.7554/eLife.41351

Zhang, M., Jiang, N., Chu, Y., Postnikova, O., Varghese, R., Horvath, A., et al. (2020). Dysregulated metabolic pathways in age-related macular degeneration. *Sci. Rep.* 10 (1), 2464. doi:10.1038/s41598-020-59244-4

Zhao, C., Yasumura, D., Li, X., Matthes, M., Lloyd, M., Nielsen, G., et al. (2011). mTOR-mediated dedifferentiation of the retinal pigment epithelium initiates photoreceptor degeneration in mice. *J. Clin. Investig.* 121 (1), 369–383. doi:10.1172/JCI44303

frontiers | Frontiers in Cell and Developmental Biology

TYPE Brief Research Report
PUBLISHED 31 October 2022
DOI 10.3389/fcell.2022.1016182



OPEN ACCESS

EDITED BY
Rajalekshmy Shyam,
Indiana University Bloomington,
United States

REVIEWED BY
Wei Liu,
Albert Einstein College of Medicine,
United States
Fei Liu,
Institute of Hydrobiology (CAS), China
Ala Moshiri,
UC Davis Medical Center, United States

*CORRESPONDENCE
Sabine Fuhrmann,
sabine.fuhrmann@vanderbilt.edu

SPECIALTY SECTION
This article was submitted to Signaling, a section of the journal Frontiers in Cell and Developmental Biology

RECEIVED 11 August 2022
ACCEPTED 04 October 2022
PUBLISHED 31 October 2022

CITATION
Fuhrmann S, Ramirez S, Mina Abouda M and Campbell CD (2022), Porcn is essential for growth and invagination of the mammalian optic cup.
*Front. Cell Dev. Biol.* 10:1016182.
doi: 10.3389/fcell.2022.1016182



# Porcn is essential for growth and invagination of the mammalian optic cup

Sabine Fuhrmann[1,2]*, Sara Ramirez[1,2], Mirna Mina Abouda[1] and Clorissa D. Campbell[1]

[1]Department of Ophthalmology and Visual Sciences, Vanderbilt Eye Institute, Vanderbilt University Medical Center, Nashville, TN, United States, [2]Department of Cell and Developmental Biology, Vanderbilt University Medical School, Nashville, TN, United States

Microphthalmia, anophthalmia, and coloboma (MAC) are congenital ocular malformations causing 25% of childhood blindness. The X-linked disorder Focal Dermal Hypoplasia (FDH) is frequently associated with MAC and results from mutations in *Porcn*, a membrane bound O-acyl transferase required for palmitoylation of Wnts to activate multiple Wnt-dependent pathways. Wnt/β-catenin signaling is suppressed in the anterior neural plate for initiation of eye formation and is subsequently required during differentiation of the retinal pigment epithelium (RPE). Non-canonical Wnts are critical for early eye formation in frog and zebrafish. However, it is unclear whether this also applies to mammals. We performed ubiquitous conditional inactivation of *Porcn* in mouse around the eye field stage. In $Porcn^{CKO}$, optic vesicles (OV) arrest in growth and fail to form an optic cup. Ventral proliferation is significantly decreased in the mutant OV, with a concomitant increase in apoptotic cell death. While pan-ocular transcription factors such as PAX6, SIX3, LHX2, and PAX2 are present, indicative of maintenance of OV identity, regional expression of VSX2, MITF, OTX2, and NR2F2 is downregulated. Failure of RPE differentiation in $Porcn^{CKO}$ is consistent with downregulation of the Wnt/β-catenin effector LEF1, starting around 2.5 days after inactivation. This suggests that *Porcn* inactivation affects signaling later than a potential requirement for Wnts to promote eye field formation. Altogether, our data shows a novel requirement for Porcn in regulating growth and morphogenesis of the OV, likely by controlling proliferation and survival. In FDH patients with ocular manifestations, growth deficiency during early ocular morphogenesis may be the underlying cause for microphthalmia.

KEYWORDS

**microphthalmia, Focal Dermal Hypoplasia, Goltz Syndrome, *Porcn*, Wnt, optic vesicle, optic cup, mouse**

## Introduction

Congenital ocular malformations—microphthalmia (small eye), anophthalmia (absent eye, also called extreme microphthalmia), coloboma (optic fissure closure defect in the ventral optic cup) (collectively hereafter MAC)—originate from defective morphogenesis during early eye development and cause 25% of childhood blindness (Clementi et al., 1992; Morrison et al., 2002; Graw, 2019). Eye development is initiated during gastrulation in a single domain in the anterior neural plate, the eye field, characterized by expression of eye field transcription factors (EFTFs) that include Pax6, Six3, Six6, Rx, Tbx3, and Lhx2 (Oliver et al., 1995; Zuber et al., 2003; Bailey et al., 2004; Motahari et al., 2016; Liu and Cvekl, 2017). In combination with secreted factors inhibiting Nodal, BMP and Wnt/β-catenin signaling, EFTFs form a gene regulatory network to promote eye field specification (Zuber et al., 2003). Subsequentially, the eye field separates into two optic pits that evaginate laterally. Bilateral optic vesicles (OVs) are formed, comprised of neuroepithelial progenitor cells giving rise to optic stalk, retina and RPE. The distal domain of the OV contacts the overlying surface (lens) ectoderm, and both OV and ectoderm invaginate to form the optic cup (OC) and the lens vesicle, respectively. While the coordinated interactions regulating regionalization of OC and OV are well studied [for reviews, see (Fuhrmann, 2010; Viczian, 2014; Miesfeld and Brown, 2019)], regulation of the morphogenetic events during OV evagination and OC invagination are less understood.

Focal Dermal Hypoplasia (FDH; Goltz Syndrome) is an x-linked dominant disorder resulting from abnormal mesodermal and ectodermal development and is frequently associated with MAC (Goltz et al., 1962; Temple et al., 1990; Wang et al., 2014; Gisseman and Herce, 2016). FDH is caused by mutations in *Porcn*, a membrane bound O-acyl transferase localized to the endoplasmic reticulum (Grzeschik et al., 2007; Wang et al., 2007). Porcn is mostly dedicated to palmitoylate the Wnt family of cysteine-rich secreted glycoproteins, and this modification is necessary for trafficking and signaling (Tanaka et al., 2000; Galli et al., 2007). Porcn is expressed in the developing mouse eye (Biechele et al., 2011). We have shown that conditional *Porcn* disruption at the OV stage results in coloboma and RPE defects in most embryos, among other abnormalities (Bankhead et al., 2015).

Wnt ligands bind to surface receptors, including Frizzled transmembrane receptors (Fzd), and activate canonical (Wnt/β-catenin) and non-canonical pathways. Wnt/β-catenin activation prevents cytoplasmic degradation of β-catenin, thereby allowing its nuclear translocation to activate Tcf/Lef1 transcription factors. Wnt/β-catenin exerts many distinct functions during different phases of eye development [for reviews, see (Fuhrmann, 2008; Fujimura, 2016)]. During early OC morphogenesis, it is required for RPE differentiation (Fujimura et al., 2009; Westenskow et al., 2009; Hagglund et al., 2013) and dorsoventral patterning (Veien et al., 2008; Zhou et al., 2008). The pathway is tightly regulated; ectopic activation by disruption of the antagonists *Dkk1* and *Axin2* can result in microphthalmia and coloboma (Lieven and Ruther, 2011; Alldredge and Fuhrmann, 2016). During forebrain development, multiple antagonists maintain anterior neural fate. Hyperactive Wnt/β-catenin frequently leads to posterization and rostral truncation of the forebrain, with concomitant severe decrease of EFTF expression. The EFTF Six3 can directly suppress Wnt/β-catenin signaling (Lagutin et al., 2003), providing another mechanism for precise coordination of pathway activity.

Non-canonical, β-catenin-independent Wnt signaling occurs *via* multiple pathways, including intracellular $Ca^{2+}$ release, activation of JNK and Planar Cell Polarity (PCP). It is essential for eye field formation in non-mammalian vertebrates by different mechanisms; it represses Wnt/β-catenin activity and promotes expression of EFTFs in frog and zebrafish (for review, see (Fuhrmann, 2008)). Close to the caudal border of the eye field, non-canonical Wnt11f2 (formerly Wnt11) and Wnt4 act through Fzd5 and Fzd3 to promote expression of the EFTFs Pax6 and Rx (Rasmussen et al., 2001; Cavodeassi et al., 2005; Maurus et al., 2005). In addition, Wnt11f2 and crosstalk between JNK/PCP and ephrinB1 are required for morphogenetic movements of ocular progenitor cells into the eye field (Heisenberg et al., 2000; Moore et al., 2004; Cavodeassi et al., 2005; Lee et al., 2006; Cavodeassi et al., 2013). However, it is unknown whether non-canonical Wnt signaling functions similarly in mammals; for example, germline disruption of *Wnt4, Wnt11, Fzd3* does not cause obvious ocular phenotypes, suggesting either redundancy of pathway components and/or context- and species-dependent mechanisms.

To investigate the role of Porcn before OV morphogenesis, we performed temporally controlled inactivation before and during the eye field stage when Wnts are expressed in the cranial region (Parr et al., 1993; Kispert et al., 1996; Yamaguchi et al., 1999; Kemp et al., 2005). Our results show that *Porcn* inactivation around eye field formation leads to severely arrested OV 3 days later. Key regulatory genes for RPE differentiation OTX2, MITF, and NR2F2 are absent, proliferation and survival of ocular progenitors in the OV is decreased, and invagination during OC morphogenesis fails. Our studies reveal a novel role for Porcn during earliest stages of mouse eye development, recapitulating severe microphthalmia in FDH.

## Materials and methods

Mouse lines were maintained on a mixed genetic C57BL/6 and CD-1 background. For temporally controlled *Porcn* inactivation, a conditional *Porcn* allele, tamoxifen-inducible, ubiquitous *Gt(ROSA)26Sor*$^{tm1(cre/ERT)Nat}$ (hereafter *ROSA26*$^{CreERT}$) and the recombination reporter *RosaR26* were utilized, with established genotyping protocols or Transnetyx (Cordova, TN) using Taqman with custom-designed primers

(Soriano, 1999; Badea et al., 2003; Barrott et al., 2011; Bankhead et al., 2015; Sun et al., 2020). Noon of the day with an observed vaginal plug was counted E0.5. Pregnant dams received tamoxifen (0.1 mg/g) by oral gavage between E6.5 and E7.5 (Park et al., 2008). To detect proliferating cells, pregnant dams received one intraperitoneal EdU injection 2 hours before sacrificing (30 μg/g; Thermofisher/Invitrogen; #E10187). Male embryos with conditional deletion of *Porcn* (hereafter $Porcn^{CKO}$) and control littermates were processed as previously published (Sun et al., 2020). For antigen retrieval, cryostat sections were treated with 1% Triton X-100 or hot citrate buffer (pH 6). Detailed antibody information is provided in Supplementary Table S1. Filamentous actin was detected using Phalloidin (1: 50; Thermo Fisher Scientific; #A12379). ApopTag Fluorescein *In Situ* Apoptosis Detection Kit (EMD Millipore, #S7110) was used to detect apoptotic cells. For EdU detection, the Click-iT® EdU Imaging Kit (Thermo Fisher Scientific; #C10637) was utilized. Cryostat sections were counter-labeled with DAPI and mounted in Prolong Gold Antifade. No obvious defects in morphology, proliferation or OV marker expression were observed in controls: conditional heterozygous female embryos (hereafter $Porcn^{CHET}$) and embryos with or without *Cre*. Unless otherwise indicated, a minimum of 3 embryos from at least 2 individual litters were analyzed per genotype, time point and marker. For analyses of E9.5 embryos induced at E6.5, 3 embryos were analyzed and 2 showed indication of ocular development.

Images were captured using a U-CMAD3 camera, mounted on an Olympus SZX12 stereomicroscope, and a XM10 camera, mounted on an Olympus BX51 epifluorescence system. For confocal imaging, the Olympus FV100 or ZEISS LSM 880 systems were used. Images were processed using ImageJ (NIH) and Adobe Photoshop software (versions CS6, 23.5.1).

Quantification of EdU-labeled and Tunel-labeled cells was performed on cryostat sections midway through the OV, with separation of dorsal and ventral subdivisions. The percentage of labeled cells was calculated by determining the number of total cells using DAPI-labeled nuclei. Statistical analysis was performed using Prism version 9 (Graphpad) for One-Way ANOVA.

# Results

## Conditional *Porcn* inactivation before eye field induction (E6.5) causes abnormal OV morphogenesis

We observed that Porcn needs to be depleted in multiple ocular and extraocular tissues at the OV stage to recapitulate consistently the ocular abnormalities found in FDH patients (Bankhead et al., 2015). In mouse, the eye field becomes established at E7.5, and Wnts are expressed in tissues adjacent to the eye field. To target both cell autonomous and non-cell autonomous Wnt production, we disrupted *Porcn* using the ubiquitous $ROSA26^{CreERT}$, allowing temporally controlled recombination. To account for delay of pathway inactivation in responding cells due to cell non-autonomous Wnt ligand production, extracellular release and downstream receptor activation, we started inactivating *Porcn* at E6.5. *RosaR26* recombination confirmed ubiquitous *Cre* activity, as expected (Supplementary Figure S1) (Soriano, 1999). At E8.5–8.75, $Porcn^{CKO}$ show severe posterior truncation (Barrott et al., 2011; Biechele et al., 2013). However, anterior regions do continue to develop, with reduced size of OVs (Figures 1B–H; 8–13 somites). In $Porcn^{CKO}$, expression of the Wnt/β-catenin readout LEF1 can be slightly decreased in the dorsal OV, consistent with decreased Wnt signaling (Figure 1D). Lhx2 is required for the transition from eye field to OV and is robustly expressed in $Porcn^{CKO}$ (Figure 1F). Otx2 is critical for rostral brain regionalization and early ocular development. In $Porcn^{CKO}$, OTX2 expression is present in the dorsal OV (Figure 1H). To determine whether the observed alterations could be due to a developmental delay, we examined $Porcn^{CKO}$ embryos 1–2 days later. We observed major developmental abnormalities on E10.5 $Porcn^{CKO}$ embryos, not suitable for further analysis (Supplementary Figure S2). Thus, we continued to examine embryos at E9.5 (20–23 somites); $Porcn^{CKO}$ exhibit more defects compared to E8.5–8.75, including abnormalities in the head region (Figures 1J,K). Morphogenesis of the OVs does not proceed properly; they are arrested and fail to contact the surface ectoderm (Figure 1M,O,Q,S). Expression of LEF1 is absent in the dorsal OV, indicating loss of Wnt/β-catenin signaling (Figure 1M). Phalloidin labeling reveals that apicobasal polarity is generally preserved (Figure 1O). Thus, it is possible that non-canonical Wnt pathways such as planar cell polarity are largely maintained. Robust LHX2 expression is maintained in $Porcn^{CKO}$ (Figure 1Q). In contrast, OTX2 is downregulated in the dorsal OV, while weak expression is detectable in the adjacent forebrain (Figure 1S). Overall, our results demonstrate that *Porcn* inactivation starts to affect eye development after approx. 2.5 days, with slightly decreased Wnt/β-catenin signaling in the dorsal OV. Evagination can occur, suggesting that OV identity is maintained, and morphogenesis initiated. However, with ongoing loss of Porcn at E9.5, dorsal regionalization and expansion of the OV is severely affected.

## *Porcn* deletion during eye field induction (E7.5) variably affects brain and eye formation

To bypass major developmental defects before OV morphogenesis (Figure 1), we administered tamoxifen 1 day later (E7.4–7.5). At E10.5, $Porcn^{CKO}$ embryos were recovered with a range of ocular abnormalities, possibly due to developmental variability between litters and embryos at the

10.3389/fcell.2022.1016182

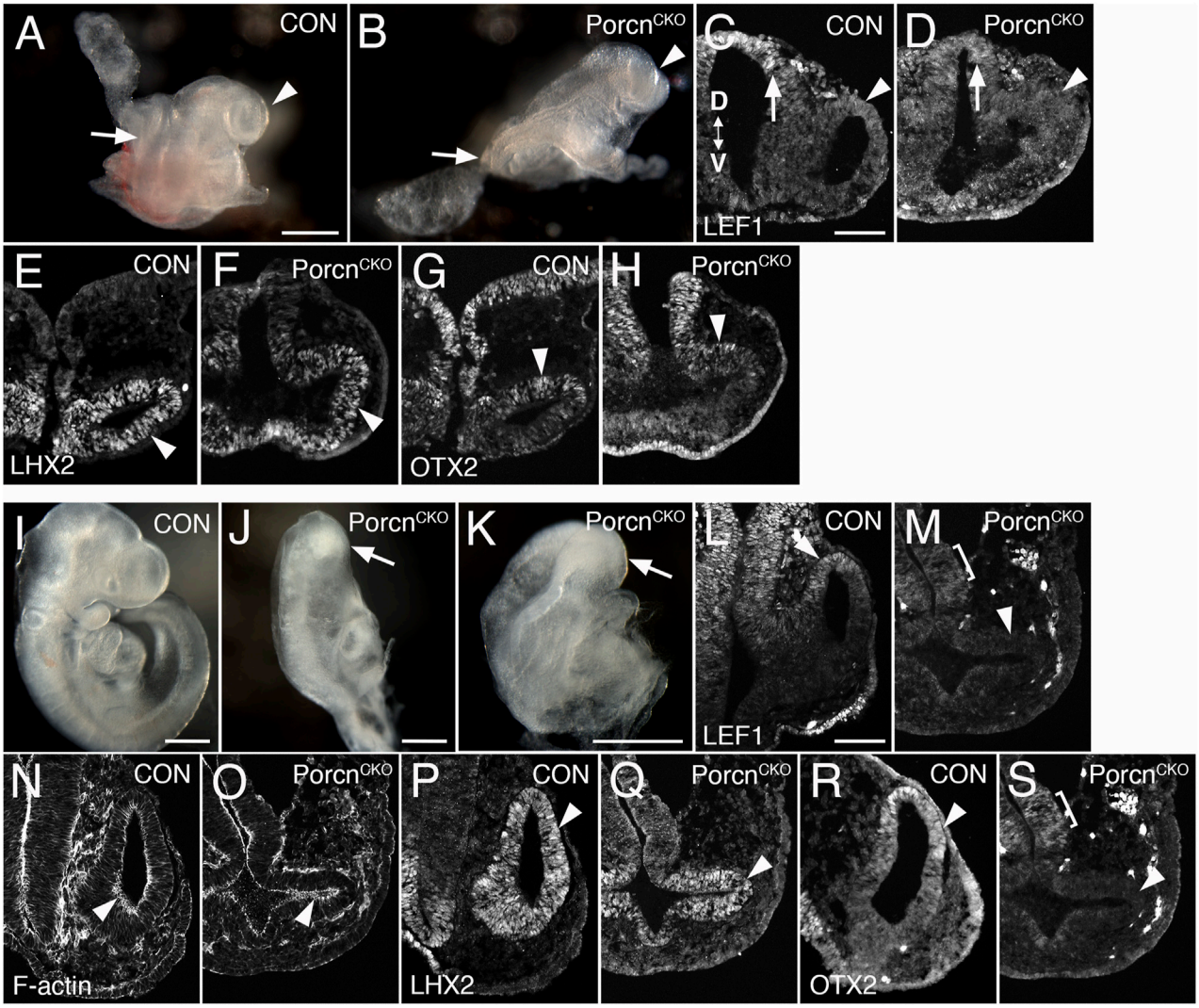


FIGURE 1
Conditional *Porcn* inactivation before eye field formation (E6.5) interferes with early OV morphogenesis. **(A–H)** Embryos at E8.75-E9.0. **(A)** Control embryo (8 somites) with OVs (arrowhead). **(B)** *Porcn*$^{CKO}$ with caudal truncation (arrow; somites not detectable). Head development proceeds at this stage and OV-like structures are present (arrowhead). **(C and D)** LEF1 expression in 13 somite embryos. Coronal cryostat sections show slightly decreased LEF1 expression in the dorsal OV of *Porcn*$^{CKO}$ (D; arrowhead), expression in the dorsal and ventral forebrain is largely maintained (D; arrow). **(E–H)**: 7-8 somite embryos. **(F)** LHX2 is robustly expressed in the mutant OV (arrowhead). **(H)** In *Porcn*$^{CKO}$, OTX2 expression is present in the dorsal OV (arrowhead). **(I–S)** Embryos at E9.5 (20–23 somites); 2 of 3 embryos showed distinct OVs, shown here in **(J–S)**. **(J–K)** Examples of *Porcn*$^{CKO}$ showing severe abnormalities throughout the body, including the heads (arrows). **(M)** LEF1 expression is absent in *Porcn*$^{CKO}$ OV (arrowhead), low expression is detectable in the adjacent diencephalon (bracket). **(O)** Phalloidin labeling shows that apicobasal polarity is largely maintained in *Porcn*$^{CKO}$ (arrowhead). **(Q)** In the mutant OV, LHX2 is robustly expressed, similar to controls (arrowhead). **(S)** OTX2 is absent in the OV of *Porcn*$^{CKO}$ (arrowhead). Weak expression is detectable in the forebrain neuroepithelium (bracket). Controls: *Porcn*$^{CHET}$. OV: optic vesicle. D < - > V: Dorsoventral orientation. Scale bars A, B, I–K: 0.5 mm; C, L: 0.1 mm.

time of tamoxifen administration (Figure 2; 9 litters with 26 *Porcn*$^{CKO}$ embryos). In 5 *Porcn*$^{CKO}$, no detectable eye phenotype was observed (19%; not shown). In mildly affected *Porcn*$^{CKO}$, telencephalic vesicles are slightly smaller (Figure 2F). Eye size can be reduced, associated with incomplete OC morphogenesis, failure of lens vesicle formation and accumulation of POM between distal OV and surface ectoderm (Figures 2G–J; 27%, n = 7). In mildly affected *Porcn*$^{CKO}$, OVs can be more closely associated with lens ectoderm, occasionally with further advanced invagination (not shown). We also observed *Porcn*$^{CKO}$ embryos with a more severe developmental and ocular phenotype (Figures

10.3389/fcell.2022.1016182

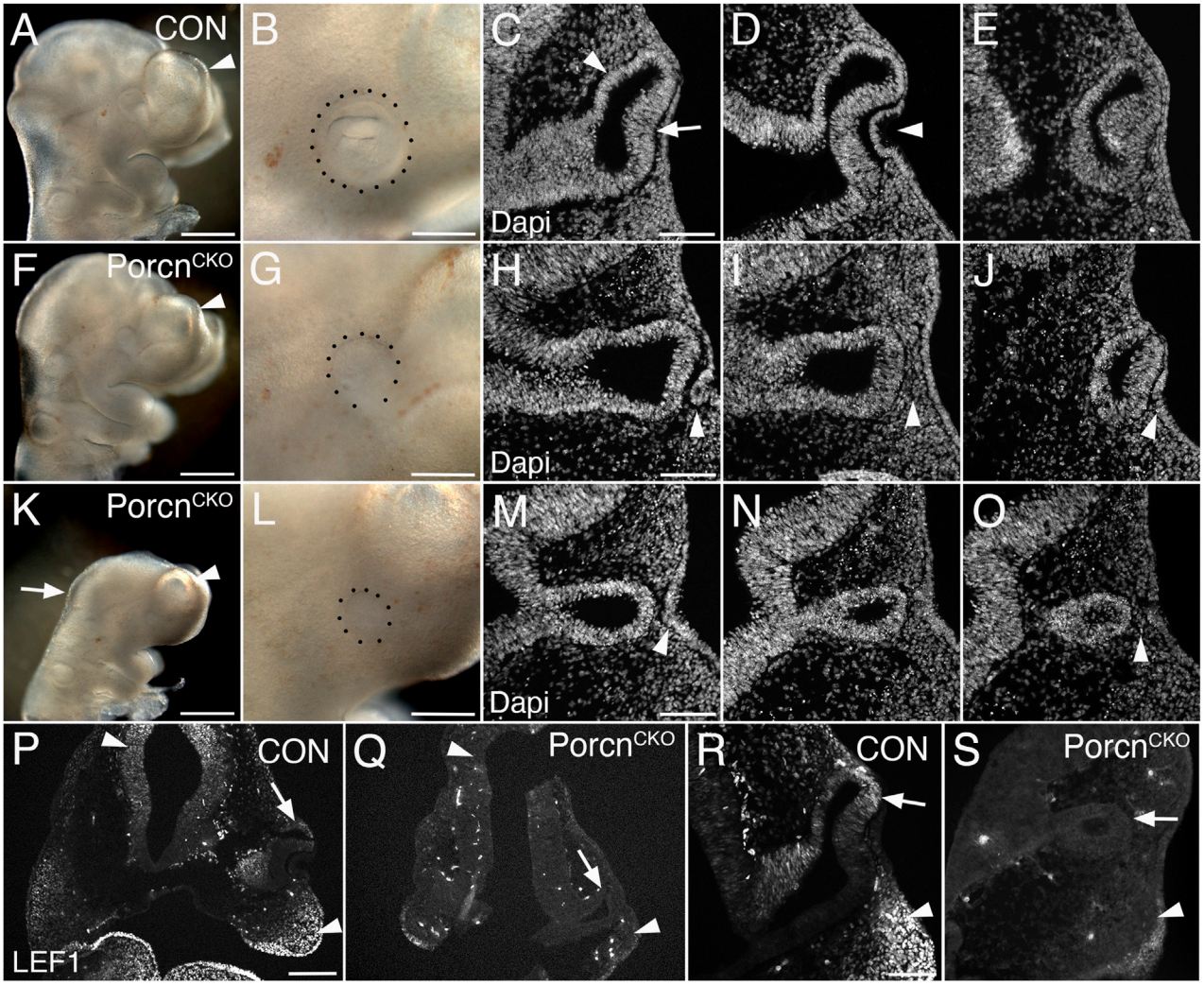


FIGURE 2
Conditional *Porcn* inactivation during eye field formation (E7.4-7.5) causes a range of brain and ocular abnormalities at E10.5. **(A–E)** Control *Porcn*$^{CHET}$ embryos showing telencephalic vesicle (A; arrowhead), early OC with lens vesicle (B; dotted outline), presumptive RPE and neural retina (C; arrowhead and arrow, respectively) and invaginating lens vesicle (D; arrowhead) in sequential Dapi-labeled coronal sections **(C–E)**. **(F–J)** *Porcn*$^{CKO}$ with mild abnormalities; reduced telencephalic vesicle size (F; arrowhead), reduced eye size **(G)**, incomplete invagination of OV and lens ectoderm (H, J; arrowheads) and accumulation of POM between distal OV and lens ectoderm (I; arrowhead). **(K–O)** *Porcn*$^{CKO}$ with major defects showing loss of the mid-hindbrain border and further reduction of telencephalic vesicles (K; arrow and arrowhead, respectively), microphthalmia (L; dotted outline, compare B, G, L), arrested OV **(M–O)** and accumulation of POM (O; arrowhead). Some thickening of the surface can occur (M; arrowhead). **(P–S)** LEF1 immunolabeling of coronal control *Porcn*$^{CHET}$ sections shows expression in the dorsal forebrain (P, left arrowhead), facial primordia mesenchyme (P; right arrowhead, R; arrowhead) and dorsal OC (P, R; arrows). In *Porcn*$^{CKO}$ embryos, LEF1 is severely reduced in the dorsal forebrain (Q; left arrowhead), facial primordia (Q; right arrowhead, S; arrowhead) and dorsal OC (Q, S; arrows). Scale bars A, F, K: 0.5 mm; B, G, L, P: 0.2 mm; C, H, M, R: 0.1 mm.

2K–S; 54%, n = 14). These *Porcn*$^{CKO}$ embryos exhibit defects in mid- and forebrain development; the mid-hindbrain border is missing and telencephalic vesicles are underdeveloped (Figure 2K). Ocular morphogenesis is consistently arrested with small OVs that fail to expand, with abnormal accumulation of anterior POM preventing close contact between distal OV and lens ectoderm (Figure 2L–O). Consequently, neither the OV nor the surface ectoderm show any signs of invagination (Figure 2M–O). Some thickening of the surface ectoderm is occasionally detectable, suggesting that early aspects of lens morphogenesis can be initiated (Figure 2M). In *Porcn*$^{CKO}$ embryos with a severe phenotype, overall LEF1 expression is decreased, specifically in the dorsal forebrain, dorsal OV and facial primordia, indicating widespread downregulation of the Wnt/β-catenin pathway (Figures 2Q,S).

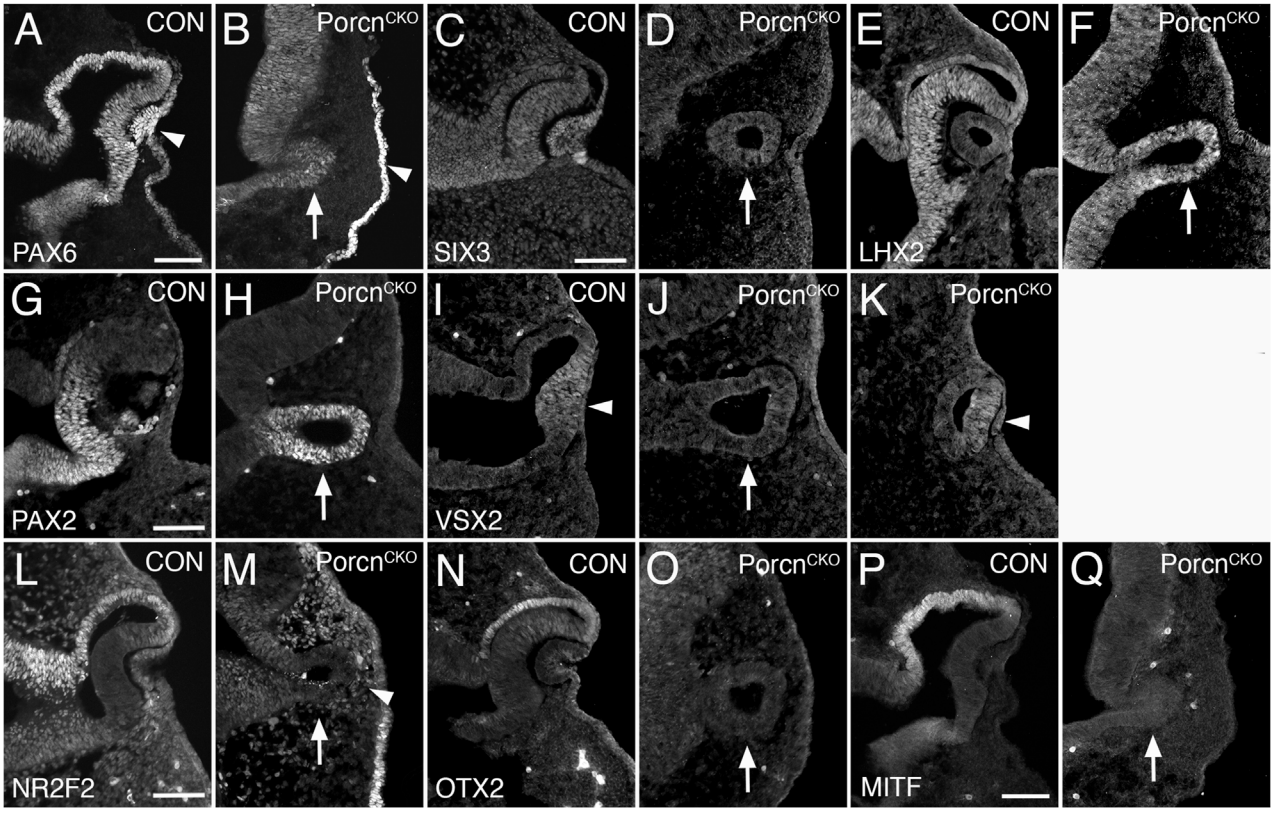


FIGURE 3
*Porcn* mutant embryos display defective regionalization at E10.5. Coronal view of control embryos **(A,C,E,G,I,L,N,P)** and *Porcn*$^{CKO}$ embryos that were treated with tamoxifen at E7.4 **(B,D,F,H,J,K,M,O,Q)**. **(A)** During normal eye development, PAX6 is expressed in ocular tissues and in the overlying surface ectoderm (arrowhead). **(B)** In the mutant OV, PAX6 expression is expressed (arrow) and is present in the surface ectoderm (arrowhead). **(C and D)** SIX3 expression is not altered in the OV and surface ectoderm of *Porcn*$^{CKO}$ (D; arrow). **(E and F)** In control (E) and in *Porcn*$^{CKO}$ (F; arrow) LHX2 is expressed throughout the OC and OV, respectively. **(G)** In control OC, PAX2 is restricted to the ventral OC. **(H)** In *Porcn*$^{CKO}$, PAX2 expression is maintained throughout the OV (arrow). **(I)** In controls, the distal OC is tightly attached to the overlying lens ectoderm and expresses VSX2 (arrowhead). **(J)** In *Porcn*$^{CKO}$ with loss of close contact, VSX2 is not detectable (arrow). **(K)** When distal OV and lens ectoderm are closely associated, some cells in the distal OV in *Porcn*$^{CKO}$ can express VSX2 (arrowhead). **(L)** NR2F2 expression shown in control embryos. **(M)** In the OV of *Porcn*$^{CKO}$, NR2F2 expression is missing (arrow). NRF2 expressing POM cells are abnormally present between distal OV and surface ectoderm (arrowhead). **(N,O)** OTX2 is normally robustly expressed in the presumptive RPE of the OC but is absent in the mutant OV (O; arrow). **(P)** MITF is an early differentiation marker restricted to the presumptive RPE. **(Q)** In the OV of *Porcn*$^{CKO}$, MITF expression is not detectable (arrow). Scale bars A, C, G, L, P: 0.1 mm.

## Eye field transcription factors are robustly expressed in the arrested OV of severely affected E10.5 *Porcn*$^{CKO}$

Since OC morphogenesis is consistently and impaired the most, we proceeded with analyzing severely affected E10.5 *Porcn*$^{CKO}$ (Figures 2F–J). The pan-ocular transcription factor PAX6 is expressed in the arrested *Porcn*$^{CKO}$ OV and also present in the surface ectoderm (Figure 3B). The eye field transcription factor Six3 is required for neuroretinal specification the mammalian eye (Liu et al., 2010; Liu and Cvekl, 2017). SIX3 expression is not altered in the OV and surface ectoderm of *Porcn*$^{CKO}$ (Figure 3D). LHX2 is not altered (Figure 3F), confirming that general ocular specification including OV identity are maintained at later stages.

## *Porcn* mutant embryos display defective regionalization of the arrested OV at E10.5

The paired homeobox transcription factor PAX2 is initially expressed throughout the OV and is later confined to the ventral OC and optic stalk (Nornes et al., 1990; Burns et al., 2008). In *Porcn*$^{CKO}$, PAX2 expression is maintained throughout the OV (Figure 3H), consistent with failure of OC formation and dorsoventral regionalization. During normal eye development, proximodistal regionalization into RPE and retina occurs in the advanced OV (Fuhrmann, 2010; Fuhrmann et al., 2014; Miesfeld and Brown, 2019). In *Porcn*$^{CKO}$ with loss of close contact due to POM accumulation between the distal OV and surface ectoderm (Figure 2), the strictly retina-specific CVC homeodomain transcription factor VSX2 is not expressed (Figure 3J)

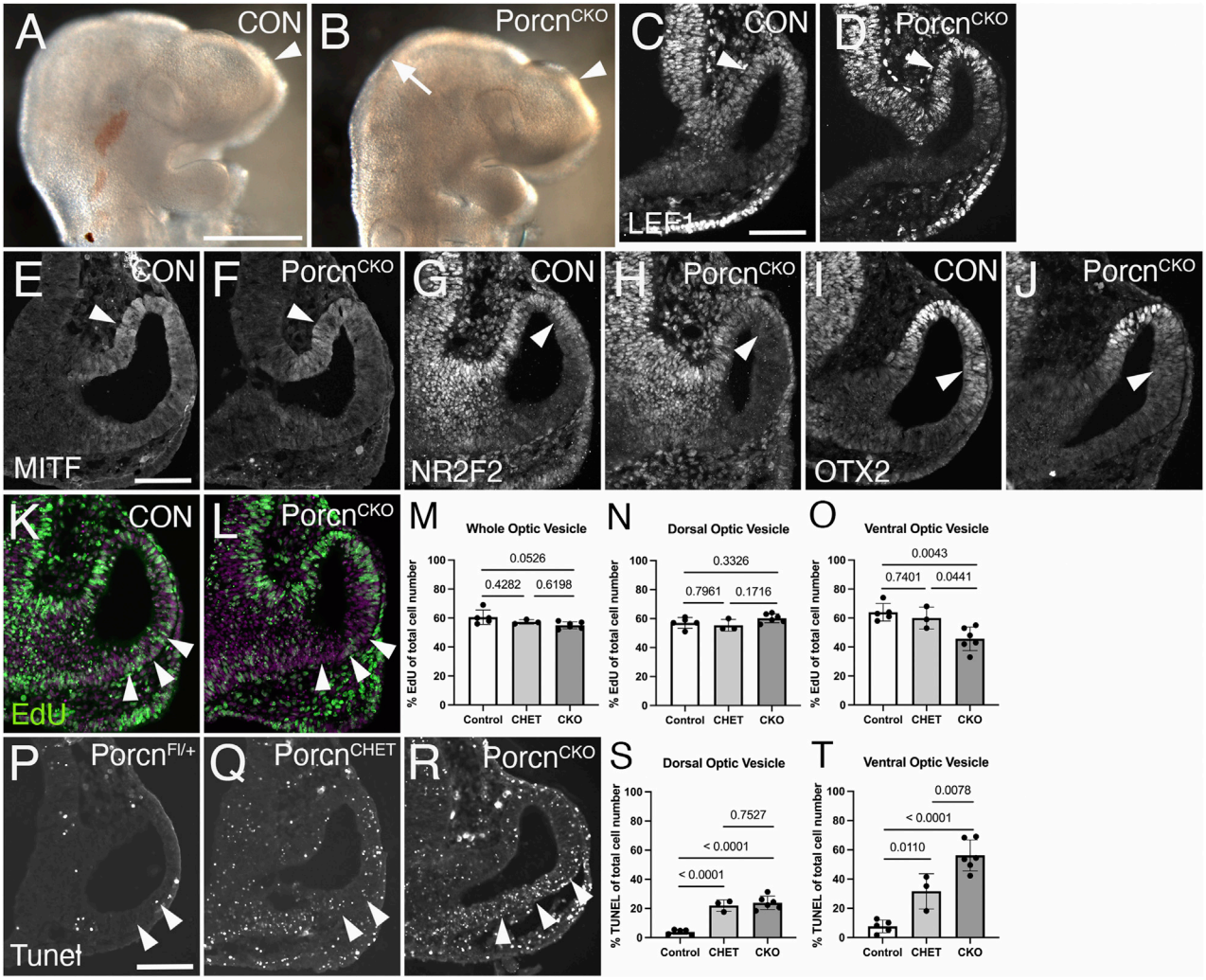


FIGURE 4
Decrease of proliferation, survival and local NR2F2 and OTX2 expression in the *Porcn*$^{CKO}$ OV at E9.5. Coronal view of control embryos (A,C,E,G,I,K; *Porcn*$^{CHET}$) and *Porcn*$^{CKO}$ embryos, induced at E7.4–7.5 (B,D,F,H,J,L). **(A)** Telencephalic vesicle in E9.5 control embryo (arrowhead). **(B)** *Porcn*$^{CKO}$ show slightly smaller telencephalic vesicles (arrowhead) and mid-hindbrain regions (arrow). **(C)** In controls, LEF1 is expressed in the dorsal OV (arrowhead). **(D)** In *Porcn*$^{CKO}$ embryos, LEF1 is unaltered (arrowhead). **(E and F)** MITF expression appears unaffected in the presumptive RPE of *Porcn*$^{CKO}$ (F; arrowhead). **(G and H)** In the mutant RPE, NR2F2 can be slightly downregulated in the dorsal OV (H; arrowhead). **(I and J)** OTX2 can start to be reduced dorsally in the distal OV domain in Porcn$^{CKO}$ (J; arrowhead). **(K,L)** Edu incorporation (green) in control **(K)** and in Porcn$^{CKO}$ OV **(L)**, showing reduced number of EdU-labeled cells in the ventral OV (L; arrowheads). Magenta: Dapi. **(M–O)** Quantification of EdU labeled cells in the entire OV **(M)**, dorsal OV **(N)** and ventral OV **(O)**. In Porcn$^{CKO}$, the number of EdU-labeled cells is significantly reduced in the ventral OV **(O)**. **(P–R)** Coronal view of representative images of Tunel-labeled E9.5 sections induced with tamoxifen at E7.4. Arrowheads mark the Tunel-labeled region in the ventral OV. Compared to *Cre*-negative controls **(P)**, overall Tunel signal is increased throughout the tissues in *Porcn*$^{CHET}$ and *Porcn*$^{CKO}$ embryos **(Q)**. In the ventral OV of *Porcn*$^{CKO}$ embryos, more Tunel-labeled cells are detectable **(R)**, compared to *Porcn*$^{CHET}$ **(Q)**. **(S,T)** Quantification of Tunel-labeled cells in the ventral OV shows a significant increase in *Porcn*$^{CKO}$ **(T)**. Quantitative data are means ± s.d. One-way ANOVA with Tukey's posthoc analysis was applied for statistical analysis, and *p*-values are indicated on the horizontal lines in each graph (significance <0.05). Scale bars A: 0.5 mm; C, E, P: 0.1 mm.

(Burmeister et al., 1996; Green et al., 2003). However, if close contact occurs in *Porcn*$^{CKO}$, some cells in the presumptive retina can express VSX2 (Figure 3K), consistent with the requirement of lens-derived FGF for retina specification (Cai et al., 2013). Concerning proximal regionalization, we observed a complete loss of the key regulatory transcription factors NR2F2, OTX2, and MITF (Figure 3M,O,Q) that are required for RPE differentiation (Hodgkinson et al., 1993; Bumsted and Barnstable, 2000; Nguyen and Arnheiter, 2000; Martinez-Morales et al., 2001; Tang et al., 2010). NR2F2 expression confirms abnormal abundance of POM between distal OV and lens ectoderm (Figure 3M). Together, our results

demonstrate that dorsoventral and proximodistal regionalization is impaired in the arrested OV of *Porcn*$^{CKO}$ at the time when OC morphogenesis normally commences.

## Decrease of proliferation, survival and local NR2F2 and OTX2 expression in the *Porcn*$^{CKO}$ OV at E9.5

To elucidate a potential mechanism underlying abnormal ocular growth obvious in E10.5 *Porcn*$^{CKO}$, we analyzed embryos 1 day earlier, following tamoxifen induction at E7.4-E7.5. At E9.5, *Porcn*$^{CKO}$ show slightly decreased telencephalic vesicles and mid-hindbrain regions (Figure 4B). LEF1 expression in the dorsal OV and adjacent dorsal forebrain neuroepithelium in *Porcn*$^{CKO}$ embryos is unaltered, suggesting that Wnt/β−catenin signaling is intact at this age (Figure 4D). MITF expression is not affected in the presumptive RPE of *Porcn*$^{CKO}$ (Figure 4F). However, other RPE markers NR2F2 and OTX2 start to be reduced dorsally in the distal OV domain (Figures 4H,J) suggesting that some aspects of regionalization can be affected at this age.

To determine effects on proliferation, we quantified the number of E9.5 OV cells incorporating EdU (Figures 4K–O). In *Porcn*$^{CKO}$, the number of EdU-labeled cells show a trend in decrease in the entire OV (Figures 4L,M). This effect is specifically due to a significant reduction in the ventral OV by 24% and 29%, compared to *Porcn*$^{CHET}$ and *Porcn*$^{Fl/+/y}$, respectively (Figure 4O). We also examined apoptotic cell death in ocular progenitors. Compared to *Porcn*$^{CHET}$, the percentage of Tunel-labeled cells is significantly upregulated by 78% in the ventral OV of *Porcn*$^{CKO}$ (Figures 4R,T). Unexpectedly, we observed a considerable effect of *Porcn* gene reduction on survival of ocular progenitors; *Porcn*$^{CHET}$ OVs show an overall significant increase in Tunel-labeled cells, compared to *Porcn*$^{Fl/+/y}$ (Figures 4Q,S,T). These results suggest that already 2 days after tamoxifen administration loss of *Porcn* negatively impacts both survival and proliferation of ocular progenitors in the ventral OV. These changes occur before major defects in expression of the Wnt/β−catenin readout LEF1, regionalization markers and abnormal morphogenesis become obvious.

# Discussion

Our results show that *Porcn* inactivation either before or during eye field formation leads to severely arrested OVs, likely due to an increase in cell death and downregulation of proliferation. In *Porcn*$^{CKO}$, the RPE key regulatory transcription factors OTX2, MITF and NR2F2 are downregulated. POM accumulates between distal OV and adjacent surface ectoderm, preventing tight association, and the retina-specific gene VSX2 is not properly expressed. Arrested eye vesicles in *Porcn*$^{CKO}$ do not invaginate, resulting in failed invagination of the OV into an OC. Our studies reveal a novel role for Porcn in the OV as the earliest obvious morphological stage of eye development and a continued requirement during OC morphogenesis, recapitulating severe microphthalmia in FHD.

## Effect of *Porcn* disruption on wnt signaling

We first determined when potential effectors of Wnt signaling are affected by *Porcn* inactivation at E6.5. Wnt/β−catenin signaling is normally not active until OV invagination starts; the pathway readouts *Axin2* and *BATgal* reporter are absent in the OV around E8.75 (8 somites) (Liu et al., 2010). Here, we observed that another readout, LEF1, starts to become weakly expressed around E9.0 in the dorsal OV of controls (13 somites; Figure 1C). In *Porcn*$^{CKO}$ embryos, LEF1 is slightly downregulated in the dorsal OV (Figure 1D) suggesting commencement of a pathway response. Indeed, in the E9.5 OV, LEF1 is absent, demonstrating complete shutdown of the pathway, and OV morphogenesis is abnormal (Figure 1M). Thus, it takes at least 2.5 days after tamoxifen treatment to detect initial effects of *Porcn* inactivation on Wnt/β−catenin signaling and approximately 3 days to observe defects in gene expression and eye morphogenesis.

Since Wnt/β-catenin signaling needs to be suppressed in the anterior neural plate, we reasoned that any requirement for Porcn would be likely due to a need for the non-canonical Wnt pathway. Inactivation of *Porcn* also prevents potentially confounding, concomitant upregulation of Wnt/β-catenin signaling. Consistent with this, arrested growth of the OV has not been observed by early Wnt/β−catenin pathway inactivation in other studies (Hagglund et al., 2013). We observed that the putative non-canonical Wnt pathway readout pJUN is normally not robustly expressed in the E9.5 OV (not shown), and F-actin shows normal apicobasal localization in *Porcn*$^{CKO}$ (Figure 1). However, we cannot exclude effects on other potential non-canonical Wnt targets in *Porcn*$^{CKO}$. In addition, Porcn can exert Wnt-independent roles in regulating cancer growth and AMPA receptor assembly and function in rate hippocampal neurons (Covey et al., 2012; Erlenhardt et al., 2016). While we cannot exclude Wnt-independent roles of Porcn during early eye development, it needs to be shown whether these functions are critical for early forebrain development.

## Porcn is not required for maintenance of EFTF expression in the OV and OC

Eye field formation with expression of EFTFs in mouse starts around E7.5. To determine Porcn's role during the

earliest stages of eye morphogenesis, we induced inactivation at E6.5. Analysis of E8.75–9.5 $Porcn^{CKO}$ embryos revealed that expression of the EFTFs LHX2 and OTX2 is unaffected at E9.0, and that LHX2 is still present 3 days after tamoxifen induction (Figures 1F,H,Q). This also applies to $Porcn^{CKO}$ induced at E7.5 and analyzed at E10.5; the EFTFs PAX6, LHX2 and SIX3 are expressed (Figures 3B,D,F). Therefore, our data demonstrates that Porcn is not required to maintain EFTF expression in the OV.

Overall, our strategy of *Porcn* inactivation may be not quick enough to affect EFTF expression in the eye field between E7.5 and E8.5. However, it could be challenging to perform *Porcn* inactivation before E6.5 without causing most severe developmental defects and allowing to determine whether Porcn promotes EFTF expression and eye field formation.

## Porcn is required for initiation of RPE differentiation in the OV

Our results are consistent with previous studies showing that *Porcn* inactivation prevents maintenance of RPE differentiation in the OC, most likely due to loss of Wnt/β−catenin signaling. RPE-specific inactivation of the pathway effector β−catenin in the early OC interferes with further RPE differentiation (Fujimura et al., 2009; Westenskow et al., 2009; Hagglund et al., 2013). Loss of RPE fate is likely caused by a failure to transactivate RPE gene expression, therefore, the mutant RPE transdifferentiates into retina (Fujimura et al., 2009; Westenskow et al., 2009). Here we show that RPE differentiation fails to initiate in $Porcn^{CKO}$ embryos induced at E6.5, since the early RPE marker OTX2 is absent in the dorsal E9.5 OV (Figure 1S). The POM is essential for RPE differentiation and a source for Wnt ligands, in addition to ocular tissues (Gage et al., 1999; Fuhrmann et al., 2000; Bassett et al., 2010; Bankhead et al., 2015; Carpenter et al., 2015). Thus, ubiquitous depletion of Porcn may interfere with RPE differentiation cell and non-cell autonomously. To examine a cell autonomous requirement, we attempted to disrupt *Porcn* using a more restricted *Cre* line, $Hes^{CreERT2}$ (Yun et al., 2009; Kopinke et al., 2011). We administered up to 0.12 mg/g tamoxifen around E6.8 and observed no obvious phenotype in *Porcn* mutant embryos (n = 4; not shown). We detected mosaic RosaR26 reporter expression in only one E10.5 embryo (n = 3; not shown) suggesting that $Hes^{CreERT2}$ may not be sufficiently activated at this time point. However, we showed in an earlier study that *Porcn* disruption causes consistent RPE differentiation defects only when performed simultaneously in ocular and extraocular tissues in the OV (Bankhead et al., 2015). We propose that Wnts are also redundantly produced and available within the eye field and adjacent tissues.

## Porcn is required for ocular growth by promoting proliferation and survival of ocular progenitors

Our study demonstrates that *Porcn* inactivation results in severe morphogenesis defects 3 days later, either at the OV (E9.5) or OC stage (E10.5). The $Porcn^{CKO}$ OV or OC is small and OV expansion or OC invagination fails, respectively. Analysis of cell death (TUNEL) and proliferation (EdU incorporation) showed robustly downregulated proliferation and survival of ocular progenitors in the ventral OV 1 day earlier when morphology and expression of the Wnt/β−catenin readout appear normal (Figure 4K–T). Wnt signaling can directly regulate proliferation and survival of ocular progenitors (Burns et al., 2008; Hagglund et al., 2013). Interestingly, during embryonic morphogenesis, Wnt signaling may support metabolic demands by preventing a cellular stress response, which could affect proliferation and survival (Poncet et al., 2020). A reduction of *Porcn* gene dosage in the embryo may impact the overall stress response and affect general survival as observed in the dorsal $Porcn^{CHET}$ OV and surrounding tissues (Figure 4Q).

Significantly reduced proliferation during OC morphogenesis has been observed in embryos with germ line mutation of early ocular regulatory genes, for example $Pax6^{sey/sey}$, *Lhx2, BMP7, Hes1* and *Mab21L2* (Grindley et al., 1995; Porter et al., 1997; Yamada et al., 2004; Lee et al., 2005; Morcillo et al., 2006; Yun et al., 2009). However, *PAX6* and *LHX2* are expressed in the OV of $Porcn^{CKO}$, and *Pax6, Bmp7, Hes1 and Mab21L2* mutants do not show a robust morphogenesis defect until E10.5. Therefore, to our knowledge, the ocular phenotype in $Porcn^{CKO}$ is unique because it shows an earlier requirement for proliferation and survival of ocular progenitors.

## *Porcn* inactivation around the eye field stage recapitulates microphthalmia and anophthalmia in FDH patients

$Porcn^{CKO}$ display severe microphthalmia 3 days after tamoxifen treatment before or during the eye field stage. $Porcn^{CKO}$ embryos induced at E6.5 and harvested at E10.5 showed severe developmental abnormalities not feasible for further analysis at later time points (Supplementary Figure S2). *Lhx2* mutants exhibit a similar OV morphogenesis defect leading to anophthalmia subsequently (Porter et al., 1997). Thus, we hypothesize that *Porcn* inactivation before the OV stage ultimately results in anophthalmia, consistent for an early role of Porcn in FDH. A case report for 18 FDH patients revealed a high incidence of ophthalmologic abnormalities (77%), including microphthalmia (44%) and anophthalmia (11%) (Gisseman and Herce, 2016). We

propose that *Porcn* inactivation around the eye field stage represents a novel mouse model recapitulating severe microphthalmia and anophthalmia in humans. $Porcn^{CHET}$ female embryos do not display an apparent ocular phenotype compared to few embryos with germline inactivation of one *Porcn* allele (Bankhead et al., 2015). The late dosage reduction of *Porcn*, combined with variable mosaic X inactivation, may cause a failure to induce ocular defects in $Porcn^{CHET}$ at this critical developmental stage.

## Conclusion

Using temporally controlled, conditional inactivation in mouse, our studies reveal a novel role for Porcn in regulating growth and morphogenesis of the optic vesicle and optic cup, *via* a requirement in proliferation, survival, and regionalization of ocular gene expression, recapitulating severe microphthalmia in FDH.

## Data availability statement

The original contributions presented in the study are included in the article/Supplementary Materials, further inquiries can be directed to the corresponding author.

## Ethics statement

The animal study was reviewed and approved by Institutional Animal Care and Use Committee at Vanderbilt University Medical Center.

## Author contributions

SF designed experiments, supervised the research, carried out experiments presented in the manuscript, analyzed the data, and wrote the manuscript. SR carried out experiments, analyzed data and edited the manuscript. MMA carried out experiments, analyzed data and edited the manuscript. CC carried out experiments, analyzed data and edited the manuscript.

## Funding

This work was supported by the National Institutes of Health (R01 EY024373 to SF, T32 HD007502 Training Grant in Stem Cell and Regenerative Developmental Biology to SR, Core Grant P30 EY14800); a Catalyst Award to SF from Research to Prevent Blindness Inc./American Macular Degeneration Foundation, an unrestricted award to the Department of Ophthalmology and Visual Sciences from Research to Prevent Blindness, Inc. Data presentation was performed in part through the use of the Vanderbilt Cell Imaging Shared Resource (supported by NIH grants CA68485, DK20593, DK58404, DK59637 and EY08126). Zeiss LSM880 Airyscan Confocal Microscope is obtained through the NIH S10 award (1 S10 OD021630 1, PI Sam Wells).

## Acknowledgments

Special thanks to Ethan Lee and Yukio Saijoh for expert advice. Many thanks to Maria Elias and Katrina Hofstetter for excellent technical support. We thank Ed Levine and his team for helpful comments and discussions. Special thanks to Charles Murtaugh (University of Utah, Salt Lake City, UT) for kindly providing the conditional *Porcn* allele and the *Cre* line $Hes1^{CreERT2}$.

## Conflict of interest

The authors declare that the research was conducted in the absence of any commercial or financial relationships that could be construed as a potential conflict of interest.

## Publisher's note



## Supplementary material

The Supplementary Material for this article can be found online at: https://www.frontiersin.org/articles/10.3389/fcell.2022.1016182/full#supplementary-material

**SUPPLEMENTARY FIGURE 1**
RosaR26 reporter activation. Coronal view of E9.0 embryonic heads, induced with tamoxifen at E6.5 **(A, B)** and E9.5 embryos **(C, D)**, induced at E7.4. **(A, B, D)** PorcnCHET and PorcnCKO embryos show widespread expression of β-galactosidase protein, in contrast to controls without Cre (C). Arrows point to OVs in each image. Scale bar: 0.1 mm.

**SUPPLEMENTARY FIGURE 2**
Developmental defects of PorcnCKO embryos 4 days after tamoxifen administration. **(A-C)** Embryos at E10.5, treated with tamoxifen at E6.5. **(A)** Control embryo (PorcnCHET; 37 somites). **(B, C)** PorcnCKO littermates with severe developmental defects (somites not detectable). Scale bar: 0.5 mm.

# References


Alldredge, A., and Fuhrmann, S. (2016). Loss of Axin2 causes ocular defects during mouse eye development. *Investigative Ophthalmol. Vis. Sci.* 57, 5253–5262. doi:10.1167/iovs.15-18599

Badea, T. C., Wang, Y., and Nathans, J. (2003). A noninvasive genetic/pharmacologic strategy for visualizing cell morphology and clonal relationships in the mouse. *J. Soc. Neurosci.* 23, 2314–2322. doi:10.1523/JNEUROSCI.23-06-02314.2003

Bailey, T. J., El-Hodiri, H., Zhang, L., Shah, R., Mathers, P. H., and Jamrich, M. (2004). Regulation of vertebrate eye development by Rx genes. *Int. J. Dev. Biol.* 48, 761–770. doi:10.1387/ijdb.041878tb

Bankhead, E. J., Colasanto, M. P., Dyorich, K. M., Jamrich, M., Murtaugh, L. C., and Fuhrmann, S. (2015). Multiple requirements of the focal dermal hypoplasia gene porcupine during ocular morphogenesis. *Am. J. Pathol.* 185, 197–213. doi:10.1016/j.ajpath.2014.09.002

Barrott, J. J., Cash, G. M., Smith, A. P., Barrow, J. R., and Murtaugh, L. C. (2011). Deletion of mouse Porcn blocks Wnt ligand secretion and reveals an ectodermal etiology of human focal dermal hypoplasia/Goltz syndrome. *Proc. Natl. Acad. Sci. U. S. A.* 108, 12752–12757. doi:10.1073/pnas.1006437108

Bassett, E. A., Williams, T., Zacharias, A. L., Gage, P. J., Fuhrmann, S., and West-Mays, J. A. (2010). AP-2alpha knockout mice exhibit optic cup patterning defects and failure of optic stalk morphogenesis. *Hum. Mol. Genet.* 19, 1791–1804. doi:10.1093/hmg/ddq060

Biechele, S., Cox, B. J., and Rossant, J. (2011). Porcupine homolog is required for canonical Wnt signaling and gastrulation in mouse embryos. *Dev. Biol.* 355, 275–285. doi:10.1016/j.ydbio.2011.04.029

Biechele, S., Adissu, H. A., Cox, B. J., and Rossant, J. (2013). Zygotic Porcn paternal allele deletion in mice to model human focal dermal hypoplasia. *PloS one* 8, e79139. doi:10.1371/journal.pone.0079139

Bumsted, K. M., and Barnstable, C. J. (2000). Dorsal retinal pigment epithelium differentiates as neural retina in the microphthalmia (mi/mi) mouse. *Investigative Ophthalmol. Vis. Sci.* 41, 903–908.

Burmeister, M., Novak, J., Liang, M. Y., Basu, S., Ploder, L., and Hawes, N. L., (1996). Ocular retardation mouse caused by Chx10 homeobox null allele: Impaired retinal progenitor proliferation and bipolar cell differentiation. *Nat. Genet.* 12, 376–384.

Burns, C. J., Zhang, J., Brown, E. C., Van Bibber, A. M., Van Es, J., and Clevers, H., (2008). Investigation of Frizzled-5 during embryonic neural development in mouse. *Dev. Dyn. official Publ. Am. Assoc. Anatomists* 237, 1614–1626. doi:10.1002/dvdy.21565

Cai, Z., Tao, C., Li, H., Ladher, R., Gotoh, N., and Feng, G. S., (2013). Deficient FGF signaling causes optic nerve dysgenesis and ocular coloboma. *Development* 140, 2711–2723. doi:10.1242/dev.089987

Carpenter, A. C., Smith, A. N., Wagner, H., Cohen-Tayar, Y., Rao, S., and Wallace, V., (2015). Wnt ligands from the embryonic surface ectoderm regulate 'bimetallic strip' optic cup morphogenesis in mouse. *Development* 142, 972–982. doi:10.1242/dev.120022

Cavodeassi, F., Carreira-Barbosa, F., Young, R. M., Concha, M. L., Allende, M. L., and Houart, C., (2005). Early stages of zebrafish eye formation require the coordinated activity of Wnt11, Fz5, and the Wnt/beta-catenin pathway. *Neuron* 47, 43–56. doi:10.1016/j.neuron.2005.05.026

Cavodeassi, F., Ivanovitch, K., and Wilson, S. W. (2013). Eph/Ephrin signalling maintains eye field segregation from adjacent neural plate territories during forebrain morphogenesis. *Development* 140, 4193–4202. doi:10.1242/dev.097048

Clementi, M., Turolla, L., Mammi, I., and Tenconi, R. (1992). Clinical anophthalmia: An epidemiological study in northeast Italy based on 368, 256 consecutive births. *Teratology* 46, 551–553. doi:10.1002/tera.1420460604

Covey, T. M., Kaur, S., Tan Ong, T., Proffitt, K. D., Wu, Y., and Tan, P., (2012). PORCN moonlights in a Wnt-independent pathway that regulates cancer cell proliferation. *PloS one* 7, e34532. doi:10.1371/journal.pone.0034532

Erlenhardt, N., Yu, H., Abiraman, K., Yamasaki, T., Wadiche, J. I., and Tomita, S., (2016). Porcupine controls hippocampal AMPAR levels, composition, and synaptic transmission. *Cell Rep.* 14, 782–794. doi:10.1016/j.celrep.2015.12.078

Fuhrmann, S., Levine, E. M., and Reh, T. A. (2000). Extraocular mesenchyme patterns the optic vesicle during early eye development in the embryonic chick. *Development* 127, 4599–4609. doi:10.1242/dev.127.21.4599

Fuhrmann, S., Zou, C., and Levine, E. M. (2014). Retinal pigment epithelium development, plasticity, and tissue homeostasis. *Exp. eye Res.* 123, 141–150. doi:10.1016/j.exer.2013.09.003

Fuhrmann, S. (2008). Wnt signaling in eye organogenesis. *Organogenesis* 4, 60–67. doi:10.4161/org.4.2.5850

Fuhrmann, S. (2010). Eye morphogenesis and patterning of the optic vesicle. *Curr. Top. Dev. Biol.* 93, 61–84. doi:10.1016/B978-0-12-385044-7.00003-5

Fujimura, N., Taketo, M. M., Mori, M., Korinek, V., and Kozmik, Z. (2009). Spatial and temporal regulation of Wnt/beta-catenin signaling is essential for development of the retinal pigment epithelium. *Dev. Biol.* 334, 31–45. doi:10.1016/j.ydbio.2009.07.002

Fujimura, N. (2016). WNT/beta-Catenin signaling in vertebrate eye development. *Front. Cell Dev. Biol.* 4, 138. doi:10.3389/fcell.2016.00138

Gage, P. J., Suh, H., and Camper, S. A. (1999). Dosage requirement of Pitx2 for development of multiple organs. *Development* 126, 4643–4651. doi:10.1242/dev.126.20.4643

Galli, L. M., Barnes, T. L., Secrest, S. S., Kadowaki, T., and Burrus, L. W. (2007). Porcupine-mediated lipid-modification regulates the activity and distribution of Wnt proteins in the chick neural tube. *Development* 134, 3339–3348. doi:10.1242/dev.02881

Gisseman, J. D., and Herce, H. H. (2016). Ophthalmologic manifestations of focal dermal hypoplasia (Goltz syndrome): A case series of 18 patients. *Am. J. Med. Genet. C Semin. Med. Genet.* 172C, 59–63. doi:10.1002/ajmg.c.31480

Goltz, R. W., Peterson, W. C., Gorlin, R. J., and Ravits, H. G. (1962). Focal dermal hypoplasia. *Archives dermatology* 86, 708–717. doi:10.1001/archderm.1962.01590120006002

Graw, J. (2019). Mouse models for microphthalmia, anophthalmia and cataracts. *Hum. Genet.* 138, 1007–1018. doi:10.1007/s00439-019-01995-w

Green, E. S., Stubbs, J. L., and Levine, E. M. (2003). Genetic rescue of cell number in a mouse model of microphthalmia: Interactions between Chx10 and G1-phase cell cycle regulators. *Development* 130, 539–552. doi:10.1242/dev.00275

Grindley, J. C., Davidson, D. R., and Hill, R. E. (1995). The role of Pax-6 in eye and nasal development. *Development* 121, 1433–1442. doi:10.1242/dev.121.5.1433

Grzeschik, K. H., Bornholdt, D., Oeffner, F., Konig, A., del Carmen Boente, M., and Enders, H., (2007). Deficiency of PORCN, a regulator of Wnt signaling, is associated with focal dermal hypoplasia. *Nat. Genet.* 39, 833–835. doi:10.1038/ng2052

Hagglund, A. C., Berghard, A., and Carlsson, L. (2013). Canonical Wnt/beta-catenin signalling is essential for optic cup formation. *PloS one* 8, e81158. doi:10.1371/journal.pone.0081158

Heisenberg, C. P., Tada, M., Rauch, G. J., Saude, L., Concha, M. L., and Geisler, R., (2000). Silberblick/Wnt11 mediates convergent extension movements during zebrafish gastrulation. *Nature* 405, 76–81. doi:10.1038/35011068

Hodgkinson, C. A., Moore, K. J., Nakayama, A., Steingrimsson, E., Copeland, N. G., and Jenkins, N. A., (1993). Mutations at the mouse microphthalmia locus are associated with defects in a gene encoding a novel basic-helix-loop-helix-zipper protein. *Cell* 74, 395–404. doi:10.1016/0092-8674(93)90429-t

Kemp, C., Willems, E., Abdo, S., Lambiv, L., and Leyns, L. (2005). Expression of all Wnt genes and their secreted antagonists during mouse blastocyst and postimplantation development. *Dev. Dyn. official Publ. Am. Assoc. Anatomists* 233, 1064–1075. doi:10.1002/dvdy.20408

Kispert, A., Vainio, S., Shen, L., Rowitch, D. H., and McMahon, A. P. (1996). Proteoglycans are required for maintenance of Wnt-11 expression in the ureter tips. *Development* 122, 3627–3637. doi:10.1242/dev.122.11.3627

Kopinke, D., Brailsford, M., Shea, J. E., Leavitt, R., Scaife, C. L., and Murtaugh, L. C. (2011). Lineage tracing reveals the dynamic contribution of Hes1+ cells to the developing and adult pancreas. *Development* 138, 431–441. doi:10.1242/dev.053843

Lagutin, O. V., Zhu, C. C., Kobayashi, D., Topczewski, J., Shimamura, K., and Puelles, L., (2003). Six3 repression of Wnt signaling in the anterior neuroectoderm is essential for vertebrate forebrain development. *Genes & Dev.* 17, 368–379. doi:10.1101/gad.1059403

Lee, H. Y., Wroblewski, E., Philips, G. T., Stair, C. N., Conley, K., and Reedy, M., (2005). Multiple requirements for Hes 1 during early eye formation. *Dev. Biol.* 284, 464–478. doi:10.1016/j.ydbio.2005.06.010

Lee, H. S., Bong, Y. S., Moore, K. B., Soria, K., Moody, S. A., and Daar, I. O. (2006). Dishevelled mediates ephrinB1 signalling in the eye field through the planar cell polarity pathway. *Nat. Cell Biol.* 8, 55–63. doi:10.1038/ncb1344

Lieven, O., and Ruther, U. (2011). The Dkk1 dose is critical for eye development. *Dev. Biol.* 355, 124–137. doi:10.1016/j.ydbio.2011.04.023

Liu, W., and Cvekl, A. (2017). Six3 in a small population of progenitors at E8.5 is required for neuroretinal specification via regulating cell signaling and survival in mice. *Dev. Biol.* 428, 164–175. doi:10.1016/j.ydbio.2017.05.026

Liu, W., Lagutin, O., Swindell, E., Jamrich, M., and Oliver, G. (2010). Neuroretina specification in mouse embryos requires Six3-mediated suppression of Wnt8b in the anterior neural plate. *J. Clin. investigation* 120, 3568–3577. doi:10.1172/JCI43219

Martinez-Morales, J. R., Signore, M., Acampora, D., Simeone, A., and Bovolenta, P. (2001). Otx genes are required for tissue specification in the developing eye. *Development* 128, 2019–2030. doi:10.1242/dev.128.11.2019

Maurus, D., Heligon, C., Burger-Schwarzler, A., Brandli, A. W., and Kuhl, M. (2005). Noncanonical Wnt-4 signaling and EAF2 are required for eye development in *Xenopus laevis*. *EMBO J.* 24, 1181–1191. doi:10.1038/sj.emboj.7600603

Miesfeld, J. B., and Brown, N. L. (2019). Eye organogenesis: A hierarchical view of ocular development. *Curr. Top. Dev. Biol.* 132, 351–393. doi:10.1016/bs.ctdb.2018.12.008

Moore, K. B., Mood, K., Daar, I. O., and Moody, S. A. (2004). Morphogenetic movements underlying eye field formation require interactions between the FGF and ephrinB1 signaling pathways. *Dev. Cell* 6, 55–67. doi:10.1016/s1534-5807(03)00395-2

Morcillo, J., Martinez-Morales, J. R., Trousse, F., Fermin, Y., Sowden, J. C., and Bovolenta, P. (2006). Proper patterning of the optic fissure requires the sequential activity of BMP7 and SHH. *Development* 133, 3179–3190. doi:10.1242/dev.02493

Morrison, D., FitzPatrick, D., Hanson, I., Williamson, K., van Heyningen, V., and Fleck, B., (2002). National study of microphthalmia, anophthalmia, and coloboma (MAC) in scotland: Investigation of genetic aetiology. *J. Med. Genet.* 39, 16–22. doi:10.1136/jmg.39.1.16

Motahari, Z., Martinez-De Luna, R. I., Viczian, A. S., and Zuber, M. E. (2016). Tbx3 represses bmp4 expression and, with Pax6, is required and sufficient for retina formation. *Development* 143, 3560–3572. doi:10.1242/dev.130955

Nguyen, M., and Arnheiter, H. (2000). Signaling and transcriptional regulation in early mammalian eye development: A link between FGF and MITF. *Development* 127, 3581–3591. doi:10.1242/dev.127.16.3581

Nornes, H. O., Dressler, G. R., Knapik, E. W., Deutsch, U., and Gruss, P. (1990). Spatially and temporally restricted expression of Pax2 during murine neurogenesis. *Development* 109, 797–809. doi:10.1242/dev.109.4.797

Oliver, G., Mailhos, A., Wehr, R., Copeland, N. G., Jenkins, N. A., and Gruss, P. (1995). Six3, a murine homologue of the sine oculis gene, demarcates the most anterior border of the developing neural plate and is expressed during eye development. *Development* 121, 4045–4055. doi:10.1242/dev.121.12.4045

Park, E. J., Sun, X., Nichol, P., Saijoh, Y., Martin, J. F., and Moon, A. M. (2008). System for tamoxifen-inducible expression of cre-recombinase from the Foxa2 locus in mice. *Dev. Dyn. official Publ. Am. Assoc. Anatomists* 237, 447–453. doi:10.1002/dvdy.21415

Parr, B. A., Shea, M. J., Vassileva, G., and McMahon, A. P. (1993). Mouse Wnt genes exhibit discrete domains of expression in the early embryonic CNS and limb buds. *Development* 119, 247–261. doi:10.1242/dev.119.1.247

Poncet, N., Halley, P. A., Lipina, C., Gierlinski, M., Dady, A., and Singer, G. A., (2020). Wnt regulates amino acid transporter Slc7a5 and so constrains the integrated stress response in mouse embryos. *EMBO Rep.* 21, e48469. doi:10.15252/embr.201948469

Porter, F. D., Drago, J., Xu, Y., Cheema, S. S., Wassif, C., and Huang, S. P., (1997). Lhx2, a LIM homeobox gene, is required for eye, forebrain, and definitive erythrocyte development. *Development* 124, 2935–2944. doi:10.1242/dev.124.15.2935

Rasmussen, J. T., Deardorff, M. A., Tan, C., Rao, M. S., Klein, P. S., and Vetter, M. L. (2001). Regulation of eye development by frizzled signaling in Xenopus. *Proc. Natl. Acad. Sci. U. S. A.* 98, 3861–3866. doi:10.1073/pnas.071586298

Soriano, P. (1999). Generalized lacZ expression with the ROSA26 Cre reporter strain. *Nat. Genet.* 21, 70–71. doi:10.1038/5007

Sun, W. R., Ramirez, S., Spiller, K. E., Zhao, Y., and Fuhrmann, S. (2020). Nf2 fine-tunes proliferation and tissue alignment during closure of the optic fissure in the embryonic mouse eye. *Hum. Mol. Genet.* 29, 3373–3387. doi:10.1093/hmg/ddaa228

Tanaka, K., Okabayashi, K., Asashima, M., Perrimon, N., and Kadowaki, T. (2000). The evolutionarily conserved porcupine gene family is involved in the processing of the Wnt family. *Eur. J. Biochem./FEBS* 267, 4300–4311. doi:10.1046/j.1432-1033.2000.01478.x

Tang, K., Xie, X., Park, J. I., Jamrich, M., Tsai, S., and Tsai, M. J. (2010). COUP-TFs regulate eye development by controlling factors essential for optic vesicle morphogenesis. *Development* 137, 725–734. doi:10.1242/dev.040568

Temple, I. K., MacDowall, P., Baraitser, M., and Atherton, D. J. (1990). Focal dermal hypoplasia (Goltz syndrome). *J. Med. Genet.* 27, 180–187. doi:10.1136/jmg.27.3.180

Veien, E. S., Rosenthal, J. S., Kruse-Bend, R. C., Chien, C. B., and Dorsky, R. I. (2008). Canonical Wnt signaling is required for the maintenance of dorsal retinal identity. *Development* 135, 4101–4111. doi:10.1242/dev.027367

Viczian, A. S. Z. (2014). "Retinal development," in *Principles of developmental genetics*. Editor S. A. Moody. second ed. (Cambridge, MA, U.S.A: Academic Press), 297–313.

Wang, X., Reid Sutton, V., Omar Peraza-Llanes, J., Yu, Z., Rosetta, R., Kou, Y. C., et al. (2007). Mutations in X-linked PORCN, a putative regulator of Wnt signaling, cause focal dermal hypoplasia. *Nat. Genet.* 39, 836–838. doi:10.1038/ng2057

Wang, L., Jin, X., Zhao, X., Liu, D., Hu, T., and Li, W., (2014). Focal dermal hypoplasia: Updates. *Oral Dis.* 20, 17–24. doi:10.1111/odi.12083

Westenskow, P., Piccolo, S., and Fuhrmann, S. (2009). Beta-catenin controls differentiation of the retinal pigment epithelium in the mouse optic cup by regulating Mitf and Otx2 expression. *Development* 136, 2505–2510. doi:10.1242/dev.032136

Yamada, R., Mizutani-Koseki, Y., Koseki, H., and Takahashi, N. (2004). Requirement for Mab21l2 during development of murine retina and ventral body wall. *Dev. Biol.* 274, 295–307. doi:10.1016/j.ydbio.2004.07.016

Yamaguchi, T. P., Bradley, A., McMahon, A. P., and Jones, S. (1999). A Wnt5a pathway underlies outgrowth of multiple structures in the vertebrate embryo. *Development* 126, 1211–1223. doi:10.1242/dev.126.6.1211

Yun, S., Saijoh, Y., Hirokawa, K. E., Kopinke, D., Murtaugh, L. C., and Monuki, E. S., (2009). Lhx2 links the intrinsic and extrinsic factors that control optic cup formation. *Development* 136, 3895–3906. doi:10.1242/dev.041202

Zhou, C. J., Molotkov, A., Song, L., Li, Y., Pleasure, D. E., and Pleasure, S. J., (2008). Ocular coloboma and dorsoventral neuroretinal patterning defects in Lrp6 mutant eyes. *Dev. Dyn. official Publ. Am. Assoc. Anatomists* 237, 3681–3689. doi:10.1002/dvdy.21770

Zuber, M. E., Gestri, G., Viczian, A. S., Barsacchi, G., and Harris, W. A. (2003). Specification of the vertebrate eye by a network of eye field transcription factors. *Development* 130, 5155–5167. doi:10.1242/dev.00723

frontiers | Frontiers in Cell and Developmental Biology

TYPE Review
PUBLISHED 09 December 2022
DOI 10.3389/fcell.2022.1058925



OPEN ACCESS

EDITED BY
Elizabeth Zuniga-Sanchez,
Baylor College of Medicine,
United States

REVIEWED BY
Ying Li,
Xi'an Jiaotong University, China
Andrea James,
University of Northern Colorado,
United States

*CORRESPONDENCE
R. Paes-de-Carvalho,
robpaesuff@gmail.com

†These authors have contributed equally to this work and share first authorship

SPECIALTY SECTION
This article was submitted to Signaling, a section of the journal Frontiers in Cell and Developmental Biology

RECEIVED 30 September 2022
ACCEPTED 28 November 2022
PUBLISHED 09 December 2022

CITATION
Duarte-Silva AT, Ximenes LGR, Guimarães-Souza M, Domith I and Paes-de-Carvalho R (2022), Chemical signaling in the developing avian retina: Focus on cyclic AMP and AKT-dependent pathways.
*Front. Cell Dev. Biol.* 10:1058925.
doi: 10.3389/fcell.2022.1058925



# Chemical signaling in the developing avian retina: Focus on cyclic AMP and AKT-dependent pathways

A. T. Duarte-Silva[1†], L. G. R. Ximenes[1†], M. Guimarães-Souza[1], I. Domith[1] and R. Paes-de-Carvalho[1,2*]

[1]Program of Neurosciences, Institute of Biology, Fluminense Federal University, Niterói, Brazil, [2]Department of Neurobiology, Institute of Biology, Fluminense Federal University, Niterói, Brazil

Communication between developing progenitor cells as well as differentiated neurons and glial cells in the nervous system is made through direct cell contacts and chemical signaling mediated by different molecules. Several of these substances are synthesized and released by developing cells and play roles since early stages of Central Nervous System development. The chicken retina is a very suitable model for neurochemical studies, including the study of regulation of signaling pathways during development. Among advantages of the model are its very well-known histogenesis, the presence of most neurotransmitter systems found in the brain and the possibility to make cultures of neurons and/or glial cells where many neurochemical functions develop in a similar way than in the intact embryonic tissue. In the chicken retina, some neurotransmitters or neuromodulators as dopamine, adenosine, and others are coupled to cyclic AMP production or adenylyl cyclase inhibition since early stages of development. Other substances as vitamin C and nitric oxide are linked to the major neurotransmitter glutamate and AKT metabolism. All these different systems regulate signaling pathways, including PKA, PKG, SRC, AKT and ERK, and the activation of the transcription factor CREB. Dopamine and adenosine stimulate cAMP accumulation in the chick embryo retina through activation of D1 and A2a receptors, respectively, but the onset of dopamine stimulation is much earlier than that of adenosine. However, adenosine can inhibit adenylyl cyclase and modulate dopamine-dependent cAMP increase since early developmental stages through A1 receptors. Dopamine stimulates different PKA as well as EPAC downstream pathways both in intact tissue and in culture as the CSK-SRC pathway modulating glutamate NMDA receptors as well as vitamin C release and CREB phosphorylation. By the other hand, glutamate modulates nitric oxide production and AKT activation in cultured retinal cells and this pathway controls neuronal survival in retina. Glutamate and adenosine stimulate the release of vitamin C and this vitamin regulates the transport of glutamate, activation of NMDA receptors and AKT phosphorylation in cultured retinal cells. In the present review we will focus on these reciprocal interactions between neurotransmitters or neuromodulators and different signaling pathways during retinal development.

KEYWORDS

cyclic AMP, calcium, adenosine, dopamine, glutamate, nitric oxide, vitamin C, Akt

# 1 Introduction

## 1.1 The chicken retina as a model for studies of central nervous system neurochemical development

The retina is a part of the Central Nervous System (CNS) involved in receiving, transducing, and modulating the light signals from the environment. The chicken retina is a very suitable model system for the study of CNS development since it can be easily obtained during most part of embryonic development and its histogenesis is relatively well known (Adler, 2000). Although few classes of cells are anatomically discernible, the chick retina differentiates more than a hundred cell types, as recently described using single cell transcriptomics, distributed among the six classes conserved across vertebrates (Yamagata et al., 2021), including photoreceptors, bipolar and ganglion cells comprising the vertical pathway, and horizontal and amacrine cells responsible for the horizontal modulation of neuronal activity. Moreover, a major glial cell type is the Muller cell which makes contact with neurons in the almost complete retinal extension (reviewed by Reichenbach and Bringmann, 2013). The chick retina is also a good model for studying nervous system development since it presents many of the neurotransmitters and neuromodulators present in the CNS (Calaza and Gardino, 2010). Figure 1 shows the general chick retina structure in three major periods of development, 7-day-old embryo (E7), E12 and E18. As can be observed, one important characteristic is the increase of plexiform layers where synaptic contacts, neurotransmitters and receptors are predominantly localized.

## 1.2 The chicken retina as a model to study retinal degenerations

Many studies discuss the advantages of using avian retina in eye disease models (Wisely et al., 2017). Studies show the use of the chick retina as a model in corneal diseases because of its anatomical and molecular similarities with the retina of humans (Fowler et al., 2004; Martínez-García et al., 2006; Mangioris et al., 2011). Many retinal diseases are related to dysfunctions in the glutamatergic system such as diabetic retinopathy, glaucoma and retinal ischemia (reviewed by Ishikawa, 2013). Retinal detachment causes changes in photoreceptors, which can degenerate and undergo apoptosis, and in Muller's glia, which proliferate and hypertrophy, contributing to the destructive scarring. Microglia can become reactive and accumulate in the retina. These events cause changes in the outer nuclear layer of the retina. Study with chicks with postnatal age between 7 and 21 days shows the advantage of this model in studies of retinal detachment (Cebulla et al., 2012). Chicken embryos were also used for studies of diabetic retinopathy in which the embryos were exposed to high concentrations of glucose on the first day of development to cause hyperglycemia and this caused damage to the embryo's eye development and the molecular mechanism of this malformation was studied demonstrating the advantages of this model (Zhang et al., 2016). In addition, there are also reports of the use of chicken embryos for retinoblastoma studies (Busch et al., 2015; Nair et al., 2022), myopia and hyperopia (Wildsoet and Schmid, 2000; reviewed by Iribarren, 2015). The participation of purinergic signaling is also addressed in retinal diseases (reviewed by Ventura et al., 2019). There is also work related to glaucoma using chicks as a study model (Lauber, 1987; Wahl et al., 2016).

## 1.3 The cAMP pathway

cAMP (Adenosine 3′,5′-Cyclic Monophosphate) is an intracellular second messenger that plays key roles in relaying first messenger information (reviewed by Zaccolo et al., 2021). Hormones, neurotransmitters and other signaling molecules use cAMP to regulate various biological processes, including cellular metabolism, ion channel activation, gene expression, cell growth, differentiation, and apoptosis reviewed by Zhang H. et al., 2020). cAMP is produced from ATP through different adenylyl cyclase (AC) isoforms which are activated by G protein-coupled receptors (GPCRs) (reviewed by Breckler et al., 2011). cAMP has four classes of effectors: Protein Kinase A (PKA), Exchange Protein Directly Activated by cAMP (EPAC), Cyclic Nucleotide Controlled Channels (CNG), and Popeye Domino-Containing Protein (POPDC) (Jakobsen et al., 2019).

Three main proteins are known to aid in the compartmentalization of cAMP signaling in cells: ACs, Cyclic Nucleotide Phosphodiesterases (PDEs) and Kinase-A Anchoring Proteins (AKAPs) (reviewed by Robichaux and Cheng, 2018). Recent work shows the existence of nanodomains of cAMP in the vicinities of GPCRs leading to independent switches of on/off activity that can eventually fuse to promote different signaling functions (Anton et al., 2022). Nine membrane-bound AC enzymes are expressed in the brain and are regulated by Gs and Gi subunits of the G protein. However, there are other modulators of AC activity, which include calcium/calmodulin, protein kinase C (PKC) and PKA. Phosphodiesterases (PDEs) play an important role in the regulation of the local concentration of cAMP, hydrolyzing it into adenosine 5′-Monophosphate (5′AMP) and cyclic guanosine-3′-5 monophosphate (cGMP) into guanosine 5′-Monophosphate (5′GMP), and this allows the return to basal concentrations of the second messenger after AC stimulation (reviewed by Gerbaud et al., 2016). More than 50 isoforms of PDEs belonging to 11 families (PDE 1-11)

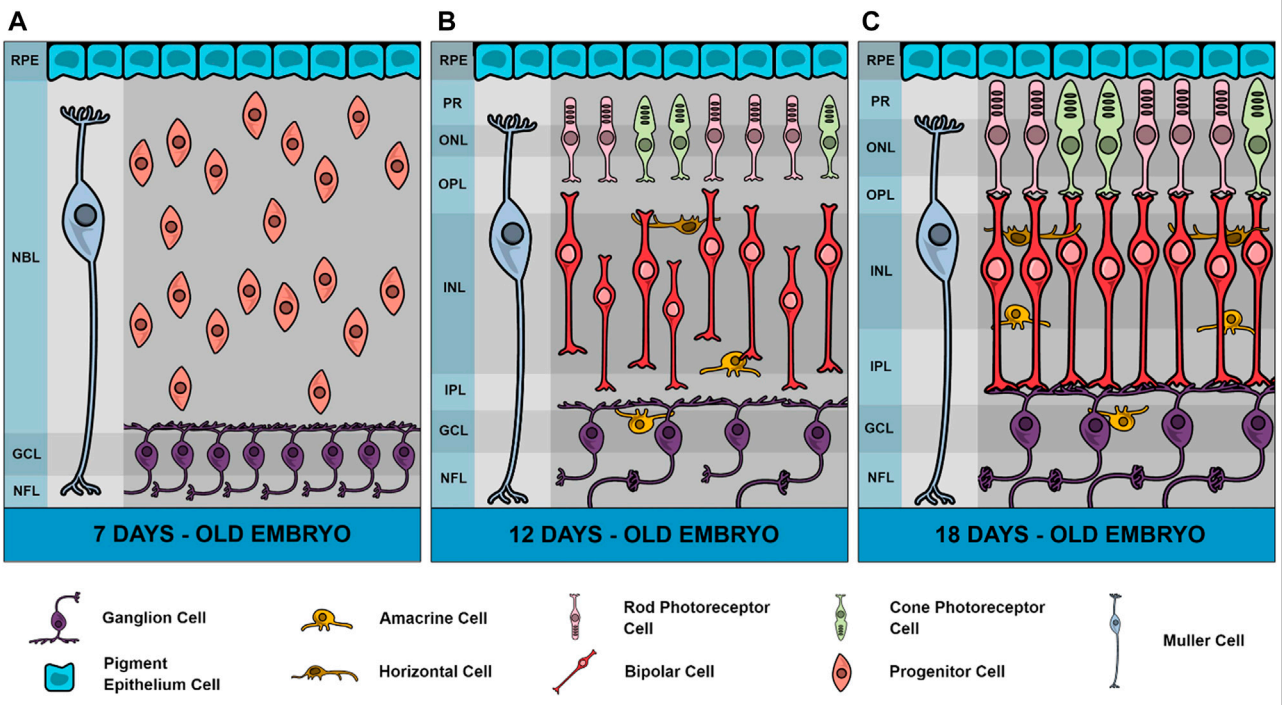


FIGURE 1
Schematic representation of chick retina in 3 different developmental stages. In embryonic day 7 (E7), neuroblasts are still dividing and a high number of ganglion cells are fully differentiated in a ganglion cell layer (GCL) and sending processes through a growing nerve fiber layer (NFL). Plexiform layers are not yet defined and instead is observed an extensive neuroblastic layer (NBL) and the retinal pigmented epithelium (RPE). Muller glial cells are also present in this stage. In E12 retinas, both inner and outer plexiform layers (IPL and OPL, respectively) are observed where neuronal processes progressively grow but synaptic contacts are observed only after E13 in IPL. Amacrine cells can be observed in both inner nuclear layer (INL) and GCL (displaced amacrine cells) and horizontal cells in the external limit of INL. From E12 to E18 there is a progressive increase of IPL and OPL thickness. Photoreceptors present a late development in the chick retina with the external segment (PR) beginning to grow in E15 and synapses between photoreceptors and bipolar cells appearing only in E17. In E19, the retina can be considered mature, and the first light responses are observed. Variations in thickness of retinal layers were drawn according to Zareen et al. (2010), but total retina thickness in different stages are not represented in this figure.

have been identified with different enzymatic and regulatory characteristics (reviewed by Calejo and Taskén, 2015). More than 50 AKAP proteins have been characterized and demonstrate the ability to bind PKA regulatory subunits (Autenrieth et al., 2016; Byrne et al., 2022). AKAPs not only present binding sites for PKA, but also to phosphatases, PDEs and other protein kinases (Nijholt et al., 2008) (Figure 2). Of the 50 AKAP proteins, one of the most important is the muscle Anchoring protein A-kinase (mAKAP), also known as AKAP 6 which is a support protein located in the nuclear envelope of neurons and myocytes. mAKAP serves as the coordinator of two cAMP effector pathways to regulate cellular processes and is the only AKAP reported to associate PKA and the exchange protein activated by cAMP type I (EPAC1) (Nijholt et al., 2008). mAKAP displays binding sites for PKA, EPAC1, AC (Type II and V) and Phosphodiesterase 4D (Wang et al., 2015).

PKA, the main effector protein of cAMP, is a serine/threonine kinase (Jakobsen et al., 2019). It was the second protein kinase to be discovered after phosphorylase kinase, a substrate of PKA. PKA is composed of two separate subunits, two catalytic (C) subunits that phosphorylate substrates and two regulatory (R) subunits that bind cAMP (Robichaux and Cheng, 2018). PKA was classically considered the only effector of cAMP, but other targets have been identified, such as EPAC (Nijholt et al., 2008). EPAC proteins function independently of PKA, acting as guanine nucleotide exchange factors (GEFs) specific for Ras GTPase Rap1 and Rap2 family members (Breckler et al., 2011). Two isoforms of EPAC have been identified, EPAC1 and EPAC2. EPAC1 is encoded by the Guanine Nucleotide Exchange Factor Rap3 (RAPGEF3) gene located on chromosome 12 in the human genome. On the other hand, EPAC2 is encoded by the Guanine Nucleotide Exchange Factor Rap 4 (RAPGEF4) located on chromosome 2 in the human genome (Breckler et al., 2011; reviewed by Gao et al., 2022). PKA and EPAC may have synergistic effects, such as in neurite extension, in the regulation of neurotensin secretion, and

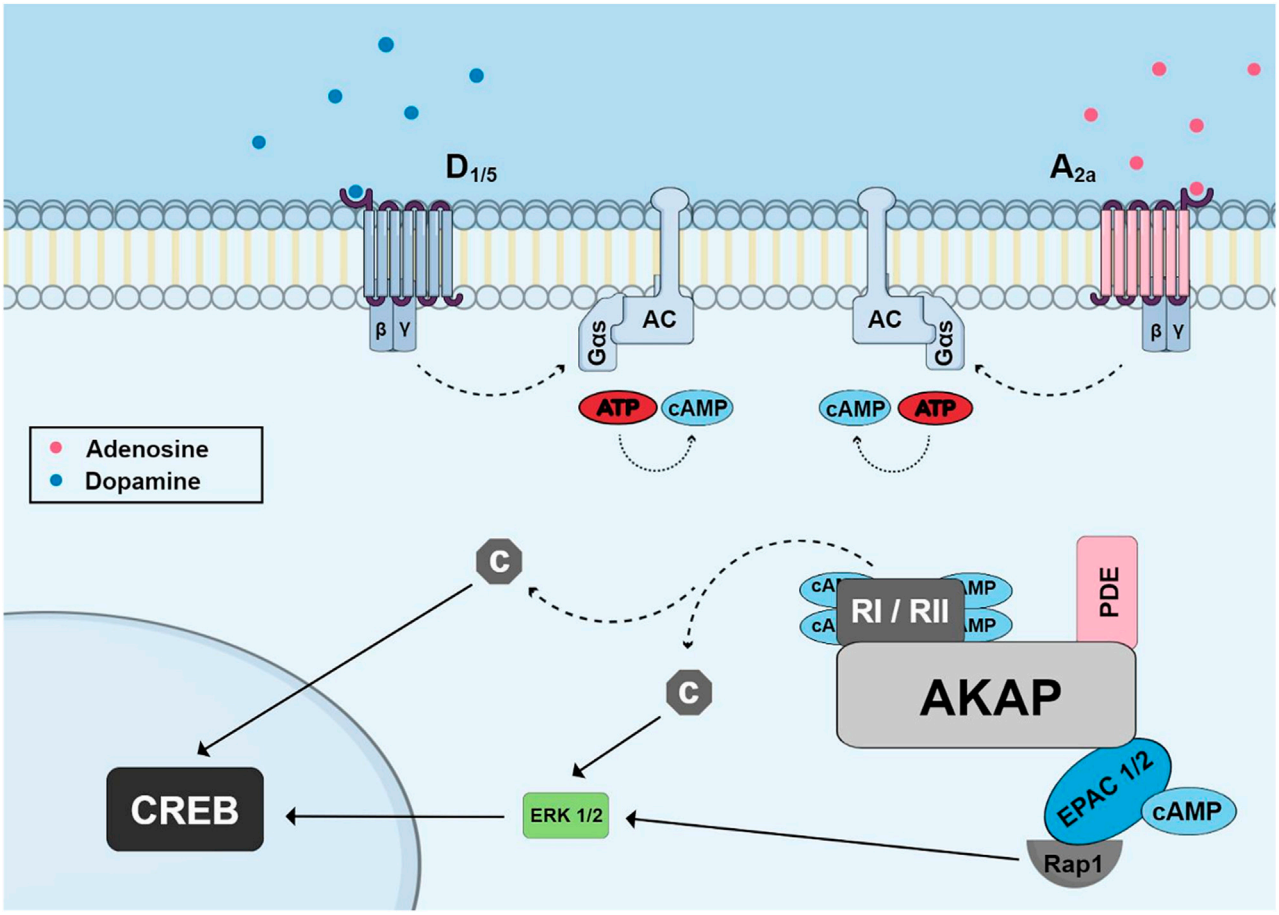


FIGURE 2
Schematic of cyclic AMP pathway to phosphorylate CREB showing accumulation of cyclic AMP induced by G-protein coupled receptors (dopamine and adenosine receptors) and highlighting the A-kinase Anchoring Protein (AKAP) and its binding sites for PKA regulatory subunits, phosphodiesterase and EPAC proteins. Dissociated catalytic PKA subunits or ERK (activated through EPAC and Rap1) can migrate to nucleus and phosphorylate CREB.

in the regulation of phosphodiesterases (Cheng et al., 2008). However, PKA and EPAC may have antagonistic effects, including regulation of AKT phosphorylation, acetylcholine regulation, and plasticity (Whitaker and Cooper, 2010).

## 1.4 The cAMP pathway in the retina

The presence of neurotransmitter systems related to cAMP pathways in the developing chick retina is discussed in section 2.1. As stated in the previous section, AKAPs (A-kinase Anchoring Proteins) belong to a family of proteins that play a key role in the intracellular targeting and compartmentalization of cAMP signaling pathways (Nijholt et al., 2008). One study in the retina provides evidence for a neuronal perinuclear cAMP compartment organized by the scaffold protein mAKAPα and shows that this protein is necessary and sufficient for the induction of neurite outgrowth *in vitro* and for the survival of retinal ganglion cells *in vivo* following optic nerve injury (Boczek et al., 2019). PKA is also present in the retina and evidence indicates that it associates with AKAP in the retina (Benz et al., 2020). The Cα subunit is distributed throughout the cell body of all cells in the retina. Cβ subunits are highly enriched in photoreceptors, interneurons, and ganglion cells. The regulatory subunits, RIIα and RIIβ are-located in photoreceptors and interneurons while RIα and Riβ subunits are present in all retinal cells (Roa et al., 2021).

An interesting study also revealed the presence of calmodulin-dependent PDE1 subtypes A, B and C during chick retina development (Deplano et al., 2008). PDE1A is highly expressed at the early stages and decreased as development proceeded. PDE1B expression remained relatively low and constant over time. PDE1C showed a prominent increase (13-fold) between embryonic day (E)

7 and E13, followed by a moderate increase between E13 and postnatal day (P) 1. This differential profile of PDE subtypes suggest distinct functions of these enzymes during chick retina development.

In brain tissue and spinal cord, Epac1 is expressed only during embryonic and neonatal development, whereas EPAC2 is highly expressed in adulthood. In the retina, Epac1 is expressed in the synaptic layers, outer plexiform layer (OPL) and inner plexiform layer (IPL). It is also expressed in the inner nuclear layer (INL) and ganglion cell layer (GCL). EPAC2 is also found in the cell bodies of INL and GCL, as well as in the cell bodies of the outer nuclear layer (ONL) and OPL (Whitaker and Cooper, 2010; Rasmussen et al., 2022).

## 1.5 The AKT pathway

AKT is a serine-threonine kinase classically activated by the PI3K family of enzymes. Receptor tyrosine kinases and GPCRs lead to the recruitment and activation of different classes of PI3K. PI3K class I phosphorylates phosphatidylinositol-4,5-bisphosphate ($PI4,5P_2$) producing phosphatidylinositol 3,4,5-triphosphate (PIP3) (reviewed by Vanhaesebroeck et al., 2010). This generated substrate can recruit cytoplasmic proteins to the plasma membrane by interacting with the homologous domain of pleckstrin (PH). AKT is a protein that contains a PH domain and, in this way, is recruited to the plasma membrane where it is phosphorylated at its residues Thr 308 and Ser 473 by PDK1 and mTORC2, respectively, and is fully active when phosphorylated at these two residues (reviewed by Fruman et al., 2017). AKT exerts functions in different signaling pathways with many cellular targets. Once activated, it activates several substrates which are involved with cell survival, metabolism, growth, proliferation and migration (Manning and Toker, 2017). The AKT activation process can be regulated by the phosphatase PTEN which dephosphorylates PIP3 to $PI4,5P_2$.

AKT promotes cell survival in a number of ways, one of which is phosphorylating and inhibiting the BAD protein, a member of the Bcl2 family that exerts pro-apoptotic functions (Datta et al., 2002; reviewed by Maiese et al., 2012). AKT also phosphorylates FOXO, another target phosphorylated by AKT, leading to inhibition of apoptosis. GSK3 can also phosphorylate the transcription factor CREB at the serine-129 residue, suppressing its transcriptional activity (Grimes and Jope, 2001; reviewed by Souder and Anderson, 2019). Inhibition of GSK3 activity by phosphorylation by AKT is then a pathway that can activate CREB. AKT also plays an important role in the activation of mTORC1, an important protein complex that regulates protein synthesis and cell growth (Scott et al., 1998; reviewed by Szwed et al., 2021). The AKT substrate TSC2 (tuberous sclerosis complex 2) downregulates mTORC1 and is inhibited when phosphorylated by AKT, i.e., AKT indirectly activates mTORC1 when it phosphorylates and inhibits TSC2 (Manning et al., 2002; reviewed by Manning and Toker, 2017). These AKT targets also play a role in cell proliferation through the translation and synthesis of proteins involved in the cell cycle (Skeen et al., 2006; reviewed by Wang, 2021).

## 1.6 AKT in the retina

AKT is phosphorylated and can modulate protein synthesis during the cell cycle of retinal progenitor cells in chick embryo retinal cultures (Ornelas et al., 2013). The cyclin D1 protein participates in the cell cycle during the G1 phase and may have its expression increased by the AKT pathway. AKT is also active during the mitosis phase and inhibition of this pathway promotes cell cycle arrest in the G2/M phase (Ornelas et al., 2013). AKT regulates neuronal survival events in the chick retina. One study shows that increased production of nitric oxide (NO) can promote retinal neuronal death in E6 retinas, while in E8 low production of nitric oxide is able to increase neuronal survival. Both events (death in E6 and survival in E8) are dependent on the activity of soluble guanylyl cyclase, PKG and AKT but with different effects on CREB phosphorylation which is inhibited in E6 and stimulated in E8 retinas (Socodato et al., 2014). The PI3K/AKT pathway was shown to be essential for neuronal survival promoted by NO in chick retina neuronal cultures (Mejía-García and Paes-de-Carvalho, 2007). Furthermore, in E8 this signaling pathway promotes the accumulation of AKT in the nucleus promoting regulation of the CREB protein. The CREB signaling pathway is critical in this process because it controls the transcription of survival factors (Socodato et al., 2014). Another study also showed the activation of PI3K and consequent translocation of AKT to the nucleus in chick retina cells in culture stimulated by exogenous NO or stimulation with the NO synthase substrate L-arginine (Mejía-García et al., 2013). This effect of NO is dependent on the sGC/cGMP/PKG pathway which can also be stimulated by the activation of NMDA receptors. Furthermore, NO blocks apoptosis of these cells induced by the toxic stimulus with $H_2O_2$ (Mejía-García et al., 2013).

In the zebrafish retina, Muller glia cells can regenerate by stimulating the signaling of growth factors that act in an autocrine/paracrine manner. The PI3K signaling pathway participates in this event and must be activated so that Muller glia cells can reprogram, proliferate, and repair the retina in response to a stimulus for injury (Wan et al., 2014). There are also works in the literature showing that PTEN, a phosphatase that controls the activation of the PI3K/AKT pathway, can regulate events in the retina. For example, in PTEN knockout models, the dendrites of amacrine cells are disorganized and AKT phosphorylation is increased in the inner plexiform layer (Sakagami et al., 2012). Furthermore, AKT phosphorylation is important for dendritic development in amacrine cells. The mutation in PTEN also affects the development and

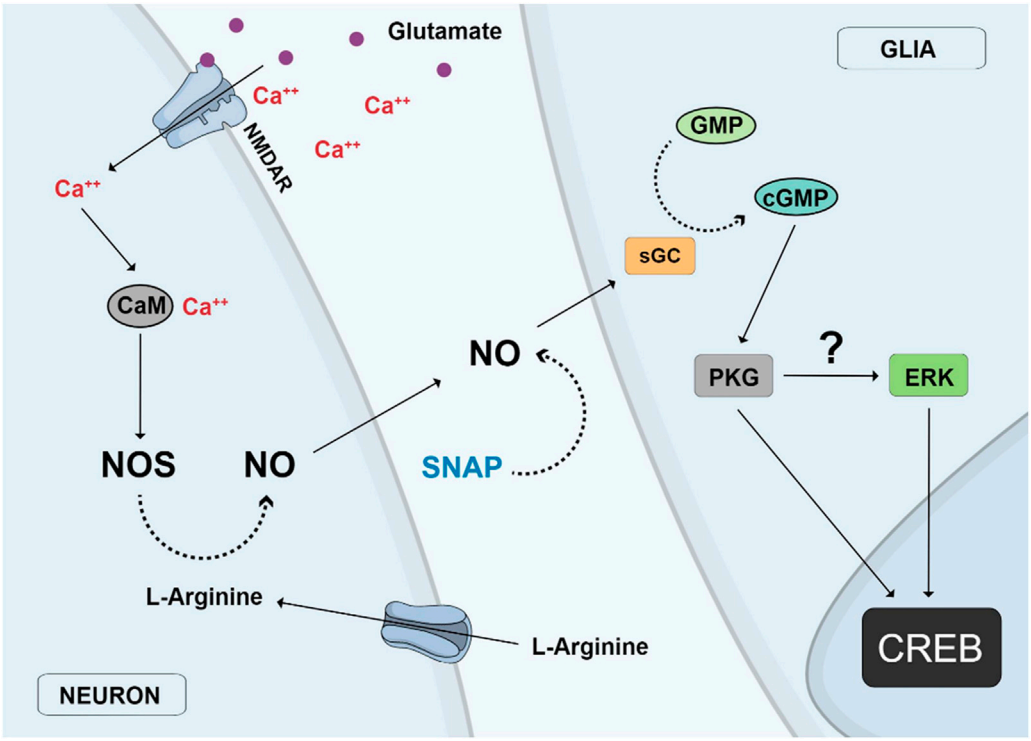


FIGURE 3
Nitric oxide (NO) neuronal-glial cycle. Activation of glutamate NMDA receptors (NMDAR) promotes calcium influx and stimulation of the calcium/calmodulin enzyme nitric oxide synthase (NOS) and NO production in neurons. NO diffuses out from neurons to glial cells where it stimulates soluble guanylyl cyclase (sGC) to produce cyclic GMP which activates protein kinase G (PKG), which then stimulates Erk and finally CREB in glial cell nuclei. The same effect is observed with the addition of the NO donor SNAP or the uptake of L-arginine, the substrate of NOS.

differentiation of photoreceptor cells. Studies show that PTEN controls important functions in the retinal circuit (Sakagami et al., 2012; Tachibana et al., 2016).

## 1.7 CREB as a hub of signaling pathways

CREB (cyclic nucleotide-responsive element binding protein) is an important transcription factor involved in many functions during CNS development such as survival and differentiation of neurons (reviewed by Belgacem and Borodinsky, 2017), as well as in cognition and memory (Morè et al., 2022).

CREB is localized in cell nuclei and is stimulated by phosphorylation of residue ser 133 by several intracellular signaling pathways including the classical cAMP/PKA but also by ERK/RSK, AKT/GSK3b and Calcium/CAMKIV (West et al., 2001; Bengtson and Bading, 2012; reviewed by Ahmed et al., 2022). In this way, it can be considered a signaling hub, converging distinct regulatory elements. Among the more studied genes regulated by CREB are the genes for antiapoptotic proteins and BDNF (Esvald et al., 2020).

## 1.8 CREB in the retina

Activation of glutamate NMDA receptors can activate ERK and CREB in chick retina cells through the accumulation of NO and stimulation of the classical guanylyl cyclase/cGMP/PKG pathway (Socodato et al., 2009). In this case, CREB activation by glutamate was found to occur in glial cell nuclei in mixed retinal cultures containing neurons and glial cells, whereas a direct CREB stimulation can be accomplished by the NO donor SNAP, implicating that NO can be produced by glutamate stimulation of neurons and released to activate CREB in glial cells (Figure 3). Ascorbate can also stimulate CREB in retinal cultures but this effect is mediated by glutamate and stimulation of NMDA receptors (Domith et al., 2018b). One study showed that nucleotides regulate CREB activity and proliferation of progenitor cells in chick retina cultures through the P2Y13 subclass of P2 purinergic receptors (Jacques et al.,

2017). Moreover, as described before, CREB phosphorylation or dephosphorylation by different pathways is fundamental for neuronal survival choices during chick retina development (Socodato et al., 2011, 2014).

## 2 Neurotransmitters and receptors in the retina

Most if not all neurotransmitter or neuromodulator systems present in other CNS regions are also present in the chicken retina, including some already described to stimulate GPCRs coupled to adenylyl cyclase such as dopamine (de Mello, 1978), adenosine (Paes-de-Carvalho and de Mello, 1982), PACAP (Fleming et al., 2013), as well as neurotransmitters linked to calcium and AKT metabolism as glutamate (Romano et al., 1998). Several neurotransmitter receptors appear very early during development in a profile consistent with the idea that some of these molecules and related neuromodulators can also function as morphogenic factors and developmental signals to regulate embryological phenomena such as neurite outgrowth and synapse formation (Lauder, 1987, 1988). Here we will discuss some of the neurotransmitter and neuromodulator systems more studied in the developing chick retina with the emphasis in the cAMP and AKT signaling pathways triggered by the activation of their specific receptors.

### 2.1 Neurotransmitter systems coupled to adenylyl cyclase in the retina

#### 2.1.1 Dopamine

Dopamine is an important neurotransmitter involved in several processes in the CNS, such as modulation of motor control, reward mechanisms and endocrine functions, as well as neurological and psychiatric disorders (reviewed by in Klein et al., 2018).

Dopamine is a major catecholamine present in retinas of several species (reviewed by Korshunov et al., 2020). In the avian retina, dopaminergic cells are found primarily in the inner nuclear layer (INL), which contains the cell bodies of amacrine neurons, whose processes extend exclusively to the inner plexiform layer (IPL) (Araki et al., 1983).

Dopamine receptors belong to the G protein-coupled receptor superfamily and are classified into two subfamilies based on their biochemical characteristics: D1-type receptors (comprising D1 and D5 receptors) and D2-type receptors (comprising D2, D3, and D4 receptors) (Mishra et al., 2018). D1-type receptors promote activation of adenylyl cyclase (AC) *via* Gs, consequently increasing the intracellular content of cAMP in retinas from several species (Figure 2). On the other hand, D2-type receptors inhibit AC activity by activating Gi or Go (Ventura and de Mello, 1990; Reis et al., 2007).

Some studies have shown dramatic variations of the cAMP content during chick embryo retina development. The basal cAMP level is low from the embryonic day 6 (E6) up to E15 but increases 3 times between E15 and E17. On the other hand, stimulation with dopamine in E7 promotes an increase in cAMP concentration of 5 times above basal level. Moreover, a 20-fold increase was observed between E8 and E16 (de Mello, 1978). Then, stimulation of dopamine receptors promotes activation of AC since E7, with a maximum observed in E14 (Lankford et al., 1988). Similarly, forskolin, a potent and direct activator of adenylyl cyclase, promotes an increase of cAMP during the period from E8 to E13, stabilizes up to E18 and decreases from E19 onwards (Paes-de- Carvalho and de Mello, 1982).

Dopamine was shown to inhibit growth cone motility and neurite outgrowth of retinal neurons in culture *via* D1 receptors and cAMP (Lankford et al., 1988), corroborating the idea that neurotransmitters are also morphogenic signaling molecules. Dopamine is also involved in regulating glutamate NMDA receptors through a PKA/CSK/Src pathway (Figure 4). Dopamine activates D1 receptors and a cAMP/PKA cascade which leads to a PKA-dependent phosphorylation of a tyrosine kinase named CSK (C-terminal Src Kinase) (Socodato et al., 2017). This kinase catalyzes the phosphorylation of residue tyr527 of Src kinase and promotes enzyme inhibition (Masato, 2012). Interestingly, this effect promotes inhibition of Src kinase-dependent posphorylation of NMDA subunit 2B and decreases receptor activity in embryonic retinal cells in culture (Socodato et al., 2017).

The presence of these systems in early stages of development suggests that they could have important functions on neuronal development. Indeed, dopamine regulates neurite growth in retinal cultures but the effects of these changes in more developed neurons are not known (Lankford et al., 1988).

Another interesting function of dopamine in retina is the modulation of vitamin C release. Dopamine *via* D1 receptors and the cAMP/EPAC pathway is able to promote the release of ascorbate in retinal cultures (da Encarnação et al., 2018). This effect of dopamine was later shown to be mediated by the release of glutamate and activation of AMPA/kainate receptors (Portugal et al., 2019) (Figure 5).

#### 2.1.2 Adenosine

Adenosine is a nucleoside that plays an important role as a neuromodulator or neurotransmitter in the CNS (reviewed by Schulte and Fredholm, 2003). It is metabolized by deamination or phosphorylation by the enzyme adenosine deaminase or adenosine kinase, respectively, and activates receptors coupled to AC in the retina during different stages of development. Four receptor subtypes, all coupled to heterotrimeric G proteins, are presently known, with subtypes A1 and A3 being classically coupled to Gi, inhibiting AC activity, while subtypes A2a and A2b are coupled to Gs protein, stimulating AC.

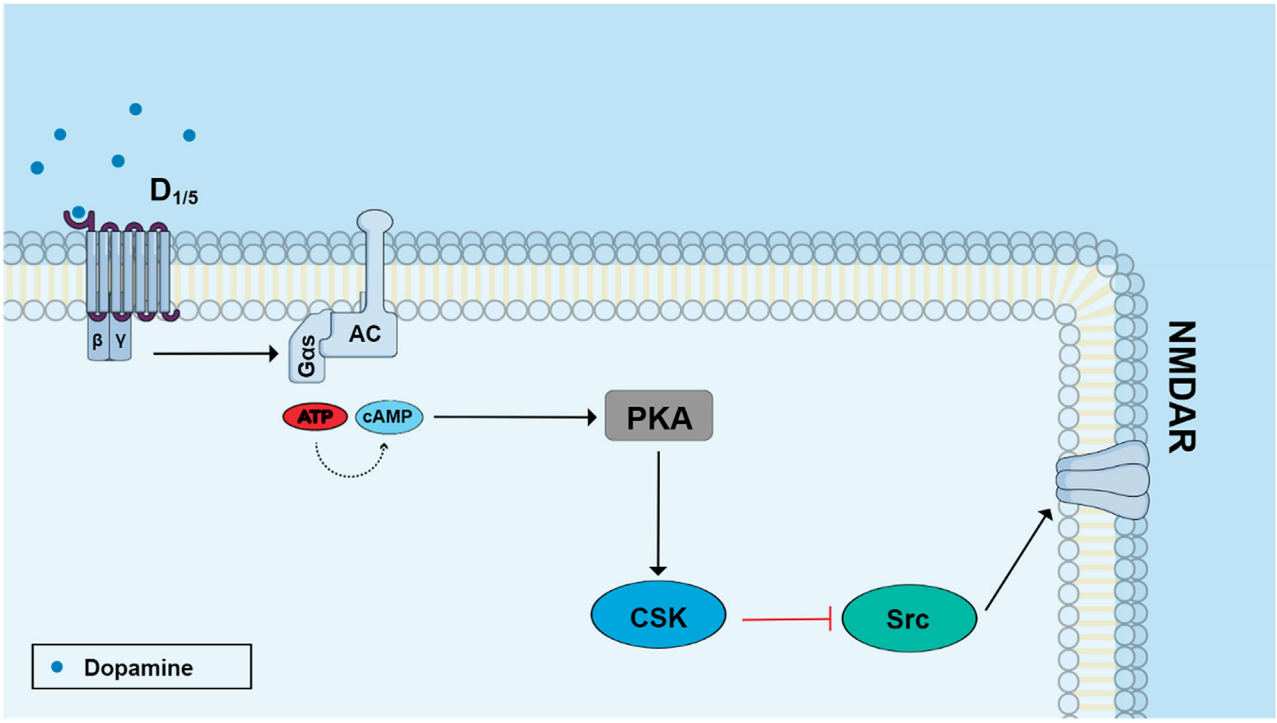


FIGURE 4
Dopamine regulates NMDA receptor function through the PKA/CSK/Src pathway. Stimulation of D1-like receptors with dopamine activates adenylyl cyclase and increases cyclic AMP production. Activated protein kinase A (PKA) induces the phosphorylation of C-terminal Src kinase (ser 364 Csk) which phosphorylates Tyr 527 Src leading to enzyme inhibition. Src phosphorylates the subunit 2B of NMDA receptor in the residue Tyr 1472 and then Src inhibition leads to diminished receptor activity.

#### 2.1.2.1 Regulation of cyclic AMP accumulation by adenosine receptors

As mentioned before, adenosine receptors have been shown to regulate AC activity and cAMP levels. In chick embryo retinas from E8 to E13, no increase in cAMP levels was observed when exposed to adenosine. Interestingly, embryos from E14 to E17 days showed a gradual adenosine-dependent increase in cAMP levels, reaching the maximum level in E17. In addition, in experiments carried out in post-hatch animals, lower levels of stimulation with adenosine were observed (Paes-de-Carvalho and de Mello, 1982). These results suggest that the increase of cAMP levels observed after stimulation of chick retinas may vary according to developmental stages (Figure 6) (reviewed by Paes-de-Carvalho, 2002).

In addition to adenosine receptors, dopamine receptors are also capable of promoting an increase in intracellular cAMP levels. One study demonstrated that in E12 chick embryo retinas, activation of D1-type dopamine receptors promotes an increase in cAMP levels, but that this effect was blocked by the use of adenosine A1 receptor agonists (Figure 6) (Paes-de-Carvalho and de Mello, 1985). Interestingly, this blocking effect upon dopamine-dependent cAMP accumulation is no longer observed in post-hatching chick retinas, but an inhibition of a cAMP increase induced by forskolin is still present (Paes-de-Carvalho, 1990). One explanation for this effect could be a developmental decrease of D1/A1 heteromers, but this possibility remains to be investigated.

#### 2.1.2.2 A1 adenosine receptor

Classically, adenosine A1 receptors are associated with the Gi protein, which inhibits AC activity, leading to a decrease in intracellular cAMP levels. However, it is already known that the adenosine A1 receptor also has the ability to modulate protein kinase C (PKC) activation (Di-Capua et al., 2003). A study using mice showed that when exposed to chronic intermittent hypoxia, the animal underwent morphological changes and a process of apoptosis in hippocampal neurons, generating a cognitive deficit. Moreover, activation of adenosine A1 receptors was able to play a neuroprotective role, in addition to modulating the Gα(i)-cAMP-PKC pathway, promoting the formation of LTP and increased synaptic plasticity (Zhang Y. et al., 2020).

In the chicken retina, adenosine A1 receptors appear throughout development at levels that vary according to embryonic age. Binding studies using [$^3$H] Cyclohexyl adenosine (CHA), an A1 receptor agonist, showed an expression of these receptors in the first stages of

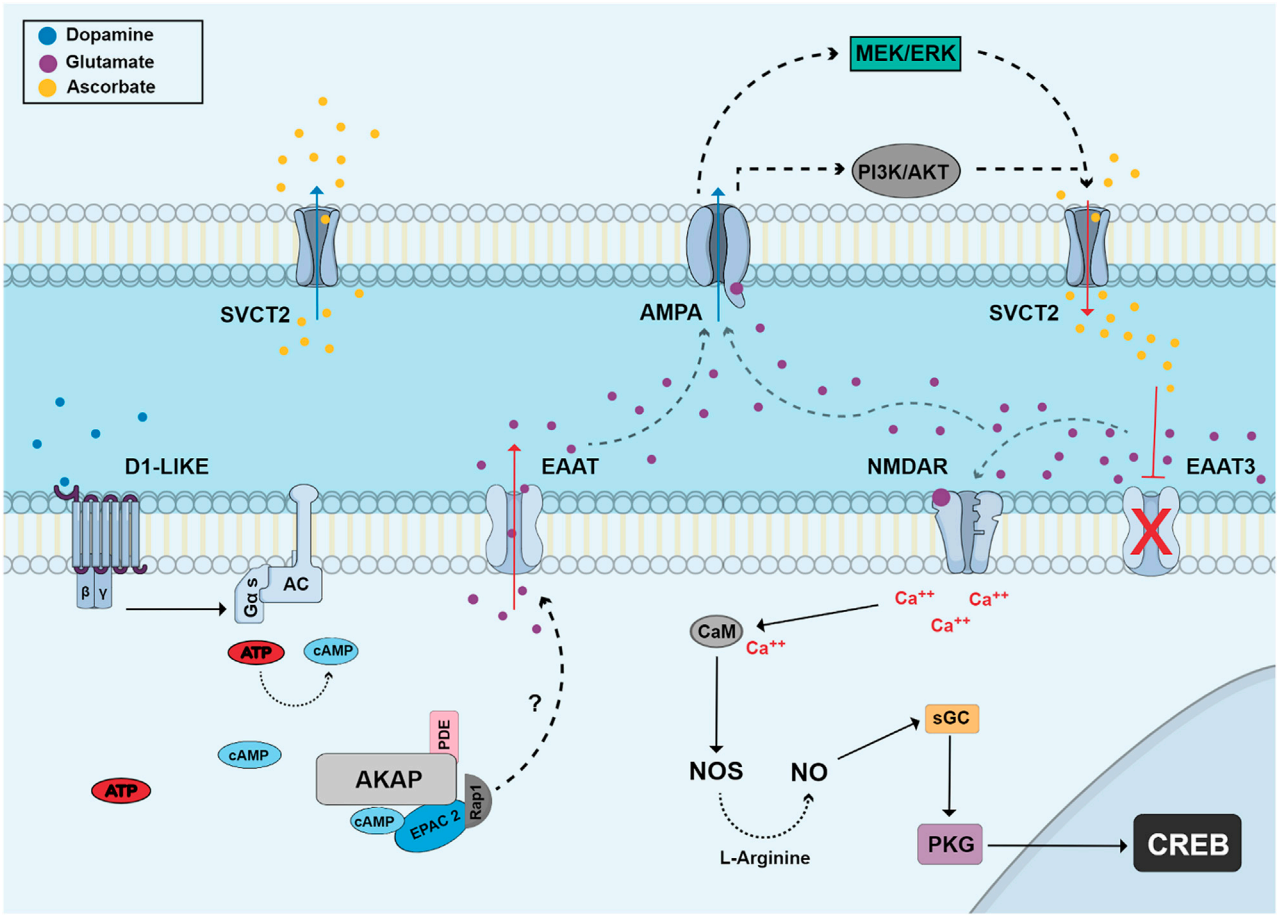


FIGURE 5
Dopamine regulates the release of vitamin C *via* EPAC and glutamate receptors. Dopamine stimulates D1-like receptors and activates adenylyl cyclase and cAMP production. cAMP stimulates EPAC2 and Rap1 which stimulates the release of glutamate by an unknown mechanism. Glutamate can then stimulate AMPA receptors in a second cell activating MEK/ERK and PI3K/AKT pathways and promoting ascorbate efflux through the sodium/vitamin C transporter 2 (SVCT2). Extracellular ascorbate promotes an increase of extracellular glutamate by inhibiting EAAT3 activity and then glutamate can stimulate NMDA receptors (NMDAR). This activation leads to calcium influx and increased NO production by calcium/calmodulin-dependent NOS, which then can stimulate the canonical PKG-dependent pathway and CREB phosphorylation.

development, but at very low levels. However, throughout development, the levels of these receptors gradually increase, reaching a peak in E16. In post-hatching animals, A1 receptor levels decrease. Autoradiographic data showed the presence of these receptors in the inner and outer plexiform layers since E12 and high labeling was observed in E18 as well in post-hatched retinas (Paes-de-Carvalho et al., 1992).

It has already been described in the literature that cell aggregation and cAMP/PKA pathways regulate A1 receptor expression in cultured retinal cells (Pereira et al., 2010). Moreover, long-term activation of adenosine A2a receptors, which promote cAMP accumulation, also has the ability to regulate A1 receptor expression in retinal cells, suggesting that regulation of extracellular adenosine levels is a key factor capable of controlling adenosine receptor expression (Pereira et al., 2010). Interestingly, long-term exposure of retinal cell in culture to adenosine promotes a decrease of cAMP accumulation stimulated by adenosine (de Mello et al., 1982).

One recent study raised the possibility that exposure to caffeine, a non-selective antagonist of adenosine A1 and A2a receptors, during the intermediate stages of development, leads retinal cells to a more ischemic-resistant state. The precise mechanism by which caffeine protects the retina still needs further study. The data presented indicate that tissue excitability modulated by the GABAergic and glutamatergic systems appears to play an important role. This protective mechanism appears to be triggered by adenosine A1 receptor, CREB phosphorylation and BDNF production (Pereira-Figueiredo et al., 2020).

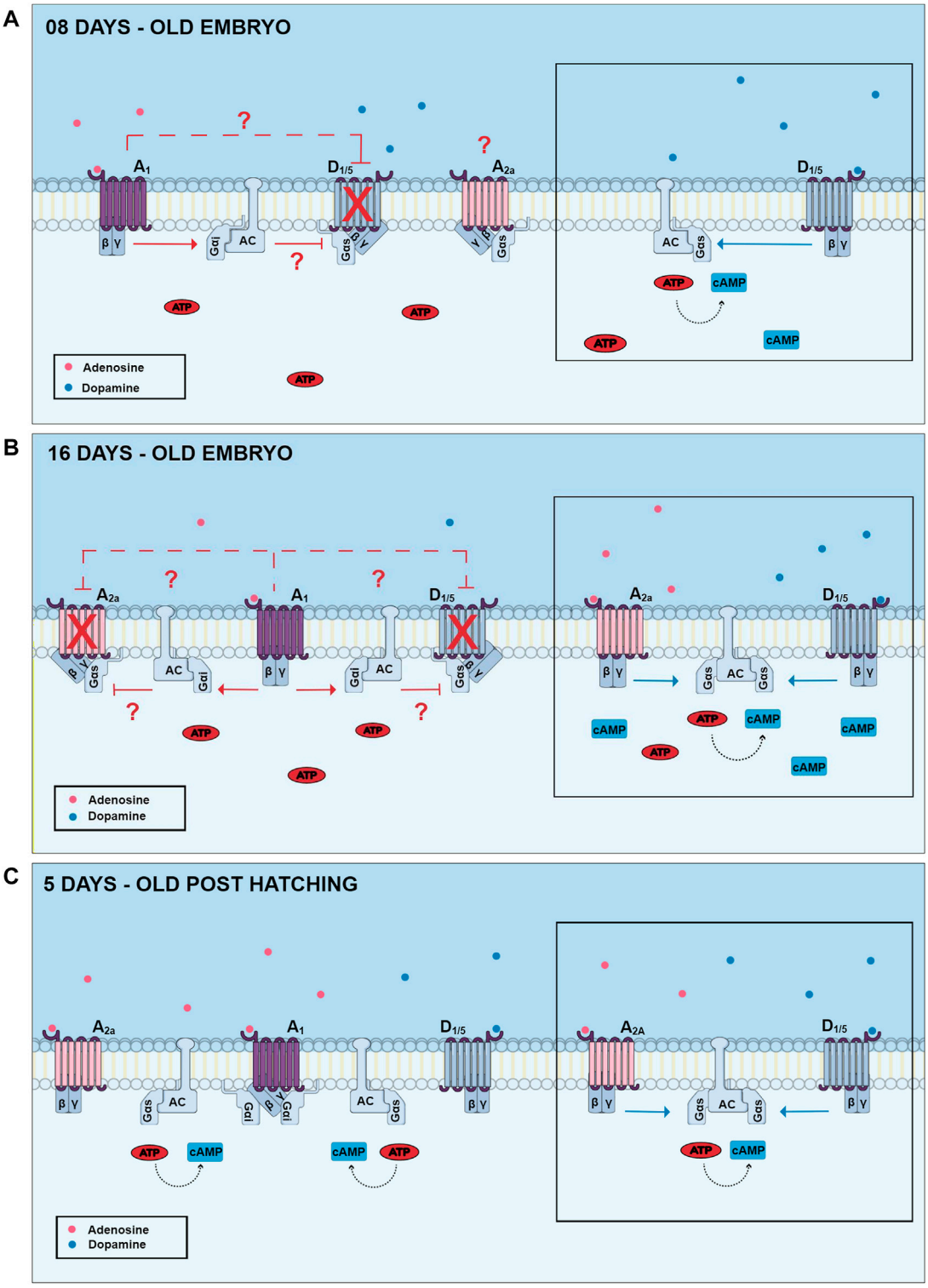


FIGURE 6
Changes of dopamine and adenosine-dependent cAMP levels in three different developmental stages of the chick retina. In E8 retinas, dopamine promotes a high increase of cAMP *via* stimulation of D1-like receptors (lateral picture), and this effect can be inhibited by activation of adenosine A1 receptors. Adenosine A2a receptors are present in this period but are not coupled to cAMP production. In E16 retinas, both D1 and A2a receptors are present and promote cAMP accumulation. However, cAMP increase is not additive due to the presence of A1 inhibitory receptors. In post-hatching retinas, dopamine and adenosine promote a lower increase of cAMP accumulation and A1 receptor-mediated decrease of dopamine-dependent cAMP accumulation is no longer observed. Gαi and Gαs are respectively inhibitory and stimulatory Gα protein subunits; AC, adenylyl cyclase.

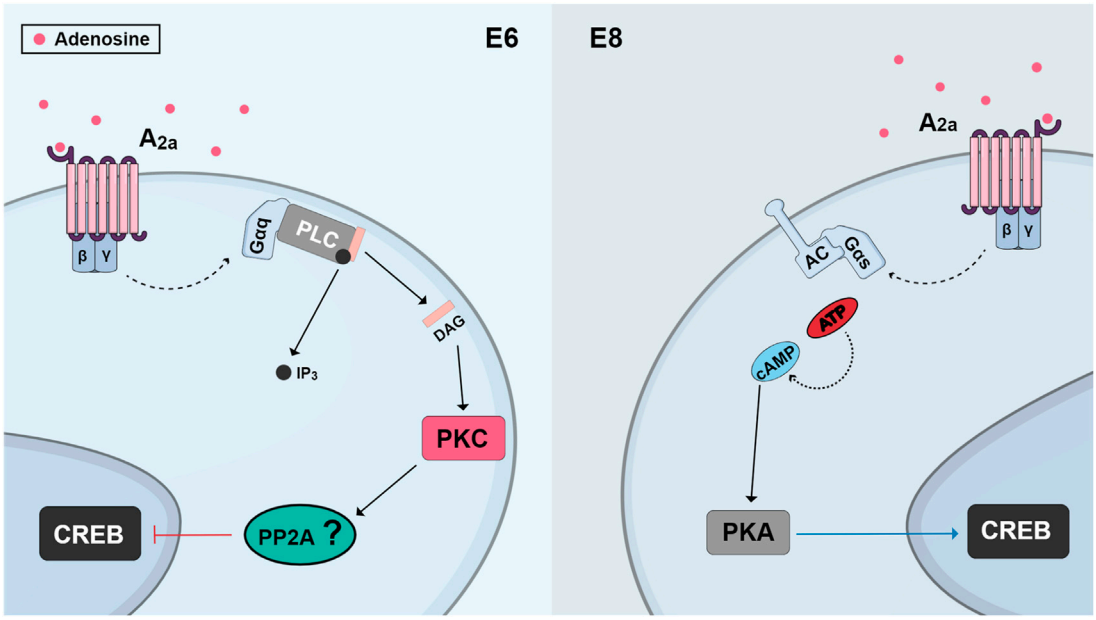


FIGURE 7
Schematic view of changes observed in CREB regulation by A2a receptors in different ages of cultures from developing chick retina. In cultures obtained from E6 retinas, activation of A2a receptors promotes phospholipase C/PKC stimulation and CREB dephosphorylation, probably through the activation of a phosphatase, leading to cell death. On the other hand, in cultures from E8 embryos, activation of A2a receptors promotes CREB phosphorylation, through a cAMP/PKA pathway, and cell survival.

#### 2.1.2.3 A2a adenosine receptor

A2a receptors are present in the retina of several animals, including rats, mice and chickens (Paes-de-Carvalho et al., 2003; Li et al., 2013). Several studies show a preeminent role of A2a receptors in the outer retina (McIntosh and Blazynski, 1994; Li et al., 2013; Huang et al., 2014; Cao et al., 2021). However, A2AR-immunoreactivity was shown to be expressed as puncta in the ganglion cell layer, inner plexiform layer, inner nuclear layer, and outer retina of the zebrafish (Grillo et al., 2019).

In purified cultures of retinal neurons, adenosine is neuroprotective against glutamate excitotoxicity or cell death induced by feeding cells with fresh medium. This effect is mediated by the activation of A2a receptors and accumulation of cyclic AMP, but it is only observed when these receptors are activated by long-term treatments of at least 24 h (Paes-de-Carvalho et al., 2003). Interestingly, as described in the previous section, these long-term treatments can promote increases in A1 receptor expression (Pereira et al., 2010), raising the possibility that the neuroprotective effect is in fact mediated by A1 receptors. Indeed, in chick retina cultures obtained from E8 embryos, activation of adenosine A2a receptors and the cAMP/PKA pathway is neuroprotective and promotes CREB phosphorylation (Socodato et al., 2011). However, activation of these receptors causes massive cell death in cultures obtained from E6 retinas, an effect mediated by increased activation of PKC and dephosphorylation of CREB (Figure 7). Activation of these receptors also can exhibit cytotoxic effects in the embryonic retina *in vivo*, where it will induce CREB dephosphorylation. These results suggest that the regulation of CREB activity and retinal neuronal survival by adenosine depends on the period of development and activation of different signaling pathways (Socodato et al., 2011).

#### 2.1.2.4 Adenosine A3 and A2b receptors

As previously reported, the adenosine A3 receptor is coupled to a Gi protein, inhibiting the activity of AC and consequently leading to a decrease in intracellular cAMP levels. Some studies show the presence of this receptor in retinal ganglion cells (RGCs). Findings related to this receptor suggest its contribution to the reversal of the toxic effect observed after stimulation of the P2X7 type of ATP receptor in RGCs (Zhang et al., 2006). When activated, the A3 receptor has the ability to modulate NMDA-dependent calcium influx into ganglion cells (Zhang et al., 2010) and also promotes neurite outgrowth *in vitro* and *in vivo* during the regeneration of mouse retinal ganglion cells. This latter effect is caused by the activation of an Akt-dependent signaling pathway (Nakashima et al., 2018).

The expression of the A3 receptor in the developing chicken retina model is still poorly characterized. A study performed in chicken retina culture showed that the adenosinergic system regulates the bioavailability of vitamin C in primary neurons and that the activation of A3R can increase the release of ascorbate in

a Sodium-Vitamin C transporter 2 (SVCT2)-dependent manner. This decrease of ascorbate content leads to an accumulation of reactive oxygen species, showing an essential and specific role of the adenosinergic system in the control of vitamin C homeostasis in a way that directly affects neuronal redox balance (Portugal et al., 2021). Although these are promising results, more studies are still needed to show the roles played by the A3-type adenosine receptor in the retina.

The adenosine A2b receptor is a G protein-coupled receptor and is activated by high concentrations of extracellular adenosine mediated by inflammation or hypoxia, for example (reviewed by Sepúlveda et al., 2016). This receptor, in addition to associating with Gs, also can associate with Gq, triggering an activation of phospholipase C and the mobilization of calcium in different animal models (reviewed by Linden, 1991). Some studies show that the A2b receptor is overexpressed in several types of tumors and in events such as angiogenesis and metastasis, which could be a suggestion that the receptor could promote the progression of these tumors (Sepúlveda et al., 2016). Regarding the A2b receptor, little is known about its presence in the chicken retina, and further studies are needed for a better characterization of this receptor and its effects in this animal model.

### 2.1.3 Neuropeptides and cannabinoids

Pituitary Adenylyl Cyclase-Activating Polypeptide (PACAP) is considered as a neuroprotective agent in several CNS tissues including in the retina of several species (Szabadfi et al., 2012). In the avian retina, PACAP activates AC since E8, and this effect desensitizes after E12. As also shown for dopamine-dependent cAMP accumulation (Paes-de-Carvalho and de Mello, 1982), chronic administration of PACAP or the PACAP antagonist (PACAP 6-38) regulates PACAP receptor/cyclase system *in vitro* and *in vivo*. Interestingly, the peptide is also able to regulate the expression of tyrosine hydroxylase positive ($TH^+$) cells, a marker of dopamine containing cells (Fleming et al., 2013).

Cannabinoid receptors are present in the retinas of several species (Straiker et al., 1999). In the chicken retina, $CB_1$ receptor is highly expressed from embryonic day 5 (E5) until post hatched day 7 (PE7), decreasing its levels throughout development. $CB_1$ is densely found in the ganglion cell layer (GCL) and inner plexiform layer (IPL). $CB_2$ receptor was also found from E5 until PE7 with a decrease in its contents from E9 afterwards (da Silva Sampaio et al., 2018). $CB_1$ is co-localized with TH and was heavily associated to dopamine $D_1$ receptor labeling in primary cell cultures. In chick retina cultures, cAMP accumulation was stimulated by the selective $D_1$ agonist SKF38393, and this effect is inhibited when cultures were treated with WIN55, 212-2 (WIN) in a $CB_1$- dependent manner. The results suggest a correlation between the endocannabinoid and dopaminergic systems (DSs) during avian retina development. Activation of $CB_1$ limits cAMP accumulation *via* $D_1$ receptor activation and may influence embryological parameters during avian retina differentiation.

# 3 Glutamate and related neuromodulator systems

## 3.1 Glutamate

The main route of glutamate synthesis in neurons is from glutamine. Glia are able to release glutamine to the neuron, which through the enzyme glutaminase converts glutamine into glutamate (reviewed by Newsholme et al., 2003). Another route of glutamate synthesis is through the mitochondrial enzyme glutamate dehydrogenase (GDH), converting α-ketoglutarate to glutamate (Dewan, 1938). Interestingly, some compounds can interfere with glutamate synthesis by regulating GDH activity. Some of them are routinely consumed in beverages around the world, such as chlorogenic acids, found in coffee, and some green tea polyphenols such as epigallocatechin gallate and epicatechin gallate (Li et al., 2006, 2011; Domith et al., 2018a).

Glutamatergic signaling occurs through a wide range of receptors. It acts on ionotropic receptors, which include NMDA (N-methyl-D-Aspartate), AMPA (alpha-amino-3-hydroxy-5-methyl-4-isoxazole-propionate) and kainate receptors (Wyllie and Bowie, 2022), as well as metabotropic receptors (reviewed by Watkins and Evans, 1981; and Ferraguti et al., 2022; Mayer and Westbrook, 1987; De Blasi et al., 2001).

## 3.2 Glutamate in the retina

As in other areas of the CNS, glutamate is also the main excitatory neurotransmitter in the retina (Mayer and Westbrook, 1987; Rauen, 2000; Bui et al., 2009; reviewed by Boccuni and Fairless, 2022). In the chick retina, a complex neurochemical network regulated by glutamate is present in the developing as well as in the mature tissue (reviewed by Paes-de-Carvalho et al., 2008). The presence of glutamate receptors was observed mainly in amacrine and ganglion cells, in addition to the inner and outer plexiform layers (Silveira Dos Santos Bredariol and Emi Hamassaki-Britto, 2001). Also, NMDA receptors has been observed in Müller cells, the only type of glial cell found in chick retina (Lamas et al., 2005).

Glutamate ionotropic receptors signaling in chick retina is involved in a wide range of cellular effects and many of these effects involve calcium signaling. In cultures of chick retina cells obtained from E8 embryos, glutamate, kainate or AMPA treatment decreases neurite outgrowth (Catsicas et al., 2001). This inhibition was due to activation of AMPA receptors, since pre-incubation of these cultures with CNQX or GYKI 52466, AMPA receptors antagonists, but not with AP5, an NMDA receptor antagonist, did prevent the inhibitory effect. Moreover, $Ca^{2+}$-permeable AMPA receptors were involved since the selective antagonist JSTX-3 was also able to block this effect (Catsicas et al., 2001). Another event involving $Ca^{2+}$ observed in chick retina is the modulation of NMDA receptor by

caffeine. Mixed retinal cultures treated with caffeine increased basal NMDA receptor activity. In addition, if these cells were pre-treated with caffeine and then stimulated with NMDA, there was an increase in intracellular $Ca^{2+}$ when compared to NMDA alone (Pereira-Figueiredo et al., 2020).

As caffeine, vitamin C also modulates NMDA receptor activity in the retina. Ascorbate, the reduced form of vitamin C, and dehydroascorbate, the oxidized form, increased NMDA receptor function in the absence of glutamate, an effect observed by measuring the increase in [$^3$H]-MK-801 binding in chick retina mixed cultures (Domith et al., 2018b). Glutamate, as expected, increased the binding to a much greater extent as [$^3$H]-MK-801 binds to an open state channel conformation. Interestingly, if the cultures were treated concomitantly with glutamate plus ascorbate or dehydroascobate, [$^3$H]-MK-801 binding was lower when compared to glutamate treatment alone (Domith et al., 2018b). Moreover, data also show that ascorbate reduces NMDA receptor levels in the cell membrane, suggesting that this vitamin prevents receptor over-activation. In addition, ascorbate started a NMDA receptor and calcium-dependent downstream signaling pathway that culminated in an increase of CREB phosphorylation (Domith et al., 2018b). Overall, these data suggest vitamin C as a NMDA receptor signaling modulator (see below).

Some studies show a relationship between glutamatergic signaling and other neurotransmitters in chick retina (Passos et al., 2019). L-glutamate decreases serotonin uptake, an effect blocked by the AMPA/kainate antagonist CNQX, but not by the NMDA receptor antagonist MK-801. In addition, this inhibitory effect was not observed in the presence of AMPA, suggesting the involvement of kainate receptors (Passos et al., 2019). Some data also support an interaction between NMDA receptors and cannabinoid signaling. Kubrusly and collaborators (2018) described in chick retina that after L-aspartate exposure, there was less $GABA^+$ amacrine cells, and that pre-incubation with the cannabinoid receptor agonist WIN 55,212-2 inhibited this effect. These data suggest the existence of some interaction between CB1 and/or CB2 and NMDA receptors in GABA release (Kubrusly et al., 2018).

Interestingly, NMDA receptors also not only modulate NO production but protein synthesis in chick retina cells (Cossenza and Paes-de-Carvalho, 2000; Cossenza et al., 2006, 2014; Gladulich et al., 2020). Stimulation of NMDA receptors activates the $Ca^{2+}$/calmodulin-dependent enzyme eEF2K, a kinase that phosphorylates the elongation factor eEF2 and inhibit its activity, promoting a decrease of protein synthesis rate (Cossenza and Paes-de-Carvalho, 2000; Cossenza et al., 2006, 2014; Gladulich et al., 2020). Experiments utilizing arginine-free solutions demonstrated that inhibition of eEF2K also promotes an increase of NMDA-dependent NO production (Gladulich et al., 2020). This effect would be due to an increase of arginine availability for NO production since this amino acid would be less directed towards protein synthesis. Some data showed that the protein Homer1b/c plays an important role in this protein synthesis regulation, since lack of this protein impairs this signaling pathway (Gladulich et al., 2021).

Metabotropic glutamate receptors (mGluRs) are divided into different subtypes that modulate several signaling pathways through G proteins. Different G protein isoforms have varied effects, so that they can promote activation ($G_s$) or inhibition of adenylyl cyclase ($G_i$), activation of phospholipase C ($G_q$), among others. Group I mGluRs comprise mGluR1 and mGluR5, coupled to the Gq protein, while group II receptors comprise mGluR2 and mGluR3 receptors, coupled to the Gi or Go protein; group III receptors comprise the mGluR4, mGluR6, mGluR7 and mGluR8 receptors, and may also be associated with Gi or Go (De Blasi et al., 2001; reviewed by Gregory et al., 2011; and Reiner and Levitz, 2018).

Previous evidence shows that activation of chick retina mGluR from group III inhibits cAMP formation during the embryonic period until hatching, demonstrating its presence and functionality early in development (Sampaio and Paes-de-Carvalho, 1998). Interestingly, presynaptic mGluR4/7 increases glutamate release in chick retina, which in turn activates postsynaptic ionotropic glutamate receptors, promoting Na + influx and GABA release *via* GAT1 (Guimaraes-Souza and Calaza, 2012). In addition, some evidence suggests that postsynaptic mGluR8 actually decreases GABA release (Guimaraes-Souza and Calaza, 2012). In relation to group I, some data indicates that mGluR5 in amacrine cells of avian retina are involved in Ca+2 release and influx *via* phospholipase C (Sosa et al., 2002). Glutamate transport occurs mainly *via* sodium-dependent excitatory amino acid transporters (EAAT). There are five isoforms of EAATs: isoforms 1 (EAAT1 or GLAST) and 2 (EAAT2 or GLT1) glial, isoform 3 (EAAT3 or EAAC1) found in neurons, isoform 4 (EAAT4) found in Purkinje cells of the cerebellum (reviewed by Shigeri et al., 2004) and isoform 5 (EAAT5) found in retina (Arriza et al., 1997; reviewed by Magi et al., 2019). There are different levels of expression of EAATs isoforms 1, 2, 3 and 4 during human development (Bar-Peled et al., 1997). During the embryonic phase, EAAT2 is the most expressed isoform in different regions of the brain, such as cortex and hippocampus (Bar-Peled et al., 1997). In the frontal cortex, expression of EAAT2 increases significantly, while in the same region EAAT4 decreases from the embryonic stage to the postnatal and adult stages (Bar-Peled et al., 1997).

In general, EAATs promote glutamate uptake, but interestingly, it has been shown that during ischemic events, the reversal of glutamate transporters can occur, causing cell death by activating NMDA receptors (Rossi et al., 2000; Camacho and Massieu, 2006). In chick retina culture, ascorbate promotes a decrease in EAAT3 surface levels in neurons, leading to glutamate accumulation at the extracellular space, but not promoting cell death in acute treatment (Domith et al., 2018b). As mentioned before, this glutamate accumulation activates NMDA receptor signaling

pathway. Interestingly, EAAT1 D-aspartate transport increases the Na+/Ca+2 exchanger activity which starts a Ca+2-dependent signaling pathway in Müller glia cells of chick retina (López-Colomé et al., 2012). This Ca+2 influx results in mTOR phosphorylation in a SRC and AKT-dependent manner (López-Colomé et al., 2012).

Overall, it is possible to verify that glutamate is an important neurotransmitter in the chick retina. The data clearly demonstrate its role in cell signaling with emphasis on calcium-dependent pathways.

## 3.3 Vitamin C

Vitamin C can be found in two forms, ascorbate, its reduced form, and dehydroascorbate, its oxidized form. Humans are not able to synthesize vitamin C, having to acquire it through the consumption of fruits and vegetables during the diet. It is estimated that 100 mg/day is sufficient to meet physiological needs. Ascorbate is absorbed in the intestine and distributed to tissues by the specific transporters named SVCTs (sodium-dependent vitamin C transporters) while dehydroascorbate is transported by glucose transporters (GLUTs) (reviewed by Lykkesfeldt and Tveden-Nyborg, 2019). SVCTs (types 1 and 2) are sodium and vitamin C co-transporters and SVCT2 is more expressed in the central nervous system. On the other hand, GLUT1 and 3 are glucose transporters that have high affinity for the transport of dehydroascorbate in the central nervous system. The distribution and different location of transporters allow physiological systems to achieve different concentrations of vitamin C (reviewed by Padayatty and Levine, 2016). It has already been shown that the SVCT2 knockout condition is incompatible with life in mice that present respiratory failure and brain hemorrhage, indicating that ascorbate transport is essential in the perinatal period (Sotiriou et al., 2002).

Vitamin C is known to act as an important antioxidant agent but has other functions such as providing electrons for enzymatic reactions, participating in the formation of the myelin band, acting as an enzymatic cofactor, hormone synthesis, modulation of the glutamatergic system, regulation of gene expression, among others (May 2012; Oudemans-van Straaten et al., 2014; reviewed by Padayatty and Levine, 2016).

## 3.4 Vitamin C in the brain

Ascorbate concentrations in the brain are high. Glial cells can reach a concentration of 1 mM while neurons can reach concentrations of 10 mM. To reach the central nervous system, vitamin C must cross the blood-brain barrier. Studies show that ascorbate can reach the choroid plexus through SVCT2 reaching the cerebrospinal fluid while dehydroascorbate crosses the blood-brain barrier by GLUTs (Nualart et al., 2014). Another mechanism to maintain the high concentration of vitamin C in the central nervous system is the recycling of dehydroascorbate by astrocytes. When ascorbate is used, formation of its oxidized form occurs. Dehydroascorbate, in turn, will be taken up by astrocytic cells *via* GLUTs where it undergoes the actions of enzymes, reducing dehydroascorbate into ascorbate. When released into the extracellular environment, ascorbate can be taken up by neuronal cells *via* SVCT2 (reviewed by Covarrubias-Pinto et al., 2015). The recycling ability of vitamin C can also be observed at the blood-retinal barrier (Hosoya et al., 2004).

## 3.5 Vitamin C as a neuromodulator in the retina

Ascorbate is present in the chick retina (Portugal et al., 2009) and, in this model, can be released by reversal of SVCT2 (Figure 5). Glutamate interacts with the NMDA receptor leading to an increase in sodium in the membrane microdomain. This inversion of the electrochemical gradient of sodium generated by NMDA allows the interaction of SVCT2 with sodium ions and intracellular ascorbate and, thus, the transporters would release vitamin C instead of capturing it (Portugal et al., 2009). Another study shows that NO promotes the increase of SVCT2 levels through the activation of its canonical cGMP/PKG pathway, stimulating NFκB translocation to the nucleus and its consequent transcription. In addition, NO can increase intracellular levels of ascorbate in retinal neurons, protecting cells from damage caused by oxidative stress (Portugal et al., 2012).

Ascorbate inhibits glutamate uptake by decreasing levels of EAAT3 (excitatory amino acid transporter 3) in the cell membrane of neurons (Figure 5). Thus, there is an accumulation of extracellular glutamate and a consequent increase in the activation of glutamate receptors and downstream signaling pathways leading to CREB activation (Domith et al., 2018b). Recent studies also show that dopamine induces ascorbate release from cultured retinal neurons in a dose-dependent manner. It was observed that dopamine pulses increased the release of ascorbate without depleting its intracellular stores, an effect also dependent on EPAC2. We can conclude that the D1/cAMP/EPAC2 signaling pathway is involved in dopamine-induced acorbate release in cultured retinal cells (da Encarnação et al., 2018). Ascorbate was also shown to increase the efficiency of dopaminergic transmission by increasing the half-life of dopamine (Neal et al., 1999) and possibly potentiating the activity of the D1 receptor (Bernstein and Dillon, 2014), an effect also dependent on EPAC2.

The release of vitamin C induced by dopamine is dependent on the activation of ionotropic glutamate receptors of the AMPA/kainate type (Portugal et al., 2019). These activated receptors

stimulate signaling pathways such as PI3K/AKT and MAP kinases that promote the reversion of the SVCT2 transporter (Figure 5), a mechanism that can explain how the cellular release of ascorbate occurs (Portugal et al., 2019). Adenosine, an important neuromodulator of the nervous system, also modulates vitamin C release in chick retinal cultures and this effect is dependent on the activation of adenosine A3 receptors, which associate with the SVCT2 transporter to modulate the transport of ascorbate, increasing its release into the extracellular environment (Portugal et al., 2021). This modulation of ascorbate transport may be important for neuronal homeostasis.

Data also show that ascorbate is able to modulate GABA receptors, potentiating its activity in goldfish retinas (Calero et al., 2011). In addition, clinical studies show that patients with proliferative diabetic retinopathy have decreased levels of vitamin C in the aqueous humor and vitreous humor when compared to non-diabetic patients. This may be due to the rapid depletion of vitamin C caused by increased oxidative stress (Park et al., 2019).

## 3.6 Vitamin C as a neuroprotective agent in retina

One study shows that exposure for 1 h to ultraviolet B radiation was able to cause damage to photoreceptor cells characterized by the presence of pyknotic nuclei and disappearance of the outer segments of these cells. However, damage by UVB exposure was blocked in the presence of vitamin C, possibly due to its antioxidant effects (Tokuda et al., 2007). Additionally, exposure to lead, present in cosmetics, fuel, and industrial processes, induces cellular apoptosis in rod and bipolar cells of the retina and exposure during pregnancy and lactation induces and increases apoptosis in the photoreceptor layer of rat offspring. The consumption of vitamin C during pregnancy and lactation of rats was able to reduce the damage caused by lead in the photoreceptor cells of the offspring of rats (Khordad et al., 2013). The use of topical ascorbate also exerts protective effects on corneal endothelial cells *via* PI3K/AKT in a rabbit phacoemulsification oxidative stress model (Hsueh et al., 2020).

## 3.7 Nitric oxide

Nitric oxide (NO) is an important cellular messenger produced from the amino acid L-arginine by enzymes called nitric oxide synthases (NOSs). The three NOS isoforms (the constitutive endothelial and neuronal, NOS I and II, and the inducible immunological, NOS III) are expressed in different cell types and have variable functions in physiological systems. The neuronal isoform nNOS is found in the central nervous system, present mainly in neurons (reviewed by in Luo and Zhu, 2011). Stimulation of NMDA receptors promotes an increase in the influx of intracellular calcium, and the complex calcium-calmodulin is able to activate nNOS that catalyzes the production of NO and citrulline in a stoichiometric way (Christopherson et al., 1999). NO exerts its effects by activating some signaling pathways, and the classical pathway involves activation of soluble guanylyl cyclase (sGC), cyclic GMP production and stimulation of protein kinase G (PKG or cGK). In the CNS, NO is involved in synaptic plasticity, neurotransmission, neuroprotection, sleep control, among others (reviewed by Calabrese et al., 2007). NO is also involved in the activation of the AKT pathway (reviewed by Contestabile and Ciani, 2004). Excessive NO production can lead to the formation of reactive nitrogen species and triggers cellular damage.

High levels of NO are present in the early stages of chick retina development (Ientile et al., 1996). Interestingly a NADPH diaphorase activity that corresponds to NOS was described during chick retina development and that can be stimulated by calcium ions (Paes-de-Carvalho and de Mattos, 1996). NO donors, such as SNAP, prevent cell death in purified cultures of retinal neurons from E8 embryos with involvement of the sGC/PKG and PI3K pathways, among others. In addition, SNAP treatment promoted neurite outgrowth that may be important for the development of the nervous system (Mejía-García and Paes-de-Carvalho, 2007). SNAP also reduced cell proliferation in purified cultures of retinal glial cells and in the "intact" retina model *via* a cGMP-independent pathway (Magalhães et al., 2006). Stimulation of NMDA receptors in cultures from E8 chick embryos promotes inhibition of protein synthesis leading to increased availability of the NOS substrate L-arginine. This increase in available L-arginine can be used for NO synthesis (Cossenza et al., 2006). Surprisingly, inhibition of protein synthesis is also able to promote L-arginine intracellular accumulation and a consequent increase of NO synthesis and activation of downstream signaling pathways including the AKT pathway (Cossenza et al., 2020). Experiments in intact retina of E8 embryos show that NO can modulate CREB phosphorylation, a transcription factor that plays a key role in many cellular functions (Socodato et al., 2009). Data show that stimulation of the calcium permeable AMPA receptor increases the activity of nNOS and the NO produced modulates the activity of Src kinases in cultures of E8 embryos. This effect is confirmed with the use of NO donors and a guanylyl cyclase activator (Socodato et al., 2012). Src is a kinase with important functions such as involvement in long-term potentiation (MacDonald et al., 2006). NO also increases the activity of the PI3K/AKT pathway and promotes translocation of AKT to the cell nucleus, in addition to protecting cells from a toxic stimulus induced by hydrogen peroxide (Mejía-García et al., 2013). As described in the previous section, NO modulates the expression of the ascorbate transporter SVCT2, increasing the ascorbate transport capacity *via* NF-κB and PKG (Portugal

et al., 2012). The viability of neuronal cells can be controlled by NO depending on the age of the embryo. SNAP promotes cell death of retinal cells from E6 embryos while it leads to decreased apoptosis in retinas from E8 embryos. These events in this time window happen *via* sGC and cGKII. Furthermore, SNAP-induced CREB phosphorylation was increased in E8 embryos while in E6 it was decreased (Socodato et al., 2014). These data show that NO is an important modulator of neuronal survival in the developing CNS.

NO and its classical activation pathway appear to be present and exert physiological roles on retinal cells (Eldred and Blute, 2005). Studies show that NO can act both on intraocular pressure and on the retinal pathophysiology of glaucoma (reviewed by Wareham et al., 2018). nNOS is expressed by pigmented epithelium, amacrine cells, ganglion cells, and photoreceptors (Blom et al., 2012), and the NO produced by this enzyme can act as a messenger between the inner cell layers of the retina and astrocytes. The eNOS enzyme is also important in controlling vascular smooth muscle tone in the eye (reviewed by Toda and Nakanishi-Toda, 2007). Data show that NO is important for correct development of retinotectal projection in chicks (Ernst et al., 1999; Wu et al., 2001). In turtle retinas, NO enhances GABA release in horizontal cells *via* cGMP (Yu and Eldred, 2005). In developing chick retinas NO can alter the cytosolic pH of amacrine cells promoting chloride release from these cells (McMains and Gleason, 2011).

## 4 Conclusion

One of the major problems in biology is how cells in multicellular organisms build the different tissues and organs in a coordinated and precise pattern. It is generally believed that this organization depends on cellular interactions and communication. Although direct cell contacts play an important role, chemical communication between cells appears to be essential to ensure correct development. The nervous system is made up of hundreds of different neurons and glial cells that develop in a coordinated fashion forming synaptic contacts in proper circuits able to perform very complex functions. Chemical signaling in the nervous system is made primarily by neurotransmitters, neuromodulators, hormones and local mediators, and their respective receptors and signaling pathways. The retina, and specially the chick retina, is a useful model to study this molecular signaling. We have reviewed here the development of some of these signaling systems in the chick retina with emphasis in those related to cyclic AMP, such as dopamine and adenosine, and to AKT, such as glutamate and related neuromodulators as vitamin C and nitric oxide. We have also discussed the role of some of these molecules in embryonic functions such as cell survival and proliferation. We conclude that these molecules are very important for retina development and that disturbances in their function can lead to neurodegenerative disorders.

## Author contributions

AD-S, LX, MG-S, and ID wrote parts of the text. AD-S perform bibliographic research, reviewed and organized the text and bibliographic information. LX organized the text and draw all figures. RP-d-C wrote many text sections and organized the final version. All authors agreed with the content of the work.

## Funding

This work was supported by CNPq, Capes, Faperj and INNT.

## Acknowledgments

We thank the members of the laboratory of Cellular Neurobiology for helpful discussions and members of the Program of post-graduation in Neurosciences from the Fluminense Federal University for the support.

## Conflict of interest

The authors declare that the research was conducted in the absence of any commercial or financial relationships that could be construed as a potential conflict of interest.

## Publisher's note

# References


Adler, R. (2000). A model of retinal cell differentiation in the chick embryo. *Prog. Retin. Eye Res.* 19, 529–557. doi:10.1016/S1350-9462(00)00008-2

Ahmed, M. B., Alghamdi, A. A. A., Islam, S. U., Lee, J. S., and Lee, Y. S. (2022). cAMP signaling in cancer: A PKA-CREB and EPAC-centric approach. *Cells* 11, 2020. doi:10.3390/CELLS11132020

Anton, S. E., Kayser, C., Maiellaro, I., Nemec, K., Möller, J., Koschinski, A., et al. (2022). Receptor-associated independent cAMP nanodomains mediate spatiotemporal specificity of GPCR signaling. *Cell* 185, 1130–1142.e11. e11. doi:10.1016/j.cell.2022.02.011

Araki, M., Maeda, T., and Kimura, H. (1983). Dopaminergic cell differentiation in the developing chick retina. *Brain Res. Bull.* 10, 97–102. doi:10.1016/0361-9230(83)90080-1

Arriza, J. L., Eliasof, S., Kavanaugh, M. P., and Amara, S. G. (1997). Excitatory amino acid transporter 5, a retinal glutamate transporter coupled to a chloride conductance. *Proc. Natl. Acad. Sci. U. S. A.* 94, 4155–4160. doi:10.1073/PNAS.94.8.4155

Autenrieth, K., Bendzunas, N. G., Bertinetti, D., Herberg, F. W., and Kennedy, E. J. (2016). Defining A-kinase anchoring protein (AKAP) specificity for the protein kinase A subunit ri (PKA-RI). *Chembiochem* 17, 693–697. doi:10.1002/CBIC.201500632

Bar-Peled, O., Ben-Hur, H., Biegon, A., Groner, Y., Dewhurst, S., Furuta, A., et al. (1997). Distribution of glutamate transporter subtypes during human brain development. *J. Neurochem.* 69, 2571–2580. doi:10.1046/J.1471-4159.1997.69062571.X

Belgacem, Y. H., and Borodinsky, L. N. (2017). CREB at the crossroads of activity-dependent regulation of nervous system development and function. *Adv. Exp. Med. Biol.* 1015, 19–39. doi:10.1007/978-3-319-62817-2_2

Bengtson, C. P., and Bading, H. (2012). Nuclear calcium signaling. *Adv. Exp. Med. Biol.* 970, 377–405. doi:10.1007/978-3-7091-0932-8_17

Benz, P. M., Ding, Y., Stingl, H., Loot, A. E., Zink, J., Wittig, I., et al. (2020). AKAP12 deficiency impairs VEGF-induced endothelial cell migration and sprouting. *Acta Physiol.* 228, e13325. doi:10.1111/APHA.13325

Bernstein, R. R., and Dillon, P. F. (2014). A common molecular motif characterizes extracellular allosteric enhancers of GPCR aminergic receptors and suggests enhancer mechanism of action. *Curr. Med. Chem.* 21, 3673–3686. doi:10.2174/0929867321666140826120604

Blom, J., Giove, T., Deshpande, M., and Eldred, W. D. (2012). Characterization of nitric oxide signaling pathways in the mouse retina. *J. Comp. Neurol.* 520, 4204–4217. doi:10.1002/CNE.23148

Boccuni, I., and Fairless, R. (2022). Retinal glutamate neurotransmission: From physiology to pathophysiological mechanisms of retinal ganglion cell degeneration. *Life* 12, 638. doi:10.3390/LIFE12050638

Boczek, T., Cameron, E. G., Yu, W., Xia, X., Shah, S. H., Chabeco, B. C., et al. (2019). Regulation of neuronal survival and axon growth by a perinuclear cAMP compartment. *J. Neurosci.* 39, 5466–5480. doi:10.1523/JNEUROSCI.2752-18.2019

Breckler, M., Berthouze, M., Laurent, A. C., Crozatier, B., Morel, E., and Lezoualc'h, F. (2011). Rap-linked cAMP signaling Epac proteins: Compartmentation, functioning and disease implications. *Cell. Signal.* 23, 1257–1266. doi:10.1016/J.CELLSIG.2011.03.007

Bui, B. V., Hu, R. G., Acosta, M. L., Donaldson, P., Vingrys, A. J., and Kalloniatis, M. (2009). Glutamate metabolic pathways and retinal function. *J. Neurochem.* 111, 589–599. doi:10.1111/j.1471-4159.2009.06354.x

Busch, M., Philippeit, C., Weise, A., and Dünker, N. (2015). Re-characterization of established human retinoblastoma cell lines. *Histochem. Cell Biol.* 143, 325–338. doi:10.1007/S00418-014-1285-Z

Byrne, D. P., Omar, M. H., Kennedy, E. J., Eyers, P. A., and Scott, J. D. (2022). Biochemical analysis of AKAP-anchored PKA signaling complexes. *Methods Mol. Biol.* 2483, 297–317. doi:10.1007/978-1-0716-2245-2_19

Calabrese, V., Mancuso, C., Calvani, M., Rizzarelli, E., Butterfield, D. A., and Giuffrida Stella, A. M. (2007). Nitric oxide in the central nervous system: Neuroprotection versus neurotoxicity. *Nat. Rev. Neurosci.* 8, 766–775. doi:10.1038/nrn2214

Calaza, K. da C., and Gardino, P. F. (2010). Neurochemical phenotype and birthdating of specific cell populations in the chick retina. *An. Acad. Bras. Cienc.* 82, 595–608. doi:10.1590/S0001-37652010000300007

Calejo, A. I., and Taskén, K. (2015). Targeting protein-protein interactions in complexes organized by A kinase anchoring proteins. *Front. Pharmacol.* 6, 192. doi:10.3389/fphar.2015.00192

Calero, C. I., Vickers, E., Cid, G. M., Aguayo, L. G., von Gersdorff, H., and Calvo, D. J. (2011). Allosteric modulation of retinal GABA receptors by ascorbic acid. *J. Neurosci.* 31, 9672–9682. doi:10.1523/JNEUROSCI.5157-10.2011

Camacho, A., and Massieu, L. (2006). Role of glutamate transporters in the clearance and release of glutamate during ischemia and its relation to neuronal death. *Arch. Med. Res.* 37, 11–18. doi:10.1016/j.arcmed.2005.05.014

Cao, J., Ribelayga, C. P., and Mangel, S. C. (2021). A circadian clock in the retina regulates rod-cone gap junction coupling and neuronal light responses via activation of adenosine A 2A receptors. *Front. Cell. Neurosci.* 14, 605067. doi:10.3389/FNCEL.2020.605067

Catsicas, M., Allcorn, S., and Mobbs, P. (2001). Early activation of Ca(2+)-permeable AMPA receptors reduces neurite outgrowth in embryonic chick retinal neurons. *J. Neurobiol.* 49, 200–211. doi:10.1002/neu.1075

Cebulla, C. M., Zelinka, C. P., Scott, M. A., Lubow, M., Bingham, A., Rasiah, S., et al. (2012). A chick model of retinal detachment: Cone rich and novel. *PLoS One* 7, e44257. doi:10.1371/JOURNAL.PONE.0044257

Cheng, X., Ji, Z., Tsalkova, T., and Mei, F. (2008). Epac and PKA: A tale of two intracellular cAMP receptors. *Acta Biochim. Biophys. Sin.* 40, 651–662. doi:10.1111/J.1745-7270.2008.00438.X

Christopherson, K. S., Hillier, B. J., Lim, W. A., and Bredt, D. S. (1999). PSD-95 assembles a ternary complex with the N-methyl-D-aspartic acid receptor and a bivalent neuronal NO synthase PDZ domain. *J. Biol. Chem.* 274, 27467–27473. doi:10.1074/JBC.274.39.27467

Contestabile, A., and Ciani, E. (2004). Role of nitric oxide in the regulation of neuronal proliferation, survival and differentiation. *Neurochem. Int.* 45, 903–914. doi:10.1016/J.NEUINT.2004.03.021

Cossenza, M., Cadilhe, D. V., Coutinho, R. N., and Paes-De-Carvalho, R. (2006). Inhibition of protein synthesis by activation of NMDA receptors in cultured retinal cells: A new mechanism for the regulation of nitric oxide production. *J. Neurochem.* 97, 1481–1493. doi:10.1111/J.1471-4159.2006.03843.X

Cossenza, M., and Paes de Carvalho, R. (2000). L-arginine uptake and release by cultured avian retinal cells: Differential cellular localization in relation to nitric oxide synthase. *J. Neurochem.* 74, 1885–1894. doi:10.1046/j.1471-4159.2000.0741885.x

Cossenza, M., Socodato, R., Mejía-García, T. A., Domith, I., Portugal, C. C., Gladulich, L. F. H., et al. (2020). Protein synthesis inhibition promotes nitric oxide generation and activation of CGKII-dependent downstream signaling pathways in the retina. *Biochim. Biophys. Acta. Mol. Cell Res.* 1867, 118732. doi:10.1016/J.BBAMCR.2020.118732

Cossenza, M., Socodato, R., Portugal, C. C., Domith, I. C. L., Gladulich, L. F. H., Encarnação, T. G., et al. (2014). Nitric oxide in the nervous system. Biochemical, developmental, and neurobiological aspects. *Vitam. Horm.* 96, 79–125. doi:10.1016/B978-0-12-800254-4.00005-2

Covarrubias-Pinto, A., Acuña, A. I., Beltrán, F. A., Torres-Díaz, L., and Castro, M. A. (2015). Old things new view: Ascorbic acid protects the brain in neurodegenerative disorders. *Int. J. Mol. Sci.* 16, 28194–28217. doi:10.3390/ijms161226095

da Encarnação, T. G., Portugal, C. C., Nogueira, C. E., Santiago, F. N., Socodato, R., and Paes-de-Carvalho, R. (2018). Dopamine promotes ascorbate release from retinal neurons: Role of D1 receptors and the exchange protein directly activated by cAMP type 2 (EPAC2). *Mol. Neurobiol.* 55, 7858–7871. doi:10.1007/s12035-018-0962-7

da Silva Sampaio, L., Kubrusly, R. C. C., Colli, Y. P., Trindade, P. P., Ribeiro-Resende, V. T., Einicker-Lamas, M., et al. (2018). Cannabinoid receptor type 1 expression in the developing avian retina: Morphological and functional correlation with the dopaminergic system. *Front. Cell. Neurosci.* 12, 58. doi:10.3389/fncel.2018.00058

Datta, S. R., Ranger, A. M., Lin, M. Z., Sturgill, J. F., Ma, Y. C., Cowan, C. W., et al. (2002). Survival factor-mediated BAD phosphorylation raises the mitochondrial threshold for apoptosis. *Dev. Cell* 3, 631–643. doi:10.1016/S1534-5807(02)00326-X

De Blasi, A., Conn, P. J., Pin, J., and Nicoletti, F. (2001). Molecular determinants of metabotropic glutamate receptor signaling. *Trends Pharmacol. Sci.* 22, 114–120. doi:10.1016/S0165-6147(00)01635-7

de Mello, F. G. (1978). The ontogeny of dopamine-dependent increase of adenosine 3′, 5′-cyclic monophosphate in the chick retina. *J. Neurochem.* 31, 1049–1053. doi:10.1111/J.1471-4159.1978.TB00146.X

de Mello, M. C. F., Ventura, A. L. M., Paes-de-Carvalho, R., Klein, W. L., and de Mello, F. G. (1982). Regulation of dopamine- and adenosine-dependent adenylate cyclase systems of chicken embryo retina cells in culture. *Proc. Natl. Acad. Sci. U. S. A.* 79, 5708–5712. doi:10.1073/PNAS.79.18.5708

Deplano, S., Giorgi, M., Maccarone, R., Santone, R., Nuccetelli, V., Basso, M., et al. (2008). Gene expression and protein localization of calmodulin-dependent phosphodiesterase during ontogenesis of chick retina. *J. Neurosci. Res.* 86, 1017–1023. doi:10.1002/JNR.21570

Dewan, J. G. (1938). The l(+)glutamic dehydrogenase of animal tissues. *Biochem. J.* 32, 1378–1385. doi:10.1042/BJ0321378

Di-Capua, N., Sperling, O., and Zoref-Shani, E. (2003). Protein kinase C-ε is involved in the adenosine-activated signal transduction pathway conferring protection against ischemia-reperfusion injury in primary rat neuronal cultures. *J. Neurochem.* 84, 409–412. doi:10.1046/J.1471-4159.2003.01563.X

Domith, I., Duarte-Silva, A. T., Garcia, C. G., Calaza, K. D. C., Paes-de-Carvalho, R., and Cossenza, M. (2018a). Chlorogenic acids inhibit glutamate dehydrogenase and decrease intracellular ATP levels in cultures of chick embryo retina cells. *Biochem. Pharmacol.* 155, 393–402. doi:10.1016/j.bcp.2018.07.023

Domith, I., Socodato, R., Portugal, C. C., Munis, A. F., Duarte-Silva, A. T., and Paes-de-Carvalho, R. (2018b). Vitamin C modulates glutamate transport and NMDA receptor function in the retina. *J. Neurochem.* 144, 408–420. doi:10.1111/jnc.14260

Eldred, W. D., and Blute, T. A. (2005). Imaging of nitric oxide in the retina. *Vis. Res.* 45, 3469–3486. doi:10.1016/J.VISRES.2005.07.033

Ernst, A. F., Wu, H. H., El-Fakahany, E. E., and McLoon, S. C. (1999). NMDA receptor-mediated refinement of a transient retinotectal projection during development requires nitric oxide. *J. Neurosci.* 19, 229–235. doi:10.1523/JNEUROSCI.19-01-00229.1999

Esvald, E. E., Tuvikene, J., Sirp, A., Patil, S., Bramham, C. R., and Timmusk, T. (2020). CREB family transcription factors are major mediators of BDNF transcriptional autoregulation in cortical neurons. *J. Neurosci.* 40, 1405–1426. doi:10.1523/JNEUROSCI.0367-19.2019

Ferraguti, F., Nicoletti, F., Klotz-Weigand, L., and Enz, R. (2022). Metabotropic glutamate receptors at ribbon synapses in the retina and cochlea. *Cells* 11, 1097. doi:10.3390/CELLS11071097

Fleming, R. L., Silveira, M. S., Santos, L. E., Henze, I. P., Gardino, P. F., De Mello, M. C. F., et al. (2013). Pituitary adenylyl cyclase-activating polypeptide receptor re-sensitization induces plastic changes in the dopaminergic phenotype in the mature avian retina. *J. Neurochem.* 124, 621–631. doi:10.1111/JNC.12121

Fowler, W. C., Chang, D. H., Roberts, B. C., Zarovnaya, E. L., and Proia, A. D. (2004). A new paradigm for corneal wound healing research: The white leghorn chicken (Gallus gallus domesticus). *Curr. Eye Res.* 28, 241–250. doi:10.1076/CEYR.28.4.241.27837

Fruman, D. A., Chiu, H., Hopkins, B. D., Bagrodia, S., Cantley, L. C., and Abraham, R. T. (2017). The PI3K pathway in human disease. *Cell* 170, 605–635. doi:10.1016/J.CELL.2017.07.029

Gao, Z., Lei, W. I., and Lee, L. T. O. (2022). The role of neuropeptide-stimulated cAMP-EPACs signalling in cancer cells. *Molecules* 27, 311. doi:10.3390/MOLECULES27010311

Gerbaud, P., Ferreira, F., and Pidoux, G. (2016). [Role and regulation of cAMP signaling in human trophoblast fusion]. *Biol. Aujourdhui* 210, 139–151. doi:10.1051/JBIO/2016017

Gladulich, L. F. H., Peixoto-Rodrigues, M. C., Campello-Costa, P., Paes-de-Carvalho, R., and Cossenza, M. (2020). NMDA-induced nitric oxide generation and CREB activation in central nervous system is dependent on eukaryotic elongation factor 2 kinase. *Biochim. Biophys. Acta. Mol. Cell Res.* 1867, 118783. doi:10.1016/j.bbamcr.2020.118783

Gladulich, L. F. H., Xie, J., Jensen, K. B., Kamei, M., Paes-de-Carvalho, R., Cossenza, M., et al. (2021). Bicuculline regulated protein synthesis is dependent on Homer1 and promotes its interaction with eEF2K through mTORC1-dependent phosphorylation. *J. Neurochem.* 157, 1086–1101. doi:10.1111/jnc.15178

Gregory, K. J., Dong, E. N., Meiler, J., and Conn, P. J. (2011). Allosteric modulation of metabotropic glutamate receptors: Structural insights and therapeutic potential. *Neuropharmacology* 60, 66–81. doi:10.1016/J.NEUROPHARM.2010.07.007

Grillo, S. L., McDevitt, D. S., Voas, M. G., Khan, A. S., Grillo, M. A., and Stella, S. L. (2019). Adenosine receptor expression in the adult zebrafish retina. *Purinergic Signal.* 15, 327–342. doi:10.1007/S11302-019-09667-0

Grimes, C. A., and Jope, R. S. (2001). CREB DNA binding activity is inhibited by glycogen synthase kinase-3β and facilitated by lithium. *J. Neurochem.* 78, 1219–1232. doi:10.1046/J.1471-4159.2001.00495.X

Guimaraes-Souza, E. M., and Calaza, K. C. (2012). Selective activation of group III metabotropic glutamate receptor subtypes produces different patterns of gamma-aminobutyric acid immunoreactivity and glutamate release in the retina. *J. Neurosci. Res.* 90, 2349–2361. doi:10.1002/jnr.23123

Hosoya, K. I., Minamizono, A., Katayama, K., Terasaki, T., and Tomi, M. (2004). Vitamin C transport in oxidized form across the rat blood-retinal barrier. *Invest. Ophthalmol. Vis. Sci.* 45, 1232–1239. doi:10.1167/IOVS.03-0505

Hsueh, Y. J., Meir, Y. J. J., Yeh, L. K., Wang, T. K., Huang, C. C., Lu, T. Te, et al. (2020). Topical ascorbic acid ameliorates oxidative stress-induced corneal endothelial damage via suppression of apoptosis and autophagic flux blockage. *Cells* 1, 943. doi:10.3390/CELLS9040943

Huang, P. C., Hsiao, Y. T., Kao, S. Y., Chen, C. F., Chen, Y. C., Chiang, C. W., et al. (2014). Adenosine A2A receptor up-regulates retinal wave frequency via starburst amacrine cells in the developing rat retina. *PLoS One* 9, e95090. doi:10.1371/JOURNAL.PONE.0095090

Ientile, R., Malecka, B., Picciurro, V., Naso, A., Pedale, S., and Macaione, S. (1996). Nitric oxide synthase in chick embryo retina during development. *FEBS Lett.* 379, 82–84. doi:10.1016/0014-5793(95)01490-X

Iribarren, R. (2015). Crystalline lens and refractive development. *Prog. Retin. Eye Res.* 47, 86–106. doi:10.1016/J.PRETEYERES.2015.02.002

Ishikawa, M. (2013). Abnormalities in glutamate metabolism and excitotoxicity in the retinal diseases. *Sci. (Cairo)* 2013, 528940–529013. doi:10.1155/2013/528940

Jacques, F. J., Silva, T. M., da Silva, F. E., Ornelas, I. M., and Ventura, A. L. M. (2017). Nucleotide P2Y13-stimulated phosphorylation of CREB is required for ADP-induced proliferation of late developing retinal glial progenitors in culture. *Cell. Signal.* 35, 95–106. doi:10.1016/J.CELLSIG.2017.03.019

Jakobsen, E., Lange, S. C., and Bak, L. K. (2019). Soluble adenylyl cyclase-mediated cAMP signaling and the putative role of PKA and EPAC in cerebral mitochondrial function. *J. Neurosci. Res.* 97, 1018–1038. doi:10.1002/JNR.24477

Khordad, E., Fazel, A., and Bideskan, A. E. (2013). The effect of ascorbic acid and garlic administration on lead-induced apoptosis in rat offspring's eye retina. *Iran. Biomed. J.* 17, 206–213. doi:10.6091/IBJ.1229.2013

Klein, M. O., Battagello, D. S., Cardoso, A. R., Hauser, D. N., Bittencourt, J. C., and Correa, R. G. (2018). Dopamine: Functions, signaling, and association with neurological diseases. *Cell. Mol. Neurobiol.* 2018, 31–59. doi:10.1007/S10571-018-0632-3

Korshunov, K. S., Blakemore, L. J., and Trombley, P. Q. (2020). Illuminating and sniffing out the neuromodulatory roles of dopamine in the retina and olfactory bulb. *Front. Cell. Neurosci.* 14, 275. doi:10.3389/fncel.2020.00275

Kubrusly, R. C. C., Günter, A., Sampaio, L., Martins, R. S., Schitine, C. S., Trindade, P., et al. (2018). Neuro-glial cannabinoid receptors modulate signaling in the embryonic avian retina. *Neurochem. Int.* 112, 27–37. doi:10.1016/j.neuint.2017.10.016

Lamas, M., Lee-Rivera, I., and López-Colomé, A. M. (2005). Cell-specific expression of N-methyl-D-aspartate receptor subunits in Muller glia and neurons from the chick retina. *Invest. Ophthalmol. Vis. Sci.* 46, 3570–3577. doi:10.1167/IOVS.04-1398

Lankford, K. L., DeMello, F. G., and Klein, W. L. (1988). D1-type dopamine receptors inhibit growth cone motility in cultured retina neurons: Evidence that neurotransmitters act as morphogenic growth regulators in the developing central nervous system. *Proc. Natl. Acad. Sci. U. S. A.* 85, 2839–2843. doi:10.1073/pnas.85.8.2839

Lauber, J. K. (1987). Light-induced avian glaucoma as an animal model for human primary glaucoma. *J. Ocul. Pharmacol.* 3, 77–100. doi:10.1089/JOP.1987.3.77

Lauder, J. M. (1987). Neurotransmitters as morphogenetic signals and trophic factors. *Model Syst. Dev. Aging Nerv. Syst.* 1, 219–237. doi:10.1007/978-1-4613-2037-1_16

Lauder, J. M. (1988). Neurotransmitters as morphogens. *Prog. Brain Res.* 73, 365–387. doi:10.1016/S0079-6123(08)60516-6

Li, C., Allen, A., Kwagh, J., Doliba, N. M., Qin, W., Najafi, H., et al. (2006). Green tea polyphenols modulate insulin secretion by inhibiting glutamate dehydrogenase. *J. Biol. Chem.* 281, 10214–10221. doi:10.1074/jbc.M512792200

Li, C., Li, M., Chen, P., Narayan, S., Matschinsky, F. M., Bennett, M. J., et al. (2011). Green tea polyphenols control dysregulated glutamate dehydrogenase in transgenic mice by hijacking the ADP activation site. *J. Biol. Chem.* 286, 34164–34174. doi:10.1074/jbc.M111.268599

Li, H., Zhang, Z., Blackburn, M. R., Wang, S. W., Ribelayga, C. P., and O'Brien, J. (2013). Adenosine and dopamine receptors coregulate photoreceptor coupling via gap junction phosphorylation in mouse retina. *J. Neurosci.* 33, 3135–3150. doi:10.1523/JNEUROSCI.2807-12.2013

Linden, J. (1991). Structure and function of A1 adenosine receptors. *FASEB J.* 5, 2668–2676. doi:10.1096/FASEBJ.5.12.1916091

López-Colomé, A. M., Martínez-Lozada, Z., Guillem, A. M., López, E., and Ortega, A. (2012). Glutamate transporter-dependent mTOR phosphorylation in Müller glia cells. *ASN Neuro* 4, e00095. doi:10.1042/AN20120022

Luo, C. X., and Zhu, D. Y. (2011). Research progress on neurobiology of neuronal nitric oxide synthase. *Neurosci. Bull.* 27, 23–35. doi:10.1007/S12264-011-1038-0

Lykkesfeldt, J., and Tveden-Nyborg, P. (2019). The pharmacokinetics of vitamin C. *Nutrients* 11, 2412. doi:10.3390/nu11102412

MacDonald, J. F., Jackson, M. F., and Beazely, M. A. (2006). Hippocampal long-term synaptic plasticity and signal amplification of NMDA receptors. *Crit. Rev. Neurobiol.* 18, 71–84. doi:10.1615/CRITREVNEUROBIOL.V18.I1-2.80

Magalhães, C. R., Socodato, R. E. S., and Paes-De-Carvalho, R. (2006). Nitric oxide regulates the proliferation of chick embryo retina cells by a cyclic GMP-independent mechanism. *Int. J. Dev. Neurosci.* 24, 53–60. doi:10.1016/J.IJDEVNEU.2005.10.004

Magi, S., Piccirillo, S., Amoroso, S., and Lariccia, V. (2019). Excitatory amino acid transporters (EAATs): Glutamate transport and beyond. *Int. J. Mol. Sci.* 20, 5674. doi:10.3390/IJMS20225674

Maiese, K., Chong, Z. Z., Shang, Y. C., and Wang, S. (2012). Targeting disease through novel pathways of apoptosis and autophagy. *Expert Opin. Ther. Targets* 16, 1203–1214. doi:10.1517/14728222.2012.719499

Mangioris, G., Chiodini, F., and Dosso, A. (2011). New strategy to study corneal endothelial cell transplantation: The chick cornea model. *Cornea* 30, 1461–1464. doi:10.1097/ICO.0B013E31821821FE

Manning, B. D., Tee, A. R., Logsdon, M. N., Blenis, J., and Cantley, L. C. (2002). Identification of the tuberous sclerosis complex-2 tumor suppressor gene product tuberin as a target of the phosphoinositide 3-kinase/akt pathway. *Mol. Cell* 10, 151–162. doi:10.1016/S1097-2765(02)00568-3

Manning, B. D., and Toker, A. (2017). AKT/PKB signaling: Navigating the network. *Cell* 169, 381–405. doi:10.1016/j.cell.2017.04.001

Martínez-García, M. C., Merayo-Llovés, J., Blanco-Mezquita, T., and Mar-Sardaña, S. (2006). Wound healing following refractive surgery in hens. *Exp. Eye Res.* 83, 728–735. doi:10.1016/J.EXER.2006.02.017

Masato, O. (2012). Regulation of the SRC family kinases by Csk. *Int. J. Biol. Sci.* 8, 1385–1397. doi:10.7150/IJBS.5141

May, J. M. (2012). Vitamin C transport and its role in the central nervous system. *Subcell. Biochem.* 56, 85–103. doi:10.1007/978-94-007-2199-9_6

Mayer, M. L., and Westbrook, G. L. (1987). The physiology of excitatory amino acids in the vertebrate central nervous system. *Prog. Neurobiol.* 28, 197–276. doi:10.1016/0301-0082(87)90011-6

McIntosh, H. H., and Blazynski, C. (1994). Characterization and localization of adenosine A2 receptors in bovine rod outer segments. *J. Neurochem.* 62, 992–997. doi:10.1046/J.1471-4159.1994.62030992.X

McMains, E., and Gleason, E. (2011). Role of pH in a nitric oxide-dependent increase in cytosolic Cl– in retinal amacrine cells. *J. Neurophysiol.* 106, 641–651. doi:10.1152/JN.00057.2011

Mejía-García, T. A., and Paes-de-Carvalho, R. (2007). Nitric oxide regulates cell survival in purified cultures of avian retinal neurons: Involvement of multiple transduction pathways. *J. Neurochem.* 100, 382–394. doi:10.1111/j.1471-4159.2006.04244.x

Mejía-García, T. A., Portugal, C. C., Encarnação, T. G., Prado, M. A. M., and Paes-de-Carvalho, R. (2013). Nitric oxide regulates AKT phosphorylation and nuclear translocation in cultured retinal cells. *Cell. Signal.* 25, 2424–2439. doi:10.1016/j.cellsig.2013.08.001

Mishra, A., Singh, S., and Shukla, S. (2018). Physiological and functional basis of dopamine receptors and their role in neurogenesis: Possible implication for Parkinson's disease. *J. Exp. Neurosci.* 12, 1179069518779829. doi:10.1177/1179069518779829

Morè, L., Privitera, L., Perrett, P., Cooper, D. D., Bonnello, M. V. G., Arthur, J. S. C., et al. (2022). CREB serine 133 is necessary for spatial cognitive flexibility and long-term potentiation. *Neuropharmacology* 219, 109237. doi:10.1016/J.NEUROPHARM.2022.109237

Nair, R. M., Revu, N. V. L., Gali, S., Kallamadi, P. R., Prabhu, V., Manukonda, R., et al. (2022). A short-term chick embryo *in vivo* xenograft model to study retinoblastoma cancer stem cells. *Indian J. Ophthalmol.* 70, 1703–1711. doi:10.4103/IJO.IJO_2348_21

Nakashima, K. I., Iwao, K., Inoue, T., Haga, A., Tsutsumi, T., Mochita, M. I., et al. (2018). Stimulation of the adenosine A3 receptor, not the A1 or A2 receptors, promote neurite outgrowth of retinal ganglion cells. *Exp. Eye Res.* 170, 160–168. doi:10.1016/J.EXER.2018.02.019

Neal, M., Cunningham, J., and Matthews, K. (1999). Release of endogenous ascorbic acid preserves extracellular dopamine in the mammalian retina. *Invest. Ophthalmol. Vis. Sci.* 40, 2983–2987.

Newsholme, P., Procopio, J., Lima, M. M., Pithon-Curi, T. C., and Curi, R. (2003). Glutamine and glutamate-their central role in cell metabolism and function. *Cell biochem. Funct.* 21, 1–9. doi:10.1002/cbf.1003

Nijholt, I. M., Dolga, A. M., Ostroveanu, A., Luiten, P. G. M., Schmidt, M., and Eisel, U. L. M. (2008). Neuronal AKAP150 coordinates PKA and Epac-mediated PKB/Akt phosphorylation. *Cell. Signal.* 20, 1715–1724. doi:10.1016/J.CELLSIG.2008.05.001

Nualart, F., Mack, L., García, A., Cisternas, P., Bongarzone, E. R., Heitzer, M., et al. (2014). Vitamin C transporters, recycling and the bystander effect in the nervous system: SVCT2 versus gluts. *J. Stem Cell Res. Ther.* 04, 209. doi:10.4172/2157-7633.1000209

Ornelas, I. M., Silva, T. M., Fragel-Madeira, L., and Ventura, A. L. M. (2013). Inhibition of PI3K/akt pathway impairs G2/M transition of cell cycle in late developing progenitors of the avian embryo retina. *PLoS One* 8, 53517. doi:10.1371/JOURNAL.PONE.0053517

Oudemans-van Straaten, H. M., Spoelstra-de Man, A. M. E., and de Waard, M. C. (2014). Vitamin C revisited. *Crit. Care* 18, 460. doi:10.1186/s13054-014-0460-x

Padayatty, S. J., and Levine, M. (2016). Vitamin C: The known and the unknown and goldilocks. *Oral Dis.* 22, 463–493. doi:10.1111/odi.12446

Paes-de-Carvalho, R. (2002). Adenosine as a signaling molecule in the retina: Biochemical and developmental aspects. *An. Acad. Bras. Cienc.* 74, 437–451. doi:10.1590/S0001-37652002000300007

Paes-de-Carvalho, R., and de Mattos, J. C. (1996). Development of nitric oxide synthase in the avian retina. *Rev. Bras. Biol.* 56 (1), 145–152.

Paes-de-Carvalho, R., and de Mello, F. G. (1982). Adenosine-elicited accumulation of adenosine 3′, 5′-cyclic monophosphate in the chick embryo retina. *J. Neurochem.* 38, 493–500. doi:10.1111/J.1471-4159.1982.TB08655.X

Paes-de-Carvalho, R., and de Mello, F. G. (1985). Expression of A1 adenosine receptors modulating dopamine-dependent cyclic AMP accumulation in the chick embryo retina. *J. Neurochem.* 44, 845–851. doi:10.1111/J.1471-4159.1985.TB12892.X

Paes-de-Carvalho, R. (1990). Development of A1 adenosine receptors in the chick embryo retina. *J. Neurosci. Res.* 25, 236–242. doi:10.1002/JNR.490250212

Paes-de-Carvalho, R., Braas, K. M., Adler, R., and Snyder, S. H. (1992). Developmental regulation of adenosine A1 receptors, uptake sites and endogenous adenosine in the chick retina. *Brain Res. Dev. Brain Res.* 70, 87–95. doi:10.1016/0165-3806(92)90106-7

Paes-de-Carvalho, R., Calaza, K. C., Cossenza, M., Magalhães, C. R., Portugal, C. C., and Socodato, R. (2008). "Glutamate receptors in the retina: Neurochemical and developmental aspects," in *Amino acid receptor research*. Editors B. F. Paley and T. E. Warfield (Nova Science Publishers, Inc.), 17–65.

Paes-de-Carvalho, R., Maia, G. A., and Ferreira, J. M. (2003). Adenosine regulates the survival of avian retinal neurons and photoreceptors in culture. *Neurochem. Res.* 2003, 1583–1590. doi:10.1023/A:1025686812298

Park, S. W., Ghim, W., Oh, S., Kim, Y., Park, U. C., Kang, J., et al. (2019). Association of vitreous vitamin C depletion with diabetic macular ischemia in proliferative diabetic retinopathy. *PLoS One* 14, e0218433. doi:10.1371/JOURNAL.PONE.0218433

Passos, A. da C. F., Herculano, A. M., Oliveira, K. R. H. M., de Lima, S. M. A., Rocha, F. A. F., Freitas, H. R., et al. (2019). Regulation of the serotonergic system by kainate in the avian retina. *Cell. Mol. Neurobiol.* 39, 1039–1049. doi:10.1007/s10571-019-00701-8

Pereira, M. R., Hang, V. R., Vardiero, E., De Mello, F. G., and Paes-de-Carvalho, R. (2010). Modulation of A1 adenosine receptor expression by cell aggregation and long-term activation of A2a receptors in cultures of avian retinal cells: Involvement of the cyclic AMP/PKA pathway. *J. Neurochem.* 113, 661–673. doi:10.1111/J.1471-4159.2010.06641.X

Pereira-Figueiredo, D., Brito, R., Araújo, D. S. M., Nascimento, A. A., Lyra, E. S. B., Cheibub, A. M. S. S., et al. (2020). Caffeine exposure ameliorates acute ischemic cell death in avian developing retina. *Purinergic Signal.* 16, 41–59. doi:10.1007/s11302-020-09687-1

Portugal, C. C., da Encarnação, T. G., Domith, I., Dos Santos Rodrigues, A., De Oliveira, N. A., Socodato, R., et al. (2019). Dopamine-induced ascorbate release from retinal neurons involves glutamate release, activation of AMPA/Kainate receptors and downstream signaling pathways. *Front. Neurosci.* 13, 453. doi:10.3389/fnins.2019.00453

Portugal, C. C., da Encarnação, T. G., Sagrillo, M. A., Pereira, M. R., Relvas, J. B., Socodato, R., et al. (2021). Activation of adenosine A3 receptors regulates vitamin C

transport and redox balance in neurons. *Free Radic. Biol. Med.* 163, 43–55. doi:10.1016/J.FREERADBIOMED.2020.11.039

Portugal, C. C., Da Encarnação, T. G., Socodato, R., Moreira, S. R., Brudzewsky, D., Ambrósio, A. F., et al. (2012). Nitric oxide modulates sodium vitamin C transporter 2 (SVCT-2) protein expression via protein kinase G (PKG) and nuclear factor-κB (NF-κB). *J. Biol. Chem.* 287, 3860–3872. doi:10.1074/jbc.M111.260166

Portugal, C. C., Miya, V. S., Calaza, K. da C., Santos, R. A. M., and Paes-de-Carvalho, R. (2009). Glutamate receptors modulate sodium-dependent and calcium-independent vitamin C bidirectional transport in cultured avian retinal cells. *J. Neurochem.* 108, 507–520. doi:10.1111/j.1471-4159.2008.05786.x

Rasmussen, M., Zhou, J., Schwede, F., and Ekström, P. (2022). Enhanced cGMP interactor Rap guanine exchange factor 4 (EPAC2) expression and activity in degenerating photoreceptors: A neuroprotective response? *Int. J. Mol. Sci.* 2022, 4619. doi:10.3390/IJMS23094619

Rauen, T. (2000). Diversity of glutamate transporter expression and function in the mammalian retina. *Amino Acids* 19, 53–62. doi:10.1007/s007260070033

Reichenbach, A., and Bringmann, A. (2013). New functions of müller cells. *Glia* 61, 651–678. doi:10.1002/GLIA.22477

Reiner, A., and Levitz, J. (2018). Glutamatergic signaling in the central nervous system: Ionotropic and metabotropic receptors in concert. *Neuron* 98, 1080–1098. doi:10.1016/J.NEURON.2018.05.018

Reis, R. A. M., Ventura, A. L. M., Kubrusly, R. C. C., de Mello, M. C. F., and de Mello, F. G. (2007). Dopaminergic signaling in the developing retina. *Brain Res. Rev.* 54, 181–188. doi:10.1016/J.BRAINRESREV.2007.01.001

Roa, J. N., Ma, Y., Mikulski, Z., Xu, Q., Ilouz, R., Taylor, S. S., et al. (2021). Protein kinase A in human retina: Differential localization of cβ, cα, RIIα, and RIIβ in photoreceptors highlights non-redundancy of protein kinase A subunits. *Front. Mol. Neurosci.* 14, 782041. doi:10.3389/fnmol.2021.782041

Robichaux, W. G., and Cheng, X. (2018). Intracellular cAMP sensor EPAC: Physiology, pathophysiology, and therapeutics development. *Physiol. Rev.* 98, 919–1053. doi:10.1152/PHYSREV.00025.2017

Romano, C., Chen, Q., and Olney, J. W. (1998). The intact isolated (*ex vivo*) retina as a model system for the study of excitotoxicity. *Prog. Retin. Eye Res.* 17, 465–483. doi:10.1016/S1350-9462(98)00008-1

Rossi, D. J., Oshima, T., and Attwell, D. (2000). Glutamate release in severe brain ischaemia is mainly by reversed uptake. *Nature* 403, 316–321. doi:10.1038/35002090

Sakagami, K., Chen, B., Nusinowitz, S., Wu, H., and Yang, X. J. (2012). PTEN regulates retinal interneuron morphogenesis and synaptic layer formation. *Mol. Cell. Neurosci.* 49, 171–183. doi:10.1016/J.MCN.2011.11.007

Sampaio, L. F., and Paes-de-Carvalho, R. (1998). Developmental regulation of group III metabotropic glutamate receptors modulating adenylate cyclase activity in the avian retina. *Neurochem. Int.* 33, 367–374. doi:10.1016/S0197-0186(98)00041-2

Schulte, G., and Fredholm, B. B. (2003). The Gs-coupled adenosine A2b receptor recruits divergent pathways to regulate ERK1/2 and p38☆. *Exp. Cell Res.* 290, 168–176. doi:10.1016/S0014-4827(03)00324-0

Scott, P. H., Brunn, G. J., Kohn, A. D., Roth, R. A., and Lawrence, J. C. (1998). Evidence of insulin-stimulated phosphorylation and activation of the mammalian target of rapamycin mediated by a protein kinase B signaling pathway. *Proc. Natl. Acad. Sci. U. S. A.* 95, 7772–7777. doi:10.1073/PNAS.95.13.7772

Sepúlveda, C., Palomo, I., and Fuentes, E. (2016). Role of adenosine A2b receptor overexpression in tumor progression. *Life Sci.* 166, 92–99. doi:10.1016/J.LFS.2016.10.008

Shigeri, Y., Seal, R. P., and Shimamoto, K. (2004). Molecular pharmacology of glutamate transporters, EAATs and VGLUTs. *Brain Res. Brain Res. Rev.* 45, 250–265. doi:10.1016/j.brainresrev.2004.04.004

Silveira Dos Santos Bredariol, A., and Emi Hamassaki-Britto, D. (2001). Ionotropic glutamate receptors during the development of the chick retina. *J. Comp. Neurol.* 441, 58–70. doi:10.1002/cne.1397

Skeen, J. E., Bhaskar, P. T., Chen, C. C., Chen, W. S., Pengding, X., Nogueira, V., et al. (2006). Akt deficiency impairs normal cell proliferation and suppresses oncogenesis in a p53-independent and mTORC1-dependent manner. *Cancer Cell* 10, 269–280. doi:10.1016/J.CCR.2006.08.022

Socodato, R., Brito, R., Calaza, K. C., and Paes-de-Carvalho, R. (2011). Developmental regulation of neuronal survival by adenosine in the *in vitro* and *in vivo* avian retina depends on a shift of signaling pathways leading to CREB phosphorylation or dephosphorylation. *J. Neurochem.* 116, 227–239. doi:10.1111/J.1471-4159.2010.07096.X

Socodato, R., Brito, R., Portugal, C. C., De Oliveira, N. A., Calaza, K. C., and Paes-de-Carvalho, R. (2014). The nitric oxide-cGKII system relays death and survival signals during embryonic retinal development via AKT-induced CREB1 activation. *Cell Death Differ.* 21, 915–928. doi:10.1038/CDD.2014.11

Socodato, R. E. da S., Magalhães, C. R., and Paes-de-Carvalho, R. (2009). Glutamate and nitric oxide modulate ERK and CREB phosphorylation in the avian retina: Evidence for direct signaling from neurons to müller glial cells. *J. Neurochem.* 108, 417–429. doi:10.1111/j.1471-4159.2008.05778.x

Socodato, R., Santiago, F. N., Portugal, C. C., Domingues, A. F., Santiago, A. R., Relvas, J. B., et al. (2012). Calcium-permeable α-amino-3-hydroxy-5-methyl-4-isoxazolepropionic acid receptors trigger neuronal nitric-oxide synthase activation to promote nerve cell death in an Src kinase-dependent fashion. *J. Biol. Chem.* 287, 38680–38694. doi:10.1074/JBC.M112.353961

Socodato, R., Santiago, F. N., Portugal, C. C., Domith, I., Encarnação, T. G., Loiola, E. C., et al. (2017). Dopamine promotes NMDA receptor hypofunction in the retina through D1 receptor-mediated Csk activation, Src inhibition and decrease of GluN2B phosphorylation. *Sci. Rep.* 71 (7), 40912–40914. doi:10.1038/srep40912

Sosa, R., Hoffpauir, B., Rankin, M. L., Bruch, R. C., and Gleason, E. L. (2002). Metabotropic glutamate receptor 5 and calcium signaling in retinal amacrine cells. *J. Neurochem.* 81, 973–983. doi:10.1046/j.1471-4159.2002.00883.x

Sotiriou, S., Gispert, S., Cheng, J., Wang, Y., Chen, A., Hoogstraten-Miller, S., et al. (2002). Ascorbic-acid transporter Slc23a1 is essential for vitamin C transport into the brain and for perinatal survival. *Nat. Med.* 8, 514–517. doi:10.1038/0502-514

Souder, D. C., and Anderson, R. M. (2019). An expanding GSK3 network: Implications for aging research. *GeroScience* 41, 369–382. doi:10.1007/S11357-019-00085-Z

Straiker, A., Stella, N., Piomelli, D., Mackie, K., Karten, H. J., and Maguire, G. (1999). Cannabinoid CB1 receptors and ligands in vertebrate retina: Localization and function of an endogenous signaling system. *Proc. Natl. Acad. Sci. U. S. A.* 96, 14565–14570. doi:10.1073/PNAS.96.25.14565

Szabadfi, K., Atlasz, T., Kiss, P., Reglodi, D., Szabo, A., Kovacs, K., et al. (2012). Protective effects of the neuropeptide PACAP in diabetic retinopathy. *Cell Tissue Res.* 348, 37–46. doi:10.1007/S00441-012-1349-0

Szwed, A., Kim, E., and Jacinto, E. (2021). Regulation and metabolic functions of mTORC1 and mTORC2. *Physiol. Rev.* 101, 1371–1426. doi:10.1152/PHYSREV.00026.2020

Tachibana, N., Cantrup, R., Dixit, R., Touahri, Y., Kaushik, G., Zinyk, D., et al. (2016). Pten regulates retinal amacrine cell number by modulating akt, tgfβ, and Erk signaling. *J. Neurosci.* 36, 9454–9471. doi:10.1523/JNEUROSCI.0936-16.2016

Toda, N., and Nakanishi-Toda, M. (2007). Nitric oxide: Ocular blood flow, glaucoma, and diabetic retinopathy. *Prog. Retin. Eye Res.* 26, 205–238. doi:10.1016/J.PRETEYERES.2007.01.004

Tokuda, K., Zorumski, C. F., and Izumi, Y. (2007). Effects of ascorbic acid on UV light-mediated photoreceptor damage in isolated rat retina. *Exp. Eye Res.* 84, 537–543. doi:10.1016/J.EXER.2006.11.005

Vanhaesebroeck, B., Guillermet-Guibert, J., Graupera, M., and Bilanges, B. (2010). The emerging mechanisms of isoform-specific PI3K signalling. *Nat. Rev. Mol. Cell Biol.* 11, 329–341. doi:10.1038/nrm2882

Ventura, A. L. M., and de Mello, F. G. (1990). D1 dopamine receptors in neurite regions of embryonic and differentiated retina are highly coupled to adenylate cyclase in the embryonic but not in the mature tissue. *Brain Res.* 530, 301–308. doi:10.1016/0006-8993(90)91299-V

Ventura, A. L. M., dos Santos-Rodrigues, A., Mitchell, C. H., and Faillace, M. P. (2019). Purinergic signaling in the retina: From development to disease. *Brain Res. Bull.* 151, 92–108. doi:10.1016/J.BRAINRESBULL.2018.10.016

Wahl, C., Li, T., and Howland, H. C. (2016). Intraocular pressure fluctuations of growing chick eyes are suppressed in constant light conditions. *Exp. Eye Res.* 148, 52–54. doi:10.1016/J.EXER.2016.05.018

Wan, J., Zhao, X. F., Vojtek, A., and Goldman, D. (2014). Retinal injury, growth factors and cytokines converge on β-catenin and pStat3 signaling to stimulate retina regeneration. *Cell Rep.* 9, 285–297. doi:10.1016/J.CELREP.2014.08.048

Wang, Y., Cameron, E. G., Li, J., Stiles, T. L., Kritzer, M. D., Lodhavia, R., et al. (2015). Muscle A-kinase anchoring protein-α is an injury-specific signaling scaffold required for neurotrophic- and cyclic adenosine monophosphate-mediated survival. *EBioMedicine* 2, 1880–1887. doi:10.1016/J.EBIOM.2015.10.025

Wang, Z. (2021). Regulation of cell cycle progression by growth factor-induced cell signaling. *Cells* 10, 3327. doi:10.3390/CELLS10123327

Wareham, L. K., Buys, E. S., and Sappington, R. M. (2018). The nitric oxide-guanylate cyclase pathway and glaucoma. *Nitric Oxide.* 77, 75–87. doi:10.1016/J.NIOX.2018.04.010

Watkins, J. C., and Evans, R. H. (1981). Excitatory amino acid transmitters. *Annu. Rev. Pharmacol. Toxicol.* 21, 165–204. doi:10.1146/annurev.pa.21.040181.001121

West, A. E., Chen, W. G., Dalva, M. B., Dolmetsch, R. E., Kornhauser, J. M., Shaywitz, A. J., et al. (2001). Calcium regulation of neuronal gene expression. *Proc. Natl. Acad. Sci. U. S. A.* 98, 11024–11031. doi:10.1073/PNAS.191352298

Whitaker, C. M., and Cooper, N. G. F. (2010). Differential distribution of exchange proteins directly activated by cyclic AMP within the adult rat retina. *Neuroscience* 165, 955–967. doi:10.1016/J.NEUROSCIENCE.2009.10.054

Wildsoet, C. F., and Schmid, K. L. (2000). Optical correction of form deprivation myopia inhibits refractive recovery in chick eyes with intact or sectioned optic nerves. *Vis. Res.* 40, 3273–3282. doi:10.1016/S0042-6989(00)00138-3

Wisely, C. E., Sayed, J. A., Tamez, H., Zelinka, C., Abdel-Rahman, M. H., Fischer, A. J., et al. (2017). The chick eye in vision research: An excellent model for the study of ocular disease. *Prog. Retin. Eye Res.* 61, 72–97. doi:10.1016/J.PRETEYERES.2017.06.004

Wu, H. H., Selski, D. J., El-Fakahany, E. E., and McLoon, S. C. (2001). The role of nitric oxide in development of topographic precision in the retinotectal projection of chick. *J. Neurosci.* 21, 4318–4325. doi:10.1523/JNEUROSCI.21-12-04318.2001

Wyllie, D. J. A., and Bowie, D. (2022). Ionotropic glutamate receptors: Structure, function and dysfunction. *J. Physiol.* 600, 175–179. doi:10.1113/JP282389

Yamagata, M., Yan, W., and Sanes, J. R. (2021). A cell atlas of the chick retina based on single-cell transcriptomics. *Elife* 10, e63907–e63939. doi:10.7554/ELIFE.63907

Yu, D., and Eldred, W. D. (2005). Nitric oxide stimulates γ-aminobutyric acid release and inhibits Glycine release in retina. *J. Comp. Neurol.* 483, 278–291. doi:10.1002/CNE.20416

Zaccolo, M., Zerio, A., and Lobo, M. J. (2021). Subcellular organization of the cAMP signaling pathway. *Pharmacol. Rev.* 73, 278–309. doi:10.1124/PHARMREV.120.000086

Zareen, N., Khan, M. Y., and Minhas, L. A. (2011). Histological stages of retinal morphogenesis in chicken – a descriptive laboratory research. *Ital. J. Zool.* 78, 45–52. doi:10.1080/11250003.2010.487075

Zhang, H., Kong, Q., Wang, J., Jiang, Y., and Hua, H. (2020a). Complex roles of cAMP–PKA–CREB signaling in cancer. *Exp. Hematol. Oncol.* 2020, 32–13. doi:10.1186/S40164-020-00191-1

Zhang, M., Budak, M. T., Lu, W., Khurana, T. S., Zhang, X., Laties, A. M., et al. (2006). Identification of the A3 adenosine receptor in rat retinal ganglion cells. *Mol. Vis.* 12, 937–948.

Zhang, M., Hu, H., Zhang, X., Lu, W., Lim, J., Eysteinsson, T., et al. (2010). The A3 adenosine receptor attenuates the calcium rise triggered by NMDA receptors in retinal ganglion cells. *Neurochem. Int.* 56, 35–41. doi:10.1016/J.NEUINT.2009.08.011

Zhang, S. J., Li, Y. F., Tan, R. R., Tsoi, B., Huang, W. S., Huang, Y. H., et al. (2016). A new gestational diabetes mellitus model: Hyperglycemia-induced eye malformation via inhibition of Pax6 in the chick embryo. *Dis. Model. Mech.* 9, 177–186. doi:10.1242/DMM.022012

Zhang, Y., Cao, H., Qiu, X., Xu, D., Chen, Y., Barnes, G. N., et al. (2020b). Neuroprotective effects of adenosine A1 receptor signaling on cognitive impairment induced by chronic intermittent hypoxia in mice. *Front. Cell. Neurosci.* 14, 202. doi:10.3389/fncel.2020.00202

frontiers | Frontiers in Cell and Developmental Biology

TYPE Original Research
PUBLISHED 07 March 2023
DOI 10.3389/fcell.2023.1058961



OPEN ACCESS

EDITED BY
Rajalekshmy Shyam,
Indiana University Bloomington,
United States

REVIEWED BY
Sudershana Nair,
New York University, United States
Deepika Vasudevan,
University of Pittsburgh, United States

*CORRESPONDENCE
Jens Rister,
jens.rister@umb.edu

†PRESENT ADDRESSES
Pamela Boodram, NYU Langone Medical Center, New York, NY, United States

SPECIALTY SECTION
This article was submitted to Signaling, a section of the journal Frontiers in Cell and Developmental Biology

RECEIVED 30 September 2022
ACCEPTED 20 February 2023
PUBLISHED 07 March 2023

CITATION
Bunker J, Bashir M, Bailey S, Boodram P, Perry A, Delaney R, Tsachaki M, Sprecher SG, Nelson E, Call GB and Rister J (2023), Blimp-1/PRDM1 and Hr3/RORβ specify the blue-sensitive photoreceptor subtype in *Drosophila* by repressing the hippo pathway . *Front. Cell Dev. Biol.* 11:1058961. doi: 10.3389/fcell.2023.1058961



# Blimp-1/PRDM1 and Hr3/RORβ specify the blue-sensitive photoreceptor subtype in *Drosophila* by repressing the hippo pathway

Joseph Bunker[1], Mhamed Bashir[1], Sydney Bailey[1], Pamela Boodram[1,2†], Alexis Perry[1], Rory Delaney[1], Maria Tsachaki[3], Simon G. Sprecher[3], Erik Nelson[4], Gerald B. Call[5] and Jens Rister[1]*

[1]Department of Biology, Integrated Sciences Complex, University of Massachusetts Boston, Boston, MA, United States, [2]NYU Langone Medical Center, New York, NY, United States, [3]Department of Biology, University of Fribourg, Fribourg, Switzerland, [4]Arizona College of Osteopathic Medicine, Midwestern University, Glendale, AZ, United States, [5]Department of Pharmacology, College of Graduate Studies, Midwestern University, Glendale, AZ, United States

During terminal differentiation of the mammalian retina, transcription factors control binary cell fate decisions that generate functionally distinct subtypes of photoreceptor neurons. For instance, Otx2 and RORβ activate the expression of the transcriptional repressor Blimp-1/PRDM1 that represses bipolar interneuron fate and promotes rod photoreceptor fate. Moreover, Otx2 and Crx promote expression of the nuclear receptor Nrl that promotes rod photoreceptor fate and represses cone photoreceptor fate. Mutations in these four transcription factors cause severe eye diseases such as retinitis pigmentosa. Here, we show that a post-mitotic binary fate decision in *Drosophila* color photoreceptor subtype specification requires ecdysone signaling and involves orthologs of these transcription factors: *Drosophila* Blimp-1/PRDM1 and Hr3/RORβ promote blue-sensitive (Rh5) photoreceptor fate and repress green-sensitive (Rh6) photoreceptor fate through the transcriptional repression of *warts*/*LATS*, the nexus of the phylogenetically conserved Hippo tumor suppressor pathway. Moreover, we identify a novel interaction between Blimp-1 and *warts,* whereby Blimp-1 represses a *warts* intronic enhancer in blue-sensitive photoreceptors and thereby gives rise to specific expression of *warts* in green-sensitive photoreceptors. Together, these results reveal that conserved transcriptional regulators play key roles in terminal cell fate decisions in both the *Drosophila* and the mammalian retina, and the mechanistic insights further deepen our understanding of how Hippo pathway signaling is repurposed to control photoreceptor fates for *Drosophila* color vision.

KEYWORDS

**rhodopsin, retina, photoreceptor, ecdysone, BLIMP-1, rorβ, color vision, hippo pathway**

10.3389/fcell.2023.1058961

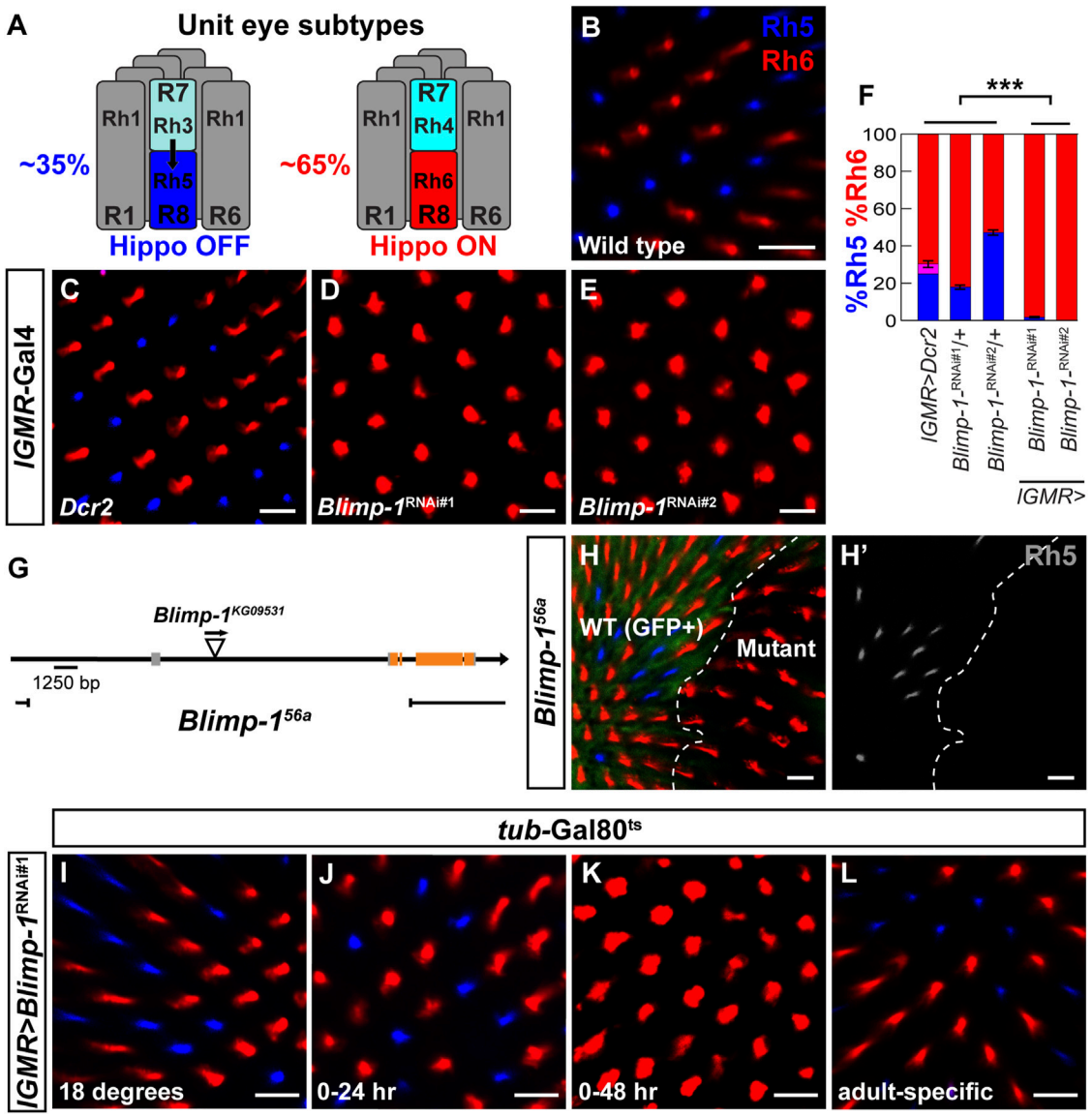


FIGURE 1
Blimp-1 is required to promote Rh5 and to repress Rh6. **(A)** Schematic side view of the two different unit eye subtypes in the *Drosophila* retina. Black arrow represents the Activin signal from Rh3-expressing R7 photoreceptors (35%, left) that induces Rh5 fate (Hippo OFF) in the proximally located R8 photoreceptors. Rh4-expressing R7 photoreceptors (65%, right) do not send the Activin signal and the corresponding R8 photoreceptors express Rh6 (Hippo ON) by default. **(B–E)** Confocal images of whole mounted adult retinas stained with antibodies for Rh5 (blue) and Rh6 (red). **(B)** A wild-type Canton S retina has an Rh5:Rh6 ratio of ~35:65. **(C)** Expression of *Dcr2* with the pan-photoreceptor driver *IGMR-Gal4* does not affect the Rh5:Rh6 ratio. **(D and E)** Expression of two independent *Blimp-1* RNAi constructs, *Blimp-1*-RNAi$^{kk}$ (*Blimp-1*$^{RNAi\#1}$) and *Blimp-1*-RNAi$^{TRiP\ \#36634}$ (*Blimp-1*$^{RNAi\#2}$), in combination with *Dcr2* causes a dramatic loss of Rh5 and a corresponding gain of Rh6. **(F)** Quantification of R8 subtypes in controls and *Blimp-1* knockdowns. Graph shows the percentage of R8 photoreceptors that express exclusively Rh5 (blue), exclusively Rh6 (red), or co-express Rh5 and Rh6 (magenta). Mean %Rh6 was compared among genotypes with an ANOVA and a *post hoc* Tukey HSD Test; ***$p < 0.0001$. 7-8 retinas were scored for each genotype. **(G)** Schematic showing the location of the *Blimp-1*$^{56a}$ deletion that was generated through imprecise P-element (triangle) excision. **(H)** Confocal image showing wild type R8 photoreceptors (GFP positive, left) exhibiting a normal Rh5:Rh6 ratio and *Blimp-1*$^{56a}$ null mutant clones (GFP negative, right) that exclusively express Rh6. The white dashed line denotes the boundary between wild-type and *Blimp-1* mutant tissue. **(H')** Rh5 channel (grayscale) shows the loss of Rh5 in the *Blimp-1* mutant tissue. **(I–L)** Confocal images of temporally restricted *IGMR* > *Blimp-1*$^{RNAi\#1}$ knockdown with *tub-Gal80*$^{ts}$. **(I)** Control flies raised throughout development and adulthood at 18°C, i.e., no *Blimp-1* knockdown, have a normal Rh5:Rh6 ratio. **(J)** Pupal *Blimp-1* knockdown from 0 to 24 h after puparium formation at 29°C does not affect the Rh5:Rh6 ratio. **(K)** Pupal *Blimp-1* knockdown from 0 to 48 h after puparium formation at 29°C causes a loss of Rh5 and gain of Rh6. **(L)** Adult-specific *Blimp-1* knockdown for 7 days at 29°C following eclosion does not affect the Rh5:Rh6 ratio. All scale bars, 10 μm.

## 1 Introduction

Color vision requires the expression of light-sensing pigments with different wavelength-sensitivities in different photoreceptor (PR) subtypes (Rister and Desplan, 2011). For instance, human color vision is based on three cone PR subtypes that express short-, medium-, or long wavelength-sensitive pigments (Nathans, 1999; Hofer et al., 2005). Likewise, the *Drosophila melanogaster* retina

10.3389/fcell.2023.1058961

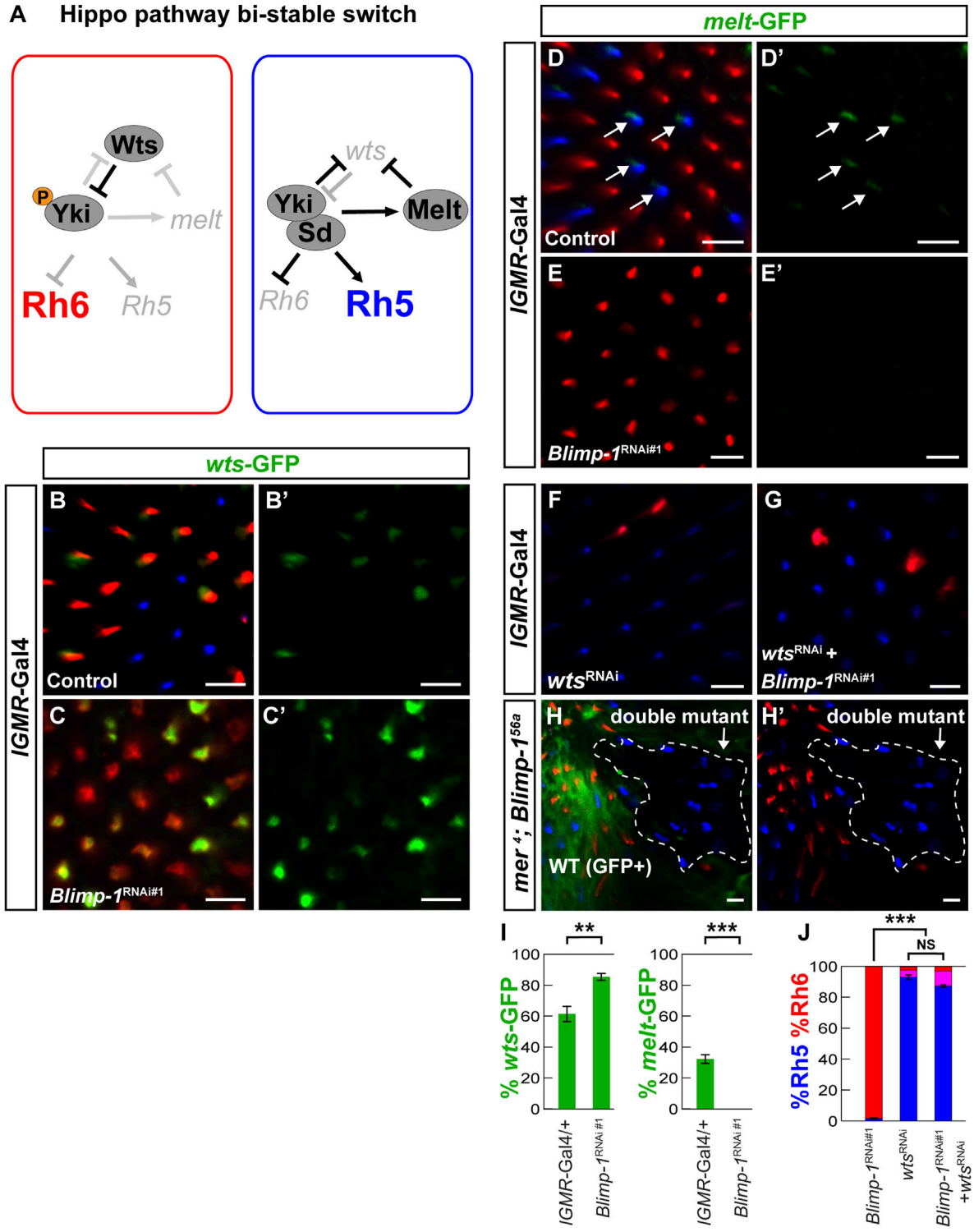


FIGURE 2
Blimp-1 is required for *warts* repression and *melted* expression. **(A)** Schematic of the repurposed Hippo pathway that controls a binary Rh5 vs. Rh6 cell fate decision in post-mitotic R8 photoreceptors. In Rh6 expressing photoreceptors (left), Wts represses Yki by phosphorylation, which prevents the expression of *melt* and *Rh5* and permits Rh6 expression. In Rh5 expressing photoreceptors (right), Yki binds to Sd, activates *melt* and *Rh5*, and represses *wts* and *Rh6*. **(B)** In the *lGMR-Gal4/+* driver control, the *wts*-GFP reporter is expressed in most Rh6 photoreceptors and absent in all Rh5 photoreceptors. **(C)** In *lGMR > Blimp-1$^{RNAi\#1}$* retinas, *wts*-GFP is de-repressed with Rh6. **(B',C')** GFP channel. **(D)** In the *lGMR-Gal4/+* driver control, the *melt*-GFP reporter is expressed in most Rh5 photoreceptors but absent in Rh6 photoreceptors. White arrows indicate *melt*-GFP expression. **(E)** In *lGMR > Blimp-1$^{RNAi\#1}$* retinas, *melt*-GFP expression is completely lost. **(D', E')** GFP channels. **(F)** Knockdown of *wts* with *lGMR-Gal4* causes a gain of Rh5 and loss of Rh6. **(G)** Knockdown of *Blimp-1* in addition to *wts* does not modify the *wts* knockdown phenotype. **(H)** *mer$^{4}$; Blimp-1$^{56a}$* double mutant clones (encircled by the white dashed line) exclusively express Rh5, which is the opposite of *Blimp-1$^{56a}$* mutant clones that exclusively express Rh6. All

(*Continued*)

FIGURE 2 (Continued)
scale bars, 10 μm. **(I)** Quantification of the *wts*-GFP-expressing R8 photoreceptors (left graph) and the *melt*-GFP expressing R8 photoreceptors (right graph) in the driver control and *Blimp-1* knockdown. Mean %*wts*-GFP (left) or %*melt*-GFP reporter (right) expression in driver control vs. knockdown was compared with an ANOVA and a *post hoc* Tukey HSD Test; ***$p < 0.0001$. 6 retinas were analyzed for each genotype. **(J)** Quantification of R8 subtypes, mean %Rh5 was compared among genotypes with an ANOVA and a *post hoc* Tukey HSD Test; ***$p < 0.0001$.5-8 retinas were scored for each genotype.

expresses five color-sensing Rhodopsin (Rh) pigments in distinct PR subtypes (Poupault et al., 2021). The "outer" PRs R1-R6 express blue/green-sensitive Rh1 and mediate dim light vision equivalent to human rods (O'Tousa et al., 1985; Zuker et al., 1985). The two 'inner' PRs R7/R8, which are arranged in tandem, each occur in two subtypes (Figure 1A) that are sensitive to different wavelengths and mediate color vision equivalent to human cones (Roorda and Williams, 1999). 35% of R7 PRs express the short UV-sensitive Rh3 and are coupled to proximally located R8 PRs that express the blue-sensitive Rh5 (Figure 1A, left), while the other 65% of R7 PRs express the long UV-sensitive Rh4 coupled with R8 PRs that express the green-sensitive Rh6 (Figure 1A, right) (Fortini and Rubin, 1990; Chou et al., 1996; Papatsenko et al., 1997; Chou et al., 1999).

The binary cell-fate decision to express either Rh5 or Rh6 in R8 PRs (Figure 1B) requires an Activin/TGFβ signal from the distally located R7 PRs (arrow in Figure 1A) (Wells et al., 2017) and differential regulation of the Hippo tumor suppressor pathway in R8 PRs (Mikeladze-Dvali et al., 2005; Jukam and Desplan, 2011; Jukam et al., 2013). In the canonical and conserved role of the Hippo pathway (Zeng and Hong, 2008; Zhao et al., 2008; Zhang et al., 2009; Chan et al., 2011; Halder and Johnson, 2011; Harvey and Hariharan, 2012; Halder and Camargo, 2013), the kinase Warts (Wts) restricts tissue growth by phosphorylating the transcriptional co-activator and oncogene Yorkie (Yki), which prevents Yki from entering the nucleus (Huang et al., 2005; Oh and Irvine, 2008). When Yki is not phosphorylated, it enters the nucleus and associates with transcription factors such as Scalloped (Sd) to activate genes that function in promoting growth, inhibiting apoptosis, and negative feedback regulation (Hamaratoglu et al., 2006; Neto-Silva et al., 2010).

In terminally differentiating *Drosophila* PRs, the Hippo pathway is repurposed to promote green-sensitive Rh6 PR fate, while its inactivation promotes blue-sensitive Rh5 PR fate (Figure 2A) (Mikeladze-Dvali et al., 2005; Jukam and Desplan, 2011; Jukam et al., 2013; Pojer et al., 2021). In this post-mitotic context, Yki/Sd promote Rh5 fate and inactivate the Hippo pathway by repressing *wts* at the transcriptional level (Mikeladze-Dvali et al., 2005; Jukam et al., 2013; Xie et al., 2019). *Wts* repression results in the activation of *melted* (*melt*), which encodes a Pleckstrin Homology domain protein (Mikeladze-Dvali et al., 2005; Teleman et al., 2005). For *wts* repression and *melt* activation, Yki/Sd require the transcription factors Orthodenticle (Otd) and Traffic Jam (Tj), which act in a coherent feedforward loop (Vandendries et al., 1996; Mears et al., 2001; Tahayato et al., 2003; Montana et al., 2011; Fichelson et al., 2012; Hao et al., 2012; Jukam et al., 2013). Conversely, when *wts* is expressed, it represses Yki; this leads to the transcriptional repression of *melt*, which allows the Hippo pathway to remain active and to promote Rh6 fate (Figure 2A). Thus, the Hippo pathway functions as a bi-stable switch in post-mitotic PRs: *wts* expression (Hippo ON) and *melt* repression specify Rh6 fate, while *melt* expression and *wts* repression (Hippo OFF) specify Rh5 fate (Figure 2A). The transcriptional regulation of *wts* in this context remains poorly understood.

Here, we show that *Drosophila* color PR subtype specification requires ecdysone signaling as well as the orthologs of transcription factors that promote rod PR fate in the mammalian retina: B lymphocyte-induced maturation protein-1/PR domain containing 1 (Blimp-1/PRDM1) and Hr3 (RAR-related orphan receptor β/RORβ) repress the Hippo pathway in post-mitotic *Drosophila* PRs, thereby promoting blue-sensitive Rh5 PR fate and repressing green-sensitive Rh6 PR fate. Moreover, we identify a novel mechanism of *wts* regulation in which Blimp-1 represses a *wts* enhancer to give rise to Rh6 PR subtype-specific *wts* expression. However, we find that this regulation of the Hippo pathway by Blimp-1 is context-specific, as Blimp-1 is required for wing growth independently of Wts. In summary, these results show that conserved transcriptional regulators play key roles in terminal PR differentiation in both *Drosophila* and mammals. Moreover, these insights deepen our understanding of the mechanisms that allow the Hippo pathway to control a binary cell-fate decision in terminally differentiating color PRs.

# 2 Materials and methods

## 2.1 Stocks and maintenance

The following *Drosophila* stocks were used in this study: *mer*$^{4}$ *FRT19A* (Fehon et al., 1997), *ey-FLP, P{ubiGFP} FRT19A* (from Jessica Treisman, NYU), *ey-FLP, P{ubiGFP} FRT80* (from Claude Desplan, NYU), *lGMR-Gal4* (Wernet et al., 2006), *UAS-Babo** (Wells et al., 2017), *sens-Gal4* (from Graeme Mardon, Baylor College of Medicine), and *ex-LacZ* (Yu and Pan, 2018). From Bloomington *Drosophila* Stock Center, we obtained: *MS1096-Gal4; UAS-Dcr2* (#25706), *UAS-Dcr2; nubbin-Gal4* (#25754), *tubP-Gal80*$^{ts}$ (#7017), *en2.4-Gal4* (#30564), *UAS-Dcr2; en2.4-Gal4, UAS-2XEGFP* (#25752), *UAS-Hr3-RNAi* #1 (TRiP.JF02542, #27253), *UAS-Hr3-RNAi* #2 (TRiP.JF02543, #27254), *UAS-wts-RNAi* (TRiP HMS00026) (#34064), *UAS-EcR-RNAi* (TRiP.HMJ22371, #58286), *UAS-EcR-A-dsRNA* (#9328), *UAS-EcR-b1-dsRNA* (#9329), *UAS-Blimp-1-RNAi* #2 (TRiP.GL00594, #36634), and *Blimp-1*$^{KG09531}$ (#15195). From Vienna *Drosophila* Resource Center, we obtained *UAS-Blimp-1-RNAi* #1 (KK #108374).

All stocks were maintained on standard lab food at 25°C, 50% humidity, and under a 12 h/12 h light/dark cycle. All experiments

and controls were conducted at 25°C with 2–5 day-old female flies, unless stated otherwise. For RNAi experiments with the *sens-Gal4* driver, third instar larvae of the experimental and control crosses were shifted from a 25°C incubator to a 29°C incubator.

For staging of pupae, newly formed white prepupae—corresponding to 0 h after puparium formation—were circled with a marker pen on the food vial (Hsiao et al., 2012). At the desired time point after puparium formation, pupae were gently removed from the vial using forceps. For Gal80$^{ts}$ experiments, white prepupae were shifted from a 25°C incubator to a 29°C incubator and then shifted at the desired time point (see Results) from the 29°C incubator to an 18°C incubator.

## 2.2 Generation of the *Blimp-1* null mutant

We used the P-element insertion *Blimp-1*$^{KG09531}$ to generate the imprecise excision allele *Blimp-1*$^{56a}$, following standard procedures (Engels et al., 1990). The deletion breakpoints of the imprecise excision allele were initially determined by Next-Generation Sequencing of the 3L chromosome from predominantly homozygous *Blimp-1*$^{56a}$ mutant first instar larvae that had reduced or no GFP expression from the *TM3, P{GAL4-Kr.C} DC2, P{UAS-GFP.S65T}DC10, Sb*$^{1}$ balancer chromosome. Initial breakpoints were determined by using the bioinformatics tool BreakDancer (Fan et al., 2014) to evaluate the chromosome for large structural variants. BreakDancer predicted a deletion from bases 3L:5624169.5645326, lining up with an area of low sequence coverage noticeable in the alignment. Subsequent Sanger sequencing surrounding this region—using the forward primer TTTTCCAGG TCATCGTTTCC and the reverse primer ATCGTCGTCTCAGGATCCAC—revealed that the chromosomal region that was deleted is 3L:5624036.5645326 (Figure 1G), based off the *D. melanogaster* genome release 6.45.

## 2.3 Generation of *warts* and *melted* reporters

The first *melt* intron was digested with KpnI and NotI to obtain a 2 kb enhancer fragment from its 3′ region (Jukam et al., 2013); the second *wts* intron (in TOPO plasmid/ThermoFisher, a gift from David Jukam) was digested with BamHI, BglII, and XhoI to obtain a 2.6 kb enhancer fragment from its 3' region. The obtained enhancer sequences were confirmed by Sanger sequencing. The following primers were used to mutate the two Blimp-1 motifs in the *wts* intron (mutated bases are in bold) with the Q5® Site-Directed Mutagenesis Kit (New England Biolabs).

*wts*-ΔBlimp-1 motif 1 forward: **aca**cgctAATCCACTTAAGCTC CTCTG
*wts*-ΔBlimp-1 motif 1 reverse: **atgcca**cGGCAATTCTACGGT TCGTG
*wts*-ΔBlimp-1 motif 2 forward: **ac**gcCAATGGGCTCACT AAATC
*wts*-ΔBlimp-1 motif 2 reverse: **tagca**AATTTGCCGTAA ATTGGC

We inserted the wild type or mutant enhancer constructs into a transformation plasmid containing an *egfp* reporter gene, a *mini-white*$^{+}$ transformation marker, an *hsp70* minimal promoter, and an *attB* site for *phiC31*-mediated transgenesis (Rister et al., 2015). The constructs were inserted in the second chromosomal landing site attP40 or the third chromosomal landing site J36 (ZH-attP-86Fb) (Bischof et al., 2007).

## 2.4 Luciferase reporter assay

The *wts-hsp70* enhancer-promoter construct (see above) was amplified using the Phusion® High-Fidelity PCR Kit (New England Biolabs) and fused to a firefly *luciferase* reporter gene (*wts-hsp70-luc*), digested with BglII and KpnI, and subcloned into the pGL3-basic vector (Promega) with the NEBuilder® HiFi DNA Assembly master mix (New England Biolabs). The following primers were used to amplify *wts-hsp70* (pGL3 overhangs are in lowercase).

*wts-hsp70* forward: atttctctatcgataggtacCTGACATATTTGG TGCTACACATGTAATCCC
*wts-hsp70* reverse: ccaagcttacttagatcgcaGGTGGCGACCGGT GGATC

To generate the *Blimp-1* expression construct (*Ac5-Blimp-1*), *Blimp-1-RA* cDNA was amplified from a *UAS-Blimp-1-RA* plasmid (*Drosophila* Genomics Resource Center #1634032) and inserted into the pAc5.1/V5-His A vector (Invitrogen) by digest with XhoI and AgeI and using the NEBuilder® HiFi DNA Assembly master mix. The following primers were used to amplify the *Blimp-1-RA* insert (pAc5.1/V5-His overhangs are in lowercase).

*Blimp-1RA* forward: tccagcacagtggcggccgcAGTTTCCCGTAAG CAACAAAAC
*Blimp-1RA* reverse: aatggtgatggtgatgatgatACGTGCATTCGA TGATCATG

To generate the *Hr3* expression construct (*Ac5-Hr3*), we ordered the *Hr3-RA* coding sequence inserted into the p-UCIDT-AMP vector from Integrated DNA Technologies (IDT). From that plasmid we amplified *Hr3-RA* and inserted it into the pAc5.1/V5-His A vector (Invitrogen) by digest with NotI and EcoRI and using the NEBuilder® HiFi DNA Assembly master mix. The following primers were used to amplify the *Hr3-RA* insert (pAc5.1/V5-His overhangs are in lowercase).

*Hr3-1RA* forward: ctactagtccagtgtggtggATGTATACGCAAC GTATGTTTG
*Hr3-1RA* reverse: agggccctctagactcgagcTTATGTCAGGTCC TGCTG

Luciferase reporter assays were performed using the Dual-Luciferase® Reporter Assay System (Promega). For all experiments and controls, 100 ng of *wts-hsp70-luc* were co-transfected with 100 ng of a *Renilla luciferase* gene fused to a *TK* promoter (*pRL-TK*) (Promega) that served as a control reporter. For controls, *wts-hsp70-luc* and *pRL-TK* were co-transfected with 100 ng of pAc5.1/V5-His A

empty vector; for experiments, *wts-hsp70-luc* and *pRL-TK* were co-transfected with 100 ng of either *Ac5-Blimp-1* or *Ac5-Hr3*. *Drosophila* S2 cells (Gibco) were maintained in Schneider's Medium with 10% fetal bovine serum (Gibco) at room temperature. 1 × 10^6 cells were plated in 6-well tissue culture dishes (Corning) 24 h prior to transfection with 7.5 µL Effectene Transfection Reagent (Qiagen). Samples were transfected in triplicate for each experiment, and each experiment was performed at least three independent times. Background luminescence was determined using non-transfected cells and subtracted from control and experimental luminescence readings. Firefly luminescence results were normalized to *Renilla* luminescence results and presented as Relative Luminescence Units (RLU). Error bars for luciferase data represent ±S.E.M.

## 2.5 Wing size assay

Adult wings of female flies raised at 25°C were removed with forceps and mounted with mounting medium–lactic acid/CMCP-10 high viscosity mountant (Polysciences) (1:3, v/v)—on a glass slide. 5 µL of isopropanol (Sigma-Aldrich) was added to the wings and allowed to evaporate without drying out the wings. Next, 10 µL of mounting medium was added to the wings on the slide, wings were oriented, and air bubbles were removed. To determine relative wing sizes, wing areas were calculated using ImageJ. At least five wings were measured per genotype, and average wing areas were normalized to the average wing area of the *MS1096-Gal4*/+ driver control. Error bars indicate the standard error of the mean (S.E.M.).

## 2.6 Imaging the *Drosophila* eye

Adult flies were embedded in an agarose gel that was prepared in a 500 mL Erlenmeyer flask by mixing 2 g of UltraPure Agarose (Invitrogen) with 100 mL of distilled water. The mixture was microwaved until bubbles were seen and the agarose was fully dissolved. Next, the Erlenmeyer flask with the dissolved agarose was transferred to a 60°C water bath (Thermo Scientific) to cool the agarose gel but maintaining it liquid. Flies were anesthetized with $CO_2$ and transferred to a 60 mm Petri dish (Falcon) filled approximately halfway with the liquid agarose gel. Wings and legs were submerged and the head was oriented with forceps such that one compound eye faced the microscope lens. Next, the Petri dish was placed on ice to allow the gel to solidify and then positioned under a Stemi 508 Trinoc microscope (model #4350649030, Zeiss); the eye was imaged using an Axiocam 208 HD/4k color camera (model #4265709000) set to auto exposure and auto white balance. Image processing was performed using Fiji (https://imagej.net/software/fiji/), Adobe Photoshop 2020, and Adobe Illustrator 2020 software.

## 2.7 Retina whole-mounts, immunohistochemistry, and confocal microscopy

We performed adult retina dissections and immunohistochemistry as previously described (Hsiao et al., 2012). We dissected adult retinas in cold phosphate-buffered saline (PBS) and fixed them in 3.7% formaldehyde solution (in PBS) for 15 min at room temperature. After two washes with PBS and one with PBST (PBS +0.2% Triton-X, Sigma), we removed the laminas. Next, we incubated the retinas overnight in the primary antibodies that were diluted in PBST (sheep anti-GFP—from AbD Serotec—1:100; mouse anti-Rh3—from Steve Britt/University of Texas—1:10; mouse anti-Rh5—from Steve Britt—1:400, guinea pig anti-Rh4—from Claude Desplan/NYU—1:1,000; or rabbit anti-Rh6—from Claude Desplan—1:1,000). After three PBST washes, we incubated the retinas overnight at room temperature in the secondary antibodies (Alexa Fluor 488-, 555-, or 647-conjugated raised in donkey; Molecular Probes) that were diluted 1:800 in PBST. Alexa Fluor (488 or 555)-coupled Phalloidin (1:150, Invitrogen) was used to visualize the photoreceptor rhabdomeres. After three PBST washes, we mounted the retinas on bridge slides with SlowFade (Molecular Probes).

We performed pupal retina dissections as previously described but with some modifications (Hsiao et al., 2012; Wang et al., 2022). We circled white prepupae, which were raised at 25°C, for staged pupal dissections. At the desired stage (after 24, 48, or 72 h, respectively), pupae were taped to a dissecting plate with double-sided tape and removed from the pupal case with forceps. The pupa was then submerged in ice-cold PBS and the head was removed using microdissection scissors. Next, the retina-brain complexes were removed using forceps and fixed in 3.7% formaldehyde solution (in PBS) for 15 min at room temperature. After two washes with PBS and one wash with PBST, the retina-brain complexes were incubated at 4°C overnight in primary antibodies (guinea pig anti-Blimp-1—from Sudipto Roy/National University of Singapore—1:400; rat anti-Elav—from DHSB—1:50) diluted in PBST and 5% normal donkey serum. After three PBST washes, we incubated the retinas overnight at 4°C for three hours in the secondary antibodies (see above). After three PBST washes, we performed a secondary fixation step by submerging retina-brain complexes in 3.7% formaldehyde solution (in PBS) for 20 min at room temperature. After washing three times with PBST, we removed the retina from the brain in PBS and mounted the retina on a slide using Slowfade. We imaged both adult and pupal retina whole mounts with a Leica SP5 or a Zeiss LSM 8 confocal microscope. We processed the confocal images with Fiji, Adobe Photoshop 2020, and Adobe Illustrator 2020 software.

## 2.8 Quantification of rhodopsin and reporter expression patterns

As previously described (Poupault et al., 2021), we manually scored the number of rhabdomeres that expressed the markers Rh5, Rh6, or a GFP reporter with the count tool in Adobe Photoshop 2020. The percentage of R8 PRs that expressed the respective marker was calculated for each retina as well as the mean percentage of all retinas within a genotype. Statistical comparisons across genotypes were performed using the Mann-Whitney *U* Test; significance levels are given as *p* values and error bars indicate the standard error of the mean (S.E.M.).

## 2.9 Conservation analysis of Blimp-1 motifs

To analyze the evolutionary conservation of Blimp-1 motifs, we obtained alignments of the *wts* second intron sequences from ten

*Drosophila* species (Clark et al., 2007) from the UCSC genome browser (https://genome.ucsc.edu/).

# 3 Results

## 3.1 Blimp-1 is required for blue-sensitive photoreceptor subtype specification

We performed a candidate RNAi screen to identify sequence-specific transcription factors that are required for the wild type 35/65 ratio of the Rh5/Rh6-expressing R8 PR subtypes and found that the knockdown of *B lymphocyte-induced maturation protein-1* (*Blimp-1*) with the pan-PR driver *lGMR-Gal4* (Wernet et al., 2006) caused a dramatic gain of Rh6-expressing PRs and a loss of Rh5-expressing PRs (Figures 1C–F). This loss of blue-sensitive PR fate and gain of green-sensitive PR fate was observed with two independent *Blimp-1*-RNAi constructs that targeted different parts of the *Blimp-1* transcript (Figures 1D,E). To validate the RNAi results, we generated a *Blimp-1* null mutant through imprecise P-element excision (see Materials and methods), which resulted in a genomic deletion that spans from 6.8 kb upstream of the *Blimp-1* transcription start site to the third coding exon (*Blimp-1*$^{56a}$, Figure 1G). Since the *Blimp-1*$^{56a}$ null allele was embryonic lethal, we used *eyeless* > Flp to generate mutant clones in the eye with the FLP/FRT recombination system (Newsome et al., 2000). Consistent with the RNAi results, *Blimp-1*$^{56a}$ null mutant clones exclusively expressed Rh6 at the expense of Rh5, confirming that Blimp-1 is required for expression of Rh5 and repression of Rh6 (Figures 1H,H'). Taken together, Blimp-1 is required for the terminal differentiation of the blue-sensitive, Rh5-expressing R8 PR subtype.

## 3.2 Blimp-1 promotes blue-sensitive photoreceptor subtype fate in mid-pupal photoreceptors

Our next goal was to determine the time window during which Blimp-1 affects R8 PR subtype specification. We detected weak Blimp-1 expression (Ng et al., 2006) in all PRs at 24 h after puparium formation (APF) and stronger expression at 48 h APF (Supplementary Figures S1A, A', B, B'), but no expression at 72 h APF and in adult eyes (Supplementary Figures S1C, C′, D, D′). Moreover, RNAi-mediated knockdown of *Blimp-1* abolished Blimp-1 expression (Figures S1E–F′). This suggests that Blimp-1 expression is transiently increased in PRs from early-to mid-pupal development, when R8 PR subtypes are distinguished (Jukam and Desplan, 2011), and is turned off in late pupal development. Interestingly, most of the Blimp-1 signal was not restricted to the nucleus, but surrounded it: at 48 h APF, we observed a partial overlap of Blimp-1 with the Elav nuclear marker in wild-type and occasional strong Blimp-1 PR nuclear localization in the driver control, suggesting that Blimp-1's nuclear localization is regulated and transient. We therefore propose that Blimp-1's nuclear entry and/or export is regulated to restrict its activity during pupal development.

Since Blimp-1 expression and nuclear localization is lost after 48 h APF, we hypothesized that Blimp-1 is required for the specification of Rh5 fate but not for its maintenance at later stages. To further investigate this transient requirement of Blimp-1 for R8 subtype specification, we used a temperature sensitive mutant of the Gal4 inhibitor Gal80 (Gal80$^{ts}$) to temporally restrict the *Blimp-1* knockdown (McGuire et al., 2004). Permissive temperature (Figure 1I), RNAi-mediated *Blimp-1* knockdown from 0 to 24 h APF (Figure 1J), or *Blimp-1* knockdown for seven days after eclosion (Figure 1L) did not affect the Rh5:Rh6 ratio. In contrast, *Blimp-1* knockdown from 0 to 48 h APF (Figure 1K) caused a dramatic loss of Rh5 and gain of Rh6. Taken together, these data suggest that Blimp-1 is required in early to mid-pupal PRs for the specification of Rh5 fate.

We next asked if Blimp-1 acts cell autonomously in R8 PRs to promote Rh5 fate. To this end, we performed an RNAi-mediated knockdown of *Blimp-1* using the R8 driver *sens-Gal4* and two copies of *UAS-Blimp-1*-RNAi. This again led to a dramatic gain of Rh6 and loss of Rh5 (Supplementary Figures S1G–J), suggesting that Blimp-1 is required cell autonomously in R8 PRs to promote Rh5 PR fate and to repress Rh6 PR fate. In a complementary approach, we took advantage of the fact that the specification of Rh5 fate requires an Activin signal from a subset of R7 PRs (Figure 1A) that activates the type I receptor Baboon (Babo) in the proximally located subset of R8 PRs (Wells et al., 2017). If Blimp-1 acts cell autonomously in R8 PRs to promote Rh5 fate, then Blimp-1 should act downstream of the Activin signal. Indeed, when we expressed a constitutively active form of Babo (Babo*) (Wells et al., 2017) in combination with an RNAi-mediated knockdown of *Blimp-1,* Babo activation was no longer able to specify Rh5 fate and we observed the *Blimp-1* mutant phenotype (loss of Rh5 and gain of Rh6; Supplementary Figures S1K, L). In summary, these data suggest that Blimp-1 specifies Rh5 fate cell autonomously in early to mid-pupal R8 PRs downstream of the Activin signal and the Babo receptor.

## 3.3 Blimp-1 is required for the activation of *melted* and the repression of *warts*

Because the Hippo pathway is inactivated in the Rh5 PRs that require Blimp-1 for their specification (Mikeladze-Dvali et al., 2005; Jukam et al., 2013) and Blimp-1 is a transcriptional repressor (Keller and Maniatis, 1991; Yu et al., 2000; Agawa et al., 2007; Ozturk-Colak et al., 2018), we asked whether Blimp-1 represses the Hippo pathway in R8 PRs. A candidate target for Hippo pathway repression is its nexus *wts,* which is transcriptionally repressed in Rh5 PRs (Figure 2A) (Mikeladze-Dvali et al., 2005; Jukam et al., 2013; Pojer et al., 2021). We identified an enhancer in the second *wts* intron (Figure 3A; see Materials and methods) that was sufficient to recapitulate PR subtype-specific *wts* expression in the Rh6 PRs when fused to an *egfp* reporter gene (*wts*-GFP); this allowed us to test whether Blimp-1 is required to repress *wts* transcription in Rh5 PRs. Indeed, *wts*-GFP was de-repressed with Rh6 upon *Blimp-1* knockdown (Figures 2B–C′, I; Supplementary Figures S2A–C), suggesting that Blimp-1 is required for the transcriptional repression of *wts*. Since *melt* is expressed in Rh5 PRs and repressed by Wts in Rh6 PRs, we tested if Blimp-1 is also

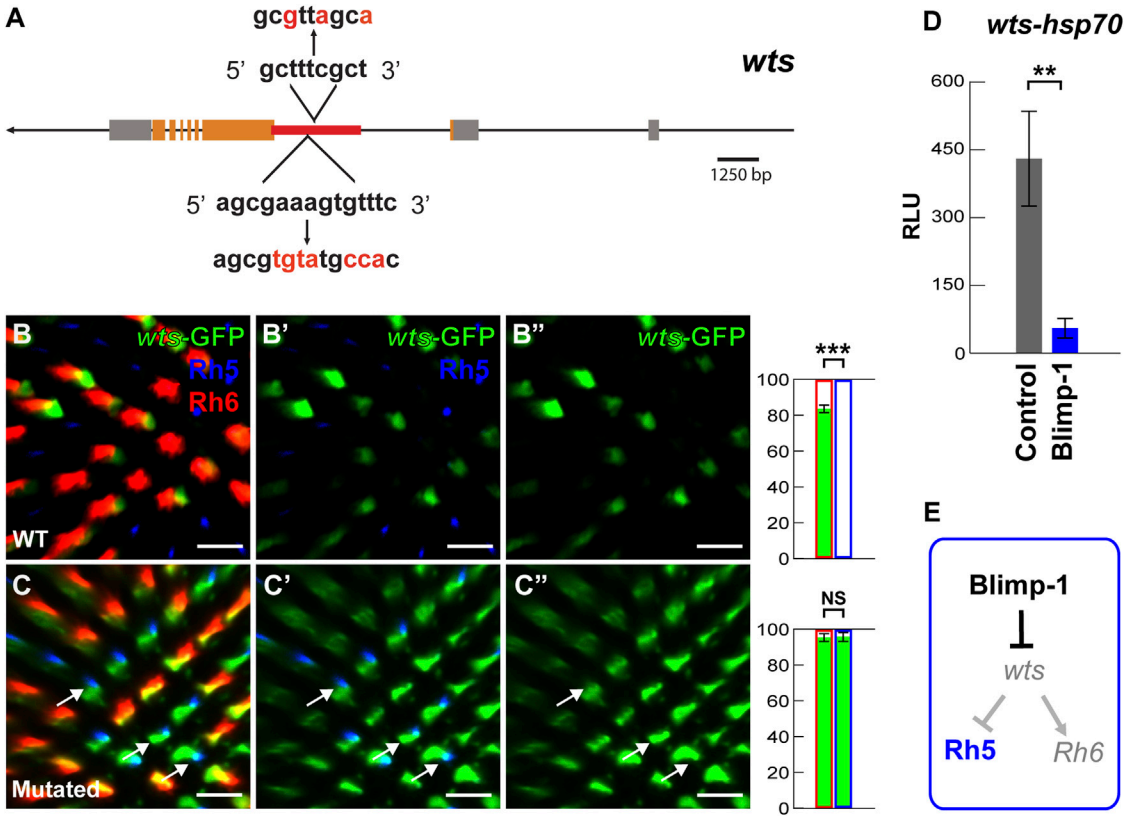


FIGURE 3
Blimp-1 represses the *warts* intronic enhancer. **(A)** Schematic of the *wts* locus. The red line indicates the location of the 2.6 kb *wts* enhancer in the second intron that contains two conserved Blimp-1 motifs. The red letters indicate introduced mutations. **(B–B')** The 2.6 kb *wts* enhancer fused to an *hsp70* promoter drives GFP (hereafter referred to as *wts*-GFP reporter) in the majority of Rh6 photoreceptors. Right: percentage of Rh6 photoreceptors (red outline) or Rh5 photoreceptors (blue outline) that co-express GFP (green bars), respectively. %Rh6/GFP co-expression vs. %Rh5/GFP co-expression was compared with an ANOVA and a *post hoc* Tukey HSD Test; ***$p < 0.0001$. $N = 5$ retinas. **(C–C')** Mutation of the two conserved Blimp-1 motifs causes *wts*-GFP reporter de-repression in Rh5 photoreceptors. White arrows indicate examples of *wts*-GFP de-repression. Right: percentage of Rh6 photoreceptors or Rh5 photoreceptors that co-express GFP, respectively. $N = 5$ retinas. All scale bars, 10 μm. **(D)** Dual luciferase reporter assay. The intronic *wts* reporter (*wts-hsp70-luc*) is active in S2 cells, but Blimp-1 strongly represses it ($N = 3$). *Y*-axis: Relative Luminescence Units (RLU) of *wts-hsp70-luc* normalized to the Renilla luciferase control reporter (see Materials and methods). **(E)** Schematic of Blimp-1 function in color photoreceptor specification: Blimp-1 represses *wts*/Rh6 fate to promote Rh5 fate.

required for *melt* activation in Rh5 PRs. Indeed, *melt* transcriptional reporter expression (Figures 2D, D′) was lost when *Blimp-1* was knocked down (Figures 2E, E', 2I). Taken together, these data suggest that Blimp-1 is required for both the repression of *wts* and the expression of *melt*.

The *wts* and *melt* reporter results suggest that Blimp-1 acts genetically upstream of *wts*. To test this hypothesis, we performed epistasis experiments. Indeed, RNAi-mediated knockdown of *wts* caused a gain of Rh5 and loss of Rh6 (Figure 2F) even with concomitant knockdown of *Blimp-1* (Figures 2G,J). Since *wts* knockdown reverses the *Blimp-1* knockdown phenotype (gain of Rh6 and loss of Rh5), this provides further support that Blimp-1 acts upstream of *wts*. To corroborate this result, we analyzed *merlin (mer)* mutant clones. Mer is a FERM domain-containing protein that is required for Wts activity in R8 PRs, and *mer* mutant clones exclusively express Rh5 (Jukam and Desplan, 2011). Likewise, we found that *mer; Blimp-1* double mutants also exclusively expressed Rh5 (Figure 2H, H'). In summary, the perturbation of Wts activity, either through RNAi-mediated knockdown of *wts* or mutation of *mer*, reverses the *Blimp-1* mutant phenotype. These data show that Blimp-1 acts genetically upstream of *wts*.

Lastly, we investigated the possibility that Blimp-1 directly represses *wts* transcription. We identified two conserved motifs (Supplementary Figure S3A) in the *wts* intronic enhancer that match the Blimp-1 consensus motif AGNGAAAG (Kuo and Calame, 2004; Ancelin et al., 2006; Katoh et al., 2010) as well as the *Drosophila* Blimp-1 Position Weight Matrix (Zhu et al., 2011) (Figure 3A) (see Materials and methods). Strikingly, the mutation of the conserved Blimp-1 motifs caused *wts*-GFP reporter de-repression in Rh5 PRs (compare Figures 3B-B", C-C"), suggesting that the Blimp-1 motifs are required for *wts* repression in Rh5 PRs. Consistent with these *in vivo* data, Blimp-1 dramatically reduced (~9-fold) *wts-hsp70-luc* reporter expression in *Drosophila* S2 cells (Figure 3D) (see Material and methods). Taken all the data together, we propose that Blimp-1 represses Rh6 fate through repression of *wts*, the nexus of the Hippo pathway, and thereby promotes Rh5 fate (Figure 3E).

10.3389/fcell.2023.1058961

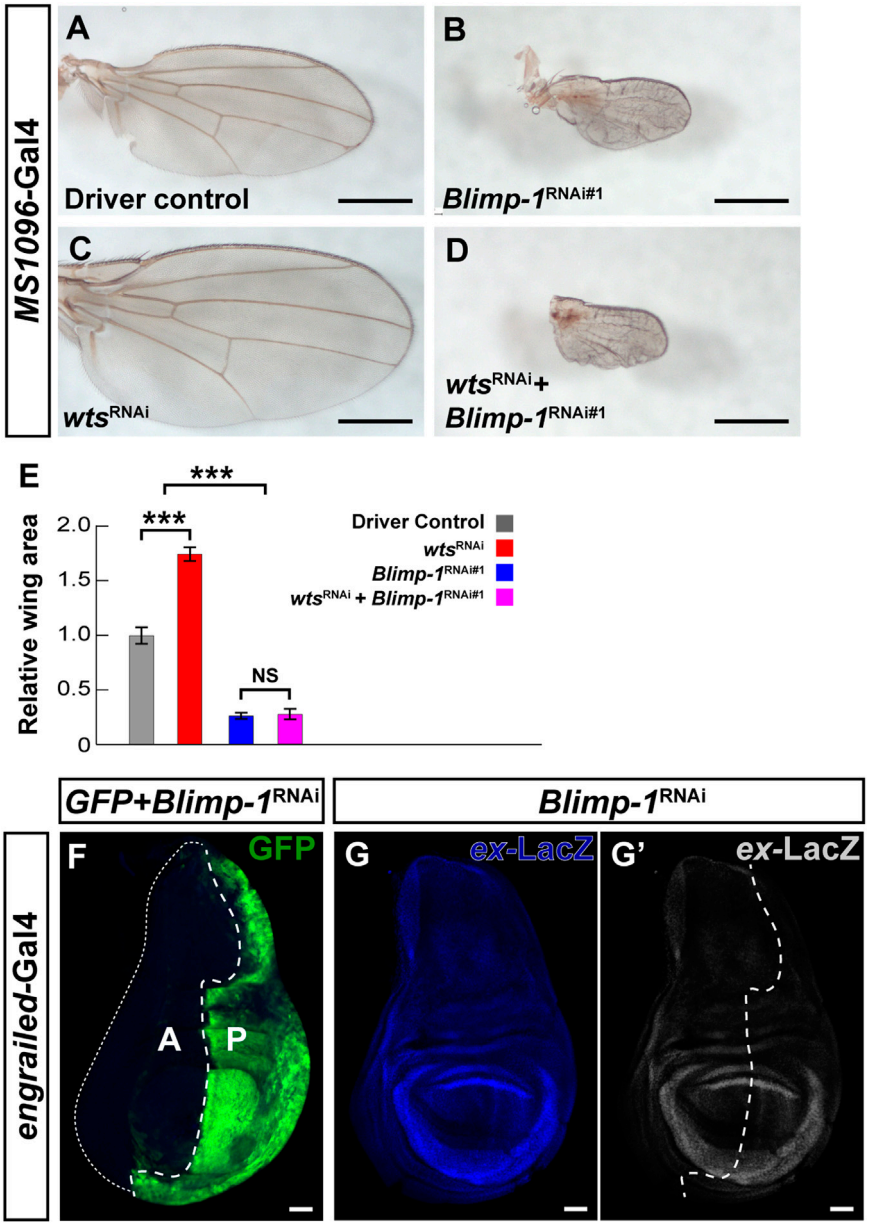


FIGURE 4
Blimp-1 plays a role in wing development independent of the Hippo pathway. **(A–D)** Wings of 2–4 days-old female flies raised at 25°C. Scale bars, 500 μm. **(A)** Wing disc driver control *MS1096-Gal4*/+. **(B)** *Blimp-1* knockdown causes a dramatic reduction in wing size. **(C)** *wts* knockdown causes an increase in wing size. **(D)** Knockdown of both *Blimp-1* and *wts* resembles the *Blimp-1* knockdown. **(E)** Quantification of wing area for each genotype normalized to the *MS1096-Gal4* driver control. Relative wing areas were compared with an ANOVA and a *post hoc* Tukey HSD Test; ***$p < 0.0001$. 6-8 wings were scored for each genotype. **(F)** Confocal image of a third instar larval wing disc with *engrailed-Gal4* driving GFP and *Blimp-1*$^{RNAi\#1}$ in the posterior half. Blimp-1 knockdown does not appear to affect the size of the posterior half of the wing disc (marked by GFP) compared to the anterior half of the wing disc (GFP negative). White dashed line encircles the anterior half of the wing disc. Anterior is labeled with "A", and posterior is labeled with "P". **(G)** *Blimp-1* knockdown does not affect *expanded*-lacZ reporter expression in the posterior wing disc. **(G')** *Expanded*-LacZ staining in grayscale. White dotted line indicates the approximate boundary between anterior and posterior halves based on the GFP staining in **(F)**. All scale bars for larval wing discs, 50 μm.

## 3.4 The role of Blimp-1 in wing growth is independent of the hippo pathway

Since the canonical role of the Hippo pathway is to regulate organ growth (Halder and Camargo, 2013) and we found that Blimp-1 represses the core component *wts* in the post-mitotic PR context, we asked whether Blimp-1 regulates the Hippo pathway in mitotically active tissue. While *Blimp-1* knockdown caused a glossy eye phenotype (Wang et al., 2022) (Supplementary Figures S4A, B), it did not decrease the size of the adult eye (Supplementary Figures S4A, B), indicating that Blimp-1 does not regulate tissue growth in the developing eye. Moreover,

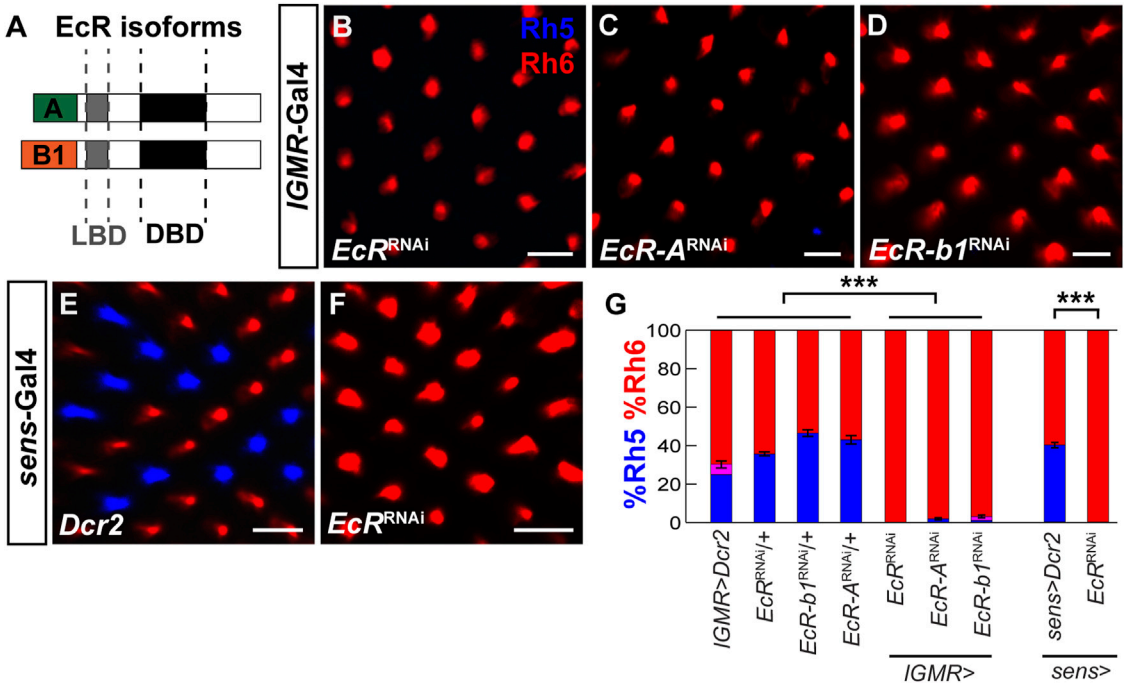


FIGURE 5
EcR is required cell autonomously to specify Rh5 fate. **(A)** Schematic of two EcR isoforms, EcR-A and EcR-b1, which contain identical DNA binding domains (DBD) and ligand binding domains (LBD) but differ in their N-terminal A/B domains. **(B)** Pan-photoreceptor knockdown of all *EcR* isoforms causes a loss of Rh5 and a gain of Rh6. **(C, D)** Pan-photoreceptor knockdown of the individual *EcR* isoforms *EcR-A* **(C)** and *EcR-b1* **(D)** causes a loss of Rh5 and gain of Rh6. **(E)** Expression of *Dcr2* with the R8 driver *sens-Gal4* at 29°C does not affect the Rh5:Rh6 ratio. **(F)** Expression of $EcR^{RNAi}$ and *Dcr2* with *sens-Gal4* at 29°C causes a loss of Rh5 and gain of Rh6. All scale bars, 10 µm. **(G)** Quantification of R8 subtypes in controls vs. *EcR* knockdowns. Mean %Rh6 was compared among genotypes with an ANOVA and a *post hoc* Tukey HSD Test; ***$p < 0.0001$. 5-8 retinas were scored for each genotype.

knockdown of *wts* did not rescue the glossy eye phenotype (Supplementary Figure S4C), indicating that this *Blimp-1* mutant phenotype is not related to the Hippo pathway. In addition, *Blimp-1* knockdown in the developing wing caused a dramatic decrease in adult wing size with two different wing disc drivers (Figures 4A, B; Supplementary Figures S4D, E). However, in contrast to the terminal PR differentiation context, and consistent with the glossy eye phenotype, the wing size defect could not be modified by concomitant knockdown of *wts* (Figures 4C–E). Moreover, knockdown of *Blimp-1* in the posterior half of the wing disc with *engrailed-Gal4* did not have any obvious effects on the size of the third instar larval wing disc in comparison to the anterior half (Figure 4F), suggesting that Blimp-1 likely regulates wing development during pupal stages, similar to its pupal role in post-mitotic PRs. Again, in contrast to post-mitotic PRs, this other role of Blimp-1 does not appear to involve regulation of Hippo pathway activity: *expanded*-LacZ (Yu and Pan, 2018), a transcriptional reporter of Yki activity, was unaffected when *Blimp-1* was knocked down in the posterior half of the developing wing disc (Figures 4G, G'). Furthermore, the intronic *wts* enhancer that is repressed by Blimp-1 in post-mitotic PRs was not detectable in the wing disc (Supplementary Figure S4F). Together, these data suggest that Blimp-1 is required for proper wing growth, but this function appears to be independent of the Hippo pathway.

## 3.5 Ecdysone signaling is cell autonomously required for blue-sensitive photoreceptor fate

Blimp-1 is activated by the steroid hormone ecdysone (Agawa et al., 2007; Akagi and Ueda, 2011; Akagi et al., 2016; Ozturk-Colak et al., 2018) and Blimp-1 expression in the pupal retina requires the ecdysone receptor (EcR) (Wang et al., 2022). Therefore, we analyzed whether ecdysone signaling is required to specify Rh5 fate by performing RNAi-mediated knockdown of *EcR* with *lGMR-Gal4*. Closely resembling the *Blimp-1* mutant phenotype, *EcR* knockdown with an RNAi construct that targets all *EcR* isoforms caused a complete loss of Rh5 PRs and a gain of Rh6 PRs (Figures 5A,B). Since there are three EcR isoforms (EcR-A, EcR-b1, and EcR-b2) that have identical DNA binding domains but differ in their N-terminal A/B domains that allow them to elicit differential transcriptional responses (Mouillet et al., 2001; Schubiger et al., 2003), we additionally performed isoform-specific knockdowns. The knockdown of *EcR-A* and *EcR-b1* (an RNAi line specifically targeting *EcR-b2* was not available) each caused a loss of Rh5 PRs and gain of Rh6 PRs (Figures 5C, D), respectively, suggesting that both isoforms are non-redundantly required to specify Rh5 fate. Similarly, *EcR* knockdown using the R8 PR driver *sens-Gal4* also caused a loss of Rh5 PRs and gain of Rh6 PRs (Figures 5E, F). Taken together (Figure 5G), ecdysone signaling is cell autonomously required in R8 PRs to specify Rh5 fate and to repress Rh6 fate.

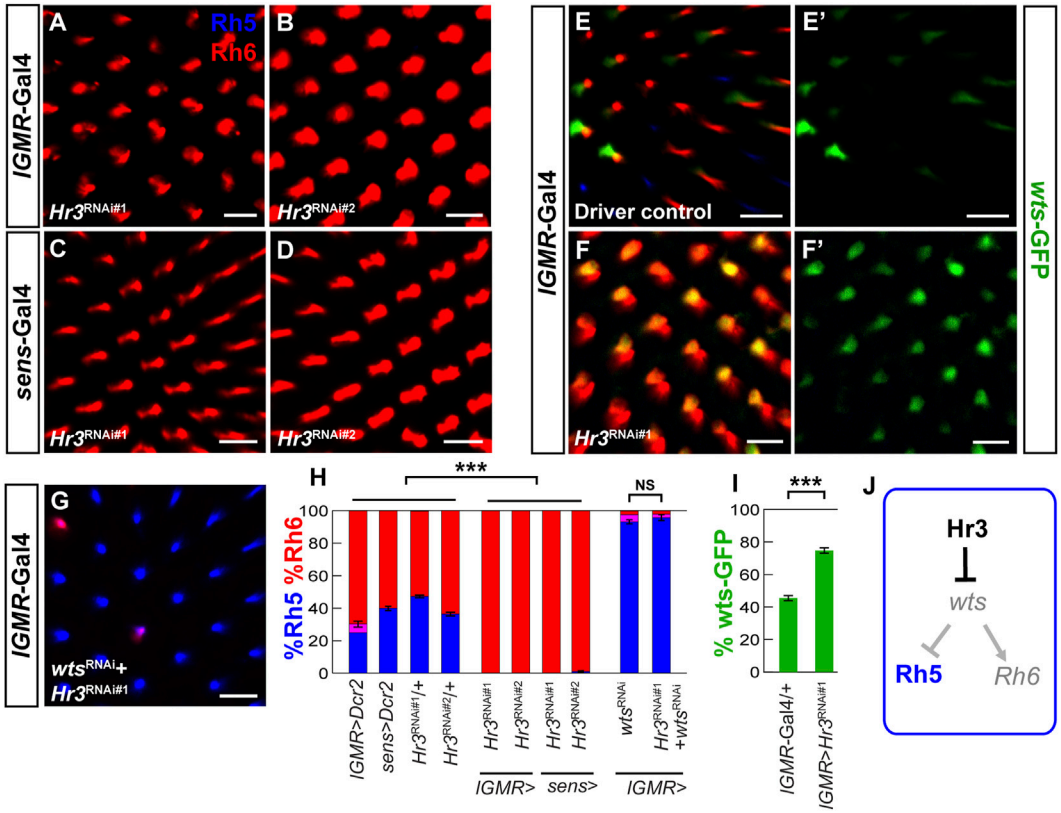


FIGURE 6
Hr3/RORβ is required to repress *warts* and to specify Rh5 fate.**(A,B)** Pan-photoreceptor knockdown of *Hr3* using two separate RNAi constructs, TRiP$^{\#27253}$ (*Hr3*$^{RNAi\#1}$) and TRiP$^{\#27254}$ (*Hr3*$^{RNAi\#2}$) causes a complete loss of Rh5 and gain of Rh6. **(C,D)** R8 photoreceptor knockdown with two separate RNAi constructs also causes a dramatic loss of Rh5 and gain of Rh6. **(E,E')** In the heterozygous *lGMR-Gal4/+* driver control, the *wts*-GFP transcriptional reporter is expressed in most Rh6 photoreceptors. **(F, F')** Pan-photoreceptor knockdown of *Hr3* causes a de-repression of the *wts*-GFP reporter together with Rh6. **(G)** Pan-photoreceptor knockdown of both *Hr3* and *wts* causes a gain of Rh5 and loss of Rh6, resembling the *wts* knockdown phenotype. All scale bars, 10 μm. **(H)** Quantification of R8 subtypes in controls and *Hr3* knockdowns. Mean %Rh6 was compared among genotypes with an ANOVA and a *post hoc* Tukey HSD Test; ***$p < 0.0001$. 5-8 retinas were scored for each genotype. **(I)** Quantification of the GFP-expressing R8 photoreceptors in the driver control and *Hr3* knockdown. Mean %*wts*-GFP reporter expression in driver control vs. knockdown was compared with an ANOVA and a *post hoc* Tukey HSD Test; ***$p < 0.0001$. 6 retinas were analyzed for each genotype. **(J)** Schematic of Hr3 function in Rh5 photoreceptors: Hr3 represses *wts* and thereby promotes Rh5 fate.

## 3.6 Hr3 acts cell autonomously in R8 photoreceptors to promote blue-sensitive photoreceptor fate

In the developing mouse retina, the nuclear receptor RORβ and the transcription factor Otx2 activate Blimp-1 in retinal progenitor cells to repress bipolar interneuron fate and promote rod PR fate (Jia et al., 2009; Brzezinski et al., 2010; Katoh et al., 2010; Brzezinski et al., 2013; Wang et al., 2014; Goodson et al., 2020). Because the *Drosophila* ortholog of Otx2, Otd, is required for Rh5 fate (McDonald et al., 2010; Jukam et al., 2013), we asked whether the *Drosophila* ortholog of RORβ, the ecdysone-responsive Hormone Receptor 3 (Hr3) (Kageyama et al., 1997; Lam et al., 1999) is also required for Rh5 fate. Indeed, RNAi-mediated knockdown of *Hr3* with two different RNAi lines combined with the *lGMR-Gal4* driver (Figures 6A, B) or the *sens-Gal4* driver (Figures 6C, D) caused a nearly complete loss of Rh5 PRs and gain of Rh6 PRs. Next, we hypothesized that Hr3 represses the Hippo pathway in Rh5 PRs. Consistent with this hypothesis, *Hr3* knockdown caused a significant de-repression of the *wts*-GFP reporter (Figures 6E–F') and concomitant knockdown of *wts* reversed the *Hr3* knockdown phenotype (Figure 6G). As expected from the gain of *wts*, *Hr3* knockdown also caused a loss of *melt*-GFP reporter expression (Supplementary Figures S5A–C). Moreover, Hr3 significantly reduced *wts-hsp70-luc* reporter expression in *Drosophila* S2 cells, albeit to a lesser extent (~3 fold) than Blimp-1 (Supplementary Figure SD). In summary (Figures 6H, I), these data suggest that both Blimp-1 and Hr3 are cell autonomously required to specify Rh5 fate in R8 PRs by repressing *wts* (Figure 6J).

We next asked whether Hr3 is required for Blimp-1 expression. To this end, we performed RNAi-mediated knockdown of *Hr3* and assessed the expression of Blimp-1 in pupal PRs. While *Blimp-1* knockdown abolished Blimp-1 expression, *Hr3* knockdown did not affect Blimp-1 expression compared to the driver control (Supplementary Figures S5E–G'). Therefore, Hr3 is not required for Blimp-1 expression in pupal PRs. Taken together, these data suggest that Hr3 promotes Rh5 fate by acting in parallel with Blimp-1 to repress *wts* (Figure 7B).

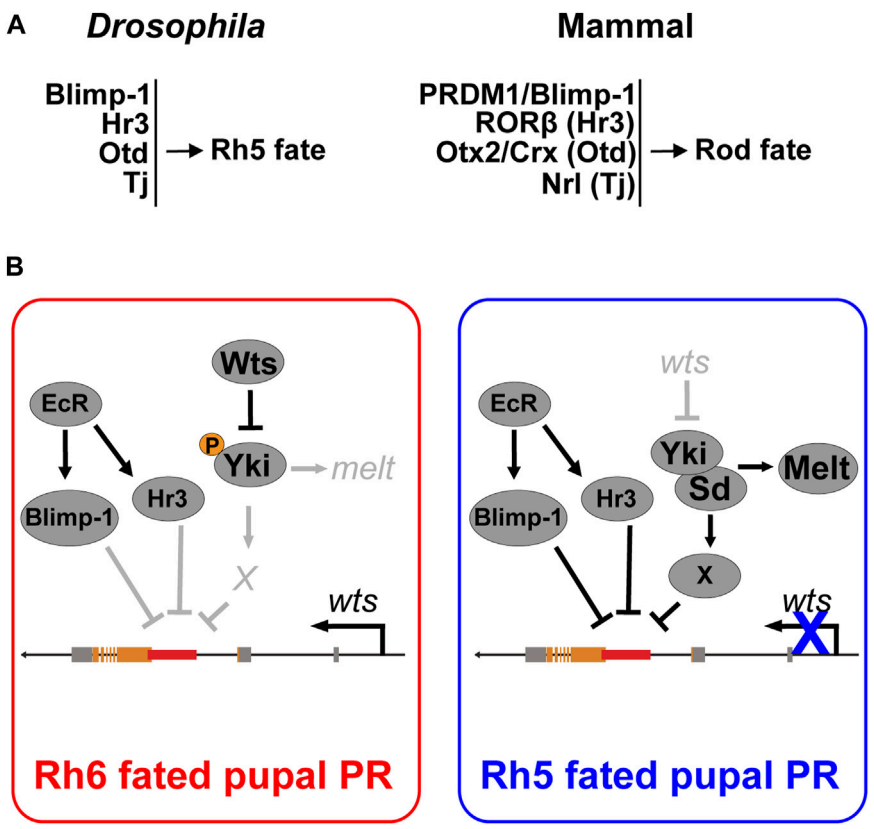


FIGURE 7
Cell fate decisions in the *Drosophila* and mammalian retina. **(A)** Summary of conserved transcription factors that are necessary to specify Rh5 photoreceptor fate in *Drosophila* and rod photoreceptor fate in mammals. **(B)** Model for Blimp-1's function as a permissive factor that represses *wts* at the transcriptional level in parallel with the ecdysone-responsive Hr3. Blimp-1 is expressed in pupal PRs in an EcR-dependent manner, but when Yki is not activated, Blimp-1 is not sufficient to repress *wts* and thereby gives rise to Rh6 fate. However, when Yki is transiently activated, possibly in response to the TGFβ signal from the distal R7 photoreceptor, Yki/Sd activate an unknown Rh5 subtype-specific transcription factor "X" that acts in combination with Blimp-1 and Hr3 to repress the *wts* enhancer, thereby silencing *wts* transcription and giving rise to robust Yki activation as well as Rh5 fate.

# 4 Discussion

## 4.1 Conserved transcription factors control binary cell fate decisions in the mammalian and the *Drosophila* retina

Here, we analyzed the regulatory mechanisms that specify two related *Drosophila* PR subtypes that express different color-sensing pigments (Rh5 or Rh6) in a mutually exclusive manner. We discovered that the *Drosophila* orthologs of the mammalian rod PR fate determinants Blimp-1/PRDM1 (Brzezinski et al., 2010; Katoh et al., 2010; Brzezinski et al., 2013; Goodson et al., 2020) and Hr3/RORβ (Wang et al., 2014) also play a role in terminal *Drosophila* PR specification, but in the cone-equivalent "inner" R8 PRs rather than the rod-equivalent "outer" R1-R6 PRs. In the binary R8 PR subtype decision, Blimp-1 and Hr3 promote the blue-sensitive/Rh5 PR fate and repress the green-sensitive/Rh6 PR fate by repressing *wts* and activating *melt*.

A previous study had unraveled that Otd, the ortholog of the mammalian PR fate determinants Otx2 and Crx (McDonald et al., 2010), and Tj, the ortholog of the mammalian rod fate determinant Nrl, are also required to specify Rh5 fate (Jukam et al., 2013). Otd and Tj form a coherent feedforward loop that allows Yki/Sd to activate *melt* and to repress *wts* (Jukam et al., 2013). In the mammalian retina, the Otd and Tj orthologs Otx2/Crx and Nrl, respectively, promote rod PR fate: Otx2 and Crx are both necessary for the expression of Nrl (Montana et al., 2011; Roger et al., 2014), which is necessary and sufficient for rod PR fate (Mears et al., 2001; Oh et al., 2007). *NRL* mutations have been associated with retinitis pigmentosa (Bessant et al., 1999) and mutations in Blimp-1, RORβ, Otx2, Crx, or Nrl are associated with a loss of rod PRs in mammals (Mears et al., 2001; Nishida et al., 2003; Daniele et al., 2005; Koike et al., 2007; Jia et al., 2009; Katoh et al., 2010). Likewise, loss of Blimp-1, Hr3, Otd, or Tj are each associated with a loss of blue-sensing PR fate (this study) (Jukam et al., 2013). Although the *Drosophila* eye and the mammalian eye seem to use different mechanisms for eye and PR development (Rister and Desplan, 2011; Cepko, 2015; Eldred et al., 2018), our current study and previous results (Jukam et al., 2013) suggest that a conserved set of transcription factors is used in both animal groups for specific binary PR fate decisions (Figure 7A).

While Blimp-1/PRDM1 and Hr3/RORβ promote rod fate in mammals and blue-sensitive/Rh5 PR fate in *Drosophila* respectively,

the mechanisms by which they regulate these cell fate decisions differ: in mammals, Hr3/RORβ is required to activate *Blimp-1/PRDM1* to repress bipolar fate and specify rod fate (Wang et al., 2014). However, in developing *Drosophila* PRs, Hr3 does not regulate *Blimp-1* expression (Supplementary Figures SE–G') but rather acts in parallel with Blimp-1 to repress *wts*. Given that conserved Blimp-1 motifs are required to repress *wts* in blue-sensitive/Rh5 PRs and Blimp-1 represses a *wts-hsp70-luc* reporter *in vitro* (Figures 3B–D), it is likely that Blimp-1 represses the *wts* enhancer directly. Since we did not find conserved Hr3 motifs in the *wts* enhancer, future studies will have to analyze the *in vivo* relevance of the Hr3-mediated *wts* repression that we found in cultured cells.

### 4.2 Blimp-1 acts as a permissive factor to promote blue-sensitive photoreceptor fate

Blimp-1/PRDM1 controls cell fate decisions in diverse developmental contexts (Bikoff et al., 2009). In pupal *Drosophila* PRs, Blimp-1 expression is ecdysone-dependent and regulates the terminal differentiation of the eye non-autonomously in non-neuronal cells (Wang et al., 2022). In the current study, we revealed a novel cell autonomous role of Blimp-1 in the terminal differentiation of color-sensing PR neurons. Blue-sensitive PR fate requires ecdysone signaling (EcR) and the ecdysone-responsive regulators Blimp-1 and Hr3, which both act to promote Rh5 PR fate. In contrast, in the larval fat body, Blimp-1 and Hr3 play antagonistic roles in regulating the regulatory gene *ftz-f1* to control pupation timing: Blimp1 represses *ftz-f1*, while Hr3 activates *ftz-f1* (Kageyama et al., 1997; Lam et al., 1999; Agawa et al., 2007).

The R8 PR specification network involves several permissive transcription factors that are not restricted to one of the two subtypes. Blimp-1 is transiently expressed during the early differentiation of both R8 PR subtypes, where it on the one hand represses *wts* in Rh5-fated PRs but on the other hand permits *wts* expression in Rh6-fated PRs. Likewise, Otd and Tj are expressed in both Rh5- and Rh6-fated PRs and act as permissive factors for Rh5 fate. Yki/Sd are unable to activate *melt* in the absence of Otd or Tj, or to activate *Rh5* in the absence of Otd (Jukam et al., 2013). However, Tj and Otd are not sufficient to activate *melt* in the absence of Yki or Sd, and Otd is not sufficient to activate *Rh5* (Jukam et al., 2013). Therefore, the conserved PR fate specification module is required to establish a post-mitotic context wherein *melt* and *wts* can function as a bi-stable switch to rewire the Hippo pathway. The proposed context-specificity is consistent with the finding that Blimp-1 represses *wts* in the post-mitotic PR context, but not in the wing growth context, and that the intronic *wts* enhancer drives expression in Rh6 PRs but not in the wing disc.

Since Blimp-1 acts as a permissive factor that represses *wts* in Rh5-fated PRs, a possible regulatory scenario is that an unknown transcription factor is specifically expressed in the Rh5-fated PRs and acts in combination with Blimp-1 to repress *wts*, analogous to how Yki/Sd activate *melt* in combination with Otd and Tj. Since Yki is active in Rh5 PRs but not in Rh6 PRs (Jukam et al., 2013), another possibility is that Yki is transiently activated in Rh5-fated pupal PRs, and then acts in combination with Blimp-1 to repress *wts* transcriptionally, permanently inactivating the Hippo pathway to give rise to robust Yki activation and Rh5 fate. Alternatively, we propose a scenario that contains an intermediate step (Figure 7B) in which Yki/Sd activate an additional transcription factor that acts with Blimp-1 to repress *wts* in a combinatorial manner.

In conclusion, the *Drosophila* color PR subtype specification is an excellent model to study how terminal cell fate decisions mediate the differential expression of sensory receptor proteins in related subsets of sensory neurons. The analysis of the underlying mechanisms gives insights into how conserved transcription factors generate sensory neuron diversity and potentially inform treatments for diseases that affect specific sensory neuron types.

## Data availability statement

The original contributions presented in the study are included in the article/Supplementary Material, further inquiries can be directed to the corresponding author.

## Author contributions

JR and JB conceived the experiments, analyzed the data, and wrote the article. JR obtained financial support. JB, JR, SB, AP, MB, PB, RD, EN, GC, MT, and SS collected the data. All authors read and approved the final article.

## Funding

This work was supported by an R00/Pathway to Independence Award (R00EY023995) to JR from the NEI/NIH. The content is solely the responsibility of the authors and does not necessarily represent the official views of the NIH. The funders had no role in study design, data collection and analysis, decision to publish, or preparation of the manuscript. Funding to SGS was provided by the Swiss National Science foundation grant 310030_188471.

## Acknowledgments

We thank Steve Britt, Claude Desplan, and Sudipto Roy for antibodies, as well as Johannes Bischof and Konrad Basler (UZH) for the J36 landing site stock.

## Conflict of interest

The authors declare that the research was conducted in the absence of any commercial or financial relationships that could be construed as a potential conflict of interest.

## Publisher's note

reviewers. Any product that may be evaluated in this article, or claim that may be made by its manufacturer, is not guaranteed or endorsed by the publisher.

## Supplementary material

The Supplementary Material for this article can be found online at: https://www.frontiersin.org/articles/10.3389/fcell.2023.1058961/full#supplementary-material

### SUPPLEMENTARY FIGURE S1

Blimp-1 acts in mid-pupal R8 photoreceptors. **(A-F')** Confocal images of whole mounted retinas from different pupal timepoints stained with antibodies for Elav (red, photoreceptor nuclei) and Blimp-1 (blue). **(A,A')** Blimp-1 is weakly expressed in photoreceptors at 24 h after puparium formation. Note the partial overlap with the Elav nuclear marker (white arrow). Inset shows ommatidium of the arrowed photoreceptor nucleus. **(B,B')** Blimp-1 is strongly expressed at 48 h after puparium formation. White arrow indicates partial Blimp-1/Elav overlap; inset shows ommatidium of the arrowed photoreceptor nucleus. **(C,C')** Blimp-1 is absent in R8 photoreceptors at 72 h after puparium formation. **(D,D')** Blimp-1 is absent in adult R8 photoreceptors. **(E,E')** Blimp-1 expression at 48 h after puparium formation in the heterozygous *lGMR-Gal4; UAS-Dcr2* driver control. Note individual strong Blimp-1-positive nuclei (one example is indicated by white arrow). **(F,F')** Pan-photoreceptor knockdown of *Blimp-1* causes a loss of Blimp-1 staining. **(G–I,K,L)** Confocal images of whole mounted retinas from adult males raised at 29°C. **(G)** In driver control males with hemizygous *UAS-Dcr2* on the X chromosome and heterozygous *sens-Gal4* on the third chromosome, the ratio of Rh5:Rh6 is normal. **(H)** *Blimp-1* knockdown with two copies of *UAS-Blimp-1$^{RNAi\#1}$*, one copy of *sens-Gal4*, and hemizygous *UAS-Dcr2* causes a loss of Rh5 and gain of Rh6. **(I)** The Rh5: Rh6 ratio is normal in the homozygous *UAS-Blimp-1$^{RNAi\#1}$* control. **(J)** Quantification of R8 subtypes in controls and *Blimp-1* knockdown. Graph shows %R8 photoreceptors that express Rh5 exclusively (blue), Rh6 exclusively (red), or co-express Rh5 and Rh6 (magenta). Mean %Rh6 was compared among genotypes with an ANOVA and a post-hoc Tukey HSD Test; *** $p<0.0001$. 8 retinas were scored for each genotype. **(K)** Pan-photoreceptor expression of a constitutively active form of Babo (Babo*) causes a gain of Rh5 and loss of Rh6. **(L)** Pan-photoreceptor *Blimp-1* knockdown causes a loss of Rh5 and gain of Rh6 even with concomitant ectopic Babo* expression. All scale bars, 10 µm.

### SUPPLEMENTARY FIGURE S2

Blimp-1 knockdown de-represses *wts*-GFP. **(A)** Longitudinal section of the heterozygous *lGMR-Gal4* driver control with a *wts*-GFP transcriptional reporter. Note that *wts*-GFP overlaps with Rh6 and not with Rh5; white arrow indicates an Rh6-expressing photoreceptor that does not express *wts*-GFP, suggesting that the heterozygous *wts* reporter is not strong enough to label all Rh6 photoreceptors. **(A')** Rh5 channel. **(A'')** Rh6 channel. **(A''')** *wts*-GFP channel (grayscale). **(B)** Longitudinal section of *Blimp-1$^{RNAi\#1}$* expressed with *lGMR-Gal4* in the presence of a *wts*-GFP transcriptional reporter. There is a loss of Rh5 and gain of Rh6, and *wts*-GFP expands with Rh6. Morphological defects caused by *Blimp-1* knockdown made it difficult to observe the *wts*-GFP reporter; longitudinal sections circumvented this issue. Similar to the driver control, there were occasional instances of Rh6-expressing photoreceptors that did not express *wts*-GFP (white arrow). **(B')** Rh5 channel. **(B'')** Rh6 channel. **(B''')** *wts*-GFP channel (grayscale). **(C)** Quantification of the percentage of Rh6 photoreceptors (red outline) that co-express GFP (green bars) in the *lGMR-Gal4* driver control and *Blimp-1* knockdown, respectively. *%wts*-GFP/Rh6 co-expression was compared for the two genotypes with an ANOVA and a post-hoc Tukey HSD Test; *** $p<0.0001$. $N = 6$ retinas.

### SUPPLEMENTARY FIGURE S3

Conservation analysis of Blimp-1 motifs in the *wts* intron. **(A)** Alignments of the two Blimp-1 motif regions located in the intronic *wts* enhancer of ten *Drosophila* species. Blue indicates parts of the Blimp-1 motifs matching the consensus AGNGAAAG.

### SUPPLEMENTARY FIGURE S4

Blimp-1 does not regulate *wts* in a growth context. **(A,B)** Knockdown of *Blimp-1* using the eye driver *GMR-Gal4* did not affect adult eye size compared to the heterozygous driver control. Note the glossy eye phenotype caused by *Blimp-1* knockdown due to its role in corneal lens formation (Wang et al., 2022). **(C)** Concomitant knockdown of *wts* with *Blimp-1* using *GMR-Gal4* did not affect the glossy eye phenotype that is caused by *Blimp-1* knockdown. **(D,E)** Knockdown of *Blimp-1* using the wing disc driver *nubbin-Gal4* causes a dramatic decrease in wing size compared to the heterozygous driver control. Scale bars, 500 µm **(E)** The intronic *wts*-GFP reporter that is expressed in post-mitotic photoreceptors is not active in the third instar larval wing disc. White dashed line indicates the edge of the wing disc. Scale bar, 50 µm.

### SUPPLEMENTARY FIGURE S5

Hr3 regulates *melt* and *wts* but not Blimp-1. **(A)** In the heterozygous *lGMR-Gal4* driver control, *melt*-GFP is expressed in most Rh5 PRs and absent from Rh6 PRs. **(A')** GFP channel. White arrows indicate examples of Rh5/*melt*-GFP co-expression. **(B)** Knockdown of *Hr3* using *lGMR-Gal4* causes a loss of *melt*-GFP. **(B')** GFP channel. All scale bars, 10 µm. **(C)** Quantification of the GFP-expressing R8 photoreceptors in the driver control and *Hr3* knockdown. Mean *%melt*-GFP reporter expression in driver control *vs.* knockdown was compared with an ANOVA and a post-hoc Tukey HSD Test; *** $p<0.0001$. 6 retinas were analyzed for each genotype. **(D)** Dual luciferase reporter assay. The intronic *wts* reporter (*wts-hsp70-luc*) is active in S2 cells, but Hr3 represses it ($N = 3$). *Y*-axis: Relative Luminescence Units (RLU) of *wts-hsp70-luc* normalized to the Renilla luciferase control reporter (see Materials and methods). **(E-G')** Pupal retinas with *lGMR-Gal4* at 48 h after puparium formation stained for Blimp-1 (blue) and the nuclear marker Elav (red). **(E)** The heterozygous *lGMR-Gal4; UAS-Dcr2* driver control shows Blimp-1 expression with occasional strong nuclear localization. White arrow indicates nuclear Blimp-1. **(E')** Blimp-1 channel. **(F)** Pan-photoreceptor knockdown of *Blimp-1* abolishes Blimp-1 signal. **(F')** Blimp-1 channel. **(G)** Pan-photoreceptor knockdown of *Hr3* does not affect Blimp-1 expression. Moreover, there was occasional strong nuclear localization, similar to the driver control, suggesting that Hr3 is neither required for Blimp-1 expression, nor its nuclear localization. White arrow indicates nuclear Blimp-1. **(G')** Blimp-1 channel.

## References


Agawa, Y., Sarhan, M., Kageyama, Y., Akagi, K., Takai, M., Hashiyama, K., et al. (2007). Drosophila Blimp-1 is a transient transcriptional repressor that controls timing of the ecdysone-induced developmental pathway. *Mol. Cell Biol.* 27 (24), 8739–8747. doi:10.1128/MCB.01304-07

Akagi, K., Sarhan, M., Sultan, A. R., Nishida, H., Koie, A., Nakayama, T., et al. (2016). A biological timer in the fat body comprising Blimp-1, βFtz-f1 and Shade regulates pupation timing in *Drosophila melanogaster*. *Development* 143 (13), 2410–2416. doi:10.1242/dev.133595

Akagi, K., and Ueda, H. (2011). Regulatory mechanisms of ecdysone-inducible Blimp-1 encoding a transcriptional repressor that is important for the prepupal development in Drosophila. *Dev. Growth Differ.* 53 (5), 697–703. doi:10.1111/j.1440-169X.2011.01276.x

Ancelin, K., Lange, U. C., Hajkova, P., Schneider, R., Bannister, A. J., Kouzarides, T., et al. (2006). Blimp1 associates with Prmt5 and directs histone arginine methylation in mouse germ cells. *Nat. Cell Biol.* 8 (6), 623–630. doi:10.1038/ncb1413

Bessant, D. A., Payne, A. M., Mitton, K. P., Wang, Q. L., Swain, P. K., Plant, C., et al. (1999). A mutation in NRL is associated with autosomal dominant retinitis pigmentosa. *Nat. Genet.* 21 (4), 355–356. doi:10.1038/7678

Bikoff, E. K., Morgan, M. A., and Robertson, E. J. (2009). An expanding job description for Blimp-1/PRDM1. *Curr. Opin. Genet. Dev.* 19 (4), 379–385. doi:10.1016/j.gde.2009.05.005

Bischof, J., Maeda, R. K., Hediger, M., Karch, F., and Basler, K. (2007). An optimized transgenesis system for Drosophila using germ-line-specific phiC31 integrases. *Proc. Natl. Acad. Sci. U. S. A.* 104 (9), 3312–3317. doi:10.1073/pnas.0611511104

Brzezinski, J. A. t., Lamba, D. A., and Reh, T. A. (2010). Blimp1 controls photoreceptor versus bipolar cell fate choice during retinal development. *Development* 137 (4), 619–629. doi:10.1242/dev.043968

Brzezinski, J. A. t., Uoon Park, K., and Reh, T. A. (2013). Blimp1 (Prdm1) prevents re-specification of photoreceptors into retinal bipolar cells by restricting competence. *Dev. Biol.* 384 (2), 194–204. doi:10.1016/j.ydbio.2013.10.006

Cepko, C. L. (2015). The determination of rod and cone photoreceptor fate. *Annu. Rev. Vis. Sci.* 1, 211–234. doi:10.1146/annurev-vision-090814-121657

Chan, S. W., Lim, C. J., Chen, L., Chong, Y. F., Huang, C., Song, H., et al. (2011). The Hippo pathway in biological control and cancer development. *J. Cell Physiol.* 226 (4), 928–939. doi:10.1002/jcp.22435

Chou, W. H., Hall, K. J., Wilson, D. B., Wideman, C. L., Townson, S. M., Chadwell, L. V., et al. (1996). Identification of a novel Drosophila opsin reveals specific patterning of the R7 and R8 photoreceptor cells. *Neuron* 17 (6), 1101–1115. doi:10.1016/s0896-6273(00)80243-3

Chou, W. H., Huber, A., Bentrop, J., Schulz, S., Schwab, K., Chadwell, L. V., et al. (1999). Patterning of the R7 and R8 photoreceptor cells of Drosophila: Evidence for induced and default cell-fate specification. *Development* 126 (4), 607–616. doi:10.1242/dev.126.4.607

Clark, A. G., Eisen, M. B., Smith, D. R., Bergman, C. M., Oliver, B., Markow, T. A., et al. (2007). Evolution of genes and genomes on the Drosophila phylogeny. *Nature* 450 (7167), 203–218. doi:10.1038/nature06341

Daniele, L. L., Lillo, C., Lyubarsky, A. L., Nikonov, S. S., Philp, N., Mears, A. J., et al. (2005). Cone-like morphological, molecular, and electrophysiological features of the photoreceptors of the Nrl knockout mouse. *Invest. Ophthalmol. Vis. Sci.* 46 (6), 2156–2167. doi:10.1167/iovs.04-1427

Eldred, K. C., Hadyniak, S. E., Hussey, K. A., Brenerman, B., Zhang, P. W., Chamling, X., et al. (2018). Thyroid hormone signaling specifies cone subtypes in human retinal organoids. *Science* 362, eaau6348. doi:10.1126/science.aau6348

Engels, W. R., Johnson-Schlitz, D. M., Eggleston, W. B., and Sved, J. (1990). High-frequency P element loss in Drosophila is homolog dependent. *Cell* 62 (3), 515–525. doi:10.1016/0092-8674(90)90016-8

Fan, X., Abbott, T. E., Larson, D., and Chen, K. (2014). BreakDancer: Identification of genomic structural variation from paired-end read mapping. *Curr. Protoc. Bioinforma.* 45, 1–11. doi:10.1002/0471250953.bi1506s45

Fehon, R. G., Oren, T., LaJeunesse, D. R., Melby, T. E., and McCartney, B. M. (1997). Isolation of mutations in the Drosophila homologues of the human Neurofibromatosis 2 and yeast CDC42 genes using a simple and efficient reverse-genetic method. *Genetics* 146 (1), 245–252. doi:10.1093/genetics/146.1.245

Fichelson, P., Brigui, A., and Pichaud, F. (2012). Orthodenticle and Kruppel homolog 1 regulate Drosophila photoreceptor maturation. *Proc. Natl. Acad. Sci. U. S. A.* 109, 7893–7898. doi:10.1073/pnas.1120276109

Fortini, M. E., and Rubin, G. M. (1990). Analysis of cis-acting requirements of the Rh3 and Rh4 genes reveals a bipartite organization to rhodopsin promoters in *Drosophila melanogaster*. *Genes Dev.* 4 (3), 444–463. doi:10.1101/gad.4.3.444

Goodson, N. B., Park, K. U., Silver, J. S., Chiodo, V. A., Hauswirth, W. W., and Brzezinski, J. A. (2020). Prdm1 overexpression causes a photoreceptor fate-shift in nascent, but not mature, bipolar cells. *Dev. Biol.* 464 (2), 111–123. doi:10.1016/j.ydbio.2020.06.003

Halder, G., and Camargo, F. D. (2013). The hippo tumor suppressor network: From organ size control to stem cells and cancer. *Cancer Res.* 73 (21), 6389–6392. doi:10.1158/0008-5472.CAN-13-2392

Halder, G., and Johnson, R. L. (2011). Hippo signaling: Growth control and beyond. *Development* 138 (1), 9–22. doi:10.1242/dev.045500

Hamaratoglu, F., Willecke, M., Kango-Singh, M., Nolo, R., Hyun, E., Tao, C., et al. (2006). The tumour-suppressor genes NF2/Merlin and Expanded act through Hippo signalling to regulate cell proliferation and apoptosis. *Nat. Cell Biol.* 8 (1), 27–36. doi:10.1038/ncb1339

Hao, H., Kim, D. S., Klocke, B., Johnson, K. R., Cui, K., Gotoh, N., et al. (2012). Transcriptional regulation of rod photoreceptor homeostasis revealed by *in vivo* NRL targetome analysis. *PLoS Genet.* 8 (4), e1002649. doi:10.1371/journal.pgen.1002649

Harvey, K. F., and Hariharan, I. K. (2012). The hippo pathway. *Cold Spring Harb. Perspect. Biol.* 4, a011288. doi:10.1101/cshperspect.a011288

Hofer, H., Carroll, J., Neitz, J., Neitz, M., and Williams, D. R. (2005). Organization of the human trichromatic cone mosaic. *J. Neurosci.* 25 (42), 9669–9679. doi:10.1523/JNEUROSCI.2414-05.2005

Hsiao, H. Y., Johnston, R. J., Jukam, D., Vasiliauskas, D., Desplan, C., and Rister, J. (2012). Dissection and immunohistochemistry of larval, pupal and adult Drosophila retinas. *J. Vis. Exp.*, 4347. doi:10.3791/4347

Huang, J., Wu, S., Barrera, J., Matthews, K., and Pan, D. (2005). The Hippo signaling pathway coordinately regulates cell proliferation and apoptosis by inactivating Yorkie, the Drosophila Homolog of YAP. *Cell* 122 (3), 421–434. doi:10.1016/j.cell.2005.06.007

Jia, L., Oh, E. C., Ng, L., Srinivas, M., Brooks, M., Swaroop, A., et al. (2009). Retinoid-related orphan nuclear receptor RORbeta is an early-acting factor in rod photoreceptor development. *Proc. Natl. Acad. Sci. U. S. A.* 106 (41), 17534–17539. doi:10.1073/pnas.0902425106

Jukam, D., and Desplan, C. (2011). Binary regulation of Hippo pathway by Merlin/NF2, Kibra, Lgl, and Melted specifies and maintains postmitotic neuronal fate. *Dev. Cell* 21 (5), 874–887. doi:10.1016/j.devcel.2011.10.004

Jukam, D., Xie, B., Rister, J., Terrell, D., Charlton-Perkins, M., Pistillo, D., et al. (2013). Opposite feedbacks in the Hippo pathway for growth control and neural fate. *Science* 342 (6155), 1238016. doi:10.1126/science.1238016

Kageyama, Y., Masuda, S., Hirose, S., and Ueda, H. (1997). Temporal regulation of the mid-prepupal gene FTZ-F1: DHR3 early late gene product is one of the plural positive regulators. *Genes cells.* 2 (9), 559–569. doi:10.1046/j.1365-2443.1997.1460344.x

Katoh, K., Omori, Y., Onishi, A., Sato, S., Kondo, M., and Furukawa, T. (2010). Blimp1 suppresses Chx10 expression in differentiating retinal photoreceptor precursors to ensure proper photoreceptor development. *J. Neurosci.* 30 (19), 6515–6526. doi:10.1523/JNEUROSCI.0771-10.2010

Keller, A. D., and Maniatis, T. (1991). Identification and characterization of a novel repressor of beta-interferon gene expression. *Genes Dev.* 5 (5), 868–879. doi:10.1101/gad.5.5.868

Koike, C., Nishida, A., Ueno, S., Saito, H., Sanuki, R., Sato, S., et al. (2007). Functional roles of Otx2 transcription factor in postnatal mouse retinal development. *Mol. Cell Biol.* 27 (23), 8318–8329. doi:10.1128/MCB.01209-07

Kuo, T. C., and Calame, K. L. (2004). B lymphocyte-induced maturation protein (Blimp)-1, IFN regulatory factor (IRF)-1, and IRF-2 can bind to the same regulatory sites. *J. Immunol.* 173 (9), 5556–5563. doi:10.4049/jimmunol.173.9.5556

Lam, G., Hall, B. L., Bender, M., and Thummel, C. S. (1999). DHR3 is required for the prepupal-pupal transition and differentiation of adult structures during Drosophila metamorphosis. *Dev. Biol.* 212 (1), 204–216. doi:10.1006/dbio.1999.9343

McDonald, E. C., Xie, B., Workman, M., Charlton-Perkins, M., Terrell, D. A., Reischl, J., et al. (2010). Separable transcriptional regulatory domains within Otd control photoreceptor terminal differentiation events. *Dev. Biol.* 347 (1), 122–132. doi:10.1016/j.ydbio.2010.08.016

McGuire, S. E., Roman, G., and Davis, R. L. (2004). Gene expression systems in Drosophila: A synthesis of time and space. *Trends Genet.* 20 (8), 384–391. doi:10.1016/j.tig.2004.06.012

Mears, A. J., Kondo, M., Swain, P. K., Takada, Y., Bush, R. A., Saunders, T. L., et al. (2001). Nrl is required for rod photoreceptor development. *Nat. Genet.* 29 (4), 447–452. doi:10.1038/ng774

Mikeladze-Dvali, T., Wernet, M. F., Pistillo, D., Mazzoni, E. O., Teleman, A. A., Chen, Y. W., et al. (2005). The growth regulators warts/lats and melted interact in a bistable loop to specify opposite fates in Drosophila R8 photoreceptors. *Cell* 122 (5), 775–787. doi:10.1016/j.cell.2005.07.026

Montana, C. L., Lawrence, K. A., Williams, N. L., Tran, N. M., Peng, G. H., Chen, S., et al. (2011). Transcriptional regulation of neural retina leucine zipper (Nrl), a photoreceptor cell fate determinant. *J. Biol. Chem.* 286 (42), 36921–36931. doi:10.1074/jbc.M111.279026

Mouillet, J. F., Henrich, V. C., Lezzi, M., and Vogtli, M. (2001). Differential control of gene activity by isoforms A, B1 and B2 of the Drosophila ecdysone receptor. *Eur. J. Biochem.* 268 (6), 1811–1819. doi:10.1046/j.1432-1327.2001.02051.x

Nathans, J. (1999). The evolution and physiology of human color vision: Insights from molecular genetic studies of visual pigments. *Neuron* 24 (2), 299–312. doi:10.1016/s0896-6273(00)80845-4

Neto-Silva, R. M., de Beco, S., and Johnston, L. A. (2010). Evidence for a growth-stabilizing regulatory feedback mechanism between Myc and Yorkie, the Drosophila homolog of Yap. *Dev. Cell* 19 (4), 507–520. doi:10.1016/j.devcel.2010.09.009

Newsome, T. P., Asling, B., and Dickson, B. J. (2000). Analysis of Drosophila photoreceptor axon guidance in eye-specific mosaics. *Development* 127 (4), 851–860. doi:10.1242/dev.127.4.851

Ng, T., Yu, F., and Roy, S. (2006). A homologue of the vertebrate SET domain and zinc finger protein Blimp-1 regulates terminal differentiation of the tracheal system in the Drosophila embryo. *Dev. Genes Evol.* 216 (5), 243–252. doi:10.1007/s00427-005-0044-5

Nishida, A., Furukawa, A., Koike, C., Tano, Y., Aizawa, S., Matsuo, I., et al. (2003). Otx2 homeobox gene controls retinal photoreceptor cell fate and pineal gland development. *Nat. Neurosci.* 6 (12), 1255–1263. doi:10.1038/nn1155

O'Tousa, J. E., Baehr, W., Martin, R. L., Hirsh, J., Pak, W. L., and Applebury, M. L. (1985). The Drosophila ninaE gene encodes an opsin. *Cell* 40 (4), 839–850. doi:10.1016/0092-8674(85)90343-5

Oh, E. C., Khan, N., Novelli, E., Khanna, H., Strettoi, E., and Swaroop, A. (2007). Transformation of cone precursors to functional rod photoreceptors by bZIP transcription factor NRL. *Proc. Natl. Acad. Sci. U. S. A.* 104 (5), 1679–1684. doi:10.1073/pnas.0605934104

Oh, H., and Irvine, K. D. (2008). *In vivo* regulation of Yorkie phosphorylation and localization. *Development* 135 (6), 1081–1088. doi:10.1242/dev.015255

Ozturk-Colak, A., Stephan-Otto Attolini, C., Casanova, J., and Araujo, S. J. (2018). Blimp-1 mediates tracheal lumen maturation in *Drosophila melanogaster*. *Genetics* 210 (2), 653–663. doi:10.1534/genetics.118.301444

Papatsenko, D., Sheng, G., and Desplan, C. (1997). A new rhodopsin in R8 photoreceptors of Drosophila: Evidence for coordinate expression with Rh3 in R7 cells. *Development* 124 (9), 1665–1673. doi:10.1242/dev.124.9.1665

Pojer, J. M., Manning, S. A., Kroeger, B., Kondo, S., and Harvey, K. F. (2021). The Hippo pathway uses different machinery to control cell fate and organ size. *iScience* 24 (8), 102830. doi:10.1016/j.isci.2021.102830

Poupault, C., Choi, D., Lam-Kamath, K., Dewett, D., Razzaq, A., Bunker, J., et al. (2021). A combinatorial cis-regulatory logic restricts color-sensing Rhodopsins to specific photoreceptor subsets in Drosophila. *PLoS Genet.* 17 (6), e1009613. doi:10.1371/journal.pgen.1009613

Rister, J., and Desplan, C. (2011). The retinal mosaics of opsin expression in invertebrates and vertebrates. *Dev. Neurobiol.* 71 (12), 1212–1226. doi:10.1002/dneu.20905

Rister, J., Razzaq, A., Boodram, P., Desai, N., Tsanis, C., Chen, H., et al. (2015). Single-base pair differences in a shared motif determine differential Rhodopsin expression. *Science* 350 (6265), 1258–1261. doi:10.1126/science.aab3417

Roger, J. E., Hiriyanna, A., Gotoh, N., Hao, H., Cheng, D. F., Ratnapriya, R., et al. (2014). OTX2 loss causes rod differentiation defect in CRX-associated congenital blindness. *J. Clin. Invest.* 124 (2), 631–643. doi:10.1172/JCI72722

Roorda, A., and Williams, D. R. (1999). The arrangement of the three cone classes in the living human eye. *Nature* 397 (6719), 520–522. doi:10.1038/17383

Schubiger, M., Tomita, S., Sung, C., Robinow, S., and Truman, J. W. (2003). Isoform specific control of gene activity *in vivo* by the Drosophila ecdysone receptor. *Mech. Dev.* 120 (8), 909–918. doi:10.1016/s0925-4773(03)00134-5

Tahayato, A., Sonneville, R., Pichaud, F., Wernet, M. F., Papatsenko, D., Beaufils, P., et al. (2003). Otd/Crx, a dual regulator for the specification of ommatidia subtypes in the Drosophila retina. *Dev. Cell* 5 (3), 391–402. doi:10.1016/s1534-5807(03)00239-9

Teleman, A. A., Chen, Y. W., and Cohen, S. M. (2005). Drosophila Melted modulates FOXO and TOR activity. *Dev. Cell* 9 (2), 271–281. doi:10.1016/j.devcel.2005.07.004

Vandendries, E. R., Johnson, D., and Reinke, R. (1996). Orthodenticle is required for photoreceptor cell development in the Drosophila eye. *Dev. Biol.* 173 (1), 243–255. doi:10.1006/dbio.1996.0020

Wang, H., Morrison, C. A., Ghosh, N., Tea, J. S., Call, G. B., and Treisman, J. E. (2022). The Blimp-1 transcription factor acts in non-neuronal cells to regulate terminal differentiation of the Drosophila eye. *Development* 149 (7). doi:10.1242/dev.200217

Wang, S., Sengel, C., Emerson, M. M., and Cepko, C. L. (2014). A gene regulatory network controls the binary fate decision of rod and bipolar cells in the vertebrate retina. *Dev. Cell* 30 (5), 513–527. doi:10.1016/j.devcel.2014.07.018

Wells, B. S., Pistillo, D., Barnhart, E., and Desplan, C. (2017). Parallel Activin and BMP signaling coordinates R7/R8 photoreceptor subtype pairing in the stochastic Drosophila retina. *Elife* 6, e25301. doi:10.7554/eLife.25301

Wernet, M. F., Mazzoni, E. O., Celik, A., Duncan, D. M., Duncan, I., and Desplan, C. (2006). Stochastic spineless expression creates the retinal mosaic for colour vision. *Nature* 440 (7081), 174–180. doi:10.1038/nature04615

Xie, B., Morton, D. B., and Cook, T. A. (2019). Opposing transcriptional and post-transcriptional roles for Scalloped in binary Hippo-dependent neural fate decisions. *Dev. Biol.* 455 (1), 51–59. doi:10.1016/j.ydbio.2019.06.022

Yu, J., Angelin-Duclos, C., Greenwood, J., Liao, J., and Calame, K. (2000). Transcriptional repression by blimp-1 (PRDI-BF1) involves recruitment of histone deacetylase. *Mol. Cell Biol.* 20 (7), 2592–2603. doi:10.1128/mcb.20.7.2592-2603.2000

Yu, J., and Pan, D. (2018). Validating upstream regulators of Yorkie activity in Hippo signaling through scalloped-based genetic epistasis. *Development* 145 (4). doi:10.1242/dev.157545

Zeng, Q., and Hong, W. (2008). The emerging role of the hippo pathway in cell contact inhibition, organ size control, and cancer development in mammals. *Cancer Cell* 13 (3), 188–192. doi:10.1016/j.ccr.2008.02.011

Zhang, L., Yue, T., and Jiang, J. (2009). Hippo signaling pathway and organ size control. *Fly. (Austin)* 3 (1), 68–73. doi:10.4161/fly.3.1.7788

Zhao, B., Lei, Q. Y., and Guan, K. L. (2008). The hippo-YAP pathway: New connections between regulation of organ size and cancer. *Curr. Opin. Cell Biol.* 20 (6), 638–646. doi:10.1016/j.ceb.2008.10.001

Zhu, L. J., Christensen, R. G., Kazemian, M., Hull, C. J., Enuameh, M. S., Basciotta, M. D., et al. (2011). FlyFactorSurvey: A database of Drosophila transcription factor binding specificities determined using the bacterial one-hybrid system. *Nucleic Acids Res.* 39, D111–D117. doi:10.1093/nar/gkq858

Zuker, C. S., Cowman, A. F., and Rubin, G. M. (1985). Isolation and structure of a rhodopsin gene from *D. melanogaster*. *Cell* 40 (4), 851–858. doi:10.1016/0092-8674(85)90344-7

frontiers | Frontiers in Cell and Developmental Biology

TYPE Review
PUBLISHED 06 April 2023
DOI 10.3389/fcell.2023.1151348



OPEN ACCESS

EDITED BY
Deepika Vasudevan,
University of Pittsburgh, United States

REVIEWED BY
Amit Singh,
University of Dayton, United States
Anadika Prasad,
University College London,
United Kingdom

*CORRESPONDENCE
Justin P. Kumar,
jkumar@indiana.edu

SPECIALTY SECTION
This article was submitted to Morphogenesis and Patterning, a section of the journal Frontiers in Cell and Developmental Biology

RECEIVED 26 January 2023
ACCEPTED 23 March 2023
PUBLISHED 06 April 2023

CITATION
Warren J and Kumar JP (2023), Patterning of the *Drosophila* retina by the morphogenetic furrow.
*Front. Cell Dev. Biol.* 11:1151348.
doi: 10.3389/fcell.2023.1151348



# Patterning of the *Drosophila* retina by the morphogenetic furrow

Jasmine Warren and Justin P. Kumar*

Department of Biology, Indiana University, Bloomington, IN, United States

Pattern formation is the process by which cells within a homogeneous epithelial sheet acquire distinctive fates depending upon their relative spatial position to each other. Several proposals, starting with Alan Turing's diffusion-reaction model, have been put forth over the last 70 years to describe how periodic patterns like those of vertebrate somites and skin hairs, mammalian molars, fish scales, and avian feather buds emerge during development. One of the best experimental systems for testing said models and identifying the gene regulatory networks that control pattern formation is the compound eye of the fruit fly, *Drosophila melanogaster*. Its cellular morphogenesis has been extensively studied for more than a century and hundreds of mutants that affect its development have been isolated. In this review we will focus on the morphogenetic furrow, a wave of differentiation that takes an initially homogeneous sheet of cells and converts it into an ordered array of unit eyes or ommatidia. Since the discovery of the furrow in 1976, positive and negative acting morphogens have been thought to be solely responsible for propagating the movement of the furrow across a motionless field of cells. However, a recent study has challenged this model and instead proposed that mechanical driven cell flow also contributes to retinal pattern formation. We will discuss both models and their impact on patterning.

KEYWORDS

***Drosophila*, eye, pattern formation, morphogenetic furrow, morphogen, diffusion-reaction, positional information, cell flow**

## Introduction

Once the fate of an initially homogeneous tissue has been specified, each cell must adopt a specialized fate—This is the process of pattern formation, a term coined by the great developmental biologist Lewis Wolpert. To explain how tissue patterning occurred, Wolpert formulated the concept of positional information (Figure 1). At its core, his model predicts that every cell can sense its relative location within an epithelium and adopt a fate that is appropriate for its position within the developing field (Wolpert, 1969). His thinking was influenced in part by the work of John Saunders who had demonstrated that the posterior margin of the chick wing bud, when transplanted to the anterior margin, would force the anterior domain into producing digits that were normally associated with the posterior half of the limb bud. As a result, a mirror-symmetry duplication of digits was generated across the anterior-posterior axis (Saunders and Gasseling, 1968). Wolpert proposed that the posterior region of the limb bud produced a long-range morphogen that established a concentration gradient across the entire posterior-anterior axis (Wolpert, 1969). He suggested that cells lying along this axis could sense and interpret negligible differences in morphogen titer or exposure time and this in turn would result in the specification of distinct cell fates (in this case, distinct digits). Support for Wolpert's ideas of patterning came from the discovery in both chick and mouse that Sonic hedgehog (Shh) is expressed within the posterior limb bud,

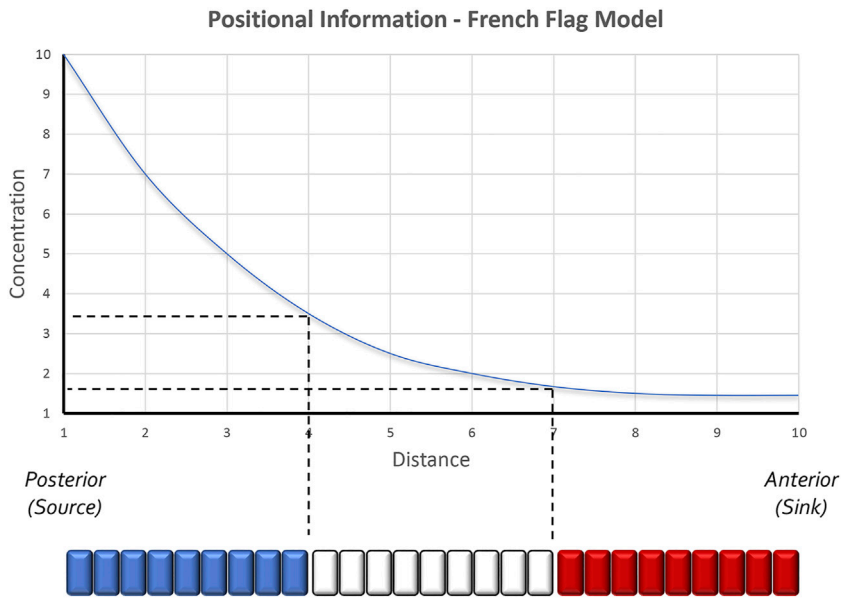


FIGURE 1
The positional information model of pattern formation. Based in part by the results of transplantation experiments conducted within the chick limb bud by John Saunders, Lewis Wolpert proposed that secreted morphogens form smooth gradients across developing tissues. Groups of cells along the gradient then capture unique amounts of the morphogen and as a result produce distinct structures. Colorized representations of this model are often represented as a French Flag where each color of the flag represents the conversion of a distinct morphogen concentration into a unique physical structure. Studies in the *Drosophila* embryo have further suggested that even 2 cells lying adjacent to each other can sense very small differences in morphogen concentrations and as a result execute different developmental programs. The schematic is adapted from Sharpe and Greene, 2015.

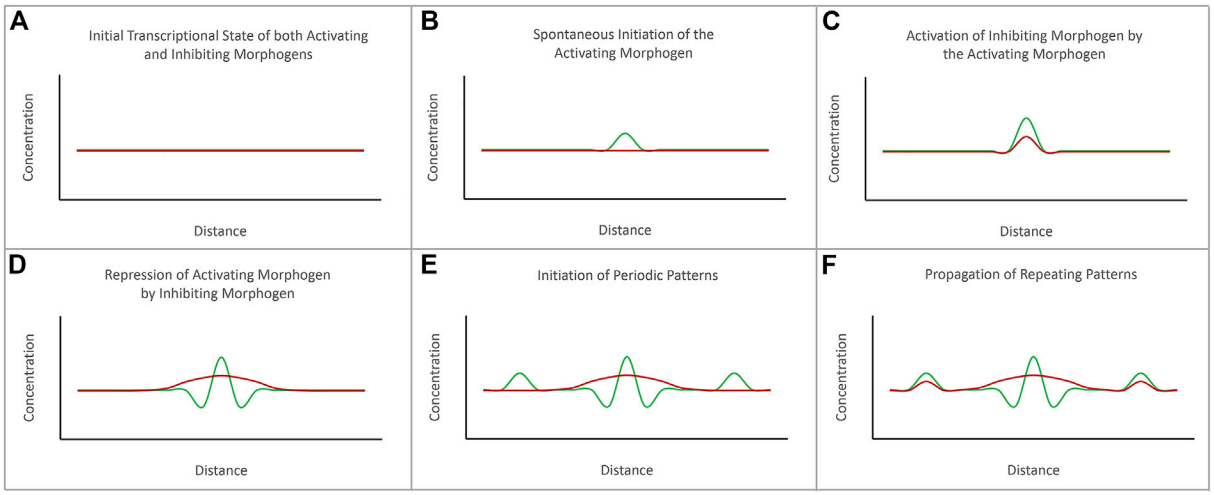


FIGURE 2
The diffusion-reaction model for the *de novo* initiation of repeated patterns. Alan Turing proposed that repeated patterns could spontaneously be generated *via* the combined activities of activating and inhibiting morphogens. **(A)** Prior to the initiation of pattern formation, the expression levels of both activating and inhibiting morphogens are at baseline levels. **(B)** The initiation of a pattern begins with the spontaneous initiation of expression of the activating morphogen. **(C)** As levels of the activating morphogen rises, it activates expression of the inhibiting morphogen. **(D)** The expression levels of the activating morphogen are higher than the inhibiting morphogen at the source. However, the inhibiting morphogen can diffuse further than the activating morphogen. **(E)** The inhibiting morphogen suppresses the expression of the activating morphogen further away from the source. However, just beyond the range of the inhibiting morphogen is seen spontaneous activation of the activating morphogens. **(F)** The process repeats itself to generate a periodically spaced pattern of repeated elements. The schematic is adapted from Sharpe and Green, 2015.

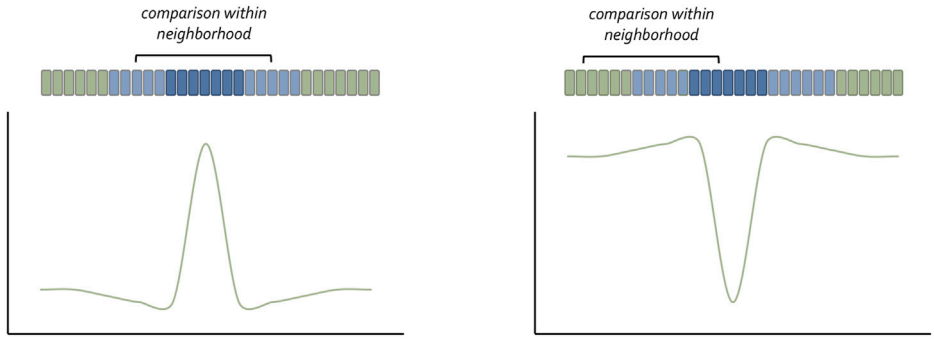


FIGURE 3
The neighborhood watch model for understanding how cells understand their position within a concentration gradient. Claudio Stern has recently proposed that a cell cannot interpret the absolute value of the morphogen it captures. Instead, it compares itself with its neighbors to make a relative calculation as to the amount of morphogen it has received. The schematic was adapted from Lee et al., 2022.

that its loss leads to the elimination of posterior digits, and that the induction of digit duplications that were seen in grafting experiments could be recapitulated if Shh expressing cells or beads soaked with Shh were transplanted into the anterior domain of the limb bud (Echelard et al., 1993; Riddle et al., 1993; Chang et al., 1994; Lopez-Martinez et al., 1995; Pagan et al., 1996; Yang et al., 1997). Additional support for Shh functioning as a morphogen came from experiments showing that the extent of digit duplications was directly proportional to the concentration of Shh (Yang et al., 1997). Manipulating exposure time demonstrated that the duration of Shh exposure is also important for limb patterning (Yang et al., 1997; Ahn and Joyner, 2004; Harfe et al., 2004).

Although Wolpert is most associated with the concept of morphogen gradients, many researchers in preceding decades had proposed that concentration gradients of secreted molecules could be the genesis for spatial patterns (Boveri, 1901; Morgan, 1901; Child, 1915; Runnstrom, 1929; Dalcq and Pasteels, 1938; Horstadius, 1939). Their ideas were based on the observation that changes in spatial patterns after tissue transplantation or extirpation were quantitative and thus might be subject to changes in the concentration of a diffusible substance. The relationship between Shh concentration and digit duplications in the chick limb (i.e., increasing Shh titer = more complete duplication) is a classic confirmation of the concentration gradient hypothesis (Yang et al., 1997). Interestingly, a recent synthesis has suggested a "neighborhood watch" model (Figure 2) in which cells interpret positional information not by autonomously sensing their address within a morphogen gradient but rather by comparing themselves to their neighbors (Lee et al., 2022). This innovative advance to Wolpert's original positional information model excellently explains how patterns can be generated across very large distances.

Alan Turing, the mathematician and World War II era codebreaker, was a notable contributor to the field of developmental biology through the publication of his diffusion-reaction model nearly two decades before Wolpert's model (Turing, 1952). He coined the term "morphogen" and proposed that the production of two morphogens (one that serves as an activator and one that serves as a repressor) could generate spatial patterns within a *de novo* homogeneous field by antagonizing each other's activity (Figure 3). But for the two signals to not simply cancel each other out, two criteria had to be met. First, the activator must be produced at a higher concentration than the repressor in order to overcome local repression. Second, the repressor needs to have long-range effects (diffuse fast and far) while the activator needs to be a short-range signal (diffuse slowly and over only a short distance). While he did not predict it, differences in the affinities for ligands and receptors can also play a role in limiting the reach of the activator. Turing's model also predicted that the size and shape of the generated pattern would correspond directly to the distribution of the activator morphogen gradients (i.e., the width of a spot or stripe would correspond to the distance that the activator morphogen diffused).

The diffusion-reaction model as proposed by Turing stands in sharp contrast to Wolpert's positional information model. Turing's interest was in explaining how a spatial pattern could be generated *de novo* from a homogenous tissue, while Wolpert was attempting to understand how patterns developed in a field in which pre-existing molecular heterogeneities already existed. Another important difference is that the diffusion-reaction model predicts that the morphogen itself produced the observed spatial pattern while the positional information model requires that cells sense and interpret the amount of morphogen to which they were exposed. In practical terms, Turing's proposal implied that the size and shape of the spatial pattern was directly correlated to the size and shape of the morphogen gradient. In contrast, Wolpert firmly believed that a smooth concentration gradient (high at the source to low at the edge of the sink) could generate any type of pattern. While these two models stand in apparent opposition to each other in the minds of many developmental biologists, a relatively recent synthesis has suggested potential avenues for how these two important ideas can be incorporated into a single model for pattern formation (Green and Sharpe, 2015).

A special circumstance in which the diffusion-reaction and positional information models have been particularly useful is the generation of simple repeated patterns. Some of the most studied examples include the scales of fishes (Bertin, 1944; Breder, 1947; Gunter, 1948), feather buds of birds (Holmes, 1935; Wessells, 1965),

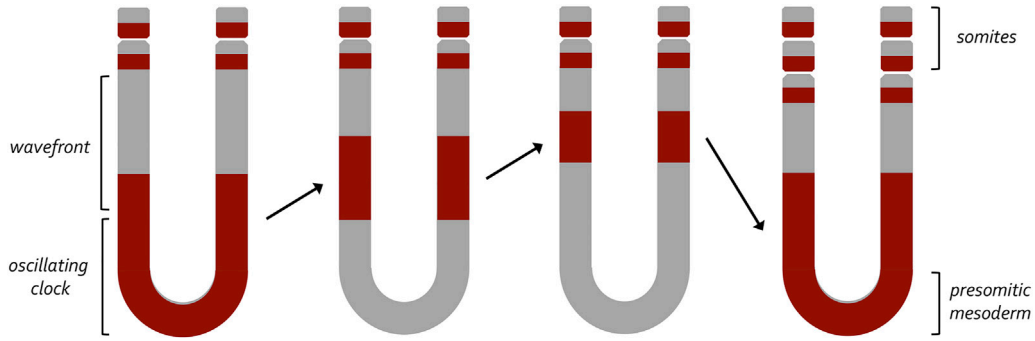


FIGURE 4
A clock and wavefront model for the generation of vertebrate somites. This model, developed by Johnathan Cooke and Erick Christopher Zeeman, proposed a two-component mechanism that would account for the periodic emergence of vertebrate somites. At its core it proposes that a wavefront of maturation (i.e., gene expression) transforms populations of undifferentiated cells into a pair of somites at periodic intervals. These periodic waves are triggered by an internal oscillator within the pre-somitic mesoderm (clock). Initially, it was thought that a similar internal oscillator could participate in the production of column of ommatidia within the fly eye. The variable rate at which these columns are now known to be produced suggests that an internal clock does not exist within the fly eye imaginal disc.

somites of vertebrates (Cooke, 1975; Cooke and Zeeman, 1976), molars and hair follicles of mammals (Gaunt, 1955; Straile, 1960; Mann, 1962; Lumsden, 1970; Mou et al., 2006; Prochazka et al., 2010; Cheng et al., 2014), and the unit eyes or ommatidia of the *Drosophila melanogaster* compound eye (Ready et al., 1976). The repeated nature of these systems means that a mutation which affects one element of the pattern affects the entire assembly. As such, mutations that disrupt repeated patterns have outsized effects that are easy to identify. Genetic screens and target gene knockdowns have shown that each of the above repeated patterns is disturbed by reductions in Shh or it orthologs (Heberlein et al., 1993; Ma et al., 1993; Fan and Tessier-Lavigne, 1994; Johnson et al., 1994; Hardcastle et al., 1998; St-Jacques et al., 1998; Chiang et al., 1999; Karlsson et al., 1999; Cobourne et al., 2004; Busby et al., 2020), which is entirely consistent with hypotheses put forth by Turing and Wolpert. Here, we will focus on how the morphogenetic furrow patterns the *Drosophila* eye. In this context, we will discuss the roles that several signaling pathways including Hedgehog (Hh), Decapentaplegic (Dpp), Wingless (Wg), Notch (N), and the EGF Receptor (EGFR) pathways play in regulating the initiation and progression of the morphogenetic furrow. We will also discuss how these signaling cascades generate interlocking columns of periodically spaced unit eyes.

The initial descriptions of the morphogenetic furrow by Donald Ready (Ready et al., 1976; Lebovitz and Ready, 1986; Wolff and Ready, 1991) and the subsequent identification of a role for the Hh morphogen in patterning by Kevin Moses and Ulrike Heberlein (Heberlein et al., 1993; Ma et al., 1993) suggested that diffusion-reaction and positional information models are likely sufficient to explain how the compound eye is patterned. Conspicuously absent from these discussions of the compound eye were models centered around mechanical forces contributing to the emergence of biological patterns. In general, mechanisms such as these were explicitly rejected by both Turing and Wolpert. However, a recent study from Richard Carthew has provided a compelling reason to consider the validity of mechanical forces such as cell flow in pattern formation. We will discuss the evidence supporting both chemical and mechanical force models for patterning.

## Structure of the adult *Drosophila* eye and the eye-antennal disc

The adult *Drosophila* eye is a simple nervous system comprised of approximately 750 ommatidia that are packed into a hexagonal array consisting of 32–34 interlocking vertical columns (Figure 4) (Ready et al., 1976). The compound eye is responsible for a wide range of visual and circadian behaviors (Grenacher, 1879; Exner, 1891; Mallock, 1894; Horridge, 1975; Strausfeld, 1976; Heisenberg and Buchner, 1977; Fischbach, 1979; Paulus, 1979; Land and Fernald, 1992; Vosshall and Young, 1995; Land, 1997; Veleri et al., 2007; Schlichting et al., 2016; Schnaitmann et al., 2020). These behaviors are augmented by the ocelli, which are three simple eyes located on the head vertex (Medioni, 1959; Fischbach and Reichert, 1978; Hu and Stark, 1980; Rieger et al., 2003; Umezaki and Tomioka, 2008; Krapp, 2009; Saint-Charles et al., 2016; Jean-Guillaume and Kumar, 2022). Each ommatidium within the compound eye contains eight photoreceptor neurons, four lens-secreting cone cells, a set of optically insulating pigment cells, and a mechanosensory bristle complex. Since each cell occupies a stereotyped position within the ommatidium, every unit eye is an exact replica of its neighbors (Waddington and Perry, 1960; Ready et al., 1976; Tomlinson and Ready, 1987; Cagan and Ready, 1989a). This is best seen in retinal sections of the adult retina with the only difference between ommatidia is that the photoreceptors within dorsal half of the eye are organized in a chiral pattern that is the mirror opposite to those within the ventral half of the eye. The two chiral versions of ommatidia meet at the equator, which is an invisible line that runs along the middle of the compound eye (Figure 4). Mutations that affect the development of individual cells within the ommatidium affect the overall structure of the

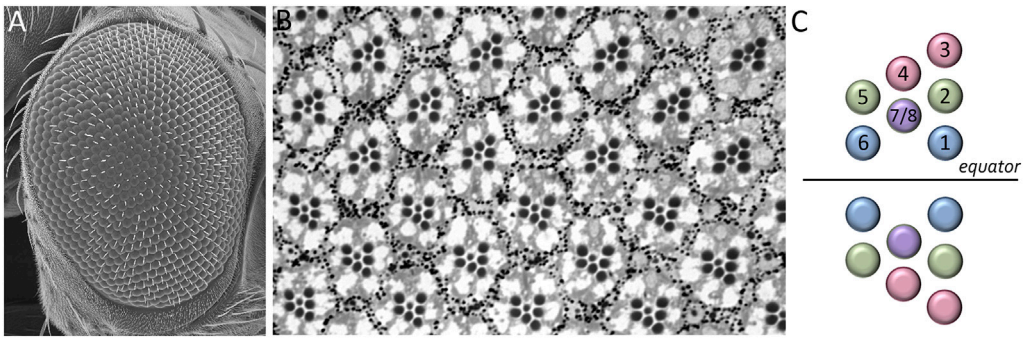


FIGURE 5
Structure of the adult *Drosophila* compound eye. **(A)** A scanning electron micrograph of the adult compound eye reveals that it consists of approximately 750 unit eyes or ommatidia that are organized into 32–34 columns. **(B)** A light microscope section of the adult retina shows that the eight photoreceptors that are contained within each unit eye are organized into an asymmetrical trapezoid pattern. The only difference between one unit eye and another is the chirality of the trapezoid within ommatidia. **(C)** A schematic showing the distinct chiral patterns of ommatidia within the dorsal and ventral compartments. These two compartments meet at the center of the eye which is called the equator.

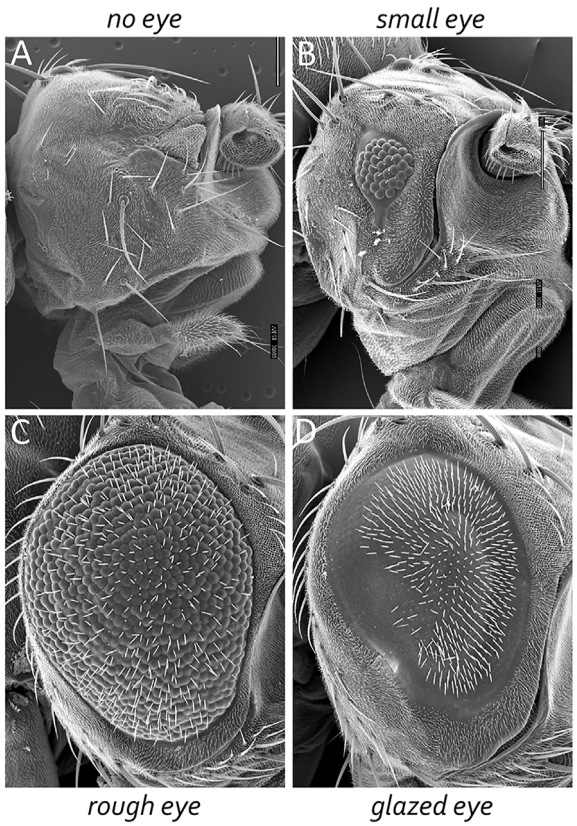


FIGURE 6
The *Drosophila* compound eye is a model system for identifying genes involved in development. Mutations that affect tissue specification, growth and proliferation, pattern formation, and cell fate specification can be identified by alterations in the crystalline-like nature of the adult compound eye. These mutant phenotypes can manifest themselves as **(A)** the absence of eyes, **(B)** small eyes, **(C)** large-roughened eyes, and **(D)** large-glazed looking eyes.

unit eye. In rare instances, a cell within a single ommatidium of a genetically normal fly will fail to develop correctly and this will manifest itself as a small, barely visible, local distortion in the array. In contrast, genetic mutations that affect the specification of one or more cells in every ommatidium can be identified by a "roughening" or "glazing" of the entire external surface and/or a reduction in the overall size of the compound eye. In some instances, the compound eye is completely lost and replaced with epidermal tissue (Figure 5).

The adult eye is derived from a sac-like structure called the eye-antennal imaginal disc (Krafka, 1924; Chen, 1929; Pilkington, 1942). In addition to the compound eye, it also gives rise to nearly all adult head structures including three simple eyes called ocelli, antennae, maxillary palps, and surrounding head epidermis (Figure 6) (Sturtevant, 1929; Bodenstein, 1938; Birmingham, 1942; Zalokar, 1943; Vogt, 1946; Schlapfer, 1963; Abaturova and Ginter, 1968; Ouweneel, 1970; Haynie and Bryant, 1986). The only structural feature of the adult head that is not derived from the eye-antennal disc is the proboscis (mouthpart), which arises from the labial and clypeo-labral imaginal discs (Wildermuth and Hadorn, 1965; Gehring and Seippel, 1967; Wildermuth, 1968; Kumar et al., 1979). The eye-antennal disc, like all other imaginal discs, is comprised of three cell layers—A sheet of columnar cells called the disc proper, a layer of squamous cells called the peripodial epithelium, and a strip of cuboidal cells referred to as the margin (Figure 7) (Atkins and Mardon, 2009; Weasner et al., 2020). The disc proper and peripodial epithelium are of the same overall size and shape and lie juxtaposed to each other. However, due to the differences in the size and shape of the two different cell types that comprise these epithelia, it is estimated that by the end of larval development the number of cells within the disc proper outnumbers those of the peripodial epithelium by a ratio of at least 20:1 (McClure and Schubiger, 2005). These two cell layers are joined together along their edges by the cuboidal margin cells (Figure 7). As such, the eye-antennal disc resembles a closed pillowcase. Enclosed within these

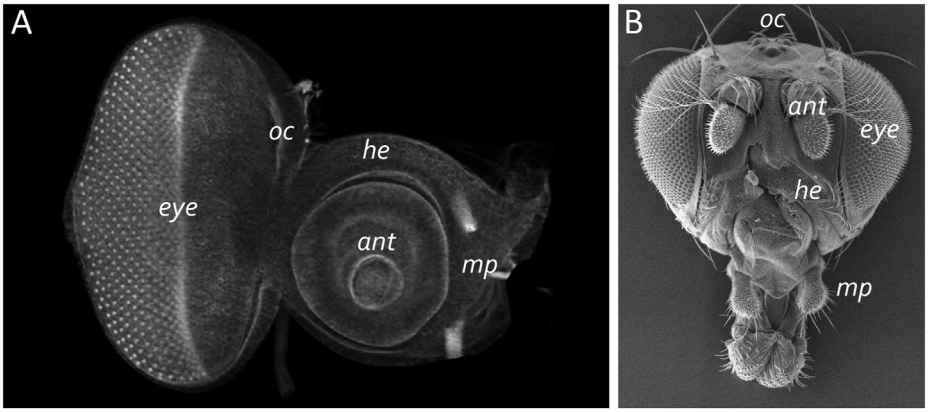


FIGURE 7
The eye-antennal disc gives rise to the adult head. **(A)** A light microscope image of a third larval instar eye-antennal disc. The disc is divided into several different neighborhoods that each give rise to a unique structure on the adult head. Each larva has two eye-antennal discs that are stitched together during pupal development. **(B)** A scanning electron micrograph of that adult head. The adult structures that are derived from the disc are labeled. oc, ocelli; ant, antenna; eye, compound eye; he, head epidermis; mp, maxillary palp.

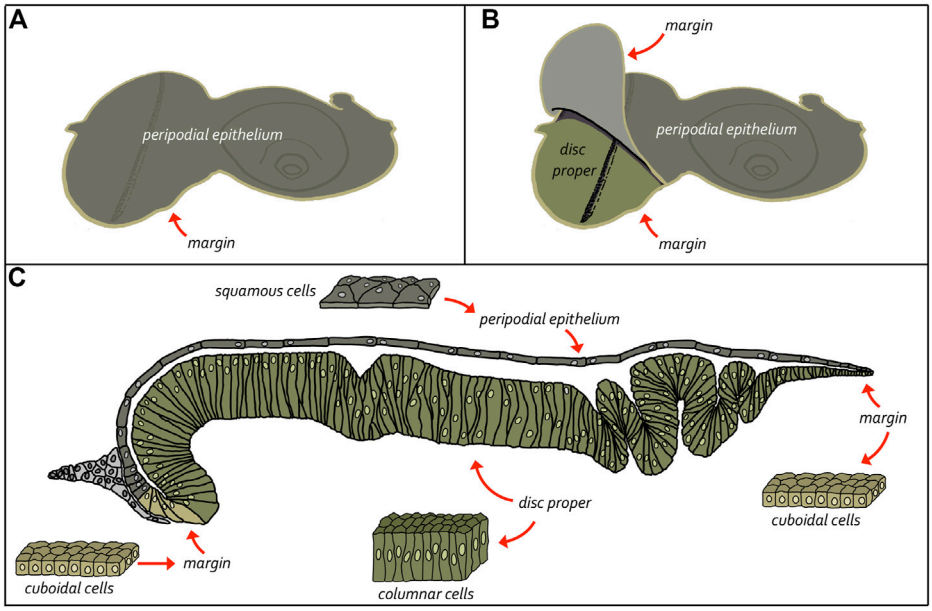


FIGURE 8
Structure of the eye-antennal disc. The eye-antennal disc is comprised of three different cell types. A layer of columnar cells comprises the disc proper while an overlying layer of squamous cells makes up the peripodial epithelium. These two equally sized tissues are joined together at the edges by a strip of cuboidal cells referred to as the margin. **(A, B)** Schematics showing the relationship between the disc proper and the peripodial epithelium. **(C)** Cross-section view of the eye-antennal disc showing the relative position of all three layers and the enclosed lumen. It also shows the cellular composition of the three cellular layers.

three cell layers is a small lumen (Auerbach, 1936) through which signaling molecules are thought to be trafficked either by simple diffusion or through two types of subcellular structures called translumenal extensions and cytonemes (Ramirez-Weber and Kornberg, 1999; Cho et al., 2000; Gibson and Schubiger, 2000; Gibson et al., 2002; Roy et al., 2011).

## Discovery of the morphogenetic furrow

The first recorded description of the eye-antennal disc can be found within August Weisman's monograph on the development of insects (Weismann, 1864). His camera lucida drawing of the disc includes all known major features including the morphogenetic

furrow, which in his drawing appears as a vertical line within the posterior oval domain of the disc. At the time, Weissman proposed that this line (which he probably envisioned as a physical fold in the tissue) demarcates the border between the developing eye and the antennal fields. Early histological methods, applied to the eye-antennal disc, appeared to confirm this prediction as developing ommatidia were only seen in the most posterior regions of the disc (Chen, 1929; Krafka, 1924; Medvedev, 1935; Steinberg, 1943a; b). This view went unchallenged for 112 years until Donald Ready and Seymour Benzer published their landmark paper on the cellular development of the *Drosophila* eye (Ready et al., 1976). They noticed that the "eye/antenna boundary" that Weissman proposed could be found at different physical positions during development. In younger discs the "line" was closer to the posterior edge of the eye field while it would be found nearer to the antenna in older discs. The shifting position of the "line" corresponded to a shift in the number of unit eyes—Younger discs had fewer ommatidia than older discs. From this it was immediately obvious that the "boundary line" was not the eye/antennal border at all but is instead the leading edge of a differentiating wave (Figure 8). They called it the morphogenetic furrow as its movement across the eye field appeared to transform a sea of undifferentiated cells into a periodic array of unit eyes and it appeared as an indentation in the epithelium (Ready et al., 1976).

## Dynamic properties of the morphogenetic furrow

If development is allowed to proceed at 25°C, the third and last larval instar stage begins at roughly 72 h after egg laying (AEL). At this stage the entire eye field is both unpatterned and undifferentiated. But approximately 6 h later at 78 h AEL the morphogenetic furrow leaves the posterior margin and begins its journey across the epithelium (Spratford and Kumar, 2013). Over the course of two and a half days the furrow patterns the retina by organizing thousands of undifferentiated cells into nearly three dozen columns of unit eyes that ultimately will make up the adult compound eye. The developing retina grows by accretion with each new column of ommatidia being added to the anterior face of the last column. The patterning of the eye resembles a growing crystal so much that, in the title of their original paper, Ready and Benzer referred to the compound eye as a "neurocrystalline lattice" (Ready et al., 1976). This level of perfection is achieved through tight regulatory control of pattern formation, cell fate specification, and planar cell polarity.

The differentiating wave was originally described as a furrow, in part, because scanning electron micrograph images of larval eye-antennal discs showed a dorso-ventral groove within the epithelium (Ready et al., 1976). Cross-sections of the disc showed that cells within the furrow were bottle-shaped with very narrow apical domains and enlarged basolateral sides. In comparison, cells on either side of the furrow are tall and columnar. Dramatic changes in cell shape, such are associated with a broad array of patterning events including tissue invagination, cell ingression, and cell extrusion. The transition from columnar to bottle-shaped cells result from the simultaneous dramatic constriction of the apical profile and the migration of nuclei towards the basal surface (Sawyer et al., 2010; Martin and Goldstein, 2014; Heer and Martin, 2017). If a cell making this transition maintains its cell-cell adhesion with its neighbors, then local deformation of the tissue will occur. In the case of the eye disc a stripe of cells along the dorso-ventral axis all constrict their apical profiles and plunge their nuclei in unison while preserving cell-cell adhesion with adjacent cells. This causes a depression in the tissue that we visualize as the morphogenetic furrow.

How and why does the furrow appear to move across the eye primordium? At the cellular level the movement of the furrow across the epithelium is akin to the "wave" done by fans within a sporting arena. At the beginning everyone in the stadium starts out sitting in their seats. For the wave to initiate, fans in one section will stand up while everyone else remains seated. For the wave to then propagate across the arena folks in the standing section all sit in unison while fans in the adjacent section simultaneously all stand up in concert. As this process repeats itself across all sections, it appears as if a wave is sweeping across the stadium. While the wave appears to move across the arena, the fans have, in reality, not moved from one section to another but instead they simply sit and/or stand in place. One can think of the moving furrow similarly. At the start of third larval instar all cells are fully extended with the apical profiles expanded. Then, at 78 h AEL, a stripe of cells at the posterior margin changes their shape in unison thereby creating a dorso-ventral groove at the posterior edge of the disc. A short time later when those cells extend themselves back into their original position, cells within an adjacent, anterior stripe concomitantly make the opposite decision and become bottle shaped. As this process repeats itself nearly three dozen times it appears as if the furrow rolls across the retinal primordium.

The developing compound eye is patterned by the morphogenetic furrow over the course of two and a half days. Several studies have provided differing accounts of how quickly the furrow produces a column of unit eyes as it traverses the eye disc. In the first study, the authors injected third instar larvae with radiolabeled thymidine which would be incorporated into the genomes of cells that were dividing at the time of injection. Cells that took up the radiolabeled thymidine would differentiate into photoreceptors and could be identified later in a retinal section of the adult compound eye. As such, one could determine when a particular column of ommatidia had been born by correlating the position of the labeled column in the adult with the time of radiolabeled thymidine injection within the larva. The authors then compared the position of labeled columns in adults to each other after larvae had been injected at different times during the third larval instar. From this it was proposed that a new column of ommatidia was generated every 120 min, and this timing did not vary across the developing eye (Campos-Ortega and Hofbauer, 1977). From this it appeared as if an intrinsic clock existed within the eye disc to produce columns of unit eyes at regular intervals. Support for this idea came from studies of somite development where a similar degree of periodicity was initially observed for the generation of somites in the frog, *Xenopus laevis* (Cooke, 1975) and then later for other species including snakes, zebrafish, chicken, and mice (Gomez et al., 2008). Johnathan Cook and E.C Zeeman proposed a clock and wavefront model to explain this periodicity (Figure 9). In this model a gradient of positional information (i.e., smooth

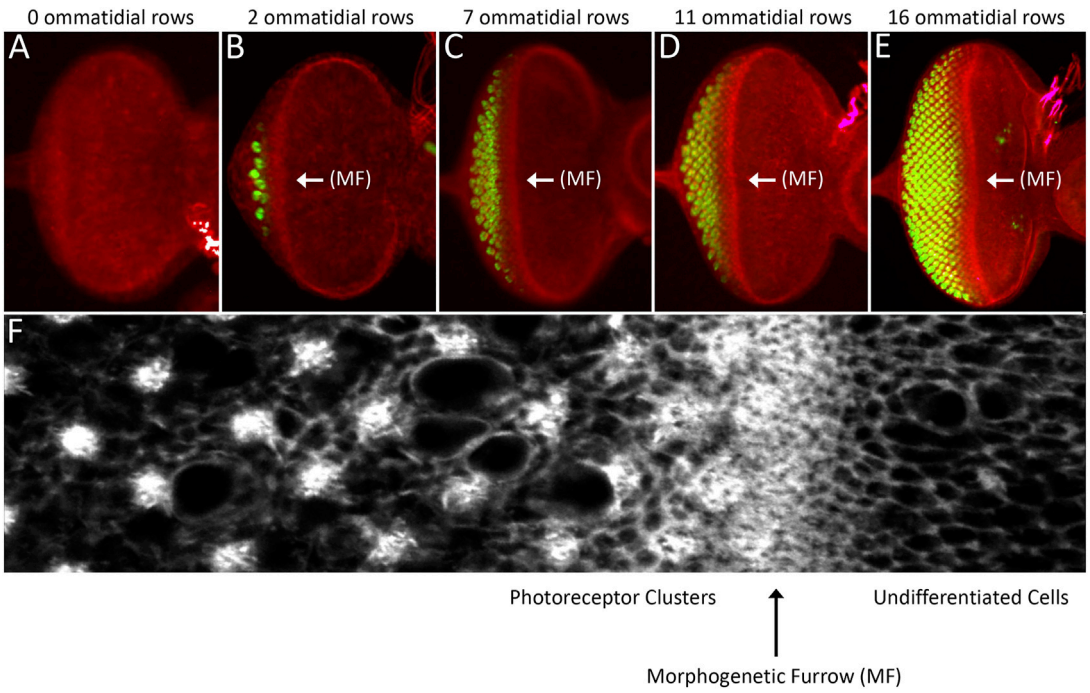


FIGURE 9
The morphogenetic furrow patterns the eye field during the third larval instar. **(A–E)** Light microscope images of different stage third larval instar eye discs showing the progression of the morphogenetic furrow. As the furrow passes across the epithelium, columns of photoreceptor clusters (ELAV, green) are produced in its wake. **(C)** High magnification view of the area surrounding the morphogenetic furrow. Cells ahead the furrow have large apical profiles and are dividing randomly. As the furrow approaches, cells constrict their apical profiles and enter G1 arrest. As cells exit the furrow groups of periodically spaced cells exist the cell cycle and form the first five photoreceptors of each unit eyes. Cells between these developing ommatidia will eventually undergo one final round of mitosis and give rise to the final three photoreceptor neuron and twelve non-neuronal accessory cells. **(F)** A high magnification image showing a region around the morphogenetic furrow.

morphogen gradients) would interact with an autonomously acting internal oscillator (i.e., cycling waves of gene expression) to produce new somites at regular intervals (Cooke and Zeeman, 1976; Saga and Takeda, 2001; Hubaud and Pourquie, 2014). Molecular evidence for the clock component first came when repeating waves of Hairy1 expression were observed within the pre-somitic mesoderm (PSM) during development (Palmeirim et al., 1997; Cooke, 1998). Likewise, support for the wavefront part of the model came from the observation that disruptions to the FGF and Wnt gradients within the PSM disrupt somite formation (Dubrulle et al., 2001; Sawada et al., 2001; Aulehla et al., 2003; Naiche et al., 2011). Similar waves and gradients of gene expression are observed in the developing eye.

A later attempt to document the velocity of the furrow suggested that patterning of the eye field was less uniform than previously thought. The authors first determined that a very brief pulse of Sevenless protein can restore R7 development to a narrow stripe of ommatidia—Sometimes just one or two columns wide. If the authors introduced a pause between two brief pulses, then the velocity of the furrow could be calculated by dividing the intervening time period by the number of ommatidial columns that lacked the R7 cell. From this method the furrow appeared to produce a column of ommatidia every 100 min within posterior regions of the eye which was consistent with the earlier report. However, in anterior half of the eye, the furrow appeared to accelerate and produce a column of unit eyes every 60–70 min (Basler and Hafen, 1989). These two methods indirectly measured the pace at which the retina is patterned. As such, it is not surprising that these studies came up with differing measurements.

A resolution to this issue came when an effort was made to directly measure the rate of patterning across the eye field. To do this, the number of ommatidial columns were directly counted in eye discs from third instar larvae that were carefully timed and dissected at 3-h intervals. From this effort, it appears that patterning is a very dynamic process with the generation time for producing a single ommatidial column ranging from 35 to 150 min. Ommatidial columns at the posterior and anterior edges of the eye field are produced more quickly than those within the center (Spratford and Kumar, 2013). Such differences in velocity suggest that molecular "accelerator and brake pedals" likely exist within the disc to either speed up or slow down the furrow depending upon its position within the disc. At least two brake pedals have been identified—One is a nuclear hormone receptor encoded by the *ultraspiracle* (*usp*) locus and the other is a helix-loop-helix transcription factor encoded by the *extramacrochaetae* (*emc*) gene (Brown et al., 1995; Zelhof et al., 1997; Spratford and Kumar, 2013). The removal of either *usp* or *emc* results in the acceleration of the furrow. In

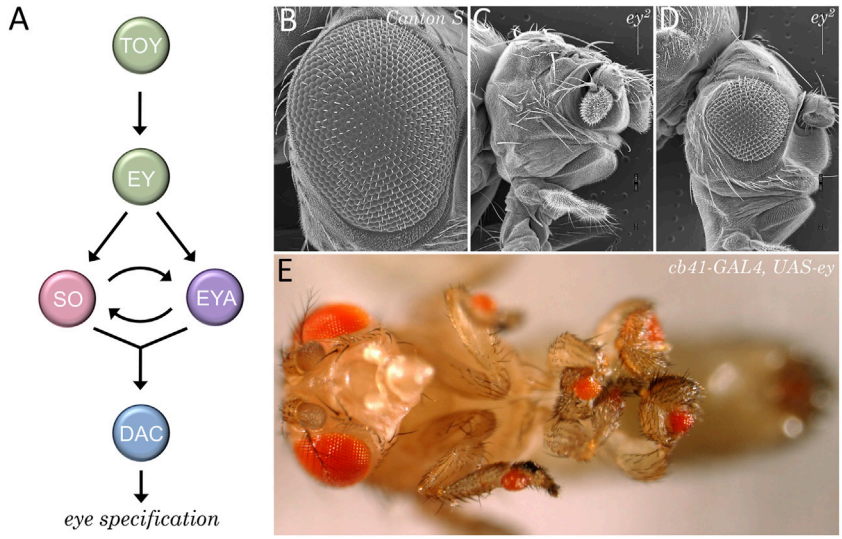


FIGURE 10
The retinal determination network specifies the fate of the eye. **(A)** The core members of the retinal determination network include the transcription factors Eyeless (Ey), Twin of Eyeless (Toy), Sine Oculis (So), Eyes Absent (Eya), and Dachshund (Dac). **(B–D)** Scanning electron micrographs of wild type **(B)** and eyeless loss-of-function mutants **(C, D)**. Disruptions to the retinal determination network result in either the loss or the severe reduction of the compound eye. **(E)** Forced expression of members of the retinal determination network can induce the transdetermination of non-ocular tissues such as legs, wings, halteres, antennae, and genitalia into eyes.

the instance of *emc*, its removal results in a furrow that moves approximately 30% faster than it does during normal development. Emc is able to control the pace of the ommatidial column production by regulating the levels of the activating form of Cubitus interruptus (Ci), the sole transcription factor of the Hh pathway (Spratford and Kumar, 2013). The variable speed at which ommatidial columns are laid down suggests that the mere presence of a repeated pattern in nature does not necessarily guarantee that it is generated with rhythmic periodicity or that it uses an oscillating molecular clock. In short, while somites are generated with a regular periodicity, such regularity does not appear to be a feature of compound eye development. Thus, one can think of the clock and wavefront mechanism as a very specific adaptation of the diffusion-reaction and positional informational paradigms that applies to the production of vertebrate somites.

Molecular accelerators and brakes are required to regulate the pace at which the furrow patterns the eye field because the eye continues to grow while it is being patterned and these two processes need to be synchronized so that 750 ommatidia are generated. If the rate at which the furrow patterns the disc outpaces the rate of cell proliferation, then the resulting adult eye will contain fewer unit eyes than required and will be disorganized. On the other hand, if the furrow moves too slowly then, even though there may be enough cells to make a normal sized eye, fewer than expected numbers of ommatidia will be created by the time larval development comes to an end. This failure to complete eye development on schedule could lead to developmental delays as the fly "waits" for the eye to finish patterning itself. It could also result in a smaller than normal eye if the fly fails to recognize the incomplete state of patterning and proceeds into the pupal stage of development. The furrow must reach the eye/antenna border before the head morphogenesis begins.

## Initiation of the morphogenetic furrow—Evidence for the positional information model

The positional information model predicts that a source of a secreted morphogen should be present at the posterior edge of the eye field. This is indeed the case in the vertebrate limb bud where Shh is expressed in and emanates from the posterior domain (Riddle et al., 1993; Chang et al., 1994). Around the same time of this discovery there was a lot of interest in understanding how the fly eye was patterned. In decades past, a considerable number of mutants with severely reduced or missing compound eyes had been identified. These mutants were starting to be examined and the underlying genes were being cloned. Several genes such as *eyeless* (*ey*), *eyes absent* (*eya*), *sine oculis* (*so*), and *dachshund* (*dac*) turned out to be core components of the retinal determination network (Kumar, 2010). In addition to the eye being lost in these mutants (Bonini et al., 1993; Cheyette et al., 1994; Hoge, 1915; Mardon et al., 1994; Milani, 1941; Serikaku and O'Tousa, 1994; Sved, 1986) forced expression of these genes in non-retinal tissues is sufficient to induce the formation of ectopic eyes within the antenna, leg, wing, and genital imaginal discs (Halder et al., 1995a; Bonini et al., 1997; Pignoni et al., 1997; Shen and Mardon, 1997). As such, these factors function as selector genes for the eye during the earliest stages of development (Figure 10).

The identification of the retinal determination network had a profound impact on our understanding of how fate of the eye is specified. Furthermore, the subsequent identification of these genes

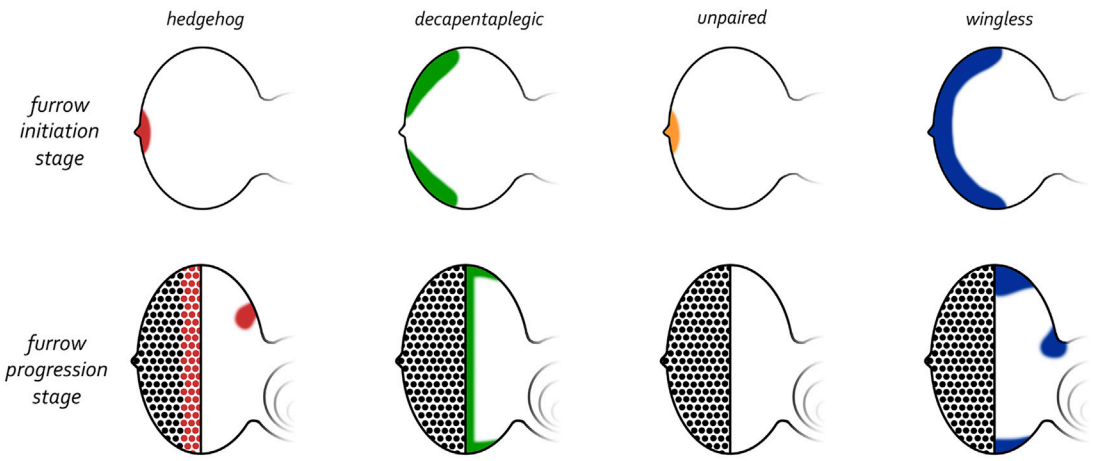


FIGURE 11
Expression patterns of morphogens that regulate patterning of the eye. (Top row) Early third larval instar just prior to the initiation of the morphogenetic furrow. Prior to the initiation of the furrow, *hedgehog* and *unpaired* are expressed at the firing point while *decapentaplegic* and *wingless* are along the posterior-lateral margins. (Bottom row) Mid third larval instar in which the morphogenetic furrow has progressed half-way across the eye field. As the furrow progresses across the eye field, the expression patterns of all four morphogens are altered dramatically. *Hedgehog* is expressed within the first few columns of photoreceptor clusters, *decapentaplegic* is expressed within cells of the furrow, and *wingless* is expressed ahead of the furrow along the posterior margins. Both *hedgehog* and *wingless* are also expressed within the developing ocellar field.

within the eyes of all seeing animals resulted in a paradigm shift in our view of how the eye evolved. The traditional view that the eye arose multiple times (Salvini-Plawen and Mayr, 1977; Land and Fernald, 1992) has been replaced with a new view that the eye originated just once during evolutionary history (Halder et al., 1995b; Gehring, 1996; Callaerts et al., 1997; Gehring and Ikeo, 1999).

Prior to the initiation of the morphogenetic furrow, *hh* is expressed at a single point along the posterior edge of the eye primordium (Figure 11) (Ma et al., 1993; Dominguez and Hafen, 1997; Borod and Heberlein, 1998). This is reminiscent of the Shh expression pattern in the limb bud and the asymmetry in *hh* expression within the disc at this stage is entirely consistent with Wolpert's positional information model. Two lines of evidence proved that the Hh pathway is required for the initiation of retinal patterning. First, a viable mutation within the *hh* locus implicates Hh signaling in the development of the eye. Like several retinal determination mutants, the $hh^{bar3}$ allele (renamed $hh^{1}$) has very small eyes—Roughly 150 out of a possible 750 ommatidia (Ives, 1950; Mohler, 1988; Renfranz and Benzer, 1989). This defect is caused by a deletion within an eye-specific enhancer element (Pauli et al., 2005; Rogers et al., 2005). It should be noted that in $hh^{1}$ mutants the expression of *hh* is severely reduced but not eliminated from the margin and/or photoreceptors neurons. Thus, pattern formation can be initiated and sustained for a short period of time before terminating. Second, if Hh signaling is completely disrupted at the posterior margin then the furrow is prevented from initiating (Dominguez and Hafen, 1997; Borod and Heberlein, 1998; Greenwood and Struhl, 1999; Curtiss and Mlodzik, 2000). Third, ectopic activation of the Hh pathway ahead of the advancing furrow induces undifferentiated cells to initiate ectopic retinal patterning (Chanut and Heberlein, 1995; Heberlein et al., 1995; Ma and Moses, 1995; Pan and Rubin, 1995; Strutt et al., 1995; Wehrli and Tomlinson, 1995; Fu and Baker, 2003). As such, the necessity and sufficiency of Hh signaling in eye development confirms that it can initiate development in a manner predicted by the positional information model.

Grafting experiments using the limb bud had suggested that Shh might function as a long-range morphogen with an activity range of as much as 200 um (approximately 20 cell diameters) (Honig, 1981; Summerbell and Honig, 1982; Riddle et al., 1993; Chang et al., 1994). Similarly, Hh establishes patterning over considerable distances across the *Drosophila* wing and leg imaginal discs (Diaz-Benjumea et al., 1994; Felsenfeld and Kennison, 1995). Initially, it was not clear if Hedgehog proteins exert their influence over such distances by directly acting as long-range gradient morphogens or by functioning as short-range inducers of other downstream signaling pathways. Evidence supporting the latter model came, in part, from studies of the wing and leg imaginal discs. In both tissues, Hh is expressed just within the posterior compartment. Several studies have demonstrated that in the wing and leg, Hh acts locally to activate *dpp* and *wg* within stripes of cells that lie adjacent to the *hh* expressing domain (Basler and Struhl, 1994; Capdevila and Guerrero, 1994; Tabata and Kornberg, 1994; Ingham and Fietz, 1995; Jiang and Struhl, 1995; Li et al., 1995; Pan and Rubin, 1995; Zecca et al., 1995). Their activation is direct as functional binding sites for Ci are present within *dpp* and *wg* disc enhancer elements (Von Ohlen et al., 1997; Muller and Basler, 2000; Parker et al., 2011). The Dpp and Wg signaling molecules in turn, then function as long-range gradient morphogens to pattern the anterior domain of the imaginal discs (Struhl and Basler, 1993; Zecca et al., 1995; 1996). (Nellen et al., 1996) These findings support the clear conclusion that Hh patterns the leg and wing imaginal discs by functioning as a short-range activator of secondary long-range morphogens.

At the start of the third larval instar *dpp* is expressed within domains along the posterior-lateral margins that flank *hh* expression

at the firing point (Figure 11). One of the few *dpp* mutants that survive to adulthood contains a deletion of an eye-specific enhancer ($dpp^{blk}$). In these mutants, expression of *dpp* along the margins is greatly reduced and as a result, the eyes of these mutants are very small with pattern formation failing to initiate at the dorsal and ventral margins (Borod and Heberlein, 1998; Chanut and Heberlein, 1997a; b). In contrast, if *dpp* expression is forcibly targeted to the anterior margin of the eye field (where it is normally absent), then it is sufficient to initiate a new morphogenetic furrow (Chanut and Heberlein, 1997b; Pignoni and Zipursky, 1997). Together these findings indicate that the Dpp pathway is integral to initiating pattern formation within the retina. In contrast to the wing and leg discs, Hh signaling is unlikely to activate *dpp* transcription within the eye as the onset of *dpp* expression predates that of *hh* during development (Ma et al., 1993; Hazelett et al., 1998; Chang et al., 2001). As we will see in in our discussion of furrow progression, the regulatory relationship between Hh and Dpp that is seen in the leg and wing will return to the retina during furrow progression.

The initiation of the morphogenetic furrow is a very complex regulatory process with several additional signaling pathways contributing to the kickstarting of pattern formation. One key morphogen is Unpaired (Upd), a ligand for the JAK/STAT pathway. At the late second larval instar Upd overlaps with Hh and is present just at the firing point (Figure 11) (Zeidler et al., 1999; Chao et al., 2004; Tsai and Sun, 2004). In contrast to Hh and Dpp, which function to directly promote the initiation of the furrow, Upd and the JAK/STAT pathway appear to control the timing of when the furrow is initiated. High levels of Upd at the firing point correlates with the loss of *wg* transcription, which, until this time, had been expressed along the posterior margin including the firing point (Ma and Moses, 1995; Treisman and Rubin, 1995; Hazelett et al., 1998). As we will see below, early in development the Wg pathway functions at the posterior margin to prevent temporally precocious initiation of the furrow. The JAK/STAT and Dpp pathways relieve this repression at the L2/L3 transition by inhibiting *wg* expression (Dominguez and Hafen, 1997; Ekas et al., 2006; Tsai et al., 2007). By expelling the Wg morphogen from the firing point and posterior margin, the Hh and Dpp cascades are free to initiate the morphogenetic furrow.

Comparing the temporal and spatial expression patterns of *hh*, *upd*, and *dpp* hinted that the initiation of the morphogenetic furrow could be divided into two phases with each chapter being controlled by unique combinations of signaling gradients. The first phase of initiation can be thought of as the primary ignition step. It takes place at the firing point, generates the first column of ommatidia, and is controlled by the Hh and JAK/STAT pathways. Mutations that affect these pathways at the firing point, as expected, often result in a complete block in pattern initiation—Imaginal discs and adult flies lack photoreceptor neurons in these instances (Dominguez and Hafen, 1997; Ekas et al., 2006). In addition to the Hh and JAK/STAT cascades, the EGF Receptor (EGFR) pathway appears to also participate in regulating this phase. Disruption of this pathway using a temperature sensitive allele ($Egfr^{tsla}$) identified a critical window where EGFR signaling is required for the initial phase of pattern formation. The furrow fails to initiate when pathway activity is eliminated during this window (Kumar and Moses, 2001). Furthermore, Hh appears to lie downstream of the EGF receptor cascade as its expression is lost when pathway activity is compromised. Furthermore, activation of EGFR pathway activity along the margins is sufficient to initiate new differentiating waves indicating that this pathway is both necessary and sufficient for the initial triggering of retinal patterning (Kumar and Moses, 2001).

The generation of each of the remaining columns of unit eyes can be conceptually thought of as being part of a second phase of pattern initiation. The production of each column involves the progression of the furrow through the middle of the disc (discussed below) *and* the re-initiation of the furrow at the margins. The combination of furrow progression and re-initiation results in a uniform straight wave of differentiation. At the margins, the second phase of patterning relies on the use of the Dpp morphogen, as lowering of Dpp signaling directly or *via* disruption of upstream regulators blocks its re-initiation from the margins (Chanut and Heberlein, 1997a; b; Hazelett et al., 1998; Pignoni et al., 1997). Likewise, blocking either EGFR and/or Notch signaling along the margins prevents the furrow from reinitiating as well (Kumar and Moses, 2001). In all three instances the furrow starts at the firing point and bulges outward—Much like toothpaste being squeezed out of a tube—Instead of appearing as a uniform line across the dorsal-ventral axis.

## Limiting pattern initiation to a single firing point

As we have seen above, prior to the initiation of pattern formation, expression of several morphogen ligands is limited to either the firing point (Hh, Upd) or the posterior margin (Dpp). This restriction is important as ectopic activation of these ligands ahead of the furrow or at any point along the dorsal, ventral, or anterior margins results in the initiation of ectopic differentiating waves (Chanut and Heberlein, 1995; 1997b; Heberlein et al., 1995; Ma and Moses, 1995; Pan and Rubin, 1995; Strutt et al., 1995; Wehrli and Tomlinson, 1995; Pignoni and Zipursky, 1997; Ekas et al., 2006; Tsai et al., 2007). The endogenous and ectopic patterning waves crash into each other within the middle of the eye field resulting in small, drastically disorganized eyes. Thus, the initiation of pattern formation, particularly in the context of an organized, repeated pattern, needs to be restricted to a single point within the epithelium. What is the mechanism(s) that restricts the sources of positional information? Initial insight into this question came from experiments in which temperature sensitive alleles of *wg* were used to inhibit pathway activity within the retina (Ma and Moses, 1995; Treisman and Rubin, 1995). Early in development, *wg* is expressed broadly along the entire posterior lateral margin (Figure 11). But at the end of the second larval instar *wg* expression is "pushed" off the posterior margin and is now restricted to the dorsal-lateral and ventral-lateral margins—These lie just ahead of and abut the *dpp* expression domain (Figure 11). The loss of Wg pathway activity at the start of the third larval instar results in the initiation of ectopic differentiating waves from the dorsal and ventral edges of the eye field. The resulting eyes are small, globe-like, and highly disorganized (Ma and Moses, 1995; Treisman and Rubin, 1995). In contrast, ectopic expression of *wg* within the eye field is sufficient to block both furrow initiation and progression

(Treisman and Rubin, 1995; Cadigan et al., 2002). Together, these results indicate that the roles of the Wg pathway is to first block precocious activation of the furrow from the posterior margin (at the L1 and L2 stages) and then later to prevent the emanation of ectopic furrows from the margins (during the L3).

Ectopic differentiating waves are also seeing igniting from the dorsal and ventral margins of eye fields that are mutant for *emc* (Spratford and Kumar, 2013). In *emc* mutants, *wg* expression is lost along the ventral margin suggesting that Emc functions to activate transcription of *wg*. Emc Is a HLH protein and its biochemical function is to bind to and sequester basic helix-loop-helix (bHLH) transcription factors away from their DNA consensus binding sites (Ellis et al., 1990; Garrell and Modolell, 1990; Van Doren et al., 1991). Thus, in this context, if Emc is directly regulating *wg* at the ventral margin, then it does so most likely by removing one or more bHLH transcriptional repressors from the locus. It is alternatively possible that Emc and its binding partner regulates an unknown upstream regulator of *wg*. Interestingly, this genetic relationship does not exist at the dorsal margin—Here *wg* expression remains unchanged suggesting that Emc and the Wg pathway function independently from each other to block differentiating waves from initiating at this margin. It is not clear why the regulatory relationship between Emc and Wg differs at the two margins. But interestingly, in two studies it is reported that the dorsal and ventral compartments of the compound eye are formed at different times and through different molecular mechanisms (Singh et al., 2002; Singh and Choi, 2003; Singh et al., 2004; Won et al., 2015). As such, patterning at the two margins (which border each compartment) could, by extension, be regulated by unique mechanisms.

## Progression of the morphogenetic furrow—Reaction-diffusion makes a temporary comeback

A central tenant of the positional information model and the more recent neighborhood watch model is that cells within a gradient adopt different fates based on the differences in morphogen concentration. This is certainly true of situations like the mammalian limb bud in which distinct types of digits are produced in response to declining amounts of Shh. However, in the developing eye, cells that are close to the original source of Hh (the firing point) as well as those that are located on other side of the disc all make the same decision—All are turned into identically constructed columns of ommatidia. How is this accomplished in the developing fly eye and are there similarities with other patterns in nature that contains repeated elements?

As the furrow begins to traverse the eye disc the expression patterns of both *hh* and *dpp* are completely reconfigured. Expression of *hh* at the firing point is lost and then reinitiated within all newly formed photoreceptor clusters. At the same time, *dpp* expression is extinguished at the margins and is instead activated within the furrow itself (Figure 11) (Heberlein et al., 1993; Ma et al., 1993). The relationship between these two genes now resembles what is seen in the wing in that *hh* and *dpp* expressing cells lie adjacent to each other. Furthermore, genetic studies suggested that Hh functions as a short-range morphogen to activate *dpp* expression within the furrow. Cells within the furrow constrict their apical profiles significantly which, as a result, increases the density of the Patched (Ptc) and Smoothened (Smo) surface receptors—These capture the Hh morphogen (Benlali et al., 2000; Corrigall et al., 2007; Schlichting and Dahmann, 2008). Strong activation of the Hh pathway within cells of the furrow results in the stabilization of the full-length activator form of Ci, which is the sole transducer of Hh signaling (Methot and Basler, 1999; 2001). It is thought to then activate several target genes within the furrow including *dpp* (Dominguez and Hafen, 1997; Greenwood and Struhl, 1999). However, other inputs into *dpp* must exist as it continues to be activated within the furrow even in the complete absence of Ci (Fu and Baker, 2003; Pappu et al., 2003). This is consistent with embryonic and wing development in which Ci appears dispensable for Hh pathway function (Hepker et al., 1999; Gallet et al., 2000). It should be noted that others have come to the opposite conclusion and report that there is an absolute requirement for Ci within the Hh signaling pathway (Methot and Basler, 2001).

Dpp, in turn, then exerts its effects over a longer range and directs a broad swathe of cells ahead of the furrow to prepare to enter a furrow-like state. As cells within the furrow initiate photoreceptor fate specifications, their nuclei rise, their apical profiles expand, they exit the cell cycle, downregulate *dpp* expression, and activate *hh* transcription. Likewise, cells that were once ahead of the furrow now enter G1 arrest, plunge their nuclei basally, constrict their apical profiles, and activate *dpp* expression in response to Hh activity from the newly created column of photoreceptor clusters. This process repeats itself until the furrow reaches the eye/antenna border. These rolling waves of *hh* and *dpp* expression ensure that all regions of the eye field are exposed to the same concentrations of both morphogens at some point during their life history. As such, in the developing eye, the Hh and Dpp pathways generate identical structures (32–34 columns of ommatidia) across the entire eye field. This is markedly different from the mouse limb bud or the leg/wing imaginal discs—In these tissues there is a concentration gradient across the epithelial field such that each cell receives a different dosage of each morphogen and contributes to the development of a unique structure.

When the Hh pathway is activated, the full-length isoform of Ci, which functions as an activator ($Ci^A$) is stabilized and prevented from being cleaved into the smaller $Ci^R$ isoform. In the wing disc the Hh morphogen gradient translates into opposing gradients of $Ci^A$ and $Ci^R$ proteins (Parker et al., 2011). Since both activator and repressor forms recognize the same DNA binding site, competition amongst these two forms results in the activation of different target genes along the Hh gradient. Regions with a high $Ci^A/Ci^R$ ratio (near the Hh source) activate *dpp* while cells with a high $Ci^R/Ci^A$ ratio (far from the Hh source) repress *dpp* (Parker et al., 2011). Surprisingly, it has shown that eye development proceeds normally in tissue that completely lacks Ci (Fu and Baker, 2003; Pappu et al., 2003). This finding suggests that, at least in the eye, the Hh pathway may not play a role in directly activating target genes in a concentration dependent manner. Instead, it suggests that the task of the upstream Hh pathway is to eliminate default repression that is caused by the inhibiting form of Ci ($Ci^R$). In essence, the role of the Hh pathway will be to prevent the $Ci^R$ from repressing target genes such as *dpp*. The conversion of the Hh pathway from a concentration gradient (in the wing) to a binary switch (in the

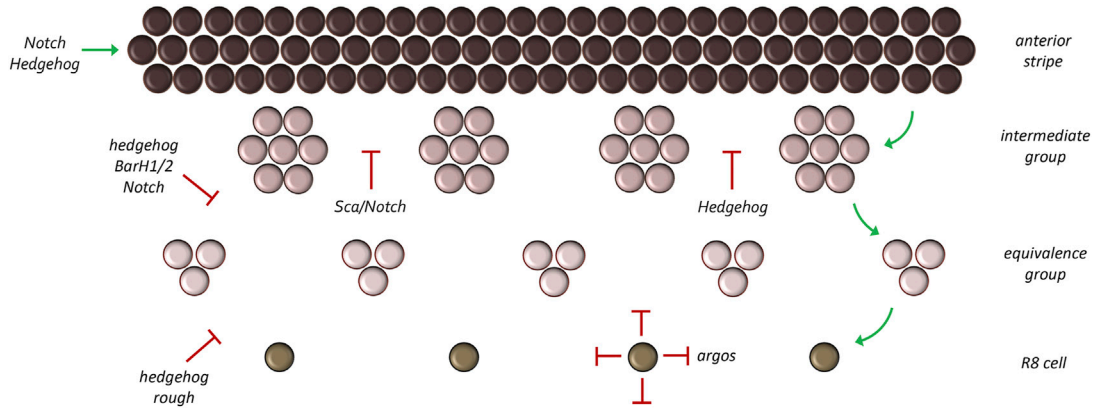


FIGURE 12
Refinement of the atonal expression pattern. Atonal is first activated in a broad stripe ahead and within the morphogenetic furrow. As development proceeds, this broad pattern is reduced to a column of single cells through a series of refinement steps. During the first step groups of 10–15 cells (called intermediate groups) retain atonal expression. In the second step, atonal expression within the intermediate groups will be eliminated from all but two to three cells—These are now called equivalence groups. In the last step, a single cell within the equivalence group will retain atonal expression. This cell, the R8 photoreceptor, is the founding cell of the ommatidium.

eye) may be essential for generating columns of repeated units as it might allow for the rapid activation and repression of *dpp*—This creates a tight, rolling wave of *dpp* expression.

Turing's reaction-diffusion model predicted that both activating and repressing signals are required to generate an array of periodically spaced repeated units. In the fly eye, how each unit eye is properly spaced within a column and how each column of unit eyes is appropriately spaced with respect to adjacent columns depends on generating a periodically spaced array of R8 photoreceptors within the eye disc. The R8 cell is the first cell of the unit eye to be specified and it serves as the founding cell for the rest of the ommatidium (Ready et al., 1976; Tomlinson and Ready, 1987; Wolff and Ready, 1991). A key regulatory molecule for R8 specification is the pro-neural transcription factor Atonal (Ato). The R8 photoreceptors fail to form in *ato* loss-of-function mutants and without the founding cell, the remaining photoreceptors, cone, and pigments cells of the ommatidium fail to develop as well (Jarman et al., 1994; Jarman et al., 1995). In contrast, ectopic *ato* expression either due to mis-expression of *ato* itself or through the manipulation of upstream regulators, results in the formation of ectopic R8 cells and a disruption of the ommatidial lattice (Baker et al., 1996; Dokucu et al., 1996; Frankfort et al., 2001; Pepple et al., 2008). Thus, a key step in producing the crystalline like array of unit eyes is to properly activate *ato* expression in a periodically spaced pattern.

Within the developing eye *ato* expression starts off in a broad pattern which is then progressively reduced to a column of evenly spaced single *ato* positive cells behind the furrow (Figure 12) (Jarman et al., 1994; Jarman et al., 1995; Baker et al., 1996; Dokucu et al., 1996; Frankfort and Mardon, 2002). *ato* is first expressed in a wide dorso-ventral stripe just anterior to and within the morphogenetic furrow. As these cells mature through the furrow and exit on the posterior side, *ato* expression is lost in small periodically spaced cell clusters. What remains are evenly spaced groups of approximately 10–15 Ato positive cells termed intermediate groups. As these cells continue to mature behind the furrow, *ato* expression is extinguished in all but two to three cells per cluster. These cells are considered the R8 equivalence group as each cell has the potential to develop into the R8 neuron. A final refinement takes place so that only a single cell is selected from this equivalence group to become an R8.

Initially, Hh signaling, first emanating from the firing point (during initiation) and later from photoreceptor clusters (during progression), plays a role in activating the broad stripe of *ato* expression (Strutt and Mlodzik, 1996; Dominguez and Hafen, 1997; Borod and Heberlein, 1998). This pattern is controlled by an enhancer element located at the 3′ end of the locus (Sun et al., 1998). As we have seen above, Hh signaling is unlikely to be directly activating target genes such as *ato*. Instead, Hh signaling most likely contributes to the activation of the broad *ato* stripe by eliminating the $Ci^R$ isoform. The independence of *ato* from direct Hh signaling is also seen within the Bolwig's organ, which is used by larvae as a phototactic organ (Suzuki and Saigo, 2000). Direct activation of *ato* in the compound eye comes from the concerted activities of several eye selector genes including Ey, So, and Eya (Tanaka-Matakatsu and Du, 2008; Zhou et al., 2014; Zhou et al., 2016). These are all expressed in broad overlapping stripes ahead of the morphogenetic furrow (Bonini et al., 1993; Cheyette et al., 1994; Quiring et al., 1994; Serikaku and O'Tousa, 1994). In addition to the RD network, the Notch pathway also contributes to the broad stripe of *ato* expression ahead and within the furrow by downregulating levels of the Emc and Hairy (H) transcription factors) which are themselves tasked with repressing *ato* (Brown et al., 1995; Baker and Yu, 1997; Ligoxygakis et al., 1998; Nagel and Preiss, 1999; Baonza and Freeman, 2001). In the eye the Hh and Notch pathways are connected to each other in that Hh signaling activates expression of the Delta ligand which then triggers Notch signaling (Baonza and Freeman, 2001).

As discussed above, the broad band of *ato* expressing cells must be refined into a column of evenly spaced single R8 cells. The process of reducing pro-neural gene expression to single cells is termed

lateral inhibition. At each refinement stage, cells that will eventually contribute to future ommatidia (intermediate groups, equivalence groups, single R8 cells) as well as the ommatidia themselves secrete inhibitory morphogens which prevent neighboring cells from becoming photoreceptor neurons. The requirement of inhibitory signals to generate a periodically spaced array of repeated units, be it ommatidia or feather buds, was predicted by Turing and is an essential component of his diffusion-reaction model. Within and behind the morphogenetic furrow, Hh signaling switches from being an activator of *ato* and now, indirectly aids in its repression (Dominguez, 1999). It does so through the default activation of the *BarH1/2* and *rough* (*ro*) genes. Although these transcriptional repressors were originally thought to be activated directly by the Hh signaling pathway (Chanut et al., 2000; Lim and Choi, 2004), the results of Nick Baker and Graeme Mardon suggest that their activation might result, in part, from the elimination of the $Ci^R$. Irrespective, both factors are expressed broadly within the furrow (Kimmel et al., 1990; Dokucu et al., 1996; Lim and Choi, 2003) and function to prune the broad band of *ato* expression into single R8 cells with BarH1/2 being responsible for the refinement to intermediate and equivalence groups and Ro for the pruning down to a single R8 cell. Loss of either repressor results in ectopic R8 formation (Heberlein et al., 1991; Dokucu et al., 1996; Chanut et al., 2000; Lim and Choi, 2003; 2004).

The Notch pathway is also redeployed for lateral inhibition and aids the Hh pathway in refining *ato* expression. Loss of Notch signaling during the different refinement stages results in extra R8 photoreceptors and abnormal spacing between ommatidia (Cagan and Ready, 1989b; Baker et al., 1990; Baker and Zitron, 1995). Since the distance between *ato* clusters is too great for Notch-Delta interactions to mediate lateral inhibition, a secreted morphogen with a much longer range is required. One such factor is encoded by the *scabrous* (*sca*) locus which encodes a secreted protein that shares homology with both fibrinogen-related and tenascin extracellular matrix proteins and binds to the Notch receptor (Lee et al., 1996; Powell et al., 2001). As with reductions in Notch signaling, loss-of-function mutations in *sca* also result in extra R8 cells that are too closely spaced to each other (Baker et al., 1990; Mlodzik et al., 1990; Ellis et al., 1994; Baker and Zitron, 1995; Gavish et al., 2016).

The Epidermal Growth Factor Receptor (EGFR) signaling cascade is an important contributor to the spacing of ommatidia but does so later than either the Hh or Notch pathways. EGFR signaling does not appear to play a role in R8 selection as both specification and spacing of this pioneer neuron are completely normal when the receptor is removed (Kumar et al., 1998; Yang and Baker, 2001). R8 specification and spacing are also unaffected if a ligand for the receptor, Spitz (Spi), is likewise removed (Tio and Moses, 1997). Spi contains a single EGF-like repeat and once secreted serves to activate the EGFR signaling cascade (Schweitzer et al., 1995b). Spi is not required for the specification of the R8 cell itself but must be secreted by the R8 for the recruitment of the R2/5 pair of photoreceptors. It is then made within and secreted from these cells to recruit the R3/4 photoreceptor pair. After the second mitotic wave generates a new pool of cells, Spi generated from the last pair of photoreceptors is sequentially used to first recruit the R1/6 and then the R7 neuron. Except for R8, all remaining photoreceptors within the ommatidium require Spi for their development (Freeman, 1994b; Tio et al., 1994; Tio and Moses, 1997). A similar requirement is seen for the EGF Receptor (Freeman, 1996; Kumar et al., 1998; Spencer et al., 1998; Yang and Baker, 2001).

To preserve the spacing between unit eyes, mechanisms must be in put in place to limit the range of Spi-EGFR interactions so that cells lying between ommatidial clusters (product of lateral inhibition) do not adopt a photoreceptor fate and join neighboring unit eyes. To do this, the same cells that secrete the activating Spi ligand also secrete a long-range inhibiting ligand called Argos (Aos), which inhibits EGFR signaling *via* two distinct biochemical mechanisms. At one level, Aos inhibits EGFR signaling by competing with Spi for binding to the receptor (Schweitzer et al., 1995a; Sawamoto et al., 1996; Jin et al., 2000). In a second layer of regulation, Aos also binds to Spi and sequesters it away from the receptor (Klein et al., 2004; Alvarado et al., 2006; Klein et al., 2008). Spi is made at higher levels than Aos but diffuses across a much smaller distance. As such, within the cluster of cells that will form the future ommatidium there is sufficient Spi to activate the EGFR pathway. However, since Aos can travel much farther than Spi, Aos-EGFR interactions are dominant in cells the lie between developing unit eyes. Amazingly, built into Turing's diffusion-reaction model was the understanding that these types of differences in levels and traveling distances of activating and inhibiting ligands are necessary for creating periodically spaced patterns (Figure 13). Loss-of-function mutations in *aos* result in cells that lie between clusters adopting a neuronal fate (Freeman et al., 1992). In contrast, over-expression of *aos* results in too few photoreceptor neurons (Freeman, 1994a; Sawamoto et al., 1994).

As a new column of ommatidia develops, the newly created photoreceptor neurons serve as a fresh source of Hh. As a result, a new band of *ato* expression is activated ahead of the morphogenetic furrow (which has advanced one column) and the entire process begins again. This process will repeat itself until the furrow reaches the eye/antennal border about half-way through the first day of pupal development. The Hh, Dpp, Notch, and EGFR signaling pathways function as the activating and repressing factors within the reaction-diffusion model and their combined activities ensure that an initially uniform field of undifferentiated cells are transformed into a crystalline array consisting of hundreds of identical unit eyes that are organized into several dozen interlocking columns.

## Mechanical cell movements dethrone diffusion-reaction

One of the hallmark features of the *Drosophila* eye is that significant cell movements and/or migrations do not take place during its development (Ready et al., 1976; Campos-Ortega and Hofbauer, 1977; Wolff and Ready, 1991). The lone exception is a set of glial cells that enter the eye field through the optic stalk (Choi and Benzer, 1994; Perez and Steller, 1996; Rangarajan et al., 1999). The cells of the eye field are thought to lie motionless while waves of morphogens pass over them like water rippling over

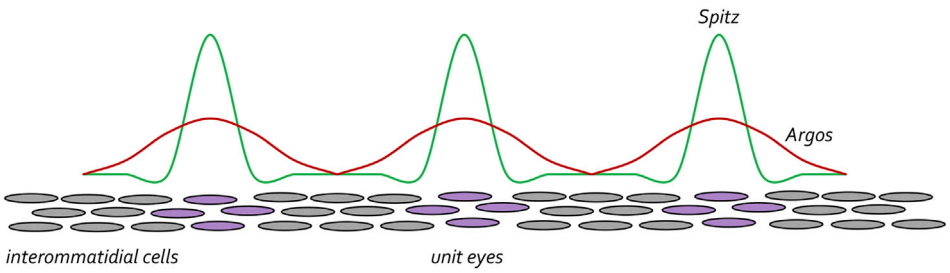


FIGURE 13
The EGF receptor pathway maintains spacing between developing ommatidial clusters. Once the R8 cell is specified the EGFR pathway is then reiteratively used to specify the remaining photoreceptor neurons (purple circles). Starting with the R8 cell, each photoreceptor secretes the Spitz ligand. This activating morphogen is expressed at high levels but only travels short distances. The photoreceptor cells also secrete the Argos inhibiting morphogen. It is expressed at lower levels than Spitz but travels farther. The differences in levels and distance travelled by the two morphogens ensures that the unit eyes are spaced at periodic intervals. This is reminiscent of the diffusion-reaction model that was proposed by Alan Turing.

river stones. The small lumen between the disc proper and the overlying peripodial epithelium (Auerbach, 1936) provides a space for morphogens to pass easily over the disc surface without undergoing excessive dilution. From this point of view, cells within the developing eye stand in place and execute their cellular behaviors in response to different combinations and concentrations of the morphogens that we have discussed. When thinking about the movement of the furrow, the optical illusion of the wave moving across a stadium is an apt visual. The static nature of the developing eye was thought to make it an ideal example of Turing's diffusion-reaction model. In fact, several mathematical models based on reaction-diffusion principles have been specifically proposed to explain how the eye is patterned (Pennington and Lubensky, 2010; Lubensky et al., 2011; Fried et al., 2016; Gavish et al., 2016).

The view that cells within the developing eye lie motionless is based in part on the absence of observable cell migration when discs are extirpated from larvae, cultured in media, and viewed using time-lapse video microscopy (Milner and Haynie, 1979; Milner et al., 1983; Milner et al., 1984; Li and Meinertzhagen, 1995; Tsao et al., 2016; Tsao et al., 2017). However, the culture media used in these assays often did not allow for significant survival times and/or disc growth. In addition, limitations in imaging technology and the absence of advanced imaging software prevented authors of earlier studies from being able to accurately assess cell movements. These technological limitations prevented a rigorous testing of the assumption that little to no cell movements take place within the developing eye field. As a result, researchers have instead relied mainly on snapshots of developing eyes that have been dissected and photographed at successive stages of development and other indirect measures such as the behavior of clonal patches of cells.

A recent study by Richard Carthew's group describes a breakthrough in developing a long-term *ex vivo* culturing system for the eye-antennal disc. It uses a unique culture media as well as cutting-edge time-lapse microscopy and image analysis to visualize the birth and development of approximately four to five columns of ommatidia over the course of 10–12 h (Gallagher et al., 2022). Their *ex vivo* system is an excellent proxy for studying *in vivo* eye development because all aspects of gene expression, tissue growth, cell fate specification, and planar cell polarity appear to be recapitulated. Surprisingly, and for the first time, the authors noted that there are extensive cellular movements throughout the eye field. Within the morphogenetic furrow itself the authors observed both "fast" and "slow" moving cell clusters—Both of which are moving in the anterior direction. These relative rates refer to the movements of these clusters in relation to each other. The faster moving cells are not yet specified as ommatidia and instead contribute to the leading edge of the morphogenetic furrow. In comparison, the slow migrating cells, by moving slower than the others, appear to emerge from the posterior side of the furrow. A subset of these cells will develop into a column of evenly spaced ommatidia and slow to a standstill. By doing so they fall further and further behind the anterior edge of the furrow. When the developing eye field is viewed in real-time, the faster moving cells appear to race ahead of the new ommatidial column and as such the furrow appears to move forward. The surprising finding that the crystalline growth of the eye is the product of complex cell movements as opposed to diffusion-reaction of morphogens across a sheet of motionless cells is only possible because new cutting-edge technology such as an *ex vivo* culturing system, time-lapse microscopy, and sophisticated image analysis tools were used to revisit a question that seemed to have been answered decades ago.

As we have discussed throughout this article, the Hh, Dpp, Notch, EGFR, and Wg signaling transduction pathways set up chemical gradients that result in repeating waves of gene expression. As a result, a completely non-patterned and undifferentiated sheet of cells is transformed into a neurocrystalline lattice of hundreds of periodically spaced unit eyes. This transformation closely resembles the process of generating the array of feathers on a bird. Based on past assumptions about the static behavior of cells within the eye field, patterning of the eye has been held up as a textbook example of the diffusion-reaction model as was proposed by Alan Turing exactly 70 years ago. However, the mechanical flow of cells that is described by Gallagher et al., 2022 makes the mechanism by which the eye develops incompatible with the diffusion-reaction model as envisaged by Turing.

But models are just that, models. In fact, the positional information model itself is undergoing a makeover as a recent study has proposed a new model to potentially replace it. In the neighborhood watch model, cells do not interpret their position within a gradient in isolation (as predicted by positional information) but instead understand their position within the gradient by comparing themselves to neighboring cells (Lee et al., 2022). In fact, even the role of Shh as a morphogen, which appeared to give proof to Wolpert's positional information model, has recently been called into question. Instead of acting as a spatial morphogen, Shh is now proposed to act transiently as a trigger for the specification of all digits of the mouse limb in a concentration independent manner (Zhu et al., 2008; Zhu et al., 2022). Similarly, Hh is seen as functioning as binary switch instead of as a morphogen gradient in the fly eye (Pappu et al., 2003). Live imaging of the eye-antennal disc has forced us to view patterning of the fly eye through a completely new lens. It will be fascinating to determine if the signaling pathways that we have discussed here contribute to the flow of cells that appear to exist within the developing *Drosophila* compound eye.

## Concluding remarks

Studies of the *Drosophila* compound eye have, for over a century, made remarkable contributions to our understanding of developmental biology including the mechanisms that underlie tissue determination, specification, and pattern formation (Weasner and Kumar, 2022). The morphogenetic furrow provides a unique opportunity to understand the molecular mechanisms underlying the generation of arrays of periodically spaced identical units, a pattern that is seen repeatedly in nature. While describing the morphogenetic furrow we have endeavored in this article to describe the models of tissue patterning that have underpinned our conceptual understanding of how the fly eye achieves its final crystal-like arrangement. By discussing the morphogenetic furrow within a historical timeline, we hope that we have impressed upon the reader how new technologies can be used to force the fly eye to give up ever more secrets to its development and thus continue to enrich our own understanding of how patterns in nature are generated. Like the initial studies of the furrow, many of the seminal discoveries using the fly eye were made before the molecular age. As such, it is exciting to wonder if applying more sophisticated tools to other aspects of the fly eye will yield new insights into specification and patterning.

## Author contributions

JK wrote the manuscript and secured external funding. JW edited the manuscript.

## Funding

This work has been funded by a research grant from the National Eye Institute (R01 EY030847) to JK and an administrative diversity supplement (R01 EY030847-S1) to support JW.

## Acknowledgments

JK would like to dedicate this manuscript to his graduate thesis advisor Donald Ready who described the cellular features of the morphogenetic furrow and to his postdoctoral advisor Kevin Moses who determined that the Hedgehog pathway controls the initiation and progression of the furrow. Both authors would like to thank Bonnie M. Weasner for comments and suggestions on the manuscript. We also thank Brandon Weasner for providing the schematic drawings for Figures 7, 11 of this article.

## Conflict of interest

The authors declare that the research was conducted in the absence of any commercial or financial relationships that could be construed as a potential conflict of interest.

## Publisher's note



## References

Abaturova, M. P., and Ginter, E. K. (1968). The transplantation of the imaginal discs of the mutation ophtalmopedia in *Drosophila melanogaster*. *Genetika* 4, 58–64.

Ahn, S., and Joyner, A. L. (2004). Dynamic changes in the response of cells to positive hedgehog signaling during mouse limb patterning. *Cell.* 118, 505–516. doi:10.1016/j.cell.2004.07.023

Alvarado, D., Evans, T. A., Sharma, R., Lemmon, M. A., and Duffy, J. B. (2006). Argos mutants define an affinity threshold for spitz inhibition *in vivo*. *J. Biol. Chem.* 281, 28993–29001. doi:10.1074/jbc.M603782200

Atkins, M., and Mardon, G. (2009). Signaling in the third dimension: The peripodial epithelium in eye disc development. *Dev. Dyn.* 238, 2139–2148. doi:10.1002/dvdy.22034

Auerbach, C. (1936). The development of the legs, wings, and halteres in wild type and some mutant strains of *Drosophila melanogaster*. *Trans. R. Soc. Edin.* LVIII. Part III, No. 27.

Aulehla, A., Wehrle, C., Brand-Saberi, B., Kemler, R., Gossler, A., Kanzler, B., et al. (2003). Wnt3a plays a major role in the segmentation clock controlling somitogenesis. *Dev. Cell.* 4, 395–406. doi:10.1016/s1534-5807(03)00055-8

Baker, N. E., Mlodzik, M., and Rubin, G. M. (1990). Spacing differentiation in the developing Drosophila eye: A fibrinogen-related lateral inhibitor encoded by scabrous. *Science* 250, 1370–1377. doi:10.1126/science.2175046

Baker, N. E., Yu, S., and Han, D. (1996). Evolution of proneural atonal expression during distinct regulatory phases in the developing Drosophila eye. *Curr. Biol.* 6, 1290–1301. doi:10.1016/s0960-9822(02)70715-x

Baker, N. E., and Yu, S. Y. (1997). Proneural function of neurogenic genes in the developing Drosophila eye. *Curr. Biol.* 7, 122–132. doi:10.1016/s0960-9822(06)00056-x

Baker, N. E., and Zitron, A. E. (1995). Drosophila eye development: Notch and Delta amplify a neurogenic pattern conferred on the morphogenetic furrow by scabrous. *Mech. Dev.* 49, 173–189. doi:10.1016/0925-4773(94)00314-d

Baonza, A., and Freeman, M. (2001). Notch signalling and the initiation of neural development in the Drosophila eye. *Development* 128, 3889–3898. doi:10.1242/dev.128.20.3889

Basler, K., and Hafen, E. (1989). Dynamics of Drosophila eye development and temporal requirements of sevenless expression. *Development* 107, 723–731. doi:10.1242/dev.107.4.723

Basler, K., and Struhl, G. (1994). Compartment boundaries and the control of Drosophila limb pattern by hedgehog protein. *Nature* 368, 208–214. doi:10.1038/368208a0

Benlali, A., Draskovic, I., Hazelett, D. J., and Treisman, J. E. (2000). Act up controls actin polymerization to alter cell shape and restrict Hedgehog signaling in the Drosophila eye disc. *eye Disc. Cell.* 101, 271–281. doi:10.1016/s0092-8674(00)80837-5

Bertin, L. (1944). Modifications proposees dans la nomenclature des ecailles et des nageories. *Bull. Soc. Zool. Fr.* 69, 198–202.

Birmingham, L. (1942). Boundaries of differentiation of cephalic imaginal discs in Drosophila. *J. Exp. Zool.* 91, 345–363. doi:10.1002/jez.1400910303

Bodenstein, D. (1938). Untersuchungen zum Metamorphose-problem. I. Kombinierte Schnurungs und Transplantations-experimente an Drosophila. *Wilhelm Roux' Arch. fur Entwicklungsmechanik Org.* 137, 474–505. doi:10.1007/BF00596626

Bonini, N. M., Bui, Q. T., Gray-Board, G. L., and Warrick, J. M. (1997). The Drosophila eyes absent gene directs ectopic eye formation in a pathway conserved between flies and vertebrates. *Development* 124, 4819–4826. doi:10.1242/dev.124.23.4819

Bonini, N. M., Leiserson, W. M., and Benzer, S. (1993). The eyes absent gene: Genetic control of cell survival and differentiation in the developing Drosophila eye. *Cell.* 72, 379–395. doi:10.1016/0092-8674(93)90115-7

Borod, E. R., and Heberlein, U. (1998). Mutual regulation of decapentaplegic and hedgehog during the initiation of differentiation in the Drosophila retina. *Dev. Biol.* 197, 187–197. doi:10.1006/dbio.1998.8888

Boveri, T. (1901). Uber die Polaritat des Seeigeleies. *Verhandl Phys. Med. Ges. Wurzbg.* 34, 145–176.

Breder, C. M. J. (1947). An analysis of the geometry of symmetry with especial reference to the squamation of fishes. *Bull. Amer Mus. Nat. Hist.* 88, 325–412.

Brown, N. L., Sattler, C. A., Paddock, S. W., and Carroll, S. B. (1995). Hairy and emc negatively regulate morphogenetic furrow progression in the Drosophila eye. *Cell.* 80, 879–887. doi:10.1016/0092-8674(95)90291-0

Busby, L., Aceituno, C., McQueen, C., Rich, C. A., Ros, M. A., and Towers, M. (2020). *Sonic hedgehog specifies flight feather positional information in avian wings*, 147.*Development*

Cadigan, K. M., Jou, A. D., and Nusse, R. (2002). Wingless blocks bristle formation and morphogenetic furrow progression in the eye through repression of Daughterless. *Development* 129, 3393–3402. doi:10.1242/dev.129.14.3393

Cagan, R. L., and Ready, D. F. (1989b). Notch is required for successive cell decisions in the developing Drosophila retina. *Genes. & Dev.* 3, 1099–1112. doi:10.1101/gad.3.8.1099

Cagan, R. L., and Ready, D. F. (1989a). The emergence of order in the Drosophila pupal retina. *Dev. Biol.* 136, 346–362. doi:10.1016/0012-1606(89)90261-3

Callaerts, P., Halder, G., and Gehring, W. J. (1997). PAX-6 in development and evolution. *Annu. Rev. Neurosci.* 20, 483–532. doi:10.1146/annurev.neuro.20.1.483

Campos-Ortega, J. A., and Hofbauer, A. (1977). Cell clones and pattern formation on the lineage of photoreceptor cells in the compound eye of Drosophila. *Wilhelm's Roux's Arch.* 181, 227–245. doi:10.1007/BF00848423

Capdevila, J., and Guerrero, I. (1994). Targeted expression of the signaling molecule decapentaplegic induces pattern duplications and growth alterations in Drosophila wings. *EMBO J.* 13, 4459–4468. doi:10.1002/j.1460-2075.1994.tb06768.x

Chang, D. T., Lopez, A., von Kessler, D. P., Chiang, C., Simandl, B. K., Zhao, R., et al. (1994). Products, genetic linkage and limb patterning activity of a murine hedgehog gene. *Development* 120, 3339–3353. doi:10.1242/dev.120.11.3339

Chang, T., Mazotta, J., Dumstrei, K., Dumitrescu, A., and Hartenstein, V. (2001). Dpp and Hh signaling in the Drosophila embryonic eye field. *Development* 128, 4691–4704. doi:10.1242/dev.128.23.4691

Chanut, F., and Heberlein, U. (1997a). Retinal morphogenesis in Drosophila: Hints from an eye-specific decapentaplegic allele. *Dev. Genet.* 20, 197–207. doi:10.1002/(SICI)1520-6408(1997)20:3<197:AID-DVG3>3.0.CO;2-2

Chanut, F., and Heberlein, U. (1997b). Role of decapentaplegic in initiation and progression of the morphogenetic furrow in the developing Drosophila retina. *Development* 124, 559–567. doi:10.1242/dev.124.2.559

Chanut, F., and Heberlein, U. (1995). Role of the morphogenetic furrow in establishing polarity in the Drosophila eye. *Development* 121, 4085–4094. doi:10.1242/dev.121.12.4085

Chanut, F., Luk, A., and Heberlein, U. (2000). A screen for dominant modifiers of ro(Dom), a mutation that disrupts morphogenetic furrow progression in Drosophila, identifies groucho and hairless as regulators of atonal expression. *Genetics* 156, 1203–1217. doi:10.1093/genetics/156.3.1203

Chao, J. L., Tsai, Y. C., Chiu, S. J., and Sun, Y. H. (2004). Localized Notch signal acts through eyg and upd to promote global growth in Drosophila eye. *Development* 131, 3839–3847. doi:10.1242/dev.01258

Chen, T. Y. (1929). On the development of imaginal buds in normal and mutant *Drosophila melanogaster*. *J. Morph.* 47, 135–199. doi:10.1002/jmor.1050470105

Cheng, C. W., Niu, B., Warren, M., Pevny, L. H., Lovell-Badge, R., Hwa, T., et al. (2014). Predicting the spatiotemporal dynamics of hair follicle patterns in the developing mouse. *Proc. Natl. Acad. Sci. U. S. A.* 111, 2596–2601. doi:10.1073/pnas.1313083111

Cheyette, B. N., Green, P. J., Martin, K., Garren, H., Hartenstein, V., and Zipursky, S. L. (1994). The Drosophila sine oculis locus encodes a homeodomain-containing protein required for the development of the entire visual system. *Neuron* 12, 977–996. doi:10.1016/0896-6273(94)90308-5

Chiang, C., Swan, R. Z., Grachtchouk, M., Bolinger, M., Litingtung, Y., Robertson, E. K., et al. (1999). Essential role for Sonic hedgehog during hair follicle morphogenesis. *Dev. Biol.* 205, 1–9. doi:10.1006/dbio.1998.9103

Child, C. M. (1915). A dynamic conception of the organic individual. *Proc. Natl. Acad. Sci. U. S. A.* 1, 164–172. doi:10.1073/pnas.1.3.164

Cho, K. O., Chern, J., Izaddoost, S., and Choi, K. W. (2000). Novel signaling from the peripodial membrane is essential for eye disc patterning in Drosophila. *Cell.* 103, 331–342. doi:10.1016/s0092-8674(00)00124-0

Choi, K. W., and Benzer, S. (1994). Migration of glia along photoreceptor axons in the developing Drosophila eye. *Neuron* 12, 423–431. doi:10.1016/0896-6273(94)90282-8

Cobourne, M. T., Miletich, I., and Sharpe, P. T. (2004). Restriction of sonic hedgehog signalling during early tooth development. *Development* 131, 2875–2885. doi:10.1242/dev.01163

Cooke, J. (1998). A gene that resuscitates a theory--somitogenesis and a molecular oscillator. *Trends Genet.* 14, 85–88. doi:10.1016/s0168-9525(98)01396-1

Cooke, J. (1975). Control of somite number during morphogenesis of a vertebrate, *Xenopus laevis*. *Nature* 254, 196–199. doi:10.1038/254196a0

Cooke, J., and Zeeman, E. C. (1976). A clock and wavefront model for control of the number of repeated structures during animal morphogenesis. *J. Theor. Biol.* 58, 455–476. doi:10.1016/s0022-5193(76)80131-2

Corrigall, D., Walther, R. F., Rodriguez, L., Fichelson, P., and Pichaud, F. (2007). Hedgehog signaling is a principal inducer of Myosin-II-driven cell ingression in Drosophila epithelia. *Dev. Cell.* 13, 730–742. doi:10.1016/j.devcel.2007.09.015

Curtiss, J., and Mlodzik, M. (2000). Morphogenetic furrow initiation and progression during eye development in Drosophila: The roles of decapentaplegic, hedgehog and eyes absent. *Development* 127, 1325–1336. doi:10.1242/dev.127.6.1325

Dalcq, A., and Pasteels, J. (1938). Potentiel morphogenetique, regualtion et axial gradients. *Child Bull Acad Roy Belg Vie Ser. Tome* III, 261–308.

Diaz-Benjumea, F. J., Cohen, B., and Cohen, S. M. (1994). Cell interaction between compartments establishes the proximal-distal axis of Drosophila legs. *Nature* 372, 175–179. doi:10.1038/372175a0

Dokucu, M. E., Zipursky, S. L., and Cagan, R. L. (1996). Atonal, rough and the resolution of proneural clusters in the developing Drosophila retina. *Development* 122, 4139–4147. doi:10.1242/dev.122.12.4139

Dominguez, M. (1999). Dual role for Hedgehog in the regulation of the proneural gene atonal during ommatidia development. *Development* 126, 2345–2353. doi:10.1242/dev.126.11.2345

Dominguez, M., and Hafen, E. (1997). Hedgehog directly controls initiation and propagation of retinal differentiation in the Drosophila eye. *Genes. Dev.* 11, 3254–3264. doi:10.1101/gad.11.23.3254

Dubrulle, J., McGrew, M. J., and Pourquie, O. (2001). FGF signaling controls somite boundary position and regulates segmentation clock control of spatiotemporal Hox gene activation. *Cell.* 106, 219–232. doi:10.1016/s0092-8674(01)00437-8

Echelard, Y., Epstein, D. J., St-Jacques, B., Shen, L., Mohler, J., McMahon, J. A., et al. (1993). Sonic hedgehog, a member of a family of putative signaling molecules, is implicated in the regulation of CNS polarity. *Cell.* 75, 1417–1430. doi:10.1016/0092-8674(93)90627-3

Ekas, L. A., Baeg, G. H., Flaherty, M. S., Ayala-Camargo, A., and Bach, E. A. (2006). JAK/STAT signaling promotes regional specification by negatively regulating wingless expression in Drosophila. *Development* 133, 4721–4729. doi:10.1242/dev.02675

Ellis, H. M., Spann, D. R., and Posakony, J. W. (1990). extramacrochaetae, a negative regulator of sensory organ development in Drosophila, defines a new class of helix-loop-helix proteins. *Cell.* 61, 27–38. doi:10.1016/0092-8674(90)90212-w

Ellis, M. C., Weber, U., Wiersdorff, V., and Mlodzik, M. (1994). Confrontation of scabrous expressing and non-expressing cells is essential for normal ommatidial spacing in the Drosophila eye. *Development* 120, 1959–1969. doi:10.1242/dev.120.7.1959

Exner, S. (1891). *Die Physiologie der facettirten Augen von Krebsen und Insecten: eine Studie*. Leipzig: Franz Deuticke, 230.

Fan, C. M., and Tessier-Lavigne, M. (1994). Patterning of mammalian somites by surface ectoderm and notochord: Evidence for sclerotome induction by a hedgehog homolog. *Cell.* 79, 1175–1186. doi:10.1016/0092-8674(94)90009-4

Felsenfeld, A. L., and Kennison, J. A. (1995). Positional signaling by hedgehog in Drosophila imaginal disc development. *Development* 121, 1–10. doi:10.1242/dev.121.1.1

Fischbach, K. F., and Reichert, H. (1978). Interactions of visual subsystems in *Drosophila melanogaster*: A behavioural genetic analysis. *Behav. Biol.* 3, 305–317.

Fischbach, K. F. (1979). Simultaneous and successive colour contrast expressed in "slow" phototactic behavior of walkign *Drosophila melanogaster*. *J. Comp. Physiology* 130, 161–171. doi:10.1007/bf00611050

Frankfort, B. J., and Mardon, G. (2002). R8 development in the Drosophila eye: A paradigm for neural selection and differentiation. *Development* 129, 1295–1306. doi:10.1242/dev.129.6.1295

Frankfort, B. J., Nolo, R., Zhang, Z., Bellen, H., and Mardon, G. (2001). Senseless repression of rough is required for R8 photoreceptor differentiation in the developing Drosophila eye. *Neuron* 32, 403–414. doi:10.1016/s0896-6273(01)00480-9

Freeman, M., Klambt, C., Goodman, C. S., and Rubin, G. M. (1992). The argos gene encodes a diffusible factor that regulates cell fate decisions in the Drosophila eye. *Cell.* 69, 963–975. doi:10.1016/0092-8674(92)90615-j

Freeman, M. (1994a). Misexpression of the Drosophila argos gene, a secreted regulator of cell determination. *Development* 120, 2297–2304. doi:10.1242/dev.120.8.2297

Freeman, M. (1996). Reiterative use of the EGF Receptor triggers differentiation of all cell types in the *Drosophila* eye. *Cell.* 87, 651–660. doi:10.1016/s0092-8674(00)81385-9

Freeman, M. (1994b). The spitz gene is required for photoreceptor determination in the Drosophila eye where it interacts with the EGF receptor. *Mech. Dev.* 48, 25–33. doi:10.1016/0925-4773(94)90003-5

Fried, P., Sanchez-Aragon, M., Aguilar-Hidalgo, D., Lehtinen, B., Casares, F., and Iber, D. (2016). A model of the spatio-temporal dynamics of Drosophila eye disc development. *PLoS Comput. Biol.* 12, e1005052. doi:10.1371/journal.pcbi.1005052

Fu, W., and Baker, N. E. (2003). Deciphering synergistic and redundant roles of Hedgehog, Decapentaplegic and Delta that drive the wave of differentiation in Drosophila eye development. *Development* 130, 5229–5239. doi:10.1242/dev.00764

Gallagher, K. D., Mani, M., and Carthew, R. W. (2022). Emergence of a geometric pattern of cell fates from tissue-scale mechanics in the Drosophila eye. *eLife* 11, e72806. doi:10.7554/eLife.72806

Gallet, A., Angelats, C., Kerridge, S., and Therond, P. P. (2000). Cubitus interruptus-independent transduction of the Hedgehog signal in Drosophila. *Development* 127, 5509–5522. doi:10.1242/dev.127.24.5509

Garrell, J., and Modolell, J. (1990). The Drosophila extramacrochaetae locus, an antagonist of proneural genes that, like these genes, encodes a helix-loop-helix protein. *Cell.* 61, 39–48. doi:10.1016/0092-8674(90)90213-x

Gaunt, W. A. (1955). The development of the molar pattern of the mouse (*Mus musculus*). *Acta Anat. (Basel)* 24, 249–268. doi:10.1159/000141046

Gavish, A., Shwartz, A., Weizman, A., Schejter, E., Shilo, B. Z., and Barkai, N. (2016). Periodic patterning of the Drosophila eye is stabilized by the diffusible activator Scabrous. *Nat. Commun.* 7, 10461. doi:10.1038/ncomms10461

Gehring, W. J., and Ikeo, K. (1999). Pax 6: Mastering eye morphogenesis and eye evolution. *Trends Genet.* 15, 371–377. doi:10.1016/s0168-9525(99)01776-x

Gehring, W. J., and Seippel, S. (1967). Die Imaginalzellen des Clypeo-Labrums und die Bildung des Rüssels von *Drosophila melanogaster*. *Rev. Suisse Zool.* 74, 589–596. doi:10.5962/bhl.part.75862

Gehring, W. J. (1996). The master control gene for morphogenesis and evolution of the eye. *Genes. cells devoted Mol. Cell. Mech.* 1, 11–15. doi:10.1046/j.1365-2443.1996.11011.x

Gibson, M. C., Lehman, D. A., and Schubiger, G. (2002). Lumenal transmission of decapentaplegic in Drosophila imaginal discs. *Dev. Cell.* 3, 451–460. doi:10.1016/s1534-5807(02)00264-2

Gibson, M. C., and Schubiger, G. (2000). Peripodial cells regulate proliferation and patterning of Drosophila imaginal discs. *Cell.* 103, 343–350. doi:10.1016/s0092-8674(00)00125-2

Gomez, C., Ozbudak, E. M., Wunderlich, J., Baumann, D., Lewis, J., and Pourquie, O. (2008). Control of segment number in vertebrate embryos. *Nature* 454, 335–339. doi:10.1038/nature07020

Green, J. B., and Sharpe, J. (2015). Positional information and reaction-diffusion: Two big ideas in developmental biology combine. *Development* 142, 1203–1211. doi:10.1242/dev.114991

Greenwood, S., and Struhl, G. (1999). Progression of the morphogenetic furrow in the Drosophila eye: The roles of hedgehog, decapentaplegic and the raf pathway. *Development* 126, 5795–5808. doi:10.1242/dev.126.24.5795

Grenacher, H. (1879). *Untersuchungen ueber das Sephorgan der Arthropoden, insbesondere der Spinnen, Insekten und Crustaceen*, 188. Gottingen: Vandenhoech & Ruprecht.

Gunter, G. (1948). A discussion of abnormal scale patterns in fishes, with notice of anotehr specimen with reversed scales. *Am. Soc. Ichthyologists Herpetologists* 4, 280–285.

Halder, G., Callaerts, P., and Gehring, W. J. (1995a). Induction of ectopic eyes by targeted expression of the eyeless gene in Drosophila. *Science* 267, 1788–1792. doi:10.1126/science.7892602

Halder, G., Callaerts, P., and Gehring, W. J. (1995b). New perspectives on eye evolution. *Curr. Opin. Genet. Dev.* 5, 602–609. doi:10.1016/0959-437x(95)80029-8

Hardcastle, Z., Mo, R., Hui, C. C., and Sharpe, P. T. (1998). The Shh signalling pathway in tooth development: Defects in Gli2 and Gli3 mutants. *Development* 125, 2803–2811. doi:10.1242/dev.125.15.2803

Harfe, B. D., Scherz, P. J., Nissim, S., Tian, H., McMahon, A. P., and Tabin, C. J. (2004). Evidence for an expansion-based temporal Shh gradient in specifying vertebrate digit identities. *Cell.* 118, 517–528. doi:10.1016/j.cell.2004.07.024

Haynie, J. L., and Bryant, P. J. (1986). Development of the eye-antenna imaginal disc and morphogenesis of the adult head in *Drosophila melanogaster*. *J. Exp. Zool.* 237, 293–308. doi:10.1002/jez.1402370302

Hazelett, D. J., Bourouis, M., Walldorf, U., and Treisman, J. E. (1998). Decapentaplegic and wingless are regulated by eyes absent and eyegone and interact to direct the pattern of retinal differentiation in the eye disc. *Development* 125, 3741–3751. doi:10.1242/dev.125.18.3741

Heberlein, U., Mlodzik, M., and Rubin, G. M. (1991). Cell-fate determination in the developing Drosophila eye: Role of the rough gene. *Development* 112, 703–712. doi:10.1242/dev.112.3.703

Heberlein, U., Singh, C. M., Luk, A. Y., and Donohoe, T. J. (1995). Growth and differentiation in the Drosophila eye coordinated by hedgehog. *Nature* 373, 709–711. doi:10.1038/373709a0

Heberlein, U., Wolff, T., and Rubin, G. M. (1993). The TGF beta homolog dpp and the segment polarity gene hedgehog are required for propagation of a morphogenetic wave in the Drosophila retina. *Cell.* 75, 913–926. doi:10.1016/0092-8674(93)90535-x

Heer, N. C., and Martin, A. C. (2017). Tension, contraction and tissue morphogenesis. *Development* 144, 4249–4260. doi:10.1242/dev.151282

Heisenberg, M., and Buchner, E. (1977). The role of retinula cell types in visual behavior ofDrosophila melanogaster. *J. Comp. Physiology* 117, 127–162. doi:10.1007/bf00612784

Hepker, J., Blackman, R. K., and Holmgren, R. (1999). Cubitus interruptus is necessary but not sufficient for direct activation of a wing-specific decapentaplegic enhancer. *Development* 126, 3669–3677. doi:10.1242/dev.126.16.3669

Hoge, M. A. (1915). Another gene in the fourth chromosome of Drosophila. *Am. Nat.* 49, 47–49. doi:10.1086/279455

Holmes, A. (1935). The pattern and symmetry of adult plumage units in relation to the order and locus of origin of the embryonic feather papillae. *Am. J. Anat.* 56, 513–537. doi:10.1002/aja.1000560308

Honig, L. S. (1981). Positional signal transmission in the developing chick limb. *Nature* 291, 72–73. doi:10.1038/291072a0

Horridge, G. A. (1975). *The compound eye and vision of insects*. Oxford, England: Clarendon Press, 595.

Horstadius, S. (1939). The mechanics of sea urchin development studied by operative methods. *Biol. Rev.* 14, 132–179. doi:10.1111/j.1469-185x.1939.tb00929.x

Hu, K. G., and Stark, W. S. (1980). The roles of Drosophila ocelli and compound eyes in phototaxis. *J. Comp. Physiology* 135, 85–95. doi:10.1007/bf00660183

Hubaud, A., and Pourquie, O. (2014). Signalling dynamics in vertebrate segmentation. *Nat. Rev. Mol. Cell. Biol.* 15, 709–721. doi:10.1038/nrm3891

Ingham, P. W., and Fietz, M. J. (1995). Quantitative effects of hedgehog and decapentaplegic activity on the patterning of the Drosophila wing. *Curr. Biol.* 5, 432–440. doi:10.1016/s0960-9822(95)00084-4

Ives, P. (1950). New mutant report: bar-3. *Dros. Info. Serv.* 24, 58.

Jarman, A. P., Grell, E. H., Ackerman, L., Jan, L. Y., and Jan, Y. N. (1994). Atonal is the proneural gene for Drosophila photoreceptors. *Nature* 369, 398–400. doi:10.1038/369398a0

Jarman, A. P., Sun, Y., Jan, L. Y., and Jan, Y. N. (1995). Role of the proneural gene, atonal, in formation of Drosophila chordotonal organs and photoreceptors. *Development* 121, 2019–2030. doi:10.1242/dev.121.7.2019

Jean-Guillaume, C. B., and Kumar, J. P. (2022). Development of the ocellar visual system in *Drosophila melanogaster*. *FEBS J.* 289, 7411–7427. doi:10.1111/febs.16468

Jiang, J., and Struhl, G. (1995). Protein kinase A and hedgehog signaling in Drosophila limb development. *Cell.* 80, 563–572. doi:10.1016/0092-8674(95)90510-3

Jin, M. H., Sawamoto, K., Ito, M., and Okano, H. (2000). The interaction between the Drosophila secreted protein argos and the epidermal growth factor receptor inhibits dimerization of the receptor and binding of secreted spitz to the receptor. *Mol. Cell. Biol.* 20, 2098–2107. doi:10.1128/MCB.20.6.2098-2107.2000

Johnson, R. L., Laufer, E., Riddle, R. D., and Tabin, C. (1994). Ectopic expression of Sonic hedgehog alters dorsal-ventral patterning of somites. *Cell.* 79, 1165–1173. doi:10.1016/0092-8674(94)90008-6

Karlsson, L., Bondjers, C., and Betsholtz, C. (1999). Roles for PDGF-A and sonic hedgehog in development of mesenchymal components of the hair follicle. *Development* 126, 2611–2621. doi:10.1242/dev.126.12.2611

Kimmel, B. E., Heberlein, U., and Rubin, G. M. (1990). The homeo domain protein rough is expressed in a subset of cells in the developing Drosophila eye where it can specify photoreceptor cell subtype. *Genes. Dev.* 4, 712–727. doi:10.1101/gad.4.5.712

Klein, D. E., Nappi, V. M., Reeves, G. T., Shvartsman, S. Y., and Lemmon, M. A. (2004). Argos inhibits epidermal growth factor receptor signalling by ligand sequestration. *Nature* 430, 1040–1044. doi:10.1038/nature02840

Klein, D. E., Stayrook, S. E., Shi, F., Narayan, K., and Lemmon, M. A. (2008). Structural basis for EGFR ligand sequestration by Argos. *Nature* 453, 1271–1275. doi:10.1038/nature06978

Krafka, J. (1924). Development of the compound eye of Drosophila melogaster and its bar-eyed mutant. *Biol. Bull.* 47, 143–149.

Krapp, H. G. (2009). Ocelli. *Curr. Biol.* 19, R435–R437. doi:10.1016/j.cub.2009.03.034

Kumar, J. P., and Moses, K. (2001). The EGF receptor and Notch signaling pathways control the initiation of the morphogenetic furrow during Drosophila eye development. *Development* 128, 2689–2697. doi:10.1242/dev.128.14.2689

Kumar, J. P. (2010). Retinal determination the beginning of eye development. *Curr. Top. Dev. Biol.* 93, 1–28. doi:10.1016/B978-0-12-385044-7.00001-1

Kumar, J. P., Tio, M., Hsiung, F., Akopyan, S., Gabay, L., Seger, R., et al. (1998). Dissecting the roles of the Drosophila EGF receptor in eye development and MAP kinase activation. *Development* 125, 3875–3885. doi:10.1242/dev.125.19.3875

Kumar, K., Ouweneel, W. J., and Faber, J. (1979). Differentiation capacities of the labial imaginal disc ofDrosophila melanogaster. *Wilhelm Roux's archives Dev. Biol.* 186, 51–64. doi:10.1007/BF00848107

Land, M. F., and Fernald, R. D. (1992). The evolution of eyes. *Annu. Rev. Neurosci.* 15, 1–29. doi:10.1146/annurev.ne.15.030192.000245

Land, M. F. (1997). Visual acuity in insects. *Annu. Rev. entomology* 42, 147–177. doi:10.1146/annurev.ento.42.1.147

Lebovitz, R. M., and Ready, D. F. (1986). Ommatidial development in Drosophila eye disc fragments. *Dev. Biol.* 117, 663–671. doi:10.1016/0012-1606(86)90335-0

Lee, E. C., Hu, X., Yu, S. Y., and Baker, N. E. (1996). The scabrous gene encodes a secreted glycoprotein dimer and regulates proneural development in Drosophila eyes. *Mol. Cell. Biol.* 16, 1179–1188. doi:10.1128/MCB.16.3.1179

Lee, H. C., Hastings, C., Oliveira, N. M. M., Perez-Carrasco, R., Page, K. M., Wolpert, L., et al. (2022). *'Neighbourhood watch' model: embryonic epiblast cells assess positional information in relation to their neighbours*, 149.*Development*

Li, C., and Meinertzhagen, I. A. (1995). Conditions for the primary culture of eye imaginal discs from *Drosophila melanogaster*. *J. Neurobiol.* 28, 363–380. doi:10.1002/neu.480280309

Li, W., Ohlmeyer, J. T., Lane, M. E., and Kalderon, D. (1995). Function of protein kinase A in hedgehog signal transduction and Drosophila imaginal disc development. *Cell.* 80, 553–562. doi:10.1016/0092-8674(95)90509-x

Ligoxygakis, P., Yu, S. Y., Delidakis, C., and Baker, N. E. (1998). A subset of notch functions during Drosophila eye development require Su(H) and the E(spl) gene complex. *Development* 125, 2893–2900. doi:10.1242/dev.125.15.2893

Lim, J., and Choi, K. W. (2003). Bar homeodomain proteins are anti-proneural in the Drosophila eye: Transcriptional repression of atonal by bar prevents ectopic retinal neurogenesis. *Development* 130, 5965–5974. doi:10.1242/dev.00818

Lim, J., and Choi, K. W. (2004). Induction and autoregulation of the anti-proneural gene Bar during retinal neurogenesis in Drosophila. *Development* 131, 5573–5580. doi:10.1242/dev.01426

Lopez-Martinez, A., Chang, D. T., Chiang, C., Porter, J. A., Ros, M. A., Simandl, B. K., et al. (1995). Limb-patterning activity and restricted posterior localization of the amino-terminal product of Sonic hedgehog cleavage. *Curr. Biol.* 5, 791–796. doi:10.1016/s0960-9822(95)00156-4

Lubensky, D. K., Pennington, M. W., Shraiman, B. I., and Baker, N. E. (2011). A dynamical model of ommatidial crystal formation. *Proc. Natl. Acad. Sci. U. S. A.* 108, 11145–11150. doi:10.1073/pnas.1015302108

Lumsden, A. G. (1970). Pattern formation in the molar dentition of the mouse. *J. Biol. Buccale* 7, 77–103.

Ma, C., and Moses, K. (1995). Wingless and patched are negative regulators of the morphogenetic furrow and can affect tissue polarity in the developing Drosophila compound eye. *Development* 121, 2279–2289. doi:10.1242/dev.121.8.2279

Ma, C., Zhou, Y., Beachy, P. A., and Moses, K. (1993). The segment polarity gene hedgehog is required for progression of the morphogenetic furrow in the developing Drosophila eye. *Cell.* 75, 927–938. doi:10.1016/0092-8674(93)90536-y

Mallock, A. (1894). Insect sight and the definign power of composite eyes. *Proc. R. Soc. Lond.* 55, 331–335.

Mann, S. J. (1962). Prenatal formation of hair follicle types. *Anatomical Rec.* 144, 135–141. doi:10.1002/ar.1091440208

Mardon, G., Solomon, N. M., and Rubin, G. M. (1994). Dachshund encodes a nuclear protein required for normal eye and leg development in Drosophila. *Development* 120, 3473–3486. doi:10.1242/dev.120.12.3473

Martin, A. C., and Goldstein, B. (2014). Apical constriction: Themes and variations on a cellular mechanism driving morphogenesis. *Development* 141, 1987–1998. doi:10.1242/dev.102228

McClure, K. D., and Schubiger, G. (2005). Developmental analysis and squamous morphogenesis of the peripodial epithelium in Drosophila imaginal discs. *Development* 132, 5033–5042. doi:10.1242/dev.02092

Medioni, J. (1959). Mise en evidence et evaluation d'un effet de stimulation du aux ocelles frontaux dans le phototropisme de *Drosophila melanogaster*. *Meigen. Compt. Rendus Soc. Biol.* 153, 1587–1590.

Medvedev, N. H. (1935). Genes and development of characters. *Z. Induk. Abst. Vererb. Lehre.* 70, 55–72. doi:10.1007/bf01741639

Methot, N., and Basler, K. (2001). An absolute requirement for Cubitus interruptus in Hedgehog signaling. *Development* 128, 733–742. doi:10.1242/dev.128.5.733

Methot, N., and Basler, K. (1999). Hedgehog controls limb development by regulating the activities of distinct transcriptional activator and repressor forms of Cubitus interruptus. *Cell.* 96, 819–831. doi:10.1016/s0092-8674(00)80592-9

Milani, R. (1941). Two new eye-shape mutant alleles in *Drosophila melanogaster*. *D. I. S.* 14, 52.

Milner, M. J., Bleasby, A. J., and Pyott, A. (1984). Cell interactions during the fusion*in vitro* of Drosophila eye-antennal imaginal discs. *Wilhelm Roux's archives Dev. Biol.* 193, 406–413. doi:10.1007/BF00848232

Milner, M. J., Bleasby, A. J., and Pyott, A. (1983). The role of the peripodial membrane in the morphogenesis of the eye-antennal disc ofDrosophila melanogaster. *Roux's Arch. Dev. Biol.* 192, 164–170. doi:10.1007/BF00848686

Milner, M. J., and Haynie, J. L. (1979). Fusion of Drosophila eye-antennal imaginal discs during differentiation *in vitro*. *Wilhelm Roux's Arch.* 185, 363–370. doi:10.1007/BF00848522

Mlodzik, M., Baker, N. E., and Rubin, G. M. (1990). Isolation and expression of scabrous, a gene regulating neurogenesis in Drosophila. *Genes. Dev.* 4, 1848–1861. doi:10.1101/gad.4.11.1848

Mohler, J. (1988). Requirements for hedgehog, a segmental polarity gene, in patterning larval and adult cuticle of Drosophila. *Genetics* 120, 1061–1072. doi:10.1093/genetics/120.4.1061

Morgan, T. H. (1901). *Regeneration*. New York: Macmillan.

Mou, C., Jackson, B., Schneider, P., Overbeek, P. A., and Headon, D. J. (2006). Generation of the primary hair follicle pattern. *Proc. Natl. Acad. Sci. U. S. A.* 103, 9075–9080. doi:10.1073/pnas.0600825103

Muller, B., and Basler, K. (2000). The repressor and activator forms of Cubitus interruptus control Hedgehog target genes through common generic gli-binding sites. *Development* 127, 2999–3007. doi:10.1242/dev.127.14.2999

Nagel, A. C., and Preiss, A. (1999). Notchspl is deficient for inductive processes in the eye, and E(spl)D enhances split by interfering with proneural activity. *Dev. Biol.* 208, 406–415. doi:10.1006/dbio.1999.9203

Naiche, L. A., Holder, N., and Lewandoski, M. (2011). FGF4 and FGF8 comprise the wavefront activity that controls somitogenesis. *Proc. Natl. Acad. Sci. U. S. A.* 108, 4018–4023. doi:10.1073/pnas.1007417108

Nellen, D., Burke, R., Struhl, G., and Basler, K. (1996). Direct and long range action of a dpp morphogen gradient. *Cell.* 85, 357–368. doi:10.1016/s0092-8674(00)81114-9

Ouweneel, W. J. (1970). Normal and abnormal determination in the imaginal discs of Drosophila, with special reference to the eye discs. *Acta embryol. Exp.* 1, 95–119.

Pagan, S. M., Ros, M. A., Tabin, C., and Fallon, J. F. (1996). Surgical removal of limb bud Sonic hedgehog results in posterior skeletal defects. *Dev. Biol.* 180, 35–40. doi:10.1006/dbio.1996.0282

Palmeirim, I., Henrique, D., Ish-Horowicz, D., and Pourquie, O. (1997). Avian hairy gene expression identifies a molecular clock linked to vertebrate segmentation and somitogenesis. *Cell.* 91, 639–648. doi:10.1016/s0092-8674(00)80451-1

Pan, D., and Rubin, G. M. (1995). cAMP-dependent protein kinase and hedgehog act antagonistically in regulating decapentaplegic transcription in Drosophila imaginal discs. *Cell.* 80, 543–552. doi:10.1016/0092-8674(95)90508-1

Pappu, K. S., Chen, R., Middlebrooks, B. W., Woo, C., Heberlein, U., and Mardon, G. (2003). Mechanism of hedgehog signaling during Drosophila eye development. *Development* 130, 3053–3062. doi:10.1242/dev.00534

Parker, D. S., White, M. A., Ramos, A. I., Cohen, B. A., and Barolo, S. (2011). The cis-regulatory logic of hedgehog gradient responses: Key roles for gli binding affinity, competition, and cooperativity. *Sci. Signal.* 4, ra38. doi:10.1126/scisignal.2002077

Pauli, T., Seimiya, M., Blanco, J., and Gehring, W. J. (2005). Identification of functional sine oculis motifs in the autoregulatory element of its own gene, in the eyeless enhancer and in the signalling gene hedgehog. *Development* 132, 2771–2782. doi:10.1242/dev.01841

Paulus, H. F. (1979). "Eye structure and the monophyly of the Arthropoda," in *Arthropod phylogeny*. Editor A. P. Gupta (New York, 299–371.

Pennington, M. W., and Lubensky, D. K. (2010). Switch and template pattern formation in a discrete reaction-diffusion system inspired by the Drosophila eye. *Eur. Phys. J. E, Soft matter* 33, 129–148. doi:10.1140/epje/i2010-10647-6

Pepple, K. L., Atkins, M., Venken, K., Wellnitz, K., Harding, M., Frankfort, B., et al. (2008). Two-step selection of a single R8 photoreceptor: A bistable loop between senseless and rough locks in R8 fate. *Development* 135, 4071–4079. doi:10.1242/dev.028951

Perez, S. E., and Steller, H. (1996). Molecular and genetic analyses of lama, an evolutionarily conserved gene expressed in the precursors of the Drosophila first optic ganglion. *Mech. Dev.* 59, 11–27. doi:10.1016/0925-4773(96)00556-4

Pignoni, F., Hu, B., Zavitz, K. H., Xiao, J., Garrity, P. A., and Zipursky, S. L. (1997). The eye-specification proteins So and Eya form a complex and regulate multiple steps in Drosophila eye development. *Cell.* 91, 881–891. doi:10.1016/s0092-8674(00)80480-8

Pignoni, F., and Zipursky, S. L. (1997). Induction of Drosophila eye development by Decapentaplegic. *Development* 124, 271–278. doi:10.1242/dev.124.2.271

Pilkington, R. W. (1942). Facet mutants of Drosophila. *Proc. Zool. Soc. Lond. Ser. A* 3, 199–222. doi:10.1111/j.1469-7998.1942.tb08482.x

Powell, P. A., Wesley, C., Spencer, S., and Cagan, R. L. (2001). Scabrous complexes with Notch to mediate boundary formation. *Nature* 409, 626–630. doi:10.1038/35054566

Prochazka, J., Pantalacci, S., Churava, S., Rothova, M., Lambert, A., Lesot, H., et al. (2010). Patterning by heritage in mouse molar row development. *Proc. Natl. Acad. Sci. U. S. A.* 107, 15497–15502. doi:10.1073/pnas.1002784107

Quiring, R., Walldorf, U., Kloter, U., and Gehring, W. J. (1994). Homology of the eyeless gene of Drosophila to the Small eye gene in mice and Aniridia in humans. *Science* 265, 785–789. doi:10.1126/science.7914031

Ramirez-Weber, F. A., and Kornberg, T. B. (1999). Cytonemes: Cellular processes that project to the principal signaling center in Drosophila imaginal discs. *Cell.* 97, 599–607. doi:10.1016/s0092-8674(00)80771-0

Rangarajan, R., Gong, Q., and Gaul, U. (1999). Migration and function of glia in the developing Drosophila eye. *Development* 126, 3285–3292. doi:10.1242/dev.126.15.3285

Ready, D. F., Hanson, T. E., and Benzer, S. (1976). Development of the Drosophila retina, a neurocrystalline lattice. *Dev. Biol.* 53, 217–240. doi:10.1016/0012-1606(76)90225-6

Renfranz, P. J., and Benzer, S. (1989). Monoclonal antibody probes discriminate early and late mutant defects in development of the Drosophila retina. *Dev. Biol.* 136, 411–429. doi:10.1016/0012-1606(89)90267-4

Riddle, R. D., Johnson, R. L., Laufer, E., and Tabin, C. (1993). Sonic hedgehog mediates the polarizing activity of the ZPA. *Cell.* 75, 1401–1416. doi:10.1016/0092-8674(93)90626-2

Rieger, D., Stanewsky, R., and Helfrich-Forster, C. (2003). Cryptochrome, compound eyes, Hofbauer-Buchner eyelets, and ocelli play different roles in the entrainment and masking pathway of the locomotor activity rhythm in the fruit fly *Drosophila melanogaster*. *J. Biol. Rhythms* 18, 377–391. doi:10.1177/0748730403256997

Rogers, E. M., Brennan, C. A., Mortimer, N. T., Cook, S., Morris, A. R., and Moses, K. (2005). Pointed regulates an eye-specific transcriptional enhancer in the Drosophila hedgehog gene, which is required for the movement of the morphogenetic furrow. *Development* 132, 4833–4843. doi:10.1242/dev.02061

Roy, S., Hsiung, F., and Kornberg, T. B. (2011). Specificity of Drosophila cytonemes for distinct signaling pathways. *Science* 332, 354–358. doi:10.1126/science.1198949

Runnstrom, J. (1929). Uber Selbstdifferenzierung und Induktion bei dem Seeigelkeim. Wilhelm Roux. *Arch. fur Entwicklungsmechanik Org.* 117, 123–145. doi:10.1007/BF02110965

Saga, Y., and Takeda, H. (2001). The making of the somite: Molecular events in vertebrate segmentation. *Nat. Rev. Genet.* 2, 835–845. doi:10.1038/35098552

Saint-Charles, A., Michard-Vanhee, C., Alejevski, F., Chelot, E., Boivin, A., and Rouyer, F. (2016). Four of the six Drosophila rhodopsin-expressing photoreceptors can mediate circadian entrainment in low light. *J. Comp. neurology* 524, 2828–2844. doi:10.1002/cne.23994

Salvini-Plawen, L., and Mayr, E. (1977). *On the evolution of photoreceptors and eyes*. Plenum Press.

Saunders, J., and Gasseling, M. (1968). "Ectodermal-mesenchymal interactions in the orgin of limb symmetry," in *Epithelial mesenchumal interactions*. Editors R. Fleischmajer and R. E. Billingham (Baltimore: William and Wilkins), 78–97.

Sawada, A., Shinya, M., Jiang, Y. J., Kawakami, A., Kuroiwa, A., and Takeda, H. (2001). Fgf/MAPK signalling is a crucial positional cue in somite boundary formation. *Development* 128, 4873–4880. doi:10.1242/dev.128.23.4873

Sawamoto, K., Okabe, M., Tanimura, T., Mikoshiba, K., Nishida, Y., and Okano, H. (1996). The Drosophila secreted protein Argos regulates signal transduction in the Ras/MAPK pathway. *Dev. Biol.* 178, 13–22. doi:10.1006/dbio.1996.0194

Sawamoto, K., Okano, H., Kobayakawa, Y., Hayashi, S., Mikoshiba, K., and Tanimura, T. (1994). The function of argos in regulating cell fate decisions during Drosophila eye and wing vein development. *Dev. Biol.* 164, 267–276. doi:10.1006/dbio.1994.1197

Sawyer, J. M., Harrell, J. R., Shemer, G., Sullivan-Brown, J., Roh-Johnson, M., and Goldstein, B. (2010). Apical constriction: A cell shape change that can drive morphogenesis. *Dev. Biol.* 341, 5–19. doi:10.1016/j.ydbio.2009.09.009

Schlapfer, T. (1963). Der Einfluss des adulten wirtsmilieus auf die entwicklung von larvalen augenanteennen-imaginalscheiben von *Drosophila melanogaster*. *Roux Arch. fur Entwicklungsmechanik* 154, 378–404. doi:10.1007/BF00582082

Schlichting, K., and Dahmann, C. (2008). Hedgehog and Dpp signaling induce cadherin Cad86C expression in the morphogenetic furrow during Drosophila eye development. *Mech. Dev.* 125, 712–728. doi:10.1016/j.mod.2008.04.005

Schlichting, M., Menegazzi, P., Lelito, K. R., Yao, Z., Buhl, E., Dalla Benetta, E., et al. (2016). A neural network underlying circadian entrainment and photoperiodic adjustment of sleep and activity in Drosophila. *J. Neurosci. official J. Soc. Neurosci.* 36, 9084–9096. doi:10.1523/JNEUROSCI.0992-16.2016

Schnaitmann, C., Pagni, M., and Reiff, D. F. (2020). Color vision in insects: Insights from Drosophila. *J. Comp. Physiology* 206, 183–198. doi:10.1007/s00359-019-01397-3

Schweitzer, R., Howes, R., Smith, R., Shilo, B. Z., and Freeman, M. (1995a). Inhibition of Drosophila EGF receptor activation by the secreted protein Argos. *Nature* 376, 699–702. doi:10.1038/376699a0

Schweitzer, R., Shaharabany, M., Seger, R., and Shilo, B. Z. (1995b). Secreted Spitz triggers the DER signaling pathway and is a limiting component in embryonic ventral ectoderm determination. *Genes. Dev.* 9, 1518–1529. doi:10.1101/gad.9.12.1518

Serikaku, M. A., and O'Tousa, J. E. (1994). Sine oculis is a homeobox gene required for Drosophila visual system development. *Genetics* 138, 1137–1150. doi:10.1093/genetics/138.4.1137

Shen, W., and Mardon, G. (1997). Ectopic eye development in Drosophila induced by directed dachshund expression. *Development* 124, 45–52. doi:10.1242/dev.124.1.45

Singh, A., and Choi, K. W. (2003). Initial state of the Drosophila eye before dorsoventral specification is equivalent to ventral. *Development* 130, 6351–6360. doi:10.1242/dev.00864

Singh, A., Kango-Singh, M., Choi, K. W., and Sun, Y. H. (2004). Dorso-ventral asymmetric functions of teashirt in Drosophila eye development depend on spatial cues provided by early DV patterning genes. *Mech. Dev.* 121, 365–370. doi:10.1016/j.mod.2004.02.005

Singh, A., Kango-Singh, M., and Sun, Y. H. (2002). Eye suppression, a novel function of teashirt, requires Wingless signaling. *Development* 129, 4271–4280. doi:10.1242/dev.129.18.4271

Spencer, S. A., Powell, P. A., Miller, D. T., and Cagan, R. L. (1998). Regulation of EGF receptor signaling establishes pattern across the developing Drosophila retina. *Development* 125, 4777–4790. doi:10.1242/dev.125.23.4777

Spratford, C. M., and Kumar, J. P. (2013). Extramacrochaetae imposes order on the Drosophila eye by refining the activity of the Hedgehog signaling gradient. *Development* 140, 1994–2004. doi:10.1242/dev.088963

St-Jacques, B., Dassule, H. R., Karavanova, I., Botchkarev, V. A., Li, J., Danielian, P. S., et al. (1998). Sonic hedgehog signaling is essential for hair development. *Curr. Biol.* 8, 1058–1068. doi:10.1016/s0960-9822(98)70443-9

Steinberg, A. G. (1943b). Studies on the development of the eye: Evidence that the Lobe$^2$, Lobe4, Lobe$^5$ and eyeless mutants of *Drosophila melanogaster* develop in a manner similar to bar. *Genetics* 30, 5–13. doi:10.1073/pnas.30.1.5

Steinberg, A. G. (1943a). The development of the wild type and bar eyes of *Drosophila melanogaster*. *Can. J. Res.* 21, 277–283. doi:10.1139/cjr43d-022

Straile, W. E. (1960). Sensory hair follicles in mammalian skin: The trlotrich follicle. *Am. J. Anat.* 106, 89–183.

Strausfeld, N. J. (1976). "Mosaic organizations, layers, and visual pathways in the insect brain," in *Neural principles of vision* (Friedrich Zettler and Reto Weiler, New York), 245–279.

Struhl, G., and Basler, K. (1993). Organizing activity of wingless protein in Drosophila. *Cell.* 72, 527–540. doi:10.1016/0092-8674(93)90072-x

Strutt, D. I., Wiersdorff, V., and Mlodzik, M. (1995). Regulation of furrow progression in the Drosophila eye by cAMP-dependent protein kinase A. *Nature* 373, 705–709. doi:10.1038/373705a0

Strutt, D. L., and Mlodzik, M. (1996). The regulation of hedgehog and decapentaplegic during Drosophila eye imaginal disc development. *Mech. Dev.* 58, 39–50. doi:10.1016/s0925-4773(96)00555-2

Sturtevant, A. H. (1929). The claret mutant type of *Drosophila simulans*: A study of chromosome elimination and cell lineage. *Z. Wiss. Zool. Abt. A* 135, 323–356.

Summerbell, D., and Honig, L. S. (1982). The control of pattern across the antero-posterior Axis of the chick limb bud by a unique signalling region. *Amer Zool.* 22, 105–116. doi:10.1093/icb/22.1.105

Sun, Y., Jan, L. Y., and Jan, Y. N. (1998). Transcriptional regulation of atonal during development of the Drosophila peripheral nervous system. *Development* 125, 3731–3740. doi:10.1242/dev.125.18.3731

Suzuki, T., and Saigo, K. (2000). Transcriptional regulation of atonal required for Drosophila larval eye development by concerted action of eyes absent, sine oculis and hedgehog signaling independent of fused kinase and cubitus interruptus. *Development* 127, 1531–1540. doi:10.1242/dev.127.7.1531

Sved, J. (1986). Report of new mutants. *D. I. S.* 63, 169.

Tabata, T., and Kornberg, T. B. (1994). Hedgehog is a signaling protein with a key role in patterning Drosophila imaginal discs. *Cell.* 76, 89–102. doi:10.1016/0092-8674(94)90175-9

Tanaka-Matakatsu, M., and Du, W. (2008). Direct control of the proneural gene atonal by retinal determination factors during Drosophila eye development. *Dev. Biol.* 313, 787–801. doi:10.1016/j.ydbio.2007.11.017

Tio, M., Ma, C., and Moses, K. (1994). spitz, a Drosophila homolog of transforming growth factor-alpha, is required in the founding photoreceptor cells of the compound eye facets. *Mech. Dev.* 48, 13–23. doi:10.1016/0925-4773(94)90002-7

Tio, M., and Moses, K. (1997). The Drosophila TGF alpha homolog Spitz acts in photoreceptor recruitment in the developing retina. *Development* 124, 343–351. doi:10.1242/dev.124.2.343

Tomlinson, A., and Ready, D. F. (1987). Neuronal differentiation in Drosophila ommatidium. *Dev. Biol.* 120, 366–376. doi:10.1016/0012-1606(87)90239-9

Treisman, J. E., and Rubin, G. M. (1995). Wingless inhibits morphogenetic furrow movement in the Drosophila eye disc. *eye Disc. Dev.* 121, 3519–3527. doi:10.1242/dev.121.11.3519

Tsai, Y. C., and Sun, Y. H. (2004). Long-range effect of upd, a ligand for Jak/STAT pathway, on cell cycle in Drosophila eye development. *Genesis* 39, 141–153. doi:10.1002/gene.20035

Tsai, Y. C., Yao, J. G., Chen, P. H., Posakony, J. W., Barolo, S., Kim, J., et al. (2007). Upd/Jak/STAT signaling represses wg transcription to allow initiation of morphogenetic furrow in Drosophila eye development. *Dev. Biol.* 306, 760–771. doi:10.1016/j.ydbio.2007.04.011

Tsao, C. K., Ku, H. Y., Lee, Y. M., Huang, Y. F., and Sun, Y. H. (2016). Long term *ex vivo* culture and live imaging of Drosophila larval imaginal discs. *PLoS One* 11, e0163744. doi:10.1371/journal.pone.0163744

Tsao, C. K., Ku, H. Y., and Sun, Y. H. (2017). Long-term live imaging of Drosophila eye disc. *J. Vis. Exp.*, 55748. doi:10.3791/55748

Turing, A. (1952). The chemical basis of morphogenesis. *Philosophical Trans. R. Soc. Lond. Ser. B, Biol. Sci.* 237, 37–72.

Umezaki, Y., and Tomioka, K. (2008). Behavioral dissection of the Drosophila circadian multioscillator system that regulates locomotor rhythms. *Zool. Sci.* 25, 1146–1155. doi:10.2108/zsj.25.1146

Van Doren, M., Ellis, H. M., and Posakony, J. W. (1991). The Drosophila extramacrochaetae protein antagonizes sequence-specific DNA binding by daughterless/achaete-scute protein complexes. *Development* 113, 245–255. doi:10.1242/dev.113.1.245

Veleri, S., Rieger, D., Helfrich-Forster, C., and Stanewsky, R. (2007). Hofbauer-Buchner eyelet affects circadian photosensitivity and coordinates TIM and PER expression in Drosophila clock neurons. *J. Biol. Rhythms* 22, 29–42. doi:10.1177/0748730406295754

Vogt, M. (1946). Zur labilen Determination der Imagin-alscheiben von Drosophila. I. Verhalten verschieden-altriger Imaginalanlagen bei operativer Defektsetzung. *Biol. Zbl.* 65, 223–238.

Von Ohlen, T., Lessing, D., Nusse, R., and Hooper, J. E. (1997). Hedgehog signaling regulates transcription through cubitus interruptus, a sequence-specific DNA binding protein. *Proc. Natl. Acad. Sci. U. S. A.* 94, 2404–2409. doi:10.1073/pnas.94.6.2404

Vosshall, L. B., and Young, M. W. (1995). Circadian rhythms in Drosophila can be driven by period expression in a restricted group of central brain cells. *Neuron* 15, 345–360. doi:10.1016/0896-6273(95)90039-x

Waddington, C. H., and Perry, M. M. (1960). The ultrastructure of the developing eye of Drosophila. *Proc. Roy. Soc. Biol. Sci.* 153, 155–178.

Weasner, B. P., and Kumar, J. P. (2022). *The early history of the eye-antennal disc of* Drosophila melanogaster, 221.*Genetics*

Weasner, B. P., Weasner, B. M., and Kumar, J. P. (2020). "Ghost in the machine: The peripodial epithelium," in *Molecular genetics of axial patterning, growth, and disease in the Drosophila eye*. Editors Singh Amit and Madhuri Kango-Singh (Switzerland: Springer), 121–141.

Wehrli, M., and Tomlinson, A. (1995). Epithelial planar polarity in the developing Drosophila eye. *Development* 121, 2451–2459. doi:10.1242/dev.121.8.2451

Weismann, A. (1864). Die nachembryonale entwicklung der Musciden nach beobachtungen an Musca vomitoria und Sarcophaga carnaria. *Zeit. Wiss. Zool.* 14, 187–336.

Wessells, N. K. (1965). Morphology and proliferation during early feather development. *Dev. Biol.* 12, 131–153. doi:10.1016/0012-1606(65)90025-4

Wildermuth, H. (1968). Differentiation, pattern formation and mechanisms of transdetermination in heteroplastic and homoplastic transplants of proboscis primordia in Drosophila. *Wilhelm Roux' Arch. fur Entwicklungsmechanik Org.* 160, 41–75. doi:10.1007/BF00573646

Wildermuth, H., and Hadorn, E. (1965). Differenzierungsleistungen der Labial-Imaginalscheibe von *Drosophila melanogaster*. *Rev. Suisse Zool.* 72, 686–694. doi:10.5962/bhl.part.75663

Wolff, T., and Ready, D. F. (1991). The beginning of pattern formation in the Drosophila compound eye: The morphogenetic furrow and the second mitotic wave. *Development* 113, 841–850. doi:10.1242/dev.113.3.841

Wolpert, L. (1969). Positional information and the spatial pattern of cellular differentiation. *J. Theor. Biol.* 25, 1–47. doi:10.1016/s0022-5193(69)80016-0

Won, J. H., Tsogtbaatar, O., Son, W., Singh, A., Choi, K. W., and Cho, K. O. (2015). Cell type-specific responses to wingless, hedgehog and decapentaplegic are essential for patterning early eye-antenna disc in Drosophila. *PLoS One* 10, e0121999. doi:10.1371/journal.pone.0121999

Yang, L., and Baker, N. E. (2001). Role of the EGFR/Ras/Raf pathway in specification of photoreceptor cells in the Drosophila retina. *Development* 128, 1183–1191. doi:10.1242/dev.128.7.1183

Yang, Y., Drossopoulou, G., Chuang, P. T., Duprez, D., Marti, E., Bumcrot, D., et al. (1997). Relationship between dose, distance and time in Sonic Hedgehog-mediated regulation of anteroposterior polarity in the chick limb. *Development* 124, 4393–4404. doi:10.1242/dev.124.21.4393

Zalokar, M. (1943). L'ablation des disques imaginaux chez la larve de Drosophile. *Rev. Suisse Zool.* 50, 17–93.

Zecca, M., Basler, K., and Struhl, G. (1996). Direct and long-range action of a wingless morphogen gradient. *Cell.* 87, 833–844. doi:10.1016/s0092-8674(00)81991-1

Zecca, M., Basler, K., and Struhl, G. (1995). Sequential organizing activities of engrailed, hedgehog and decapentaplegic in the Drosophila wing. *Development* 121, 2265–2278. doi:10.1242/dev.121.8.2265

Zeidler, M. P., Perrimon, N., and Strutt, D. I. (1999). Polarity determination in the Drosophila eye: A novel role for unpaired and JAK/STAT signaling. *Genes. Dev.* 13, 1342–1353. doi:10.1101/gad.13.10.1342

Zelhof, A. C., Ghbeish, N., Tsai, C., Evans, R. M., and McKeown, M. (1997). A role for ultraspiracle, the Drosophila RXR, in morphogenetic furrow movement and photoreceptor cluster formation. *Development* 124, 2499–2506. doi:10.1242/dev.124.13.2499

Zhou, Q., DeSantis, D. F., Friedrich, M., and Pignoni, F. (2016). Shared and distinct mechanisms of atonal regulation in Drosophila ocelli and compound eyes. *Dev. Biol.* 418, 10–16. doi:10.1016/j.ydbio.2016.08.025

Zhou, Q., Zhang, T., Jemc, J. C., Chen, Y., Chen, R., Rebay, I., et al. (2014). Onset of atonal expression in Drosophila retinal progenitors involves redundant and synergistic contributions of Ey/Pax6 and So binding sites within two distant enhancers. *Dev. Biol.* 386, 152–164. doi:10.1016/j.ydbio.2013.11.012

Zhu, J., Nakamura, E., Nguyen, M. T., Bao, X., Akiyama, H., and Mackem, S. (2008). Uncoupling Sonic hedgehog control of pattern and expansion of the developing limb bud. *Dev. Cell.* 14, 624–632. doi:10.1016/j.devcel.2008.01.008

Zhu, J., Patel, R., Trofka, A., Harfe, B. D., and Mackem, S. (2022). Sonic hedgehog is not a limb morphogen but acts as a trigger to specify all digits in mice. *Dev. Cell.* 57, 2048–2062.e4. doi:10.1016/j.devcel.2022.07.016

# Frontiers in
# Cell and Developmental Biology

**Explores the fundamental biological processes of life, covering intracellular and extracellular dynamics.**

The world's most cited developmental biology journal, advancing our understanding of the fundamental processes of life. It explores a wide spectrum of cell and developmental biology, covering intracellular and extracellular dynamics.

---

## Discover the latest Research Topics

See more →


**Frontiers**

Avenue du Tribunal-Fédéral 34
1005 Lausanne, Switzerland
frontiersin.org

**Contact us**

+41 (0)21 510 17 00
frontiersin.org/about/contact